# Experimental Studies of Performance and Emissions in a 2/4-Stroke Engine with Gasoline and Ethanol

A thesis submitted for the degree of Doctor of Philosophy

By

**Mohammed Moore Ojapah**

School of Engineering and Design
Brunel University London
United kingdom

February 2014

Brunel University London

School of Engineering and Design
United Kingdom

**Experimental Studies of Performance and Emissions in a 2/4-Stroke Engine with Gasoline and Ethanol**

February 2014

**Abstract**

Direct Injection (DI) gasoline engines are staging a come-back because of its potential for improved fuel economy through principally the engine down-sizing by boosting, stratified charge combustion and Controlled Auto Ignition (CAI) at part load operations. The problem with the Spark Ignition (SI) engine is its inherent low part-load efficiency. This arises due to the pumping loses that occur when the throttle closes or partially opens. One way of decreasing the pumping losses is to operate the engine lean or by adding residual gases. It is not possible to operate the engine unthrottled with a very lean or diluted mixture at low loads due to misfire. However, the load can also be controlled by changing the valve timing. This reduce the pumping loses and hence increase the efficiency.

Due to the limited time available for complete fuel evaporation and the mixing of fuel and air mixture, locally fuel rich mixture or even liquid fuel can be present during the combustion process. This causes a significant increase in Particulate Matter (PM) emissions from direct injection gasoline engines compared to the conventional port fuel injection gasoline engines, which are of major concern because of its health implications.

In the meantime, depleting reserves of fossil fuels and the increasing environmental pollution caused by burning of fossil fuels, have paved the way for fuel diversification. Cleaner and renewable fuel is being introduced worldwide. The use of ethanol as an alternative transportation fuel shows promise for several reasons. While ethanol can be produced from several types of biomass, it offers properties such as high octane number, higher oxygen content and high heat of evaporation, which make it a most attractive alternative fuel, in particular for the direct injection gasoline engine.

In this research, a single cylinder camless engine equipped with an electro-hydraulic valve train system has been used to study and compare different engine operation modes in the SI

and CAI combustion. The fuel consumption, gaseous and particulate emissions of gasoline and its mixture with ethanol (E15 and E85) were measured and analysed at the same engine operating condition. The heat release analysis and performance characteristics of CAI and SI combustion were carried out by the in-cylinder pressure measurement. The effect of load and valve timings on the gaseous and Particulate Matter (PM) emissions was investigated for both 4-stroke SI and CAI combustion. Within the achieved CAI operational ranges, particle emissions were found to be dominated by smaller particles (<50nm). Hotter charge and better mixing are the main parameters affecting the soot particles in the exhaust irrespective of the combustion modes and valve timings.

At part-load conditions investigated, it was found that the CAI combustion produced the lowest NOx emissions of 0.4g/KWh in all fuel blends and lower fuel consumption 223g/KWh with improved combustion efficiency of 94.7% in ethanol fuel E15 and E85. The positive valve overlap was found to produce lowest fuel consumption of 222.8 g/KWh in all fuel blend and respond better to ethanol fuel in E15 and E85 with improved indicated efficiency of 40.5% compared to the other modes investigated. The early intake valve throttled SI operation led to a moderate improvement in the fuel consumption of 243.5g/KWh over the throttled SI operation but it was characterised by the slowest combustion and highest CO (33.5g/KWh) and HC (16.8g/KWh) emissions . Less and smaller particles numbers were detected for Early Intake Valve Closure (EIVC) from the combustion of E0 and E15 (4.0E+07#/cm3 less than 50nm in diameter) fuel blends. The particulate emission results showed that soot was the dominant particles in the exhaust, which could be reduced by leaner mixture combustion

.

**Acknowledgements**

I will like to express my greatest gratitude to my Supervisor Professor Hua Zhao for all the help, guidance and assistance I got from the first day he asked me to join this project. By accepting me as his PhD student in the Centre for Advanced Powertrain and Fuels (CAPF) and the early encouragement he gave to me to publish and present in international and local conference. I owe him for all the knowledge and experience acquired during the past 4 years.

I am highly grateful to the Tertiary Education Trust Fund and University of Portharcourt Nigeria for the financial support that made it possible for my study and stay in the UK.

I will like to thank Dr Yan Zhang for all his assistance in operating the engine, use of software and data analysis. I am most grateful to him.

My sincere thanks go to my second supervisor Dr Lionel Ganippa for all his assistance.

I want to express my sincere thanks to all the technicians: Andy Selway, Clive Barrett, Ken Anstiss in the laboratory for all their assistance and advice.

I will like to thank all my good friends and colleagues. Dr Seong-Ho Gin, Dr Barnaby Coates, Dr Cho-Yu Lee, Dr MohammedReza Attas, Nehemiah Alozie Sabinus, Pin Lu, and Maclene.

I owe great gratitude to my big brother, Chris Mendoza Ojapah, who has never failed to support me and help me out in all possible way throughout my academic career.

I am deeply indebted to my little daughter Oyiza Nelissa Ojapah, for having to stay away from me so early in her life. I owe you a great deal and your daddy loves you.

Last but not the least I am highly indebted to my very special darling wife, Suzanne, for all direct and indirect support and affection she has shown throughout the good and bad times that I have gone through during this PhD programme. You are more than a darling.

## Nomenclature

### General Abbreviations

| | |
|---|---|
| AFR | Air/Fuel Ratio |
| AI | Auto-Ignition |
| ATAC | Active Thermo-Atmospheric Combustion |
| ATDC | After Top Dead Centre |
| BDC | Bottom Dead Centre |
| BMEP | Brake Mean Effective Pressure |
| BSCO | Brake Specific Carbon Monoxide |
| BSFC | Brake Specific Fuel Consumption |
| BSHC | Brake Specific Hydrocarbon |
| BSNOx | Brake Specific Nitric Oxide |
| BTDC | Before Top Dead Centre |
| CA | Crank Angle |
| CA10 | 10% mass fuel burnt crank angle |
| CA50 | 50% mass fuel burnt crank angle |
| CA90 | 90% mass fuel burnt crank angle |
| CAI | Controlled Auto Ignition |
| CI | Compression Ignition |
| COV_imep | Coefficient of Variation in IMEP |
| CR | Compression Ratio |
| DAQ | Data Acquisition |
| DI | Direct Injection |
| ECU | Engine Control Unit |
| ECM | Engine Control Module |
| ECR | Effective Compression Ratio |
| EGR | Exhaust Gas Recirculation |
| EGT | Exhaust Gas Temperature |
| EIVC | Early Intake Valve Close |
| EV | Electric Vehicle |
| EVC | Exhaust Valve Close |
| EVO | Exhaust Valve Open |
| FFVVA | Fully Flexible Variable Valve Actuation |
| FMEP | Friction Mean Effective Pressure |
| GDI | Gasoline Direct Injection |
| HC | Hydrocarbon |
| HCCI | Homogeneous Charge Compression Ignition |
| HRR | Heat Release Rate |
| ICE | Internal Combustion Engine |
| IEGR | Internal Exhaust Gas Recirculation |
| IMEP | Indicated mean Effective Pressure |
| ISCO | Indicated Specific Carbon Monoxide |
| ISFC | Indicated specific fuel consumption |
| ISHC | Indicated specific hydro carbon |
| ISNOx | Indicated specific NOx |
| IVL | Intake Valve Lift |
| IVO | Intake Valve Open |

| | |
|---|---|
| IVC | Intake Valve Close |
| KW | Kilowatts |
| LEV | Low Emission Vehicles |
| LHV | Lower Heating Value |
| MBT | Minimum Spark Advance for Best Torque |
| MFB | Mass Fraction Burned |
| NVO | Negative Valve Overlap |
| PAH | Polyschyclic Aromatic Hydrocarbons |
| PFI | Port Fuel Injector |
| PM | Particulate Mass |
| PMEP | Pumping Mean Effective Pressure |
| PN | Particulate Number |
| PPM | Parts Per Million |
| PRF | Primary Reference Fuel |
| PVO | Positive valve overlap |
| RGF | Residual Gas Fraction |
| RON | Research Octane Number |
| RPM | Revolution Per Minute |
| SGDI | Stratified Gasoline Direct Injection |
| SI | Spark Ignition |
| SOI | Start of Ignition |
| SULEV | Super Low Emission Vehicle |
| TDC | Top Dead Center |
| ULEV | Ultra Low Emission Vehicle |
| UHC | Unburnt Hydrocarbon |
| VCU | Valve Control Unit |
| VOC | Volatile Organic Fraction |
| VVA | Variable Valve Actuation |
| VVT | Variable Valve Timing |
| WOT | Wide Open Throttle |
| ZEV | Zero Emission Vehicle |

**General Notation**

| | |
|---|---|
| E0 | Pure Gasoline |
| E15 | 15% ethanol gasoline blend |
| E85 | 85% ethanol gasoline blend |
| Pi | Indicated Power |
| $\lambda$ | Relative air/fuel ratio |
| $\theta$ | Crank Angle |
| V | Volume |
| Vc | Clearance Volume |
| Vd | Displaced Volume |
| $\eta_c$ | Combustion efficiency |

**Contents** **Page**

## List Of Figures

## List Of Tables

# Chapter 1 Introduction

## 1.1 Introduction

Human civilization is facing significant socioeconomic and environmental challenges created by mankind. The invention and production of the internal combustion (IC) engine that powered the motor vehicles for more than a century ago had enabled rapid development socioeconomically worldwide. However, the emissions resulting from incomplete combustion of fuel used in engines and the release of chemicals, such as Carbon monoxide (CO), carbon dioxide ($CO_2$), oxides of nitrogen (NOx), unburnt hydrocarbon (UHC) and Particulate matter (PM) are still major issues affecting the society globally by way of global warming, and locally in the form of acid rain, and health effect.

Over the years extensive research and development of the internal combustion engines have enabled the car manufacturers to introduce new technology that had led to lower emissions, reduced fuel consumption and improved the engine performance. However, as the number of people using motor vehicles continue to increase and their energy needs. Governments on one hand monitoring the environmental impact on emissions from road vehicles have continue to enact stringent regulations on emissions from road vehicles.

Additionally, as fuel costs reach new levels and limited availability, the economic repercussions of business as usual could be devastating. With increasing annual population growth rates and more corresponding number of vehicle demand, resulting in substantial fuel consumptions, there is little evidence that emissions reduction will occur through a decrease in the amount of vehicle use. There is a substantial opportunity to reduce the amount of carbon and smog-generating chemicals released into the atmosphere by concentrating on cleaner and more efficient transportation strategies.

The $CO_2$ legislation due to global warming has mandated the development of more efficient IC engines. There are several options for realizing more efficient and less polluting or cleaner transportation powerplants or IC engines, including continued advancement in internal combustion (IC) strategies, hybrid power train and fuel cells.

Advanced IC engines and hybrid power-trains are more practical today than fuel cells and will likely continue to be so for the foreseeable future. Among advanced IC engine strategies, the gasoline direct injection (GDI) are staging a come-back and variable valve timing (VVT) engine because of its potential for improved fuel economy principally through the engine

down-sizing by boosting or 2-stroke operation, and possibly stratified charge combustion or Controlled Auto Ignition (CAI) or homogeneous charge compression ignition (HCCI) at part-load operations where vehicles are operated most times. The most promising is the HCCI/CAI combustion, where the compression induced auto-ignition of a uniform fuel and air mixture. This is achieved by control of the in-cylinder operational parameters such as pressure and temperature with high residual dilution using wide open throttled (WOT) position.

The HCCI engine combines features of both gasoline and diesel engines utilising the advantages of GDI and VVT. The fuel and air are premixed either prior to entering the engine cylinder in port-fuel injection (PFI) engines or mixed in the cylinder such as in GDI engine. However, the mixture is compression-ignited like a diesel rather than a spark-ignited engine. HCCI/CAI engine run well on lean fuel/air mixture which leads to lower combustion temperature favouring ultra-low NOx emissions and good thermal efficiency. In PFI engine the fuel/air mixture is premixed, there are no locally fuel-rich regions that are conducive to soot formation. However, in GDI engines due to the limited time available for complete fuel evaporation and the mixing of fuel and air mixture, locally fuel rich mixture or even liquid fuel can be present during the combustion process. This causes significant increase in particulate matter (PM) emissions from direct injection gasoline engines compared to the conventional port fuel injection gasoline engines, which are of major concerns because of its health implications

Although experimental HCCI/CAI engines have shown good thermal efficiencies and low emission of NOx and soot, several technical hurdles stand in the way of their commercialisation. In particular HCCI/CAI engines operate stably over a fairly narrow range of operating conditions. For very lean fuel-air mixtures (used at low power and idle conditions), the engine can misfire. For near-stoichiometric mixtures (used at high power), significant pressure waves develop in the combustion leading to noisy operation (knock) and possibly structural damage.

In the meantime, depleting reserves of fossil fuels and the increasing environmental pollution caused by burning of fossil fuels, have paved the way for fuel diversification. Cleaner and renewable fuel is being introduced worldwide. The use of ethanol as an alternative transportation fuel shows promise for several reasons. While ethanol can be produced from several types of biomass, it offers properties such as high octane number, higher oxygen

content and high heat of evaporation, which make it as a most attractive alternative fuel, in particular for the direct injection gasoline engine.

The primary goal of this work was to develop a better understanding tool that could predict and control the stable operating range in different SI and HCCI/CAI combustion modes and use the tool to design an engine that is stable over a broad range of operations.

### 1.2 Objectives

In response to the above challenges, an extensive research programme has been set up at Brunel University where all experiments were conducted in a newly commissioned single cylinder engine research facility. It comprises of a unique state of the art single cylinder direct injection gasoline camless engine. The single cylinder camless Engine is coupled to an AC dynamometer for motored and firing operations. The engine is capable of 2 and 4 stroke cycle operations through the flexible electro-hydraulic actuated intake and exhaust valves. The main objectives of this research work are;

1. To operate the engine in different SI and CAI combustion modes and cycles and evaluate their effect on the engine efficiency, the gaseous and particulate emissions.

2. To investigate the effect of bio-fuels in ratio of 15% and 85% gasoline-ethanol blends on the combustion and emissions by measuring the engine efficiency, the gaseous and particulate emissions.

3. To investigate the effect of the relative air fuel ratio on efficiency and emissions in SI and CAI modes at a typical part load condition of 3.2 bar IMEP_net and 1500rpm**.**

4. To study the effect of early intake-valve closure (EIVC) on part-load performance and emissions with different air/fuel mixtures and blends of gasoline and ethanol.

### 1.3 Outline of Thesis

Following the introduction in Chapter 1, Chapter 2 summarises in six parts the literature review published in relations to the objectives of this research. The first part provides overview of automotive powertrain technology, by looking at the different powertrains and where they stand in terms of practical applications and future directions in powertrain developments. The second part of the chapter introduces the internal combustion engines, the

associated emissions and the legislation internationally on global warming and the local legislations, and the expectations from engine manufacturers on emission reduction from their fleets. The third part looks at recent developments in spark ignition engines in the form of gasoline direct injection (GDI) and variable valve timing (VVT). The fourth part review the history and development of HCCI/CAI combustion, the combustion operating strategies, the residual gas trapping methods to initiate auto-ignition and the challenges in commercialising HCCI/CAI combustion.

The fifth part gives general overview of work done on the fuel effects on HCCI/CAI combustion, gasoline and its ethanol blends. This is important as efforts are now focused on diversification from gasoline, and ethanol seems the most promising candidate in terms of availability and sustainability.

Part six of this chapter examines the work done on particulate emissions to date in SI and CAI combustion using gasoline and its ethanol blends are discussed.

Chapter 3 gives a general overview of the engine set-up and its components. The engine specifications and the test bed are discussed, along with the electro-hydraulic valve actuator. The engine has the capability of varying the four valve timing and lift independently according to the engine load and speed for optimum performances. The cylinder head, the fuel injector, the ignition, the gaseous and particulate analyser are discussed.

Chapter 4 details the experiments performed in thirteen different operational modes with special emphasis on particulate emissions at full load. The test procedures and modes using 4-stroke and 2-strokes, the valve and injection timing are given in the first section. This is followed by the particulate number emissions and the total particulate number. The efficiency, the gaseous emissions, the heat release rate and mass fraction burned, the combustion temperature and exhaust temperature, and the fuel consumption charts then follow to support explanations for the particulate emissions results obtained.

Chapter 5 details the experiment in three operational modes of throttled SI, positive valve overlap (PVO) SI and CAI negative valve overlap (NVO) combustions at 3.2 bar IMEP_net at MBT and 1500rpm engine speed. Lambda was varied between 1 and 1.2 using pure gasoline, gasoline ethanol blends in ratio of 15% (E15) and 85% (E85). The throttle was wide opened in PVO and CAI combustion. The combustion was first analysed, followed by the engine efficiency, then the gaseous, the fuel consumption and particulate emissions.

Chapter 6 contains discussions of the result obtained by early intake valve closing (EIVC) in part-load with reduced intake valve-lift to 2mm in height, at the same engine operational conditions as in chapter 5 and their effects on combustion, performances, fuel consumption, gaseous and particulate emissions was discussed.

Chapter 7 summarises the conclusions that have been drawn from the previous chapters on the investigations carried out on CAI and SI combustion in different engine operational modes, loads and fuel blends. Recommendations for additional work and suggestions are also given for future research work and development into CAI and SI combustions.

# Chapter 2 Literature Review

## 2.1 Overview of Automotive Powertrain Technologies

Over the last few decades, the increasing shortage of fossil fuel reserves, stringent emissions legislation and global warming has increased pressure on manufacturers to develop a more efficient, clean and environmentally friendly powertrain for vehicles. The car manufacturers' ultimate aim is the development of zero emission vehicles (ZEVs) capable of acceptable performance. Although this technology has already been introduced onto the market (the electric vehicle), there are still many challenges to be met before it can be used in production vehicles.

Some of the challenges currently being faced include developing new fuel-cell technologies, modifying present infrastructure, addressing storage problems and the cost. As such it is very unlikely that this technology can be fully implemented in the near future.

Electric vehicles (EV's) have been around since before the turn of the century. They were very popular and sold reasonably well until about 1918 [1]. However, this form of propulsion lost favour as gasoline powered internal combustion engines (ICE) continued to improve. By 1933, the number of EV's had reduced drastically due to their slow speed and greater manufacturing costs.

These challenges, which hindered the early development of EVs and prevented it from becoming a viable automotive powertrain, have not yet been totally overcome. However, advances in power electronics, computer and microelectronics have enabled EVs to compete with ICEs. Nevertheless, the advances in battery energy storage are still insufficient, despite extensive on-going research in this area.

The rising price of fossil fuel coupled with its supply dependency has prompted the re-introduction of cleaner, less environmentally damaging EVs. In fact, some major cities in Europe and America have set aside emission-free zones and have enforced stricter emission regulations, encouraging the use of EVs.

The EVs are propelled by an electric motor or motors powered by rechargeable battery packs. The battery can be charged by an on-board power source, such as the ICE (hybrid electric) such as the Chevy Volt by General Motors, or by plugging into an external power source (plug-in hybrid), such as grid connected electric outlet [2].

Many models of hybrid electric vehicle using ICE and battery cells are currently widely used in the market such as Toyota Prius, Honda Insight and Fiat. These vehicles have limited market penetration to date, this is as a result of their higher cost due to the complexity and control of the powertrains, extra battery weight and electric motors.

Whilst hybrid vehicles may satisfy the market in the short term and move it towards ZEV, there has been substantial improvement in performance and emissions achieved in internal combustion engine technology.

## 2.2 Internal Combustion Engines

The internal combustion engine was invented more than a century ago to produce mechanical power from the chemical energy contained in fuel. It has been in a state of constant development, which has led to a deeper understanding of engine processes and inspired new technological breakthroughs [3]. In particular, the development of the internal combustion engine has played a key role in motor vehicle applications and is responsible for shaping the modern world both economically and socially [4]. The global success of the internal combustion engine lies in its suitability for the purpose of motor vehicle propulsion. With a dwindling supply of fossil fuels and their associated link to air pollution, research has recently taken on a new sense of urgency. The internal combustion engine is considered to be one of the major contributors to environmental pollution due to the gaseous and particulate emissions generated and released from its operation.

### 2.2.1 Source of Pollutants and Emission Legislation for Light Duty Vehicles

The emission from petrol and diesel engine combustion includes carbon monoxide (CO), nitrogen oxide (NOx), unburnt hydrocarbons (UHC) and particulate matter (PM).

The sources of the listed pollutants vary and depend on the engine operating conditions and the type of fuel used.

**Carbon monoxide** is produced as a result of rich fuel/air-mixture combustion of carbon compounds such as fossil fuel, its formation rate is controlled primarily by the air-fuel ratio or lambda (λ). The process that governs the formation of CO is kinetically controlled. The formation process may be represented by

$$RH \rightarrow R \rightarrow RCO_2 \rightarrow RCHO \rightarrow RCO \rightarrow CO$$

Here R stands for the hydrocarbon radical. The CO formed in the combustion process is then oxidised to $CO_2$ at a slower rate [3].

The formed CO in exhaust increases rapidly when lambda is less than 1.0. Some of the improvements in reduced CO emissions were achieved by injecting fuel into mixture of hot residuals for better fuel evaporation.

Carbon monoxide gas is very dangerous to human health. In respiration it combines with the haemoglobin in the blood hindering the body ability to absorb oxygen. It causes respiratory conditions and heart disease.

**Nitrogen Oxides** are formed as a result of high temperature combustion in engines. The nitric oxide (NO) and nitrogen dioxide ($NO_2$) are usually grouped together as NOx emissions, Nitric oxide is the predominant oxide of nitrogen produced inside the engine cylinder. These gases are responsible for acid rain. Nitrogen dioxide ($NO_2$) is toxic and is known to cause and aggravate human respiratory diseases. The nitrous oxide contributes directly to global warming. It is generally accepted that in combustion in the region of lambda 1.0 the reaction mechanism of NO formation is

$O + N_2 = NO + N$

$N + O_2 = NO + O$

$N + OH = NO + H$

The temperature and pressure distribution in the cylinder during combustion and expansion process affects the NOx formation. The most important parameters affecting NOx formation are the fuel-air ratio, burned gas fraction and the spark-timing. Substantial reduction of 90-95% in NOx emissions was achieved using hot residuals. Advanced spark-timing led to higher NOx formation.

**The Unburnt Hydrocarbon** (UHC) is a volatile organic compound consisting of a number of different chemicals, which are produced during combustion of fossil fuel as a result of incomplete combustion of the hydrocarbon fuel. The values range between 1000 to 3000 ppm [3].

**Particulate Matters** (PM) are small particles formed by incomplete combustion, the burning of lubrication oil and by the presence of impurities in the fuel. They are known to cause and aggravate human respiratory diseases and are thought to be carcinogenic.

The negative environmental impact of the combustion engine has resulted in many governments imposing stringent conditions stipulating the level of pollutant that may be emitted from vehicles. As a result of the increasing restrictions for spark-ignition and compression-ignition engines, there is an urgent need to develop an alternative combustion system for the automotive powertrain.

The emissions from the gasoline combustion engine include carbon dioxide ($CO_2$) and carbon monoxide (CO), partially burnt fuel present in the exhaust (UHC) such as methane ($CH_4$), nitric oxide (NOx) and particulate matter (PM).

Recent data [5] showed that vehicle emissions contribute to the increasing concentration of gases that are leading to climate change. In order of significance, the principal greenhouse gases associated with road vehicles are $CO_2$, $CH_4$ and nitrous oxide ($N_2O$). Road transport constitutes the third largest source of UK greenhouse gases and accounts for over 20% of total emissions.

The data shows that over 85% of emissions from motor vehicles are as a result of CO2 emissions, which contribute to the greenhouse effect. The rise in vehicle usage and ownership is directly proportionate to the amount of pollution being released. Furthermore, the motor vehicle also constitutes the major source of local emissions, including benziene, 1,3-butadiene, CO, NOx and PMs.

The alarming increase in emissions has prompted many nations to agree to reduce the production of greenhouse gases. Kyoto protocol attempts to address this issue by requiring each nation to meet an annual percentage target.

The UK was required to reduce the production by 12.5% below base year levels over the 2008-2012 period. This translates to annual emissions of 682.4 million tonnes carbon dioxide equivalent ($MtCO_2e$) on average over the period.

In performance, excluding emissions trading, UK exceeded the target, achieving 26.7% below the baseline. With emission trading included, the result was 24.9% below the baseline by 2012 [6].

The European Union (EU) directives have been instrumental in reducing what is called regulated emissions. These include CO, NOx, UHC, and PM less than 10 microns [5]. This was first introduced in 1992, these forms a rolling regulations designed to become more stringent year on year. New cars and light-duty vans must conform to 'Euro VI' standards to be introduced in 2014-2015.

The effect of tighter Euro standards on vehicle emissions has been to accelerate the introduction of greener vehicle technologies. In gasoline engine this had been achieved in part through the use of the three-way catalytic converter and the move to fuel injection systems, and mostly through engine downsizing.

The results of these regulations have resulted in advanced engine technology improvement, together with the cleaner fuels that made these developments possible. These have resulted to a dramatic reduction in regulated pollutants.

Table 2.1 provides the summary of the emissions legislation currently in the EU for passenger cars

Euro VI regulation will be introduced in 2014-2015. In addition, a new standard for particle numbers has been set to 6E+11 #/km for Euro VI in 2015 for light duty vehicles, including both gasoline direct injection (GDI) and diesel engines.

**Table 2.1 Present and Proposed Emission Levels Legislated in the EU for light duty vehicles**

| Euro Standard | Year of Implementation | CO (g/km) | THC (g/km) | NMHC (g/km) | NOx (g/km) | HC+NOx (g/km) | PN (#/km) |
|---|---|---|---|---|---|---|---|
| **Diesel** | | | | | | | |
| **Euro I** | 1993 | 2.72 | - | - | - | 0.97 | |
| **Euro II** | 1997 | 1.00 | - | - | - | 0.70 | |
| **Euro III** | 2001 | 0.64 | - | - | 0.5 | 0.56 | |
| **Euro IV** | 2006 | 0.50 | - | - | 0.25 | 0.30 | |
| **Euro V** | 2010 | 0.500 | - | - | 0.180 | 0.230 | 6E+11 |
| **Euro VI** | 2014 | 0.500 | - | - | 0.080 | 0.170 | 6E+11 |
| **Petrol** | | | | | | | |
| **Euro I** | 1993 | 2.72 | - | - | - | 0.97 | - |
| **Euro II** | 1997 | 2.20 | - | - | - | 0.50 | - |
| **Euro III** | 2001 | 2.30 | 0.20 | - | 0.15 | - | - |
| **Euro IV** | 2006 | 1.00 | 0.10 | - | 0.08 | - | - |
| **Euro V** | 2010 | 1.000 | 0.100 | 0.068 | 0.060 | - | 6E+11** |
| **Euro VI** | 2014 | 0.100 | 0.100 | 0.068 | 0.060 | - | 6E+11** |

** GDI

### 2.2.2 CO2 Emission and CO2 Legislation for Light Duty Vehicles

#### 2.2.2.1 CO2 Emission

Carbon dioxide ($CO_2$) is nontoxic, and it was expected to have high emission of $CO_2$ as evidence of good combustion. However, the main environmental effect is as a greenhouse gas. By enhancing the greenhouse effect, the greenhouse emissions are leading to increases of the Earth's atmospheric temperature, land and sea temperature [5,6]. Road transport was reported to contribute about one –fifth of the EU's total emissions of carbon dioxide [5]. It was also reported that this increased by nearly 23% between 1990 and 2010, and without any economic downturn growth it could have been higher. The transport sectors are reported as the only major sector in the EU where greenhouse gas emissions are still rising.

It was reported by [5, 6] that light-duty vehicles such as vans and passenger cars are a major source of greenhouse gas emissions, producing around 15% of the EU's emissions of $CO_2$**.**

#### 2.2.2.2 CO2 Legislation

Following up on a European Commission strategy adopted in 2007, the EU has put in place a comprehensive legal framework to reduce $CO_2$ emissions from new light duty vehicles as part of efforts to ensure it meets its greenhouse gas emission reduction targets under the Kyoto Protocol and beyond.

The legislation sets binding emission targets for new car and van fleets. As the automotive industry works towards meeting these targets, average emissions are falling each year.

For cars, manufacturers are obliged to ensure that their new car fleet does not emit more than an average of 130 grams of $CO_2$ per kilometre (g $CO_2$/Km) by 2015 and 95g by 2020. This compares with an average of almost 160g in 2007 and 135.7g in 2011.

In terms of fuel consumption, the 2015 target is approximately equivalent to 5.6 litres per 100 km (l/100 km) of petrol or 4.9 l/100 km of diesel. The 2020 target equates approximately to 4.1 l/100 km of petrol or 3.6 l/100 km of diesel [5,6]. This

For vans the mandatory target is 175 g $CO_2$/Km by 2017 and 147g by 2020. This compares with an average of 203g in 2007 and 181.4g in 2010 [5,6]. In summary the key solution to control of $CO_2$ is to reduce fuel consumption.

## 2.3 Recent Developments in Spark Ignition Gasoline Engines

### 2.3.1 Direct Injection and Engine Downsizing

Engine downsizing reduces the fuel consumption of a vehicle by shifting the IC engine operation points to the most efficient region at high load and reducing the percentage of mechanical loss through the use of a smaller engine. In order to maintain the vehicle performance, the downsized engine is normally boosted by a turbo and/or a supercharger and the engine remains operational in the 4-stroke cycle. Furthermore, direct-injection gasoline engines have been developed recently because of their potential for better fuel economy and better performance through unthrottled part-load operation and, in particular, engine downsizing technology. Direct injection is often used to take advantage of its charge-cooling

effect for high-compression operations without knocking combustion. In addition, engine downsizing can be achieved by operating an engine in the 2-stroke mode.

The direct injection technology was first applied in 1952 by Goliath and Gutbrod [7] to improve power output. The DI has become more attractive because of the flexibility of fuel injection, either early-for homogeneous mixture or late-for stratified combustion at part-load to improve fuel economy and reduce emissions.

Stratified charge enables optimal process efficiency at part-load operation of a gasoline engine with direct injection. Fuel is injected during or only towards the end of the compression stroke. This makes it possible to ensure stratification of the charge in the combustion chamber. An ignitable mixture is required in the vicinity of the spark plug at point of ignition. In areas further away from the spark plug, either a very lean but still combustible mixture or pure air or pure exhaust gas through systematic exhaust-gas recirculation should be available [8]. This is to reduce fuel consumption and emissions at part-load operations typical of urban traffic driving.

The flexibility in injection-timing enables fuel-injection during the negative valve overlap (NVO) in CAI/HCCI for fuel reforming that allows a better mixture preparation.

### 2.3.2 Variable Valve Actuation

In recent years, different mechanical variable valve-lift systems have been implemented in production engines. They range from the 2-step cam profile switching [9, 10] to continuous mechanical variable lift mechanisms, such as BMW Valvetronics and Fiat's multi-air valve actuation system. Such mechanical and electro-hydraulic systems allow the valve-lift and duration to be changed, although not independently. Fully Flexible Variable Valve Actuation (FFVVA) systems are capable of independent control over the valve-lift, opening and closing timings, and duration. The FFVVA camless system can be either electro-magnetic, electro-pneumatic or electro hydraulic and drive individual engine valves directly [11- 20]. They offer more control and freedom while improving engine performance and emissions. They have been used to operate the 2/4-stroke switchable gasoline engine [21] and air-hybrid engine [22]. But high energy consumption, cost, packaging and durability issues have limited FFVVA to research engines.

#### 2.3.2.1 Early Intake Valve Closing (EIVC)

In addition, Early Intake Valve Closing (EIVC) can be effective in reducing the pumping loss at part-load operation of a SI gasoline engine. The EIVC timing is a technique where the intake-valve is closed before BDC when the required quantity of air has been admitted into the cylinder, instead of closing the intake throttle. The EIVC can be achieved by both reduced valve-lift and duration with a low lift cam lobe using a mechanical variable valve actuation system or a shorter duration with a camless valve actuation system.

Several studies have been undertaken on the effectiveness of EIVC to reduce fuel consumption. An early study by Kreuter et al [23] suggested that the EIVC with a maximum valve-lift of 2mm or less could result in higher flow-in velocities even at low engine load and speed. The resulting micro-turbulences in the area between valve and valve seat effectively support a mechanical mixture preparation and help to compensate for the reduction of in-cylinder turbulence, which is principally associated with unthrottled load control by means of early intake-valve closing.

Vogel et al [24] investigated the effect of EIVC on fuel consumption and pumping losses using a Ford Zetec, 4 cylinder, 2.0l engine fitted with a secondary valve assembly between the cylinder head and the original intake manifold of the engine. The aim was to implement EIVC with the secondary valve. Such a strategy enabled a 70% reduction in pumping loss and a 4% improvement in fuel economy.

Kreuter et al [25] recorded a noticeable improvement in fuel consumption at low speed and low load conditions. It was also reported that the EIVC resulted in poor combustion as a result of reduced in-cylinder turbulence, temperature, and reduced mixing through the inlet valve.

Soderberg and Johansson [26] investigated the load control by the EIVC and LIVC control using symmetric and asymmetric valve-timings. Their results indicated a longer flame development period with EIVC than the throttled SI, while varied combustion duration results were found for LIVC. The pumping mean effective pressure (PMEP) was reduced for both EIVC and LIVC compared to throttled SI.

Urata et al [27] developed Hydraulic Variable-valve Train (HVT) that can be closed at arbitrary timings and capable of withstanding engine speeds up to 6000rpm, they reported a

reduced pumping loss of 80% and about a 7% reduction in fuel consumption. Lower in-cylinder compression temperature and increased combustion fluctuation under low load was also observed.

More recently, Patel et al [28] reported that the EIVC could be used to improve part-load fuel efficiency in a direct-injection gasoline engine.

#### 2.3.2.2 Late Intake Valve Closing (LIVC)

The major challenge of the conventional throttled SI engine at part-load is the throttling process and the consequential low pressure at the end of the compression stroke. In late intake valve closing (LIVC), the inlet valve is

Gasoline engine downsizing allows for improvement in fuel consumption by load point shifting, operating the engine at lower pumping loss regions of the operating map for a given power demand.

Miklanek et al [29] used a 1-D code to calculate the in-cylinder pressure and fuel economy improvement for both unconventional cycles with and without mixture heating. They observed significant improvement in fuel economy compared to Otto cycle, especially due to Miller cycle.

Hong et al [30] Simulated a single-cylinder engine by GT-Power software. They analysed different VVT philosophies and concluded that with proper VVA mechanism design and control, it can be expected that PV cycle of any VVT engine can achieve near-zero pumping loses, maximum gas-exchange efficiency and minimization of exhaust pollutants.

Xin He et al [31] investigated the benefit of the LIVC on particulate emissions due to the longer ignition delay time and a subsequent reduction in local fuel-rich combustion zones, more than 95% reduction in particulates was observed at some operating conditions.

Wang et al [32] implemented the LIVC using DMF, Bio-Ethanol and pure gasoline. The result indicated that the gasoline-fueled Miller cycle has a higher efficiency of 6.9% at 7.5bar IMEP_net and lower emissions compared with the Otto cycle under the same condition. However, the improvement is not evidenced with bio-ethanol or DMF and to take advantage of Miller cycle for bio-ethanol and DMF higher compression ratios and/or boosting are needed.

Taylor et al [33] achieved high-load combustion-phasing improvements through a reduced effective compression ratio and improvements at part-load through pumping reduction.

Other researchers have conducted several tests on LIVC. Asmus [34] stated that the volumetric efficiency increases in LIVC at higher speeds because the mixture high-flow momentum continues to charge the cylinder even though the piston is travelling upwards. But at lower speeds it will penalize the volumetric efficiency because the intake manifold and cylinder pressures are equal at BDC, and this will result in some fresh charge being pushed back into the intake manifold.

Rabia and Korah [35] investigated the knocking phenomena and established that knocking onset in LIVC increases with decreasing engine speed. This is as a result of a lower air-fuel ratio and richer mixture, which decreases the flame speed and thus cause knocking. It was also established that the maximum pressure inside the cylinder of LIVC is lower than in conventional engines. This is because the amount of effective mixture left for combustion after the intake is less in LIVC engines.

## 2.4 CAI Combustion in Gasoline Engines

### 2.4.1 Introduction

A controlled Auto Ignition (CAI) gasoline engine is an attempt to combine the high efficiency of a diesel engine with the low emissions of an SI engine.

CAI combustion is a spontaneous and fast, chemical reaction driven by the elevated charge temperature. This high temperature is produced by compression through a high geometric compression ratio and by the presence of substantial hot exhaust gas residuals that have been trapped using an advanced exhaust valve closing (EVC) strategy. This trapping of exhaust gas residuals represents the predominant method of load control since, in CAI mode; the engine is run with a wide-open throttle to minimize pumping loss. Increasing or decreasing the mass of exhaust gas residual in the cylinder decreases or increases the mass of fuel and air that can be inducted thereby leading to lower or higher engine load.

In general, combustion in the CAI engine is not limited to stoichiometric fuel-air equivalence ratios. However, in a typical urban driving cycle, the CAI/SI engine frequently operates in the SI mode. In this mode, emission reduction through the three-way catalyst is necessary. In order to ensure optimal performance of the catalyst immediately following transitions from

CAI mode to SI mode, the ($O_2$) storage capacity of the catalytic converter must be maintained. This requirement is most easily accomplished by requiring that lambda (λ) in the CAI regime be stoichiometric. This strategy will be followed in this work.

By design, CAI/SI engine is a dual mode engine that operates in SI mode wherever CAI mode is neither feasible nor possible.

At high loads, the CAI regime is limited by knock brought about by insufficient dilution of the in-cylinder charge and high overall temperature. As speed increases, heat transfer to the cylinder walls, piston and cylinder head decreases thereby exacerbating knock and further lowering the CAI boundary. At low loads, the charge is overly diluted by exhaust gas residuals leading to misfire. As speed increases, this low load limit improves; the engine can be operated at lower loads because of the decrease in cycle heat transfer, until the excess dilution effects overpowers the heat transfer effect. At high speeds, insufficient reaction times lead to misfire. Finally, at low engine speeds, excessive heat transfer leads to misfire since there is insufficient thermal energy remaining to initiate the reaction.

CAI combustion represents a practical implementation of the more general homogeneous charge compression ignition (HCCI) combustion.

### 2.4.2 Historical Background

The history of HCCI/CAI combustion and the subsequent development of the SI/CAI engine is briefly described as follows. HCCI/CAI combustion was first demonstrated in internal combustion engines by Onishi et al [36] for use in two-stroke engines, through the use of hot residual gas retained in the cylinder. Since then a large number of studies of CAI from experimental and modelling point of view have been completed. More recently, control of the process has become another focus of the research community.

Thring [37] suggested that a passenger car engine could be designed that would use HCCI at idle and light load to obtain fuel economy like that of diesel, along with smooth operation, while switching to a conventional gasoline engine at full power for good specific power output and noted that high in-cylinder temperatures were needed to auto-ignite the combustible mixture of the air and fuel. In his work Thring used intake air heating with a relatively low compression ratio to achieve the required in-cylinder temperatures. Unfortunately, intake air heating is not a method of control suitable to most internal combustion engine applications since the large thermal inertia of the intake air stream, the

intake manifold system, the cylinder head and the power cylinder components make transient engine operation and control difficult.

Later investigators of four-stroke gasoline HCCI engines, notably Aoyama et al [38], used high compression ratios to achieve in-cylinder temperatures. This, too, was not a practical method of control since the engine would be limited to only HCCI combustion, as its high compression ratio would make it prone to knock when run in SI mode. Meanwhile, Investigators of two-stroke HCCI combustion, notably Ishiobashi and Asai [39], had determined that residual exhaust gas could be used to initiate and control HCCI combustion.

Kontarakis et al [40] were the first to use modified valve timing; specifically, early EVC and late IVC, to trigger CAI combustion in a four-stroke gasoline engine by entrapment of hot exhaust gas. They concluded that practical application of this HCCI concept will require variable valve timing.

Allen and Law [41] was one of the first to use an elecro-hydraulic active valve train (AVT) to trap exhaust-gas residuals leading to spontaneous combustion of a stoichiometric air-fuel ratio. Numerous other investigators notably Koopmans et al. [42], Zhao et al. [43] and Wolters et al. [44], have demonstrated CAI combustion using variable-valve-timing (VVT) mechanisms to trap hot exhaust gas. In most investigations, advanced EVC and retarded intake valve opening (IVO) were used to trap hot exhaust gas. Subsequent mixing of the fuel and air with hot gas creates localised hot spots throughout the mixture. Compression further increases the mixture temperature leading to auto-ignition.

However, Zhao et al. [45], and other researchers have shown that, in contrast to SI operation, the CAI/HCCI combustion process produces near zero NOx, and can be operated with very lean or diluted mixtures, which leads to significantly improved fuel economy. The use of residual gas trapping is currently considered as one of the most appropriate methods to achieve CAI combustion in a gasoline engine and a large amount of residual gas has to be used in order to obtain CAI combustion in a reciprocating engine. This residual gas is required for two reasons; firstly, to use this high temperature to heat up the intake charge for auto-ignition, and secondly, to control combustion through its dilution effects. It has been shown that a large negative valve-overlap, which involves early exhaust-valve-closing and late intake valve-opening, is a very effective method in retaining sufficient hot residual gases for CAI combustion in the 4-stroke gasoline engine. The results have shown that the NOx emission could be reduced by about 95% lower than that of SI.

However, the current operational range of CAI combustion in a 4-stroke gasoline engine is relatively small and there is no effective means to alter the onset of auto-ignition and the subsequent heat release. The 2-stroke cycle in a poppet-valve engine is inherently more able to retain residual gas, it is ideally suited to operate with CAI combustion. More importantly, with the same maximum indicated mean effective pressure (IMEP) achievable for CAI combustion, the road load operating range in the 2-stroke mode will be twice as much as that in 4-stroke mode because of doubling of the engine output torque in the 2-stroke, offering much greater fuel economy and lower exhaust emissions.

Despite the availability of other methods for achieving CAI, such as intake air pre-heating or some combinations of methods, the EGR strategies through variable valve actuation will be the main area of interest in CAI combustion control for the following reasons:

1. Using Variable Valve Actuation to achieve CAI is more feasible than pre-heating.

2. Residual-affected CAI can be achieved with lower peak in-cylinder pressures than pre-compression strategies, reducing the strength requirements of the engine.

3. No throttling is required to modulate the work output in residual-affected CAI achieved through exhaust re-induction. This leads to increased efficiency of the CAI process

### 2.4.3 CAI Combustion Operation Strategies

#### 2.4.3.1 Exhaust Gas Residual Trapping

The CAI operation with residual gas trapping is used to initiate CAI combustion and to control the subsequent heat release rate by trapping large and variable amounts of residual gases in the cylinder. The burned gases from the previous cycle are trapped in the cylinder by closing the exhaust valves relatively early. The trapped burned gases or residuals as its sometime called are then compressed during the final stage of the exhaust stroke. The inlet valves are opened late and normally symmetry is created between EVC and IVO (to avoid exhaust gas sucking back into the intake), during the last stage of the exhaust stroke [3]. As the piston descends on the induction stroke, the inlet valves are opened so that fresh air is inducted into the cylinder (GDI) that has already been partially filled with trapped residuals. The cold fresh charge mixes with the hot residual gases and gains the thermal energy from the residual gases. Then the intake valves are closed and the in-cylinder charge is compressed by

the ascending piston, resulting in auto-ignition of the air-fuel mixture and the subsequent combustion about TDC.

The exhaust valve should ideally be opened normally towards the end of expansion, while their closing should be earlier to enable trapping enough residual gases that initiate CAI combustion. The intake valve should be closed as normal while their opening should be advanced. To achieve the ideal valve lift curves for CAI operation, a fully flexible valve actuation using electro-hydraulic was used.

#### 2.4.3.2 Direct Fuel Injection

During CAI operation, engine output is principally controlled by the EVC timing. As the engine load or speed increases, combustion starts earlier and burns faster, leading to too fast a rate of heat release and very high peak combustion pressure as well as increased fuel consumption. At the low or part-load region, the very retarded combustion causes very large cyclic variation and even partial burning. It then becomes necessary to find other means of control independent of the combustion phasing from the engine load. It has been shown by the work done in the lab of Zhao [4] that DI can be used as an effective means of controlling combustion phasing for optimised engine performance and emissions. This is achieved by; early-injection during the negative valve overlap (NVO) for fuel-reforming, mid-injection during intake for homogeneous mixture at high-load, and late-injection during intake (stratified) for part- and low-load operations.

### 2.4.4 CAI Combustion Challenges

Irrespective of the methods chosen, CAI combustion exhibits some challenges with regards to combustion timing and dilution limits. Additionally, for residual-affected approaches, cycle-to-cycle coupling through the exhaust-gas temperature plays a critical role.

#### Combustion Timing Challenges

Since CAI has no specific initiator of combustion, making sure that combustion takes place with acceptable timing, or at all, is more complicated than in the case of either SI or CI combustion. Combustion timing in CAI is dominated by chemical kinetics, which depends on the in-cylinder concentrations of reactants and products, their temperature and the level of compression.

### Cycle-to-cycle Coupling Challenges

When CAI is achieved through trapped or re-inducted residual gases, subsequent engine cycles are coupled through the residual temperature. Since the inducted reactant gas is heated by the residual, the residual temperature from an engine cycle directly affects the chemical kinetic-dominated combustion event on the subsequent cycle. The cyclic coupling plays an important role in steady state operation and during operation point changes. However, if care is not taken during transient and mode transition, combustion timing can become unstable, leading to misfire and this condition is not acceptable.

### Dilution Limit Strategies

The main Challenges for CAI operation is obtaining sufficient thermal energy to trigger auto-ignition late in the compression stroke. The most practical means to trigger auto-ignition in SI engines where compression ratio is limited is through the use of large levels of EGR. For any practical CAI strategy, the reactants are diluted with residual gas or air. This dilution leads to the presence of upper and lower load limits. Furthermore, the dilution process decreases the amount of work that can be extracted for a given engine geometry. For these reasons practical CAI will be accompanied with either conventional SI or CI strategies in a multi-mode engine. At very low and high load conditions the engine runs in the conventional mode. Then at low to moderate load conditions the engine runs in CAI mode. A key problem is how to transit from the conventional mode to CAI. For residual-affected strategies, the cyclic coupling exists during transition into the CAI mode.

To control CAI through VVA it is necessary to understand how the valves influence the induced gas composition, combustion timing and cycle-to-cycle coupling during steady state, transients and mode transition. This will require experimental, simulation and mathematical modelling.

## 2.5 Fuel Effects on CAI/HCCI Combustion

The CAI/HCCI combustion can be operated on a wide range of gaseous and liquid fuels. Scott et al [46] conducted an experiment and simulation that detail the sensitivity of natural gas in CAI/HCCI combustion. Noraz Khairi et al [47] compared HCCI and SI combustion of direct injection CNG at low load conditions. Hydrogen fuel was used to operate a single cylinder

engine in HCCI mode by Anil Singh Bika et al [48], in addition Rosati and Aleiferis [49] used hydrogen in SI and HCCI combustion mode in a single-cylinder direct-injection optical engine. The use of gasoline, ethanol, methanol and ethanol-gasoline blends will be discussed below.

### 2.5.1 Gasoline

Gasoline presently is the dominant fuel used in CAI/HCCI combustion in 2 and 4-stroke engines. Zhao et al [50] achieved CAI combustion in a production type 4-stroke 4-cylinder gasoline engine using standard components with modified camshafts to restrict the gas-exchange process. Yan et al [51] achieved a wider range of CAI combustion in a 2-stroke operation in a GDI engine with poppet valves. Cao et al [52] investigated the effects of thermal and residual gas inhomogeneous distribution on auto-ignition using gasoline in CAI/HCCI combustion using CFD. This is because gasoline is a volatile fuel and homogeneous mixtures can be readily formed. However, there are drawbacks in using gasoline in CAI combustion due to its resistance to auto-ignition. In the work done by Amman et al [53] on HCCI fuel evaluations-gasoline boiling range, it was observed that the largest operating range with practical compression ratios is achieved with the medium octane rating (77.0 RON).

### 2.5.2 Ethanol and its Blends with Gasoline

The use of ethanol as an alternative transportation fuel shows promise for several reasons. Firstly, ethanol has the potential to mitigate greenhouse gases, as a result of its production method. Secondly, it is a renewable fuel source with the potential to substitute fossil fuel oil. While ethanol can be produced from several types of biomass, it offers properties such as a high octane number, higher oxygen content and high heat of evaporation, which make it a most attractive alternative fuel, in particular for the CAI combustion in the direct injection gasoline engine [7,54].

Larsen et al [55] produced an extensive report on ethanol as a fuel for road transportation. In their report, ethanol was examined as an alternative fuel to gasoline from well-to-wheel, including its production, the economical, environmental and social aspects. It was concluded that wet ethanol was a suitable candidate for CAI/HCCI combustion with about 34% reduction in production cost compared to anhydrous ethanol.

Ethanol as a gasoline blend is being used world-wide because of its energy security potential, and the potential to mitigate greenhouse gas. Much has been written on the usage of ethanol in varying ratios as a gasoline blend, its emissions and effects on engine performance in throttled SI engines.

Bayraktar [56] theoretically investigated the flame propagation process in an SI engine running on gasoline-ethanol blend, it was observed that blending ethanol-gasoline up to 25% by volume positively affects the geometric properties of the flame and mass burning rate, leading to faster burning. In addition, it also produces higher cylinder pressures and temperatures compared to gasoline. It was concluded that the IMEP, the engine output power, and the thermal efficiency may ultimately increase.

Craig et al [57] developed a naturally aspirated SI direct-injection flex-fuel engine, which was used to extensively investigate ethanol and gasoline mixtures ranging from 0% (pure gasoline or E0) to 85% (E85) in volume. Cold start, part and full-load performance were also investigated. At part-load they recorded a 3-6% improvement in efficiency over the optimised gasoline engine, this result was due to a reduction in heat rejection and increased EGR tolerance. At full-load, a 13-15% improvement was observed in the specific output because of the use of E85.

Nakata et al [58] investigated the use of ethanol as it affects SI engine performance and emission. It was observed that ethanol improves the engine torque and thermal efficiency. The reason for this improvement was because of the higher anti-knock quality of ethanol due to its high octane number and the decreasing heat loss at the lower combustion temperature. The NOx level was observed to be lower when compared to that of gasoline, also as a result of the reduced combustion temperature. In addition, there was a reduction in THC emission because the components of ethanol do not boil at a high temperature, unlike those in gasoline.

In an internal combustion engine, a high compression ratio is desirable since the engine's ability to convert fuel energy into mechanical energy depends on the compression ratio (CR)[3,4]. Therefore, it will be of great advantage to set the compression ratio as high as possible. However, the fuel octane number provides a constraint when increasing the CR, only those fuels with a higher octane number can be used in engines using a high compression ratio. This results in greater engine efficiency, which currently makes ethanol as best alternative fuel source to gasoline.

However, increasing the compression ratio has effects on both the emission and the engine operating condition as a higher compression ratio causes NOx formation to intensify due to the increased combustion temperature [59]. Interestingly, a higher compression ratio with ethanol use enables high EGR, which can reduce $NO_X$ formation.

In compressing gas in an SI engine, its temperature increases; if the temperature becomes too high during the compression stroke, the possibility of premature self-ignition (known as auto-ignition) of the fuel-air mixture occurs and shockwaves can be formed in the cylinder. This is known as knocking combustion and is a design and operating constraint parameter in SI gasoline and ethanol fuel engines [3]. This knocking combustion is undesirable in an engine because it decreases the engine efficiency and could lead to engine damage. The two deciding parameters in engine design are the compression ratio and the ability of the fuel to withstand auto-ignition. This fuel characteristic is known as the anti-knock index or octane number. Hence fuel with high octane number could be used in an SI engine with a high compression ratio, offering a higher overall efficiency, improved fuel economy, and reduced $CO_2$ emission [60].

Blending ethanol with gasoline raises the overall octane number of the fuel blend [61], thus guarding against engine knock, which can have damaging effects on the engine. It enables a higher compression ratio and advanced spark-timing to be applied in SI engines. In addition, ethanol is able to replace more costly octane boosting components such as alkylate.

Another important fuel property of ethanol is its high latent heat of vaporisation, this is a measure of the amount of energy required to evaporate the fuel [62]. The vaporisation of the fuel in an engine absorbs the heat energy from the surroundings thus lowering the temperature in the intake manifold, combustion-chamber materials and air, depending on whether it is port or direct injection being used. Ethanol has a higher heat of vaporisation than that in gasoline. The engine temperature tends to be lower using ethanol fuel. This property complements the high octane number because auto-ignition or knocking is very unlikely to occur with a cooler running engine.

The benefit of the high latent heat of vaporisation in direct injection (DI) engine, widely known as the charge-cooling effect, has been demonstrated successfully on knock limits by [63, 64, 65]. A cooling of the intake air/fuel mixture, due to use of large percentage of ethanol, and high latent heat of vaporisation, increases the air density, thus enabling more air to enter the fixed or variable cylinders. Inducting more air enables more fuel injection and

more power is generated for the same engine size, resulting in increased efficiency due to the lower internal heat losses. The induction of more air also lowers exhaust-gas heat losses, which is observed as a lower exhaust temperature using ethanol fuels. Work needed during the compression stroke has also been shown to decrease due to high latent heat thus contributing to improved efficiency. However, the high latent heat of vaporisation has the major disadvantage of further worsening the engine cold start properties of ethanol fuels, a method to control this using intake valve-timing control was reported by Tsunooka et al [66].

Ethanol as an oxygenated fuel with a high octane number and high heat of vaporisation suggests that the fuel may not be suitable in HCCI/CAI combustion. However, CAI combustion has been demonstrated successfully in 4-stroke engine using ethanol by Zhang et al [67] in a Port Injection HCCI through changing exhaust and inlet-valve timing.

Rahbari A [68] demonstrated the effect of EGR on HCCI engines using ethanol as a fuel, the result shows that the increase of EGR delays the ignition timing, slows down the combustion reaction rate, reduces the temperature and pressure in cylinder, and decreases the NOx emission.

Yufeng Li et al [69] investigated the CAI combustion with methanol and ethanol in an air assisted DI SI engine. The results confirm that both oxygenated fuels, ethanol and methanol, can lead to CAI combustion. The load of CAI was increased, and emissions were lower.

Similarly, Tongroom et al [70] investigated the combustion characteristics of CAI combustion using alcohol fuels in an optical engine and compared the result to gasoline. The resulting images showed that CAI combustion was characterised by fast and early autoignition combustion compared to gasoline.

Zhang et al [71] demonstrated CAI combustion on a 2-stroke gasoline direct-injection engine using gasoline and a gasoline mixture with ethanol. The presence of ethanol enabled the CAI combustion to be extended to higher loads in E15 and E85. The CO, UHC and NOx emission are significantly reduced by injecting ethanol blend fuels. E85 has a greater effect on emission reduction than E15. The presence of ethanol improves the combustion and thermodynamic efficiency due to optimum combustion phasing and lower heat loss. In addition he confirmed that E85 improved indicated conversion efficiency by over 5% at 2000rpm.

## 2.6 Particulate Emissions from direct injection gasoline engines

Due to the limited time available for complete fuel evaporation and the mixing of fuel and air mixture in a direct-injection gasoline engine, locally fuel rich mixture or even liquid fuel can be present during the combustion process. Due to this incomplete combustion various undesirable products such as CO, NOx, hydrocarbons including PAH, CO and particulates are formed in larger quantities in direct-injection gasoline engines compared to the conventional port fuel-injection gasoline engines.

These pollutants all have a detrimental impact on the environment, and as such are a cause of great concern. Pollutants may lead to decreased visibility and the soiling of buildings as well as causing adverse health effects. Much attention worldwide is being paid to the influence of fine airborne particles on human health [72].

Particulate formation is a complex process involving many chemical and physical processes in stages. Detail kinetic model of particulate formation usually contains two general parts, gas-phase chemistry, initiating the particulate precursors, and particulate-phase model, which is the less explored area in soot formation theory.

Recent investigation had confirmed that the PAH are the most probable particulate precursors [3,73, 74]. The authors also suggested that particle formation or inception process takes place through formation of aromatic-aliphatic-linked hydrocarbons with five membered rings, which graphitize together forming more compact structures. The particulate size increases in reactions of surface growth by the active sizes on the particles surface. Coagulation forms larger particles. Where during agglomeration the primary particles stick together, forming chain-like aggregates.

Decarlo et al [75] developed theoretical particle morphology and density characterization by combined mobility and aerodynamic diameter measurement. In this work, the effective diameters are related within an analytical framework, allowing constraints to be placed on the relationships between the equivalent diameters, density, and shape (in the form of dynamic shape factor). This important framework enables important particle properties such as mass and volume to be estimated from a combination of diameter measurements.

Several authors [76, 77] have investigated the exhaust particulate-emissions from GDI and PFI and it has been established that the GDI emits a greater number of particles due to the

short duration time of mixture preparation. This may have resulted in regions of pockets of rich air-fuel mixture in the cylinder and the wall-wetting effects.

With the increasing implementation of the GDI engine, PM emissions have become a source of concern for engine manufacturers and the gasoline industry [72]. Several studies have been undertaken to understand the mechanism by which GDI systems yield increased PM emission [75,76].

Kim et al [78] investigated fuel effects on particle emissions of a direct-injection gasoline engine. Test vehicles of 2012 were used, using three different types of gasoline and LPG. In the gasoline engine, measurements were performed over NEDC using domestic fuel from South Korea and Euro 5 certification fuel, also FTP 75 cycle using domestic fuel and Indolene. Domestic fuel is the most volatile, followed by Indolene and Euro 5 fuel. It was observed through all gasoline tests that most PN emissions were generated from the cold phase, especially cold start and catalyst heating range. It was concluded that in cold conditions, the fuel-evaporation rate is lower due to the low temperature and larger amount of injected fuel. Another contributing factor to the generation of PM emissions was the increase in fuel requirement during cold starting events which requires a larger amount of injected fuel.

The NEDC tests, Euro 5 fuel resulted in 77% higher PN emissions, this was as a result of lower volatility and the higher aromatic content of Euro 5 fuel. In high speed and high-load conditions, fuel combustion in liquid form was observed to increase due to a shorter evaporation time and more wall impingement.

Khalek et al [79] analysed particle emissions from a 2009 GDI engine using different commercially available fuels with similar results [77] of increased PN number emissions observed for cold-start and acceleration. It was also concluded that this increase may be due to slow droplet evaporation and the presence of fuel enrichment zones during combustion and may be the major contributor to PM formation.

Whelan et al [80] investigated the effect of fuel temperature on particulate matter in a GDI engine, using fuel at an ambient temperature and chilled fuel. Injection of the chilled fuel into the combustion chamber led to a higher in-cylinder pressure, longer duration of combustion and lower PM number emissions than the injection of fuel at ambient temperature, though their results were obtained from a limited amount of data. The result could be due to the charge-cooling effect of the injected chilled fuel.

Sakaiet et al [81] examined the effect of equivalence ratio on the particulate emissions from a single-cylinder GDI. It was observed that as the equivalence ratio increases, a larger fraction of particles with a diameter greater than 100nm were formed due to agglomeration. For a decreasing equivalence ratio, smaller particles dominate the distribution. The total particle number and mass increased non-linearly with the increasing equivalence ratio. They concluded that the changes observed may be due to changes in fuel and oxygen availability, as well as changes in the flame temperature and heat release.

Hedge et al [82] investigated the effects of cooled and uncooled internal EGR to provide insight into the role of bulk temperature on PM formation. It was observed that cooled EGR was very effective in reducing mass by as much as 65%, compared to engine baseline. However, they observed that internal EGR was much more effective than cooled EGR in reducing particulate mass and solid-particle number at part-load, low-temperature combustion. EGR increased engine-out volatile particles that are mainly formed during dilution and cooling of hot exhaust.

Zhou et al [83] analysed the effects of hot exhaust EGR on combustion characteristics and particle emissions of a Pilot-Ignited natural gas engine. A decrease in particle number concentration with the increasing EGR rate was observed and the total number of particles sharply decreased to 57%. However, an increase in the particle mass concentration was also observed. The peak of the particle distributions gradually shifts downwards and towards the larger particle size. They attributed several reasons that could have been responsible for the result as follows. Firstly, the intake charge temperature is increased by employing the hot EGR. The HC emission, which constitutes the soluble organic fraction (SOF) of the particle, is reduced. This leads to a great reduction in the particle number concentration. Secondly, as the hot EGR is increased, the ignition period is shortened. The shorter delay ignition-period provides less mixing time for the total charge (exhaust gas, natural gas-air mixture and diesel fuel), resulting in a heterogeneous mixture. This heterogeneous mixture can raise the possibility of large particle formation, while it may decline the potential in producing smaller particles. Thirdly, the introduction of hot EGR (dilution effect) reduces the amount of natural gas-air mixture. Hence, the total fuel which participates in the combustion is reduced. It virtually reduces the particle number concentration. Furthermore, the continuously increasing dilution effect of EGR leads to the reduction of the cylinder temperature. The introduction of the hot exhaust-gas partially offsets the effect of dilution and thereby remedies the decrease of the charge-temperature to a certain degree. This declining availability of $O_2$ might strengthen

the particle coagulation rate and generate an amount of larger particles. In brief, the particle mass concentration increases and the number concentration decreases with raising the hot EGR rate.

Aikawa et al [84] investigated the relationship between gasoline properties and vehicle particulate matter emissions, they created a PM index based on fuel properties, which is of great importance in GDI because it enables modelling of air and fuel mixture and the sooting tendency

Price et al [85] compared the PM emissions of the first and second generation DISI with PFI in an optical engine. It was found that the first generation (wall guided) DI SI engine emits more PM than the SGDI. In addition, it was observed that the PM emitted by the SGDI was dominated by nucleation mode particles like PFI-SI, but the accumulation mode normally associated with DISI engine was not detected. They concluded that fuel type had the biggest effect on PM emissions, followed by air-fuel ratio, injection timing and ignition timing.

Arsie et al [86] investigated the effect of engine control parameters on particle number and size in a PFI. They highlighted the impact of injection time and spark-timing, which also affects in-cylinder oxygen content and temperature. Their result indicates that operating the engine under lean conditions decreases the particle number concentration by an order of magnitude with respect to the lambda. However, for a rich mixture, the result was comparable to the case of lean mixtures, except that it showed a slight increase in PN at a higher speed, probably due to the shorter time available for particle oxidation. The impact of the ignition timing on in-cylinder and exhaust temperatures affects the precursors of particle formation and the oxidation process. They observed an increase in particles smaller than 20nm as the ignition timing was advanced. However, as spark was reduced, they observed at low and high engine speed a different behavior, in particular, at 1500rpm particle number was observed to decrease significantly while at 2000rpm a slight increase was observed, which they believe was likely to be caused by the concurrent effect of post flame oxidation temperature and residence time of particles. The effect of EGR was also investigated, similar to [82] and as expected promotes particle formation because of lower temperature and in-cylinder oxygen content.

Several studies have been undertaken to understand the mechanism by which direct-injection combustion generates gaseous and particulate emissions [78-85] but very little has been done on particulate-matter emissions in CAI operational modes.

Price et al [87] investigated the particulate emissions from a gasoline HCCI engine, they observed that under both SI and HCCI operation, where comparison was possible, the number concentrations from HCCI combustion were slightly higher than from SI. In addition the magnitude of the accumulation mode was observed to be inversely proportional to the amount of residual gas trapped.

In particular, no measurement and comparison has been made on the PM emission between SI and CAI (2-stroke and 4-stroke using negative valve overlap) combustion operations in the same engine in different operational modes using a camless engine and varying gasoline ethanol fuel blends.

Di Iorio et al [88] investigated the particle size distribution from a DI engine fuelled with gasoline-ethanol blends E0, E50, E85 and E100, using two-fuel injection strategies; homogeneous and stratified injection. The study focused on fuel injection and ethanol on particulate emission. They observed that smaller particles and lower total mass were emitted from the engine fuelled with pure ethanol compared to gasoline. In addition, when using E50 and E85 blends, a large increase of the number concentration of particles in the accumulation mode was observed. The size distribution was also observed to be strongly affected by the mode and fuel properties, the addition of ethanol shifts the size distribution towards lower sizes, but the engine emits significantly more particles.

Several authors [89-91] have investigated the effects of oxygenated fuel blends on particle emissions in GDI, it was observed in all the findings that the resence of oxygen in the fuel molecules reduces the concentrations of key intermediate species required for the formation of aromatic soot precursors.

Fatouraie et al [92] investigated the in-cylinder particulate-matter emission and spray-imaging of ethanol-gasoline blends in a GDI engine using E50 and E85 blends. They recorded a significant reduction in in-cylinder soot formation with the higher ethanol content in the fuel, regardless of the fuel injection-timing. In addition fuel impingement was documented in the spray imaging, and it was observed as a large factor affecting the level of PM emissions.

Di Iorio et al [93] investigated the use of oxygenated fuels in order to reduce particle emissions from a GDI engine, with one of the cylinders of the engine optically accessible. She observed that the particle size distribution for pure gasoline and its blend with ethanol shows the same trend, suggesting a common route for the particle formation. The bio-ethanol

accumulation mode was observed to have shifted towards smaller sized, which they ascribed to the chemical and physical properties of the fuel as observed by optical investigation of the fuel injection and combustion process.

## 2.7 Summary

This chapter has reviewed the background, current and future emission legislations of the internal combustion engines. Since IC engines are operated mostly at part-load, engine downsizing, VVA, stratified charge lean-burn combustion as well as CAI/HCCI can lead to significant improvement in fuel consumption. The potential of ethanol as future alternative fuel has been highlighted regarding its availability and sustainability, higher octane rating and charge cooling effects. The increased particulate emissions experienced in GDI over PFI have also been examined and highlighted. The HCCI/CAI has shown from all the work reviewed to have ultra-low NOx emissions and low fuel consumption but increased in some cases UHC and CO and limited operational range. However, limited work was done on particulate emissions in HCCI/CAI in 2-stroke and 4-stoke modes. In Particular, injection of fuel during the NVO period and the use of E15 and E85 have received very little or no attention. This was highly noted.

# Chapter 3 Experimental Test Equipment Set-Up

## 3.1. Introduction

All experiments were conducted in a newly commissioned single-cylinder engine research facility, as shown in Figure 3.1. It comprises a unique single-cylinder direct-injection gasoline camless engine, the high pressure hydraulic pack for the electro-hydraulic actuators, an AC dynamometer, a supercharger unit, emission measurement and analysers, data logging and analysis system.

## 3.2 Engines and Accessories

### 3.2.1 Single Cylinder Engine

A camless single-cylinder Ricardo Engine is coupled to an AC dynamometer, supplied by CP Engineering. The engine is capable of both 2 and 4 stroke combustion modes of operation through the flexible electro-hydraulic actuated intake and exhaust valves. The engine set-up is presented in Fig 3. 2. The engine has a bore of 81.6mm and a stroke of 66.94mm. This is capable of producing 76Nm torque at 28KW. Additional engine details are given in Table 3.1.

All experiments were conducted in a research facility, newly commissioned to test single-cylinder engines. The facility is home to a unique camless single-cylinder direct-injection engine and also makes available electro-hydraulic actuators and high pressure pack, an AC dynamometer, a supercharger unit, emission measurement and analysers, data logging and analysis system as research equipment.

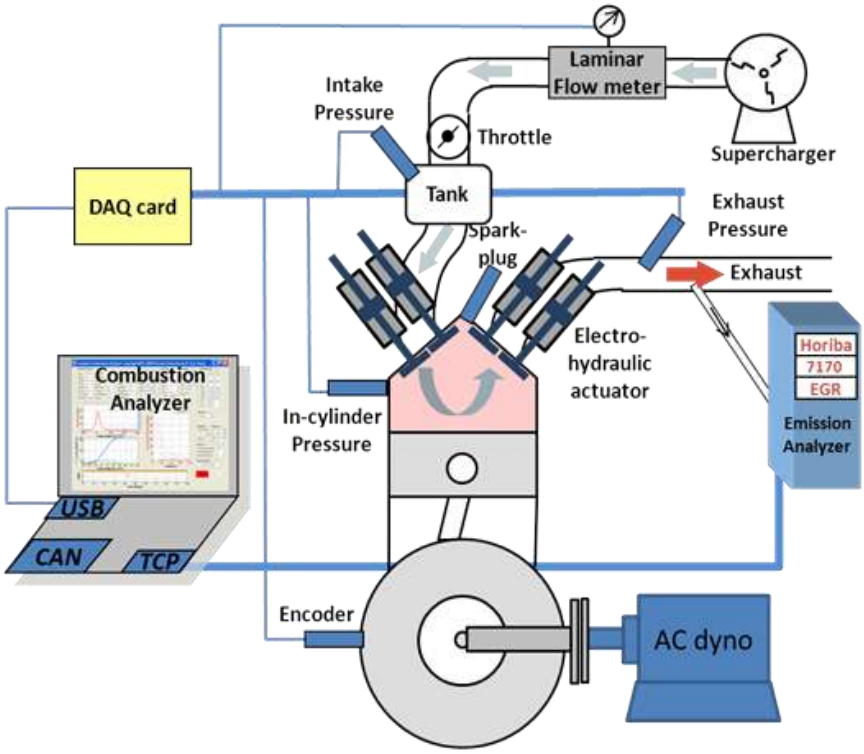


**Figure 3.1 Schematic Drawing of the Single-Cylinder Engine Testing Facility**

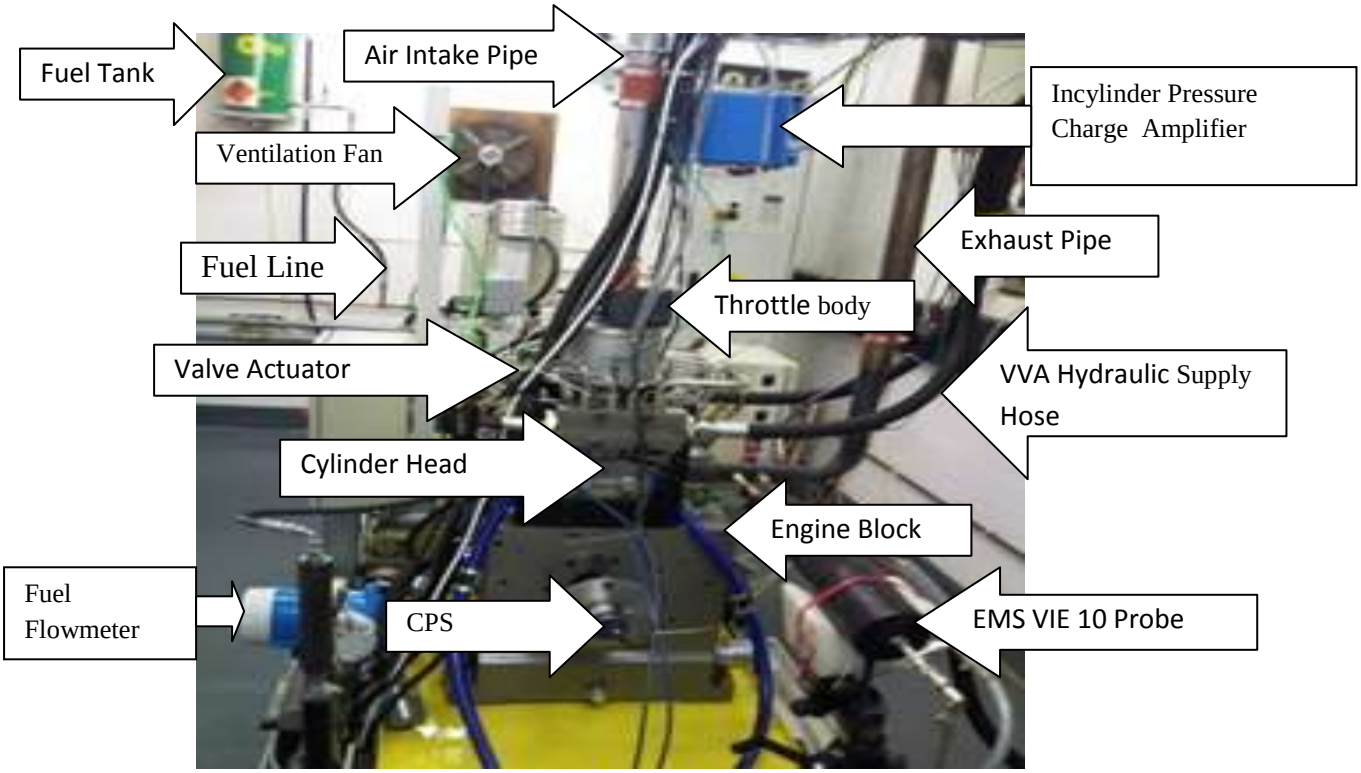


**Figure 3.2 A Photograph of the Single-Cylinder Engine on the Test Bed**

**Table 3.1 Engine Specification**

| | |
|---|---|
| Bore×Stroke | 81.6mm×66.94mm |
| Compression ratio | 11.78:1 |
| Combustion Chamber | Pent roof / 4 valves |
| Valve train | Electro-hydraulic actuation |
| Fuel Injection | Direct Injection |
| Fuel | Standard Gasoline (RON 95), E15, and E85 |
| Air/Fuel Ratio | Stoichiometric or lean |
| Intake Temperature | 25 degree celsius |

The engine speed range is 0-6500 rev/min in the four-stroke mode and up to 4000rpm in the two-stroke mode. The engine was developed for Brunel University by Ricardo as part of a consortium project on the downsized 2/4-stroke switchable engine. The combustion system was based on the 2-stroke poppet-valve Flagship Hydra SI engine. The original Flagship Hydra was run purely as a 2-stroke and the top of the piston was flat. However, this resulted in a low compression ratio (CR) which was not suitable for CAI operation.

Figure 3.3 shows the cylinder head and valves, the intake and throttle, and the piston crown. As shown in Fig.3.4, two piston crown profiles were designed and the one on the right-side was adopted in this single-cylinder engine. This gives an 11.78 CR in engine firing mode. During the commission and calibration of the electro-hydraulic valves, spin free engine operation was achieved by the installation of a spacer plate between the cylinder-head and engine-block. In this case, there was no possibility of the valves striking the piston, even if the valves were to stick in their fully-open position whilst the piston continued to reciprocate.

Another important feature of the cylinder-head design is the vertical intake ports, similar to the two-stroke flagship engine development in the late 1990s [94] and the recent 2/4-stroke projects [21], the amount of air short-circuiting, i.e. the air-flow into the exhaust during the positive valve overlap period, can be minimised by the introduction of the reversed tumble flow in the cylinder through the use of upright intake ports. In this case, the air flows preferentially through the far side of the intake valves away from the exhaust valves, so that a clockwise vertical flow structure, i.e. tumble, is set up and most air travels the furthest distance before reaching the exhaust valves. In order to reduce the air-flow to the exhaust valves through the near side of intake-valves, a ridge is incorporated between the intake and exhaust valves to act as a valve shroud.

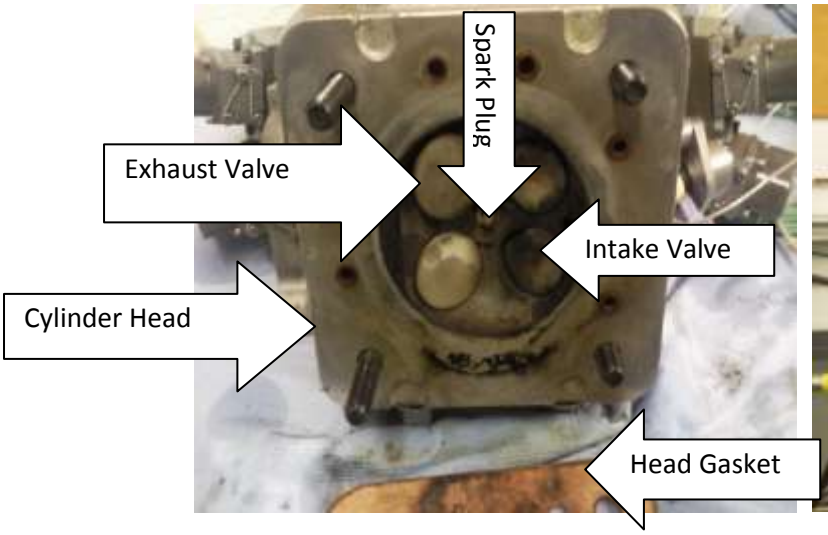


**(a) Cylinder Head**

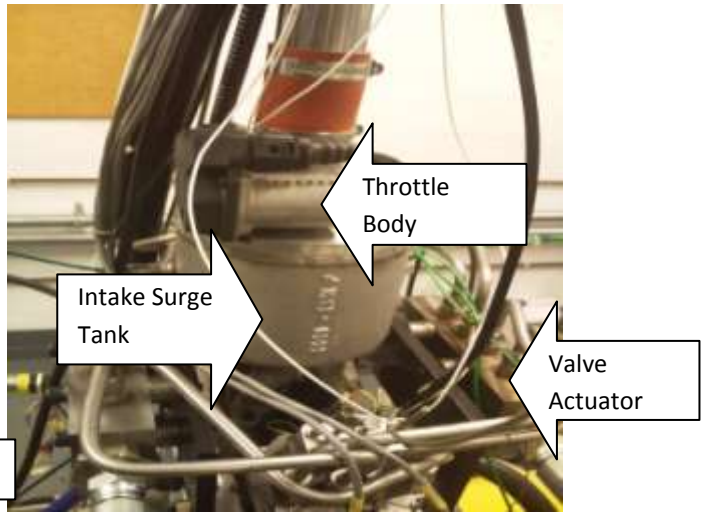


**(b) Intake System**

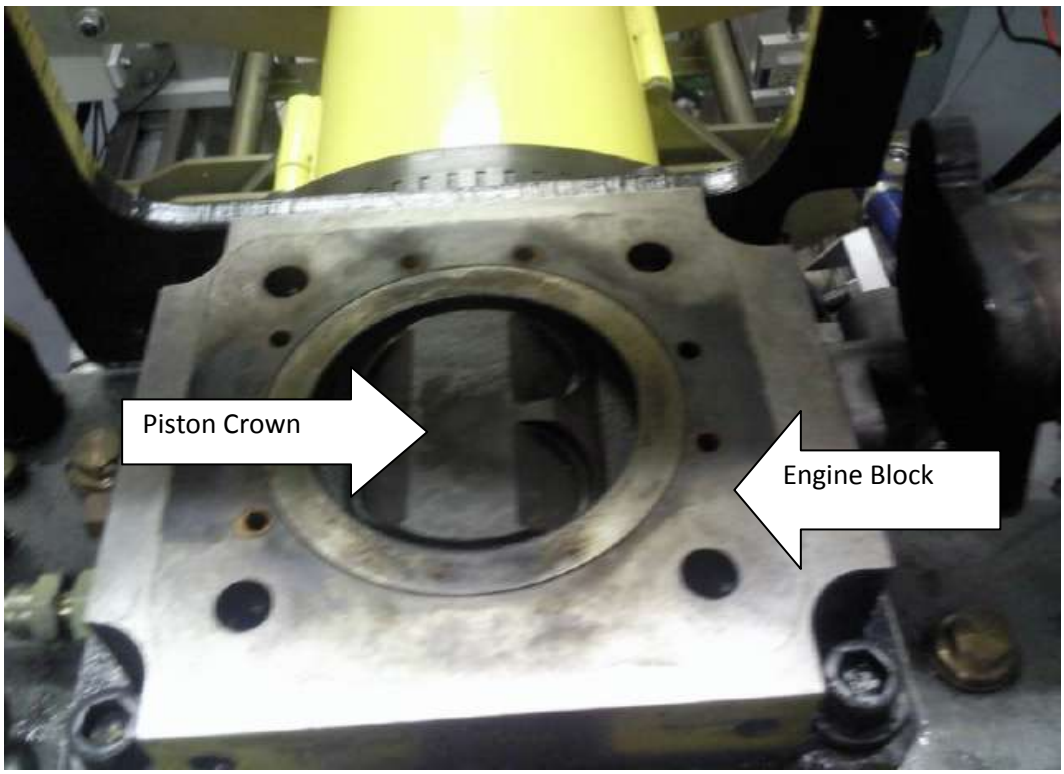


**(c) Engine Block and Piston Crown**

**Figure 3.3 Port and Pent Roof Profile**

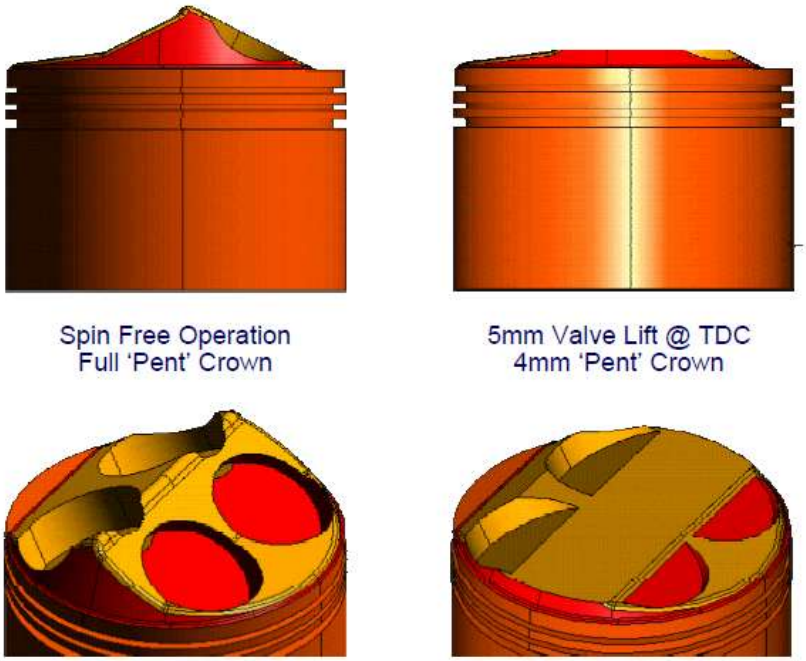


**Figure 3.4 Piston Crown Detail**

### 3.2.2 Valve Train System

A fully flexible valve train system is mounted on the cylinder-head and capable of independent control of valve-timing and lift in both 4-stroke and 2-stroke modes. It is enabled by the electro-hydraulic actuators supplied with the high-pressure oil and controlled by the high-speed solenoid valves.

#### 3.2.2.1 Hydraulic Pump Unit (HPU)

The high-pressure oil is supplied by a hydraulic pump unit shown in Fig. 3.5. It comprises a variable delivery piston hydraulic pump rated at 18.5KW power and 34 l/min delivery at 280bar. It is equipped with 3 micron on-line and 10 micron off-line filtration systems, using ISO 32 hydraulic oil from a 225l oil tank supplied by DGB Hydraulics Ltd. It includes a 10l bladder accumulator to maintain pressure during a power cut out and a load control valve powered by UPS. Feeds and drain manifolds are mounted on the engine with oil pressure sensor incorporated into feed manifold.

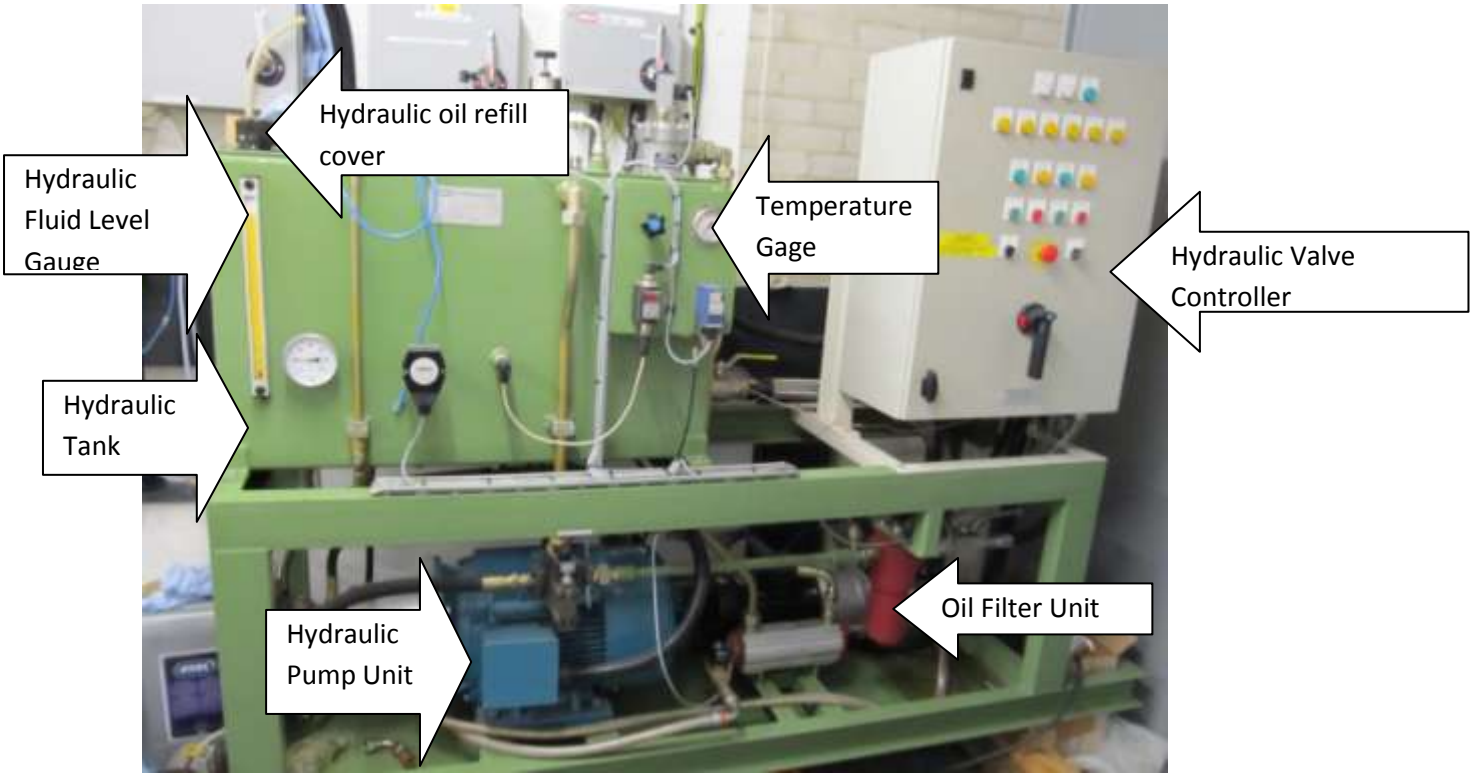


**Fig 3.5 Hydraulic Pump Unit**

### 3.2.2.2 Electro Hydraulic Valve Actuator

Each of the four valve actuators in the electro-hydraulic valve system consists of a hydraulic piston attached to the poppet valve, which moves inside a hydraulic cylinder. Movement of the piston, and thus the engine poppet valve, is controlled by flow of hydraulic fluid either above or below the piston. This hydraulic flow control allows controlled valve velocities up to engine speed of 6000rpm maintaining soft touchdown capabilities. It is essentially made up of three base components (Fig.3.6):

1) Hydraulic Actuator Unit,
   Designed by Helipebs (11mm bore /12mm stroke),
   Hydrostatic bearings.
2) Servo Valve
   Fast response Moog servo valve
   Max pressure 280bar
   Mechanically biased
3) Linear Variable Differential Transformer (LVDT)
   Stated 8KHz bandwidth
   Separate amplifier stage

Each hydraulic actuator is fixed to the cylinder head via a mounting block, and the engine poppet valve is attached to the actuator via a rigid, threaded connector.

The hydraulic valve train enables valve motion to vary with engine speed to meet set limits at every speed and position. The maximum allowable peak valve velocity is about 4.5 m/s. Although hydraulic valve train does not have a physical cam ramp to control opening and closing events a common "ramp" with the following properties was incorporated in the motion designs because the hydraulic valve train must control seating velocity somehow.

Height 0.32mm height

Velocity 0.009mm/deg

0.054 m/s @ 1000rpm

0.243 m/s @4500rpm

0.351 m/s @6500rpm

Positional feed-back from the piston and engine valve assembly is continually provided by the LVDT, which allows actual profiles to be continually monitored and corrected from cycle-to-cycle, to ensure accuracy and repeatability.

The electro-hydraulic valve actuation system has full flexible control over valve timing, lift and velocity including precision valve closing. The system is inherently capable of controlling each individual valve separately and can operate different profiles on different valves. The system is also capable of opening and closing valves more than once per engine cycle, and is limited only by hydraulic fluid delivery in terms of valve velocity and hence operating strategy.

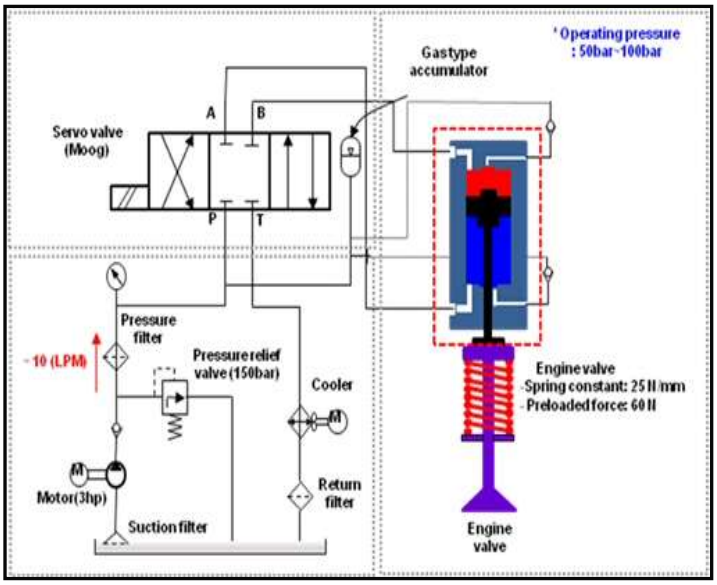


**Fig 3.6 Electro Hydraulic Valve Actuator (Ricardo Inc UK)**

### 3.2.2.3 Valve Controller

The variable valve-timing system used in this study was an electro-hydraulic system. The valve control are operated by INCA software. A Valve Control Unit (VCU) controls the operation of four electro-hydraulic actuators. It is equipped with a Freescale Processor, operating at a bus clock of 25Mhz, the VCU supports two CAN lines adapters for serial communication between this unit and the engine control module (ECM) and the four VCUs. In the event of a power loss, all VCUs have UPS power back-up. The UPS guarantees a continuous supply of electric power, in order to maintain continuous control of the hydraulic valves for safety reasons. Figure 3.7(a) shows camless engine controllers and data aquisition units and Figure 3.7(b) is the VCU showing the inner components and Figure 3.7(c) is the VCU circuit board

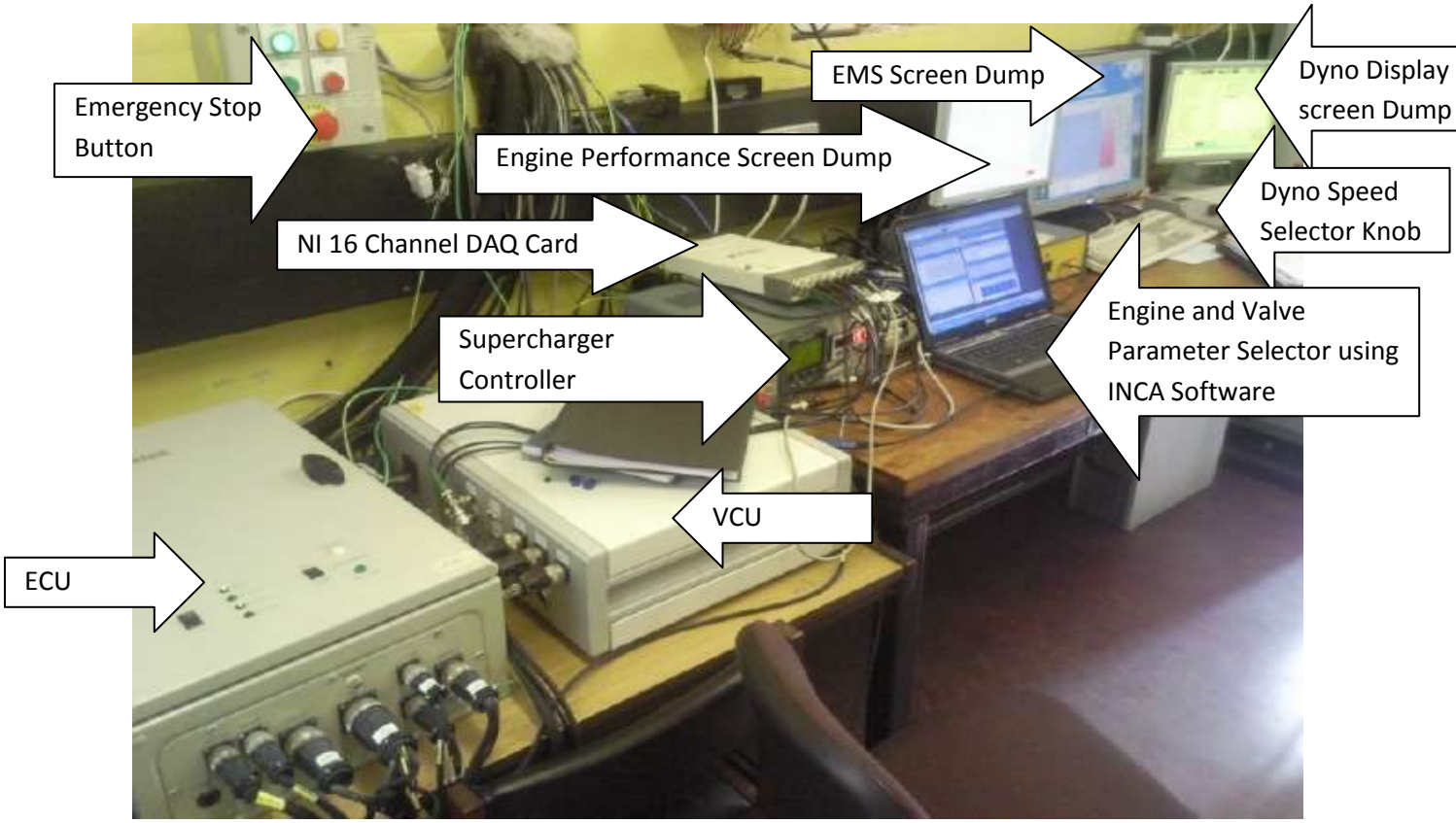


**(a) Camless Engine Controllers and Data Aquisition Units**

**(b) VCU Inner Components**

**(c) VCU Electronic Circuit Board**

**Fig 3.7 Valve Control Unit**

### 3.2.3 Fuel Delivery and Injection System

The injection system comprises a direct gasoline injector installed in the centre and under the 2 intake valves, a low-pressure fuel pump, a high-pressure fuel pump, a pressure regulator, a common rail and a fuel heat exchanger, as shown schematically in Figure 3.8. Fuel is supplied from a 25 litre tank mounted in the engine test cell and pressurised by a low-pressure pump and then pumped to 100bar in the common rail. When ethanol blended fuel is used, it is first pre-mixed and then poured into the tank.

The low-pressure pump used in this study is maintained at 2.5 bar. The low-pressure system has a pressure regulator, which is located between it and the high-pressure pump. When the fuel pressure exceeds the required value, excess fuel is released from the regulator and is allowed to flow back into the tank.

The high-pressure pump is electrically driven by a fixed speed AC electric motor and the fuel pressure is monitored by the ECU using a fuel rail pressure sensor and regulated by a high-pressure relief valve, set at 100 bar. A heat exchanger is used to remove the excess heat from the pressurised-fuel return in order to maintain a constant fuel temperature.

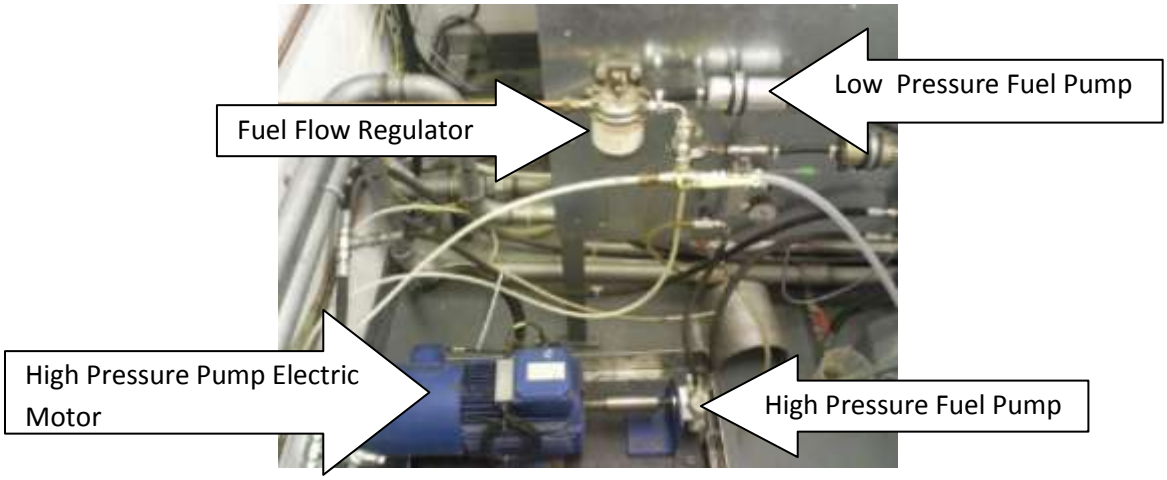


**Figure 3.8 Fuel Supply System Diagram**

The injectors used in this study were the Single and Double Slit Denso GDI injectors driven by a GDI driver. The single slit injector was used in the tests in chapter 4, and the double slit was used in chapter 5 and 6. The injector is constructed with a solenoid that opens the injector valve by moving the needle off its seat, thus allowing fuel to flow through the nozzle. The opening time and opening duration of the solenoid are controlled by the ECU so that the required quantity of fuel is injected at exactly the correct time based on the engine load and conditions. Figure 3.9 shows the injectors used in this study.

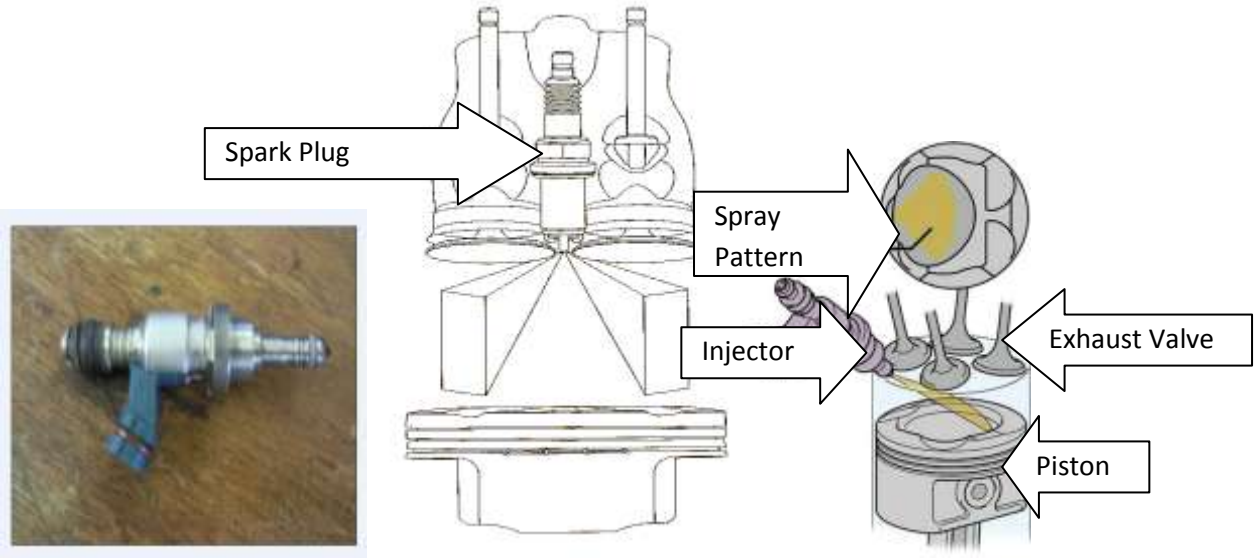


**(a) Denso Slit Injector (b) Double slit Spray Pattern (c) Incylinder Spray Pattern**

**Figure 3.9 Direct Injection High-Pressure Injector and Spray Pattern**

### 3.2.4 Engine controller

The Engine Control Module (ECM) is based on the Ricardo rapid prototype unit R-Cube, equipped with Dual PowerPC microcontrollers, Fig. 3.10. It controls all the engine functionalities such as the ignition, injection, throttle drive and valve timings and lifts via VCU. The advanced functionalities of the R-Cube are used to control the valve operating devices by means of interrupting signals via Control Area Network (CAN) communication.

**Figure 3.10 Engine Control Module**

### 3.2.4.1 Operation of the Engine Control System

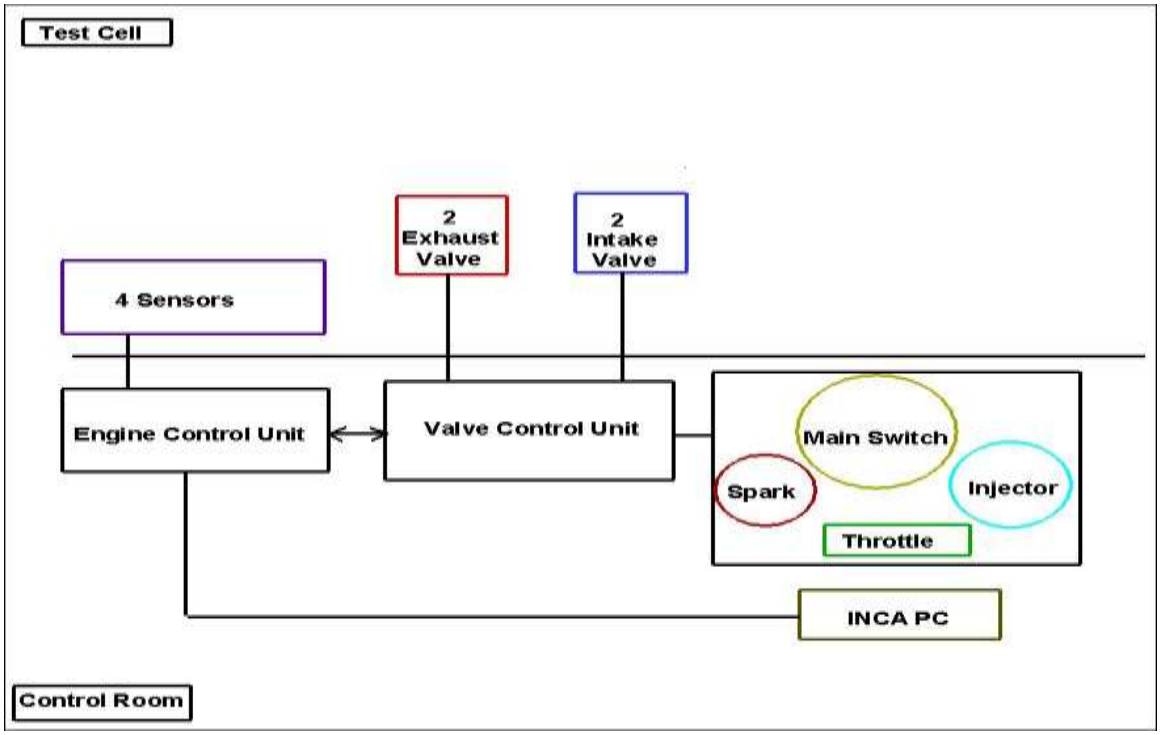


**Figure 3.11 Operation of the engine control system**

The communication structure between the ECU and VCU to the engine is shown in Fig. 3.11. The communication protocol between the ECM and the VCU box is both synchronous and asynchronous with engine's crankshaft position. The VCU is connected to the control switch that controls the main engine ignition switch, the ignition coil injector driver and the throttle control for varying engine load.

The ECU is connected to a Laptop PC for data logging and actuation using the INCA software. The valve timing, injection timing, injection pulse width and valve lifts are varied from look-up tables depending on engine speed and operational mode, i.e, two or four strokes. The ECU is also connected to the throttle, ignition coil and GDI driver to actuate them. For the valve-timing control, synchronous communication is assured through the use of hardwired interrupting signals, sent to the VCUs simultaneously to ascertain the crankshaft position. The first interruption signal initiates the VCU valve-opening sequence, while the second interruption initiates the VCU valve-closing sequence.

The asynchronous communication is supported by CAN serial line. CAN communication transmits all the essential parameters to define the correct valve motion, the parameters need to be transmitted by the ECU and received by the VCUs once per engine cycle.

The INCA software enables the various operational modes and strategies to be effected on the engine and the change from two to four strokes through calibration mode. These are made possible from the look-up tables for valve-timing, valve-lift, injection timing, injection pulse width, and spark-timing based on the selected engine speed. Figure 3.12 shows the engine control user interface display.

**(a) Data Display Screen** **(b) INCA Engine Controller Look Up Tables**

**Figure 3.12 Engine Control User Interface**

### 3.3 Engine Test Bed Set-Up

The engine test-bed comprises a AC dynamometer rated at 40KW power and 6000rpm maximum speed capable of motoring and regeneration modes. A coolant and oil condition system was used to regulate coolant and oil temperature. An external oil pump was employed to supply pressurised oil of 3.5bar pressure gauge to the engine.

The dynamometer was controlled by a PC operating with CADET V12 software. The software enabled the automatic and manual control modes of the dyno, data logging, low and high alarm level shut down and the dyno speed selection. It also allowed the coolant heating temperature to be monitored.

### 3.4 Supercharger System

The supercharger system used for this study was the AVL supercharging equipment type 515, which enables the temperature and pressures of the charged air to be controlled. The control

range of the charged air temperature began at 15 $^{o}$C above the cooling water temperature and extended up to 130 $^{o}$C. The control range of the air pressure extended from 1.1 bar to 3.2 bar absolute. The supercharging equipment provided air flow up to a maximum of 300m$^{3}$/h at 20 $^{o}$C and 1 bar absolute. measured on the suction side of the compressor.

The compressor used in this supercharger was a rotary vane type with cylindrical shaped rotor unusually mounted in the cover of a cylindrical casing. Thin steel vanes were inserted in slots which were radically arranged along the circumference of the rotor. By means of the centrifugal force, these sliding vanes were pushed outwards so that the crescent-shaped space between the rotor and the casing was divided into individual compartments. Owing to the revolving motion of the rotor, the volumetric capacity of the individual compartments was enlarged from zero to a maximum value and subsequently once again reduced to zero. These cyclical changes in volume caused the air to be sucked in, compressed and delivered.

The supercharger system was remotely controlled by a Programmable Logic Controller unit installed in the control room in order to protect it from condensation in the outside shed where the supercharger was located. The boost pressure was regulated by a linear plate valve controlled by the PID controller. The boost temperature control was carried out by a water cooler and heating rods, which are located at the entrance of the tank and can be operated alternatively.

### 3.5 Measurement System

During the course of the experiments, a number of sensors and pieces of measuring equipment were connected to the engine providing necessary data on important engine operation parameters such as in-cylinder pressure, intake and exhaust pressure, speed, load, fuel consumption, exhaust emission, lambda, intake and exhaust-gas temperature.

#### 3.5.1 In-Cylinder Pressure Measurements

In-cylinder pressure measurement is an effective research parameter widely used amongst engine research workers. Its popularity lies primarily within its capability of accurately determining vital combustion operational parameters such as combustion phasing, burn duration and burn rates. It also allows knocking combustion, misfiring conditions, and CAI/HCCI combustion to be defined with high precision under all engine operating conditions. Further analysis of the pressure data can be very effective in terms of defining engine load as well as cycle to cycle variation. In this study, in–cylinder pressure

measurements were extremely important in determining CAI/HCCI operation points and distinguishing misfire and knocking phenomena from normal combustion. To provide real-time in-cylinder pressure measurement, a water cooled piezoelectric pressure transducer (Kistler 6061B) with a measurement range of 0-250 bars gauge and sensitivity of -2.5 PC/bar was installed on the cylinder head and the pressure signals were amplified by a charge amplifier (Kistler Type 5011) and then transferred to a PC via a NI data acquisition card.

### 3.5.2 Intake and Exhaust Pressure and Temperature

The instantaneous intake-pressure readings in this study were measured with a Kistler piezo-resistive pressure sensor Type 4007BA5F of up to 5bar absolute pressure and capable of continuous high-temperature operation up to 200$^{o}$C. This is connected to a Kistler amplifier, Type 4618AO with pressure and intake temperature output.

The real-time exhaust pressure was measured with a Kistler piezo-resistive pressure sensor Type 4007BA20F in absolute pressure ranges up to 20 bar. The sensor was water cooled because of the high exhaust-gas temperature it was being exposed to. The sensor was connected to a Kistler Type 4618A2 amplifier with pressure and temperature output. Exhaust temperature was measured by a standard K- type thermocouples at a position of 50 mm from the exhaust port.

### 3.5.3 Fuel and Air Flow Measurement

The fuel-flow rate was measured by a PROMASS 83A fuel mass flow meter that works on the principle of the Corioli's effect. It has a high level of accuracy and reliability, but care is required in their installation to avoid the effects of external vibration which may adversely affect the reading.

A Teledyne Laminar air flow meter was installed in the middle of the intake pipe line and used to measure the air-mass flow.

## 3.6 Data Acquisition and Analyse System

Many calculations can be performed on in-cylinder pressure with the appropriate data acquisition and analysis system. Such a system consists of two parts: physical hardware and data processing software. The following input was normally recorded by the data acquisition system: cylinder pressure, manifold pressure, command voltages for valve-timings, fuel-injection pulse, spark charging/discharging pulse, engine speed, torque output from the

dynamometer, and exhaust lambda sensor. An in-house built Labview based subroutine programme was used to load, process and plot the necessary data.

### 3.6.1 Hardware

A PC was used to store the data and perform the calculations. The DAQ card was a National Data Acquisition Card Instrument type NI USB 6251. There are 16 input channels to the DAQ cards; among them, the charge amplifier output from the in-cylinder pressure transducer, the clock signal and the trigger signals from the shaft encoder. The clock and trigger signals to the DAQ system were required so that the in-cylinder pressure output could be sampled at every crank angle (1deg CA) and its phasing relative to the 2/4-stroke cycle could be established. The phasing signals (clock and reference) coming from the shaft encoder were used to send signals through the logic box and provide the reference signal for fuel-injection timing, as well as for spark timing. Clock signal was used to provide the data acquisition sampling interval (1 degree CA for the current configuration) while the reference signal determined the phasing of the data acquired based on the 4-cycle engine operation.

### 3.6.2 Software

Labview software was used in conjunction with the DAQ card for the real-time data acquisition and data analysis. The program used for the experimental work with this study was developed by Dr Yan Zhang. The program performs an array of functions, such as heat-release analysis, IMEP, COVimep, knocking and misfiring combustion analysis and the data were displayed on the screen as shown in Figure 3.13. The data could also be copied and converted into excel format for off-line processing and analysis.

#### 3.6.2.1 IMEP. PMEP and FMEP Calculation

The Indicated Mean Effective Pressure (IMEP) was the best indication of engine load in the single-cylinder research engine used for this study. It was very important to know how the cylinder pressure behaved in relation to cylinder volume as determined by the engine geometry. The IMEP was calculated from the indicated work, this is the specific work done on the piston by the expanding combustion-gas over the four-stroke cycle and was numerically determined by the ratio of the area enclosed by the pressure volume curve and the cylinder displaced volume.

$$\boldsymbol{IMEP = \frac{1}{V_d}\int_0^{720} P.dv} \quad (1)$$

Calculation of IMEP is done directly through numerical integration of the area bounded by the line in the pressure-volume diagram (P-V) over the entire engine cycle at a step interval of 1 deg CA that equals to the sampling rate of cylinder pressure. Figure 3.13 shows the screen display of the Data Acquisition Computer.

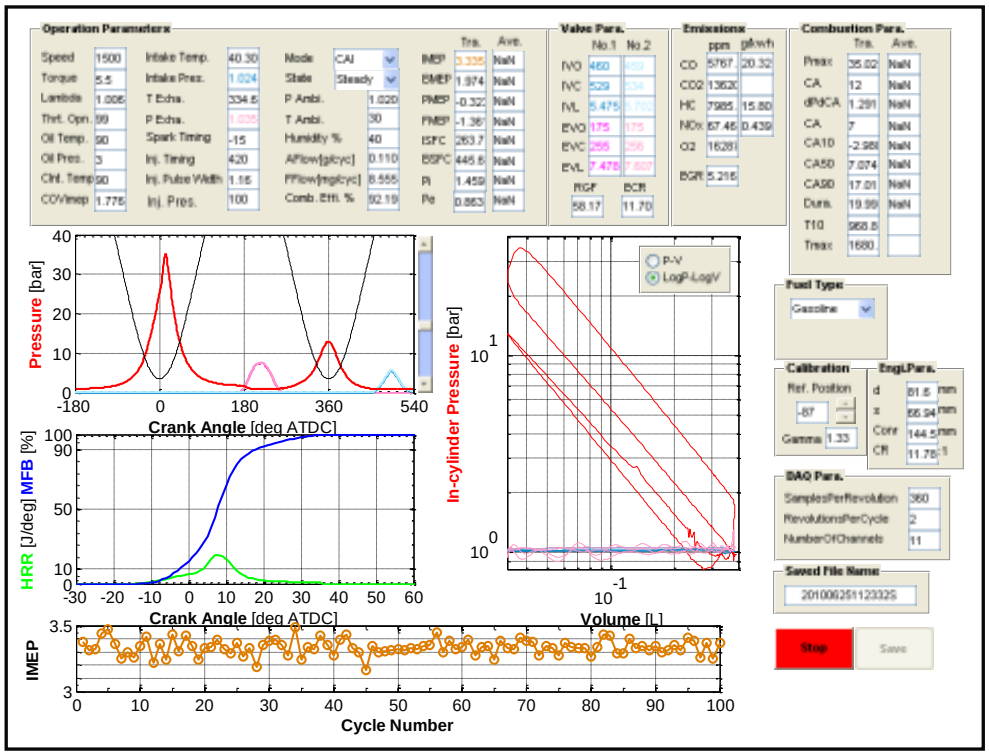


**Figure 3.13 Screen Display of the Data Acquisition Computer**

The Pumping Mean Effective Pressure (PMEP) is the work done on the gas during the intake and exhaust stroke.

The Friction Mean Effective Pressure is the work to overcome friction internal to the engine and to power essential auxiliaries such as an oil pump.

The Brake Mean Effective Pressure (BMEP) is the workout from the crank shaft engine.

By definition it follows that

$$\boldsymbol{FMEP = IMEP_{gross} - PMEP - BMEP} \quad (2)$$

But $$\boldsymbol{IMEP_{gross} - PMEP = IMEP_{net}} \quad (3)$$

Hence $$\boldsymbol{FMEP = IMEP_{net} - BMEP} \quad (4)$$

### 3.6.2.2 Heat Release Rate Analysis

Heat-release analysis was the most effective method to characterize combustion events of both SI, and CAI combustion in terms of combustion phase, speed and peak rate. It also enabled the determination of parameters affecting combustion phasing and initiation. All calculations were based on cylinder pressure measurements after calibration and referencing of the pressure transducer.

The first law of thermodynamics was implemented to the control volume of the cylinder contents. A single zone was assumed, where no temperature gradients exist and the reactants and products were completely mixed. The reactants and products were also assumed to have the same properties.

$$\boldsymbol{\delta Q_{hr} = dU + \delta W + \delta Q_{ht}} \quad \textbf{(5)}$$

Where $\delta Q_{\text{hr}}$ is the heat released in the combustion chamber during combustion, dU is the internal energy raised, $\delta W$ is the work on the piston by the considered system and $\delta Q_{\text{ht}}$ is the heat exchange occurring within the combustion chamber wall.

Analytically:

$$\boldsymbol{\delta W = PdV} \quad \textbf{(6)}$$

$$\boldsymbol{dU = mC_v dT} \quad \textbf{(7)}$$

The ideal gas law states the equation:

$$\boldsymbol{mdT = \frac{1}{R}(pdV + VdP)} \quad \textbf{(8)}$$

The net heat-release rate is now presented on an incremental angle basis

$$\boldsymbol{\frac{dQ_{net}}{d\theta} = \frac{dQ_{hr}}{d\theta} - \frac{dQ_{ht}}{d\theta} = \left(\frac{\gamma}{\gamma-1} P \frac{dV}{d\theta}\right) + \left(\frac{1}{\gamma-1} V \frac{dP}{d\theta}\right)} \quad \textbf{(9)}$$

Where $\boldsymbol{\gamma}$ (the ratio of specific heats) = $\frac{Cp}{Cv}$ and $\theta$ is the crank angle

The heat-release rate could thus be calculated from the measured pressure trace with respect to the crank angle using the estimated average ratio of specific heat values. A cumulative heat release could then be calculated from the heat-release rate and presented using Mass Fraction

Burned (MFB). This quantifies ignition timing, combustion duration, defined as the 10-90% MFB CA respectively

### 3.6.2.2.1 Start of Combustion, End of Combustion, Combustion Phase and Duration (CA10, CA50, CA90, CA10-90)

The net heat-release profile obtained from integrating the two terms on the right-hand side of equation 6 was normalized to give unity for maximum value. A mass fraction burned versus crank angle curve could be drawn after integration, as shown in Fig. 3.14 and through this curve a number of useful combustion parameters could be quantified for combustion analysis, as shown in Table 3.2.

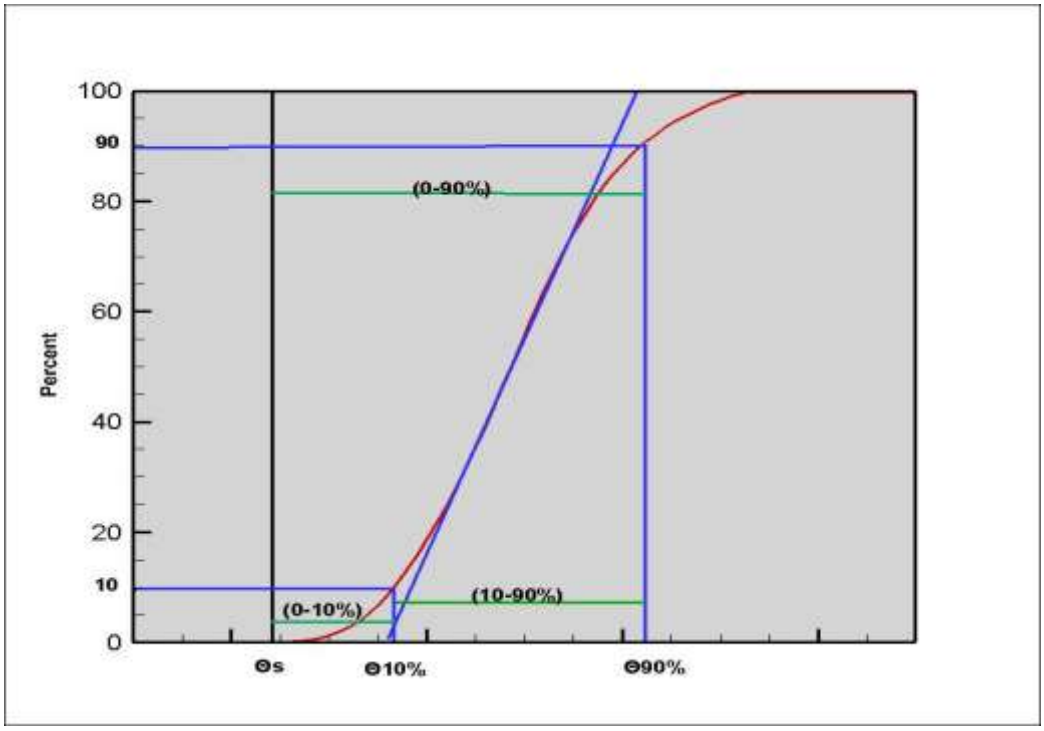


**Figure 3.14 Definition of flame-development angle on mass fraction burned versus crank angle curve**

**Table 3.2 Lists definitions commonly used to describe the various energy release stages in SI and CAI combustion in relation to MFB**

| Mass Fraction Burned | Spark Ignition | Controlled Auto-Ignition |
|---|---|---|
| 0-10% | Flame development angle | - |
| 10% | Start of rapid burn rate | Ignition |
| 10-90% | Rapid – burning angle | Combustion duration |
| 0-90% | Overall burn rate | - |
| 90% | End of combustion | End of combustion |

#### 3.6.2.2.2 Combustion Stability $COV_{imep}$

The coefficient of variation of indicated mean effective pressure ($COV_{imep}$) is a good indicative parameter for defining the cyclic variability for the combustion engine. It is the standard deviation in IMEP divided by the mean IMEP, and it is usually expressed as percentage:

$$\boldsymbol{COV_{imep} = \frac{\sigma_{imep}}{imep} \times 100} \qquad \textbf{(10)}$$

The IMEP value is calculated over 100 consecutive cycles in this study, and $\sigma_{imep}$ is the standard deviation in IMEP. A maximum value of 10% is normally defined as acceptable for vehicle drivability.

#### 3.6.2.2.3 Knocking Combustion Detection

The occurrence of knocking combustion is detected as the acoustic noise transmitted through the engine structure due to an excessive heat-release rate. The excessive rate of pressure rise not only leads to noise problem but also causes structural damage. One major objective in this experimental work was to enlarge the operating range of CAI combustion in the 4 stroke mode. To enlarge the operating range, knocking combustion which is experienced in the high-load operating region has to be correctly defined.

The data acquisition and analysis programme calculates the rate of pressure rise and uses it to determine the occurrence of knocking combustion during engine testing. The maximum allowable rate of the pressure rise was 8bar/CA but we limit it to 5bar/CA. In addition, the

upper load boundary was also limited by the level of cyclic variation as defined by the coefficient of variation in IMEP ($COV_{imep}$).

### 3.6.2.3 Fuel Consumption and Efficiency

In engine tests, the fuel consumption is measured as a flow-rate and mass-flow per unit time $m_{f,}$ but the specific fuel consumption (sfc) was a preferable parameter since it is a measurement of how efficiently an engine is using the fuel supply to produce work.

The indicated specific fuel consumption is expressed as:

$$\mathbf{ISFC} = \frac{\mathbf{m_f}}{\mathbf{P_i}} \qquad \textbf{(11)}$$

Where $m_f$ is mass flow per unit time, and $P_i$ is the indicated power.

The brake-specific fuel consumption is a measure of the overall engine efficiency. The BSFC and the engine efficiency are inversely related, hence the lower the BSFC, the better the engine. By definition the BSFC is the fuel -flow rate $m_{f,}$ divided by the brake power $P_b$ it is expressed as

$$\mathbf{BSFC} = \frac{\mathbf{m_f}}{\mathbf{P_b}} \qquad \textbf{(12)}$$

**The indicated engine efficiency** ($\eta_f$) represents how efficiently the fuel energy was converted into indicated work. It is expressed as

$$\boldsymbol{\eta_f} = \frac{\boldsymbol{P_i}}{\boldsymbol{m_f Q_{lhv}}} \qquad \textbf{(13)}$$

Where $P_i$ is the indicated power, $m_f$ is the fuel flow rate and $Q_{lhv}$ is the lower heating value of the fuel.

**The combustion efficiency** ($\eta_c$) is defined by the percent of actual energy derived from fuel combustion (fuel energy minus energy waste from CO and HC emissions) and the fuel energy supplied to the engine. It was calculated from Equation 14

$$\boldsymbol{\eta_c} = \mathbf{1} - \sum_{\mathbf{i}} \frac{\frac{\boldsymbol{X_i Q_{lhi}}}{\boldsymbol{m_f Q_{lhv}}}}{\boldsymbol{m_a + m_f}} \qquad \textbf{(14)}$$

Where $X_i$ is the mass fraction of CO and HC. $Q_{lhv}$ represents the lower heating values of these specie, ma is the air mass flow rate and mf fuel mass-flow rate

**The volumetric efficiency** ($\eta_v$) was used in this study as an overall indication of the effectiveness of a four-stroke engine and its intake and exhaust systems as an air pumping device. The volumetric efficiency is affected by the fuel, engine design and engine operating variables i.e. valve-timing, valve-lift and valve sizes. It is expressed as

$$\boldsymbol{\eta_v = \frac{2\dot{m}_a}{\rho_a V_d \, N}} \qquad \textbf{(15)}$$

where $\dot{m}_a$ is the air mass-flow rate, $\rho_a$ is the air density evaluated at atmospheric conditions, $V_d$ is the engine displaced volume and N the engine speed, then $\eta_v$ is the overall volumetric efficiencies.

**The thermal efficiency** of the engine, which defines the upper limit of the efficiency obtainable from the complete combustion and is calculated from the ratio of indicated mean effective gross (IMEPgross) to the heat liberated (QhrMEP) as follows:

$$\boldsymbol{\eta_{therm} = \left(\frac{IMEP_{gross}}{Q_{hr}MEP}\right)} \qquad \textbf{(16)}$$

### 3.7 Emission Analyser

The instantaneous relative air to fuel ratio, Lambda was measured by a lambda sensor comprising a Bosch sensor connected to a MOTEC lambda meter. In parallel, exhaust gas was sampled from the exhaust pipes for gaseous and particulate emission measurements.

#### 3.7.1 Horiba Analyser

A Horiba 7170DEGR gas analyser system was used to measure the levels of carbon monoxide (CO), carbon dioxide ($CO_2$), total unburnt hydrocarbons (THC), and nitrogen oxides (NOx) from the exhaust. The second $CO_2$ channel could be used to measure the EGR if needed. The Horiba analyser was span before running test every morning then allow it to warm up for about an hour before taking readings. The Horiba Screen display is shown in Figure 3.15.

The measurement of CO and $CO_2$ was conducted by the AIA-72X module using non-dispersive infrared analysis (NDIR). NDIR works on the principle that molecules absorb infrared radiation at specific wavelengths. The level of absorption is proportional to the concentration of the molecule. Different molecules have different absorption spectra.

The measurement of the oxygen contained in the exhaust gas was achieved by magneto-pneumatic detection within the MPA-720 unit in the Horiba analyser. The magneto-pneumatic

detection works by applying an alternating current to the electromagnet. AC current flows in the electromagnet so an alternating field appears between the poles of the electromagnet. When the sample gas flows in the magnetic field, the pressure around the magnetic poles changes according to the concentration of oxygen, because the oxygen is attracted to the poles. A condenser microphone is used to detect the changes in pressure.

The measurement of NOx is achieved by chemiluminescence (detector CLD) within the CLA-720 module of the Horiba analyser. Chemiluminescence works by reacting the nitrogen oxides with ozone. This converts the NO to $NO_2$. A proportion of the $NO_2$ created in this manner will produce an excited $NO_2$ molecule. The excited molecules emit light on return to the ground state. This light emitted is proportional to the number of nitrogen oxides present in the original gas sample.

The FIA-720 module of the Horiba analyser measures the concentration of total hydrocarbon (THC) using hydrogen Flame Ionisation Detection (FID). When hydrocarbons are introduced to a hydrogen flame, the number of ions produced is proportional to the number of carbon atoms. This in effect gives the THC as an equivalent number of methane ions.


**Figure 3.15 Horiba Screen of Gaseous Emission Analyser**

### 3.7.2 Particle Size Distribution Analyzer

The exhaust particle measurement in this study was performed with Electromobility Spectrometer EMS VIE, which is an automated system for the size classification and size analysis of airborne particles within the size range of subnano to 1000 nm. Figure 3.16 shows the layout of the EMS. Figure 3.16(a) shows the engine connected to the particulate analyser. The dilution process is shown in Figure 3.16(b). The EMS heating and dilution probe set up is shown in Figure 3.16(c).

The size separation of particles is based on the principle of electrical mobility. The electrical mobility of a particle determines the drift velocity of a charged particle under the influence of an electrical field. The Differential Mobility Analyser, DMA within the EMS was used for this purpose.

Within the DMA, the particles in the input exhaust flow are transferred to the output sample flow according to their electrical mobility, gas flow velocity, geometry of the DMA and the strength of the electrical field. The strength of the electric field is varied by changing the voltage between the electrodes of the DMA. The particles are passed through additional devices before being introduced into the DMA. For size analysis, an impactor is frequently used to discriminate against particles larger than the upper size limit of the DMA. The elimination of larger particles is necessary for the reconstruction of the unknown size distribution from the measured data. Another device used is a charger or neutraliser to establish a well defined distribution of electrical charges on the particles.

After classification, the concentration of the particles in the output sample flow is determined by a particle sensor. The instruments used for concentration measurements are the Condensation Nuclei Counter CNC and the Faraday–Cup Electrometer FCE. While the CNC can be used for low concentrations, the electrometer is of advantage with very small particles and high aerosol concentrations. The performance of the DMA is critical to the stability of these flows, which are supplied from the control unit. Electrode voltages and the reading of the particle sensor is controlled by dedicated electronics and a microcomputer, which is also used for data reduction, display and storage.

Typically it takes up to four minutes for a single sample reading. The data is displayed as shown in Figure 3.16(d) and converted into Excel format for post-processing and analysis of

the particle size distribution as a function of the engine operating conditions and variables being investigated.

**(a) Engine and Analyser Set Up**

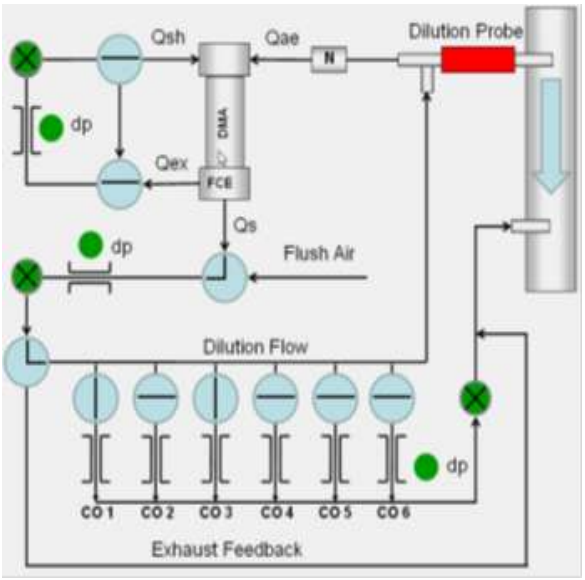


**(b) EMS VIE 10 Dilution Process**

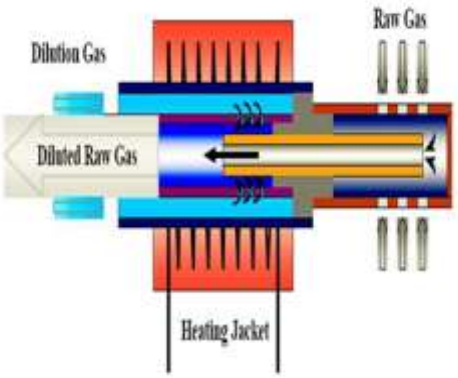


**(c) EMS Heating and Dilution Probe**

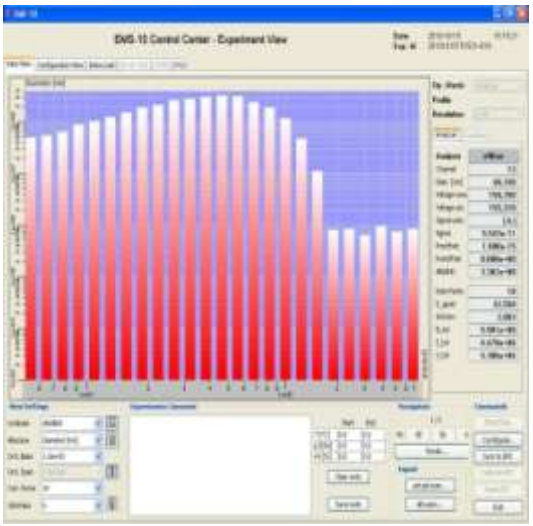

**(d) EMS Particulate Emission Display**

**Figure 3.16 Display of particle measurement results**

### 3.8 Sensors Calibration

The sensors calibration was done by the supplier and the results and certificate is attached in the Appendix.

## Chapter 4 Particulate Matter Emissions from Different Combustion Modes

### 4.1 Introduction

In this chapter the Particulate Matter (PM) emissions of pure gasoline and ethanol/gasoline blends are investigated in different SI and CAI combustion modes. A Horiba Mexa 7100DEGR exhaust-gas analyser was used to analyse unburnt hydrocarbon (UHC), carbon monoxide (CO) and nitric oxide (NO).

In this chapter the PM emissions of different combustion modes were measured from a camless direct-injection gasoline engine that could be operated in both spark-ignition and CAI combustion modes in either the 4-stroke or 2-stroke cycle using DMA EMS VIE 10. In this test both pure gasoline (E0) and a 15% ethanol blend (E15) were tested and the PM emission was sampled directly from the exhaust pipe and DMA. The effect on PM emissions when operating the engine in 2 and 4-stroke SI and CAI using E0 and E15 are presented and analysed.

### 4.2 Engine Operating Conditions

Because of the flexibility of the camless system and engine control software, seven engine operational modes were achieved through different combinations of valve timings and durations. Figure 4.1 shows the valve timings and injection timings used in different operational modes. During the 4-stroke mode operations, the supercharger was turned off and the intake air was drawn from ambient. For the 2-stroke mode operations, the compressed air supply from the supercharger was connected to the intake system to provide the boost air. The engine speed was maintained at 1500rpm during the duration of this investigation.

#### Mode 1: 4-Stroke Throttle-Controlled SI Mode

This is the conventional spark-ignition mode used in the production gasoline engine. Engine load is controlled by the throttle opening, and its combustion process is initialized by the spark discharge followed by flame propagation. The engine was operated in this mode to obtain the baseline data. At part load, the partially closed throttle results in a significant increase in the pumping loss, the main cause for the poor fuel economy of current SI gasoline engines. In this engine operational mode, fuel was injected earlier in the intake stroke to obtain a homogeneous mixture. To prevent wetting the piston top, injection-timing used in this paper was set to 412degCA ATDC.

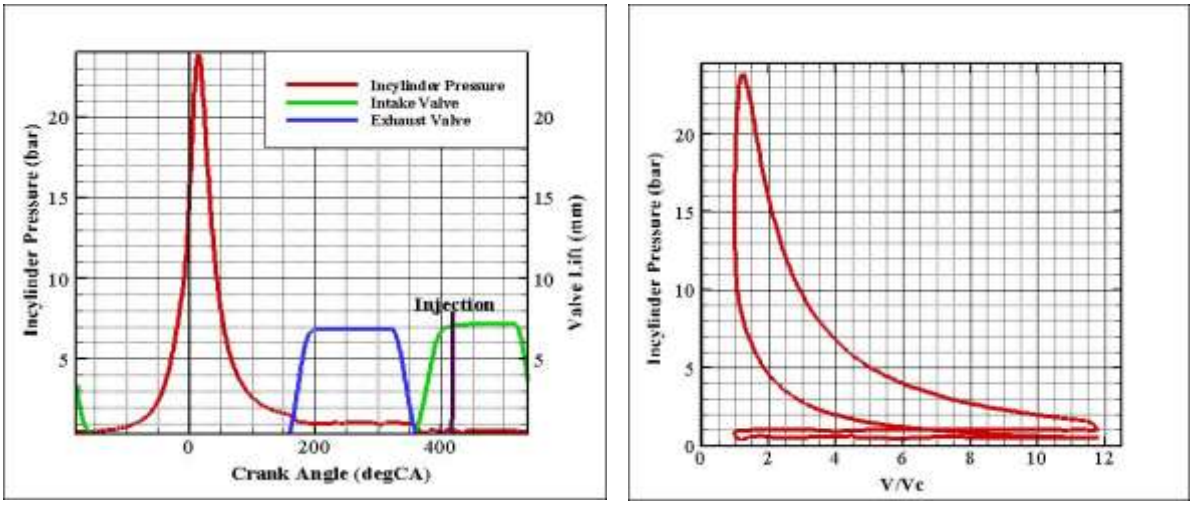


**(a) 4-Stroke throttle SI valve timing and P-V diagram**

**Figure 4.1 Valve Timing and Operation Modes Used in this Experiment**

**Mode 2: 4-Stroke Intake Valve Throttled SI Mode**

In order to reduce the pumping loss caused by the partially closed intake-throttle at part load, intake-valve opening duration can be used to regulate the amount of air into the cylinder with WOT. In this work, the intake-valve opening (IVO) was fixed at standard timing and the intake-valve closing (IVC) was varied to throttle the intake air-flow, the valve lifts was set to 4mm, injection-timing was set to 412degCA ATDC.

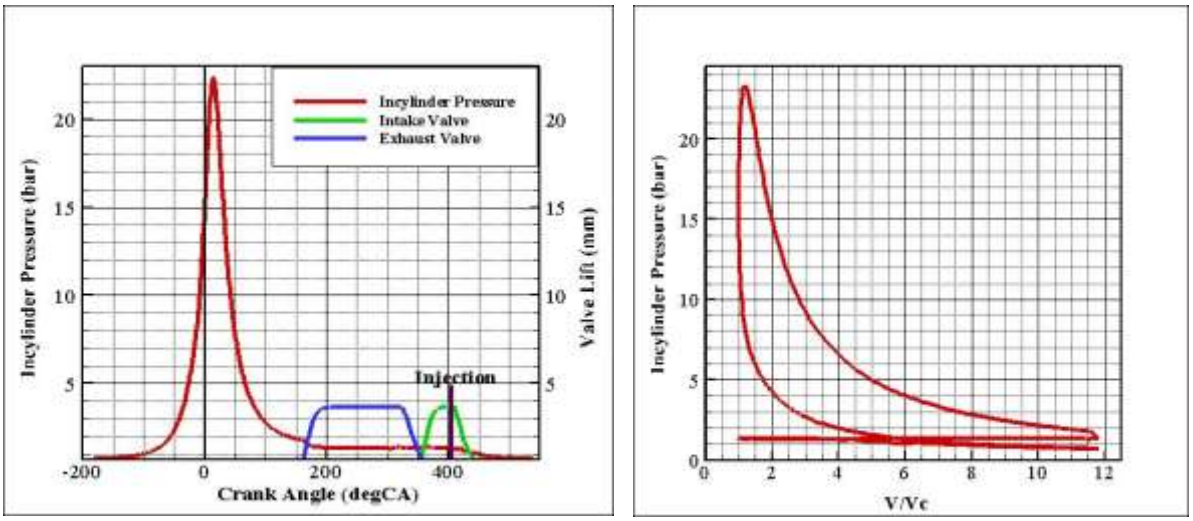


**(b) 4-Stroke Early Intake valve Closure SI valve timing and P-V diagram**

**Figure 4.1 (ctd) Valve Timing and Operation Modes Used in this Experiment**

**Mode 3: 4-Stroke Positive Valve Overlap SI Mode**

In this case IVO takes place before TDC and EVC after TDC to create a positive overlap between the intake and exhaust-valve opening period. As the intake-valves open in the exhaust stroke, a portion of exhaust-gas enters the intake port and is sucked back into the cylinder in the intake stroke. The exhaust-valves close after TDC so that some exhaust-gas is also sucked back into the cylinder. In this work, the exhaust-valve lift was maintained at 7.2mm and the intake-valve lift was reduced from full lift of 7.2mm to 3mm to avoid any contact between the piston and valves at TDC during the gas exchange. The intake throttle was used as the principal means of controlling the engine load but it was adjusted to a wider opening position than that used in the 4-stroke throttle-controlled SI mode. This was in order to maintain the same amount of air in the cylinder with recycled exhaust-gas. The fuel injection was set to 412degCA ATDC.

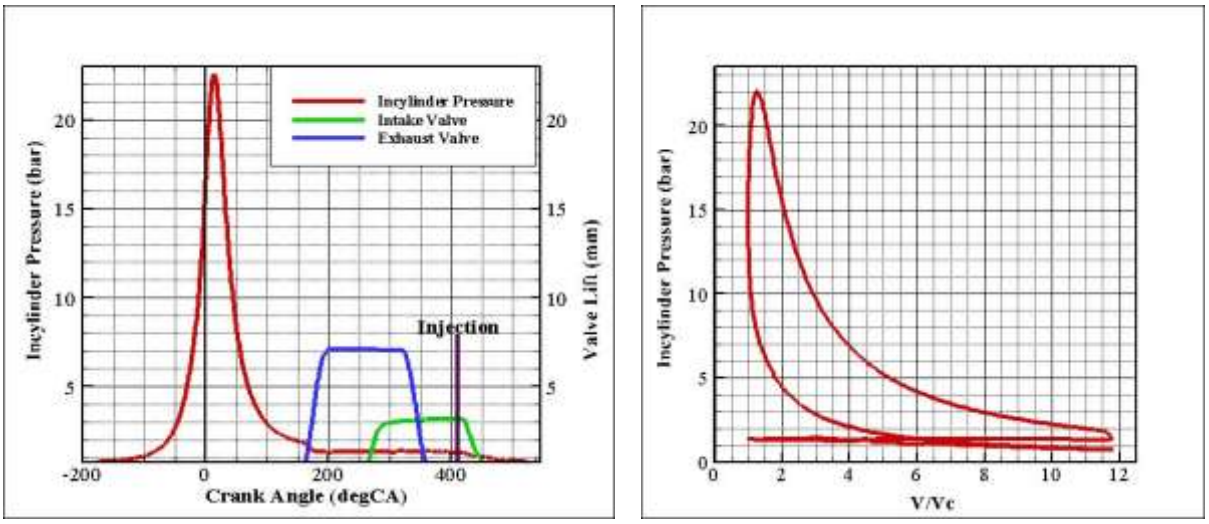


**(c) 4-Stroke Positive Valve Overlap SI valve timing and P-V diagram**

**Figure 4.1 (ctd) Valve Timing and Operation Modes Used in this Experiment**

**Mode 4: 4-Stroke Negative Valve Overlap CAI Mode**

Another way to obtain internal EGR is to trap a portion of the burnt gas in the cylinder by earlier closing of the exhaust-valves. To minimise the backflow, the intake-valve opens later. The intake and exhaust-valve lifts was maintained at 7.2mm.Then a negative valve overlap period is formed and the residuals are recompressed around the gas-exchange near TDC. In this case, the intake air-flow rate is dependent on the amount of trapped residuals, which can be controlled by varying the exhaust-valve closing. This allows the throttle to be kept wide open and reduce pumping loss. As the exhaust-valve closes earlier, the fuel-injection timing

can be advanced into the exhaust stroke for better evaporation and mixing. In this work, the fuel was injected at 280degCA ATDC.

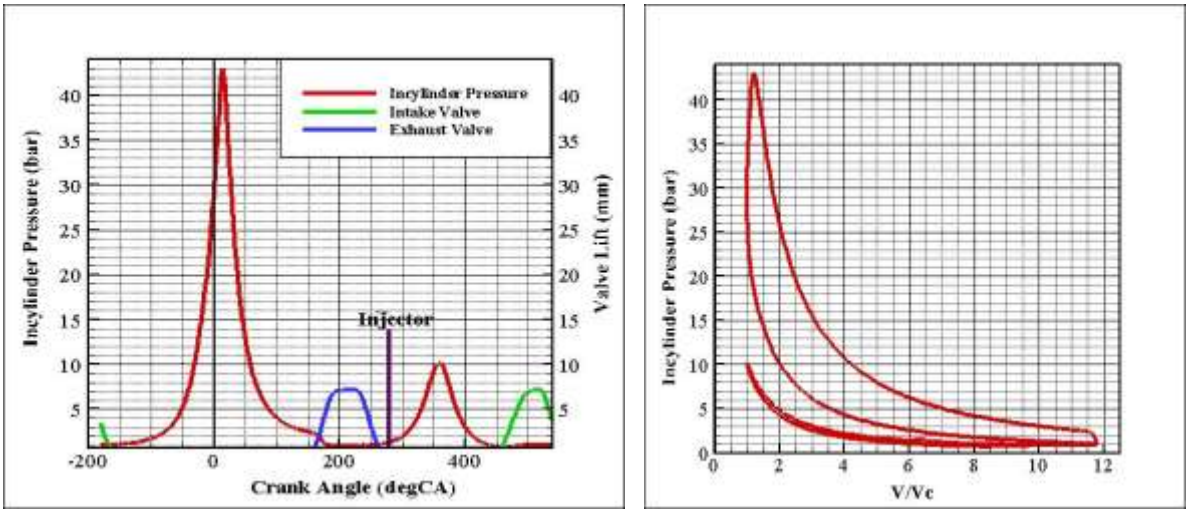


**(d) 4-Stroke CAI Negative Valve Overlap valve timing and P-V diagram**

**Figure 4.1 (ctd) Valve Timing and Operation Modes Used in this Experiment**

**Mode 6: 2-Stroke SI Mode**

As a basis for comparison, 2-stroke SI mode was also studied in this work. It was realised by an extended exhaust period to maximise the scavenging efficiency. Engine load, similar to 2-stroke CAI mode, was also determined by the boost pressure. As less burnt gas was retained in the cylinder, the boost pressure requirement was reduced to maintain the same engine load as in the 2-stroke CAI mode. Injection timing was set to 109degCA BTDC

**Mode 6: 2-Stroke SI Mode**

As a basis for comparison, 2-stroke SI mode was also studied in this work. It was realised by an extended exhaust period to maximise the scavenging efficiency. Engine load, similar to 2-stroke CAI mode, was also determined by the boost pressure. As less burnt gas was retained in the cylinder, the boost pressure requirement was reduced to maintain the same engine load as in the 2-stroke CAI mode. Injection timing was set to 109degCA BTDC

**Mode 5: 2-Stroke CAI Mode**

When both the intake and exhaust valves open once around each BDC within one engine crankshaft revolution, the engine operational mode becomes a 2-stroke operation. On the poppet-valve engine, due to incomplete scavenging in the 2-stroke mode, a large amount of

the residual gas is trapped in the cylinder when the exhaust-valves close earlier. In this mode the engine load was determined by the boost pressure. Fuel was injected after the exhaust valves closed but before the intake valves closed for better mixing through a longer mixture preparation period and the interaction between the intake air and fuel injection. The injection timing was set to 140degCA BTDC.

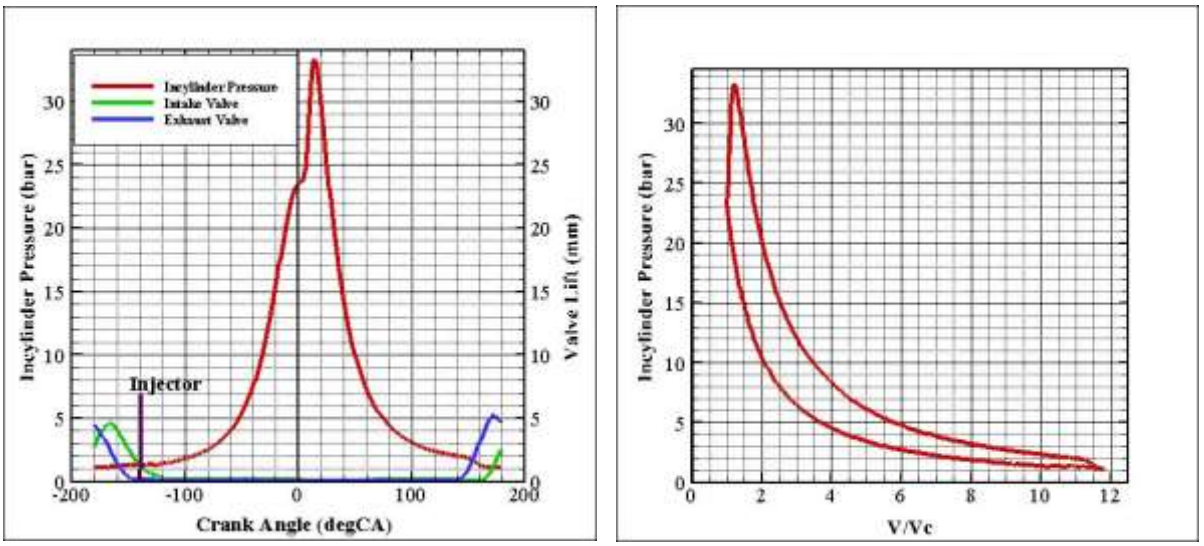


**(e) 2-Stroke CAI valve timing and P-V diagram**

**Figure 4.1 (ctd) Valve Timing and Operation Modes Used in this Experiment**

**Mode 6: 2-Stroke SI Mode**

As a basis for comparison, 2-stroke SI mode was also studied in this work. It was realised by an extended exhaust period to maximise the scavenging efficiency. Engine load, similar to 2-stroke CAI mode, was also determined by the boost pressure. As less burnt gas was retained in the cylinder, the boost pressure requirement was reduced to maintain the same engine load as in the 2-stroke CAI mode. Injection timing was set to 109degCA BTDC

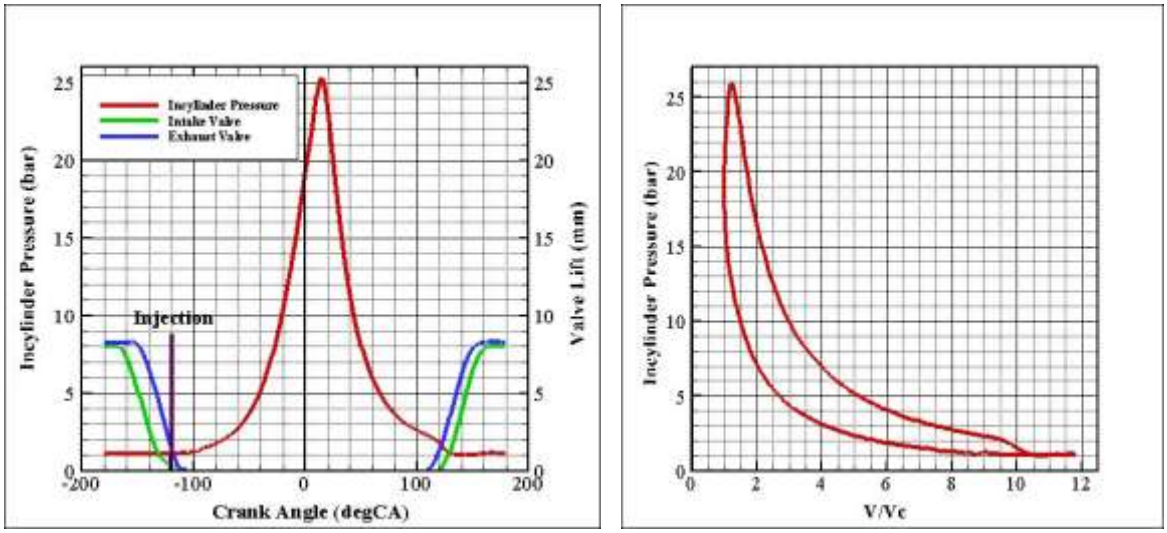


**(f) 2-Stroke SI valve timing and P-V diagram**

**Figure 4.1 (ctd) Valve Timing and Operation Modes Used in this Experiment**

### 4.2.1 Particulate Measurement Set-Up and Experimental Procedure

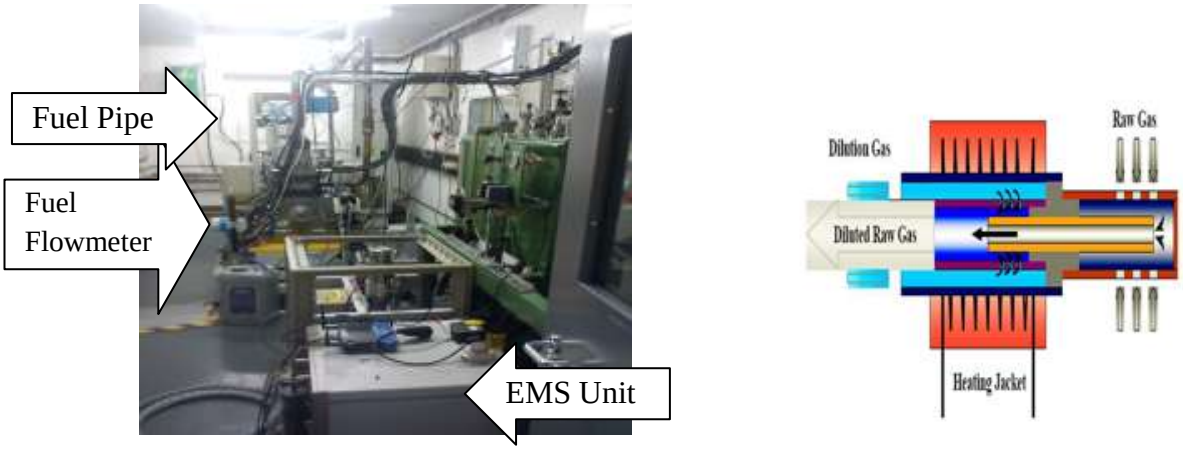


**(a)** **(b)**

**Figure 4.2 (a) EMS Connected to the Exhaust port (b) The Sampling Probe**

It is widely known that first-generation wall-guided direct-injection engines generate a greater quantity of particulates than emitted from the port fuel injection engine (PFI) [76, 77, 87]. The particulate emissions from GDI engine have been regulated from Euro V (2010 onwards) on mass basis. However, the Euro VI (2014 onwards) will limit the particulate volume. In GDI engines, a significant amount of the emissions is made up of soluble organic fractions (SOF). The increase in particulate emissions in GDI over PFI is due to the limited time available for mixture preparation and spark discharge, coupled with cylinder wall-wetting and fuel-impingement on the piston crown [87].

In CAI operational mode using high residual gas to initiate combustion, fuel is injected during the negative valve overlap period for better fuel reforming, the temperature is very high with reduced oxygen to support oxidation and pyrolysis dominates. In addition, during compression processes the temperature is reduced and subsequently the combustion pressure is low, hence pyrolysis dominates. Therefore there is a high possibility of increased particulate emissions in this combustion mode compared to other modes in direct injection. Unfortunately this area of research has not received much attention.

The PM number was measured using an Electromobility Spectrometer (EMS) Vienna type 10. The EMS is an automated measurement system for the size analysis of fine and ultrafine aerosols using Differential Mobility Analysers (DMA) for the classification of particles and an electrical sensor for their detection. The EMS used for this work has a nominal diameter size range of 5-700nm. For a detailed description of the EMS operation and set-up in this work see Chapter 3 Section 3.7.2, as well as the work of Winklmayr et al [95] and Reischl [96].

The aerosol sample is admitted through the sampling probe shown in figure 4.2(b) connected to the exhaust pipe 130mm from the combustion chamber. An essential critical point in operation of the DMA is the supply of accurate and stable gas flows. The need to control a variable gas flow was eliminated by operating the DMA at pre-determined and fixed flow rate of 100% dilution. To avoid water condensation in the sample, an additional drier is activated before the sample enters the DMA. The instrument is computer controlled. Size distribution measurement takes about 3-4 minutes. The system is flushed intermittently for better and accurate reading, an average being taken when in doubt.

The raw data obtained is processed using Excel format and the corresponding chart can be plotted using Excel or similar software. For more detail on the PM measuring device, the sampling handling and conditioning process, the measurement procedures, etc see [95,96,97].

### 4.3 Mode 1: 4-Stroke Throttled SI Mode

In this mode three different tests were performed as follows:

#### 4.3.1: 4-Stroke Throttled SI Operation with Varying Engine Loads

Fig 4.3(a) and (b) compares particulate emissions under varying engine loads in number and mass. These data were obtained at a speed of 1500rpm, no EGR, The coolant temperature was set to 80˚C. The figures display the changes in particle-size distribution as load is increased from low load of 2.2 bar to full load of 8.5 bar in Figure 4.3(a). The size distribution shows a monomodal distribution peaking at 5nm and then falls steeply for particulates of less than 5nm in diameter. The particlate number continued to increase as the load was increased. However, at 2.9 bar IMEP_net load the particulate emissions and the total Particulate Number emissions result was greatest (Figure 4.3b). This apparent disparity may have been due to the increased fuel injection rate from 0.8ms to 0.95 ms in 2.9 bar IMEP_net (Table 4.1), in addition the COVimep was greater than 10% which means the combustion was not stable. The mean particle size increased from 2.5nm at 2.2 bar IMEPnet to 5nm at 8.5 bar IMEP_net. The majority of the particles were shown to be in the 10nm size range.

The particulate emission results from this SI operation are more complicated. As shown in Figure 4.3 (a)-(d). At 2.2 bar IMEPnet, the particle number and mass were the lowest, as expected with less fuel injected. The maximum particle number and mass were detected at 2.9 bar IMEPnet and particles peaked at 2.5nm diameter. As the load was increased from 2.9 bar IMEPnet both particle mass and number decreased with load before they started to increase after about 6 bar IMEPnet. Such results are counterintuitive to the fact that the injection of more fuel is likely to form an inhomogeneous mixture and hence, produce more soot. However, according to Figure 4 (c), the small particles in the range of a few nanometres are not soot but more likely to be liquid condensates. Therefore, the reduced particle emissions between 2.9 bar and 6.0 bar IMEPnet would be a result of more homogeneous and complete combustion of hydrocarbons, which is consistent with the unburned HC emission shown in Figure 4.3(f). Such improvement in homogeneity and combustion is likely to have been caused by the better mixing from the interaction of fuel injection and in-cylinder flow during the intake stroke, which could only be confirmed through detailed in-cylinder measurement of fuel injection and mixture formation process using PIV, LIF, LDV.

Finally, as shown in Figure 4(c) despite the large number of smaller particles, the particle mass is heavily biased by the presence of large particles. Figure 4(c) is dominated by soot

emissions in the accumulation mode (50-150nm). As a result, more surface area is available for absorbing the nucleation PM, and this could then cause a reduction of particulate number in the nucleation mode (<50nm).

**Table 4.1 Engine outputs of 4-stroke throttle SI operaiton**

| IMEP_net | SparkTiming | InjTiming | InjPulseWidth |
|---|---|---|---|
| bar | BTDC | ATDC | ms |
| 2.21 | -23 | 419 | 0.8 |
| 2.90 | -22 | 421 | 0.95 |
| 4.92 | -18 | 423 | 1.22 |
| 6.21 | -19 | 425 | 1.22 |
| 7.36 | -18 | 426 | 1.61 |
| 8.58 | -17 | 428 | 1.81 |

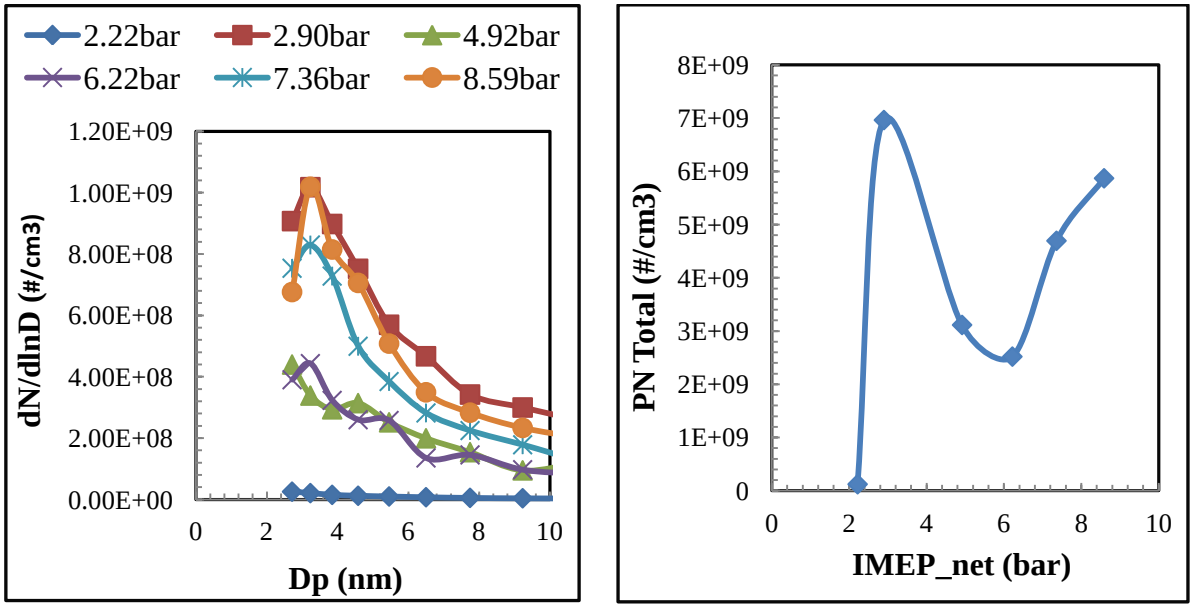


**(a) Particulate Number Emission** **(b) PN Total Number Emission**

**Figure 4.3 Particulate Emissions with Varying Engine Load**

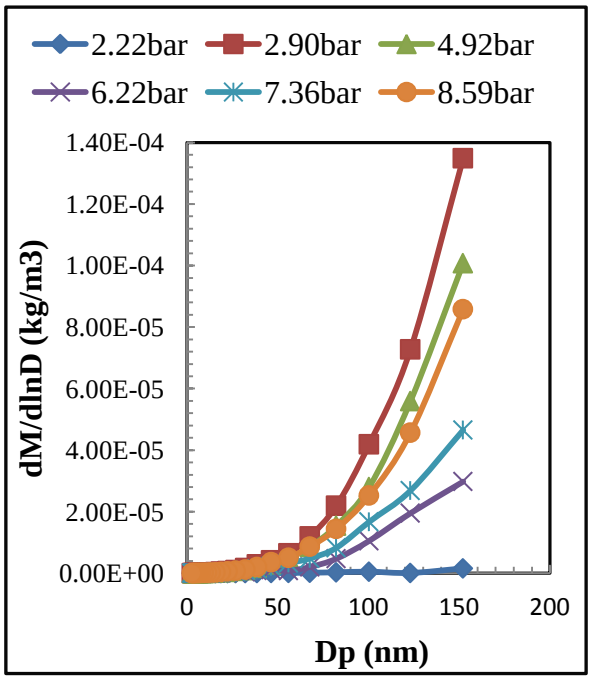


(c) Particulate Mass Emission

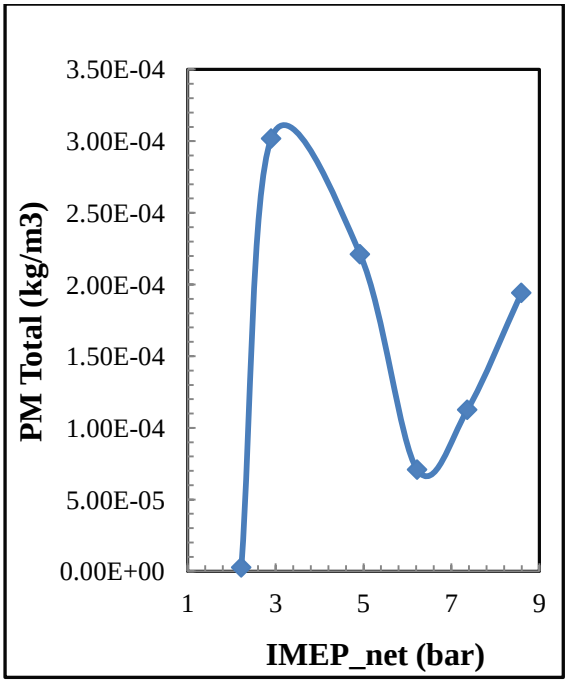


(d) PM Total Number Emission

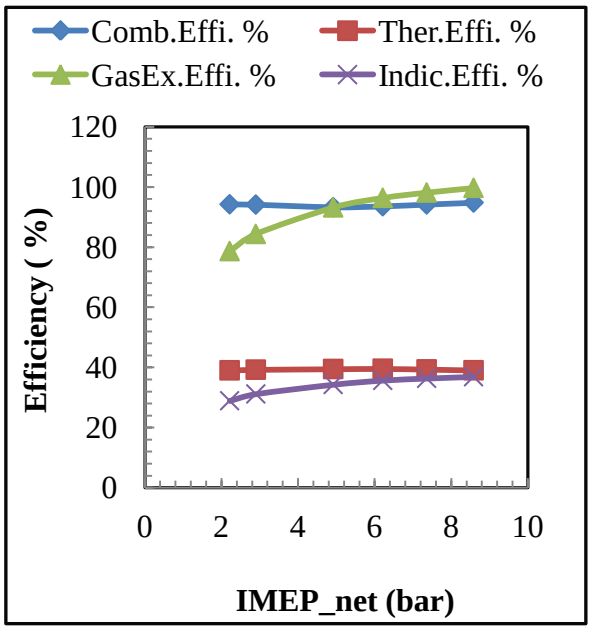


(e) Efficiency

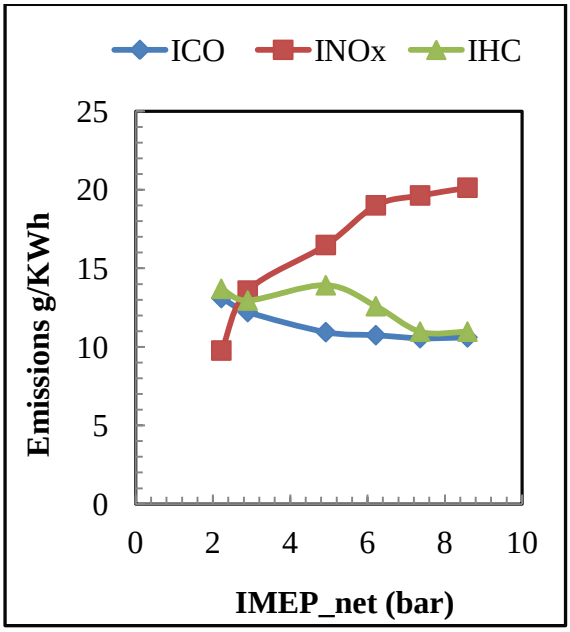


(f) Gaseous Emissions

**Figure 4.3 (ctd) Particulate Emissions with Varying Engine Load**

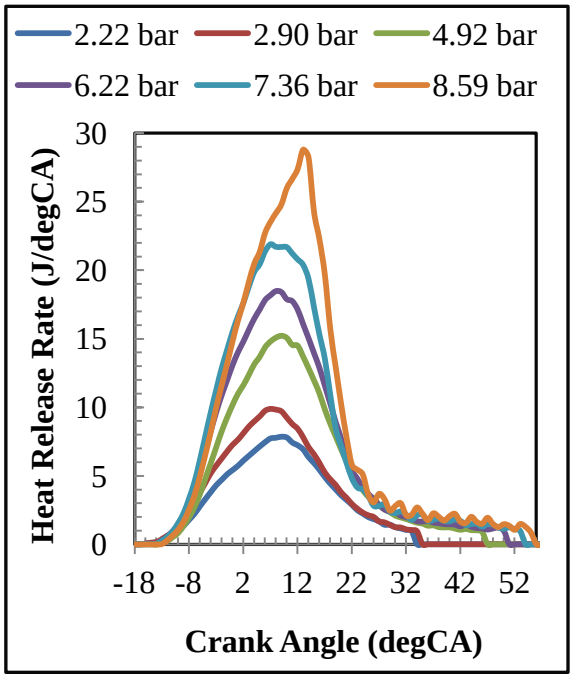


**(g) Heat Release**

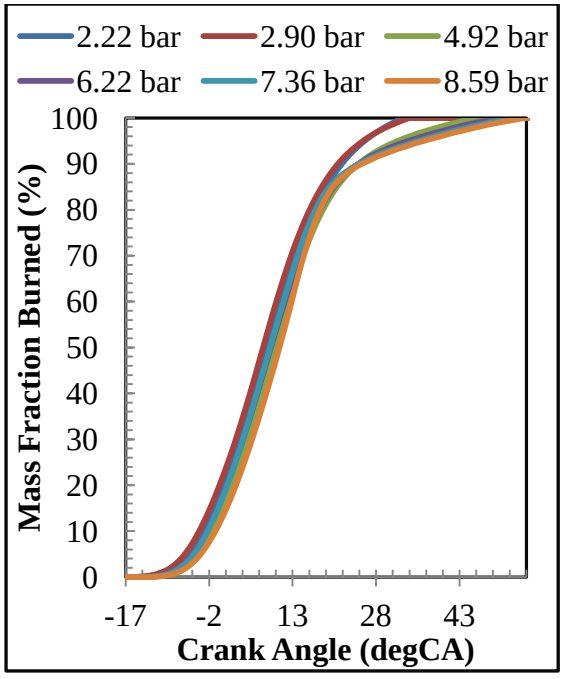


**(h) Mass Fraction Burned**

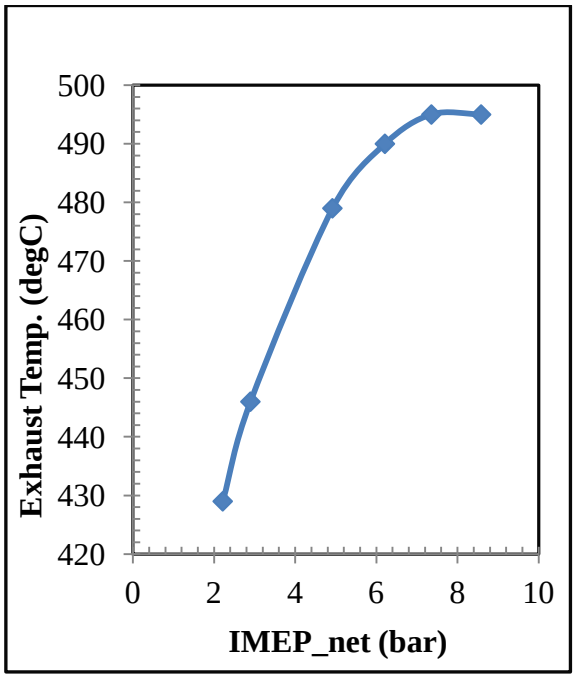


**(i) Exhaust Temperature**

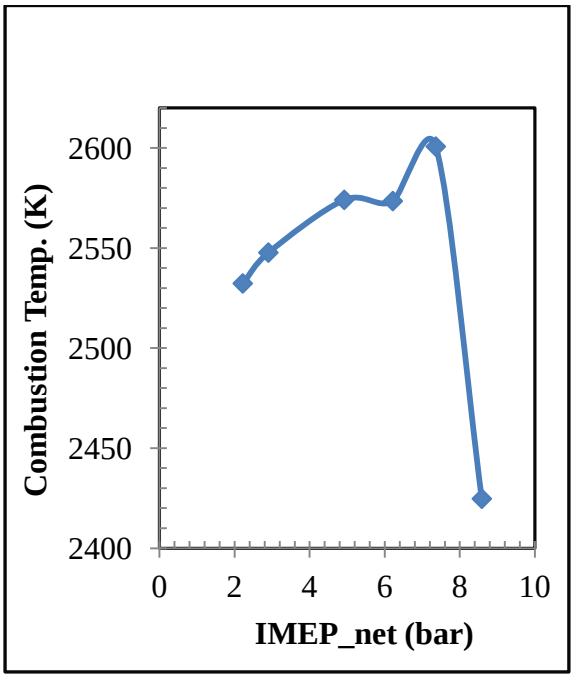


**(j) Combustion Temperature**

**Figure 4.3 (ctd) Particulate Emissions with Varying Engine Load**

### 4.3.2: 4-Stroke Throttle SI with Varying Injection Pressures

Figures 4.4 (a) and (b) shows the particulate number and total number emission as the injection pressure increased from 100bar to 150bar at constant load of 3.5 bar IMEP_net. The injection and spark timing used was fixed at 422 deg ATDC and -19 deg BTDC. The injection pressure was from 100bar to 150bar at 10bar incremental rate.

In this experiment the injection pressure was varied for its effects on particulate emissions. The mixture quality was expected to have improved due to more effective atomisation at a higher injecton pressure, a reduction in particulate emissions was predicted.

The experiment showed that whilst the number of larger particulates measuring between 10nm and 25nm did increase with the rising pressure, the number of particulates emitted between 5nm and 10nm actually decreased. The increase in particulates emitted at high injection pressure could be due to piston impingement (high ISHC figure (4.4(d)) caused by a higher penetration of fuel spray following the increased fuel-injection pressure.

In addition, the injection durations are the same 1.07ms (Table 4.2), the influence of injection timing is a very important factor. Slight deviation could cause wall impingement or inhomogeneous mixture preparation such as must have happened at 146 bar injection pressure. One would have expected that the high combustion temperature (figure 4.4(g)) would have enabled proper oxidation and the high exhaust temperature (figure 4.4(h)) should have burnt out all the remaining particles.

**Table 4.2 Injection pressure variations**

| Inj Press | Spark Tim | Inj Tim | InjPulseWidth |
|---|---|---|---|
| Bar | BTDC | ATDC | ms |
| 103 | -19 | 422 | 1.07 |
| 116 | -19 | 422 | 1.07 |
| 123 | -19 | 422 | 1.07 |
| 134 | -19 | 422 | 1.07 |
| 140 | -19 | 422 | 1.07 |
| 146 | -19 | 422 | 1.07 |

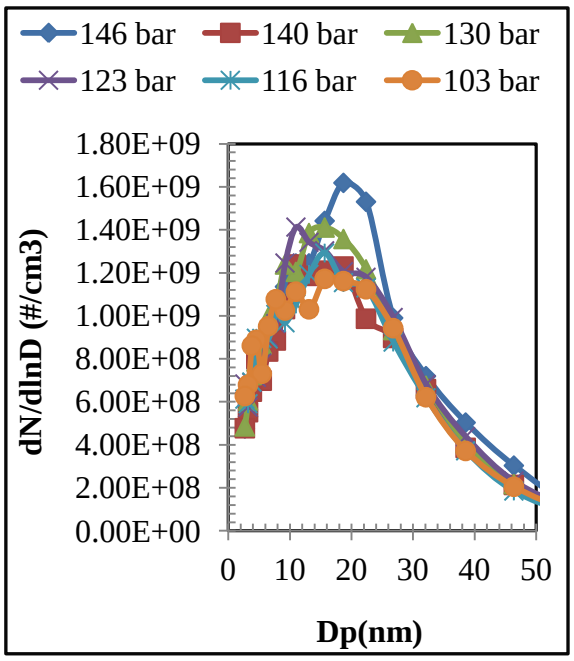


(a) Particulate Number

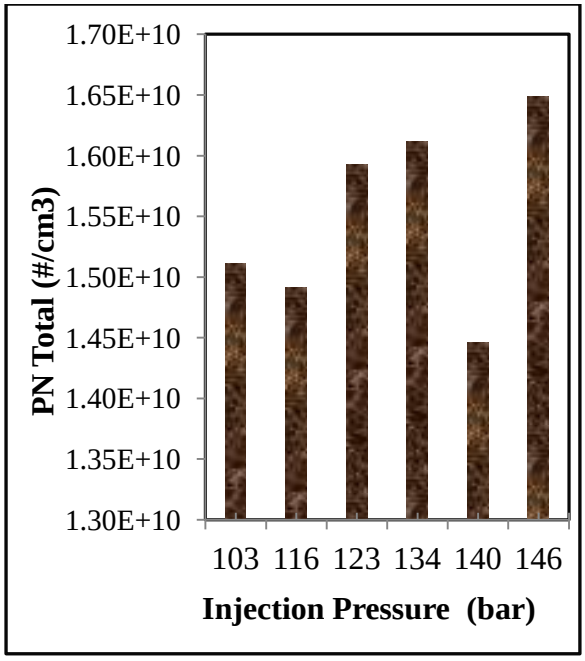


(b) PN Total

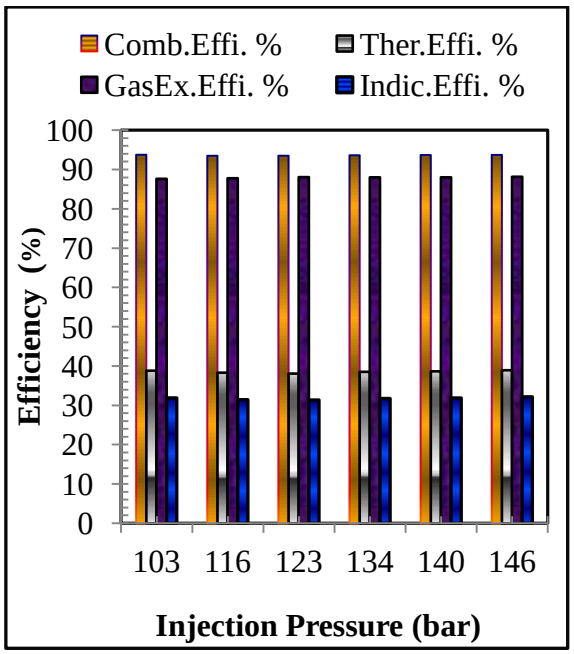


(c) Efficiency

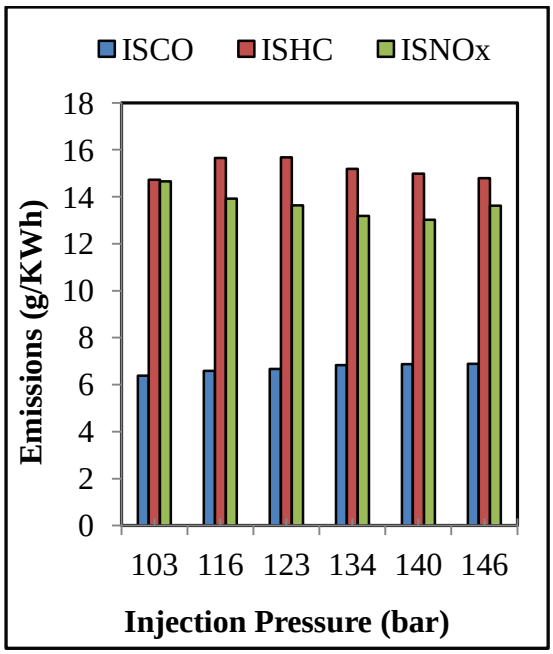


(d) Emissions

**Fig 4.4 Particulate Emissions with Varying Injection Pressure**

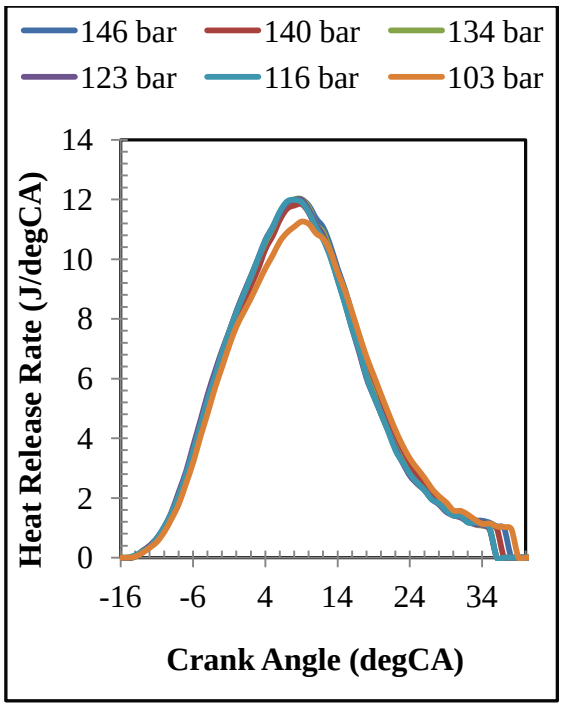


(e) Heat Release Rate

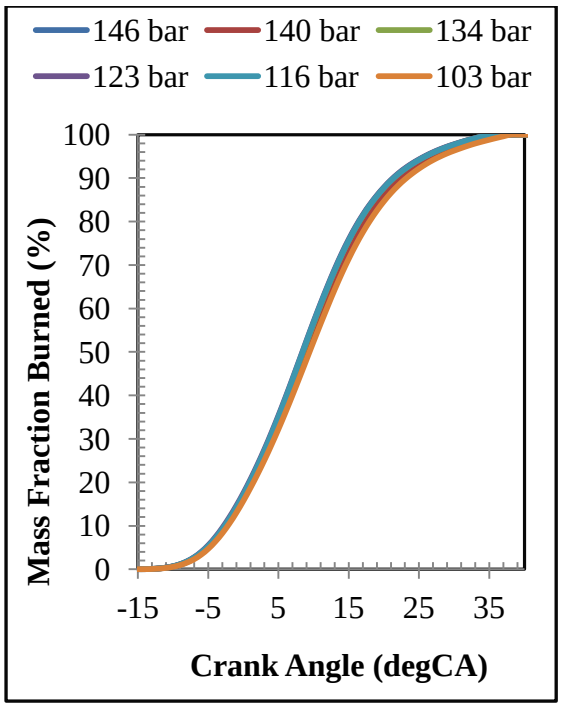


(f) Mass Fraction Burned

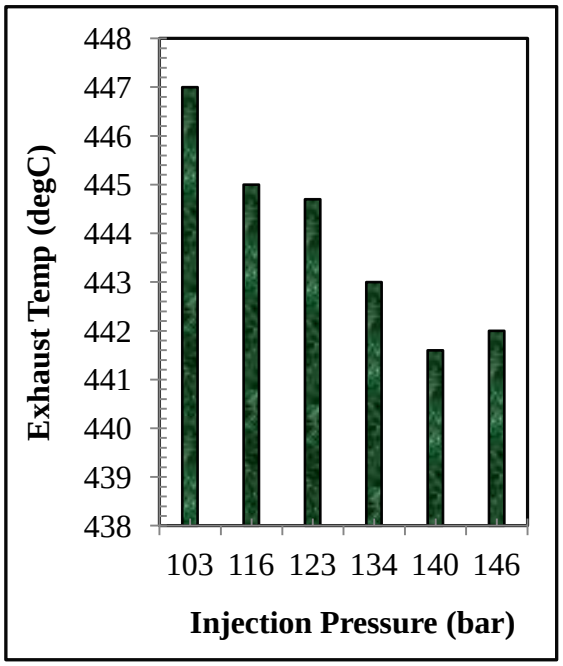


(g) Exhaust Temperature

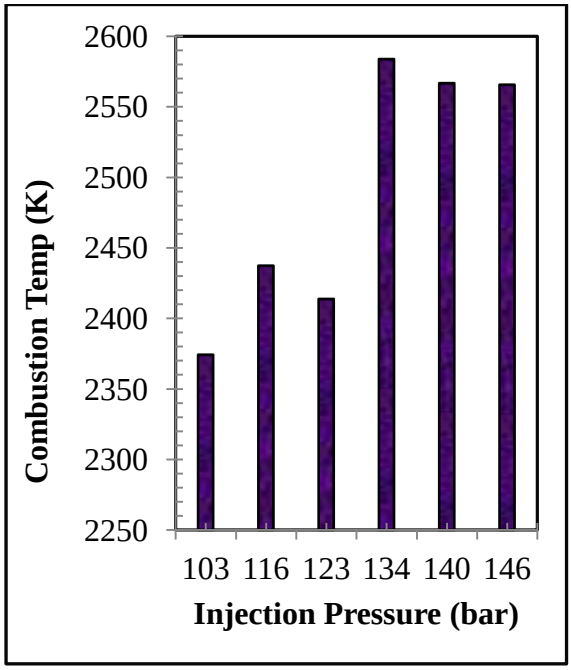


(h) Combustion Temperature

**Fig 4.4 (ctd) Particulate Emissions with Varying Injection Pressure**

### 4.3.3: 4-Sroke Throttle SI with Varying Lambda

Figure 4.5(a) and (b) shows the particle emissions and total number distribution measured at 1500 rpm. Seven different values of Lambda ranging from 1.03 to 1.54 were used. The injection timing was maintained at 422 deg ATDC, while the spark timing was advanced as lambda was increased (Table 4.3).

It can be seen that regardless of the mixture strength, the particle size distribution is unimodal. As lambda increased, the particulate number decreased by 3.5 times in the 5nm particle size range to 2.5 times in the 15nm particle size range to 2 fold in the 30nm range (Figure 4.5(b)).

The lower particle concentration observed here under lean mixtures could be attributed to the higher oxygen content in the combustion chamber that had a twofold effect on particle emission. Firstly, it led to more efficient combustion (Figure 4.5(d)), limiting the formation of the key intermediate species required for the formation of the initial aromatic ring for particle inceptions. Secondly, the reduced amount of fuel quantity injected would have resulted in better fuel droplet and evaporation resulting in improved mixture preparation and reduced emissions of CO and UHC (Figure 4.5 (c)). In addition, the reduced lambda resulted in reduced heat transfer from the engine (Figure 4.5(e)). The advanced spark-timing used as lambda increased enabled a longer burn duration (Figure 4.5(f)) resulting in improved fuel economy (Figure 4.5(i)).

**Table 4.3 Variations of the relative air/fuel ratio**

| Lambda | IMEP_net | SparkTiming | InjTiming | InjPulseWidth |
|---|---|---|---|---|
| λ | Bar | BTDC | ATDC | ms |
| 1.02 | 3.54 | -11 | 422 | 1.09 |
| 1.07 | 3.64 | -12 | 422 | 1.09 |
| 1.1 | 3.72 | -13 | 422 | 1.09 |
| 1.2 | 3.80 | -14 | 422 | 1.09 |
| 1.28 | 3.84 | -16 | 422 | 1.09 |
| 1.37 | 3.87 | -20 | 422 | 1.09 |
| 1.46 | 3.84 | -26 | 422 | 1.09 |
| 1.54 | 3.62 | -30 | 422 | 1.09 |

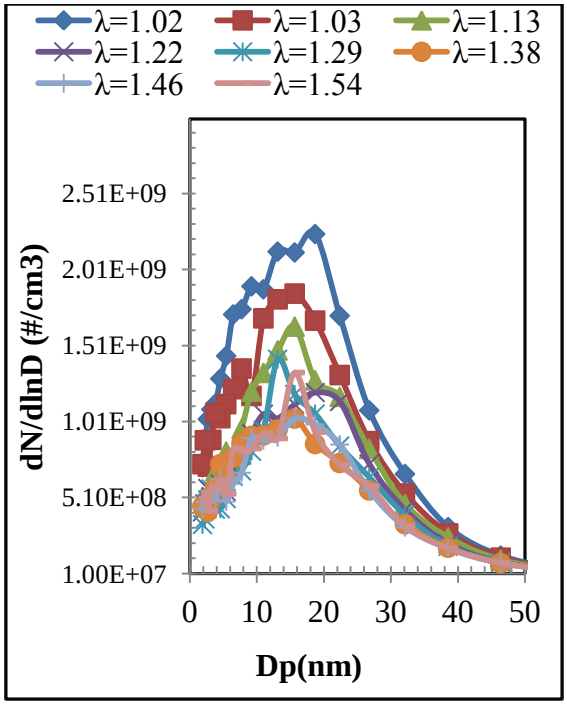


(a) Particulate Number Emission

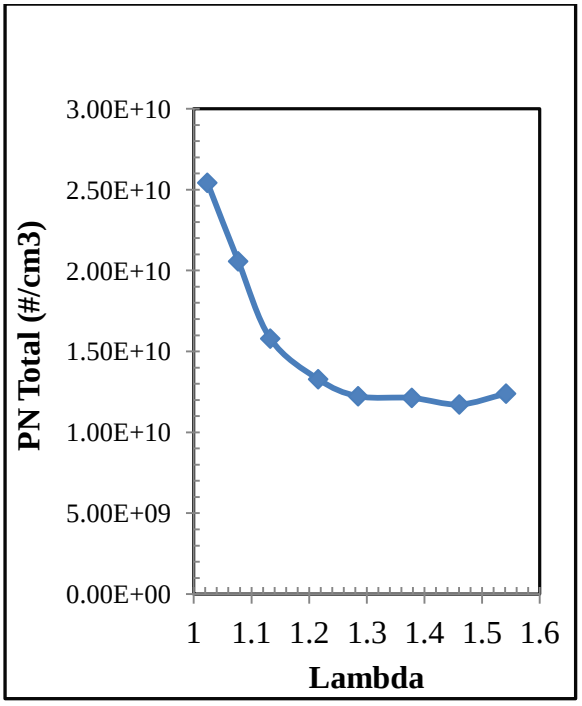


(b) PN Total

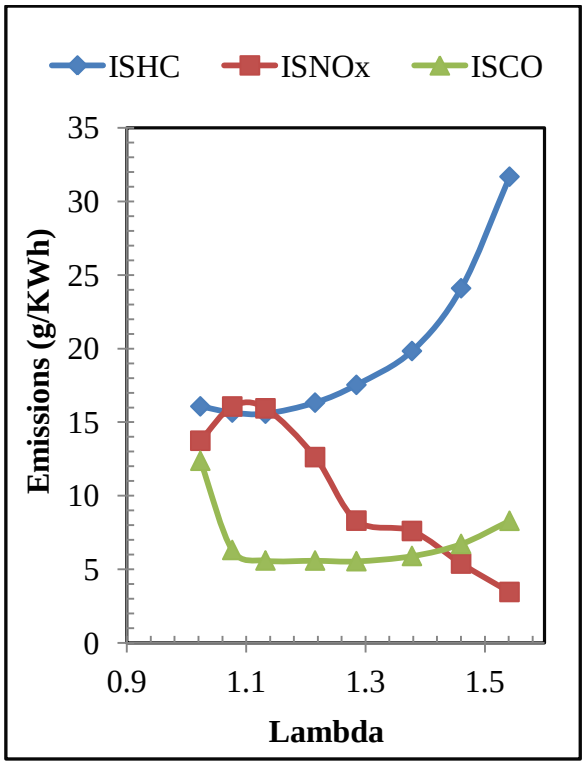


(c) Emissions

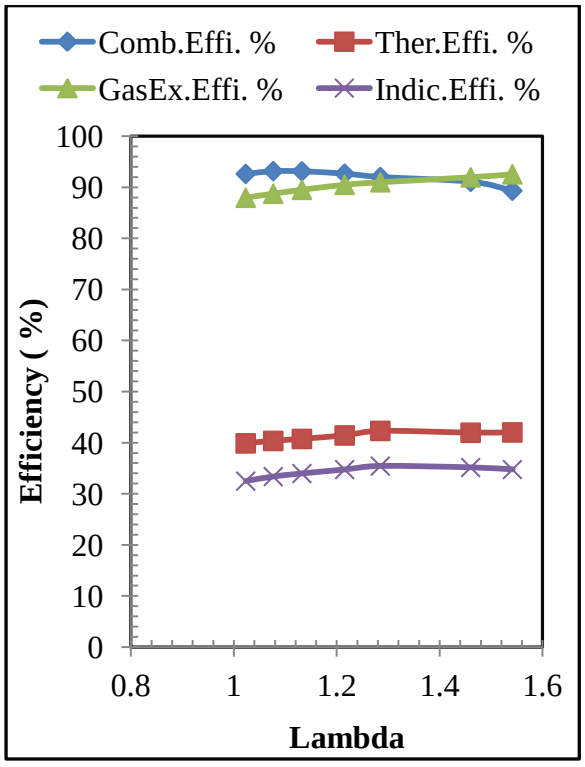


(d) Efficiency

**Figure 4.5 Effects of varying Lambda on Particulate Emissions**

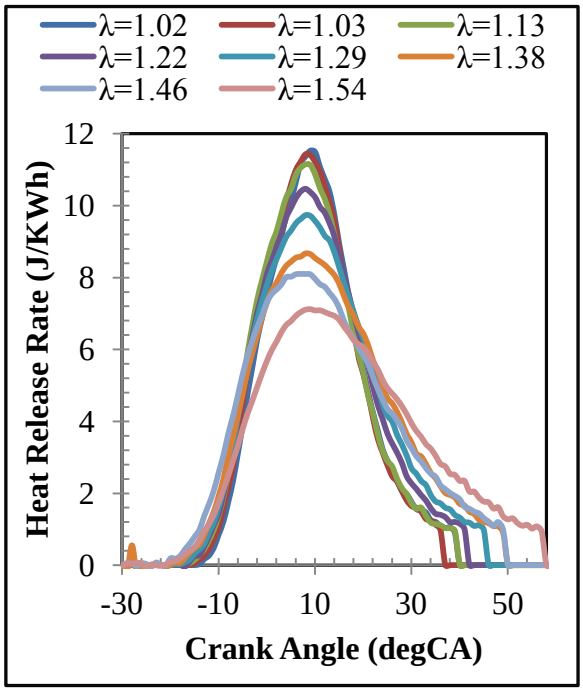


**(e) Heat Release Rate**

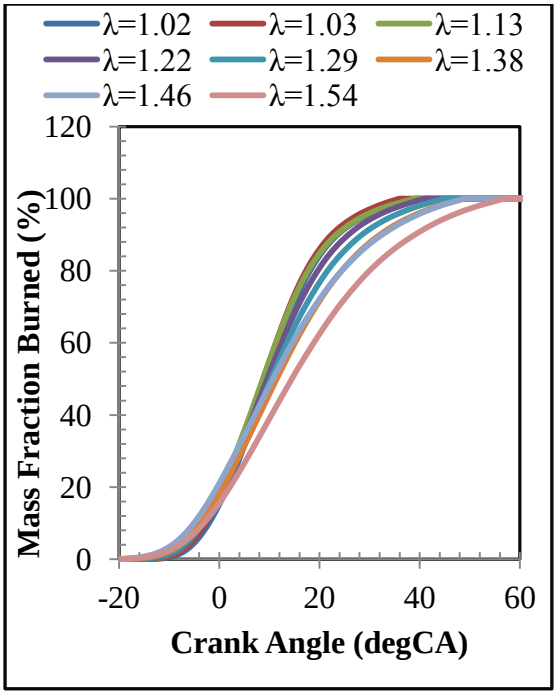


**(f) Mass Burned Fraction**

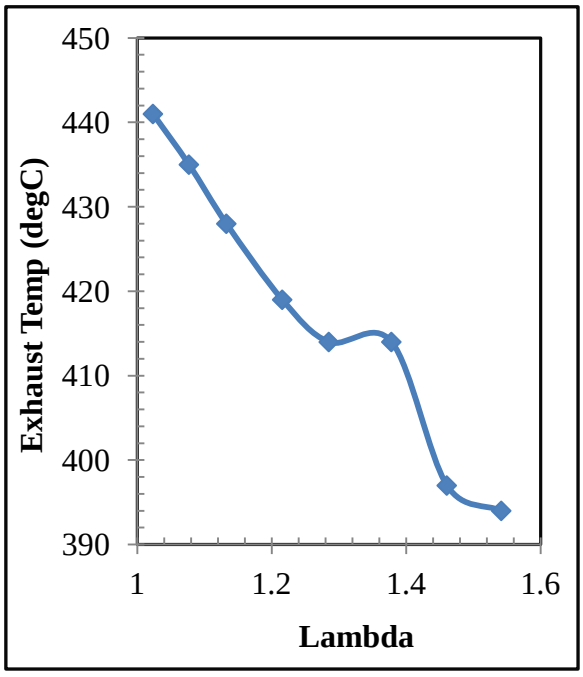


**(g) Exhaust Temperature**

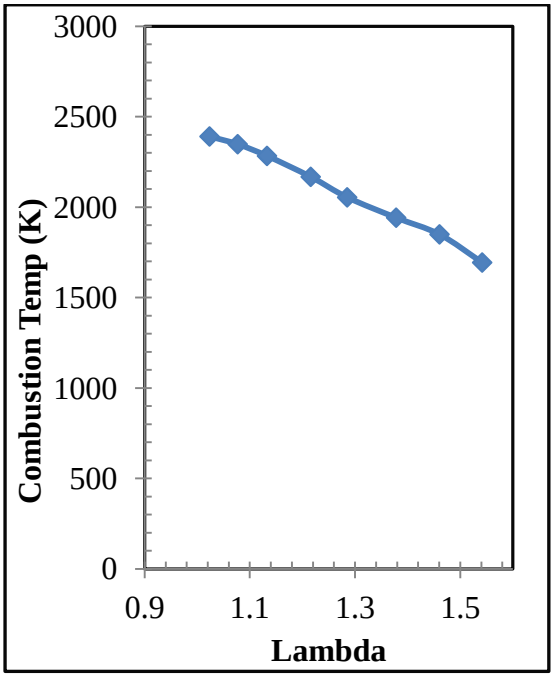


**(h) Combustion Temperature**

**Figure 4.5 (ctd) Effects of varying Lambda on Particulate Emissions**

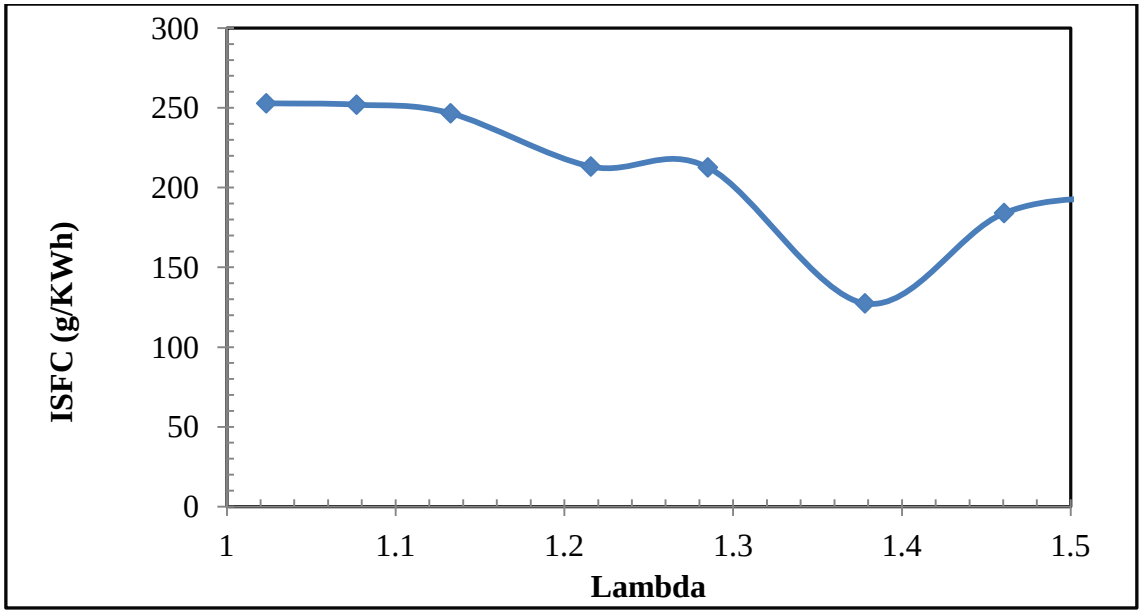


**(i) ISFC**

**Figure 4.5 (ctd) Effects of varying Lambda on Particulate Emissions**

### 4.4: Mode 2, 4-Stroke SI Intake Valve Throttled

The particulate emissions results for this test mode are shown in Figure 4.6.using intake-valve timing and durations to throttle the engine. The valve-timing and lifts used in this test are shown in Table 4.4. The result shows a unimodal trend which is peculiar to E0 in all the tests. In cases #1 and #2, the mixture was slightly rich. Moreover, the reduced valve-lift of 3mm must have resulted in micro-turbulence, which helps to raise the heat necessary for fuel evaporation. However, the closing of the intake-valve early resulted in the expansion of the mixture, resulting in reduced temperature and pressure insufficient to enhance evaporation and enable better combustion. This may have caused the increased particulate emissions for the two cases shown in figure 4.6(a) and (b). This is evidenced from the high CO emissions (figure 4.6 (c)) and reduced combustion efficiency (figure 4.6(b)). One would have expected the particulate to be oxidised during the high temperature combustion of the two cases, however, this was not possible.

In early IVC, the air admitted into the intake is reduced, meaning that during the high temperature combustion (Figure 4.6 (h)) there is not enough oxygen to support oxidation, hence pyrolysis will likely dominate. This is further worsened by the reduced exhaust-temperature (Figure 4.6(g)) resulting in the poor fuel efficiency (Figure 4.6(i)).

Case #3 shows different trends, this may be due to the value of lambda=1 used here. In addition, the intake and exhaust-valve lift was twice that of cases #1 and #2. The combustion phasing for case #3 was later than in #1 and #2, hence combustion must have continued into the expansion stroke, this is evidenced by the higher exhaust-temperature (Figure 4.6(g)) which may have helped to oxidise the particulate during the exhaust stroke.

### 4.4.1: 4-Stroke Intake Valve Throttled Valve Lift Variation

**Table 4.4 Intake valve lifts**

| VLS | IVO | IVC | IVL | EVO | EVC | EVL | SpkTim | InjTim | InjPW | ECR |
|---|---|---|---|---|---|---|---|---|---|---|
| | ATDC | ATDC | mm | ATDC | ATDC | mm | BTDC | ATDC | ms | |
| #1 | 353 | 446 | 3.7 | 160 | 359 | 3.6 | -31 | 422 | 1.06 | 6.0 |
| #2 | 352 | 447 | 3.7 | 160 | 361 | 3.6 | -29 | 422 | 1.06 | 6.0 |
| #3 | 356 | 441 | 6.9 | 160 | 359 | 7.1 | -29 | 421 | 1.05 | 5.8 |

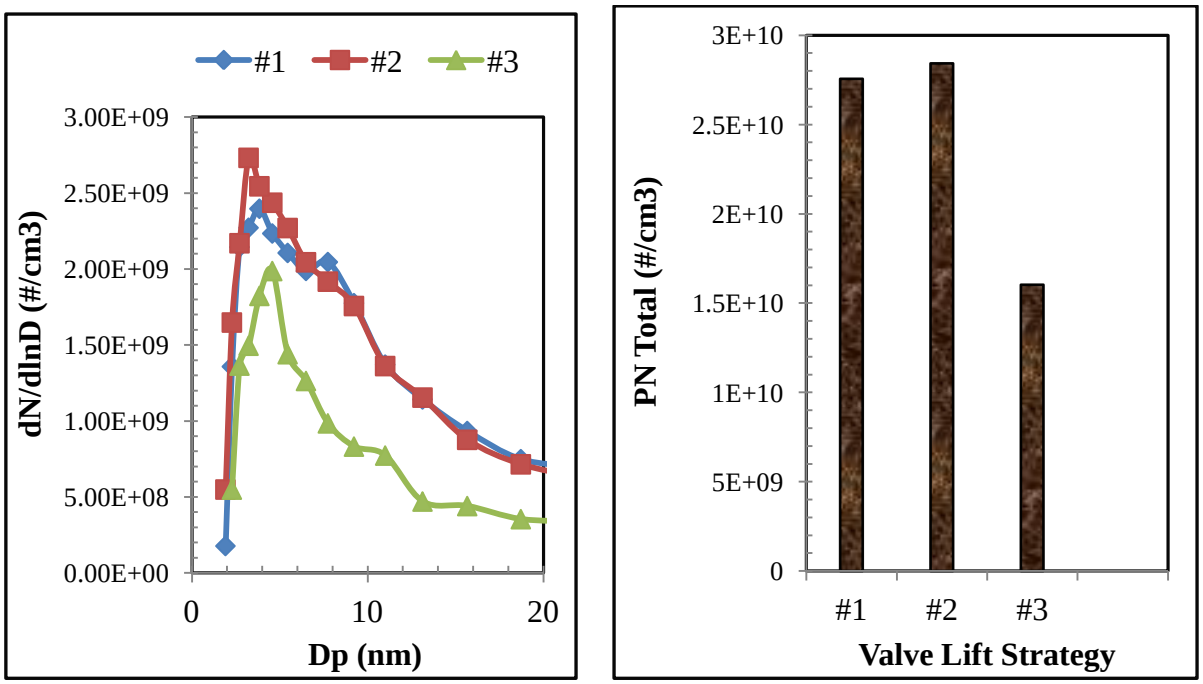


**(a) Particulate Number Emissions** **(b) PN Total**

**Figure 4.6 Effects of Intake-Valve Throttling on Particulate Emissions**

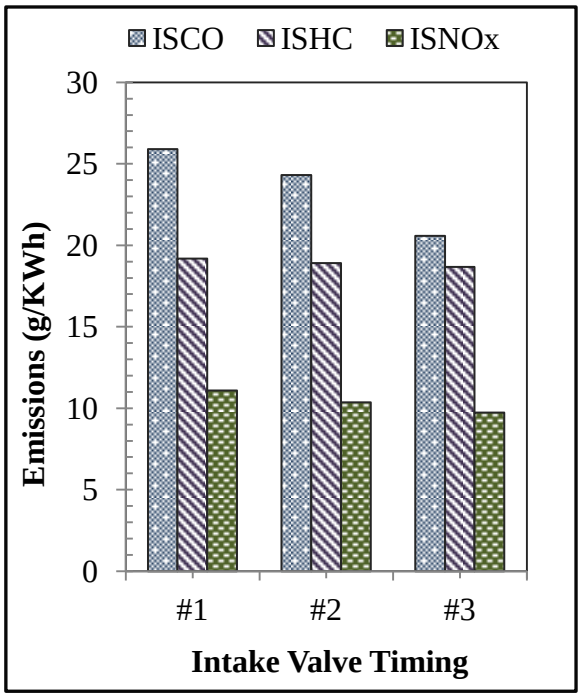


**(c) Emissions**

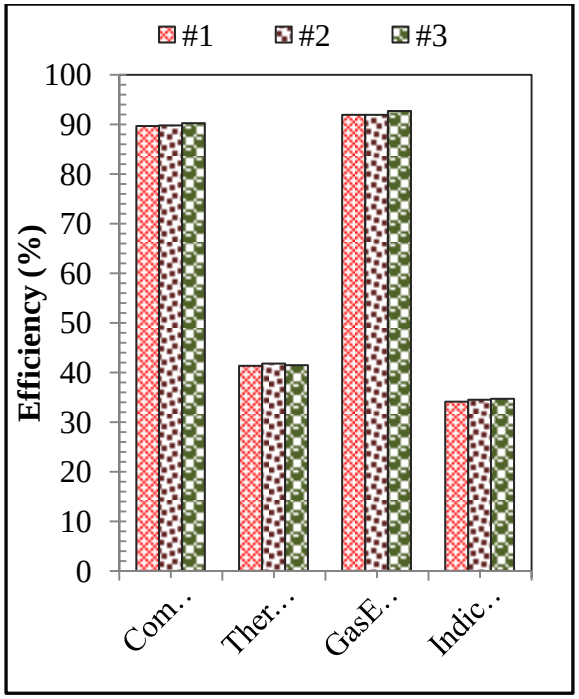


**(d) Efficiency**

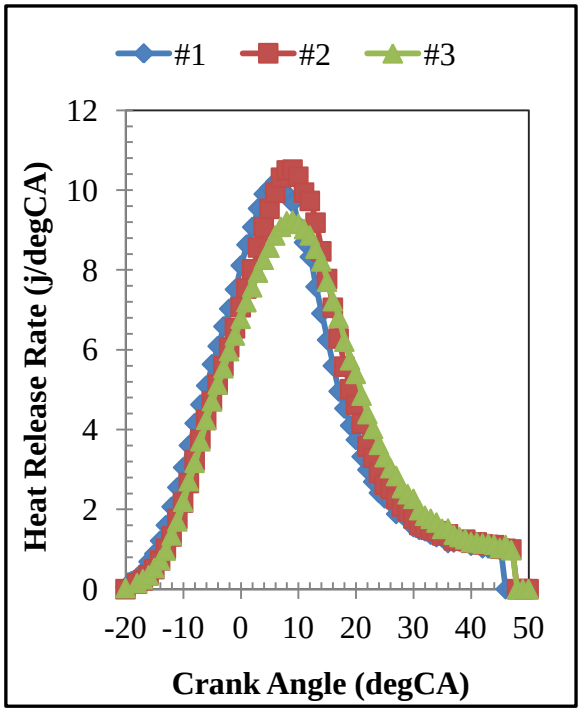


**(e) Heat Release Rate**

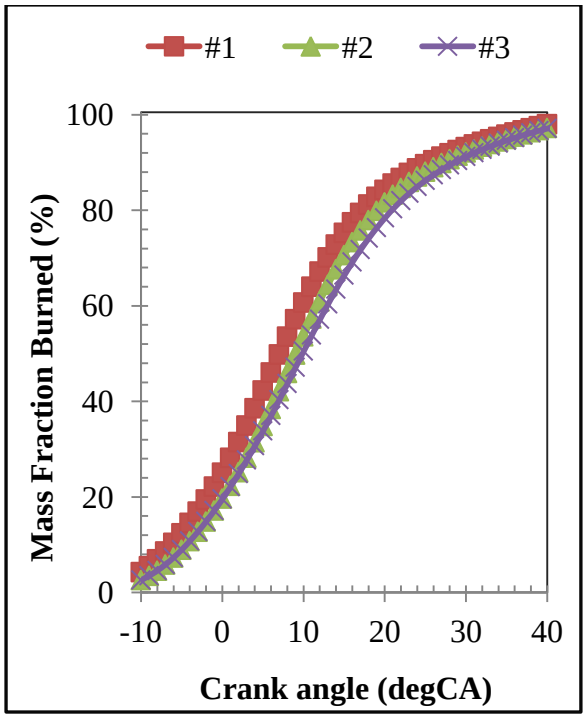


**(f) Mass Fraction Burned**

**Figure 4.6 (ctd) Effects of Intake-Valve Throttling on Particulate Emissions**

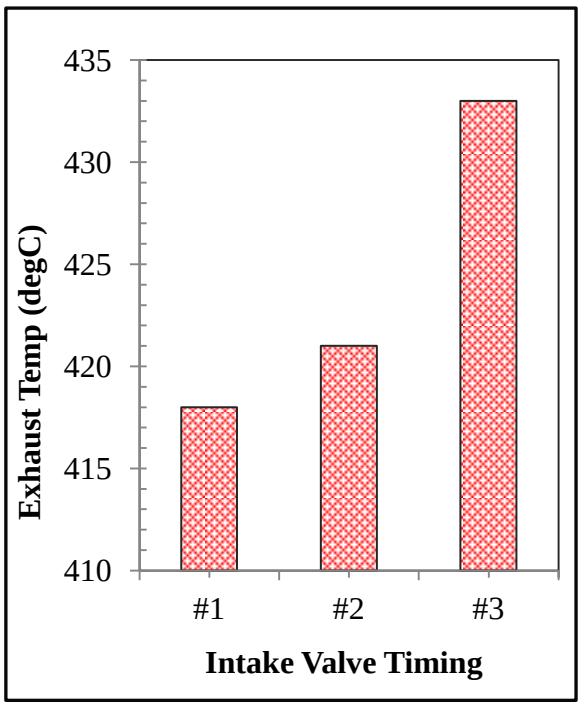


**(g) Exhaust Temperature**

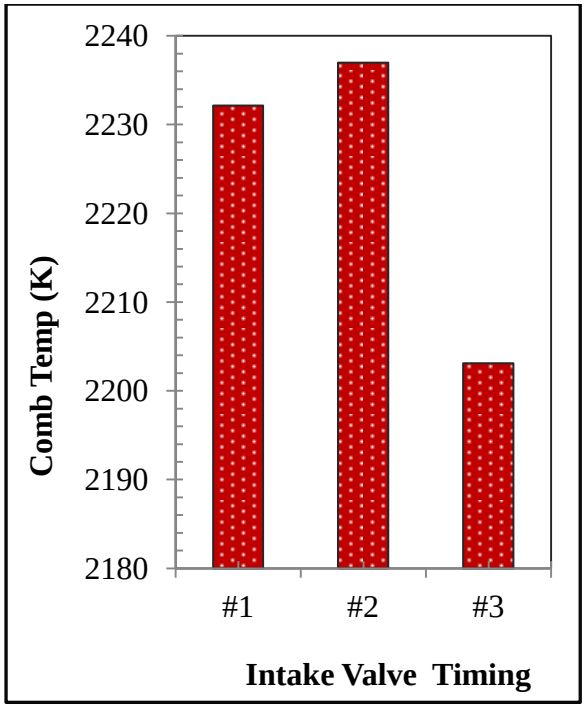


**(h) Combustion Temperature**

**Figure 4.6 (ctd) Effects of Intake-Valve Throttling on Particulate Emissions**

### 4.4.2: 4-Stroke E15 Intake Valve Throttling

Table 4.5 and Figure 4.7 show the results for particulate emissions when gasoline is blended with 15% ethanol (E15). Results are shown for the speed of 1500rpm, lambda=1 for nine load ranges 2.4 to 7bar IMEPnet, valve durations of 73 to 120 deg CA and valve lifts varied from 4.8 to 6.2mm. The exhaust-valve lift was locked at 7mm height. The throttle position was set at wide-open position. The injection pressure was set to 150 bar. Table 4.5 shows this intake-valve throttling strategy. For case #1 the trend was different from the rest, the particulate number emitted was almost double. The peculiar trend in case #1 may have been due to the high instability encounter in combustion due to misfiring (COV of 10.4%, shown in Table 4.5).

For cases #2 to #9 the trends are similar. The particulate emissions are shifted towards small size particles with no peak but with increased particle number as the load was increased. The increase in the particulate number as load is increased using E15 may likely be due to the oxygenate-property of ethanol. These can be explained on the effect of ethanol addition to the distilation curve of fuel and hence the condensation process.

The distillation curve of ethanol-gasoline blends provides insight into the boiling range of the fuel and can be used to predict its operation in engines, according to Anderson et al [98] the

addition of ethanol in 5-25% range leads to little, or no discernible change in initial boiling point (IBP). There is a substantial decrease in distilation temperature (i.e increase in volatility) over the middle portion of the distillation curve. This increase in volatility may have assisted in the mixture preparations, as evidenced in the reduced CO emissions (Figure 4.7(c)). As load is increased more fuel is injected, which implies better mixture preparation. In addition, the advanced spark-timing used in low load may have lead to reduced mixture preparation leading to the high total PN numbers observed (Figure 4.7(b)).

The higher oxygen content reduces the concentration of key aromatic intermediate species that are required for the formation of the initial aromatic ring [93], which in turn contributes to the surface growth of particles. The absence of the aromatic ring results in formation of particles in the 10nm range.

In ethanol-gaoline blends, the diffusive nature of the burning fuel that may have impinged on the cylinder walls and piston crown, does not produce soot. Less surface area is therefore available for the adsorption of the condensing organic species that are more likely to nucleate homogeneously, forming high concentrations of nucleation mode particles.

**Table 4.5 Variations in Intake valve lift and duration**

| IVL | IMEP_net | Spark Timing | Inj Timing | Inj Pulse Width | IVO | IVC | IVL | EVO | EVC | EVL | COVimep | ECR |
|---|---|---|---|---|---|---|---|---|---|---|---|---|
| # | bar | BTDC | ATDC | ms | ATDC | ATDC | mm | ATDC | ATDC | mm | % | |
| #1 | 2.43 | -58 | 420 | 0.91 | 358 | 432 | 4.83 | 170 | 361 | 7.06 | 10.40 | 4.9 |
| #2 | 2.47 | -58 | 420 | 0.91 | 358 | 431 | 4.84 | 170 | 361 | 7.06 | 4.61 | 5.0 |
| #3 | 3.04 | -43 | 421 | 1.0 | 358 | 439 | 5.00 | 170 | 361 | 7.07 | 1.81 | 5.4 |
| #4 | 3.64 | -32 | 422 | 1.09 | 358 | 445 | 5.07 | 170 | 361 | 7.07 | 1.47 | 5.9 |
| #5 | 4.05 | -26 | 422 | 1.15 | 357 | 449 | 5.13 | 170 | 361 | 7.07 | 1.12 | 6.3 |
| #6 | 4.35 | -24 | 423 | 1.21 | 358 | 452 | 5.15 | 170 | 361 | 7.08 | 1.12 | 6.8 |
| #7 | 5.14 | -21 | 425 | 1.4 | 357 | 458 | 6.14 | 170 | 361 | 7.08 | 0.94 | 7.4 |
| #8 | 6.27 | -19 | 426 | 1.6 | 358 | 470 | 6.19 | 170 | 361 | 7.06 | 0.98 | 8.5 |
| #9 | 6.99 | -16 | 428 | 1.8 | 358 | 478 | 6.21 | 170 | 361 | 7.06 | 0.72 | 9.1 |

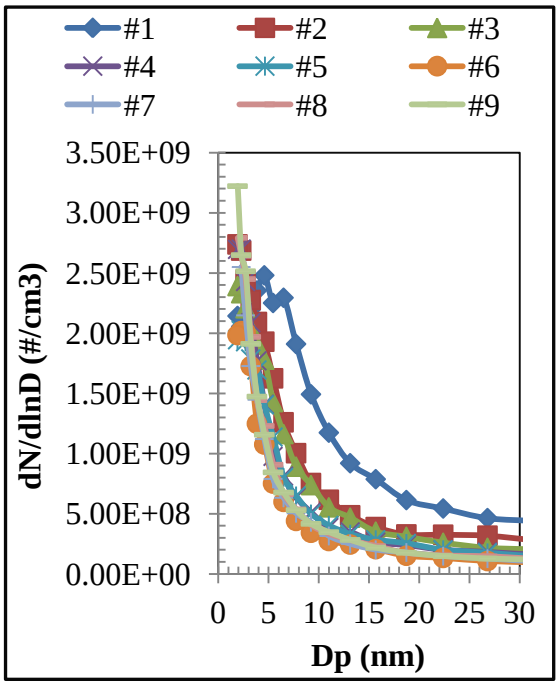


(a) Particulate Number Emissions

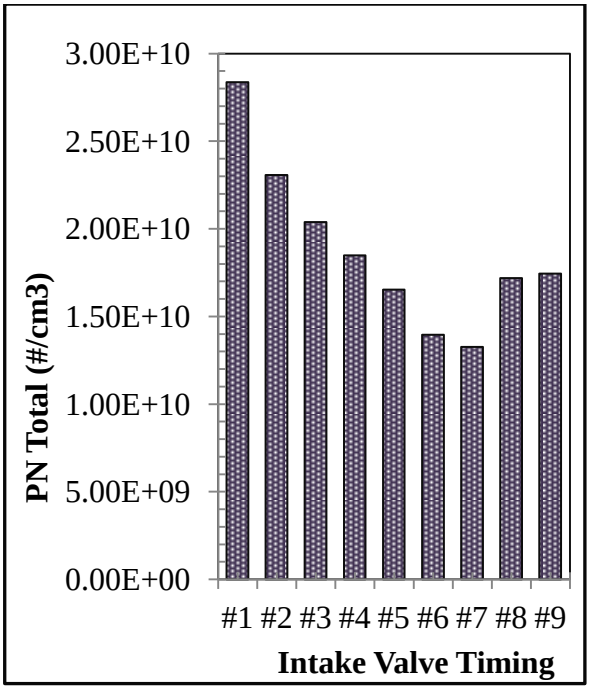


(b) PN Total

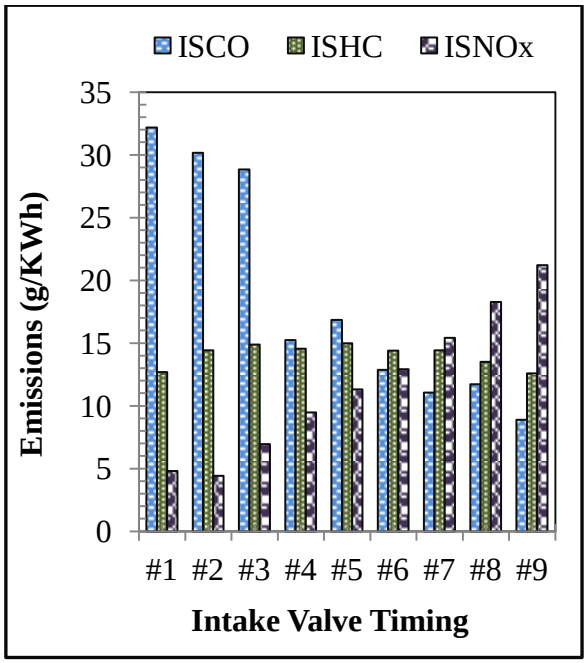


(c) Emissions

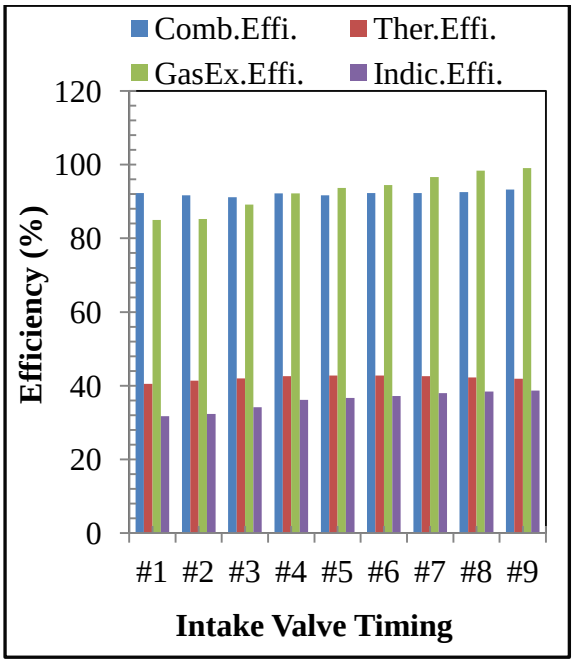


(d) Efficiency

**Fig 4.7: Effects of E15 on Particulate Emissions with Intake Valve Throttling**

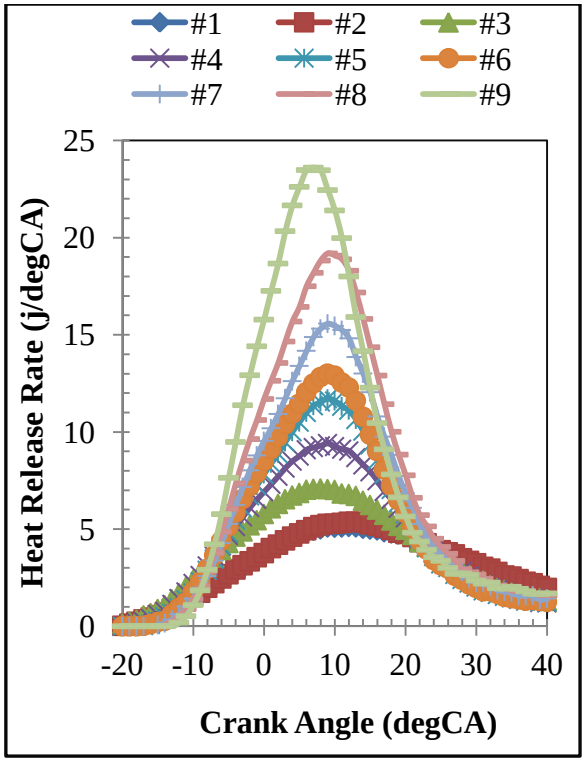


**(e) Heat Release Rate**

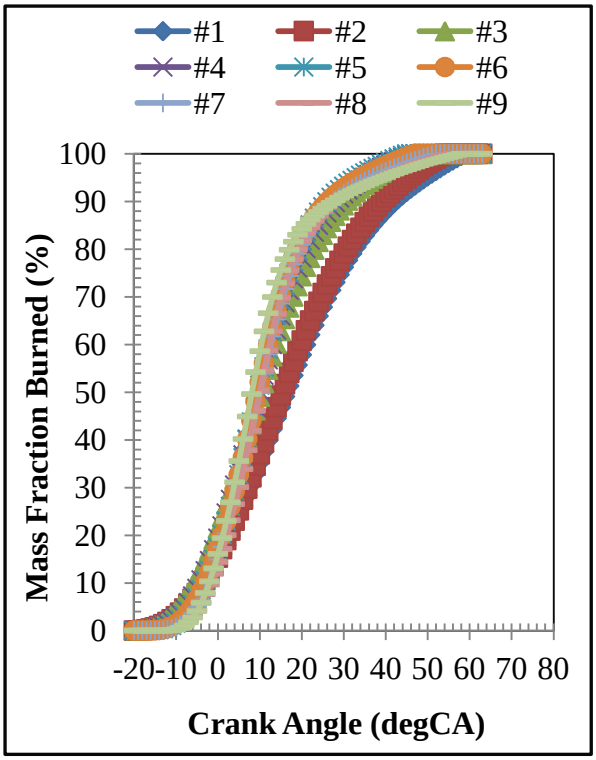


**(f) Mass Fraction Burned**

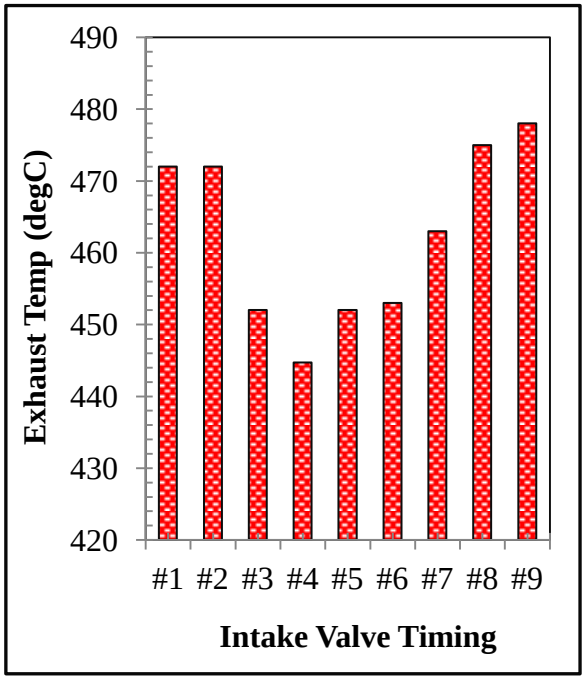


**(g) Exhaust Temperature**

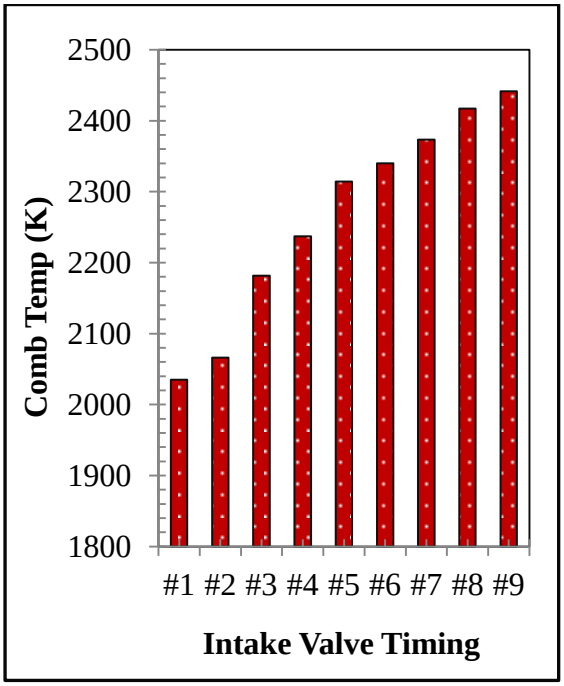


**(h) Combustion Temperature**

**Fig 4.7: (ctd) Effects of E15 on Particulate Emissions with Intake Valve Throttling**

### 4.5: Mode 3: 4-Stroke PVO SI

#### 4.5.1: 4 Stroke PVO SI Varying Intake Opening

In this test the speed was maintained at 1500rpm with wide-open throttle (WOT) using lambda=1. The valve, injection and spark timings used are shown in Table 4.6,

The intake-valve lift was reduced to 3mm, while the valve timing was varied from IVO 293 deg CA ATDC to 253 deg CA ATDC. The IVC was varied from 449 deg CA ATDC to 459 deg CA ATDC. This gives the PVO durations of 66 deg CA to 106 deg CA. The engine load was maintained at 3.5 bar IMEPnet. Spark timing was retarded from -27 to -36 deg CA BTDC from #1 to #5. The fuel injection was set to 422 deg CA BTDC. From Figure 4.8(a) and (b) the Particulate formation was concentrated in nucleation mode with unimodal mode. However as the dilution rate increased, the particulate formations shifted to a smaller size particle and increased in number, peaking around 20nm. This could be a result of the interaction of fuel injection and the gas-exchange process**.**

In the positive valve overlap (PVO), the gas-exchange process starts with the IVC before TDC and it is characterised by the reversed flow of hot burned gas into the intake port during the positive overlap period around TDC. Fuel injection takes place soon after the EVC, during which the exhaust-gas in the intake port flows back into the cylinder together with air, and fuel is injected into the hot incoming mixture. The enhanced evaporation of gasoline fuel leads to fewer fuel-rich regions in the combustion process (Figure 4.9(c) reduced CO emissions) and so shifts soot particles towards the smaller size range of less than 20nm and increases their amount. The high dilution rate used implies that reduced fuel quantity will be injected, thereby reducing the aromatics responsible for soot formation. In addition, the high exhaust temperature (Figure 4.8(g)) recorded must have promoted post- combustion oxidation in the exhaust stroke.

**Table 4.6 variations in the intake valve timing**

| | IMEP_net | Spark Timing | Inj Timing | InjP Width | IVO | IVC | EVO | EVC | IVL | EVL | PVO | IV Duration |
|---|---|---|---|---|---|---|---|---|---|---|---|---|
| | bar | BTDC | ATDC | ms | ATDC | ATDC | ATDC | ATDC | mm | mm | CA | CA |
| #1 | 3.64 | -27 | 422 | 1.06 | 293 | 449 | 160 | 359 | 3.1 | 7.1 | 66 | 156 |
| #2 | 3.57 | -29 | 421 | 1.05 | 283 | 451 | 160 | 359 | 3.1 | 7.1 | 76 | 168 |
| #3 | 3.62 | -31 | 421 | 1.05 | 273 | 454 | 160 | 359 | 3.1 | 7.1 | 86 | 181 |
| #4 | 3.64 | -33 | 421 | 1.05 | 263 | 457 | 160 | 359 | 3.1 | 7.1 | 96 | 194 |
| #5 | 3.62 | -36 | 421 | 1.05 | 253 | 459 | 160 | 359 | 3.1 | 7.1 | 106 | 206 |

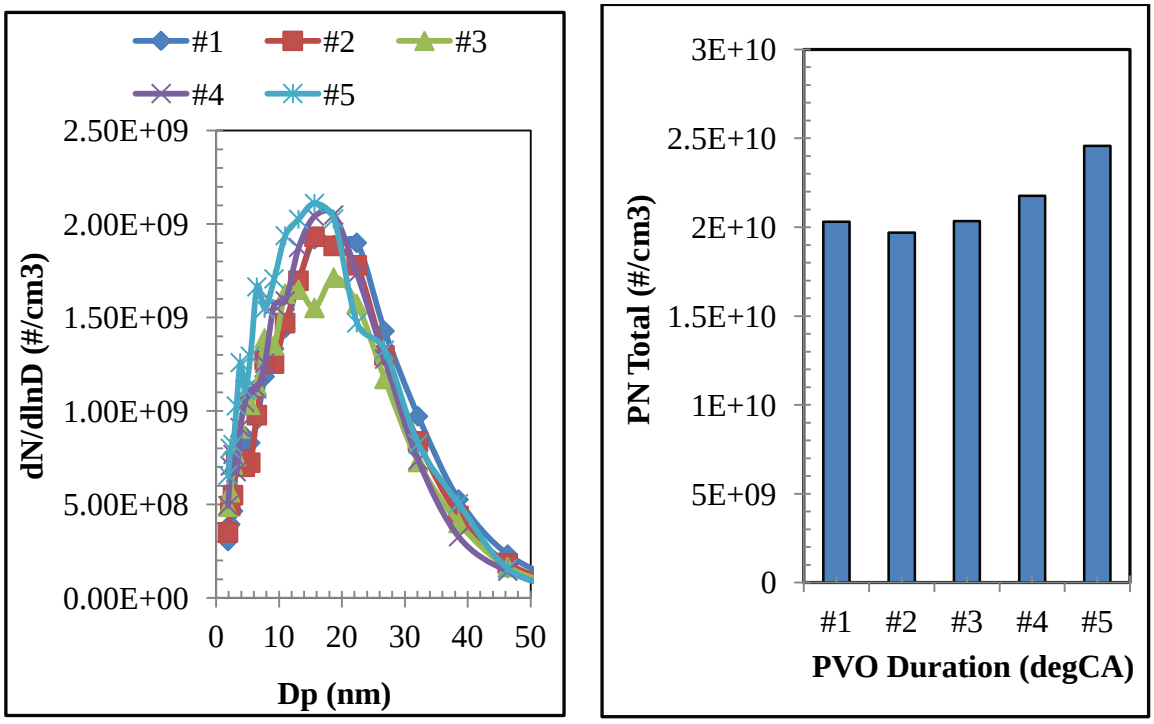


**(a) Particulate Number Emissions** **(b) PN Total**

**Figure 4.8 Effects of Positive Valve Overlap on Particulate Emissions**

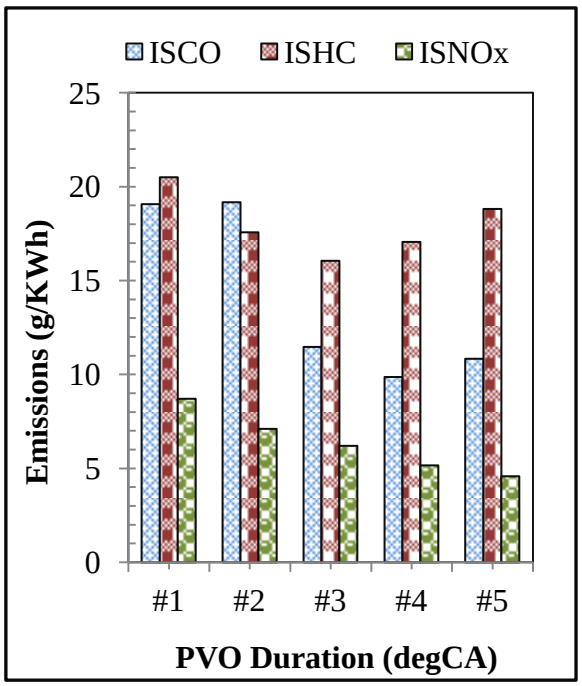


(c) Emissions

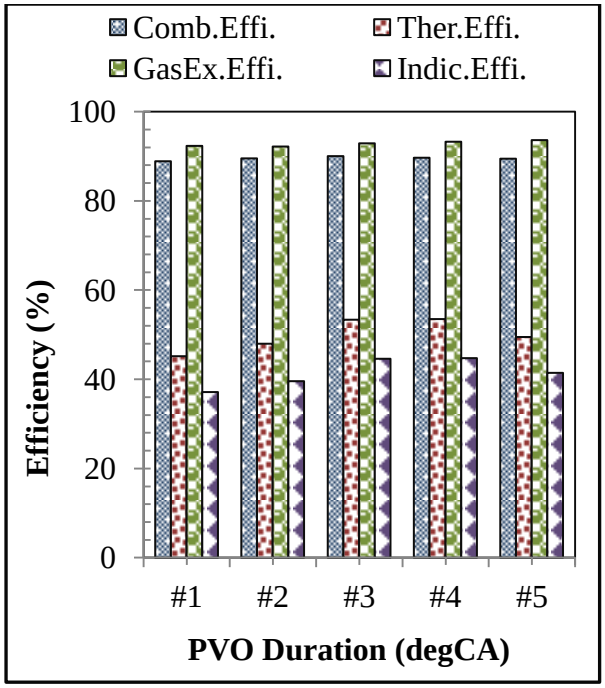


(d) Efficiency

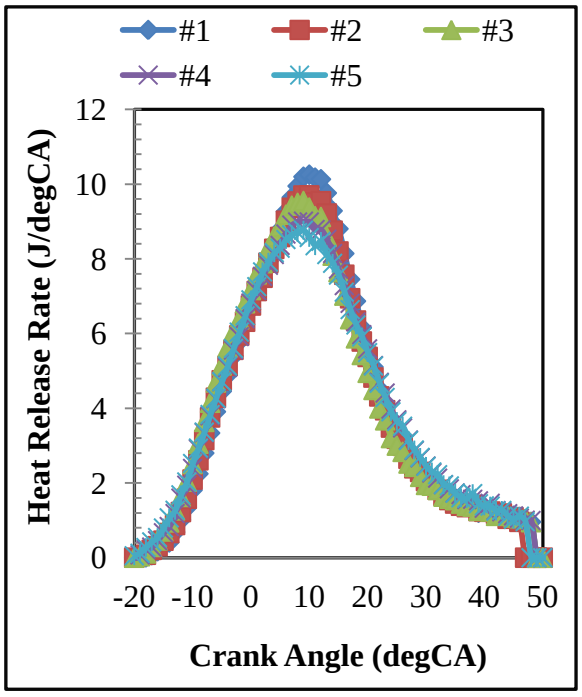


(e) Heat Release Rate

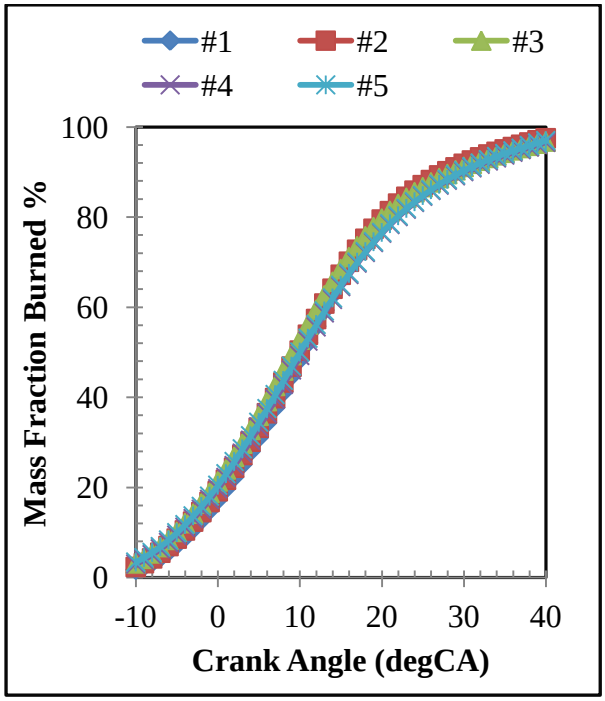


(f) Mass Fraction Burned

**Figure 4.8 (ctd) Effects of Positive Valve Overlap on Particulate Emissions**

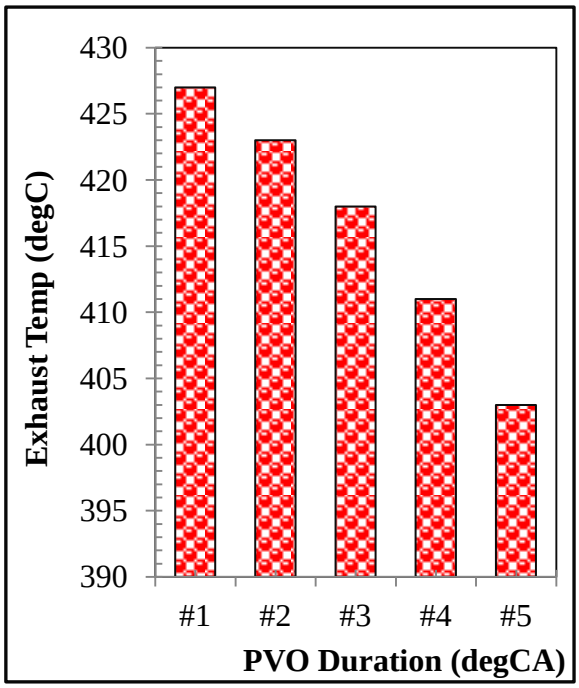


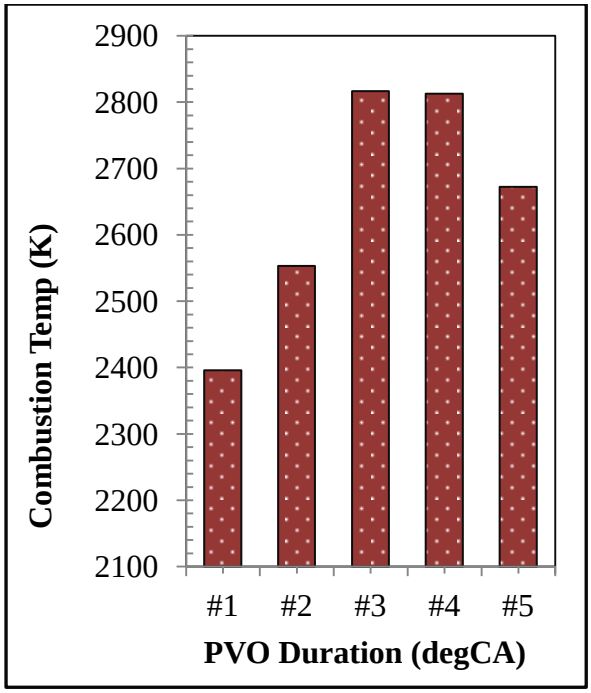


**(g) Exhaust Temperature** **(h) Combustion Temperature**

**Figure 4.8 (ctd) Effects of Positive Valve Overlap on Particulate Emissions**

### 4.5.2: 4-Stroke E15 PVO SI

This test is similar to the previous test on PVO SI, here the fuel is blended with 15% ethanol (E15) to investigate the effects on particulate emission. However, the loads here are much higher than those used in pure gasoline.The exhaust and intake-valve lifts were reduced to 3mm to avoid piston-valve clash. The exhaust valve-timing was set to170 deg CA ATDC of opening, and closing was varied between 477 deg CA ATDC and 511 deg CA ATDC of closing. Intake valve-timing was set to 224deg CA deg ATDC of opening, and 549 deg CA ATDC of closing, which means 221 to 287 deg CA PVO period duration.

Figure 4.9(a) and (b) shows the particle number and total emissions from the 4-stroke SI operation with the positive valve overlap. In contrast to the previous case of PVO, gasoline produces much fewer particle emissions, while the E15 generates a similar quantity of particles to the other cases of E15 blend. This could be as a result of the interaction of fuel injection and gas-exchange process.

The PN total for case #4 was higher than the others because the combustion was not stable (COVimep 11.1%), this reflected in highest CO emissions, indicated and thermal efficiency.

**Table 4.7 4-Stroke E15 PVO SI experiments**

| | IMEP_net | SparkTiming | InjTiming | InjPulseWidth | IVO | IVC | IVL | EVO | EVC | EVL | PVO |
|---|---|---|---|---|---|---|---|---|---|---|---|
| | bar | BTDC | ATDC | ms | ATDC | BTDC | mm | ATDC | ATDC | mm | CA |
| #1 | 6.89 | -15 | 427 | 1.71 | 256 | -171 | 3.2 | 171 | 477 | 3.1 | 221 |
| #2 | 6.51 | -17 | 426 | 1.6 | 256 | -171 | 3.2 | 171 | 482 | 3.1 | 226 |
| #3 | 5.61 | -21 | 425 | 1.47 | 224 | -171 | 3.2 | 170 | 495 | 3.1 | 271 |
| #4 | 5.19 | -36 | 425 | 1.4 | 224 | -171 | 3.2 | 170 | 511 | 3.2 | 287 |

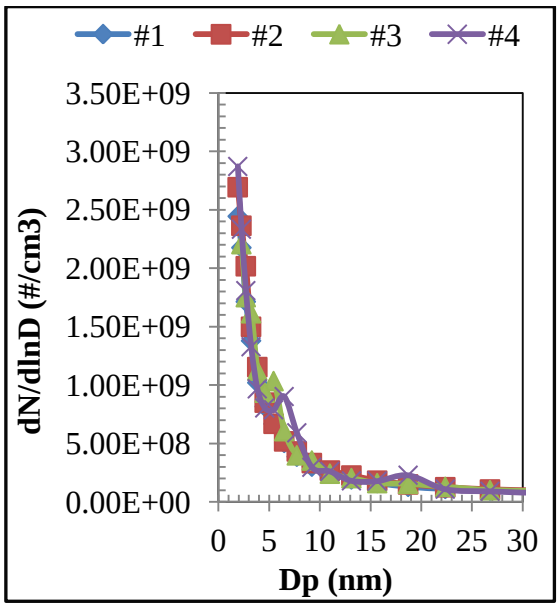


**(a) Particulate Number Emissions**

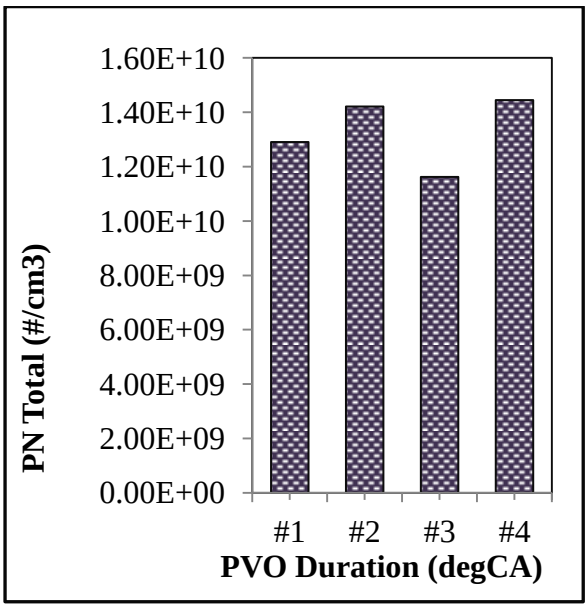


**(b) PN Total**

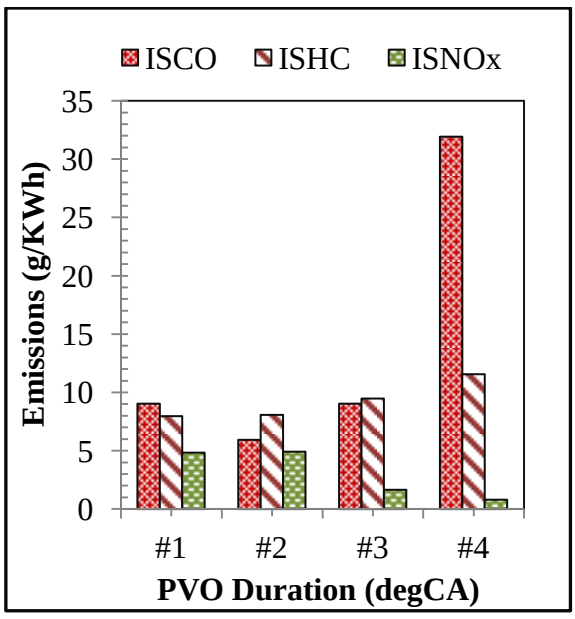


**(c) Emissions**

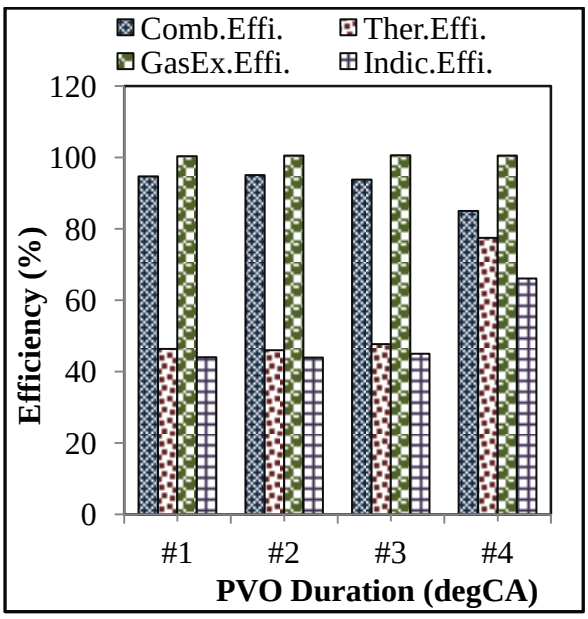


**(d) Efficiency**

**Figure 4.9 Effects of E15 on Particulate Emissions in PVO SI Operation**

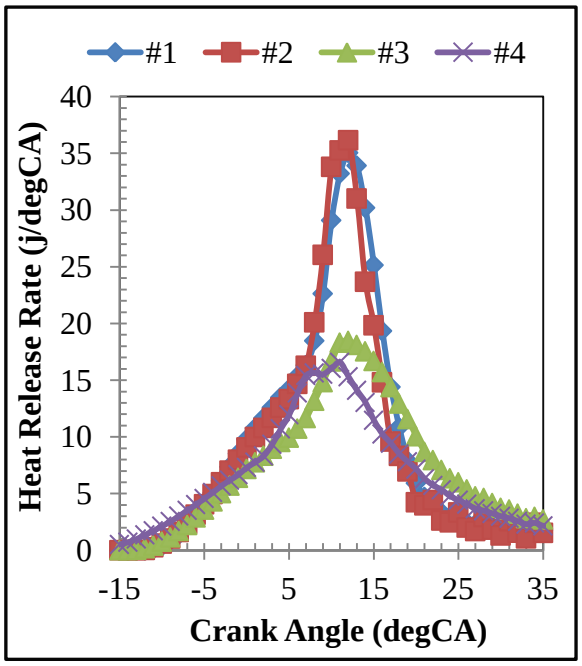


(e) Heat Release Rate

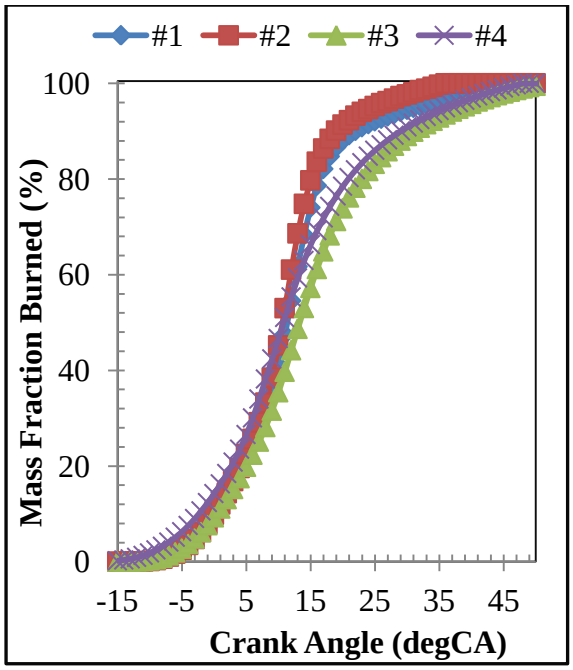


(f) Mass Fraction Burned

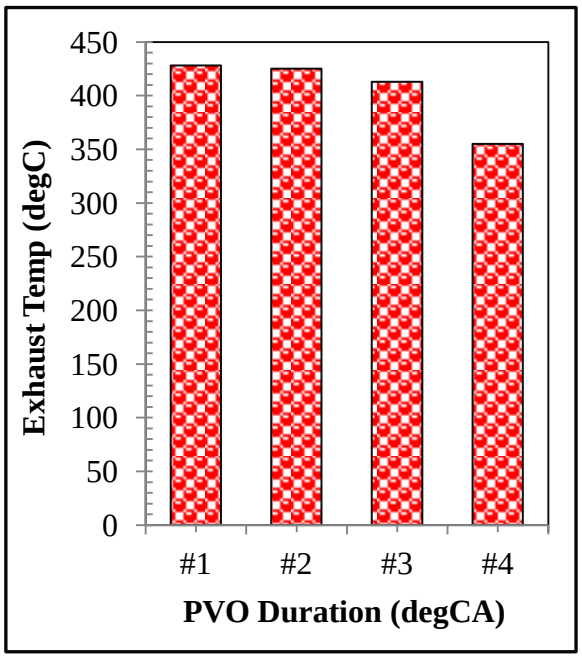


(g) Exhaust Temperature

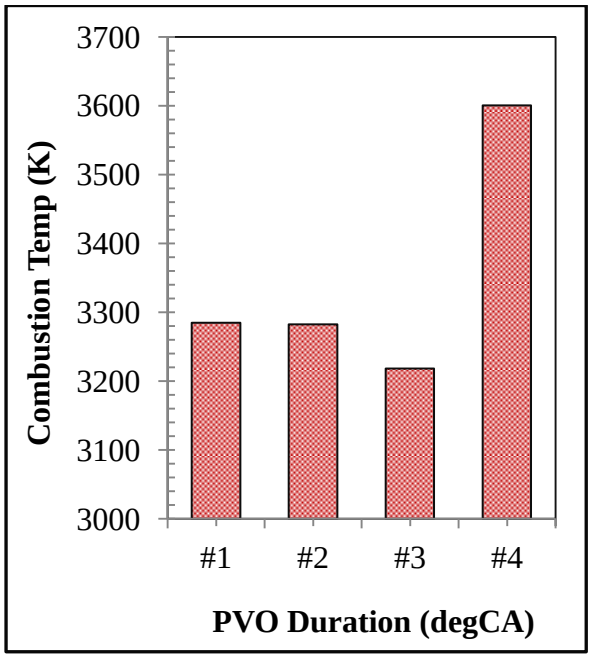


(h) Combustion Temperature

**Figure 4.9 (ctd) Effects of E15 on Particulate Emissions in PVO SI Operation**

### 4.6: Mode 4: 4-Stroke CAI

#### 4.6.1: 4-stroke CAI NVO

Figure 4.10(a) and (b) shows the results for the particulate number and total emissions when operating the engine in NVO CAI mode using pure gasoline (E0). The engine is operated at 1500rpm, using lambda 1 and the injection pressure set to 150bar. The curves are for different EVCs, each curve represents a different load and residual-gas fraction.

The particulate emissions were measured and analyzed in mass, number and their size distributions. It is noted that from Figure 4.10 (a),(b), (c) and (d) the CAI mode is characterized by both greater particulate mass, as measured by the particulate mass (PM) and total PM; and greater number of particles. Figure 4(a) shows that there are more particles in the CAI exhaust with particle size peaking at around 20nm. Therefore, the greater mass of particulate matter in the CAI exhaust may likely be as a result of more and larger particles, as shown in figure 4.10(c).

There are two plausible causes to the production of larger particles at greater numbers in the CAI combustion mode. In the case of CAI operation, fuel was injected into the hot burned gas at a high temperature but with little oxygen. This would cause hydrocarbons in gasoline to undergo thermochemical decomposition at elevated temperatures without the participation of oxygen, known as pyrolysis, in which soot particles could be produced. Although most of such soot particles would have been oxidized during the combustion process, the lower combustion temperature in CAI mode rendered the soot oxidation process less effective. It is known that such soot particles are typically in the size range of 20-40nm and defined as the nucleation mode in the particulate measurement, it comprises mostly volatile organic matters. In this test a high production of particulates was recorded, the sizes of which were indicative of nucleation mode particles. These particles are due to pyrolysis and less oxidation at a lower combustion temperature. Additionally, reduced post-combustion oxidation in the exhaust, due to low exhaust temperature, contributed to the higher particulate emissions from the CAI operation.

During the CAI operation, the load was varied by altering the exhaust valve timing (EVC). The earlier the EVC the lower the load, as more residual gas was trapped. It can be seen from Figure 4.10(a) that the particles were dominated by soot particles measuring between 10-30nm in diameter. The concentration of smaller particles of less than 20nm decreased with increasing load (Figure 4.10(b)), while the number of larger particle do not show a consistent

trend. Both particle numbers and mass tend to decrease with the load (Figure 4.10(b) and (d)). The mass distribution in Figure 4.10(c) shows the same trend of decrease with increasing load except for the 5.2 bar IMEPnet load, while the number distributions in size remained the same (Figure 4.10(a)). However, due to the presence of some larger particles at 5.2bar (Figure 4.10 (d)), it caused a jump in the particle mass curve in Figure 4.10(a). The reduction in smaller particles may be due to faster evaporation of liquid fuel due to higher residual-gas temperature at higher load operations.

**Table 4.8 CAI results with NVO**

| IMEP_net | SparkTiming | InjTiming | InjPulseWidth | IVO | IVC | IVL | EVO | EVC | EVL | RGF |
|---|---|---|---|---|---|---|---|---|---|---|
| bar | BTDC | ATDC | ms | ATDC | BTDC | mm | ATDC | ATDC | mm | % |
| 4.89 | -23 | 283 | 1.2 | 460 | -158 | 7.1 | 158 | 260 | 7.1 | 49 |
| 5.22 | -22 | 283 | 1.24 | 455 | -158 | 7.1 | 158 | 265 | 7.1 | 46 |
| 5.96 | -18 | 284 | 1.37 | 445 | -158 | 7.2 | 158 | 274 | 7.1 | 39 |
| 6.85 | -12 | 286 | 1.53 | 435 | -158 | 7.2 | 159 | 284 | 7.1 | 30. |
| 7.59 | -9 | 287 | 1.67 | 425 | -159 | 7.2 | 159 | 294 | 7.1 | 20 |

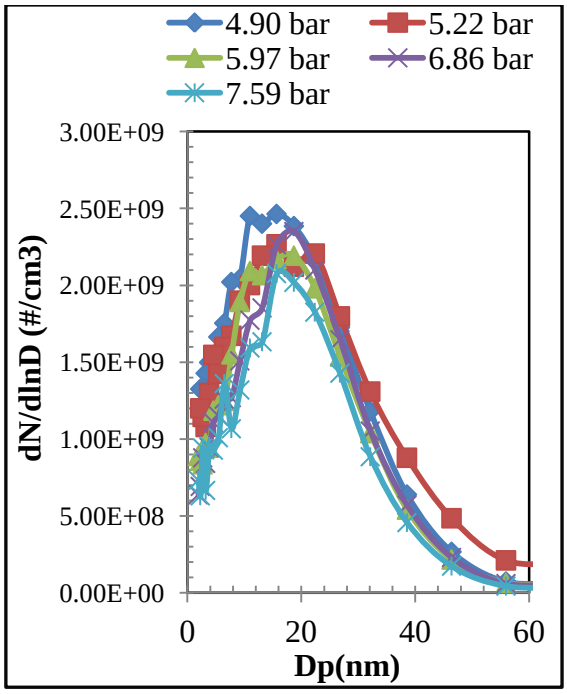


(a) Particulate Number Emissions

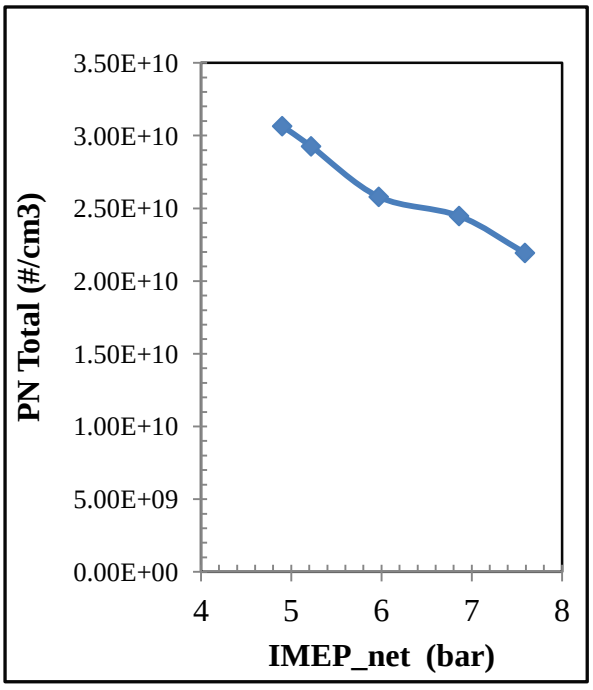


(b) PN Total Emissions

**Figure 4.10 Effects of Load in CAI NVO on Particulate Emissions**

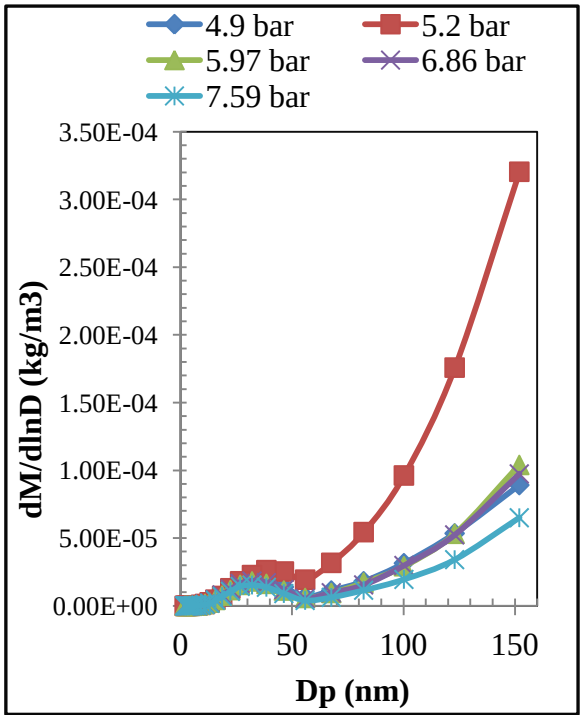


**(c ) Particulate Mass Emissions**

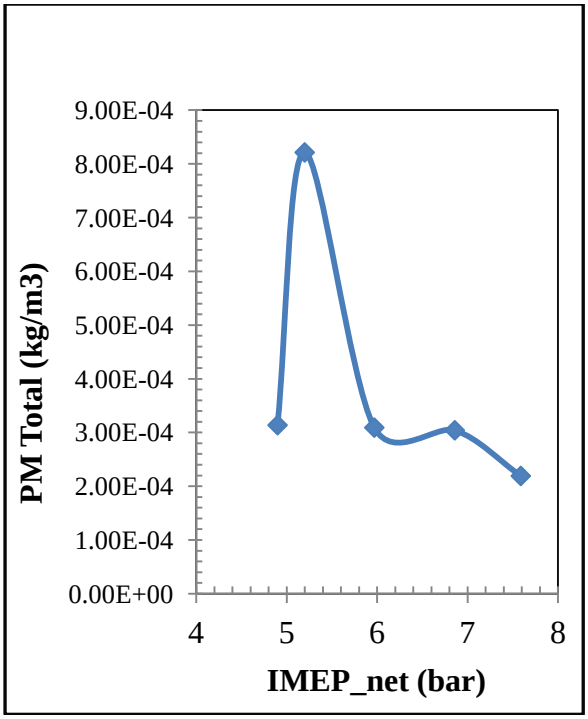


**(d) PM Total**

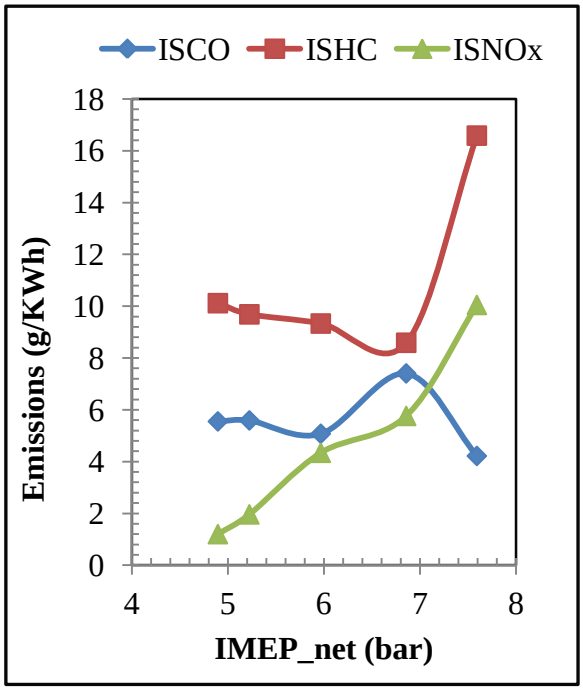


**(e) Emissions**

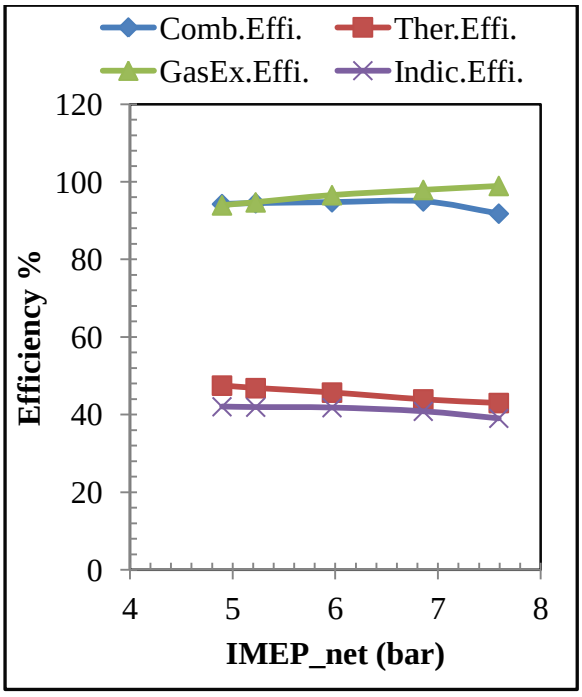


**(f) Efficiency**

**Figure 4.10 (ctd) Effects of Load in CAI NVO on Particulate Emissions**

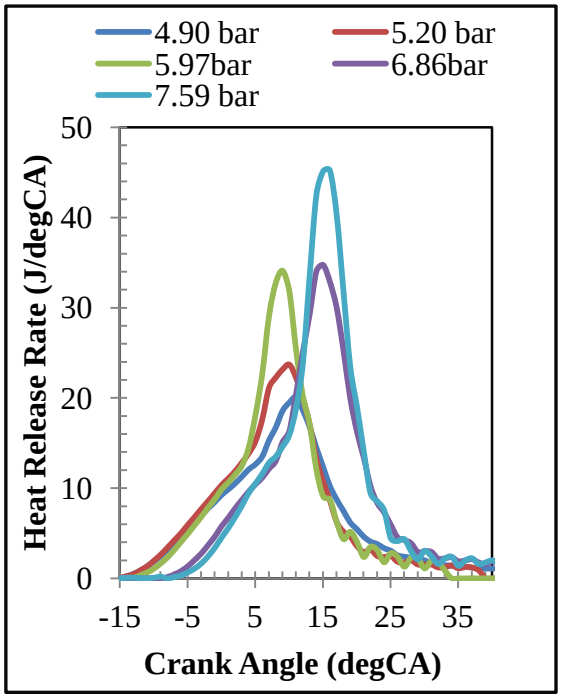


**(g) Heat-Release Rate**

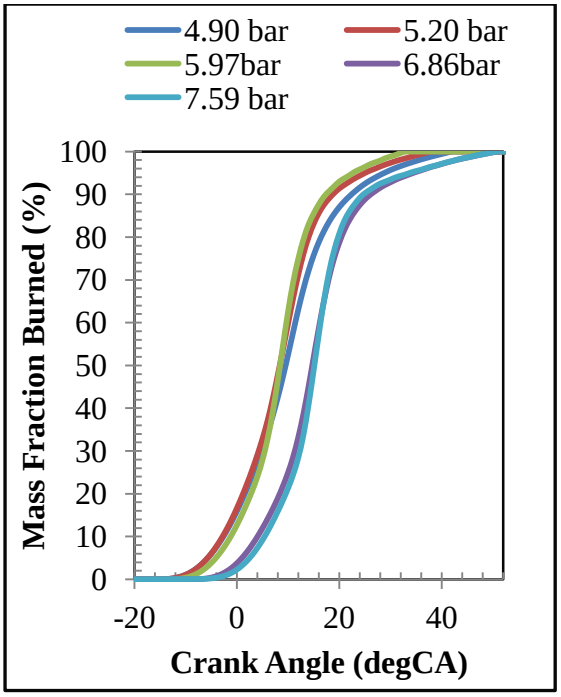


**(h) Mass Fraction Burned**

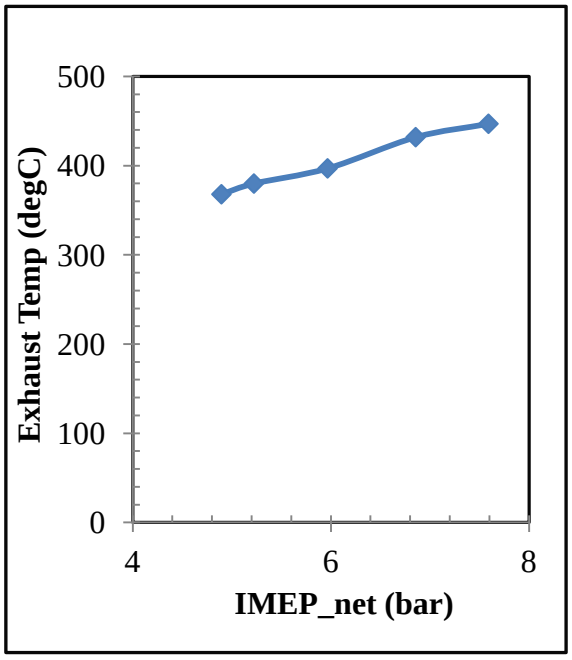


**(i) Exhaust Temperature**

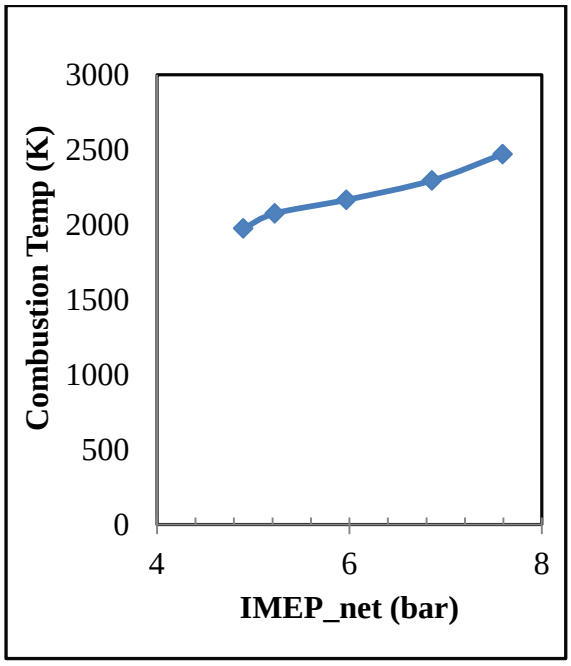


**(j) Combustion Temperature**

**Figure 4.10 (ctd) Effects of Load in CAI NVO on Particulate Emissions**

### 4.6.2: 4-stroke CAI NVO Varying Injection Pressure

The test was performed at a fixed engine speed of 1500rpm. The spark timing was fixed to operate at maximum brake torque (MBT) condition. The duration of injection was set to obtain stoichiometric lambda, as measured by a lambda sensor installed at the engine exhaust.

The start of injection was fixed in order to set the time between the injection and start of spark for each regime, thereby fixing the time available to the fuel to evaporate for all injection pressures. This enabled similar IMEP_net (3.2bar) and to achieve the optimum combustion stability. The fuel-injection pressure was increased from 100bar to 150 bar, the injection timing was set to 281 deg CA ATDC. The NVO duration was set to 300deg CA.

As predicted, an increase in injection pressure increases penetrations and better spray atomisation, whereas reducing the injection pressure generally increases the fuel droplet size. Larger fuel droplets takes longer to vaporize and mix, resulting in an increased amount of soot and unburned hydrocarbons [3,7,8] and corroborated by [99].

In Figure 4.11(a), (b) and (c) the particulate emission result was contrary to expectations. In using injection pressures of 100 bar and 115 bar, there was no peak and the particles emitted were lower in quantity and shifted to lower sized particles (Figure 4.11(c)). This can be explained as follows; fuel was injected during the negative valve overlap, which is associated with high temperatures. Furthermore, due to the large size of droplets of fuel injected at low pressure, the evaporation period was delayed.

The HC emission (Figure 4.11(e)), which constitutes the volatile organic fraction increases and there was reduced oxygen to support oxidation and, hence pyrolysis dominated. During the combustion process because of the high dilution rate, the combustion temperature was not high enough (ultra low NOx figure 4.11(e) and figure 4.11(j)) for the complete oxidation of the HC and CO, hence the observed particulate emitted in this study was likely to be in nucleation mode in sizes of less than 20nm.

In using injection pressures of 130-150 bar, the particle emission displayed a unimodal mode peaking at 2.62E09 particles/cm3 at 20nm particle diameter reducing rapidly to very low soot number for particulates in diameter of less than 10nm. This behaviour is expected and it agrees with previous experiments and expectations. This can be explained as follows, as the injection pressure increases the fuel droplet size reduces and this takes less time to vaporise and mix resulting in the decrease in particulate number, as evidenced in figure 4.11(a).

However, the high particulate emission observed peaking at 20nm was because fuel was injected into hot residual gas. Because of better spray atomisation associated with high pressure injection, the ignition delay period was shortened [83]. The shorter delay ignition

period provide less mixing time for the total charge preparation resulting in a pocket of rich mixture. This could have possibly raised the possibility of large particle formation.

Moreover, the low combustion temperature (figure 4.11(j)) may have inhibited oxidation. In addition the low exhaust temperature (Figure 4.11(i)) may have further reduced post-oxidation in the exhaust stroke.

Finally, the use of hot residual-gas fraction reduces the amount of air inducted into the engine, further reducing the total amount of fuel that participates in the combustion. This improves the ISFC, and consequently reduces the particle number concentrations. However, it was observed in the tests performed that injecting during NVO period lead to a reduction in the quantity of fresh charge inducted into the engine. The reduced availability of fresh charge may restrict the availability of $O_2$ to participate in oxidation. This may have increased the particle coagulation rate and generated an amount of larger particles, so the particle mass concentration increases and the number concentration decreases, as corroborated by [83].

**Table 4.9 CAI results with varying injection pressures**

| Inj. Pres. | IMEP_ net | Spark Timing | Inj Timing | Inj Pulse Width | IVO | IVC | IVL | EVO | EVC | EVL |
|---|---|---|---|---|---|---|---|---|---|---|
| bar | bar | BTDC | ATDC | ms | ATDC | BTDC | mm | ATDC | ATDC | mm |
| 103 | 3.12 | -26 | 281 | 1.05 | 467 | -161 | 6.9 | 159 | 253 | 6.9 |
| 115 | 3.29 | -26 | 281 | 1.05 | 467 | -161 | 6.9 | 159 | 253 | 6.9 |
| 129 | 3.33 | -26 | 281 | 1.05 | 467 | -160 | 6.9 | 159 | 253 | 6.9 |
| 143 | 3.20 | -26 | 281 | 1.05 | 466 | -160 | 6.9 | 159 | 253 | 6.9 |
| 151 | 3.12 | -26 | 281 | 1.05 | 466 | -160 | 6.9 | 159 | 253 | 6.9 |

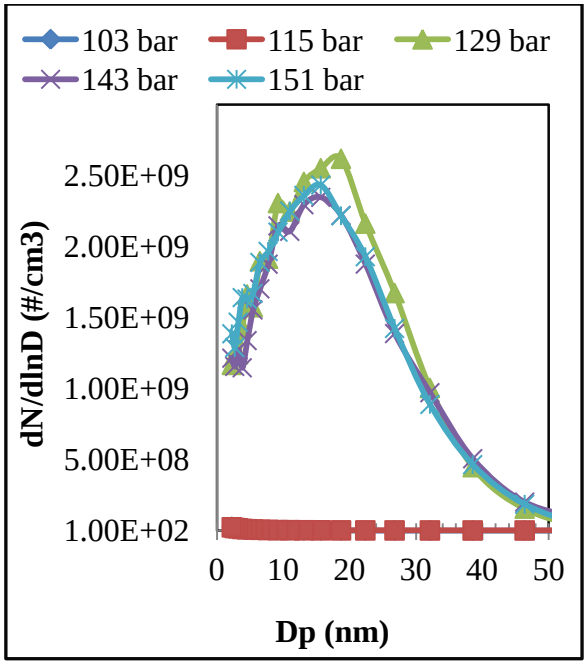


(a) Particulate Number Emission

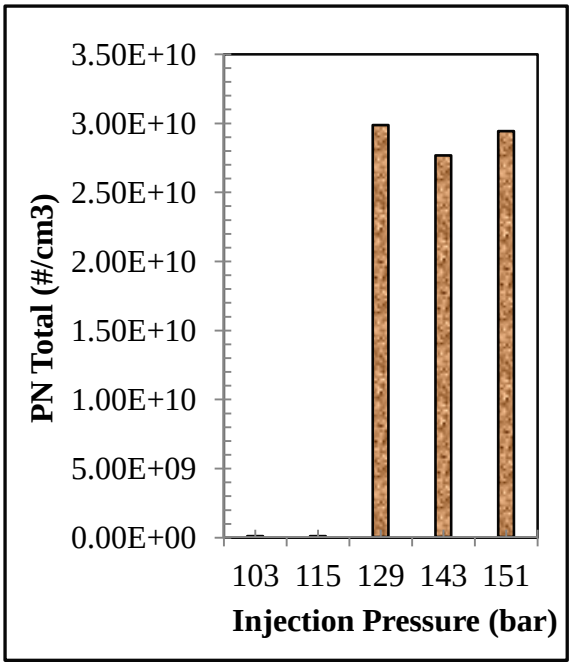


(b) PN Total

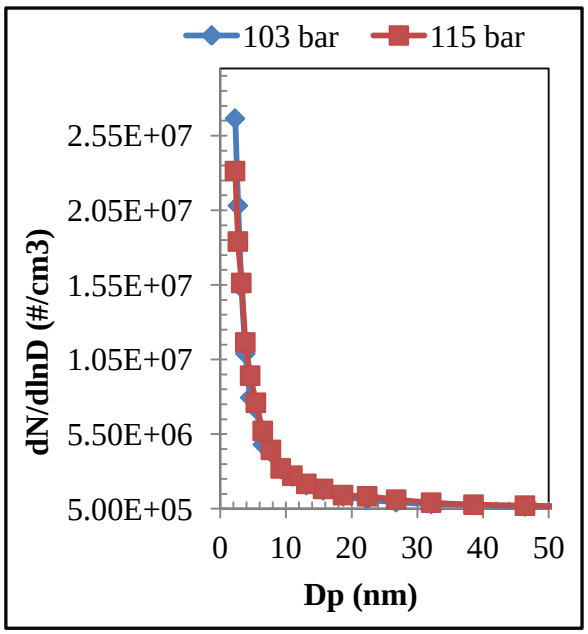


(c) Particulate Number Emissions

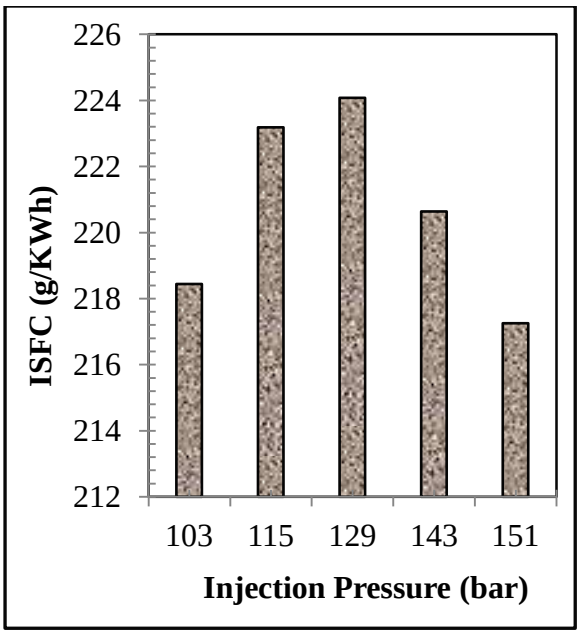


(d) ISFC

**Figure 4.11 Effects of Injection Pressure in CAI (NVO) on Particulate Emissions**

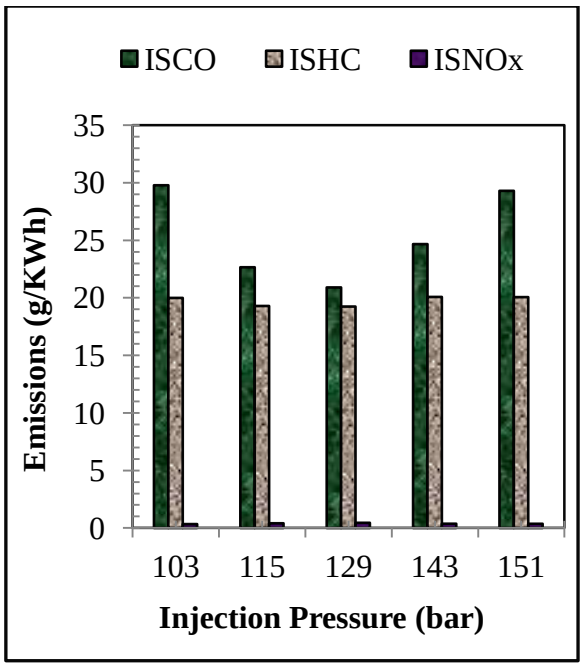


(e) Emission

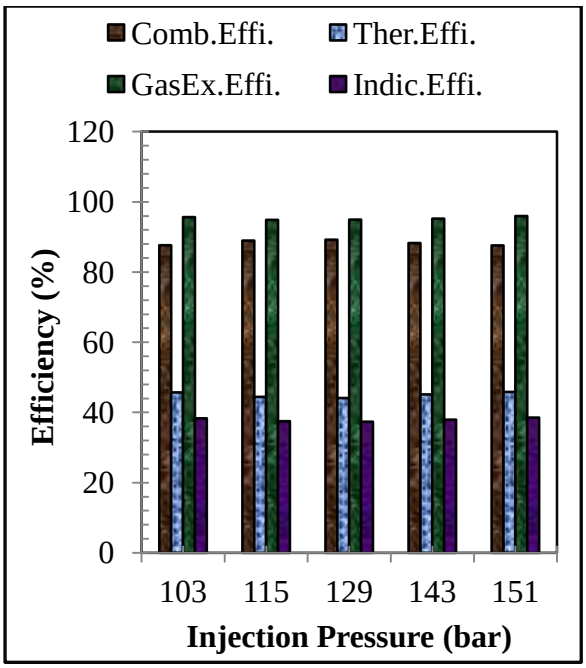


(f) Efficiency

**Figure 4.11 Effects of Injection Pressure in CAI (NVO) on Particulate Emissions**

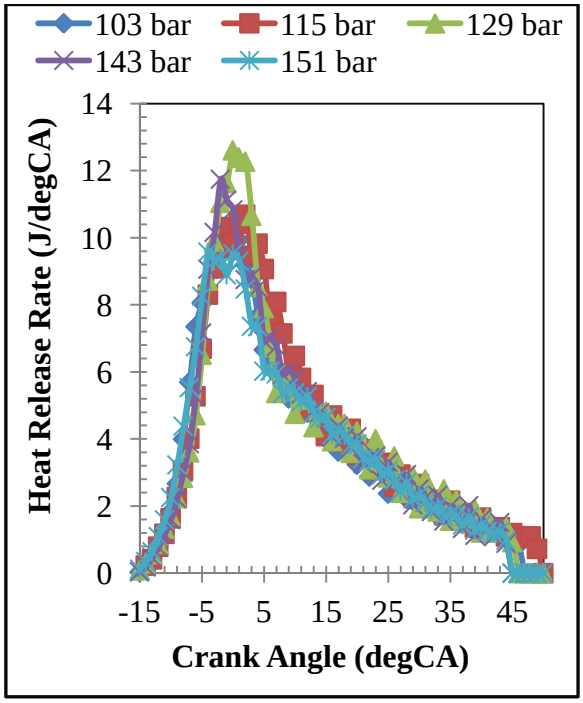


(g) Heat Release Rate

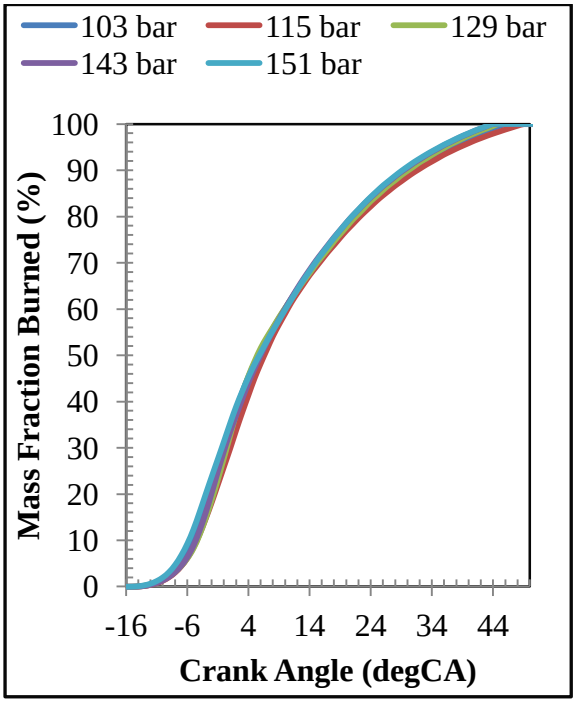


(h) Mass Fraction Burned

**Figure 4.11 (ctd) Effects of Injection Pressure in CAI (NVO) on Particulate Emissions**

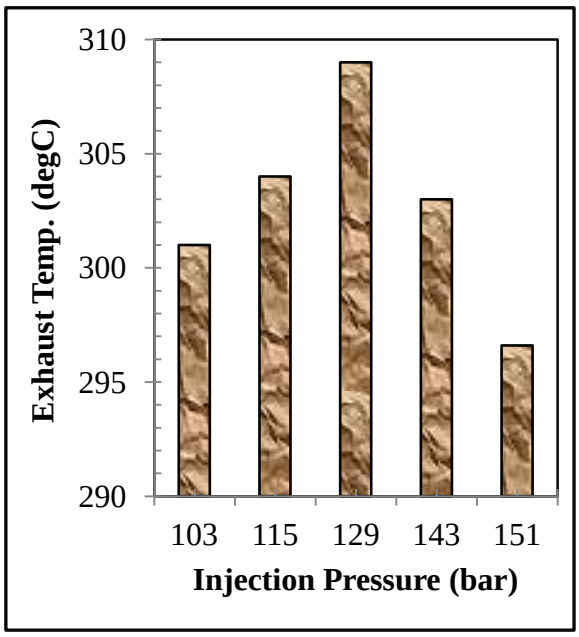


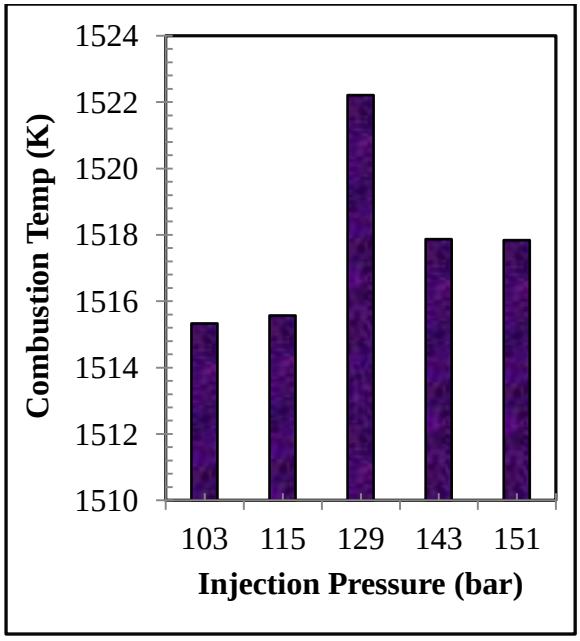


**(i) Exhaust Temperature** **(j) Combustion Temperature**

**Figure 4.11 (ctd) Effects of Injection Pressure in CAI (NVO) on Particulate Emissions**

### 4.6.3: 4-Stroke E15 CAI NVO

In this test seven different NVO durations were used (Table 4.10) to vary the load from 3.95 bar to 7.64 bar. The valve durations are from 200deg CA for minimum load corresponding to about 55%RGF to 126 deg CA corresponding to 24% RGF. The speed was maintained at 1500rpm, lambda=1, WOT position, spark timing was retarded from -23 deg CA BTDC to -9 deg CA bTDC. Injection timing was varied from 423 deg ATDC to 429 deg ATDC as the load increases for optimum emissions and performances. The injection pressure was set to 150 bar.

According to Di Ioro et al [88] the effects of using ethanol blends on the exhaust particulate emissions could be explained by considering the volatility properties of the blends. The addition of ethanol to gasoline significantly affects the vapour pressure of the fuel and its distillation curve [98, 100]. Ethanol forms positive azeotropes with the lighter compounds of gasoline, which determine a higher volatility of blends with respect to the source gasoline.

Figure 4.12 (a) and (b) show the particulate emissions using E15, the particle size distribution shifts towards smaller sizes, but higher particles were emitted as the load increases. This can be explained as follows; in accordance to the nature of the ethanol fuel as an oxygenate, as load is increased more fuel is injected, the NVO duration was reduced, this may likely have led to improved oxidation.

As is widely reported, the main sources of particles in gasoline direct-injection engines are the regions of rich spots caused by poor mixture preparation, and pool fires caused by fuel impingement on piston crown and cylinder walls.The low particle number concentration and sizes are reported to be due to the chemical and physical properties of the fuel [89].

Ethanol is a mono-component fuel with a low molecular weight. Injection of fuel during the NVO period enhances mixture formation. In addition, the higher oxygen content reduces the concentration of key intermediate species that are required for formation of the aromatic ring [89], which contributes to the surface growth of particles.The absence of this ring results in the formation of particles of sizes smaller than 20nm in diameter.

Maricq et al [76] reported an increase in particle number as load increased because more fuel was injected. The hotter residual in high loads further enhances fuel evaporation, thereby reducing ignition delay. However, as load was increased spark timing was retarded (Table 4.10) thereby enabling longer time for mixture preparation, but increased combustion duration (Fig 4.12(e) and (f)) extending into expansion stroke (increased NOx (Fig 4.12(c))), high exhaust temp (Fig 4.12(g)). This post combustion oxidation further helped to burn off the VOF the likely reason for reduced UHC (Figure 4.12(c)).

**Table 4.10 CAI results with E15**

| IMEP_net | Spark Timing | Inj Timing | Inj Pulse Width | RGF | IVO | IVC | IVL | EVO | EVC | EVL |
|---|---|---|---|---|---|---|---|---|---|---|
| bar | BTDC | ATDC | ms | % | ATDC | BTDC | mm | ATDC | ATDC | Mm |
| 3.95 | -23 | 422 | 1.14 | 58 | 455 | -170 | 5.1 | 170 | 255 | 3.1 |
| 4.18 | -21 | 423 | 1.2 | 55 | 450 | -169 | 5.1 | 170 | 259 | 3.1 |
| 4.52 | -19 | 424 | 1.3 | 51 | 447 | -169 | 5.1 | 170 | 262 | 3.1 |
| 5.29 | -16 | 425 | 1.45 | 45 | 437 | -169 | 5.1 | 170 | 272 | 3.1 |
| 5.67 | -14 | 425.85 | 1.51 | 41 | 442 | -169 | 5.1 | 171 | 276 | 3.1 |
| 6.68 | -11 | 428 | 1.74 | 31 | 432 | -168 | 5.2 | 171 | 286 | 3.1 |
| 7.64 | -9 | 429.59 | 1.94 | 24 | 422 | -169 | 5.2 | 171 | 296 | 3.1 |

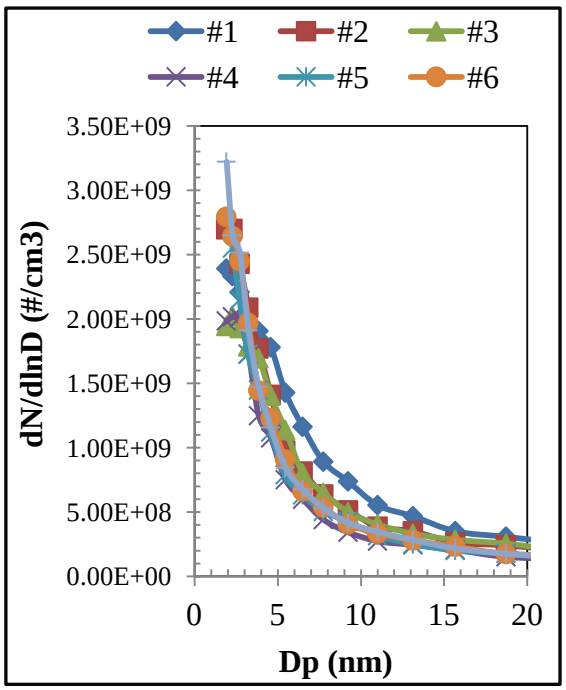


(a) Particulate Number Emission

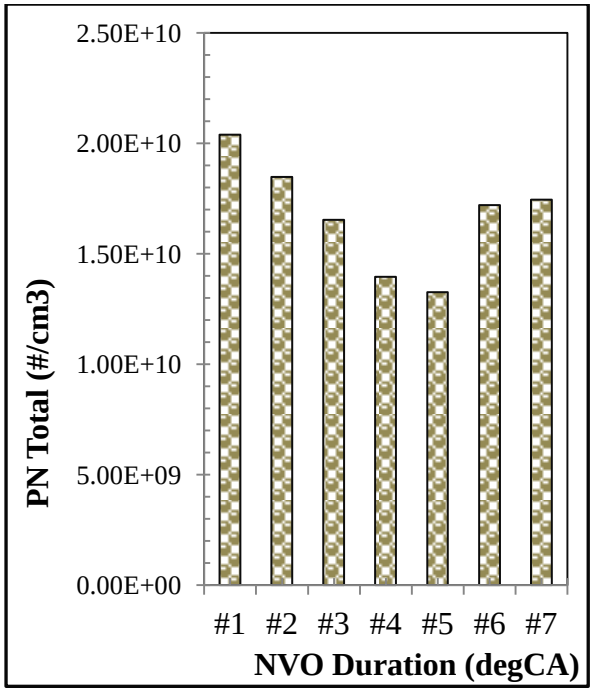


(b) PN Total

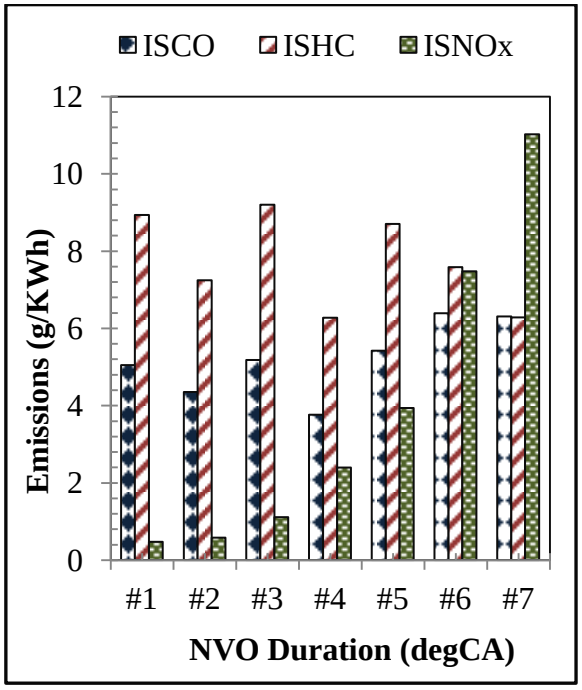


(c) Emission

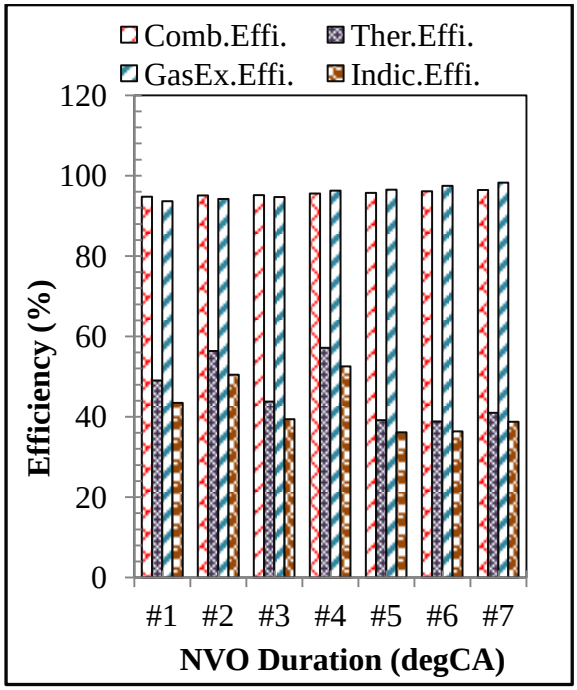


(d) Efficiency

**Fig 4.12 Effects of E15 CAI (NVO) on Particulate Emission**

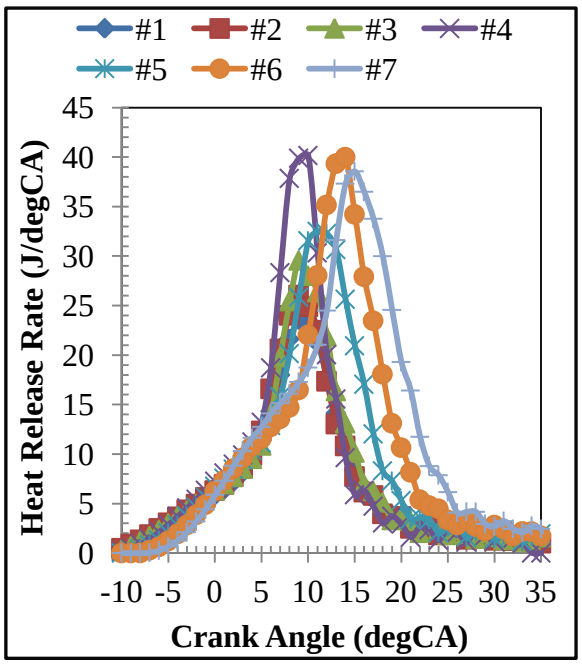


**(e ) Heat Release Rate**

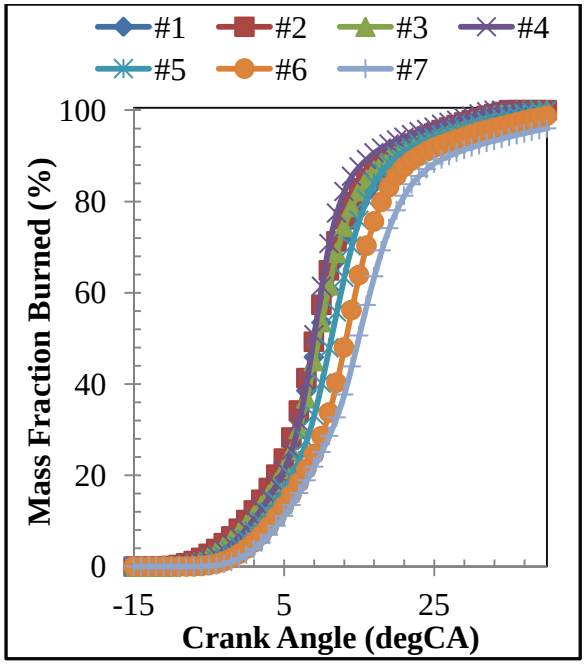


**(f) Mass Fraction Burned**

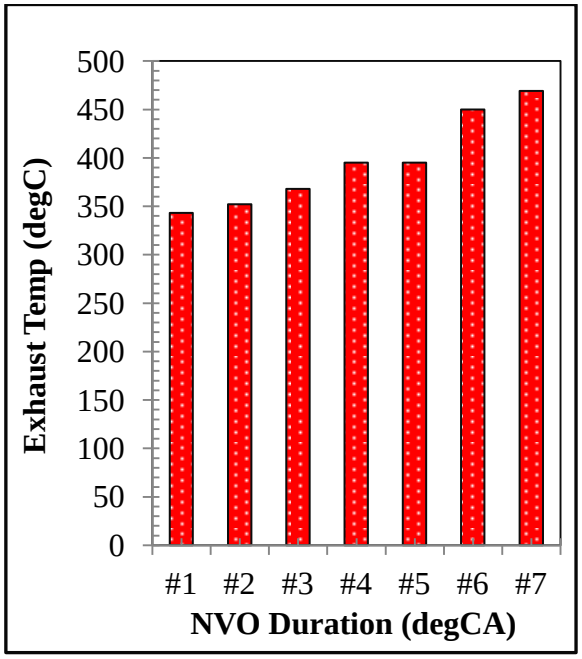


**(g) Exhaust Temperature**

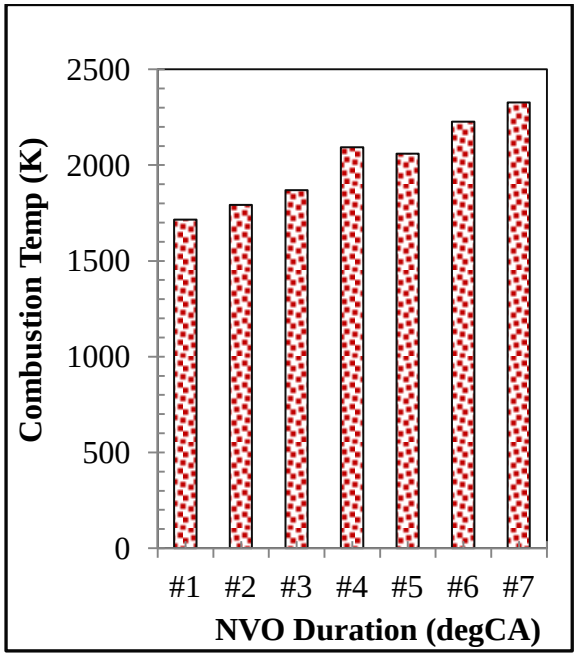


**(h) Combustion Temperature**

**Fig 4.12 (ctd) Effects of E15 CAI (NVO) on Particulate Emission**

### 4.7: Mode 6: 2-Stroke CAI Mode

#### 4.7.1: 2-Stroke Lean-Burn CAI Combustion

Table 4.11 reports the IMEP_net, lambda, intake pressure, injection timing and the valve timing used in this investigation. Figure 4.13(a) and (c) showed the particulate number and

mass emission, and Figure 4.13(b) and (d) showed the total particle number in 2-Stroke CAI mode using 15 operational load points.

Three trends are visible from the particulate emissions. In the load range of IMEPnet of 1.46bar and 2.06 bar, in lean mode there was no peak, but instead the volume of particulates of small sized particles measuring less than 7nm in diameter was 7 fold higher. At the loads of 2.20bar to 6.75 bar IMEP_net the particulates showed similar trends with concentrations around 20nm and peak value of 12nm diameter. At the 7.399 bar IMEP_net load, the particulate emissions were the lowest recorded, peaking about 6.59E+08#/$cm^3$ at about 2.5nm.

The discussion of the results will be considered in mixture phases (lambda values) according to the trends revealed. The particulate emission obtained for low loads of 1.46bar and 2.06 bar considered to be in lean mode may be explained by the interaction of spark, valve and fuel-injection timing diagram. In the low load fuel injection starts at the beginning of the compression stroke, the time for evaporation is short. The injection timing plays a very significant role in particulate emission.

During this operation, the exhaust valves are shown to close at around-164 and -158 deg ATDC and the intake valves remain open until -138degATDC. The air-flow rate is shown to decrease [101] for the two load cases as the fuel injection is retarded from EVC at -143degATDC, as the amount of charge cooling is reduced with less time available for mixture preparation during the intake process.

Some of the fuel is injected into hot residual gases as well as the fresh air and this enhances fuel evaporation. The retarding of the fuel injection to the compression stroke to avoid short circuiting reduces the fuel evaporation and atomisation time thereby resulting in poor mixture preparation and subsequent too rich combustion in some spots in the combustion chamber.

In addition, the engine is designed with vertical intake ports so that a reverse tumble flow can be formed to avoid short-circuiting during 2-stroke operations. When fuel-injection timing coincides with opening of the intake valves, the fuel spray is subject to incoming air flows at high speeds and deflected towards the piston, hence liquid fuel impingement on the piston crown. Hence the reason for higher ISHC and ISCO (Figure 4.13(g)) and poor combustion efficiency (Figure 4.13(h)) .

The rise in the CO and HC emissions with injection timing during the compression stroke is caused by the inhomogeneous mixture due to insufficient mixing time of late injections. Due to the high dilution rate, the NOx is ultra low and indicative of a very low combustion and exhaust temperature (Figure 4.13(k) and (l)).

The anslysis of the in-cylinder pressure provides additional information on the particulate formation process. Figures 4.13(e), (i) and (j) show the pressure traces of the above test and their thermodynamic analysis in terms of heat-release rate and mass-fraction burned.

After the spark, the heat release (Figure 4.13(i)) is lowest for the two load cases considered, which indicates a smaller mass-fraction burned (Figure 4.13(j)). This suggests that a greater amount of fuel fraction bypasses the combustion phase, because of a higher fuel wetting in this combustion mode.

In addition, as the mixture is made further lean, the main combustion phase slows down. In this stage the main source of soot particles is residual fuel droplets and fuel-rich zones of the combustion chamber.

However, as the mixture becomes leaner, this leads to a decrease in the particulate emissions both in number and mass as shown in Figure 4.13(b) and (d). This can be ascribed to fewer fuel-rich zones and an improved oxidation of particles as they come in contact with excess oxygen during the expansion stroke.

Interestingly, an exceptional case at 2.85 bar IMEP_net can be observed, this may require further investigation using an optical engine.

**Table 4.11 2-Stroke lean-burn CAI results**

| IMEP_net | Lambda | IntakePres | SparkTim | InjTiming | InjPulseW | IVO | IVC | IVL | EVO | EVC | EVL |
|---|---|---|---|---|---|---|---|---|---|---|---|
| bar | | bar | degBTDC | degBTDC | ms | degATDC | degBTDC | mm | degATDC | degBTDC | mm |
| 1.46089 | 1.10226 | 1.14526 | -13 | -143 | 0.558 | 158 | -138 | 4.54563 | 145 | -164 | 3.25655 |
| 2.06052 | 1.11346 | 1.13822 | -3 | -143 | 0.57 | 158 | -138 | 4.51605 | 145 | -158 | 4.41753 |
| 2.20344 | 1.09597 | 1.24522 | -3 | -142 | 0.7 | 167 | -133 | 4.2745 | 145 | -164 | 3.2654 |
| 2.85448 | 1.2216 | 1.2139 | -3 | -141 | 0.83 | 167 | -127 | 4.62048 | 146 | -154 | 4.96598 |
| 3.18698 | 1.3559 | 1.32012 | -3 | -140 | 0.9 | 167 | -127 | 4.61093 | 146 | -152 | 5.19265 |
| 4.03579 | 1.49771 | 1.44461 | -16 | -139 | 1.01 | 168 | -131 | 4.60902 | 147 | -155 | 4.31283 |
| 4.10992 | 1.47179 | 1.44195 | -16 | -139 | 1.02 | 168 | -131 | 4.61592 | 146 | -154 | 4.35982 |
| 4.63076 | 1.48162 | 1.52636 | -16 | -138 | 1.1 | 167 | -129 | 4.63027 | 146 | -154 | 4.36107 |
| 4.72692 | 1.43822 | 1.53814 | -11 | -138 | 1.1 | 168 | -129 | 4.61313 | 146 | -155 | 4.34021 |
| 4.5856 | 1.41138 | 1.50523 | -8 | -138 | 1.13 | 168 | -129 | 4.61826 | 147 | -155 | 4.29283 |
| 5.23424 | 1.41477 | 1.58807 | -13 | -137 | 1.13 | 168 | -129 | 4.61531 | 147 | -155 | 4.31096 |
| 5.41221 | 1.43 | 1.62438 | -13 | -136 | 1.3 | 168 | -129 | 4.61536 | 147 | -156 | 4.19101 |
| 6.43685 | 1.45065 | 1.79046 | -18 | -135 | 1.46 | 168 | -123 | 4.8242 | 147 | -154 | 4.28804 |
| 6.74956 | 1.45943 | 1.88642 | -13 | -134 | 1.52 | 167 | -123 | 4.81154 | 147 | -154 | 4.25115 |
| 7.399 | 1.47355 | 1.88284 | -13 | -133 | 1.65 | 167 | -122 | 4.83361 | 145 | -153 | 4.61533 |

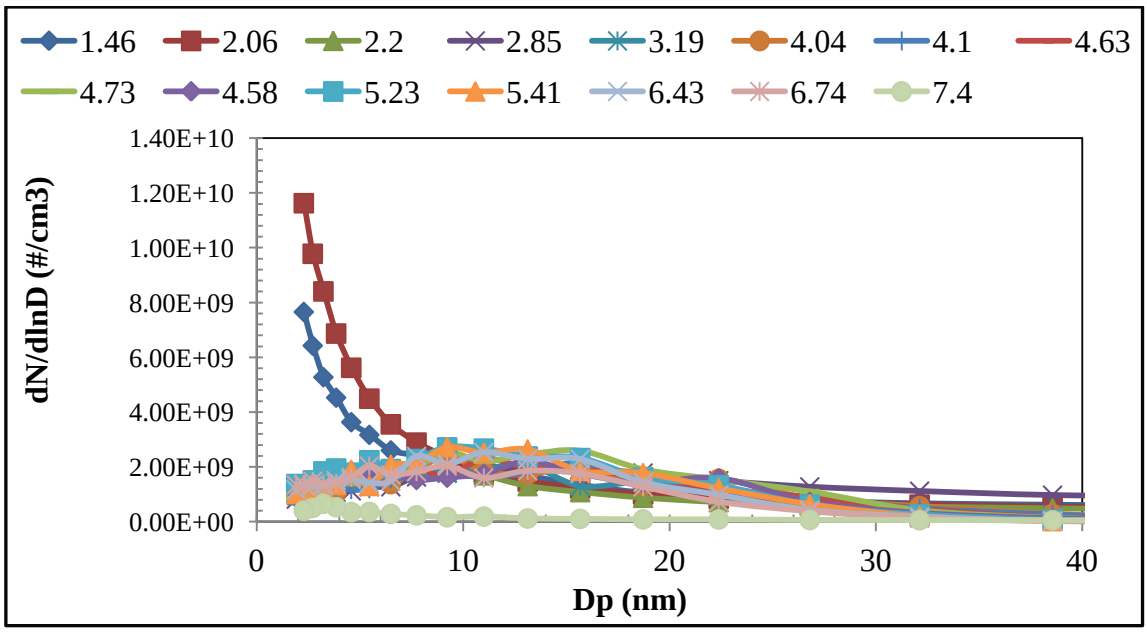


**(a) Particulate Number Emission**

**Figure 4.13. Particulate Emission in 2-Stroke CAI Operation**

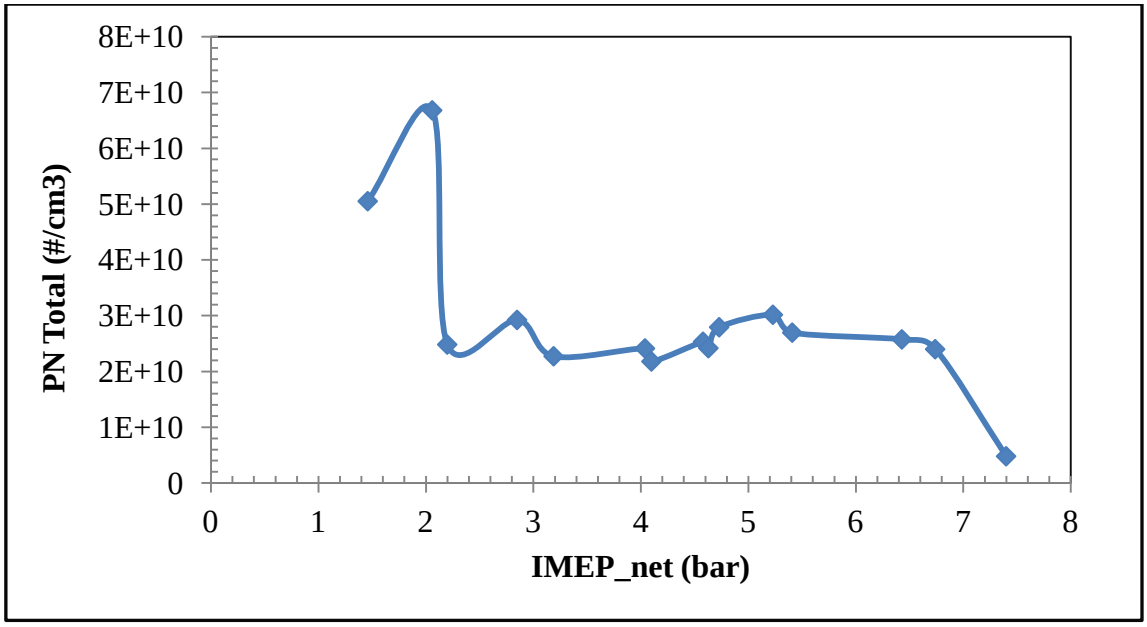


**(b) PN Total**

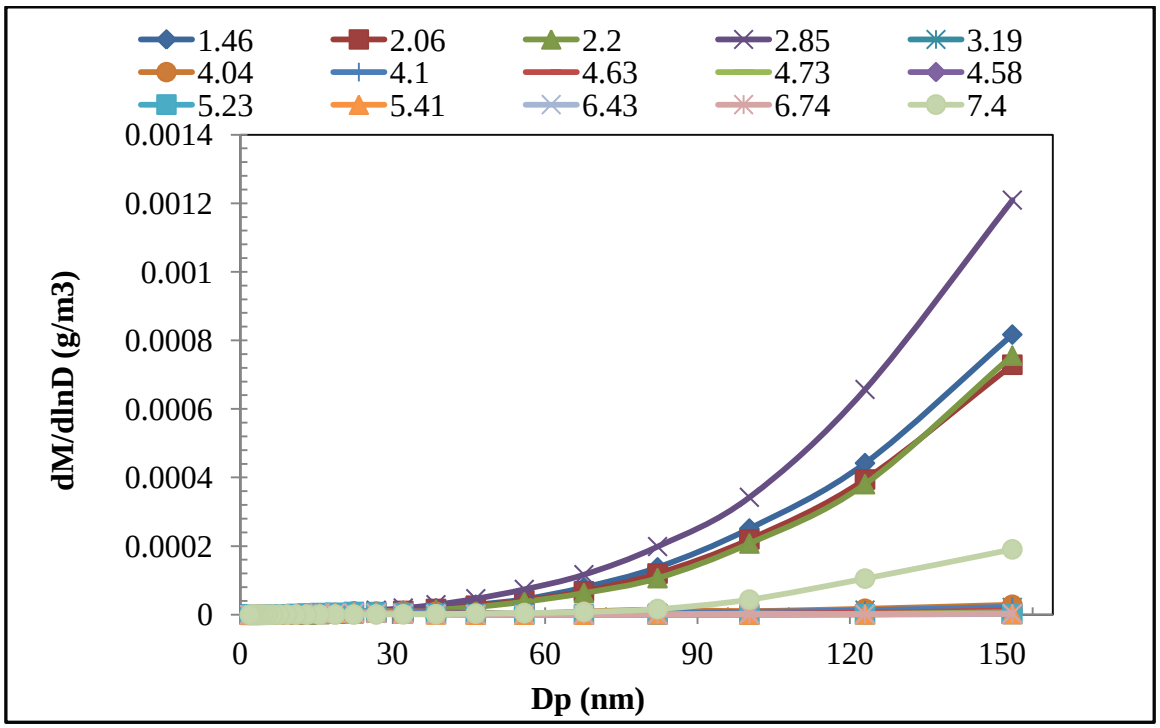


**(c) Particulate Mass Emission**

**Figure 4.13. Particulate Emission in 2-Stroke CAI Operation**

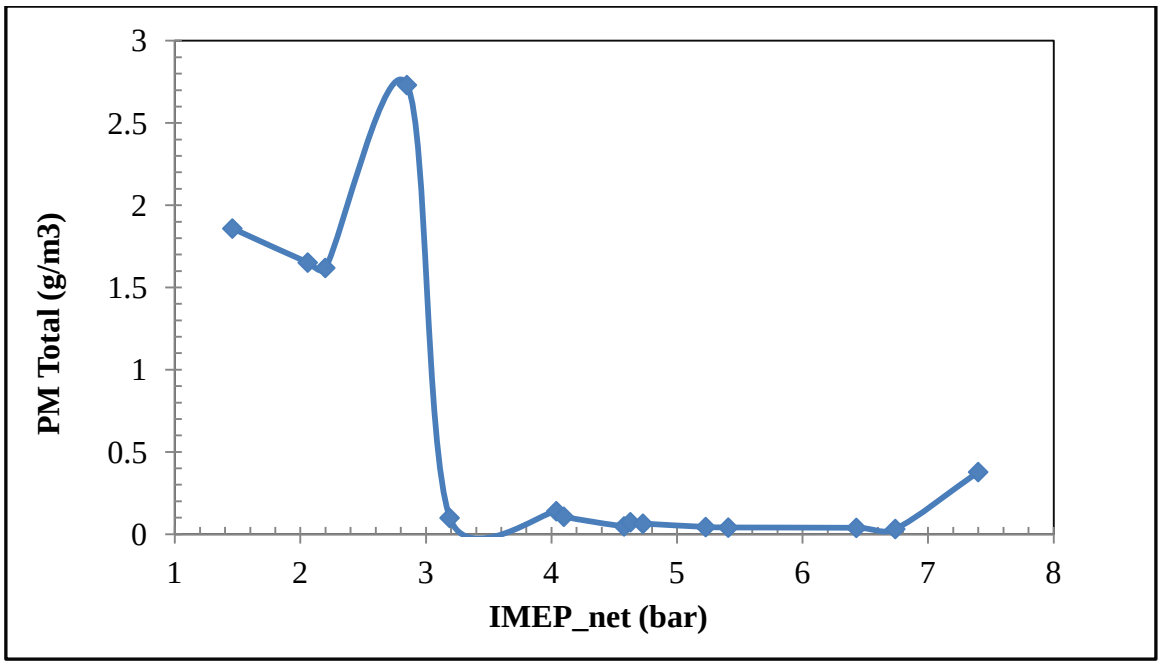


**(d) PM Total**

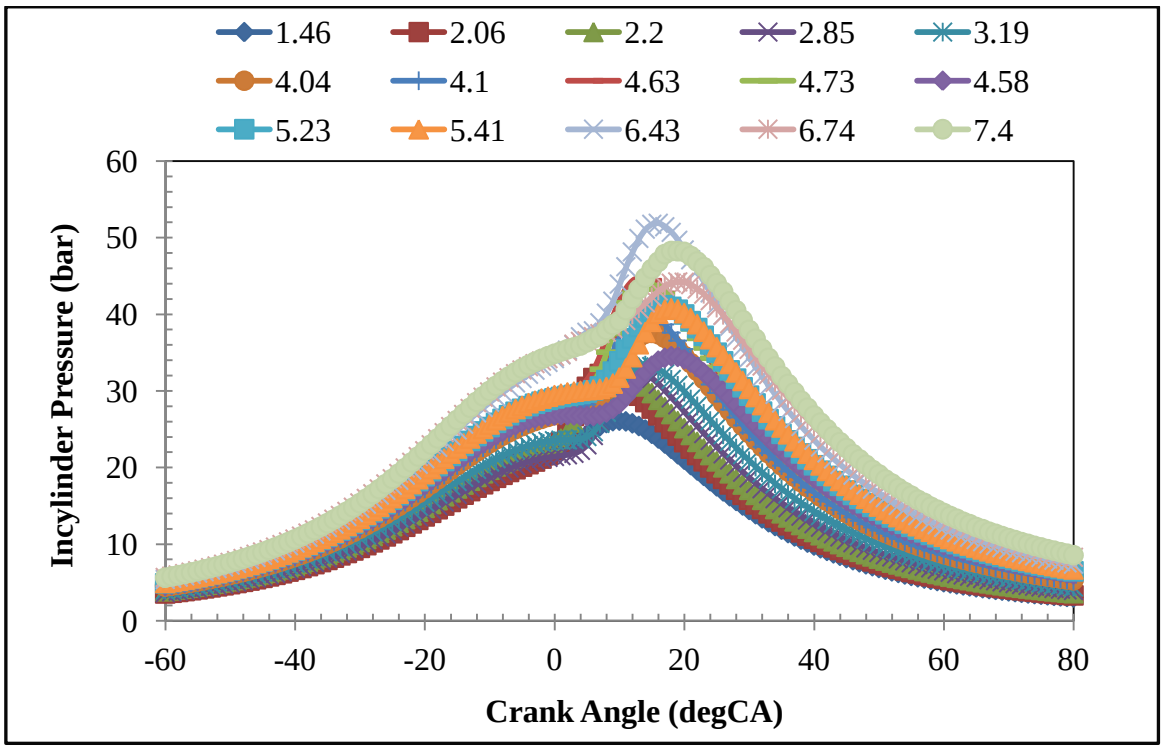


**(e) In-cylinder Pressure**

**Figure 4.13. (ctd) Particulate Emission in 2-Stroke CAI Operation**

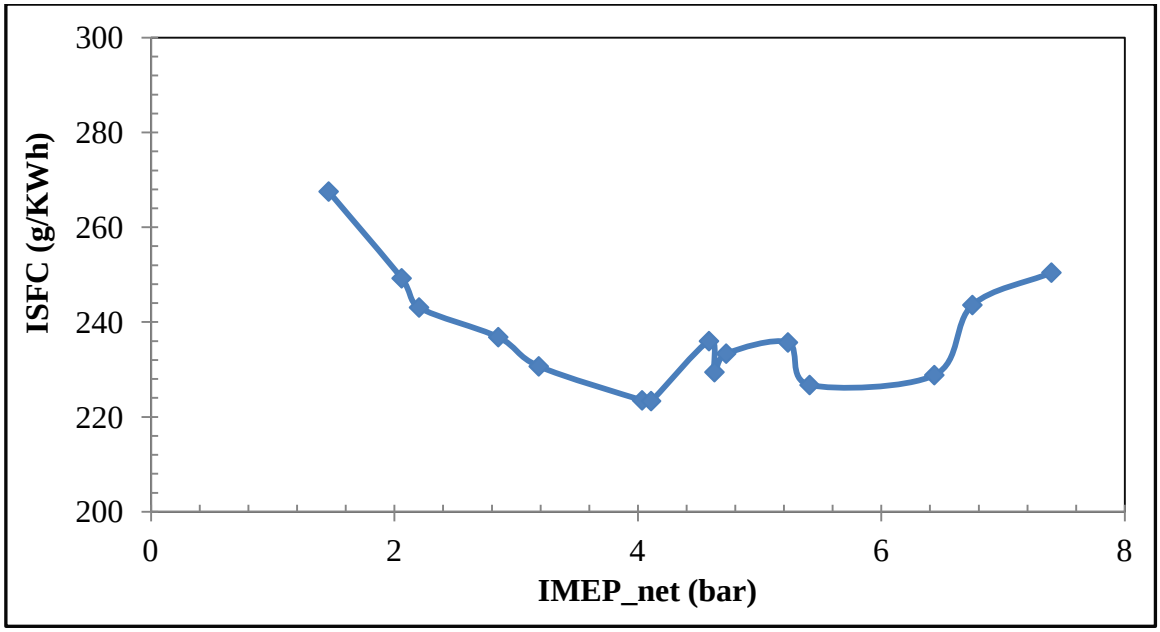


**(f) ISFC**

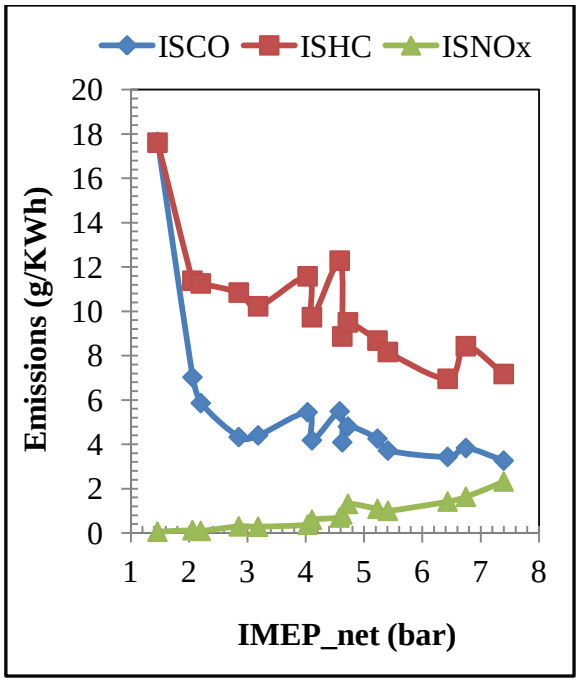


(g) **Emission**

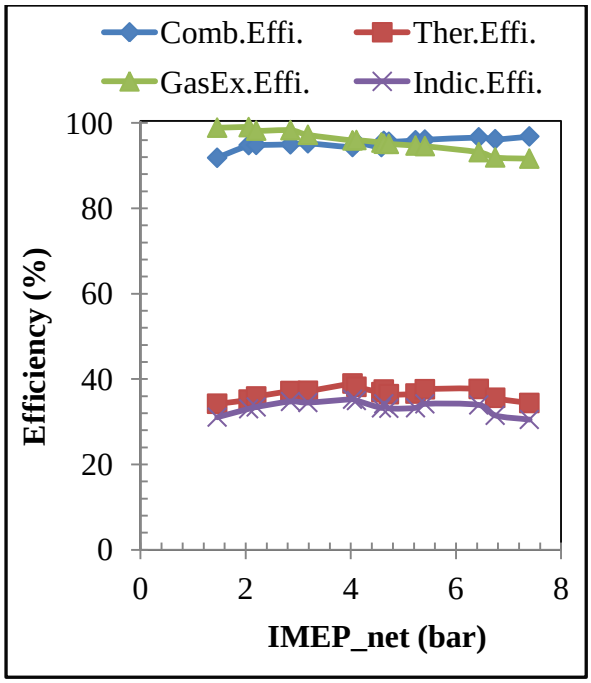


**(h) Efficiency**

**Figure 4.13. (ctd) Particulate Emission in 2-Stroke CAI Operation**

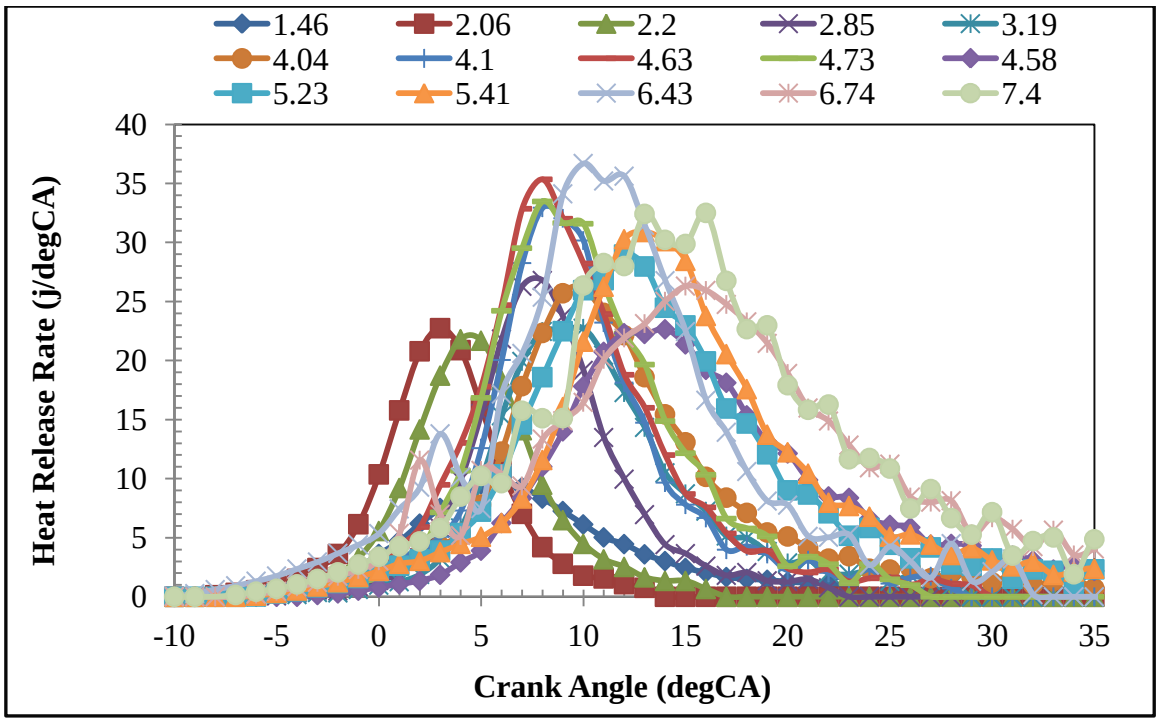


**(i) Heat Release Rate**

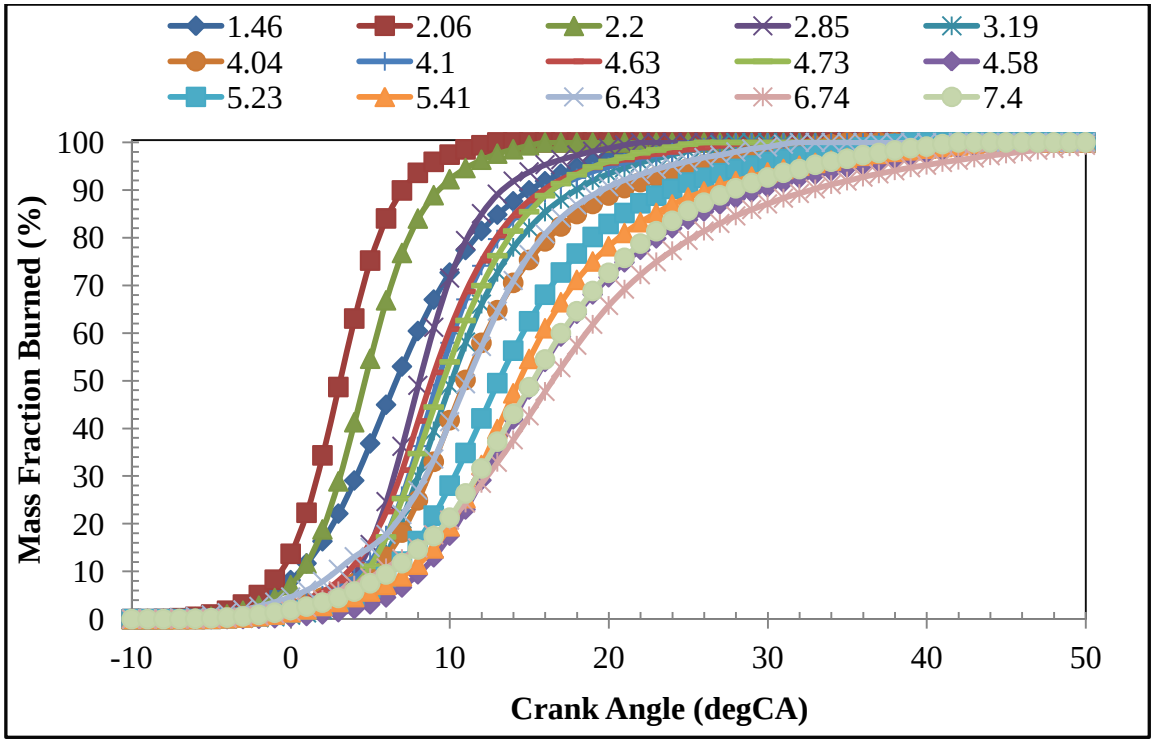


**(j) Mass Fraction Burned**

**Figure 4.13. (ctd) Particulate Emission in 2-Stroke CAI Operation**

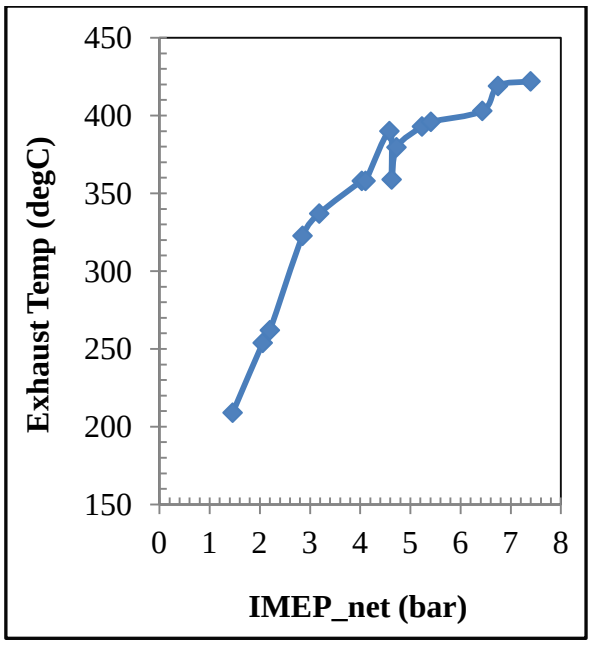


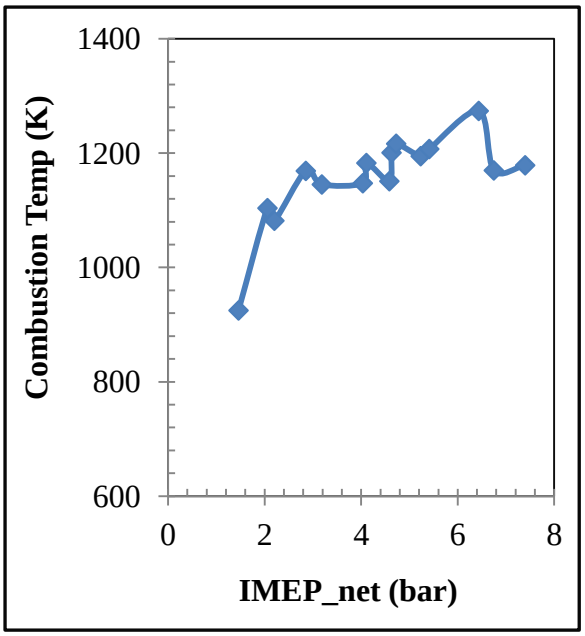


**(k) Exhaust Temperature** **(l) Combustion Temperature**

**Figure 4.13. (ctd) Particulate Emission in 2-Stroke CAI Operation**

### 4.7.2: 2-stroke E15 CAI with Boosting

Figure 4.14 shows the particulate emissions in number and mass (figure 4.14(a) and (c)) and the total particulate in number and mass (figure 4.14(b) and (d)). The heat-release rate and corresponding mass-fraction burned are shown in figure 4.14(g) and (h) in 2-stroke E15 CAI with boosting operation.

The particulate emission is similar to the previous cases, except when using 15% ethanol blend. The E15 generates a similar quantity of particles to the other cases of 4-Stroke by removing the peak and shifting the particle size towards smaller particles in diameter and increasing the volume of particulate emitted. This could be a result of the interaction of fuel injection and gas-exchange process.

In this test using E15 in the 2-stroke CAI operation, fuel injection takes place during the compression processes. Some residual gas and fuel mixture can be stratified or less well mixed with air because of the shorter time duration, causing locally fuel-rich combustion and hence the formation of soot particles seen in the peak of the exhaust particle emissions for the two stroke CAI. However, the addition of ethanol and the high residual air mixture temperature promotes faster evaporation that removes the peak associated with the soot particles due to the inherent tendency of oxygenates to produce less soot.

**Table 4.12 2-Stroke CAI results with E15**

| IntakePres | IMEP_net | SparkTim | InjTiming | InjPulseW | IVO | IVC | IVL | EVO | EVC | EVL |
|---|---|---|---|---|---|---|---|---|---|---|
| bar | bar | degBTDC | degBTDC | ms | degATDC | degBTDC | mm | degATDC | degBTDC | mm |
| 1.14881 | 1.16762 | -18 | -143 | 0.553 | 167 | -136 | 3.5195 | 143 | -161 | 3.40452 |
| 1.15082 | 1.39157 | -18 | -143 | 0.556 | 167 | -136 | 3.52078 | 143 | -161 | 3.38657 |
| 1.17043 | 1.718 | -8 | -143 | 0.56 | 167 | -136 | 3.55653 | 143 | -161 | 3.37931 |
| 1.16007 | 1.98187 | -5 | -142 | 0.696 | 167 | -135 | 3.53176 | 143 | -156 | 3.72215 |
| 1.17853 | 2.33898 | -5 | -141 | 0.79 | 166 | -132 | 3.68906 | 143 | -157 | 3.71319 |
| 1.21865 | 2.69959 | -5 | -140 | 0.89 | 166 | -123 | 3.93037 | 143 | -157 | 3.70618 |
| 1.3912 | 3.43772 | -5 | -139 | 1 | 168 | -112 | 3.98445 | 141 | -162 | 3.56227 |
| 1.52891 | 4.14188 | -3 | -137 | 1.2 | 168 | -105 | 4.02364 | 141 | -162 | 3.55084 |
| 1.63371 | 4.53876 | -3 | -136 | 1.3 | 168 | -97 | 4.06066 | 136 | -162 | 3.84937 |
| 1.63675 | 5.26849 | -7 | -134 | 1.5 | 163 | -97 | 4.07974 | 136 | -163 | 3.81706 |
| 1.71647 | 5.69228 | -7 | -133 | 1.68 | 163 | -95 | 4.08966 | 137 | -163 | 3.8214 |

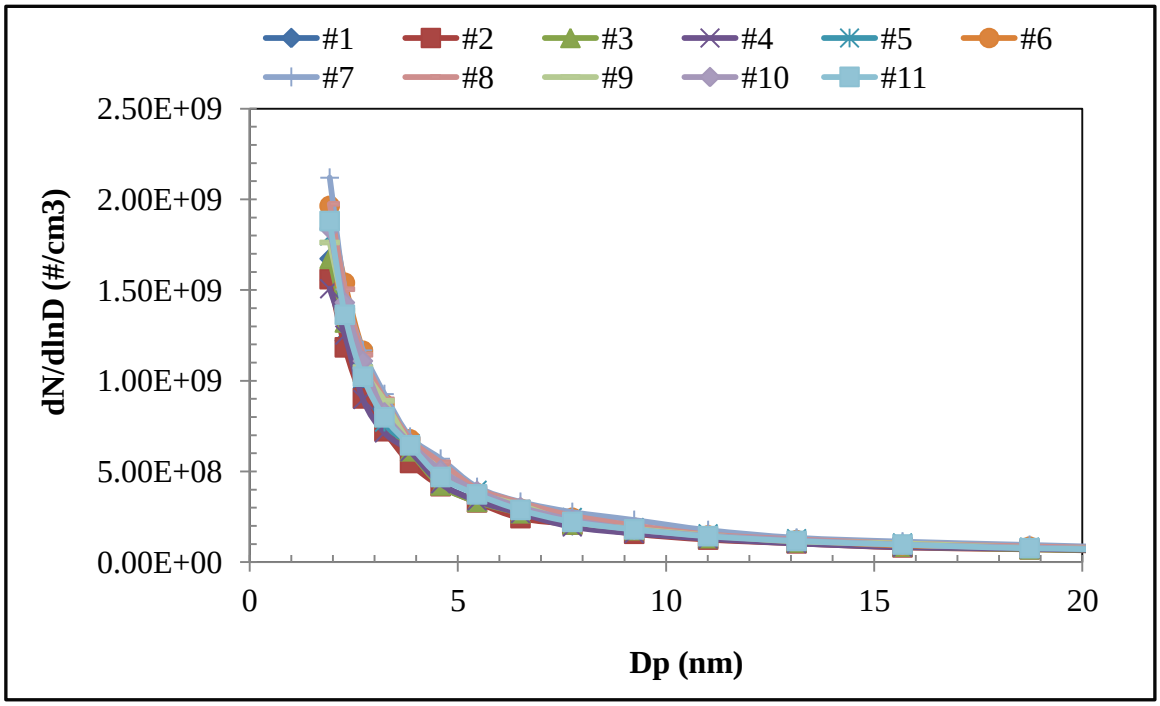


**(a) Particulate Number Emission**

**Figure 4.14 Particulate Emission in 2-Stroke E15 CAI**

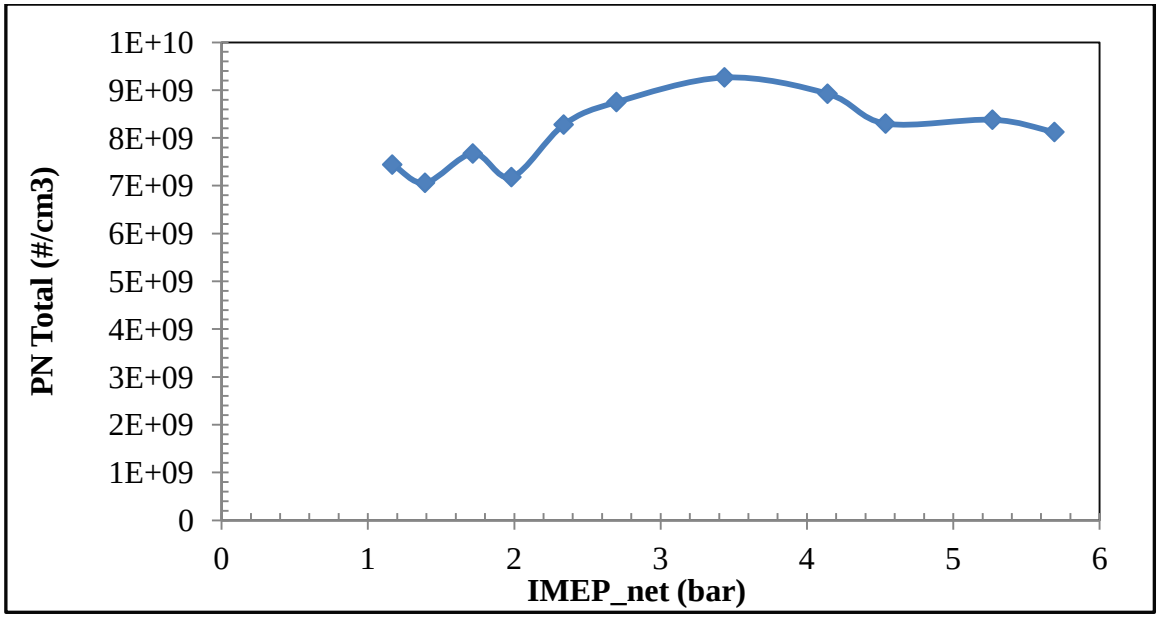


**(b) PN Total**

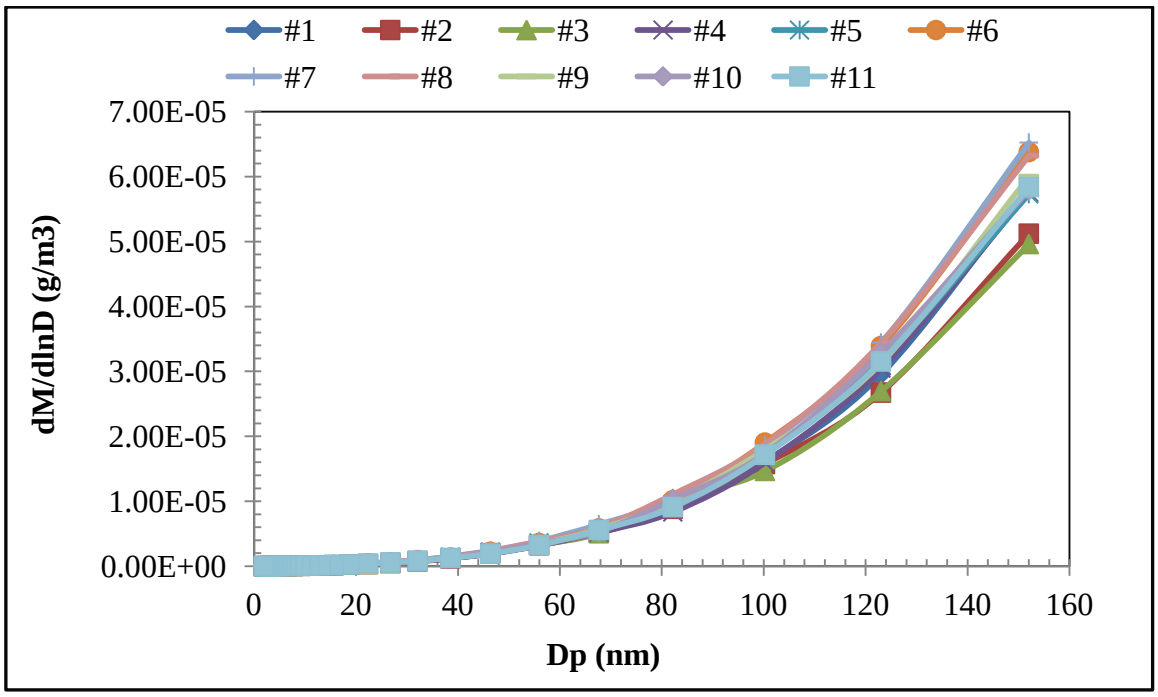


**(c) Particulate Mass Emission**

**Figure 4.14 (ctd) Particulate Emission in 2-Stroke E15 CAI**

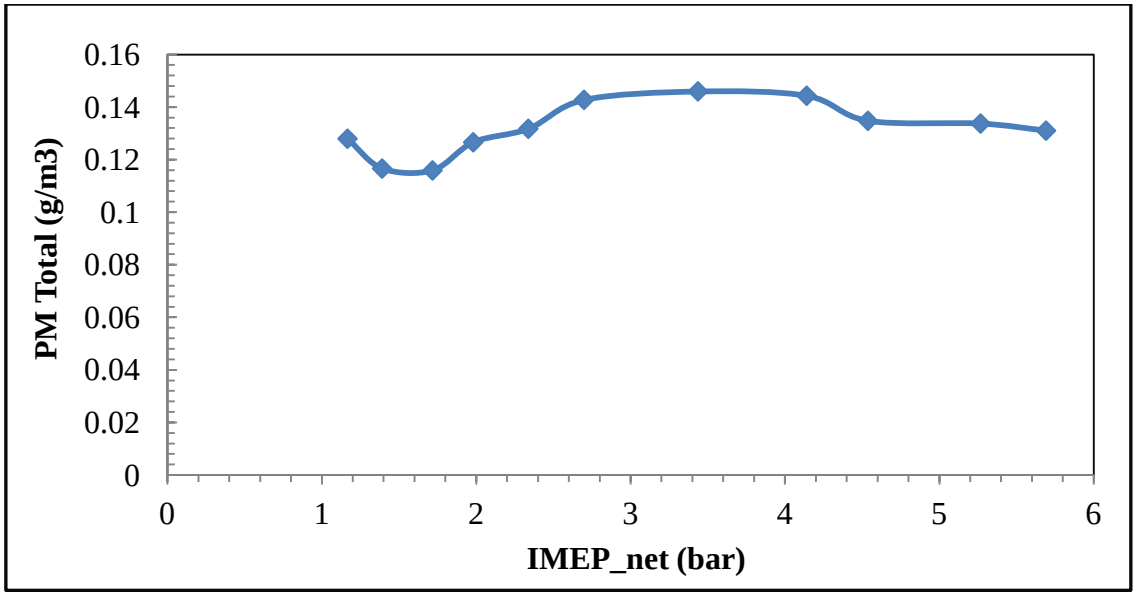


**(d) PM Total**

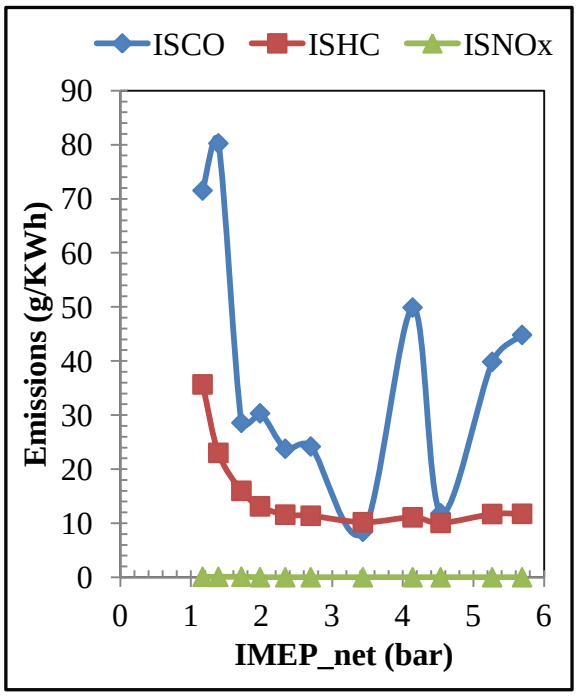


**(e) Emission**

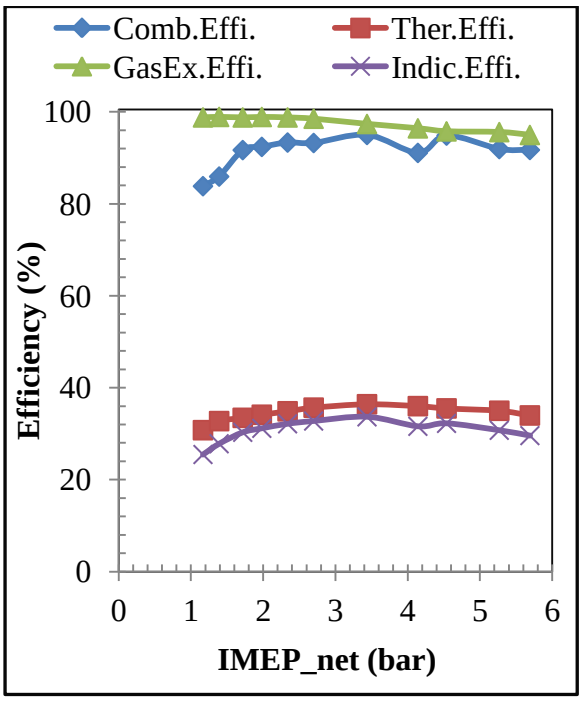


**(f) Efficiency**

**Figure 4.14. (ctd) Particulate Emission in 2-Stroke E15 CAI**

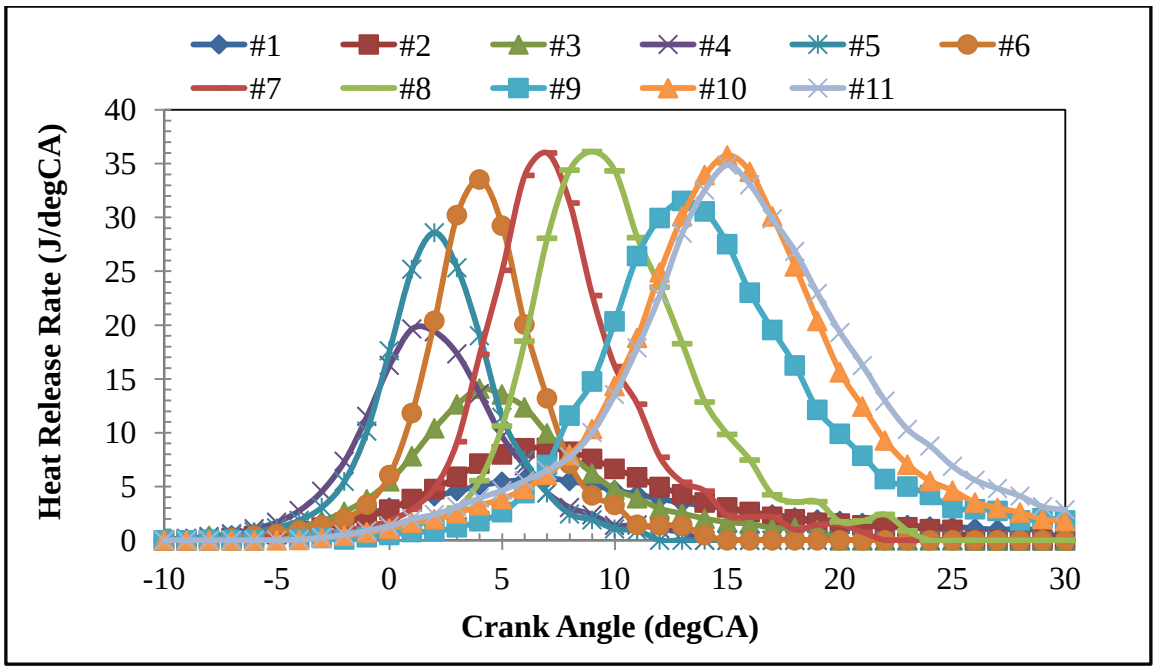


**(g) Heat-Release Rate**

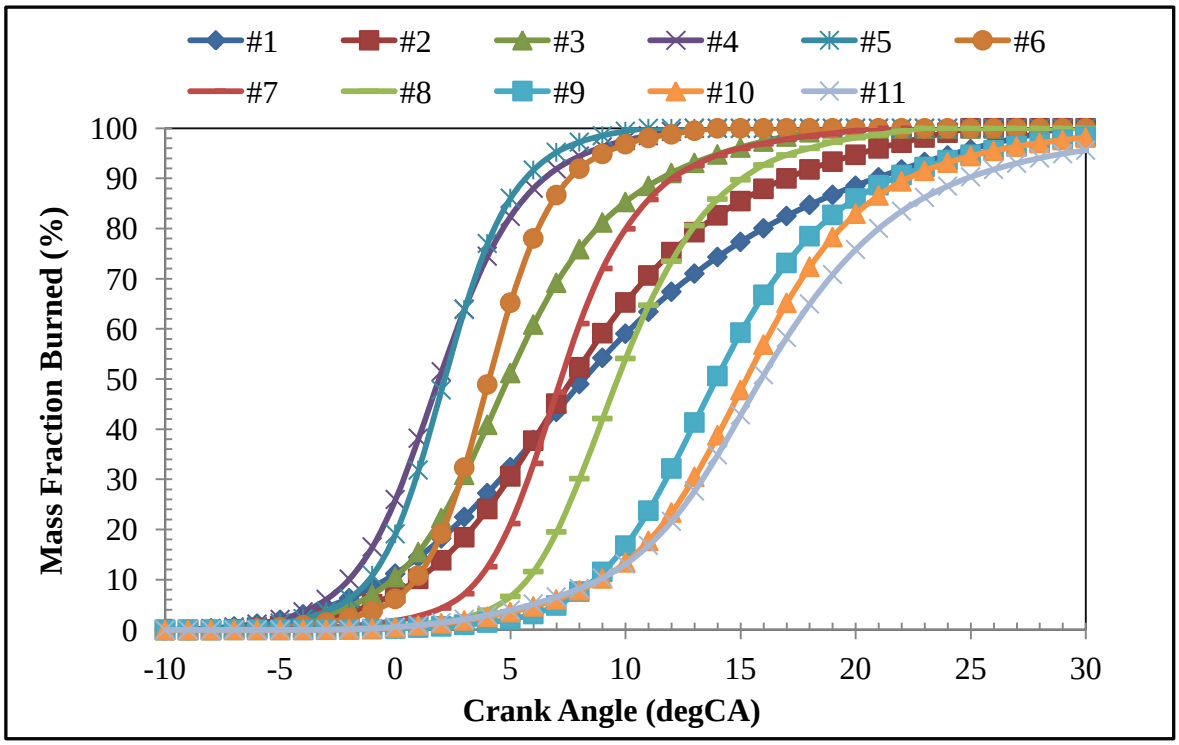


**(h) Mass-Fraction Burned**

**Figure 4.14. (ctd) Particulate Emission in 2-Stroke E15 CAI**

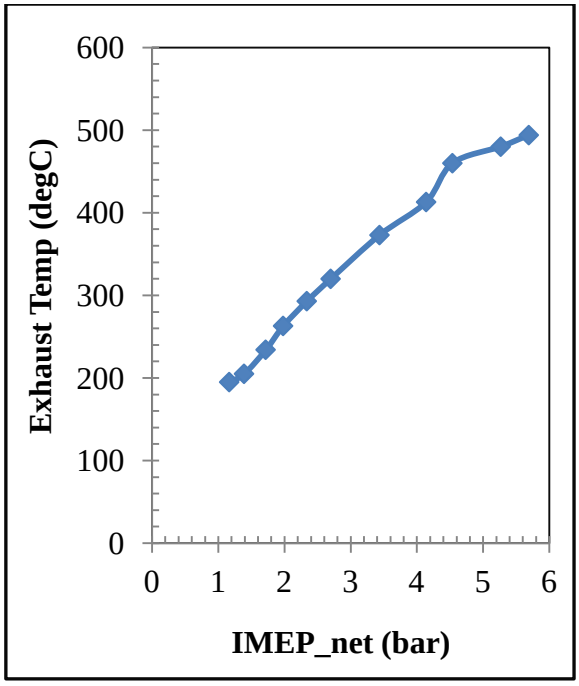


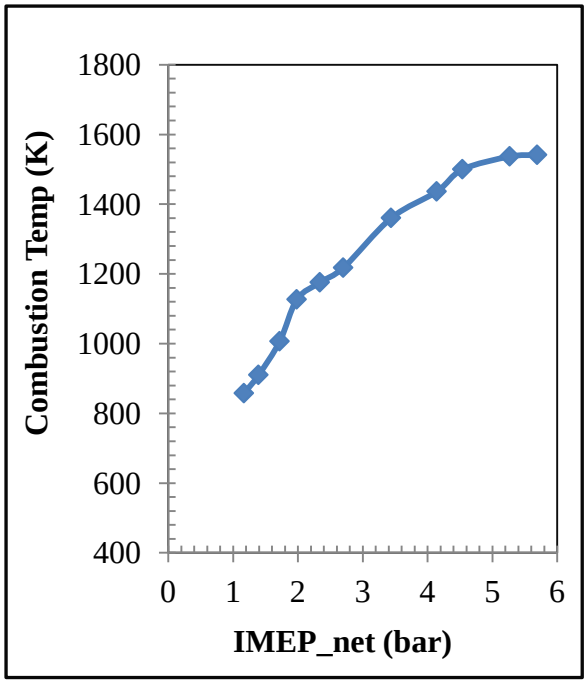


**(i) Exhaust Temperature** **(j) Combustion Temperature**

**Figure 4.14. (ctd) Particulate Emission in 2-Stroke E15 CAI**

### 4.8: Mode 7: 2-stroke Throttle SI

Figure 4.15 shows the particulate emissions from the 2-stroke throttled SI operation. The injection timing was maintained at -109deg BTDC, valve timing was set to IVO 125deg ATDC, IVC -125deg ATDC, EVO 115deg ATDC, and EVC -115deg ATDC and the lifts were maintained at 8.0mm.

The effects of varying Lambda on particulates are shown. As discussed previously, as the mixture is made leaner the peak remained at about 2nm in diameter, but the number of particulates drops rapidly. This can be explained from the process of soot formation, which is due to a locally fuel-rich mixture or even liquid fuel that can be present during the combustion process.

**Table 4.13 2-Stroke Throttled SI results**

| IMEP_net | Lambda | SparkTim | InjTiming | InjPulseW | IVO | IVC | IVL | EVO | EVC | EVL |
|---|---|---|---|---|---|---|---|---|---|---|
| bar | | degBTDC | degBTDC | ms | degATDC | degBTDC | mm | degATDC | degBTDC | mm |
| 4.43338 | 1.02946 | -21 | -109 | 1 | 125 | -125 | 8.06017 | 115 | -115 | 8.33814 |
| 2.92338 | 1.14623 | -23 | -109 | 1 | 125 | -125 | 8.05991 | 115 | -115 | 8.32454 |
| 3.05755 | 1.23202 | -22 | -109 | 1 | 124 | -123 | 8.04351 | 115 | -115 | 8.30892 |
| 3.17762 | 1.29411 | -20 | -109 | 1 | 124 | -123 | 8.04092 | 114 | -115 | 8.31014 |
| 3.43694 | 1.47537 | -17 | -109 | 1 | 124 | -122 | 8.03753 | 115 | -115 | 8.29457 |
| 3.50806 | 1.59473 | -18 | -109 | 1 | 124 | -123 | 8.06284 | 115 | -115 | 8.31496 |
| 3.64286 | 1.79584 | -21 | -109 | 1 | 124 | -123 | 8.04122 | 114 | -115 | 8.32147 |

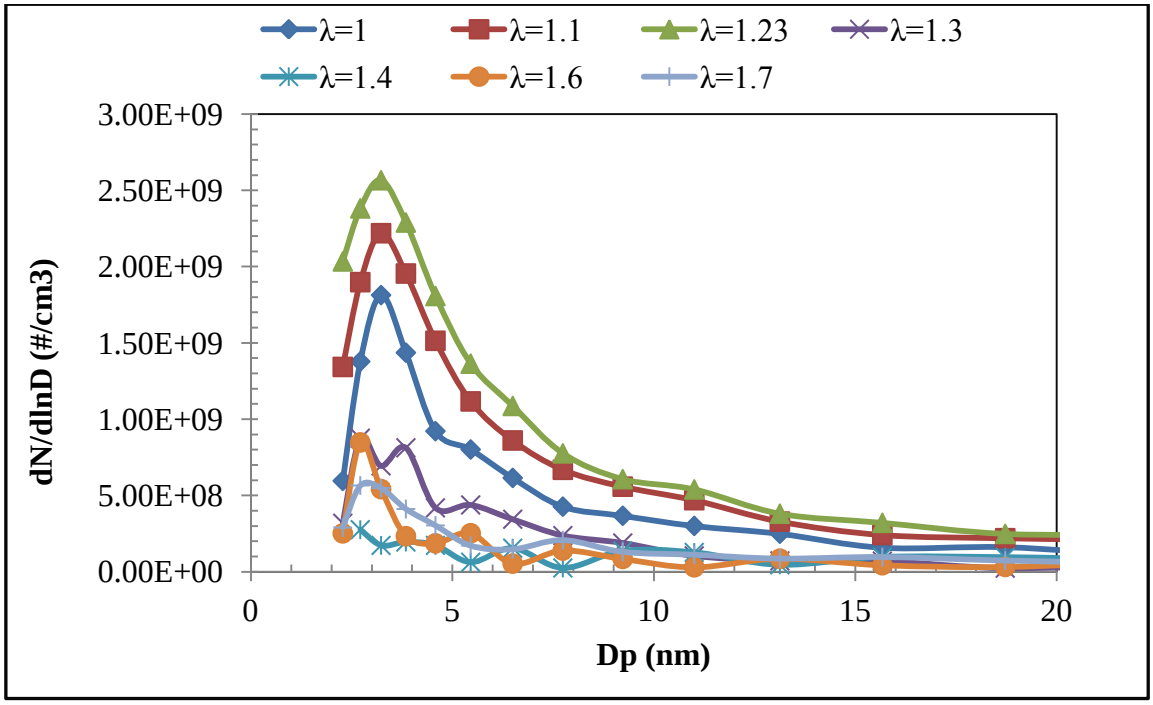


**(a) Particulate Number Emission**

**Figure 4.15. Particulate Emission in 2-Stroke Throttle SI**

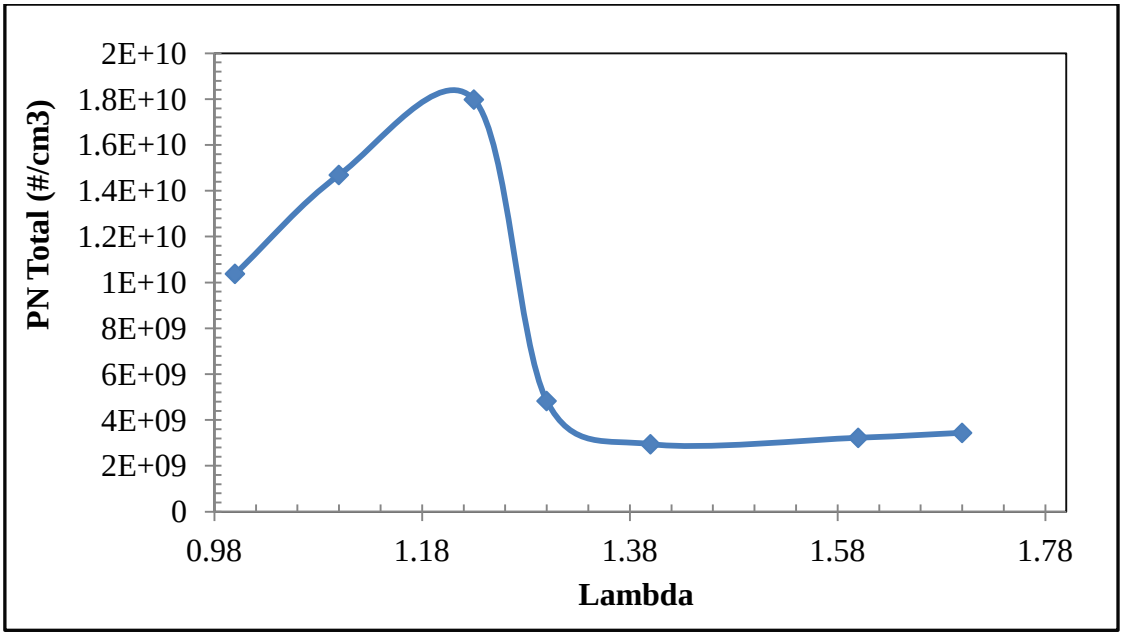


**(b) PN Total**

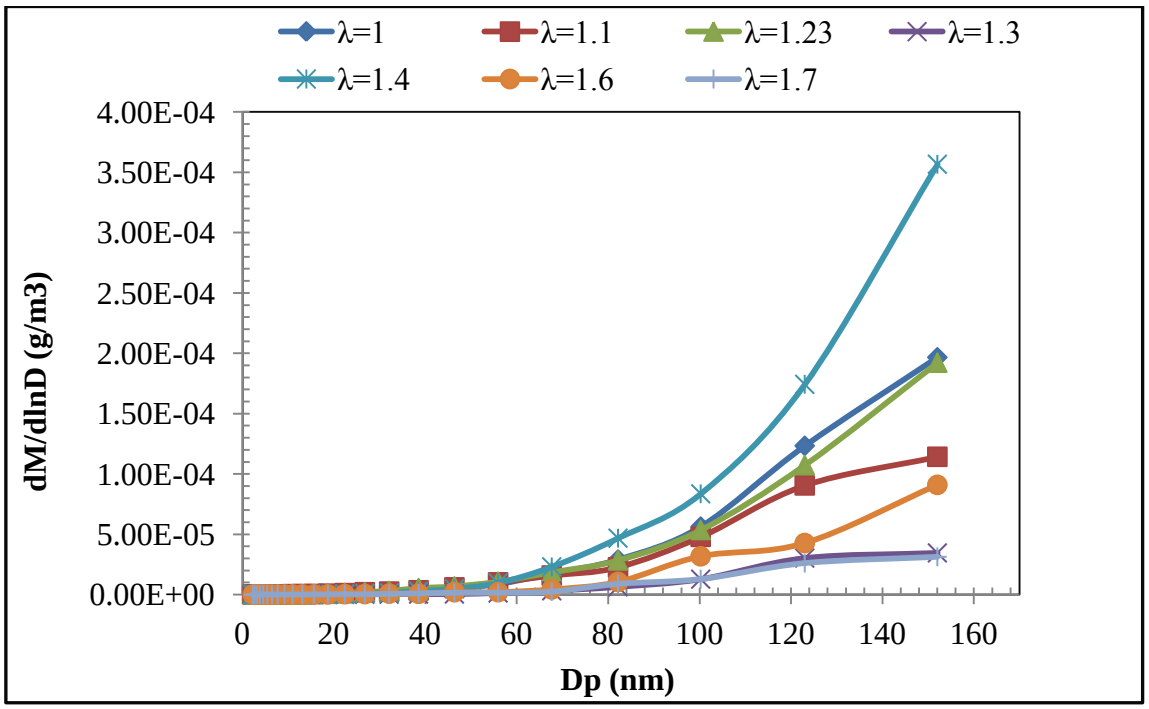


**(c) Particulate Mass Number**

**Figure 4.15. (ctd) Particulate Emission in 2-Stroke Throttle SI**

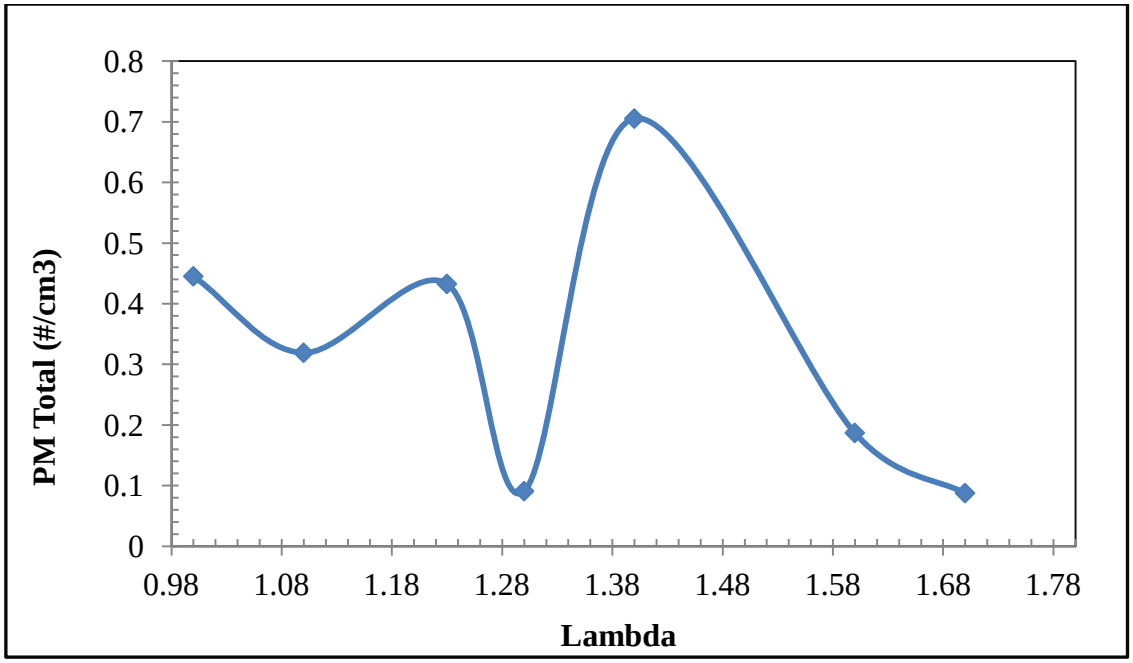


**(d) PM Total**

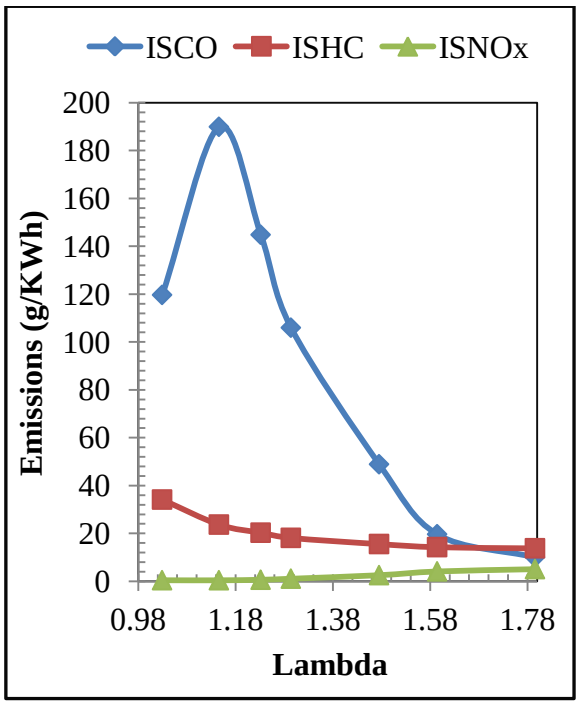


**(e ) Emission**

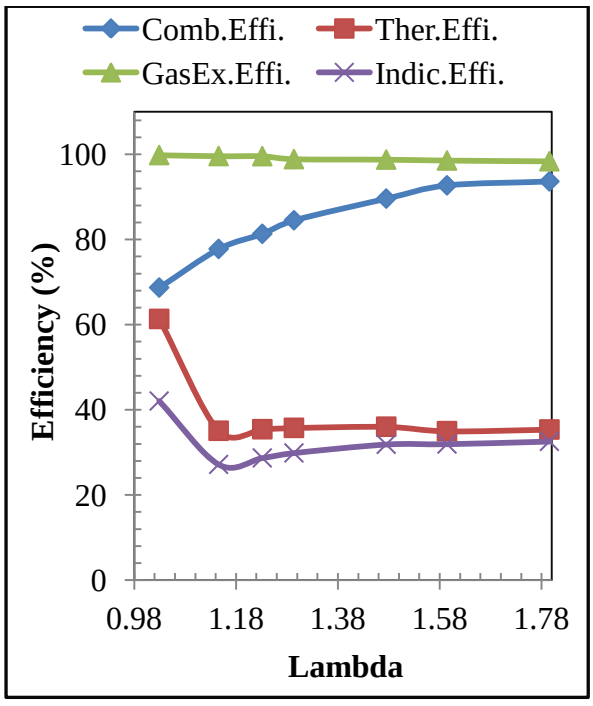


**(f) Efficiency**

**Figure 4.15. (ctd) Particulate Emission in 2-Stroke Throttle SI**

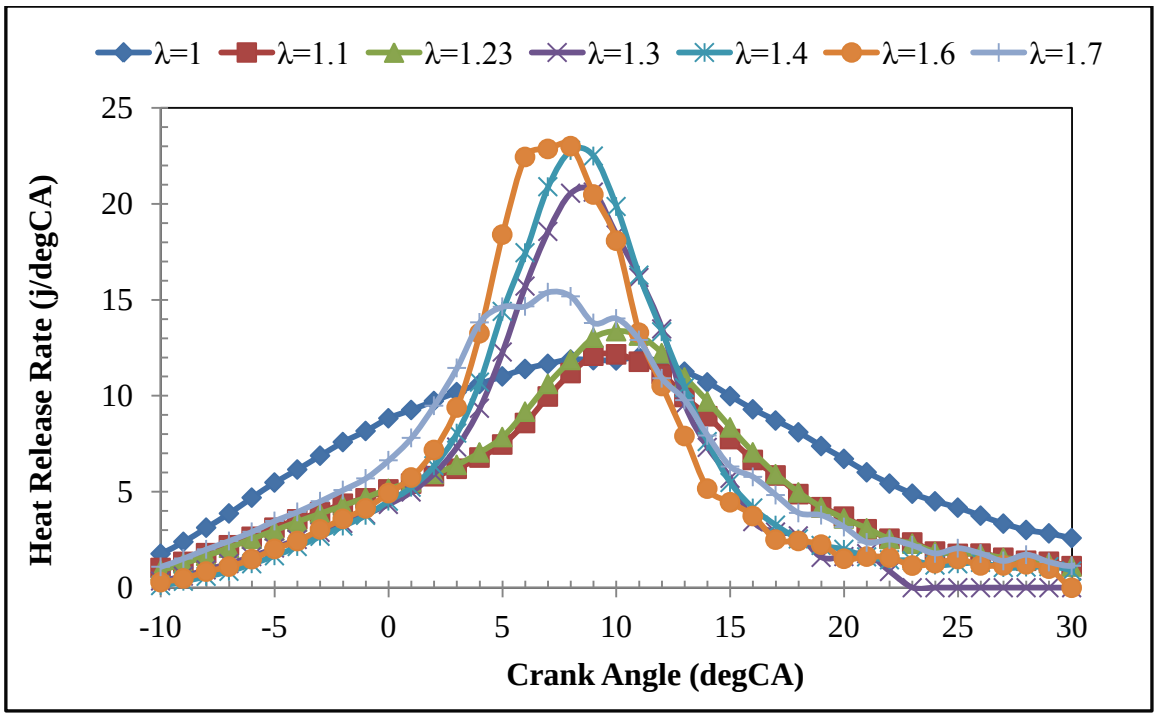


**(g) Heat-Release Rate**

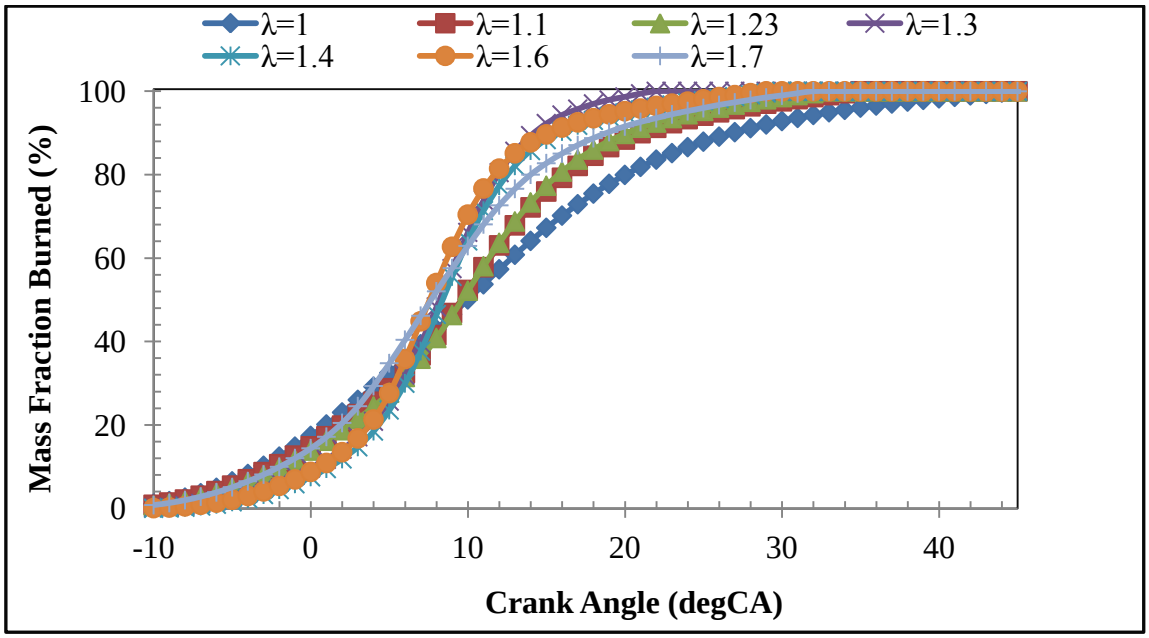


**(h) Mass-Fraction Burned**

**Figure 4.15. (ctd) Particulate Emission in 2-Stroke Throttle SI**

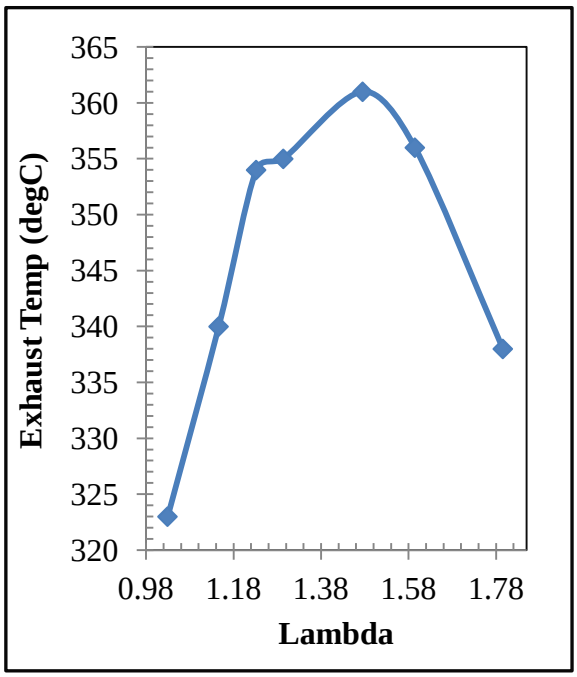


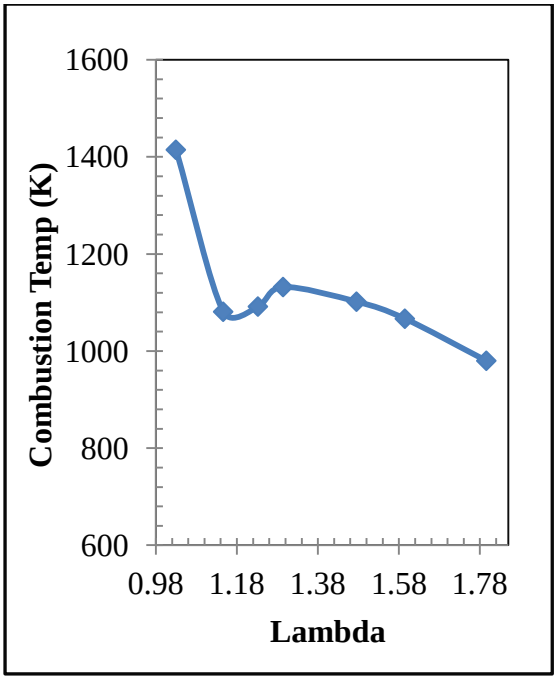


**(i) Exhaust Temperature** **(j) Combustion Temperature**

**Figure 4.15. (ctd) Particulate Emission in 2-Stroke Throttled SI**

## 4.9 Summary

In this chapter, particulate matter emissions in selected combustion modes were measured and analysed. The following observations were made:

1. The particle emissions from the DI gasoline engine are dominated by smaller particles.
2. The presence of ethanol tends to reduce the formation and emission of soot particles. The effect of ethanol content on soot reduction becomes very obvious, as particles are shifted to small-sized particles and a greater quantity of particulates is emitted, irrespective of the combustion modes.
3. The particle size distribution of gasoline combustion is normally characterised by a peak between 10nm to 30nm in diameter. The combusiton of ethanol and gasoline blends minimises the presence of soot particles in such peak regions.
4. The exhaust-particle size concentration and distribution is affected by the in-cylinder conditions at the time of injection and the subsequent mixture formation procees. Hotter charge and better mixing are the main parameters affecting the soot particles in the exhaust, irrespective of the combustion mode.

## Chapter 5 Analysis of Part-load Combustion, Performance and Emissions

### 5.1 Introduction

In this Chapter, the heat release and performance characteristics of Throttled SI, positive valve overlap (PVO) SI and CAI combustion, were investigated and compared at a typical 4-stroke part-load condition in the DI gasoline engine described in Chapter 3. The effect of such operating modes on the gaseous and particulate emissions were also analysed by means of an Electrostatic Mobility Spectrometer (EMS) based particle sizer and Horiba exhaust gas emission analyzers. In particular, the addition of ethanol on the particulate emissions was studied and compared for the three operating modes**.**

### 5.2 Engine Operating Conditions

Because of the flexibility of the camless system and engine control software, different engine operation modes could be achieved through variable valve timings and durations. Figure 5.1 shows the valve timings and injection timings used in the 4-stroke mode operations in this study. In order to compare the results in different operation modes, the engine was operated at a typical condition of 1500rpm and 3.2 bar IMEPnet. The ignition timing was set at MBT for each fuel. The three operational modes investigated in this chapter was similar to that in chapter 4. In this chapter the load was maintained constant at MBT spark timing.

**Mode 1: 4-Stroke Throttle-Controlled SI Mode**

This similar to chapter 4 but speed and load was fixed at 1500rpm and 3,2 bar IMEPnet.

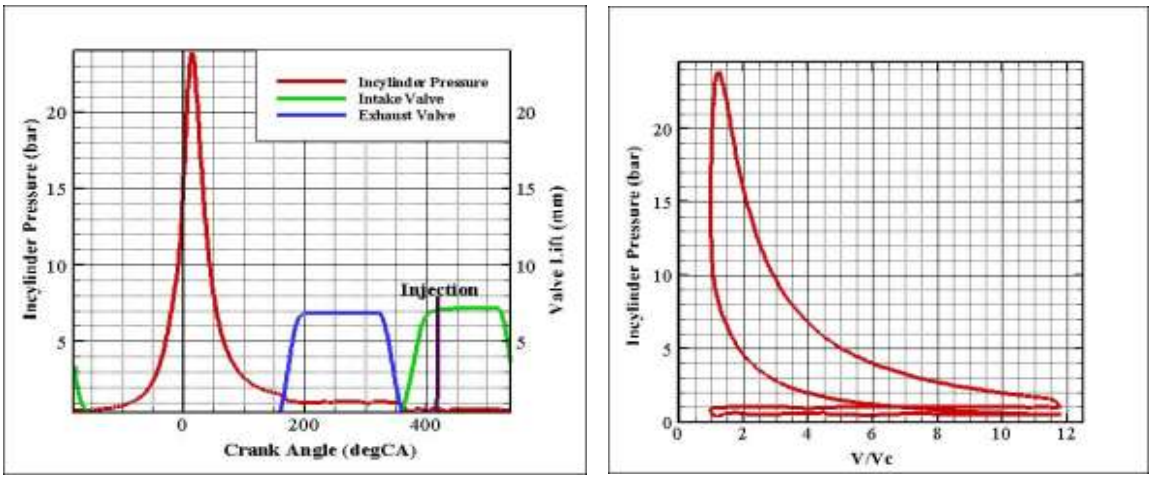


**(a) 4-Stroke throttled SI valve timing and P-V diagram**

**Figure 5.1 Valve Timings and Injection Timings for the 3 Operation Modes**

**Mode 2: 4-Stroke Positive Valve Overlap SI Mode**.

This similar to Chapter 4 the speed was maintained at 1500rpm and the intake and exhaust-valve lift reduced to 3mm because of the part load operation.

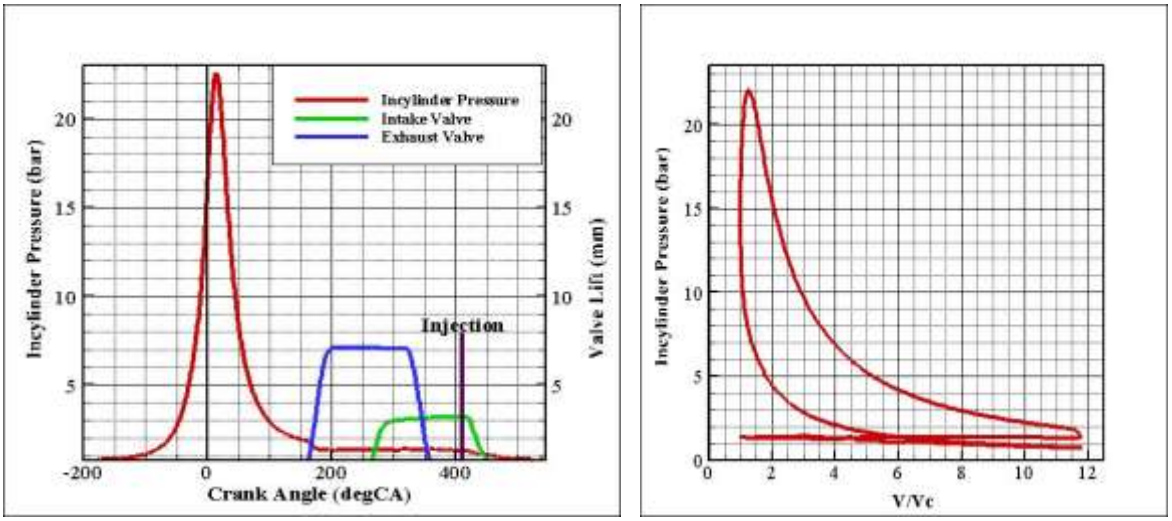


**(b) 4-Stroke Positive Valve Overlap valve timing and P-V diagram**

**Figure 5.1 (ctd) Valve Timings and Injection Timings for the 3 Operation Modes**

**Mode 3: 4-Stroke Negative Valve Overlap CAI Mode**

In this investigation the valve lifts were reduced to 5mm and the speed maintained at1500rpm. The load was maintained at 3.2bar IMEP_net.

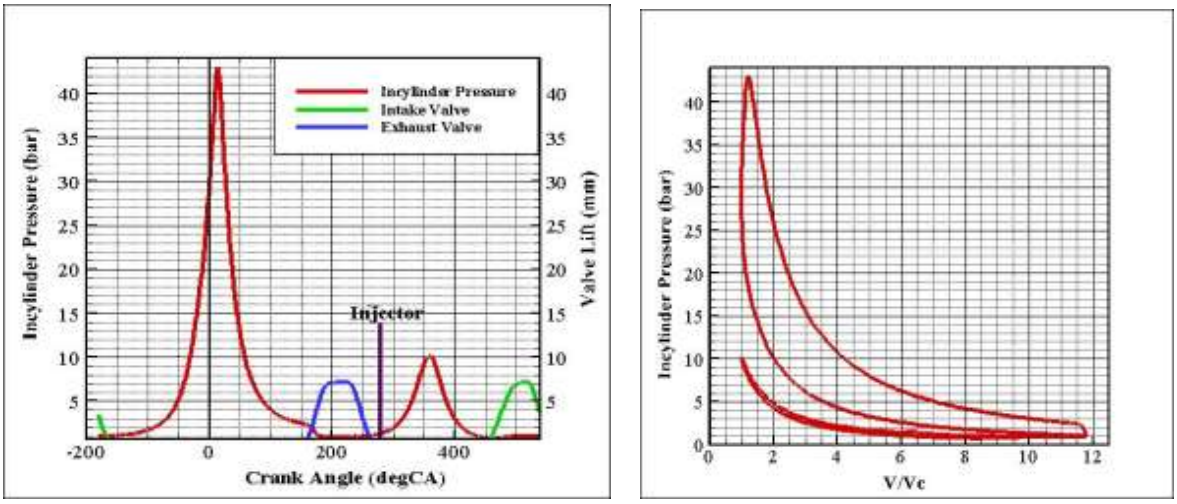


**(c) CAI Negative Valve Overlap valve timing and P-V diagram**

**Figure 5.1 (ctd) Valve Timings and Injection Timings for the 3 Operation Modes**

### 5.3 Gasoline SI and CAI Combustion

In order to compare the results in different operation modes, the engine was operated at a typical condition of 1500rpm and 3.2 bar IMEPnet. The ignition timing was set at MBT for each fuel. The 3.2 bar IMEPnet was used because it is equivalent to that generated in a comparable multi-cylinder production engine at a reference brake load of 2.62bar BMEP (a popular mapping point used by many vehicle OEMs). The oil and coolant temperature were held at 80 degree celsius. In investigating the effect of air to fuel ratios, the experiment was performed using pure gasoline (E0) at different engine operational modes with lambda 1.0, 1.1, and 1.2.

The particle size distribution and the effect of ethanol in reducing particle number (PN) from different combustion modes were analysed and displayed with the x-axis as the particle diameters, equally spaced on a log scale from 2.5nm up to 500nm, and the PN concentration on the y-axis as dN/dlnD (#/$cm^3$).

#### 5.3.1 Combustion Analysis

Figure 5.2 shows and compares the combustion characteristics of the three operation modes with different lambda values using pure gasoline (E0). It should be noted that in the throttled SI combustion the throttle was partly opened, the PVO SI while for the CAI NVO combustion modes were operated with wide open throttle (WOT).

Figure 5.2(a) shows the maximum pressure-rise rate (MPRR) as a function of lambda, which affects combustion noise in both CAI and SI combustion. It can be seen that the maximum pressure rise rate for CAI was about 10 times higher than SI in the knocking region at lambda 1.0. Although CAI combustion could be realized without spark ignition using the NVO method, it was found that spark ignition could affect the timing of the main heat release reactions, in particular in leaner mixtures. The retarded spark timing used in CAI combustion helped to reduce the peak cylinder pressure by about 40%, but the maximum in-cylinder pressure was 75% higher than in the throttled SI and PVO SI engine operation at the same load.

As shown in Figure 5.2(b), the MBT spark timings were more advanced in the PVO SI mode than the throttled SI mode because of slower flame speed of diluted mixture with internal EGR.

The heat release rate in Figure 5.2(c) and the corresponding mass burned fraction curves in Figure 5.2(d) show that the main CAI combustion takes place earlier than in the other two modes and it is slightly retarded with the leaner mixture. Although the CAI operation starts later than the other two modes, (Figure 5.2c) it is much faster than the PVO SI and throttled SI combustion, due to the simultaneous burning of the in-cylinder mixture during the CAI combustion process. Of all three modes, the PVO SI mode was characterized by the longest combustion duration.

The coefficient of variation in IMEP (COVimep) is used to measure the combustion stability and cycle-to-cycle variability of the engine operation. As shown in Fig. 5.2(e), the COVimep for all modes were below 3.0 % and did not vary significantly with the lambda and combustion modes studied.

As shown in Figure 5.2(f), the throttled SI and PVO SI operations are characterized by higher exhaust temperature at all lambda values. In particular, it is noted that the CAI combustion reduced exhaust temperature by about 130 $^{o}$C. This is due to early and fast combustion as well as heavy dilution with residual gas.

Figure 5.2(g) shows that crank angles of 10% MFB were earlier for PVO SI and throttled SI with CAI combustion being the fastest with increasing lambda values. This is also reflected by 50% MFB crank angles shown in Figure 5.2(h). As shown in Figure 5.2(i) and (j), CAI combustion processes were characterized by shorter combustion duration even though the mixture was highly diluted, because of the simultaneous burning of mixtures. With PVO, the internal EGR resulted in the slower combustion speed.

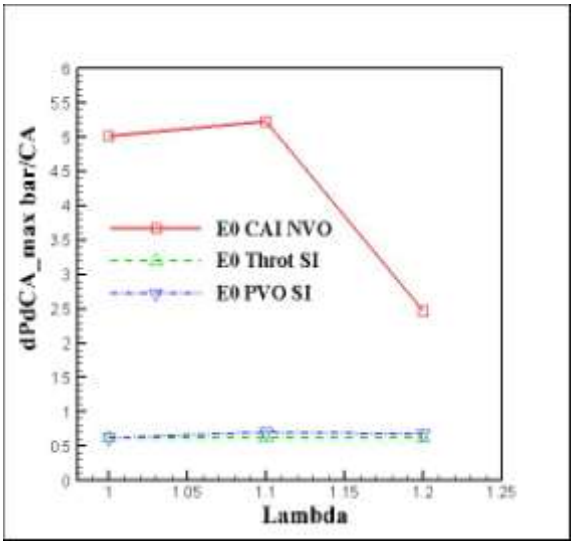


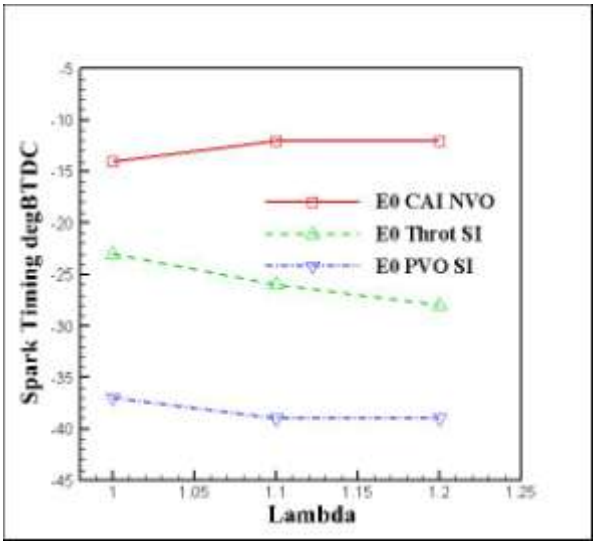


**(a) Maximum Pressure Rise Rate** **(b) MBT Spark Timing**

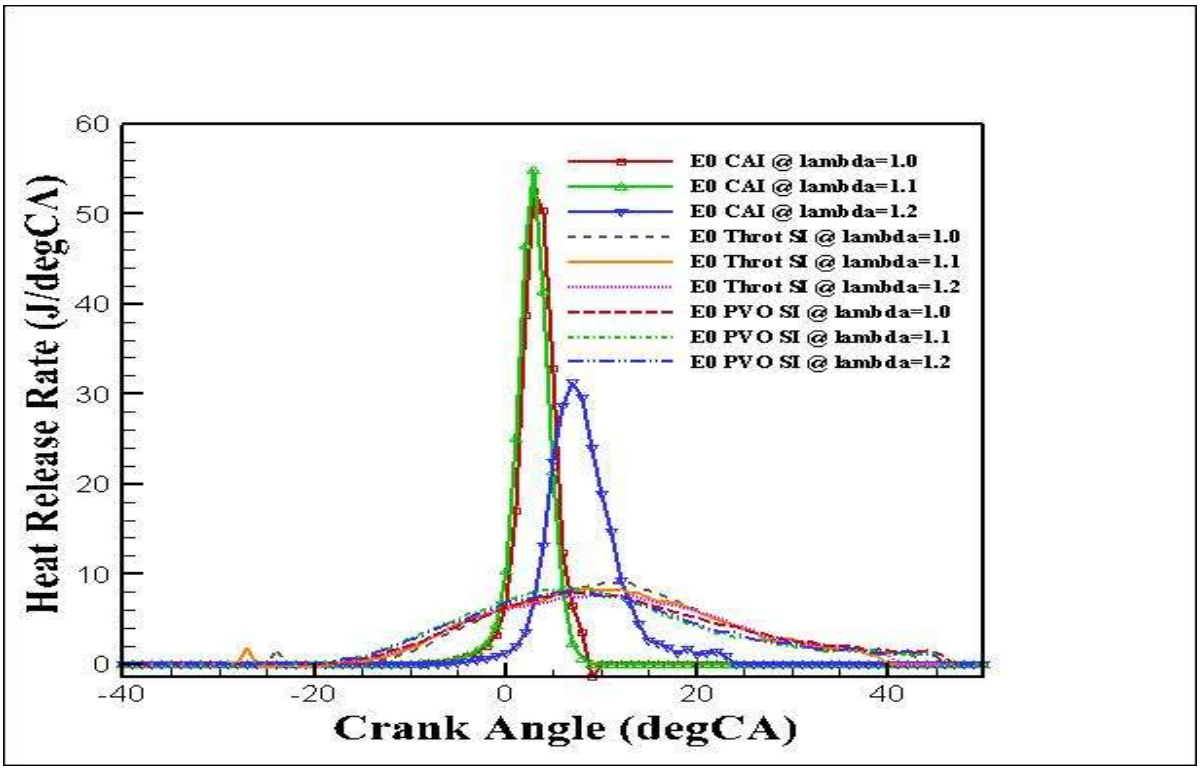


**(c) Heat Release Rate**

**Figure 5.2 Combustion Analysis**

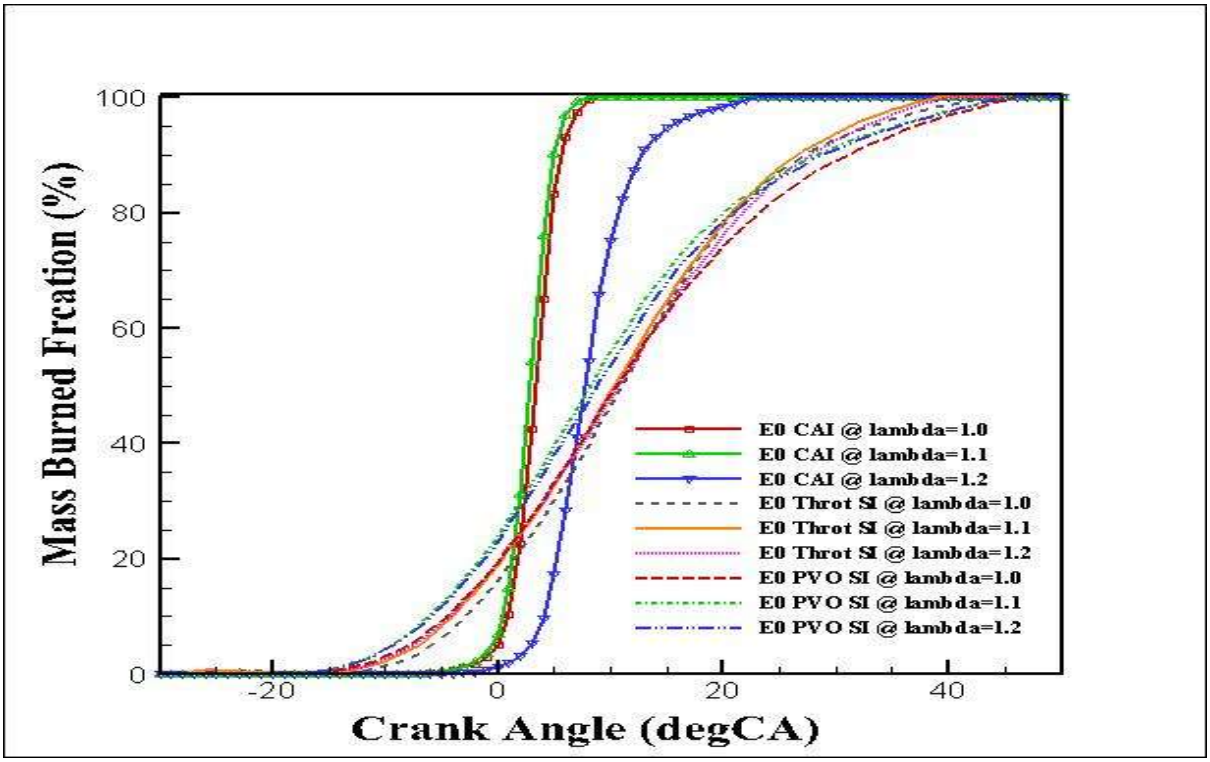


**(d) Mass Burned Fraction**

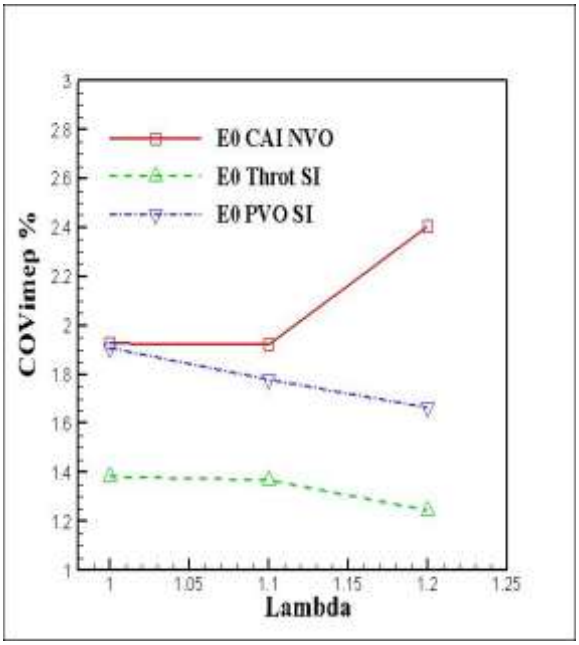


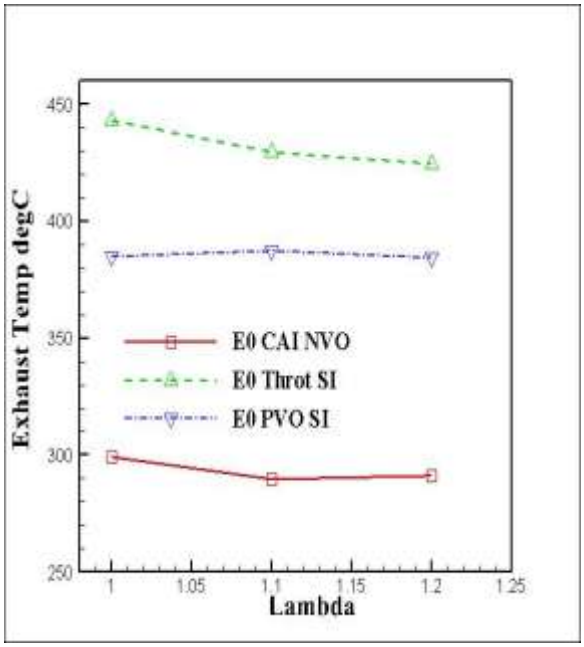


**(e) COV of IMEP** **(f) Exhaust Temperature**

**Fig. 5.2. (ctd) Combustion Analysis**

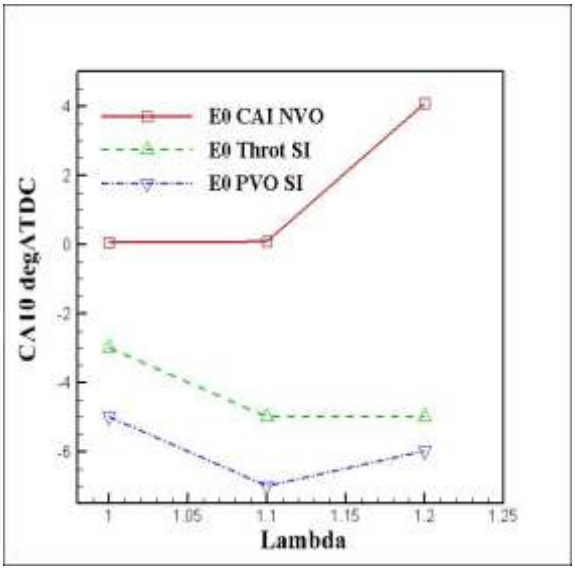


**(g) CA10**

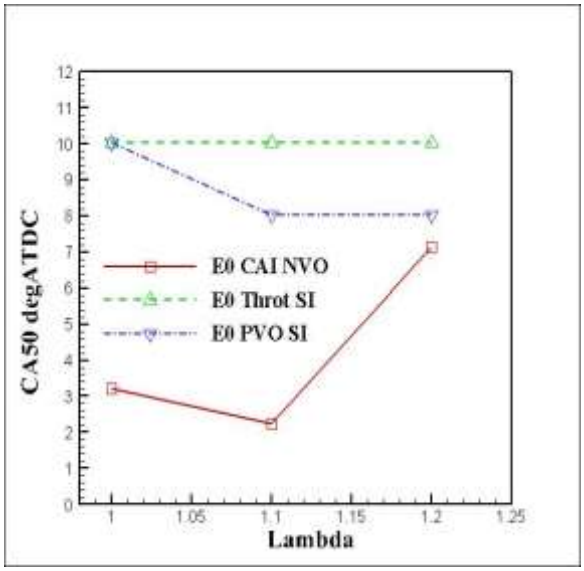


**(h) CA50**

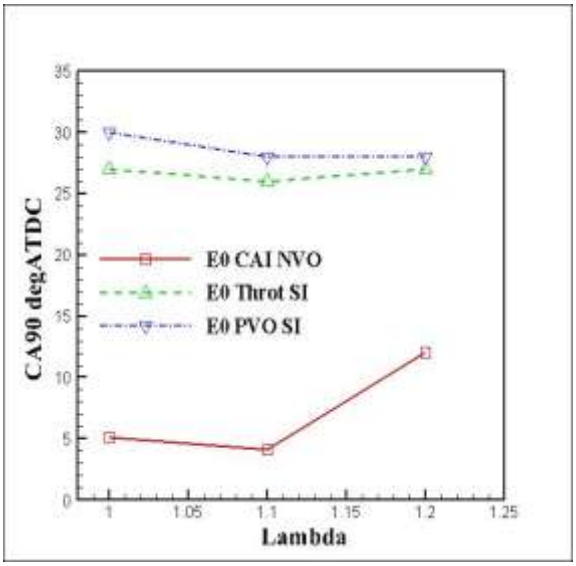


**(i) CA90**

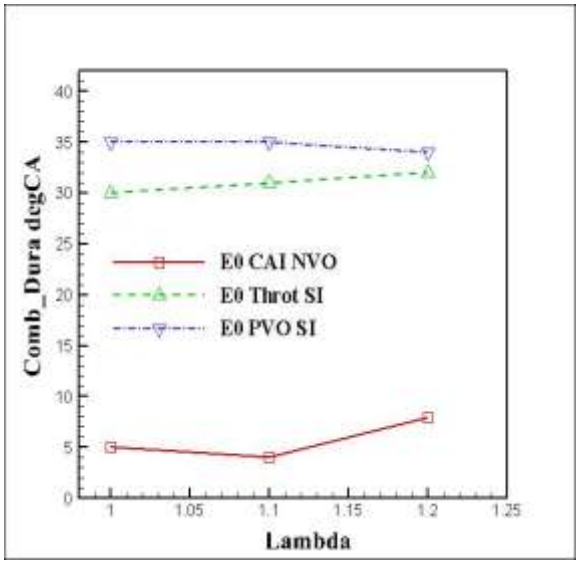


**(j) Combustion Duration**

**Figure 5.2. (ctd) Combustion Analysis**

### 5.3.2 Engine Performance and Efficiency Analysis

The combustion efficiency is the ratio of heat liberated (QhrMEP) to the theoretical heat in the fuel (FuelMEP). The amount of heat liberated is less than the theoretical value because of incomplete combustion resulting in UHC and CO emissions. Therefore, the combustion efficiency can be calculated from the exhaust gas analysis as:

$$\eta_{comb} = \left(1 - \frac{(G_{CO} * 10.1 + G_{HC} * 43)}{(Fuel\ Flow\ rate * LHV)}\right) \quad (5.1)$$

Where G_CO is the CO emission mass flow rate, G_HC is the HC emission mass flow rate, and LHV the Low heating value of the fuel.

Figure 5.3(a) shows the combustion efficiency in throttled SI, PVO SI and CAI combustion modes. It can be seen that the combustion efficiency in the PVO SI is 89% with lambda 1.0 and increasing to 94% with lambda 1.2. This could be the result of the interaction of fuel injection and gas exchange process. The gas exchange process started at IVC and it is characterised by the reversed flow of hot burned gas into the intake port during the positive overlap period around TDC. Fuel injection took place soon after the EVC, during which the exhaust gas in the intake port flowed back into the cylinder together with air. As a result, fuel was injected into the hot incoming mixture. The enhanced evaporation of gasoline fuel led to fewer fuel-rich regions in the combustion process.

The theoretical thermal efficiency of the engine is shown in Figure 5.3(b), which defines the upper limit of the efficiency obtainable from the complete combustion and is calculated from the ratio of IMEPgross to the heat liberated (QhrMEP) as follows:

$$\eta_{therm} = \left(\frac{IMEP_{gross}}{Q_{hr}MEP}\right) \quad \textbf{(5.2)}$$

Where

$$\boldsymbol{Q_{hr}MEP} = \left(\frac{\textbf{Fuel Flow Rate}\times\textbf{LHV}}{V_s\times\textbf{Combustion Efficiency}}\right) \quad \textbf{(5.3)}$$

$$\boldsymbol{IMEP_{gross}} = \int_{-180}^{180} \frac{P}{Vs}\dot{V}(\varphi)d\varphi \quad \textbf{(5.4)}$$

Where $V_{s,}$ is the displacement of the engine.

The throttled SI and CAI NVO have average thermal efficiencies of 41% for all lambda values. The PVO SI mode exhibits the highest theoretical thermal efficiency of 43% with lambda 1.0 and 1.2 and 45% with lambda 1.1, athough the combustion process was characterised by the longest combustion duration.

The gas exchange efficiency in Figure 5.3(c) shows that the PVO SI has an average of 91% efficiency. CAI combustion has the highest gas exchange efficiency of 91% with lambda 1.0 and it increases linearly with the leaner mixture to 96.6% with lambda 1.2. The throttle SI has the lowest gas exchange efficiency 86.6%, the reason for the largest pumping loss seen in Figure 5.3 (f).

The net indicated engine efficiency ($\eta_{ind}$) represents how efficiently the fuel energy is converted into the net indicated work. It takes into account the effects of combustion duration and phasing, combustion and thermal efficiency as well as the pumping work of the cycle. It is calculated from the ratio of the net work of the cycle to the theoretical heat in the fuel (FuelMEP) as follows:

$$\boldsymbol{\eta_{ind} = \left(\frac{IMEPnet}{m_f Q_{LHV}}\right)} \quad \textbf{(5.5)}$$

Where

$$\boldsymbol{IMEP_{net} = \int_{-180}^{540} \frac{P}{Vs} \dot{V}(\varphi) d\varphi} \quad \textbf{(5.6)}$$

$m_f$ = Fuel Flow rate

$Q_{LHV}$ = Lower Heating Value of Fuel

Figure 5.3(d) compares the net indicated efficiency of the PVO SI, throttled SI and CAI modes for the lambda sweep of 1 to 1.20. The figure shows average indicated efficiency of 37% in the PVO SI, 33.7% in the throttled SI and 36.7% in CAI combustion. The indicated efficiency is similar for PVO SI and CAI combustion with lambda 1.0 and 1.2, except with lambda 1.1 where PVO SI has a 1.4% improvement over CAI combustion.

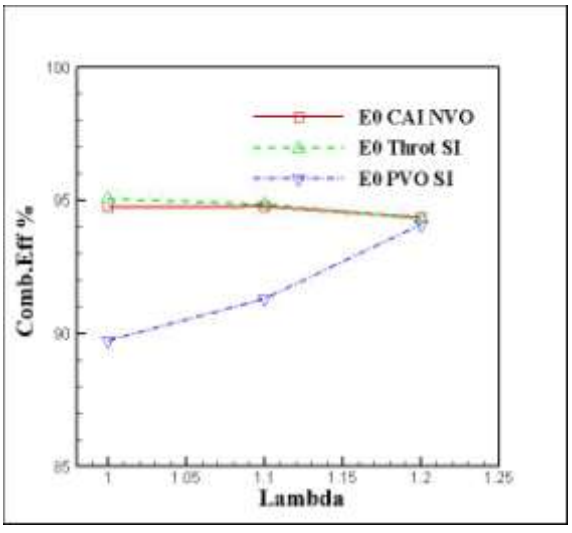


**(a) Combustion Efficiency**

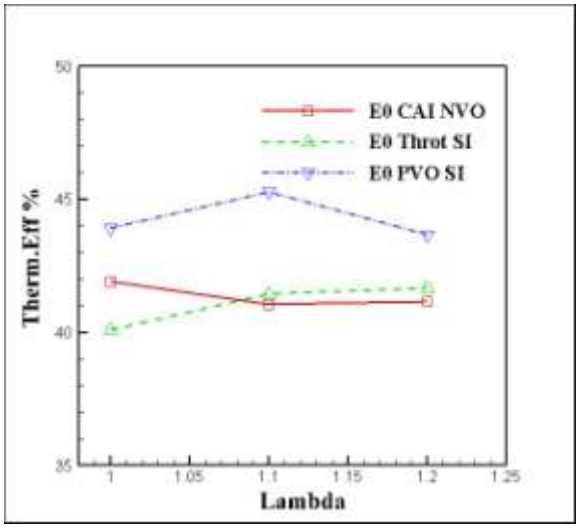


**(b) Thermal Efficiency**

**Figure 5.3 Performance Analysis**

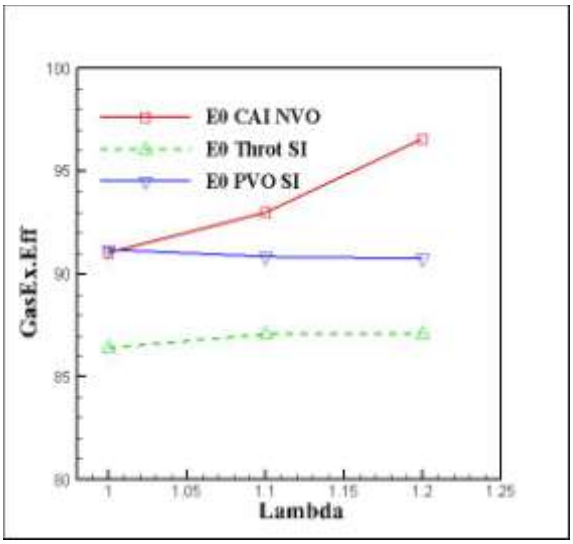


**(c) Gas Exchange Efficiency**

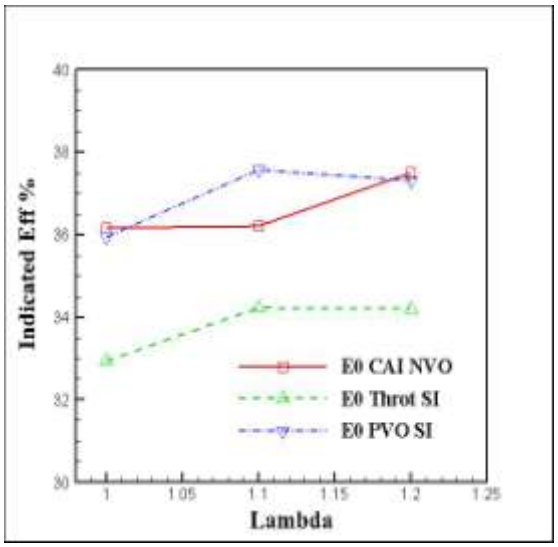


**(d) Indicated Efficiency**

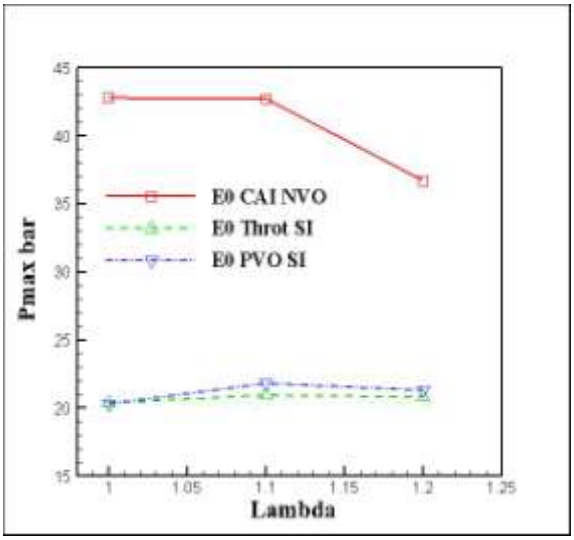


**(e) Maximum Cylinder Pressure**

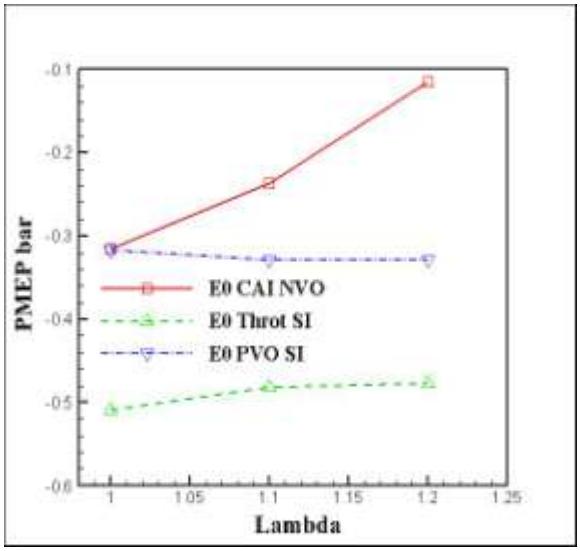


**(f) Pumping Mean Effective Pressure**

**Figure 5.3 (contd) Performance Analysis**

### 5.3.3 Emissions and Fuel Consumption

All gaseous emissions were measured and converted into the indicated specific values (g/KWh). Figure 5.4(a) shows the CO emissions from the throttled SI, PVO SI and CAI combustion at 3 different lambda values. As seen in Figure 5.4(a), the ISCO emission is higher in the PVO SI mode than the throttled SI and CAI combustion and it decreases with increasing lambda, reaching a minimum with lambda=1.2. For throttled SI and CAI

combustion the CO emission is about 50% lower than in PVO SI with lambda 1.0. With lambda 1.1, the ISCO for CAI is same level as that in PVO SI. As the lambda value is further increased to 1.2, there is about a 16% improvement on CO emissions of PVO SI over CAI combustion. Figure 5.4(b) shows the results for ISHC emission for the three modes of operations. The PVO SI operation doubles the amount of ISHC emissions compared to throttled SI and CAI combustions at lambda 1.0 and decreasing to same value with lambda 1.2.

The higher CO and HC emissions results suggest that there are more locally rich mixtures formed in the PVO SI mode with lambda 1.0 and 1.1. In the case of CAI combustion, fuel was injected into hot residual gas during the negative valve overlap period and hence could evaporate quickly and had more time to mix with air. However, the interaction of fuel injection and intake air flow during the PVO SI mode could have caused more fuel impingement on the piston and is the likely reason for higher ISCO and ISHC emissions.

Figure 5.4(c) shows the NOx emissions in the three combustion modes. It can be seen that the NOx emission for PVO SI and throttled SI are around 8-13g/KWh and the CAI combustion is about 10 times less at about 1g/KWh. The NOx formation depends strongly on the combustion temperature. As the combustion temperature increases above $1500^{o}$C, NOx formation rates increase rapidly. The formation of NOx is also dependent on the combustion duration at elevated temperatures. In CAI combustion, the peak combustion temperature and duration are much reduced due to the high dilution ratio and the simultaneous burning of autoignited mixture, resulting in the ultra-low NOx emission seen in Figure 5.4(c). The earlier completion of combustion leads to the lower exhaust temperature in Figure 5.2(f) as a result of a longer effective expansion process.

The CAI NVO and PVO SI were operated with wide-open throttle (WOT) and throttled SI at part-open throttle. As shown in Figure 5.4(e), the PVO SI and CAI NVO combustion results in a 9% improvement in fuel consumption with lambda 1.0 and 1.2 over throttled SI. In addition with lambda 1.1 the PVO SI shows a 4.5% improvement in ISFC over CAI combustion.

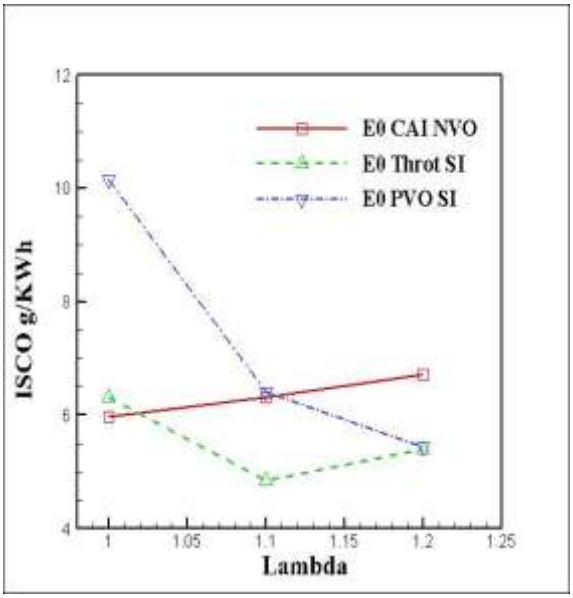


**(a) ISCO**

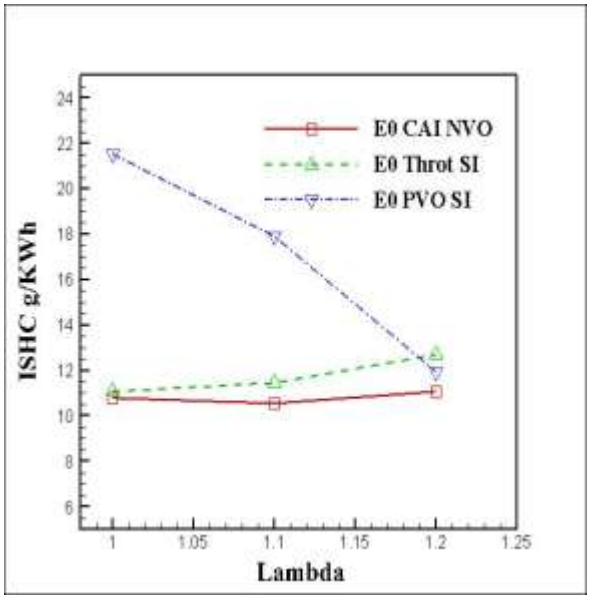


**(b) ISHC**

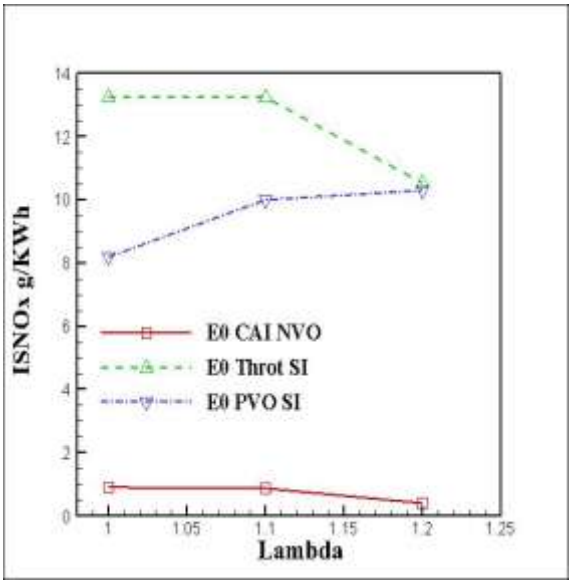


**(d) ISNOx**

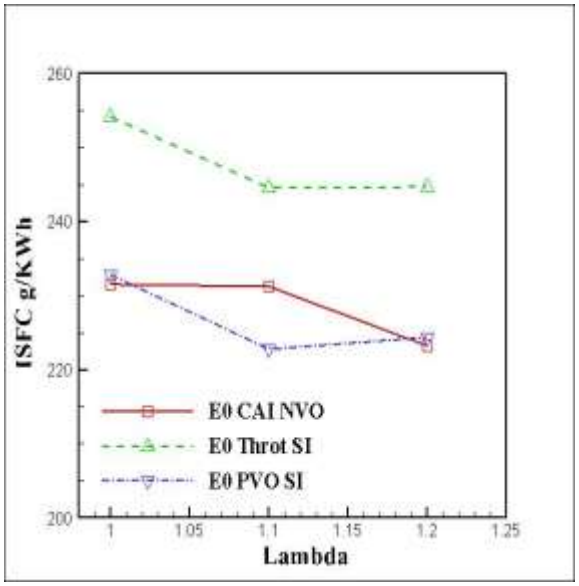


**(e) ISFC**

**Figure 5.4 (ctd) Emissions and Fuel Consumption**

### Particulate Emission

The particulate emissions were measured and analyzed in number and their size distributions. It can be seen from Figure 5.5(a) and Figure 5.5(b), with lambda 1.0, 1.1, and 1.2, the CAI mode is characterized by the greatest number of particles in total, while the PVO SI showed the least number of particles. For all cases examined, the particles are dominated by small

particles in the range of 20nm, which are typically associated with soot particles in the nucleation mode.

There are two plausible causes to the production of soot particles in greater numbers in the CAI combustion mode. In the case of CAI operation, fuel was injected into the hot burned gas at high temperatures but with little oxygen. This causes hydrocarbons in gasoline to undergo thermochemical decomposition at elevated temperatures without the participation of oxygen, known as pyrolysis, in which soot particles could be produced. Although most of such soot particles would have been oxidized during the combustion process, the lower combustion temperature in CAI mode rendered the soot oxidation process less effective.

In the PVO SI and throttled SI operation, fuel was injected into air and residual gas at much lower temperature, there is enough oxygen present to improve oxidation, this mixture preparation does not favour pyrolysis, this may be the likely causes of reduced particulate emissions in this mode compared to the Throttled SI and CAI combustion. The particles emitted as detected in the exhaust were likely to be liquid condensates, as indicated by their much smaller particle sizes. The same reason given in chapter 4 for particulate emission in CAI combustion when injecting fuel during late exhaust stroke in NVO is also responsible for the higher particulate emissions observed here.

In addition to the soot particles, there was a significant number of very small particles as small as 5nm in diameter. Such particles are typically liquid fuel condensates in the exhaust.

Furthermore, due to the reduced fuel-rich combustion the leaner mixture helped reduce the particle emissions of all sizes in all three combustion modes, except for a small range of particle sizes in the throttled SI engine where lambda 1.1 mixture caused a rise in particle emissions.

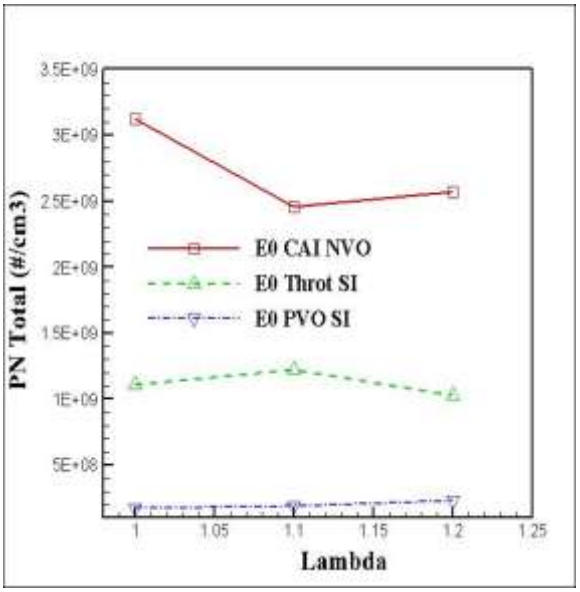


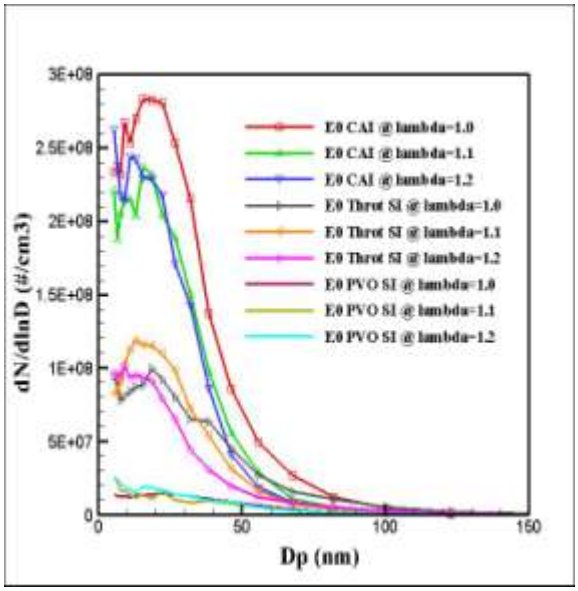


**(a) PN Total** **(b) PN Emission**

**Figure 5.5 PN Total and PN Emission**

**Summary**

Of all three operational modes at 3.2bar IMEP load condition, CAI and PVO SI operations had the lowest fuel consumption and highest indicated engine efficiency with lambda 1 and 1.2 mainly due to reduced pumping loss. In addition, the fastest heat release rate of CAI combustion further increases the thermodynamic efficiency. PVO SI and CAI NVO operations resulted in a 9% improvement in fuel consumption over the throttled SI operation at lambda 1.0 and 1.2. At lambda 1.1 PVO SI showed a further 4.5% improvement in ISFC over CAI combustion, because of better combustion timing.

The engine-out ISCO and ISHC emissions of the PVO operation decreased linearly with leaner mixtures and was about 50% higher than those of the throttled SI and CAI combustions at lambda 1, which was because of the poorer air and fuel mixing in the presence of the recycled exhaust gas flowing back into the cylinder .

The particle size distribution was characterised with a peak between 15nm to 20nm in diameter, indicating the presence of nucleation mode particles. The leaner mixture helped to reduce the total particle emissions for all combustion modes.

The fuel injection during the NVO period was assumed to lead to the production of soot particles (<50nm in size) in the CAI combustion mode due to hydrocarbon pyrolysis. The soot oxidation was rendered less effective by the lower combustion temperature.

Less and smaller particles were detected from the PVO SI and throttled SI combustion. Most particles were in the range of a few nanometers related to the unburned hydrocarbons.

However, there is still window of improvement on all three combustion modes by optimising the injection strategy, combustion chamber design, as well as the valve timing and duration used.

### 5.4 Heat Release Analysis and Emission Results with E15

In order to study the effect of ethanol, the engine was operated with E15 at the same speed and load condition under the three combustion modes.

#### 5.4.1 Combustion Analysis

Figure 5.6(a) shows the maximum pressure-rise rate in E15 as a function of lambda for both CAI and SI operations. Compared with gasoline, E15 resulted in a noticeable reduction in the pressure-rise rate from 5 to 1.1bar/CA during CAI combustion, about 1.6 times the value in SI combustion. In addition, figure 5.6(b) shows clearly that the increasing value of lambda did not affect ignition timing in CAI combustion, rather it increased the burn duration. Similarly, in the PVO SI mode, the spark timing was slightly retarded with lambda 1.1 and remained at this value with lambda 1.2. In contrast the throttled SI operation was continuously advanced as the lambda value increased from 1.0 to 1.2.As shown in Figure 5.6(b), the MBT spark timings were more advanced in the PVO SI mode than the throttled SI mode due to slower burning velocities as evidenced by the heat-release rate curves in Figure 5.6(c) and the corresponding mass fraction burned curves in Figure 5.6(d). The CAI NVO operations were characterized by the fastest combustion because of multiple auto-ignition sites. Furthermore, E15 blend enabled a reduction in the heat-release rate and combustion phase-shift in the CAI NVO operation.

As shown in Figure 5.6(e), the COVimeps for all modes were below 3.0 % and did not vary significantly with the fuel blends and combustion modes studied but showed a similar trend in the three modes and lambda values.

As shown in Figure 5.6(f), there was an increase in E15 exhaust temperature over E0 in the three modes, possibly due to the spark retard. For similar reason, the E15 exhaust temperatures for throttled SI and PVO SI operations were 100 $^{o}$C and 60 $^{o}$C higher than CAI NVO. In particular, CAI reduced exhaust temperature by about 110 $^{o}$C. This is due to early and fast combustion as well as heavy dilution by residual gas.

Figure 5.6(g) shows that the overall combustion period tended to increase from the throttled SI to PVO whilst the CAI combustion was the shortest. In the case of PVO SI, the slower burning process was likely to have been caused by decreased turbulence and lower end of compression temperatures. The CAI combustion process was characterized by shorter combustion duration Figure 5.6(j) despite the mixture being highly diluted through the simultaneous burning of mixtures.

The effect of ethanol on combustion was mode-dependent and did not show any consistent trend except for the CAI combustion.

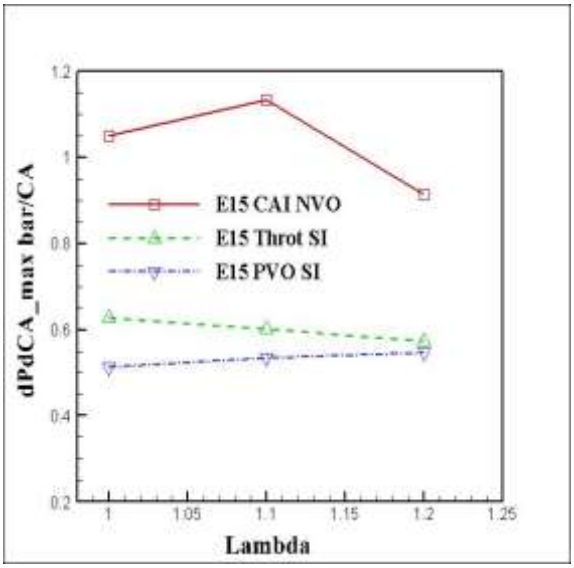


**(a) Maximum Pressure Rise rate**

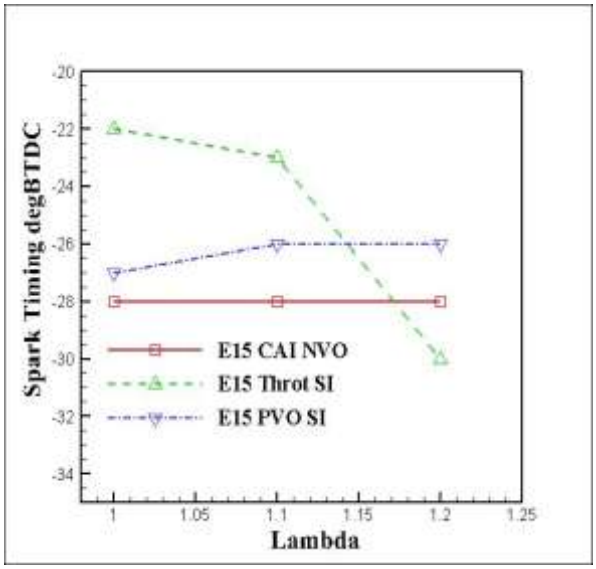


**(b) MBT Spark timing**

**Figure 5.6 Combustion Analysis**

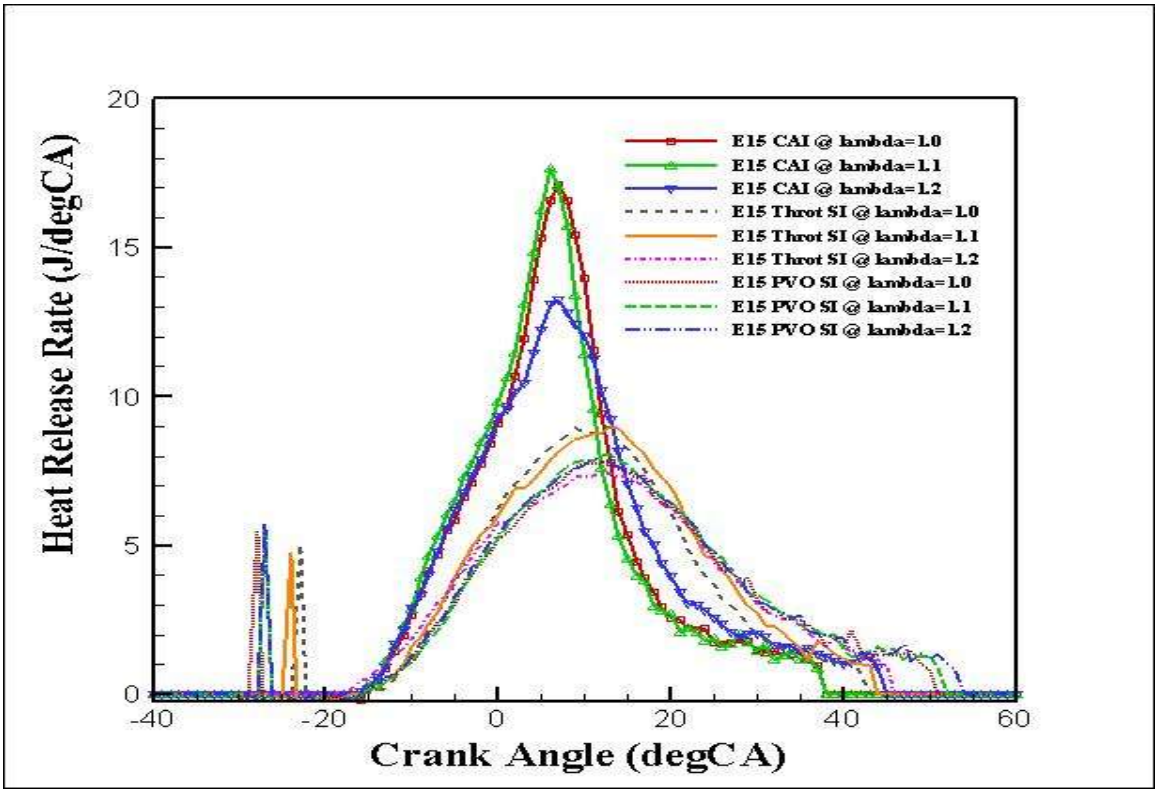


**(c) Heat Release Rate**

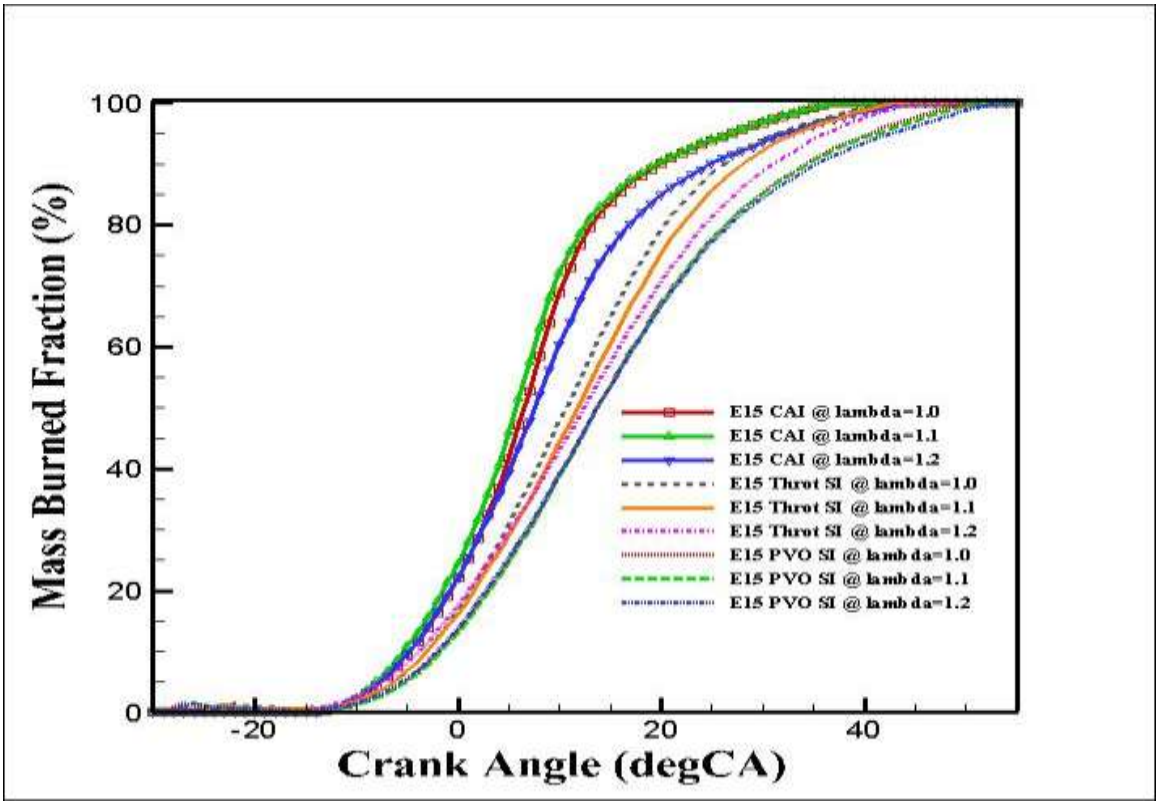


**(d) Mass Burned Fraction**

**Figure 5.6 (ctd) Combustion Analysis**

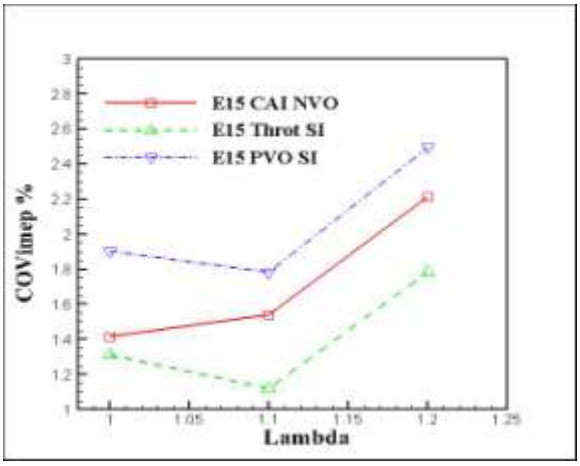


**(e) COV of IMEP**

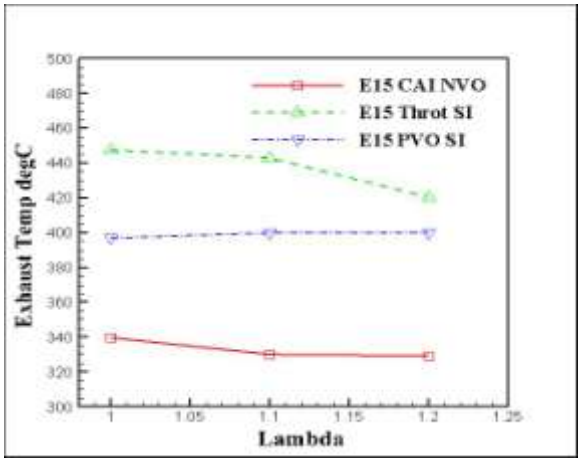


**(f) Exhaust Temperature**

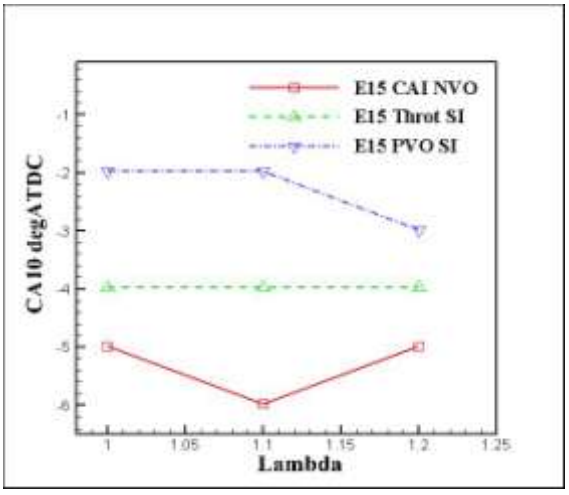


**(g) CA10**

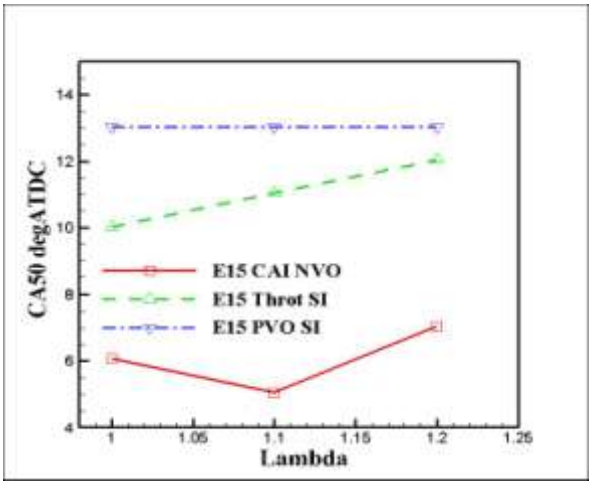


**(h) CA50**

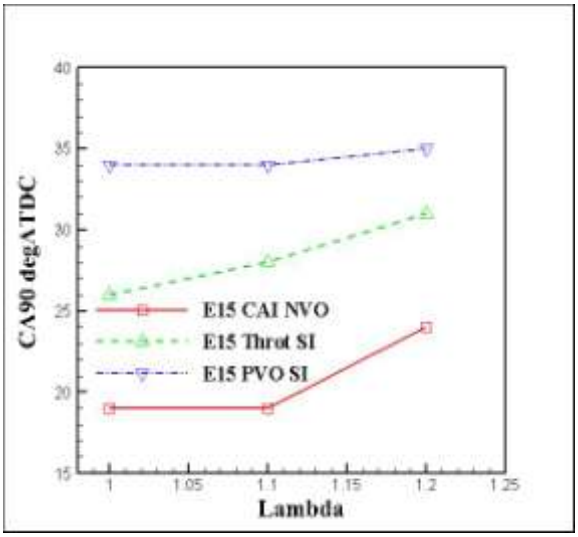


**(i) CA90**

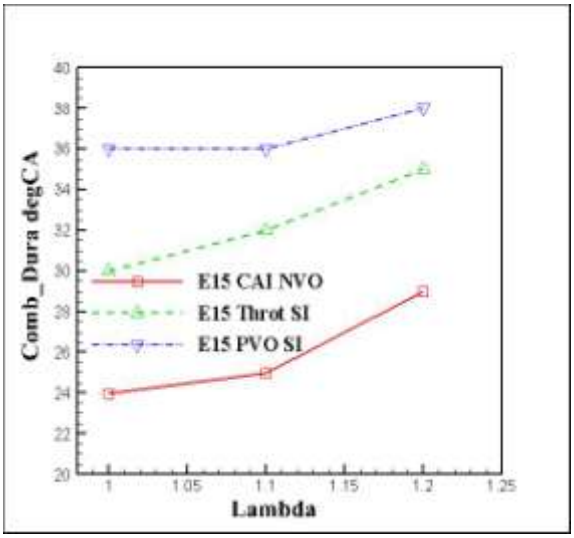


**(j) Combustion Duration**

**Figure 5.6 (ctd) Combustion Analysis**

### 5.4.2 Engine Performance and Efficiency Analysis

Figure 5.7(a) shows the combustion efficiency in E15 throttled SI, PVO SI and CAI combustion modes. It can be seen that the combustion efficiency of the PVO SI combustion was slightly lower than the other two modes.

The theoretical thermodynamic efficiency results in Figure 5.7(b) show that the PVO SI mode exhibited the highest theoretical thermodynamic efficiency even if the combustion process was assumed complete.

The gas exchange efficiency in Figure 5.7(c) shows that the throttle SI operation had the lowest gas exchange efficiency of 86.6%, the reason for the largest pumping loss seen in Figure 5.7(e).

Figure 5.7(d) shows that the net indicated efficiencies of the PVO SI and CAI NVO modes were 2.9% higher than the throttled SI operation.

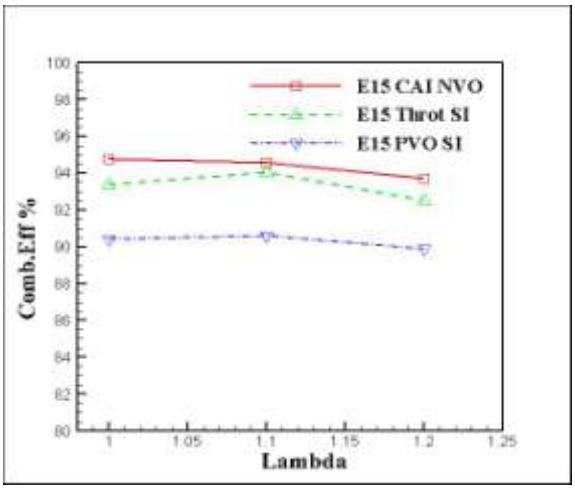


**(a) Combustion Efficiency**

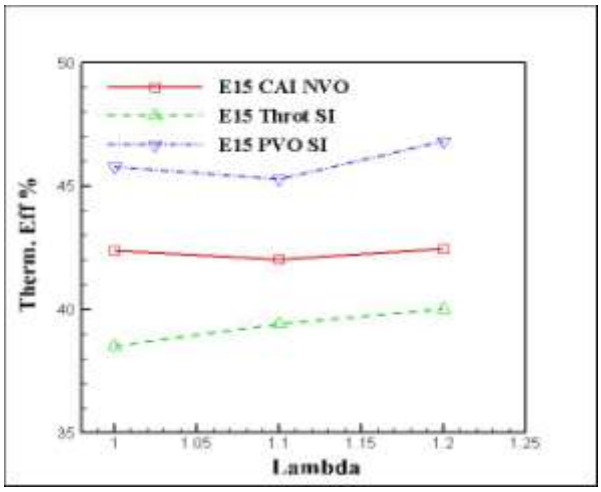


**(b) Thermal Efficiency**

**Figure 5.7 Performance Analysis**

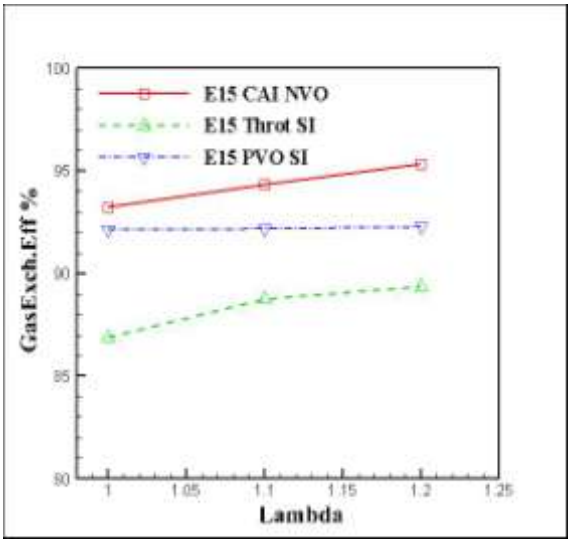


**(c) Gas Exchange Efficiency**

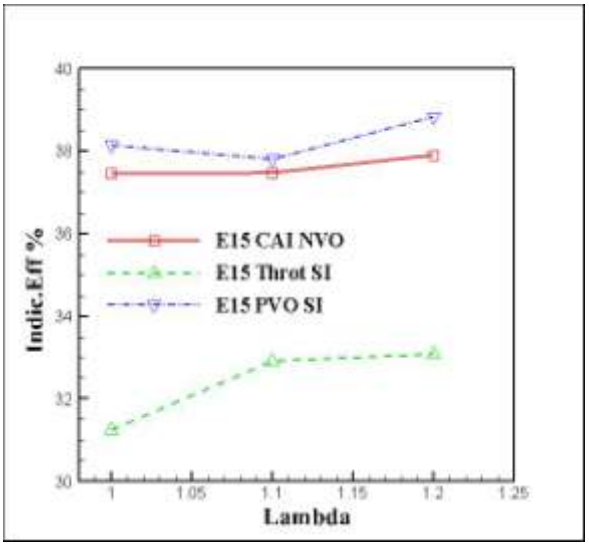


**(d) Indicated Efficiency**

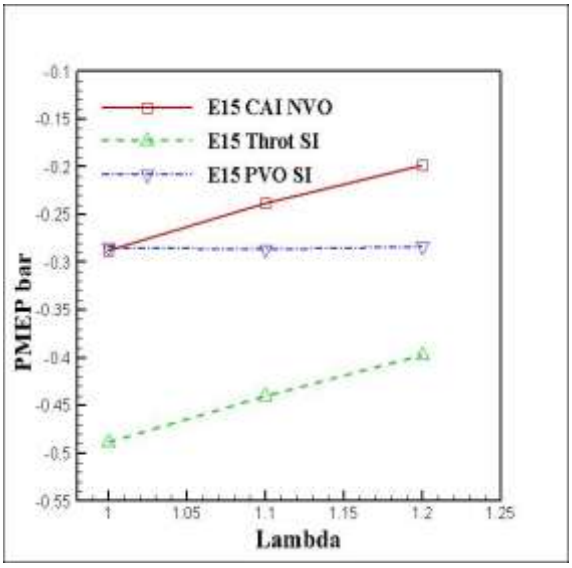


**(e) PMEP**

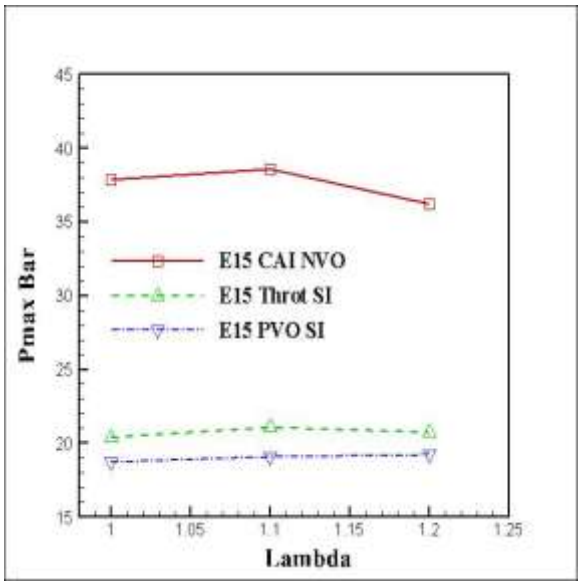


**(f) Pmax**

**Figure 5.7 (ctd) Performance Analysis**

### 5.4.3 Fuel Consumption and Emissions

Figure 5.8 (a) and (b) shows the CO and UHC emission for the three combustion modes with E15. CO is one of the notable emissions formed during combustion process, the quantity depends on the local air to fuel ratio and the combustion temperature. Low temperature combustion hampers the complete oxidation of CO into $CO_2$. Another major factor responsible for increased CO formations could be attributed to locally fuel-rich regions. As seen in Figure 5.8(a), the ISCO was higher in throttled SI and PVO SI than CAI NVO combustion. In the throttled SI combustion CO decreased from 19.0 g/KWh with lambda 1.0 to 9.3 g/KWh with lambda 1.2. In PVO SI it decreased from 15.8g/KWh with lambda 1.0 to

8.0g/KWh with lambda 1.2. In contrast in CAI combustion it increased from 5.6g/KWh with lambda 1.0 to 7.0g/KWh.

The HC emissions are significantly affected by mixture formation and post oxidation in the exhaust manifold and thus, by the exhaust gas temperature, as shown in Figure 5.8(b). The PVO exhibited the most pronounced change in ISHC with varying values of lambda. It produced about 70% higher ISHC than CAI NVO and about 40% higher on average over the lambda range in throttle SI. Overall, the CAI NVO produced the least ISCO and ISHC with lambda 1.0 to 1.2.

Figure 5.8(c) shows the NOx emissions in the three combustion modes. It can be seen that the NOx emission in CAI NVO with all the lambda values were less than 1.0g/KWh. NOx emission in the PVO SI operation varied from 3.8g/KWh at lambda 1.0 to 5.6g/KWh with lambda 1.2 and the throttled SI NOx emissions were 10g/KWh and 11g/KWh with lambda 1.0 and 1.1 decreasing to 7.3g/KWh with lambda 1.2. In CAI combustion, as explained in earlier section the peak combustion temperature is much reduced due to the high dilution ratio and the simultaneous burning of autoignited mixture produces much shorter combustion duration, resulting in the ultra-low NOx emission seen in Figure 5.8(c). The earlier completion of combustion leads to lower exhaust temperature in Figure 5.6(f) due to longer effective expansion process.

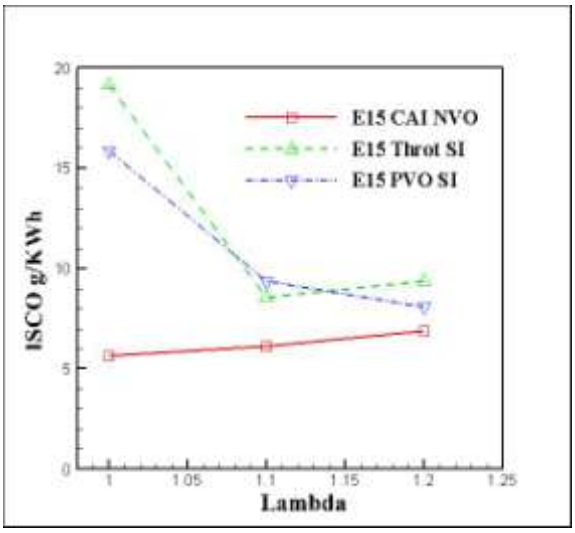


**(a) ISCO**

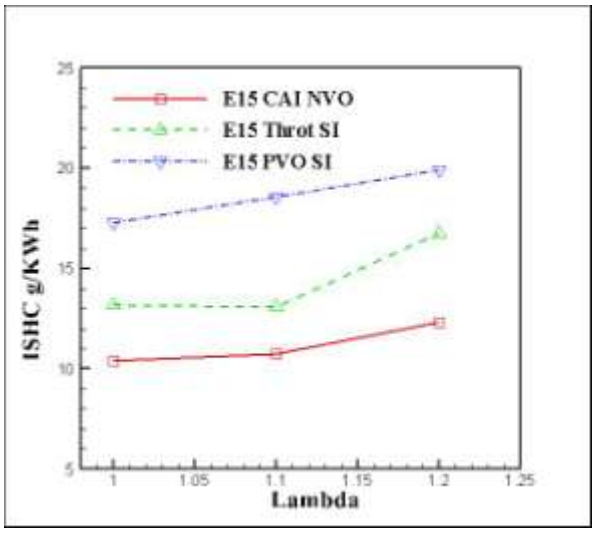


**(b) ISHC**

**Figure 5.8 (ctd) Gaseous Emissions and Fuel Consumption**

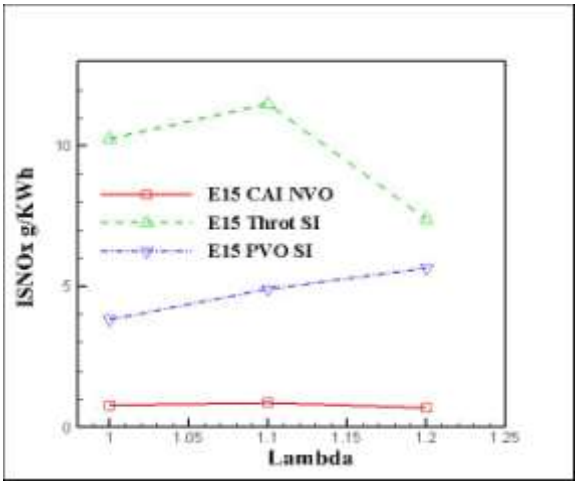


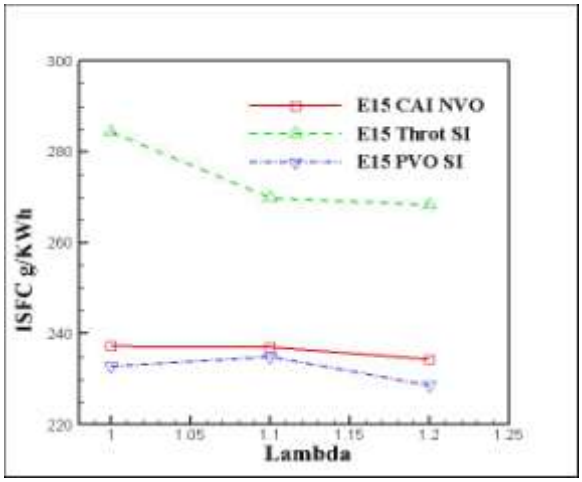


**(c) ISNOx** **(d) ISFC**

**Figure 5.8 (ctd) Gaseous Emissions and Fuel Consumption**

**Particulate Emissions**

Figures 5.9(a) and (b) show that the particle number and total number of particles varied between different operational modes and the effect of ethanol on particle numbers was dependent on the combustion mode. However, it is obvious that the value of lambda did not have noticeable effects on particulate emissions. In the case of PVO SI and throttled SI operations, the number of particles shifted to smaller particles without any noticeable peak. However, even though the CAI NVO particulate emissions also shifted towards smaller size particles, it still peaked at 20nm. As shown in Figure 5.9(a), the majority of particles were around 20nm in diameter. As it is generally accepted that the smallest particles are mainly condensates and that the larger particles are soot particles, the appearance of peaks in the number of particles of around 20nm with gasoline suggests a greater number of soot particle of this size were formed and emitted under such operating conditions. The presence of oxygen in E15 helped to reduce the soot formation.

As shown in Figure 5.9(b), the PVO mode was characterised by the lowest number of particles out of the three operational modes. This was most likely to have been caused by the higher charge temperature of internally recirculated burned gases.

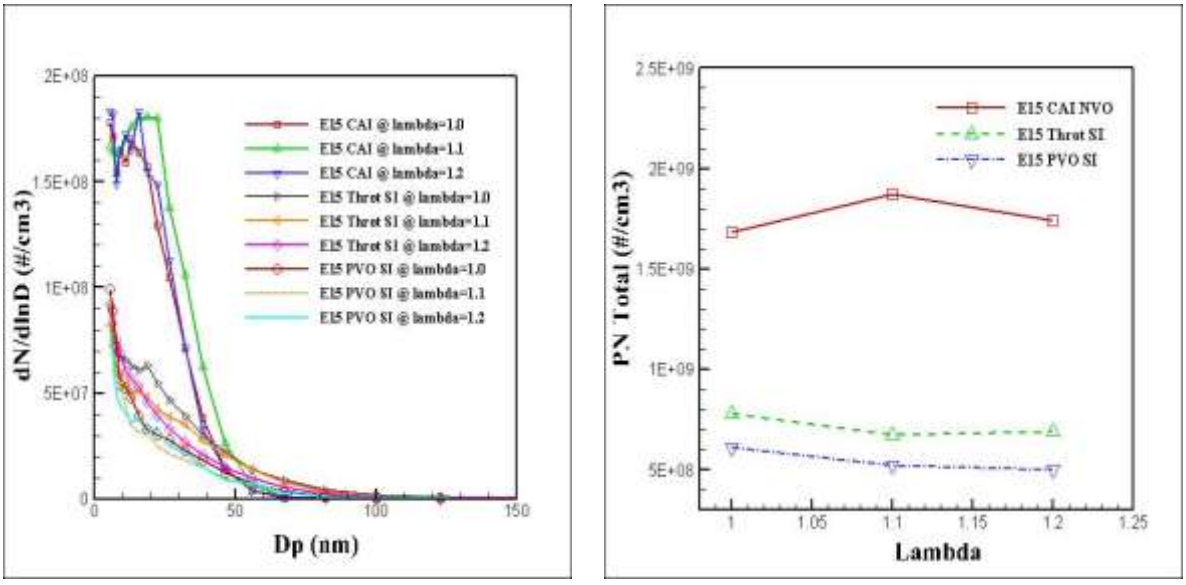


**(a) Particle Number Emission** **(b) Total Particle Number**

**Figure 5.9 Particulate Emissions**

**Summary**

When operated with E15, similar trends were observed for the three engine operation modes to gasoline' The PVO SI shows the lowest ISFC resulting in about 18% improvement in ISFC over throttled SI and highest indicated engine efficiency with all lambda values. The engine out ISCO, ISHC and NOx emissions in the three modes was lowest for CAI NVO combustion. The PVO mode was characterised by the lowest number of particles out of the three operational modes. This was most likely to have been caused by the higher charge temperature of internally recirculated burned gases. Most particles were in the range of a few nanometers related to the unburned hydrocarbons.

## 5.5 Combustion and Emission Results with E85

### 5.5.1 Combustion Analysis

Figure 5.10(a) shows the maximum pressure-rise rate as a function of combustion modes and lambda in E85. It can be seen that the maximum pressure-rise rate for all the SI combustion modes was less than 0.8 bar/CA and the CAI NVO was below 1.4 bar/CA. As shown in Figure 5.10(b), the MBT spark timings were more advanced in PVO mode than the throttled SI mode due to dilution by residual gases and slower burning velocities as evidenced by the mass burned fractions in Figure 5.10(d) and the corresponding heat-release rate shown in Figure 5.10(c). The E85 CAI NVO operations were characterized by the fastest combustion

because of heavy dilution by residual gas, charge cooling effect of E85 and multiple auto-ignition sites. Furthermore, there was a noticeable reduction in the heat-release rate with increasing lambda and combustion phase shift in the CAI NVO operation (figure 5.10(c)).

The PVO operations were characterized by the most advanced and slowest combustion because of internal EGR. Furthermore, E85 showed a noticeable reduction in the heat-release rate.

As shown in Figure 5.10 (e), the COVimeps for all modes were low and did not vary significantly with lambda 1.0 and 1.1 with the fuel blends and combustion modes studied. However, with lambda 1.2 the COV of IMEP in throttled SI was 4.5%, and although the engine was stable, poor fuel efficiency resulted. Hence, COV of IMEP was maintained at less than 3%.

As shown in Figure 5.10(f), E85 exhaust temperature in the CAI NVO was relatively constant at 340 $^{o}$C with lambda 1.0 to 1.2. In the PVO SI it was 385 $^{o}$C with lambda 1.0 and increased to 390 with lambda 1.1 and 1.2. In throttled SI mode the exhaust temperature decreases linearly from 460 $^{o}$C with lambda 1.0 with increasing lambda value to 380 with lambda 1.2 due to spark retard.

Figure 5.10(g) shows that the overall combustion period tended to increase from the throttle SI to PVO SI. In the PVO, the internal EGR resulted in the slower combustion speed. The CAI combustion was the fastest.

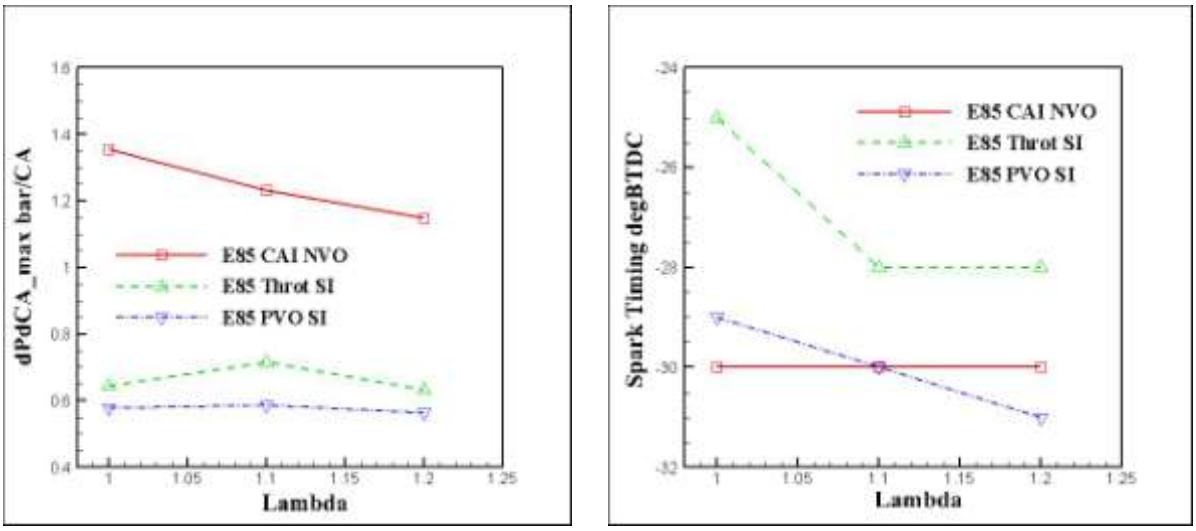


**(a) Maximum Pressure Rise Rate** **(b) Spark Timing**

**Figure 5.10 Combustion Analysis**

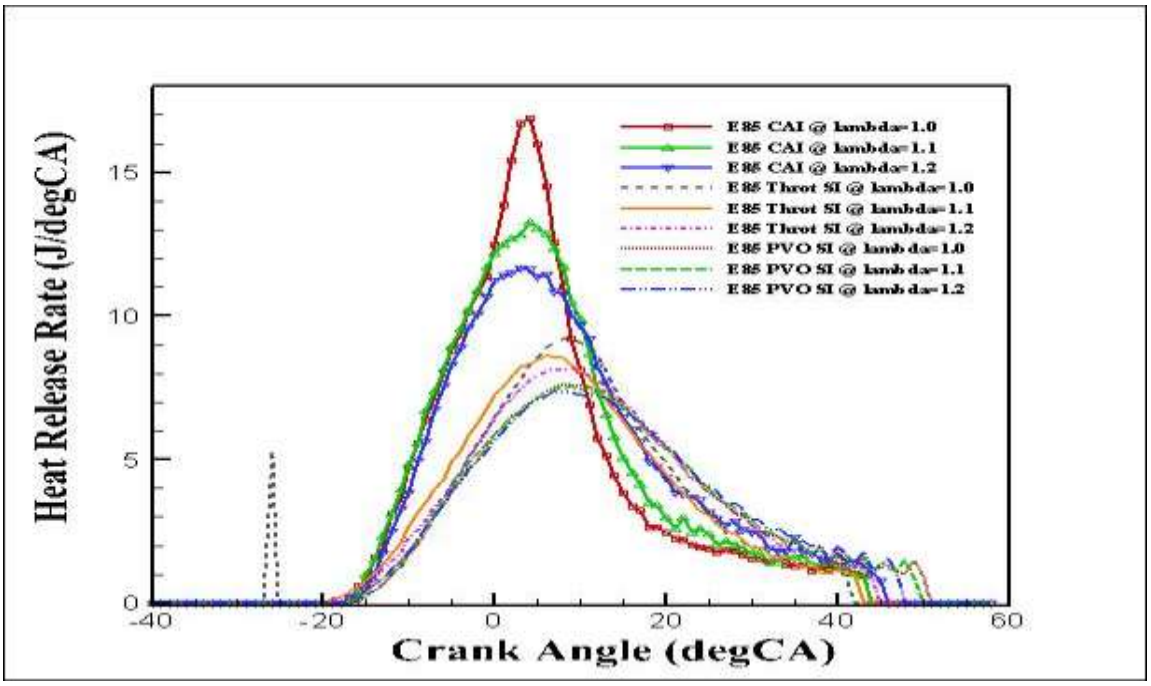


**(c) Heat Release Rate**

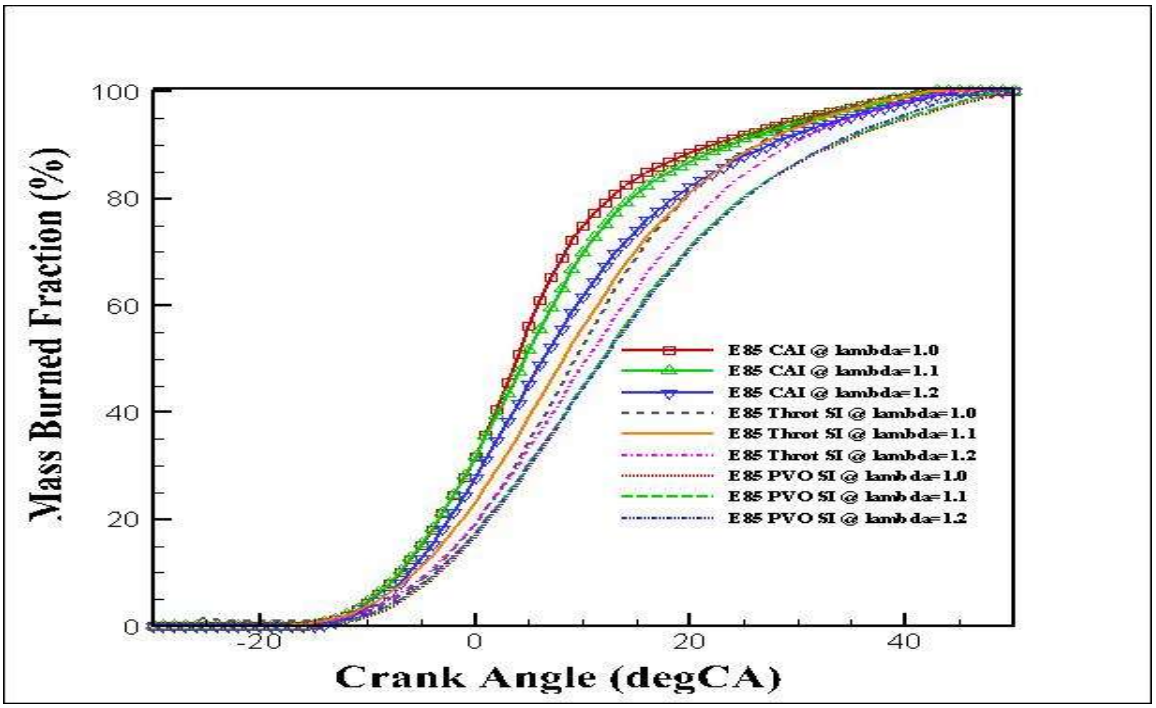


**(d) Mass Burned Fraction**

**Figure 5.10 (ctd) Combustion Analysis**

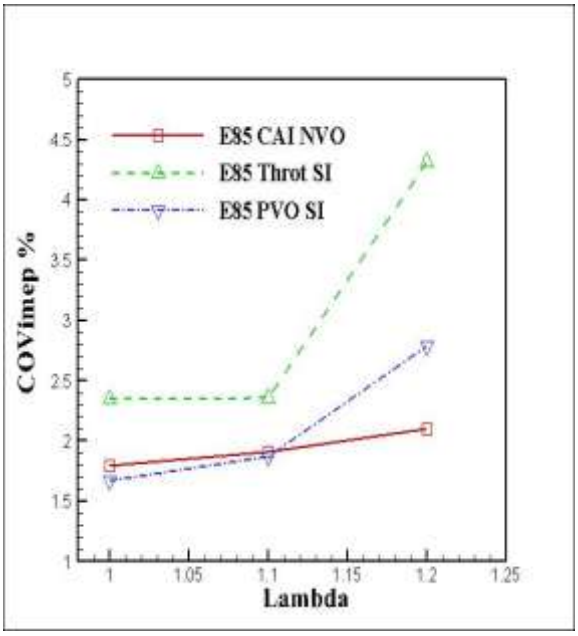


**(e) COV of IMEP**

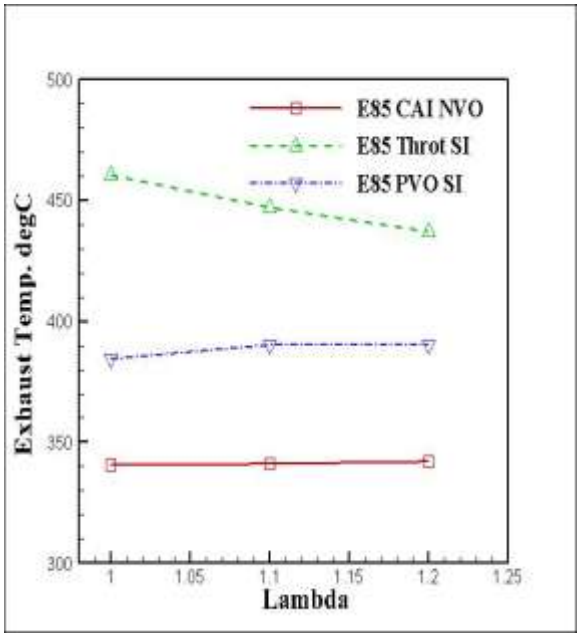


**(f) Exhaust Temperature**

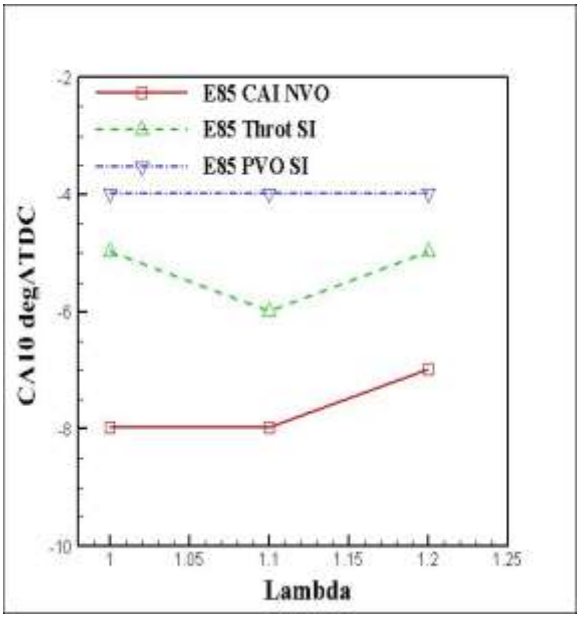


**(g) CA10**

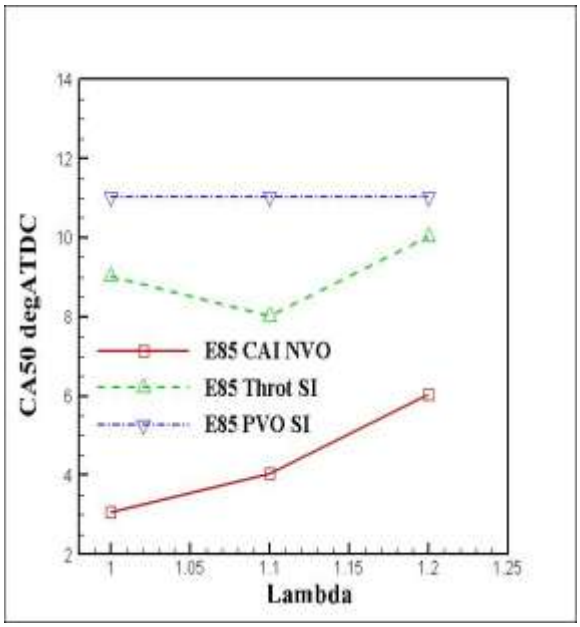


**(h) CA50**

**Figure 5.10 (ctd) Combustion Analysis**

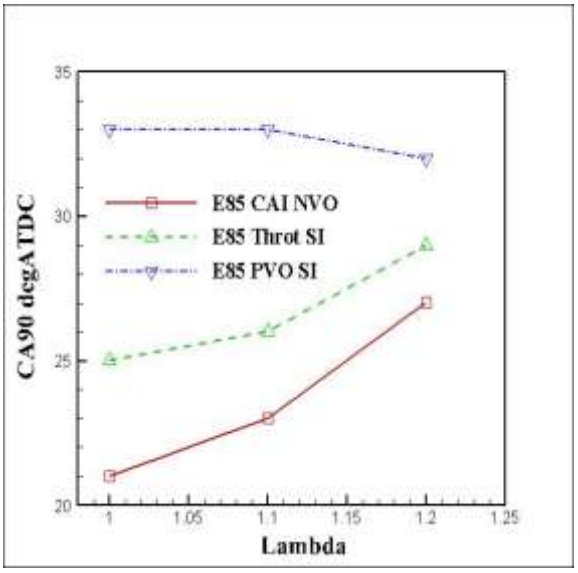


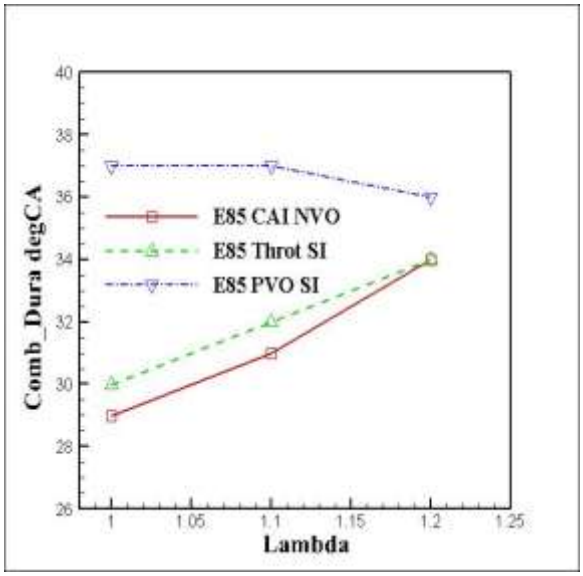


**(i) CA90** **(j) Combustion Duration**

**Figure 5.10 (ctd) Combustion Analysis**

### 5.5.2 Engine Performance and Efficiency Analysis

Figure 5.11(a) shows the combustion efficiency in throttled SI, PVO SI and CAI NVO combustion modes. It can be seen that there is no appreciable difference in combustion efficiency of the three modes with lambda 1.0 and 1.1, while with lambda 1.2 the combustion efficiency of CAI NVO was slightly lower than in the other two modes. The increased charge cooling effects of the E85 and heavy dilution may have resulted in reduced in-cylinder temperature and heat that would have enhanced evaporation when fuel was injected in NVO.

The theoretical thermodynamic efficiency of the engine is shown in Figure 5.11(b), The throttle SI mode exhibited the lowest theoretical thermodynamic efficiency even if the combustion process were assumed complete.

Figure 5.11(c) shows that the throttle SI operation was characterised by an average gas exchange efficiency of 91% compared to 92% in PVO and 95% in CAI.

Figure 5.11(d) compares the net indicated efficiency in the PVO SI, throttled SI and CAI NVO modes with lambda values of 1 to 1.20. The figure shows an average indicated efficiency of 40% in PVO SI, 31.6% in throttled SI and 36.3% in CAI combustion. Compared to the CAI operation, the PVO SI operation was on average 3.7% better in indicated efficiency.

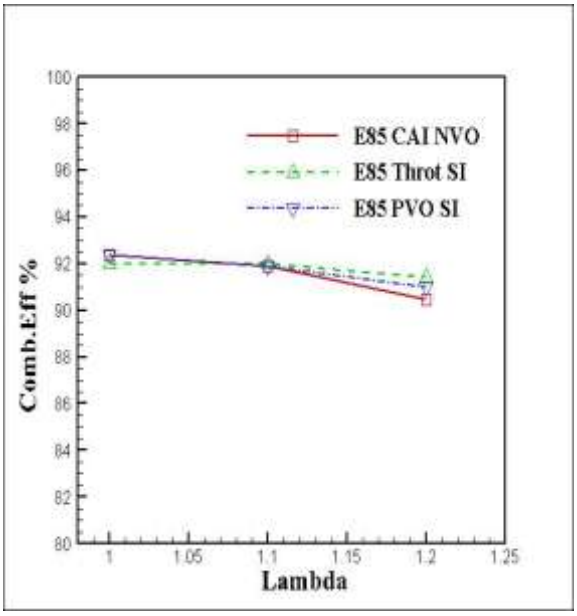


**(a) Combustion Efficiency**

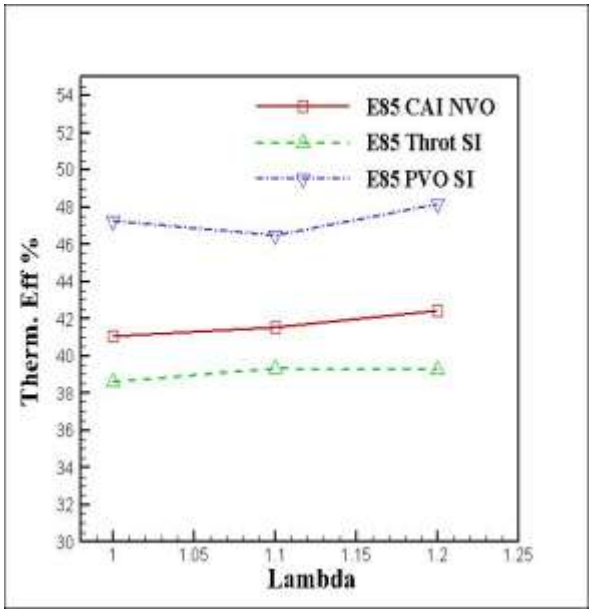


**(b) Thermal Efficiency**

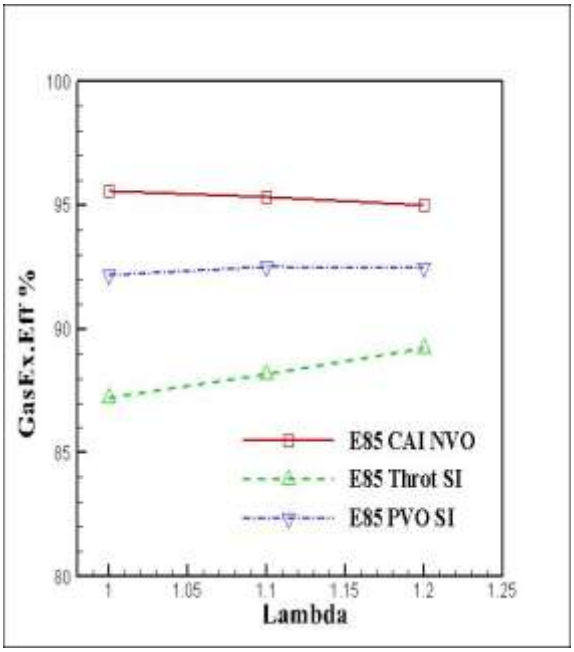


**(c) Gas Exchange Efficiency**

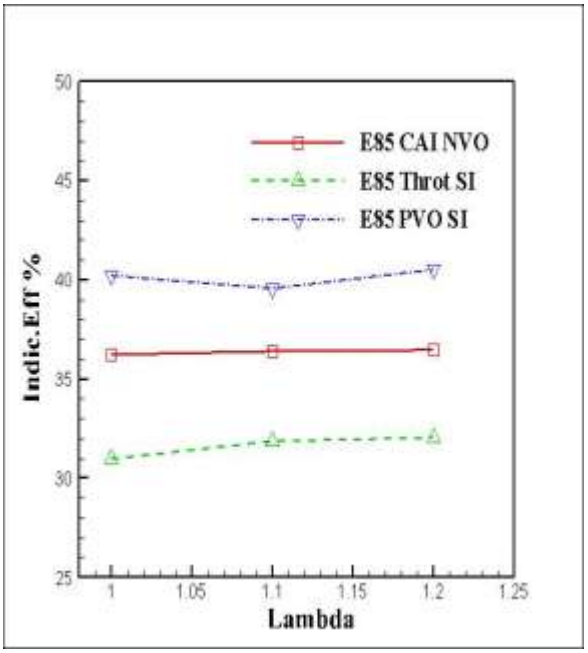


**(d) Indicated Efficiency**

**Figure 5.11 Performance Analysis of Throttled SI, PVO SI, and CAI NVO**

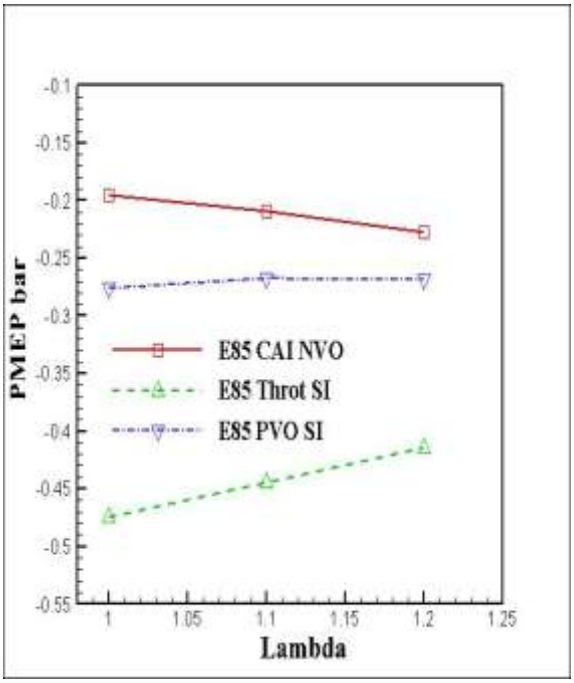


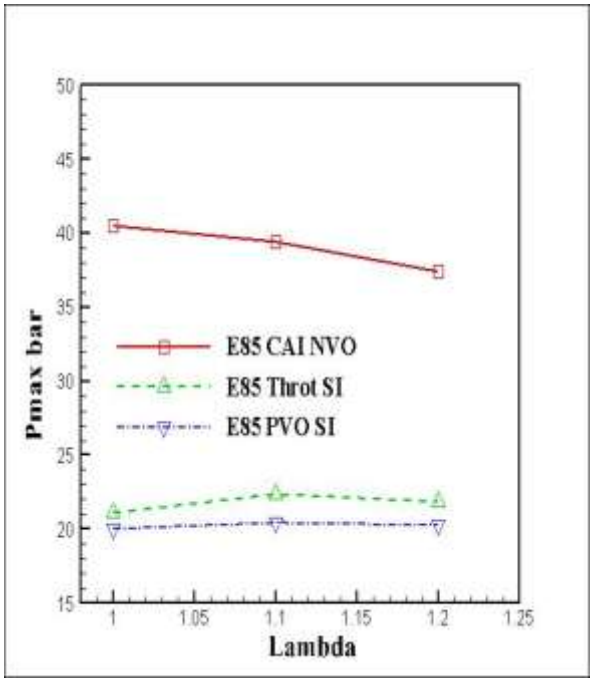


**(e) PMEP** **(f) Maximum cylinder pressure**

**Figure 5.11 (ctd) Performance Analysis of Throttled SI, PVO SI, and CAI NVO**

### 5.5.3 Fuel Consumption and Emissions

Figure 5.12(a) shows the CO emission from the throttled SI, PVO SI and CAI NVO combustion with lambda 1.0, 1.1, and 1.2. As shown in Figure 5.12(a), the ISCO emission is three times higher in the throttle SI mode than in the PVO SI and CAI NVO. The ISCO decreased as lambda increased, reaching a minimum with lambda 1.2. In the PVO SI and CAI NVO combustion the CO emission is about 70% lower than in throttle SI with lambda 1.0 and 30% lower with lambda 1.1 and 1.2. This improved CO emission of unthrottled operation over the throttled SI is due to the gas-exchange. In the PVO SI fuel was injected into re-inducted hot residuals which enabled better and faster fuel evaporation, the same as in CAI NVO in which fuel was injected during the late part of the exhaust stroke, this facilitated mixture preparation and faster fuel evaporation. The increased CO emission of the throttled SI may be due to the reduced evaporation temperature as a result of the increased charge cooling effects of E85 in the in-cylinder creating pockets of rich mixture.

The HC emissions are significantly affected by mixture formation and post oxidation in the exhaust manifold and by the exhaust gas temperature. The PVO display the most pronounced change in ISHC with ethanol content. It seemed likely that complete fuel evaporation had taken place with the E85 as evident in Figure 5.12(b) which shows the results for ISHC

emission for the three modes of operations. The PVO SI operation produces the least ISHC emissions compared to throttled SI and CAI combustion. However, all the three modes show linearly increasing ISHC emissions for increasing lambda.

The higher CO and HC emissions results suggest that there were more locally rich mixtures formed in the throttle SI mode. In the case of CAI NVO combustion, fuel was injected into hot residual gas during the negative valve overlap period and so could evaporate quickly and had more time to mix with air. In the PVO SI when fuel injection took place early in the intake stroke into hot incoming residuals, it resulted in better fuel evaporation and more complete mixing due to the higher charge temperature. This helped to eliminate regions of rich mixture that were responsible for the increased CO formations.

Figure 5.12(c) shows the NOx emissions for the three combustion modes. It can be seen that the NOx emission during the CAI NVO operation was below 1g/KWh for all the lambda values. PVO SI also displayed low ISNOx of 4.7g/KWh for lambda1.0, 1.1 and 1.2 in comparison with NOx emissions of 12-7g/KWh during the throttled SI operation.

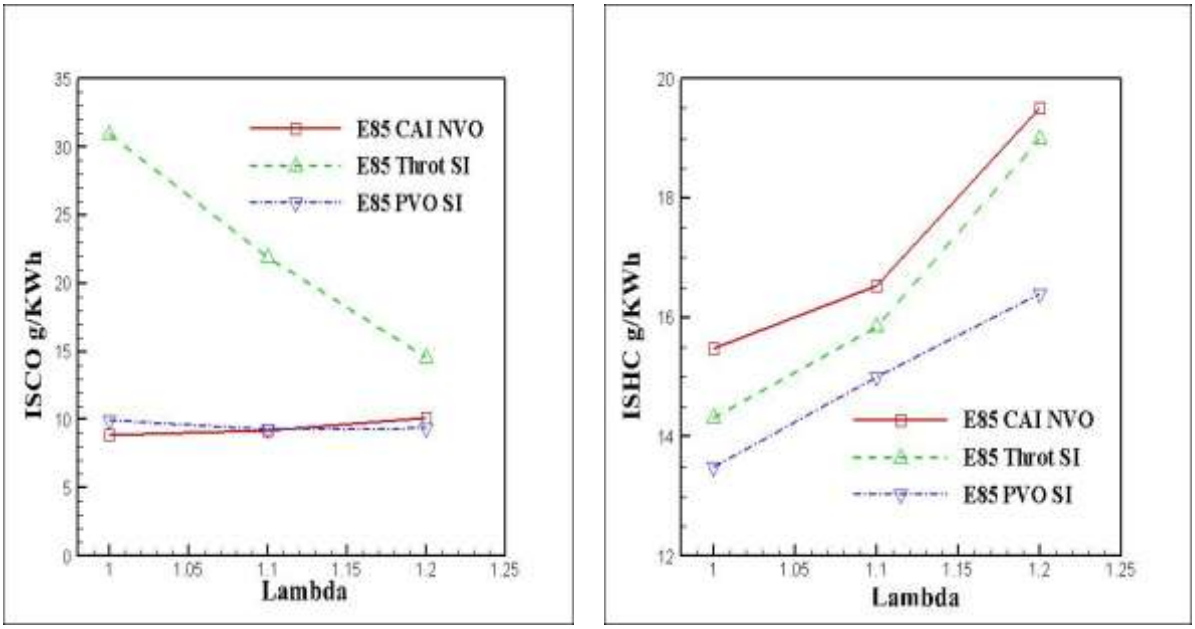


**(a) ISCO** **(b) ISHC**

**Figure 5.12 Gaseous Emission and Fuel Consumption**

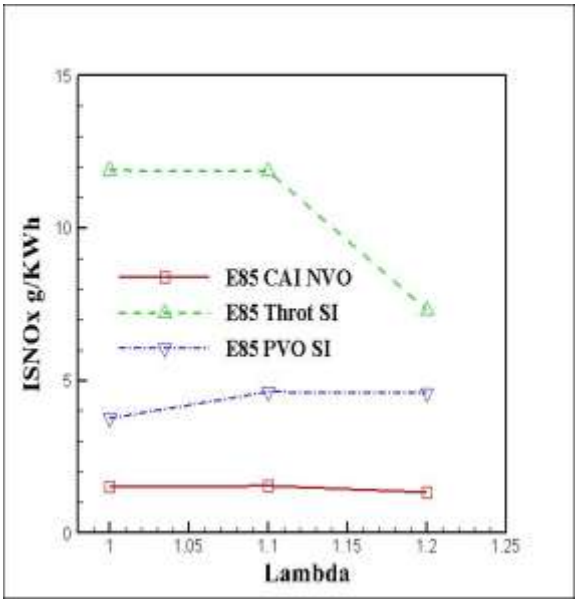


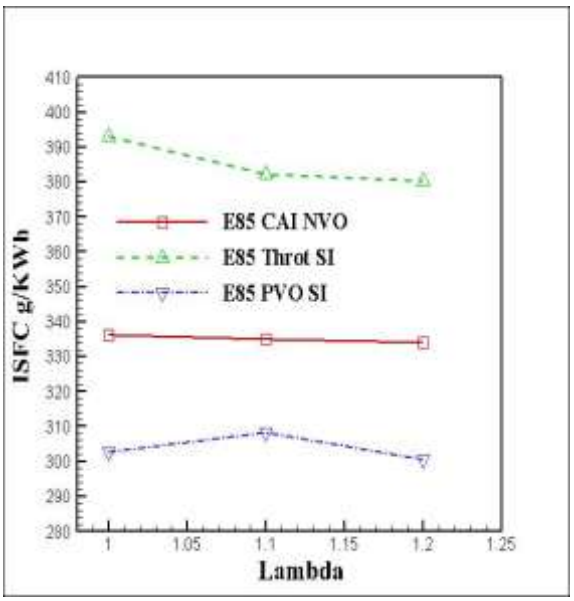


**(c) ISNOx** **(d) ISFC**

**Figure 5.12 (ctd) Gaseous Emission and Fuel Consumption**

**Particulate Emission**

Figure 5.13(a) and (b) show that the total number of particle vary between different operational modes and the effect of ethanol on particle numbers is also mode dependent. In the case of E85 throttled SI and PVO SI operations, the number of particles decreased rapidly and shifted to smaller size particles. As shown in figure 5.13(a), the majority of particles were around 20nm in diameter. As it is generally accepted that the smallest particles are mainly condensates and that the larger particles are soot particles, the appearance of peaks in the number of particles of around 20nm with gasoline suggests that a greater number of soot particle of this size were formed and emitted under such operating conditions. The presence of oxygen in E85 helped to reduce the soot formation.

Figure 5.13(a) and (b) with lambda 1.0, 1.1, and 1.2 show that in the CAI NVO mode the highest quantity of particles in total could be found in CAI NVO combustion mode. For all cases examined, the particulates are dominated by the nucleation mode particles in the range of 20nm size.

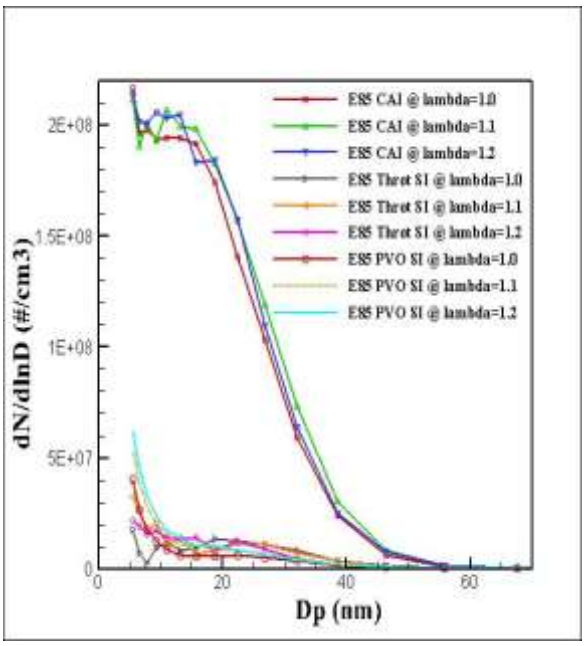


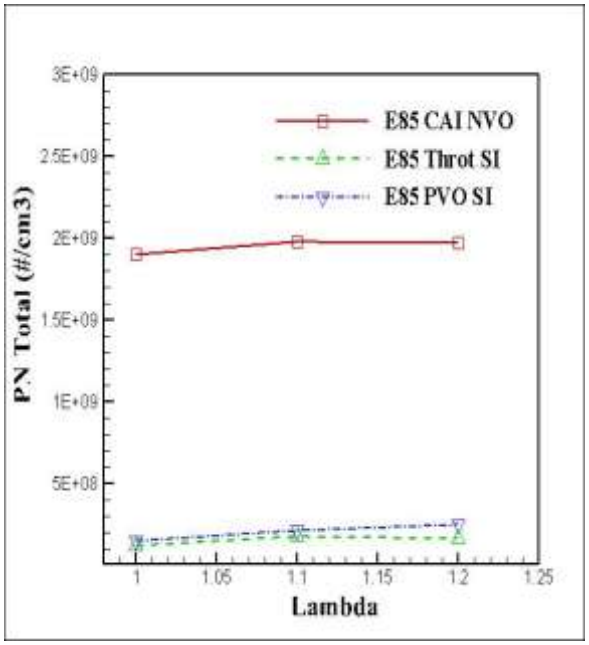


**(a) Particulate Number Emission** **(b) Total PN Emission**

**Figure 5.13 Particulate Emissions**

**Summary**

In the case of E85, the PVO SI operation showed the lowest ISFC and highest indicated engine efficiency. The engine-out ISHC emissions in CAI was on average 10% higher than the PVO SI and about 7% higher than the throttled SI operation.

The particle size distribution was characterised with a peak between 15nm to 20nm in diameter in CAI combustion, indicating the presence of nucleation mode particles. However the addition of E85 removed the soot peaks during the PVO SI and throttled SI operations. The leaner mixture did not have appreciable effect in the reduction of the total particle emissions in all combustion modes.

The E85 blend resulted in increased fuel consumption in all the three modes due to reduced energy content of E85.

## 5.6 Comparison of Gasoline E0, E15 and E85 at Lambda 1.0

### 5.6.1 Combustion Analysis

Figure 5.14(a) shows the maximum pressure-rise rate as a function of combustion modes and fuel blends at lambda 1. It can be seen that E15 and E85 resulted in a noticeable reduction in the pressure-rise rates during the CAI operation from more than 5 with gasoline to 1.4bar/CA. There was slight reduction in the rate of maximum pressure rise in PVO operations. However, the increase of E15 to E85 blends does not have any appreciable effects on the rate of reduction in pressure rise rate.

The effect of E15 and E85 on spark timing shown in Figure 5.14(b) indicates that ethanol blending have appreciable effect in advancing ignition timing in cases of CAI. In the PVO SI the effects of E15 and E85 lead to spark retard, but no appreciable effect was observed on throttle SI.

The effects of ethanol on heat release rate and mass burned fraction are shown in figure 5.14(c) and (d). The effect of ethanol on heat release rate is very obvious from CAI combustion. This could be explained as follows: alcohol fuels are partially oxidized hydrocarbons and they have lower heating values than gasoline, hence, the heating values of alcohol-gasoline blends are lower than that of pure gasoline [102]. This decreases the combustion heat energy and lowers the maximum combustion temperature, in addition because of their higher heat of vaporization, have high tendency to decrease the flame speed when they burn in lambda =1, hence the longer burn durations shown in figure 5.14(d)

As shown in Figure 5.14(e) and (f), the effects of E15 and E85 do not have appreciable effects on COVimep, in all the blends in the operational modes the value of COVimep was below 3% which is an indication of stable combustion. On ethanol blending effects on the exhaust temperature, there was no appreciable increase observed in using E15 and E85 in throttled SI and PVO SI except in CAI mode where we have slight increase in exhaust temperature.

The anti-knock performance of ethanol blends is excellent under CAI combustion, the overall effects of ethanol blends in E15 and E85 on combustion delay (CA10 and CA50 were delayed as ethanol fraction increased) shown in Figure 5.14(g), (h) and (i). The use of E85 have more appreciable delay effects on the CA10 and the combustion phasing CA50. However, the effects of E15 and E85 on the combustion duration, have appreciable effects only in CAI combustion where the durations for ethanol blends are longer (Figure 5.14(i))

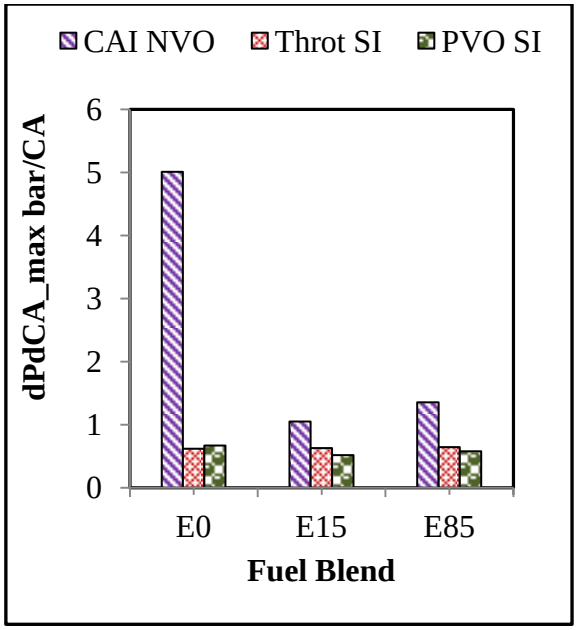


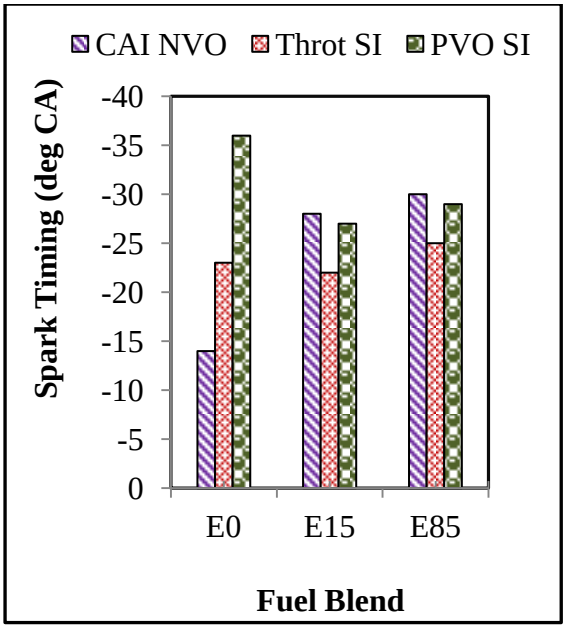


**(a) Maximum Pressure Rise Rate** **(b) Spark Timing**

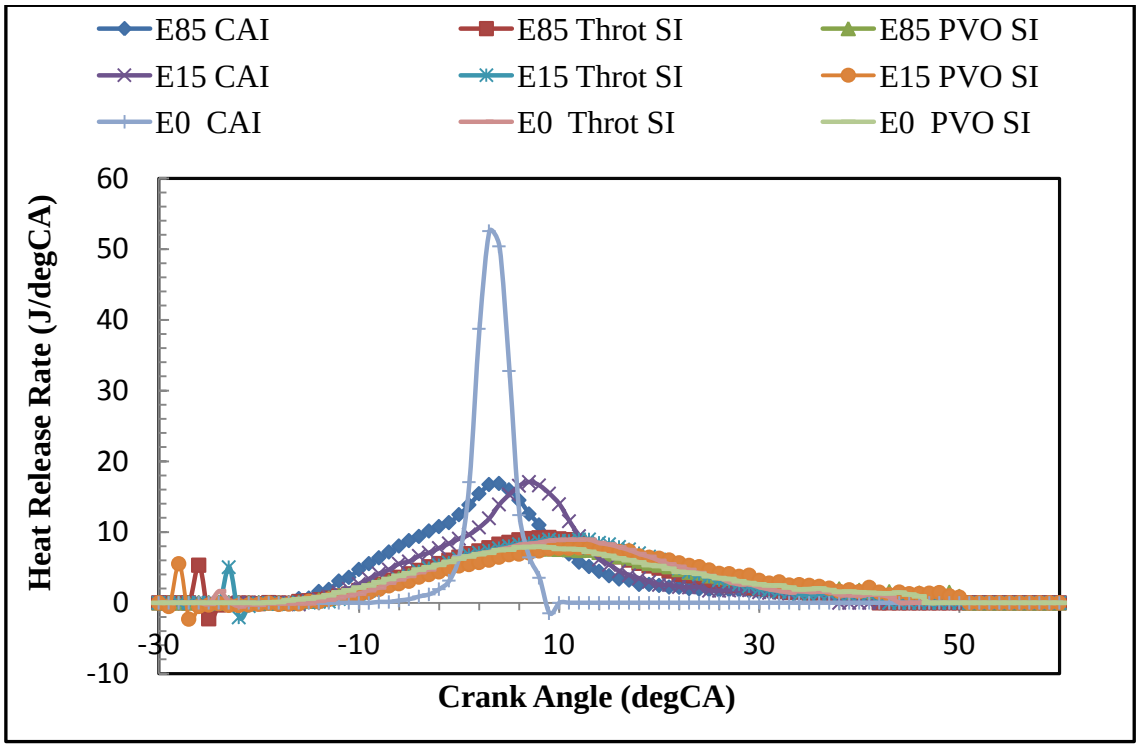


**(c) Heat Release Rate**

**Figure 5.14 Combustion Analysis**

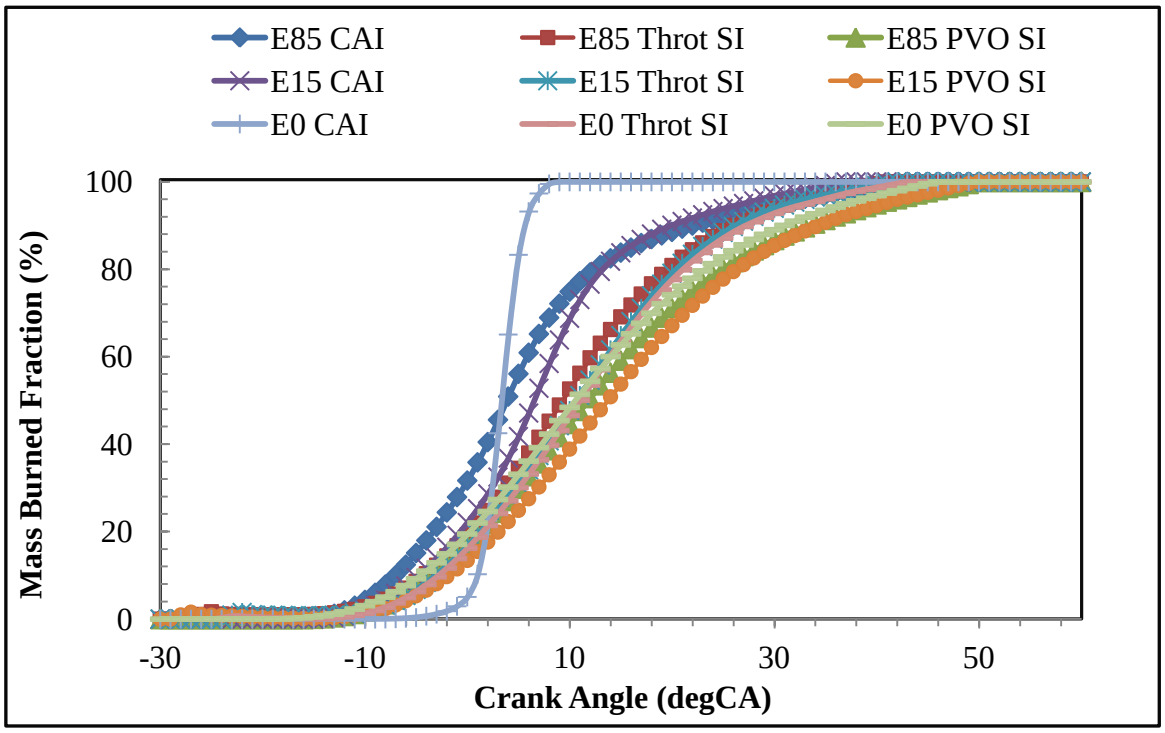


**(d) Mass Burned Fraction**

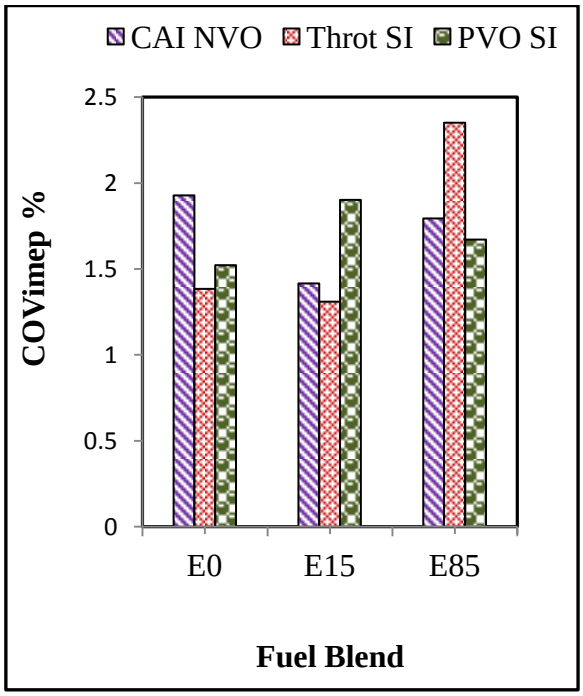


**(e) COV of IMEP**

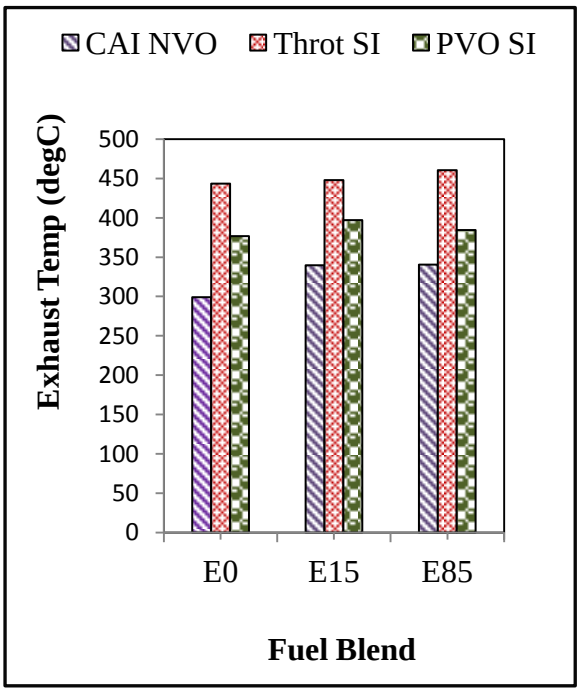


**(f) Exhaust Temperature**

**Figure 5.14 (ctd) Combustion Analysis**

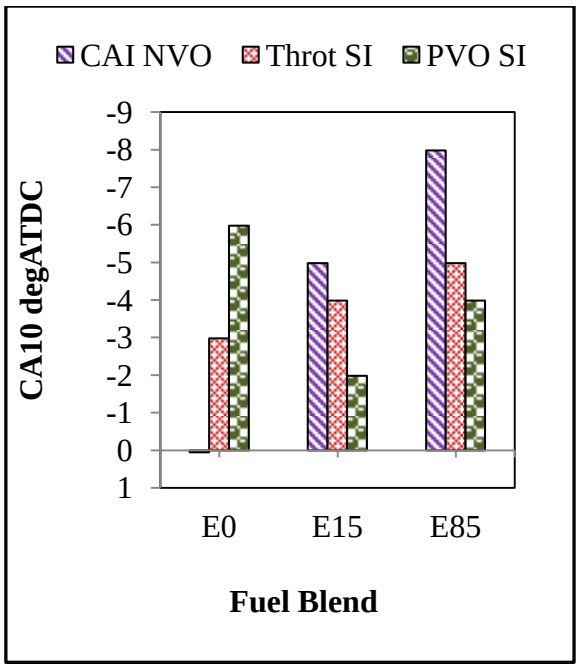


(g) CA10

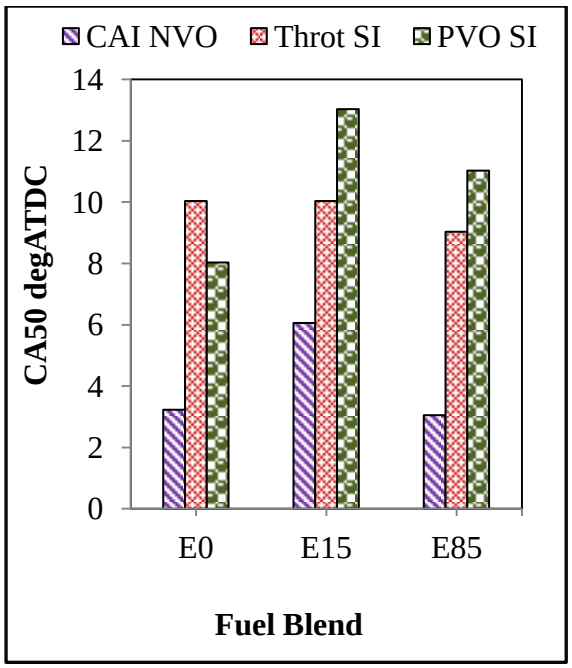


(h) CA50

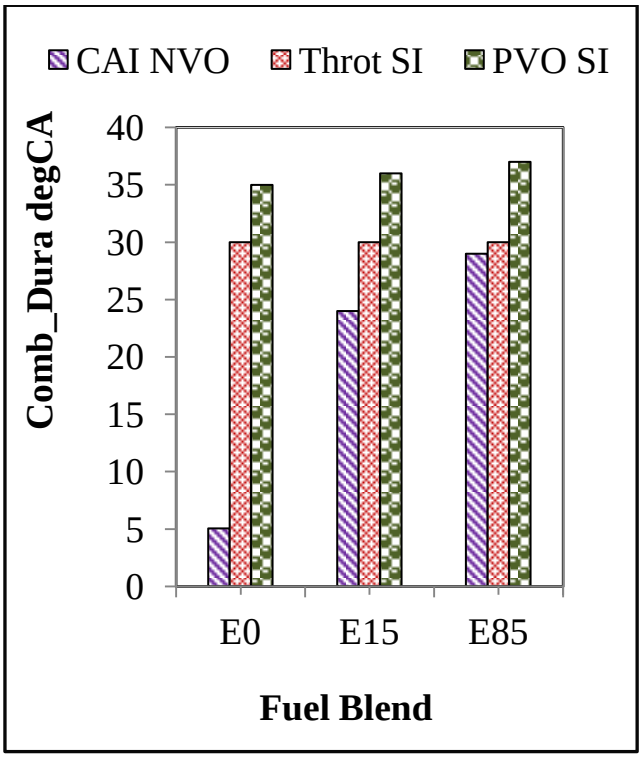


(i) Combustion Duration

**Figure 5.14 (ctd) Combustion Analysis**

### 5.6.2 Engine Performance and Efficiency Analysis

Figure 5.15(a) shows the combustion efficiency for the combustion modes using E15 and E85 blends. In using E15, there was a slight decrease in the combustion efficiency of the throttled SI. The CAI combustion efficiency decreases slightly as the ethanol is increased to E85. The lower combustion efficiency was likely to be related to the charge cooling effects of ethanol, and increasing the injection quantity of ethanol to E85 would have increased the cooling charge effect of ethanol thereby leading topoor mixture formation that resulted in pockets of rich mixture, as indicated by the higher CO emissions in Figure 5.16(a).

As the percentage of ethanol increases from E15 to E85 the PVO SI combustion efficiency increased to 92% shown in Figure 5.15(a). This could be a result of the interaction of fuel injection and gas-exchange process. This would have led gasoline fuel to less fuel rich regions in the combustion process in using E15 and E85 and hence the reduced CO and UHC emissions see Figure 5.16(a) and (b).

The thermodynamic efficiency of the engine is shown in Figure 5.15(b). There was no appreciable effects on ethanol blends in the thermodynamic efficiency of CAI combustion. In the PVO SI mode the use of E15 lead to a light increase in thermodynamic efficiency, but using E85 does not have any appreciable effect on thermodynamic efficiency. Similar trends were observed in the throttled SI mode,using E15 and E85 ethanol blends efficiency was observed to average around 40%.

Figure 5.15(c) shows the effects of E15 and E85 on gas exchange in the three operational modes, using ethanol blends improves the gas exchange of the CAI NVO and PVO SI combustion, this may be as a result of the cooling charge effects of the increased ethanol blends that enables more charge to be inducted into the engine, because fuel was injected into hot residuals in the PVO SI and CAI NVO.

Figure 5.15(d) compares the indicated efficiency of the modes and fuel blends. As the ethanol blends is increased from E15 to E85 the throttled SI indicated efficiency shows a slight decrease from 33% in E0 to 31.0% in E85, whilst the PVO SI increase from 35.9% in E0 to 40.2% in E85. In the CAI operation there was slight decrease in efficiency in E15 and E85.

Figure 5.15 (e) and (f) shows the PMEP and ISFC using E15 and E85. There was a noticeable improvement in the PMEP in using E15 and E85, which may likely be due to the charge cooling effects of ethanol blends and WOT used in PVO SI and CAI NVO. Similar trend was

observed in throttled SI but not as large as in the two other modes. There was no improvement in the fuel consumptions, this was expected as the energy content of ethanol is lower than pure gasoline, which implies that more gallons of ethanol will be needed for same energy output as pure gasoline.

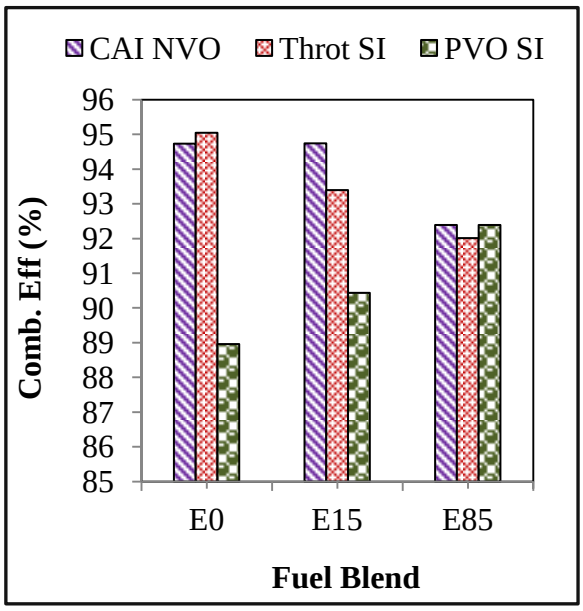


**(a) Combustion Efficiency**

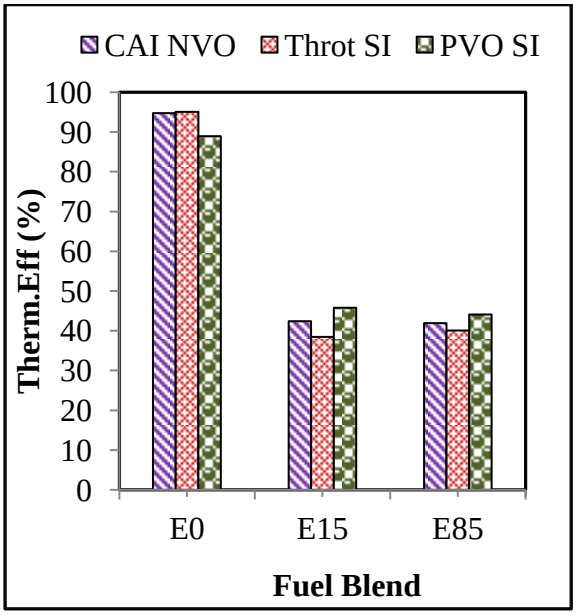


**(b) Thermal Efficiency**

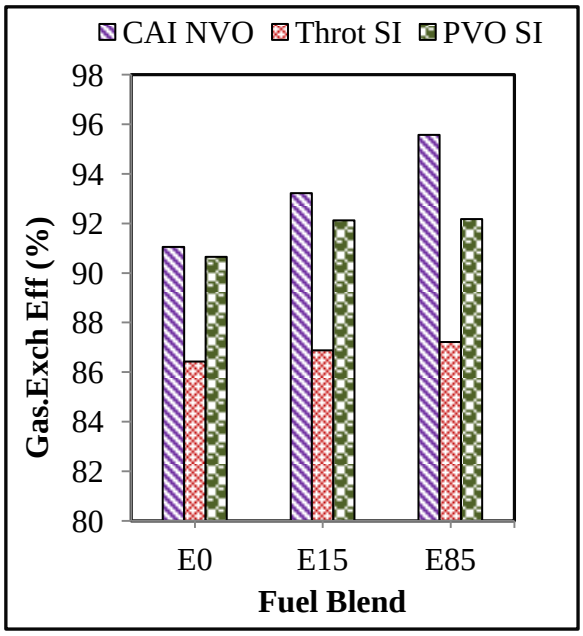


**(c) Gas Exchange Efficiency**

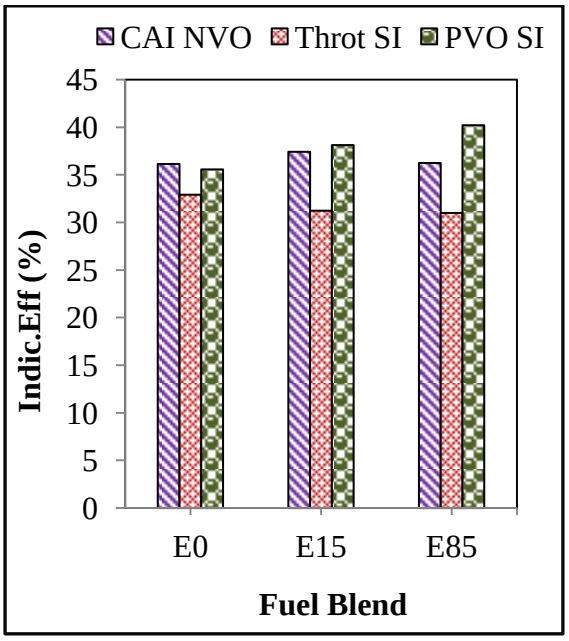


**(d) Indicated Efficiency**

**Figure 5.15 Performance Efficiency**

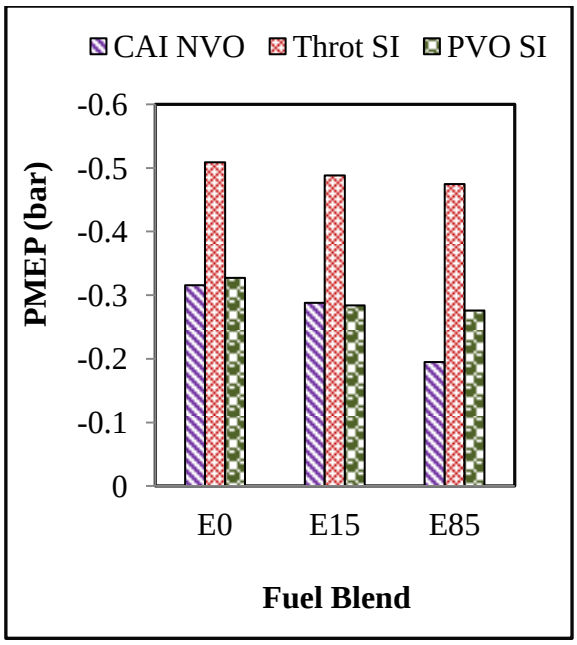


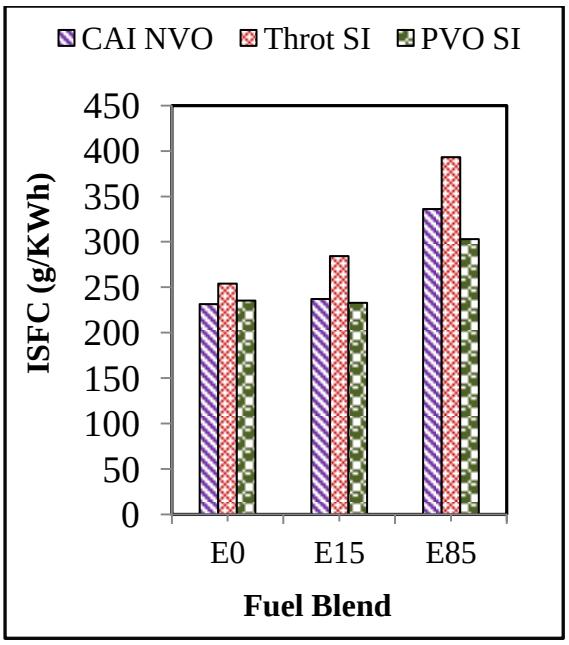


**(e) PMEP** **(f) ISFC**

**Figure 5.15 (ctd) Performance Efficiency**

### 5.6.3 Emissions and Fuel Consumption

In this analysis, the effects of E15 and E85 on exhaust emissions such as CO, UHC, and NOx are studied.

Figure 5.16(a) shows that increasing ethanol blends from E15 to E85 lead to increased CO emissions in the throttled SI (CO increased from 6.0 g/KWh in E0 to 31.0 g/KWh in E85) and slight increase was noticeable in CAI in using E85.

In contrast in PVO SI, the CO emission decreased from 33.0g/KWh in E0 to 12.0g/KWh in E85. As discussed previously, such a decrease may be caused by better ethanol fuel-mixture quality, due to the interaction of the valve-timing, injection-timing and gas exchange process.

The HC emissions shown in figure 5.16(b) display similar trends with the ISCO emissions for the three modes. Increased ethanol blends from E15 to E85 lead to increase in ISHC emissions for the throttled SI and CAI NVO combustion. This may be explained as follows, in the burning of ethanol-gasoline blends, the lighter fractions will burn earlier while, the heavier hydrocarbon will still continue to burn far into the expansion process, the likely reason we have higher HC emissions.

The PVO SI exhibited the most pronounced change in ISHC with increased added ethanol content. This result showed that more complete fuel evaporation had taken place with the E85.

It can be seen from Figure 5.16(c) that the CAI NVO mode using E15 produced the lowest NOx compared to E85.

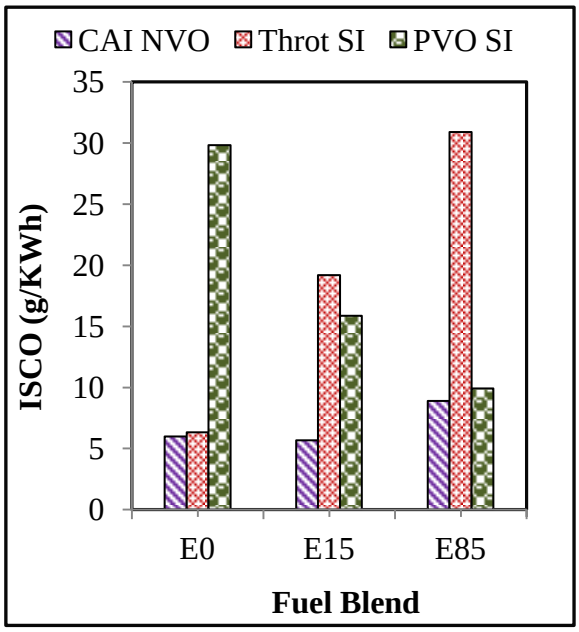


**(a) ISCO**

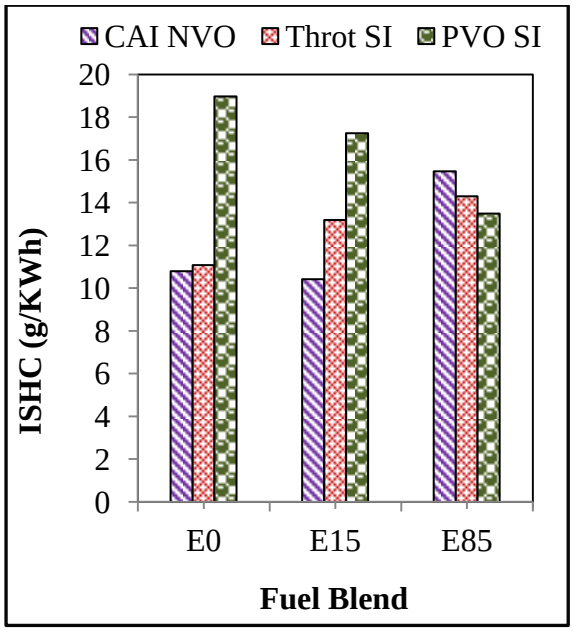


**(b) ISHC**

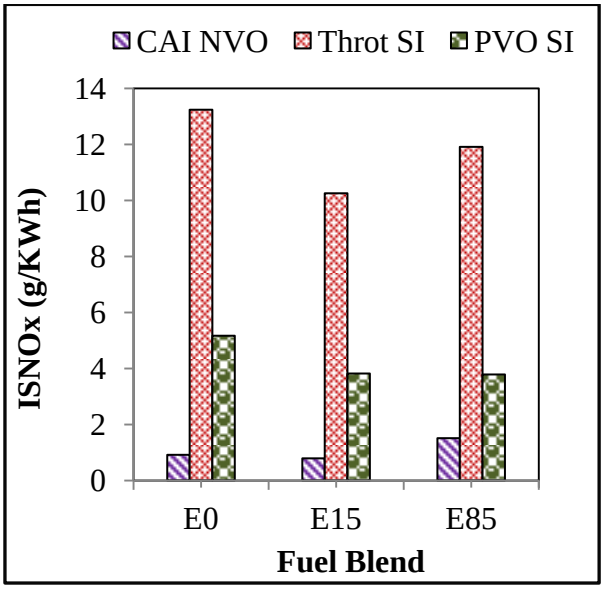


**(c) ISNOx**

**Figure 5.16 Gaseous Emissions and Fuel Consumption**

**Particulate Emissions**

Figure 5.17(a) and (b) shows the effects of increasing the quantity of ethanol blends from E15 to E85 on particulate number and total number emitted. The effects of the blend ratio in CAI NVO was the shifting of the particulates towards smaller size particles, however increasing the ethanol contents from E15 to E85 increases the particle numbers. Interestingly, figure 5.17(b) shows that the total particles number decreased in blending with E15, but increasing the ethanol content to E85 slightly increased the total particles numbers.

In the case of throttled SI operations, similar trend was observed as in CAI NVO regarding the particulate number and total number emissions in using E15 and E85.

However, in the case of PVO SI, the addition of E15 and E85 lead to increase in particulate numbers and total emissions. This may have been due to the interaction of the valve-timing, injection-timing and gas-exchange process. Injecting into re-inducted hot exhaust and fresh air must have improved mixture formations. However, injecting E15 and E85 may have led to excessive charge cooling effects leading to some pockets of rich mixtures and incomplete combustion evidenced by high ISHC emissions shown in figure 5.16(b)

We can conclude that the presence of oxygen in E15 and E85 helped to reduce the particle formation in CAI NVO and throttled SI modes.

However, in the case of PVO SI, the presence of E15 and E85 seems to have affected combustion negatively, resulting in higher particulate emissions, this may require further investigations using optical engines.

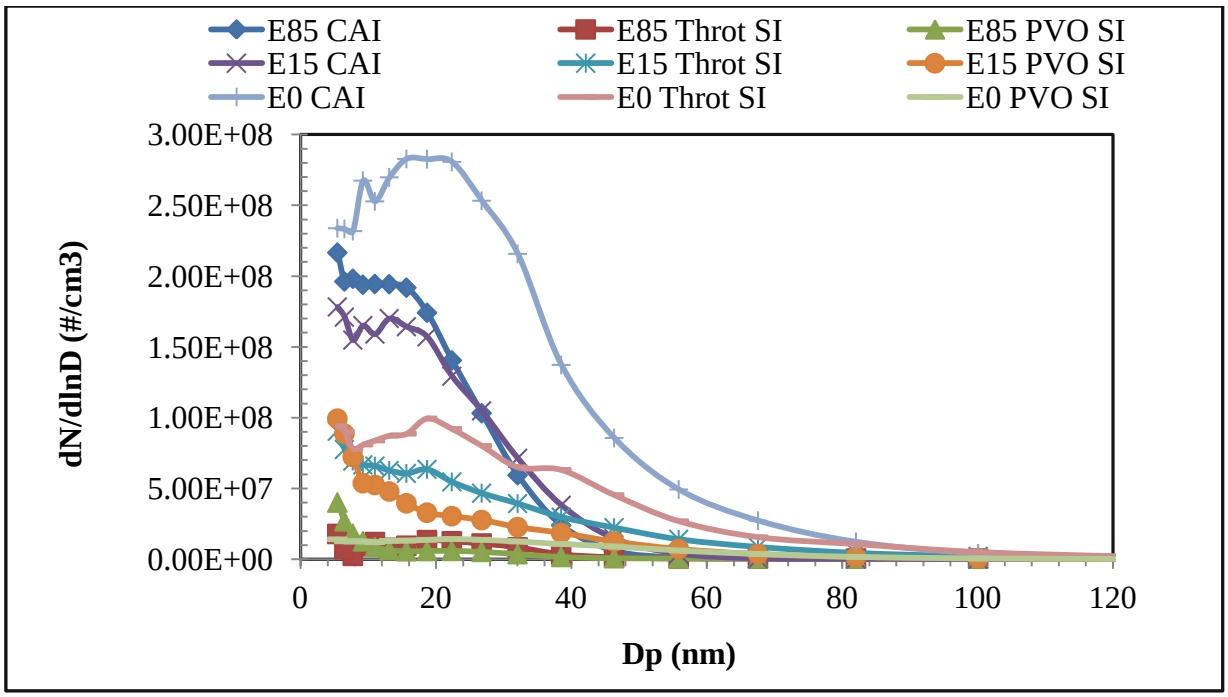


**(a) Particulate Number Distribution**

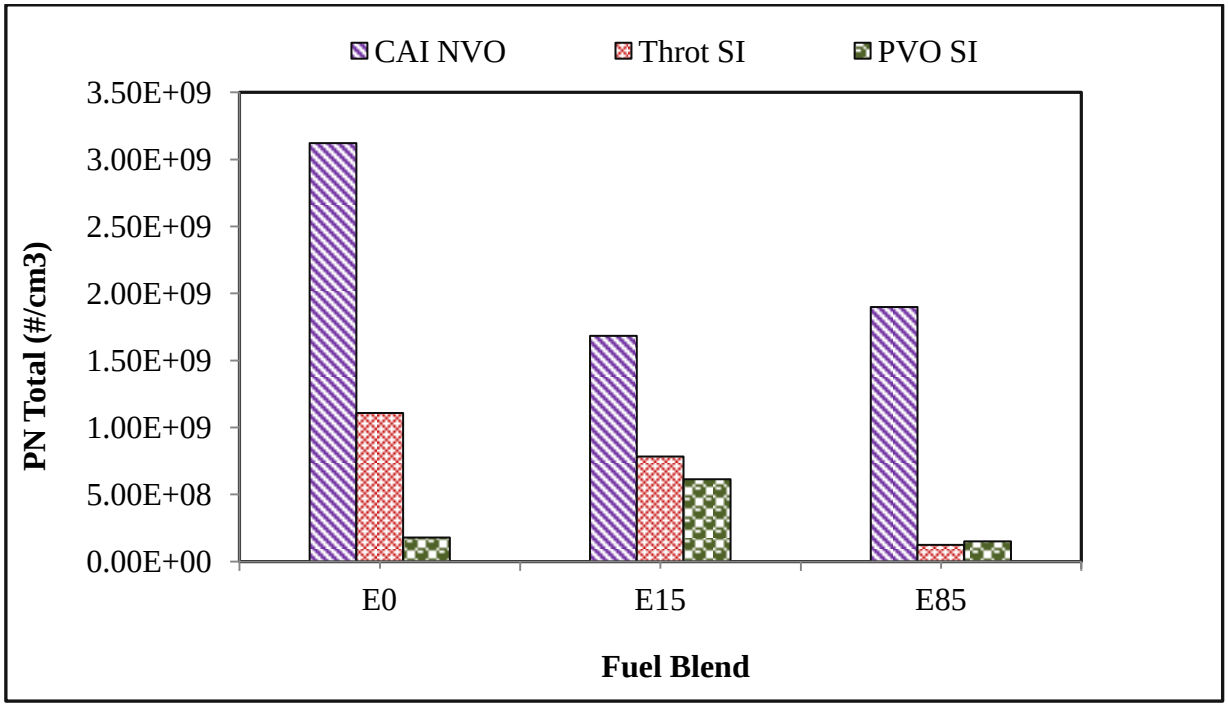


**(b) Total Particulate Number**

**Figure 5.17 PN and Total PN Emissions**

**Summary**

**The use of E15 and E85**

The use of E15 and E85 in lamda 1.0 resulted in reduction in pressure rise rate and longer burn duration in CAI combustion. There was reduction in combustion efficiency in throttle SI and PVO SI. In contrast, there was increase in combustion efficiency in PVO SI as ethanol blend increases from E0 to E85. The ISCO and ISHC were higher in E15 and E85 compared to E0. In the case of PVO SI the ISCO and ISHC decreased as ethanol increases from E0 to E85. In CAI use of ethanol led to slight increase in NOx, but a reduction was recorded in NOx for cases of PVO and throttled SI.

The use of E15 and E85 resulted in higher particulate number emissions but reduced in size.

### 5.7 Comparison of gasoline, E15 and E85 at Lambda 1.1.

#### 5.7.1 Combustion Analysis

Figure 5.18 shows and compares the combustion characteristics of the three operation modes with lean mixture (lambda = 1.1) using E15 and E85. It should be noted that in the throttled SI combustion the throttle was partly opened, the PVO SI and CAI NVO combustion modes were operated with the wide-open throttle (WOT). Here lambda was maintained at 1.1 that is lean combustion and readings are taken when the engine operating conditions have stabilized.

Figure 5.18(a) shows the effects of E15 and E85 on maximum pressure-rise rate as a function of combustion modes in lean-mixtures. The blends of E15 and E85 resulted in noticeable reduction in the pressure rise rate of CAI combustion from value of 5bar/CA to 1.4bar/CA.

The effects of E15 and E85 on MBT spark timing is shown in Figure 5.18(b), in PVO SI and CAI NVO operations lead to spark retard and advance.

In the throttled SI mode E15 lead to slight retard, however in E85 the spark was further advanced, this may likely be due to slower burning velocities, as evidenced by the mass fraction burned in Figure 5.18(d) and the corresponding heat-release rate in Figure 5.18(c). Furthermore, addition of E15 and E85 showed a noticeable reduction in the heat-release rate and combustion-phase shift in the CAI NVO operation similar to the case of stoichiometric mixture.

As shown in Figure 5.18(e), E15 and E85 does not have appreciable effect on the combustion stability, the COVimep for all modes were below 3.0 % and did not vary significantly with the fuel blends and combustion was stable in all the test..

Using E15 and E85 as shown in Figure 5.18(f) in lean-mixture in MBT timing does not have appreciable effects on the exhaust temperature.

Figure 5.18(g) shows that using E15 and E85 in CAI combustion, advances the ignition timing. In the case of throttled SI and PVO SI using E15 lead to ignition delay however addition of E85 lead to further ignition advance.

The use of E15 and E85 in lean mixtures causes the overall combustion period to increase appreciably in CAI combustion compared to the PVO SI and throttled SI whilst the CAI combustion was the shortest.

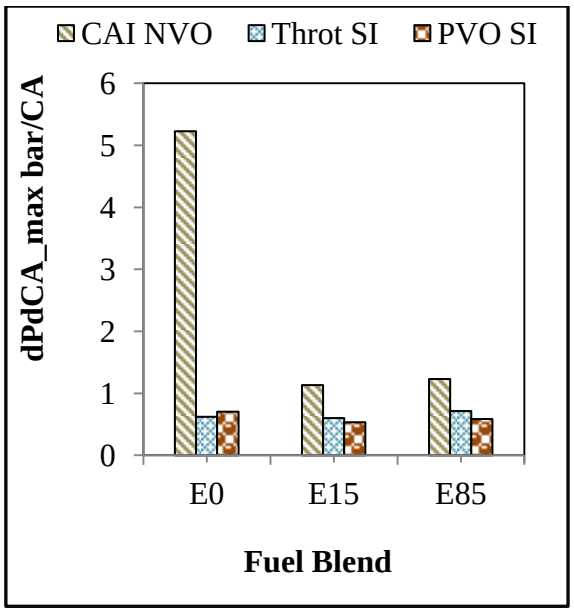


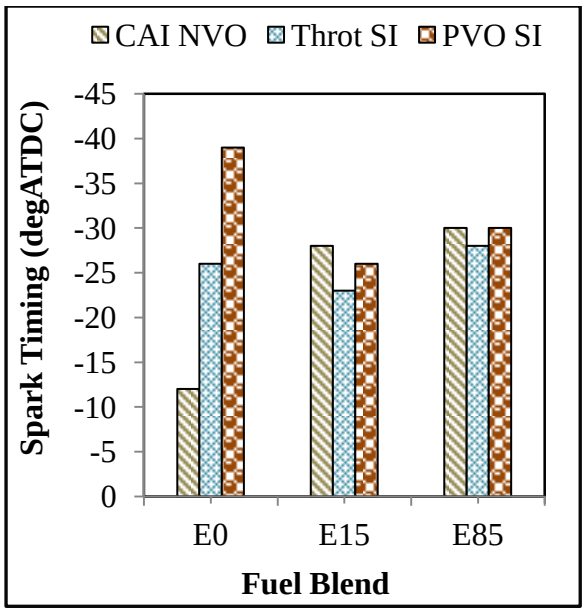


**(a) Maximum Pressure Rise Rate** **(b) Spark Timing**

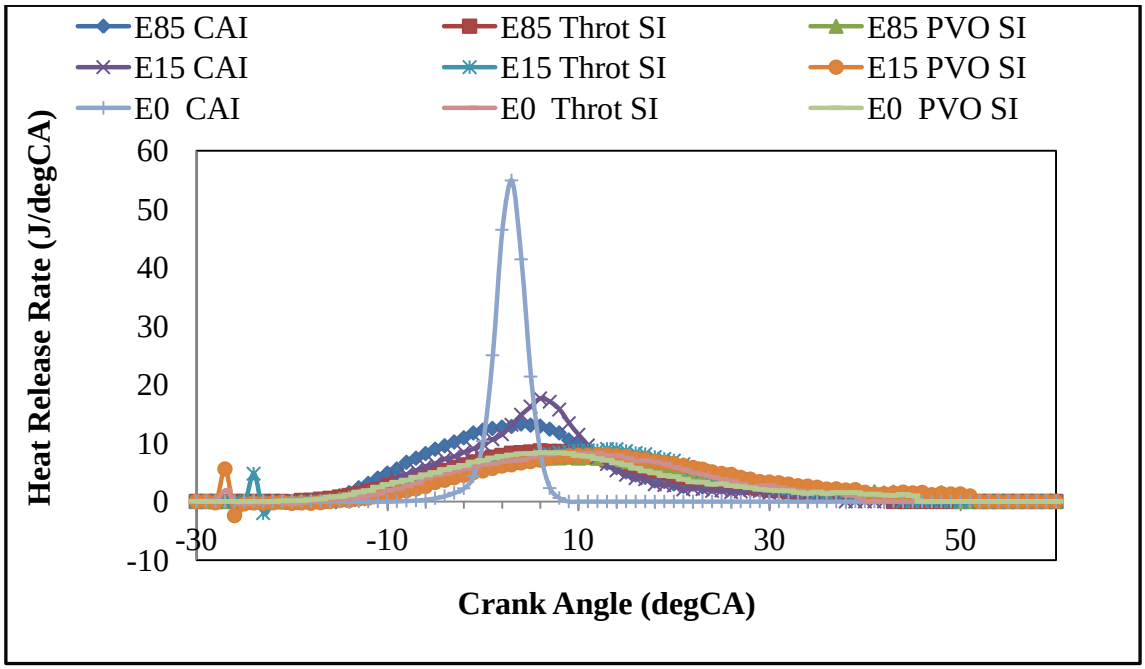


**(c) Heat Release Rate**

**Figure 5.18 Combustion Analysis**

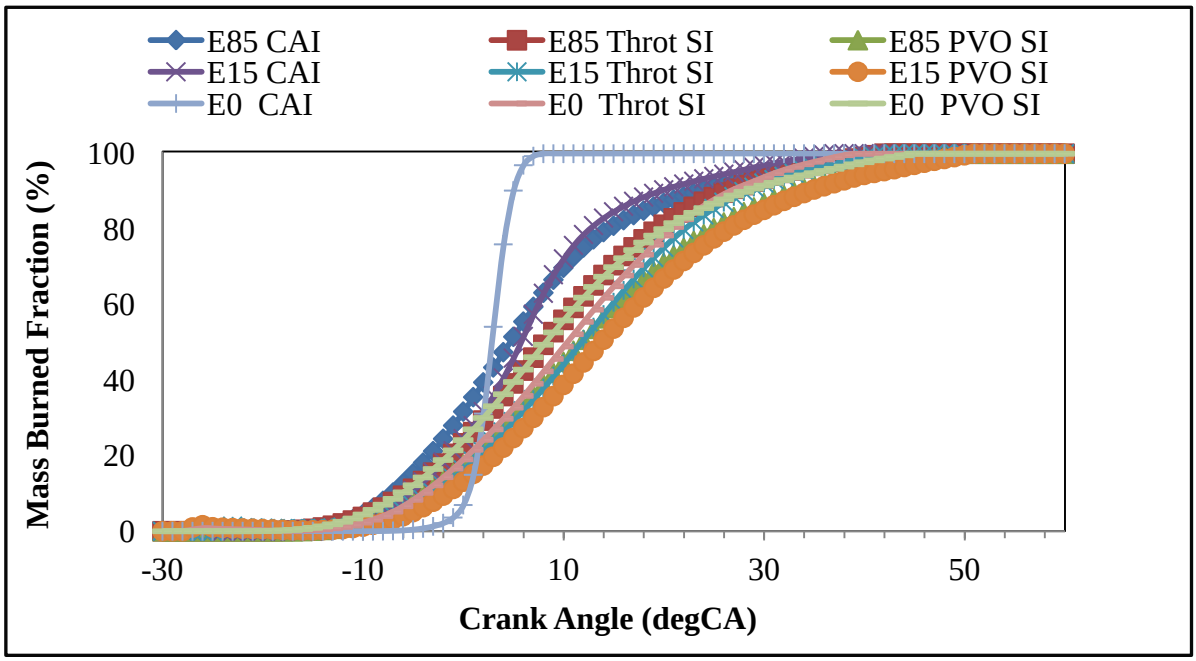


**(d) Mass Burned Fraction**

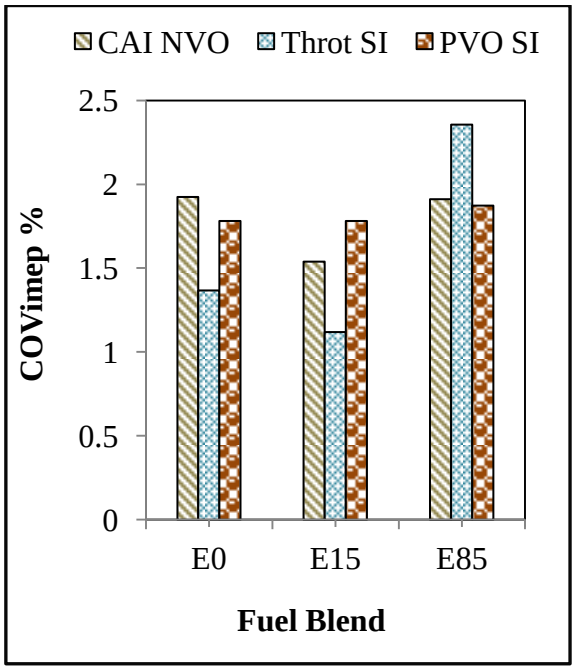


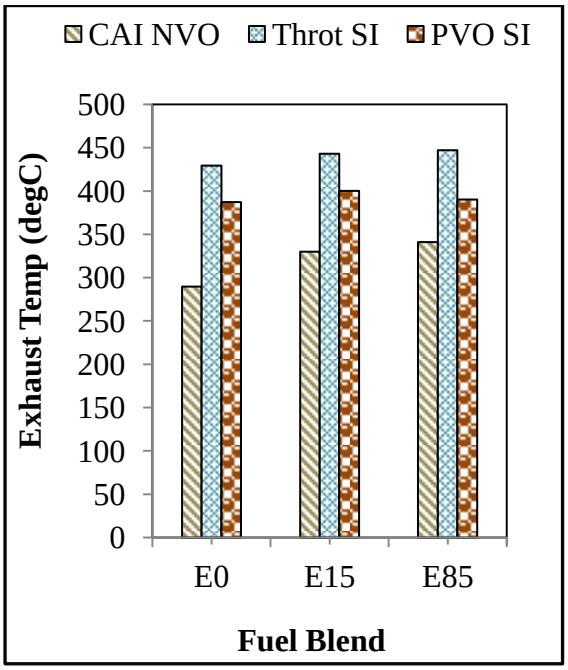


**(e) COV of IMEP**

**(f) Exhaust Temperature**

**Figure 5.18 Combustion Analysis (ctd)**

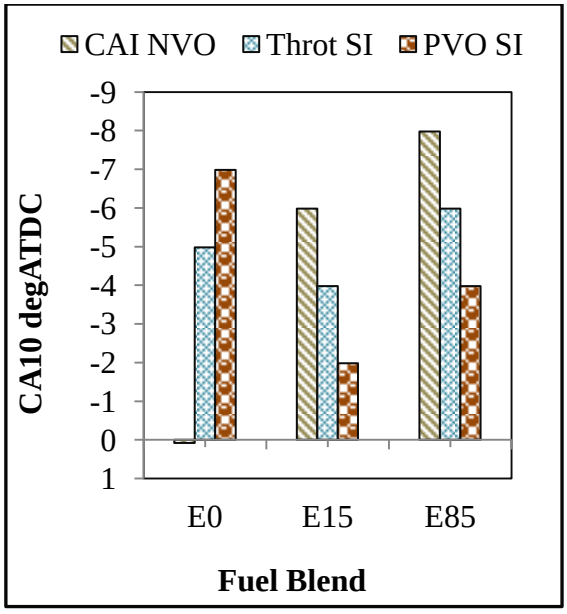


**(g) CA10**

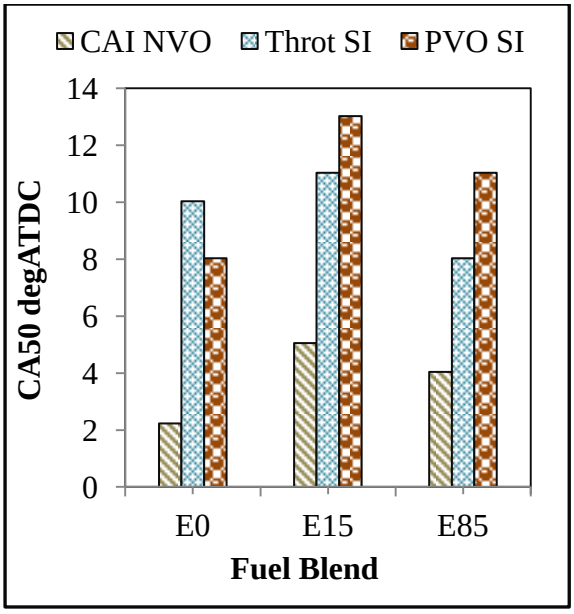


**(h) CA50**

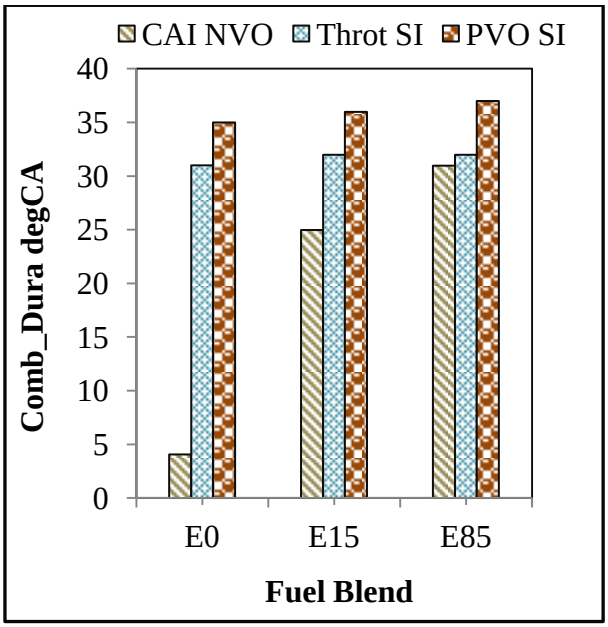


**(i) Combustion Duration**

**Figure 5.18 (ctd) Combustion Analysis**

### 5.7.2 Engine Performance and Efficiency Analysis.

Shown in Figure 5.19(a) is the combustion efficiency result using E15 and E85 fuel blends. The use of E15 have slight effects on the combustion efficiency, this may be as a result of the vapour pressure and distillation curve of ethanol-gasoline blends in ratio of 15% and higher as in E15 and E85. Using lean mixture of lambda = 1.1 resulted in reduced fuel injection, this

would have affected the combustion process. However, as the ethanol content is increased to E85, the combustion efficiency of CAI NVO and throttled SI reduced by about 3%, but the combustion efficiency of the PVO SI increased by about 1.2%. The lower combustion efficiency is likely to be related to the charge-cooling effects of the ethanol on lean mixture.

The thermodynamic efficiency of the engine is shown in Figure 5.19(b) using E15 and E85. In CAI NVO, the use of E15 and E85 does not have any appreciable effects on the efficiency, however in throttled SI the blends did cause slight reduction in the efficiency. In PVO SI E15 does not have any effects, but E85 resulted in slight increase.

Figure 5.19(c) shows the effect of using E15 and E85 in lean-mixtures on the indicated efficiency. The use of ethanol blends in throttled SI mode lead to reduced indicated efficiency (34% in E0 to 33% in E15 and 32% in E85), while in the PVO SI the indicated efficiency increased from 37.6% in E0 to 38% in E15 and to 39.5% in E85.

The use of E15 and E85 in CAI NVO combustion in lean mixture did not display any particular trend on indicated efficiency it was relatively constant at 36%.

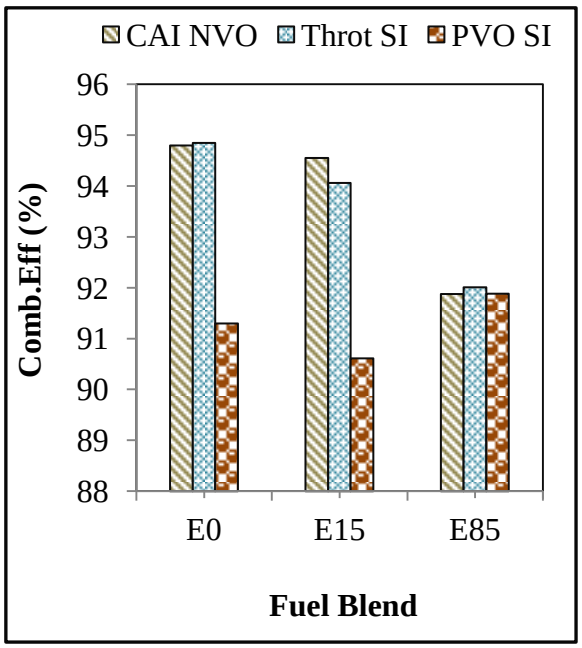


**(a) Combustion Efficiency**

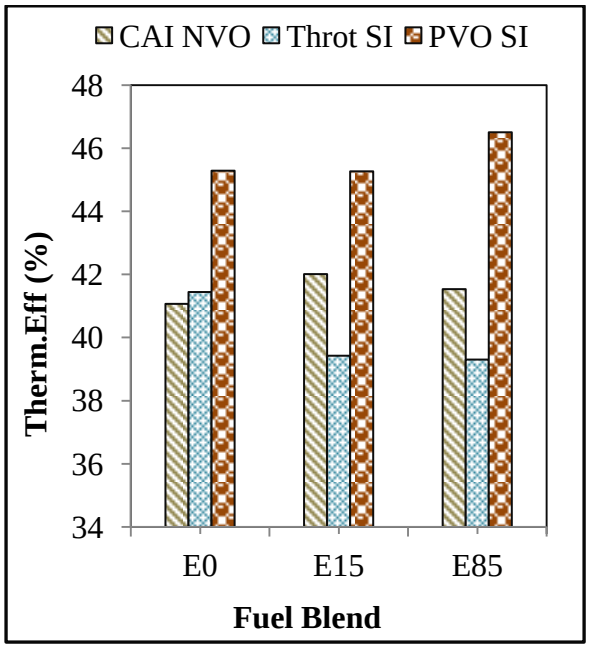


**(b) Thermal Efficiency**

**Figure 5.19 Performance Analysis**

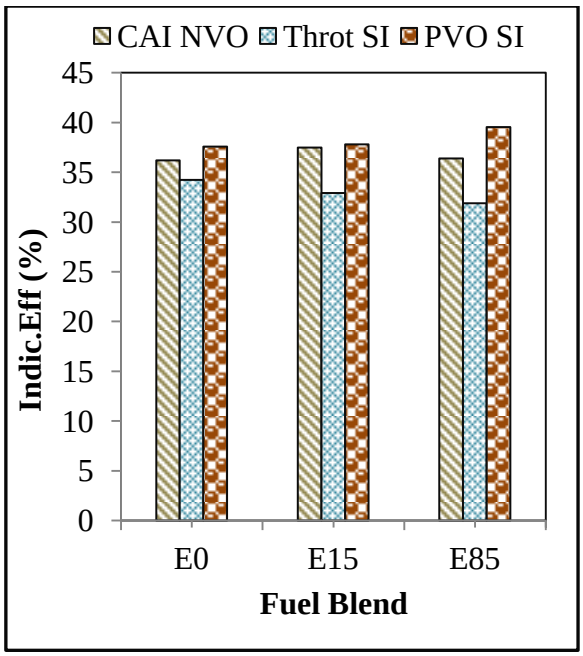


**(c) Indicated Efficiency**

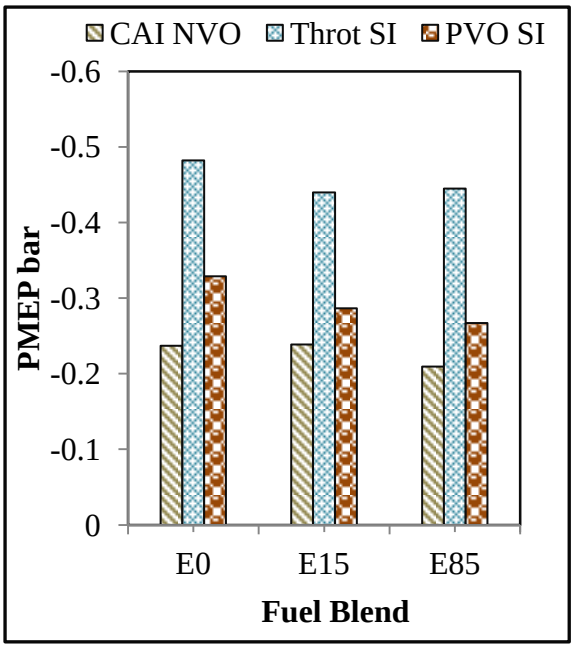


**(d) PMEP**

**Figure 5.19 (ctd) Performance Analysis**

### 5.7.3 Emissions and Fuel Consumption

In this part of the analysis, the exhaust emissions such as CO, UHC, and NOx are analysed in the three combustion modes and fuel blends with lambda 1.1. All emission results were converted into the indicated specific values (g/KWh).

The effect of E15 and E85 lean-mixture as it affects CO emissions in all the modes are shown in Figure 5.20(a). In the throttled SI using E15 and E85 lead to increased CO emissions from 5.0 g/KWh in E0 to 22.0 g/KWh in E85 which was twice that recorded in any other modes.

The PVO SI CO emissions increased from 6.4g/KWh in E0 to 9.0g/KWh in E15 and remained the same in E85. In CAI NVO the CO emissions recorded was 6.3g/KWh in E0 and E15, then increased to 9.3g/KWh in E85. Overall, the use of E15 and E85 in lean mixture, may have led to poor mixture preparation, which may likely be caused by the charge cooling effect of increased ethanol-gasoline blend in E85.

Shown in Figure 5.20(b) is the change in ISHC using E15 and E85 in lean-mixtures. The use of ethanol in lean-mixture lead to increased UHC, this may likely have been caused by the reduced availability of enough fuel to participate in the combustion, thereby leading to incomplete combustion, the likely reason for the increased UHC emissions in all the modes.

It can be seen from Fig.5.20(c) that the CAI NVO mode produced the lowest NOx emission as a result of high dilution rate, reduced combustion temperature due to lean mixture (lambda 1.1).

The ISFC shown in Figure 5.20(d) was similar to the case of stoichiometric mixture (lambda=1.0) in the previous section, however there was slight improvement over the case of lambda 1.0, because of the reduced quantity of injected fuel.

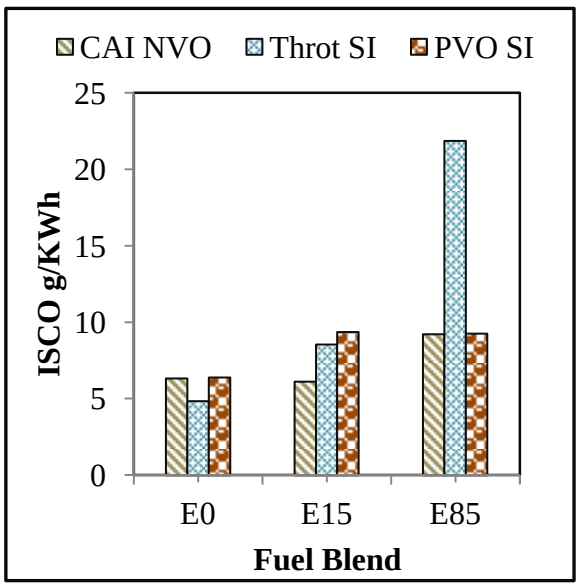


**(a) ISCO**

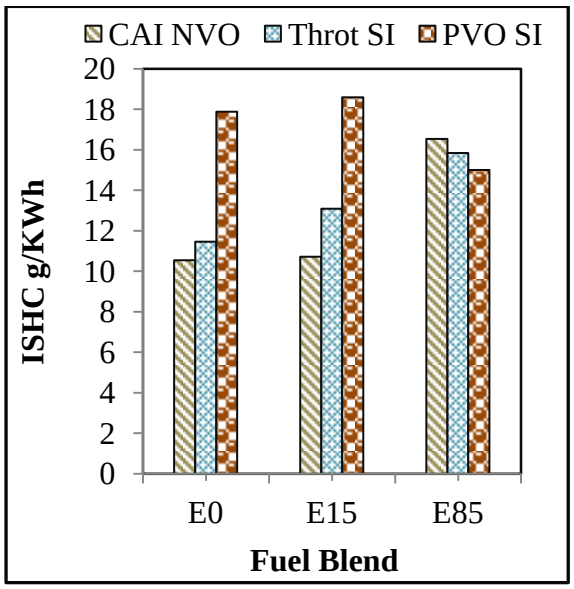


**(b) ISHC**

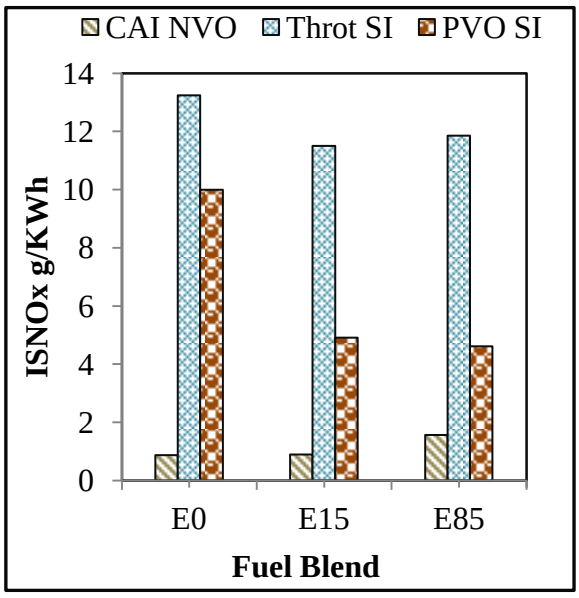


**(c) ISNOx**

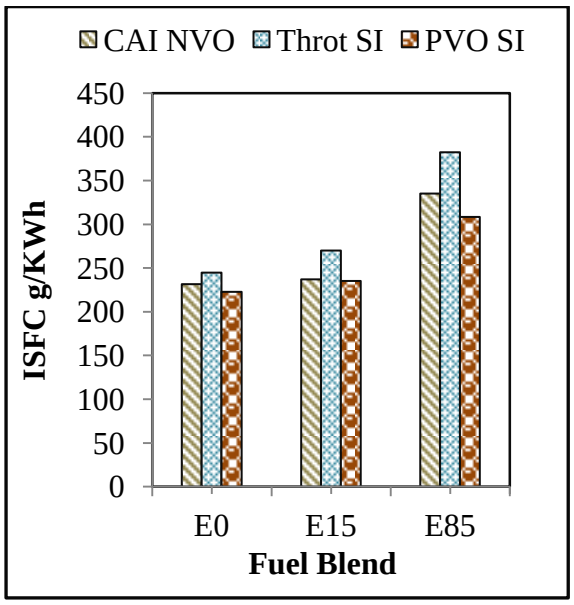


**(d) ISFC**

**Figure 5.20 Gaseous Emissions and Fuel Consumption**

**Particulate Emissions**

The effect of using E15 and E85 on the particulate emissions in their total numbers and size distributions are shown Figure 5.21(a).

In the case of throttled SI operations, the number of particles (PN) decreased rapidly when the ethanol content was increased from E15 to E85. In CAI NVO the use of E15 lead to reduction in particulate number and shifts to particles of smaller size, however as the ethanol content was increased to E85, the particles shifted further to smaller sizes but higher volume of particulate was emitted. The presence of oxygen in E15 and E85 helped to reduce the particle formation.

As shown in Figure 5.21(a), the PVO mode was characterised by the same trend as in the previous cases, the use of E15 and E85 lead to increased particle number emissions.

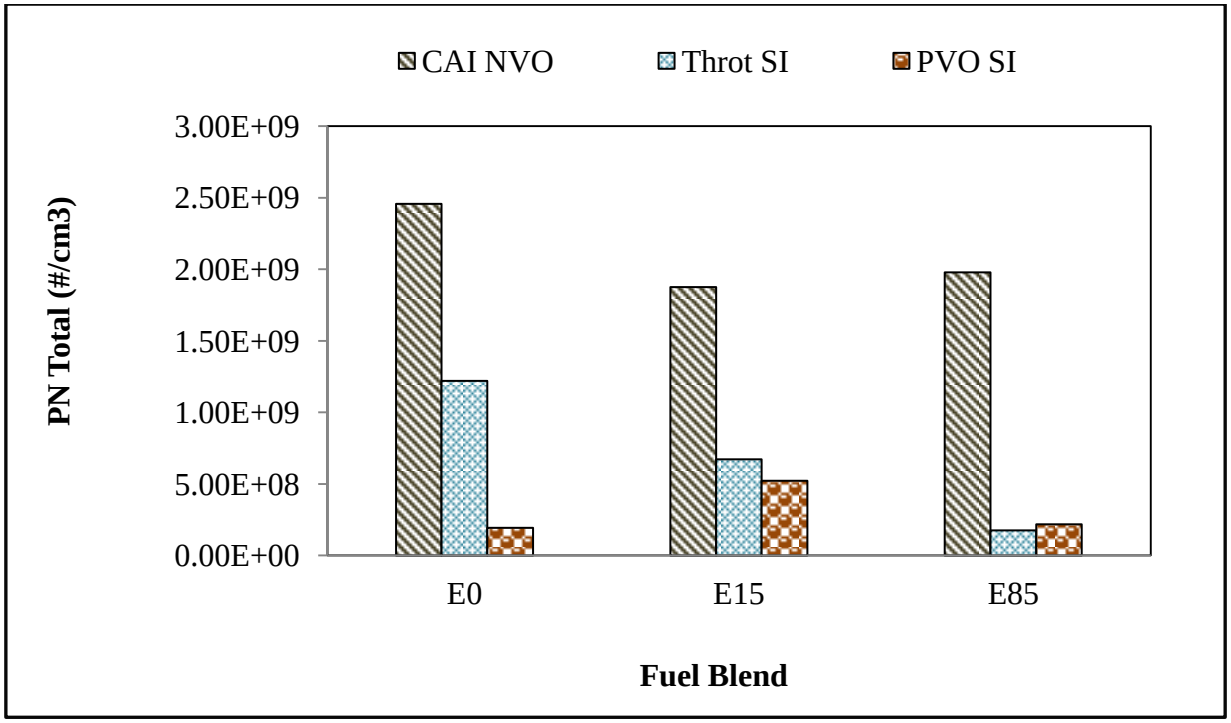


**(a) PN Total**

**Figure 5.21 Particulate Emissions**

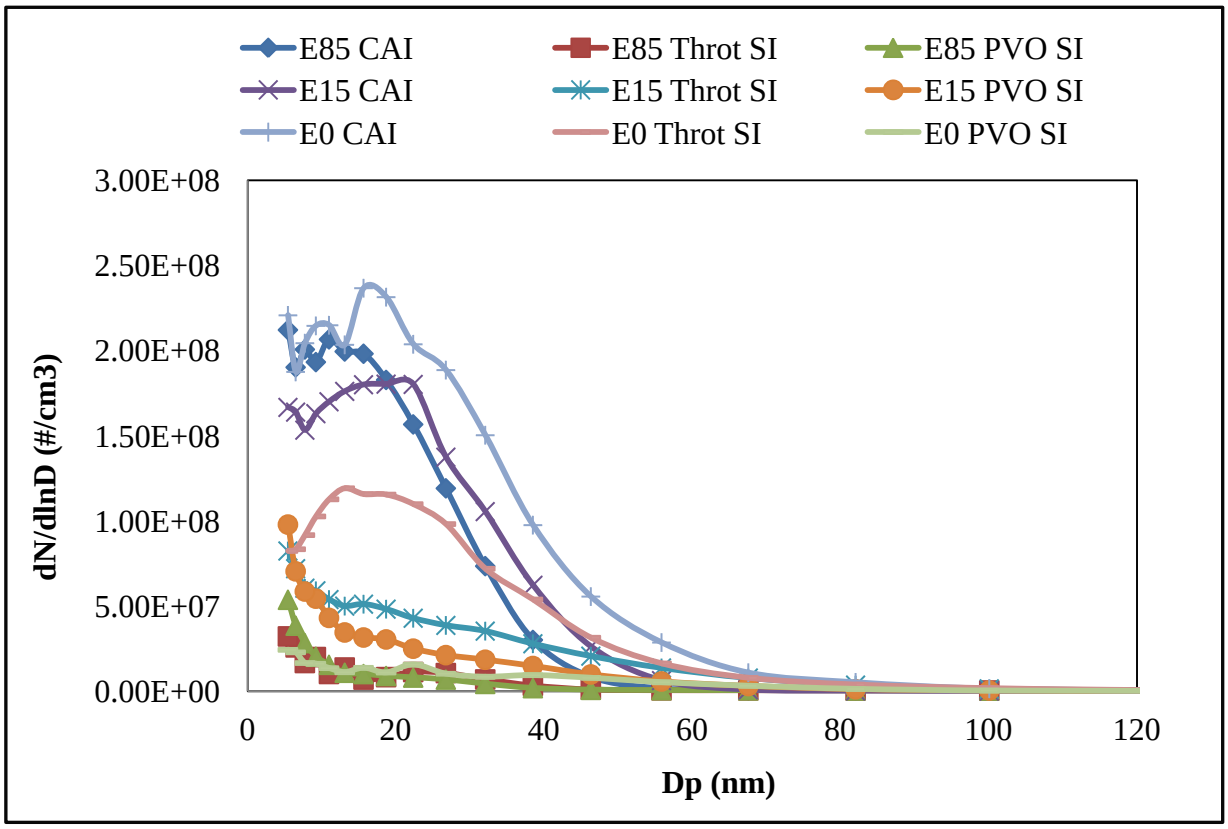


**(b) Particulate Number Emission**

**Figure 5.21 (ctd) Particulate Emissions**

**Summary**

In the PVO SI 3%, 5% and 8% higher indicated efficiencies were obtained in E0, E15 and E85 with corresponding higher fuel savings of 9%, 13% and 19.5% respectively compared to the baseline throttled SI and CAI combustion.

The PVO SI suffered from the lowest combustion efficiency but improved gas exchange and indicated efficiencies, and the lowest ISFC over Throttled SI. The addition of ethanol had the most pronounced effect on improving the pressure rise rate of CAI NVO combustion mode.

The CAI NVO mode produced the least CO in E0, E15, and E85 and least ISHC in E15 and E85. The injection of fuel during NVO period enabled better mixture preparation, this helped to eliminate regions of rich mixture that were responsible for higher CO formations in the E15 and E85 fuel blends.

The addition of ethanol caused significant increase in CO emissions from locally rich mixtures due to increased injection durations during Throttled SI mode. In the Throttled SI mode, the presence of ethanol led to significant reduction in particulates.

The PVO mode was characterised with the lowest number of particles amongst the three operational modes because of the higher in-cylinder charge temperature, the effect of ethanol was the least evident in the formation and emission of particlulates.

The fuel injection during the NVO period was assumed to lead to the production of soot particles (<50nm in size) in the CAI combustion mode due to hydrocarbon pyrolysis. The soot oxidation was rendered less effective by the lower combustion temperature. The presence of ethanol led to reduction of particulate number in CAI combustion because of the oxygenate nature of Ethanol**.**

## 5.8 Comparison of gasoline E0, E15 and E85 at Lambda 1.2

### 5.8.1 Combustion Analysis

In this test the mixture was made leaner by increasing lambda to 1.2. Like in the previous work the effects of using E15 and E85 on pressure rise rate was investigated in three operational modes of throttled SI, PVO and CAI NVO as shown in Figure 5.22(a), the MPRR in the CAI combustion was 2.5 bar/CA in E0 which was 5 times higher compared to the value in throttled SI and PVO. The addition of E15 and E85 resulted in noticeable reduction in the pressure-rise rate of CAI to 1.4bar/CA. No noticeable effect was observed for the PVO and throttled SI.

As shown in Figure 5.22(b), the use of E5 and E85 in leaner mixture resulted in a significant spark advance in MBT timing in CAI combustion.

The use of E15 and E85 in PVO SI mode led to spark retarding. In the throttled SI the use of E15 and E15 does not have any noticeable effects on the spark timing, due to slower burning velocities, as evidenced by the mass fraction burned (Figure 5.22(f)) and the corresponding heat-release rate (Figure 5.22(e)).

The effects of E15 and E85 using lambda 1.2 on the COVimep shown in Figure 3(e) for all modes were below 3.0% and did not vary significantly with the fuel blends and combustion modes studied. However, the COVimep for throttle SI was quite high about 4.5%. The reason for the high value of COVimep in E85 throttled SI was likely due to occasional misfire cycles encountered in operating the engine with too lean a mixture (lambda 1.2).

As shown in Figure 5.22(d), in using E15 and E85 in the throttled SI combustion mode, PVO SI, and the CAI NVO, there was no appreciable effects on the exhaust temperature observed..

Figure 5.22(i) shows like in the previous section (when lambda was 1.1) that in using E15 and E85 the overall combustion period increased from the CAI NVO to PVO SI. The CAI combustion was the latest to commence but with the shortest duration. The long combustion duration may likely be due to, the heavy dilution with fresh air and the charge cooling-effects of the E15 and E85 blends in a lean mixture, must have led to poor mixture preparation and incomplete combustion ( Figure 5.24(a) and (b)).

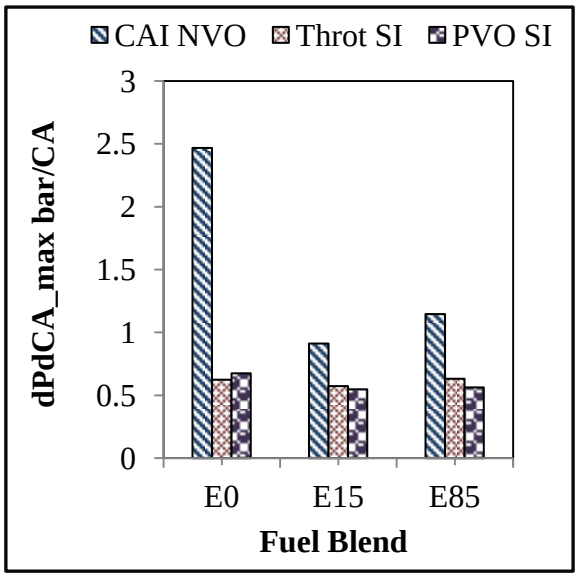


**(a) Maximum Pressure Rise Rate**

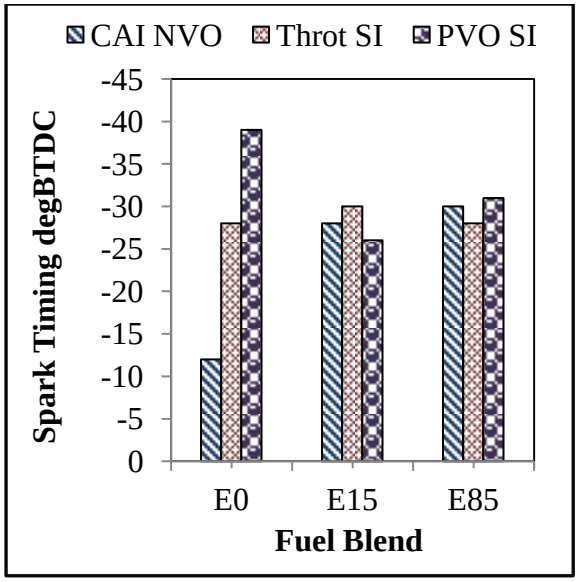


**(b) Spark Timing**

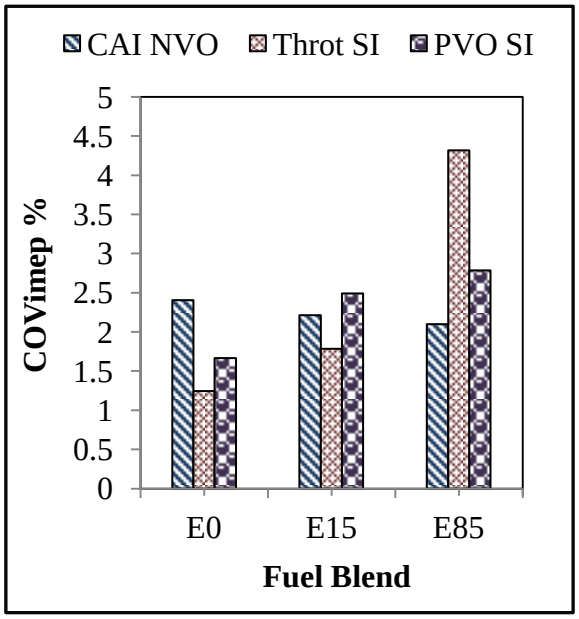


**(c) COV of IMEP**

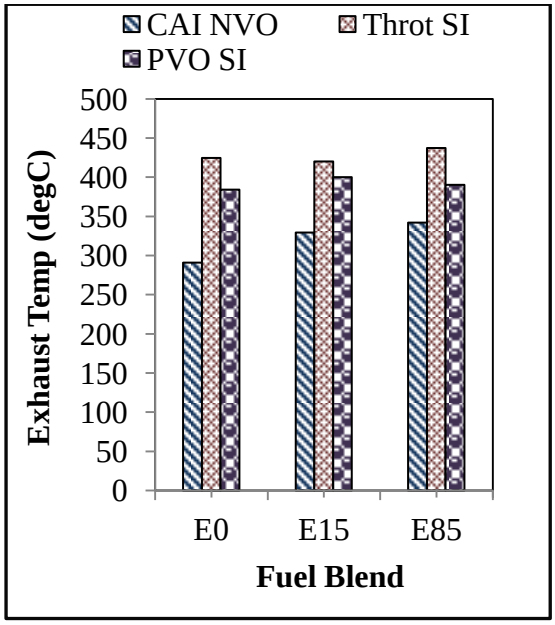


**(d) Exhaust temp**

**Figure 5.22 Combustion Analysis**

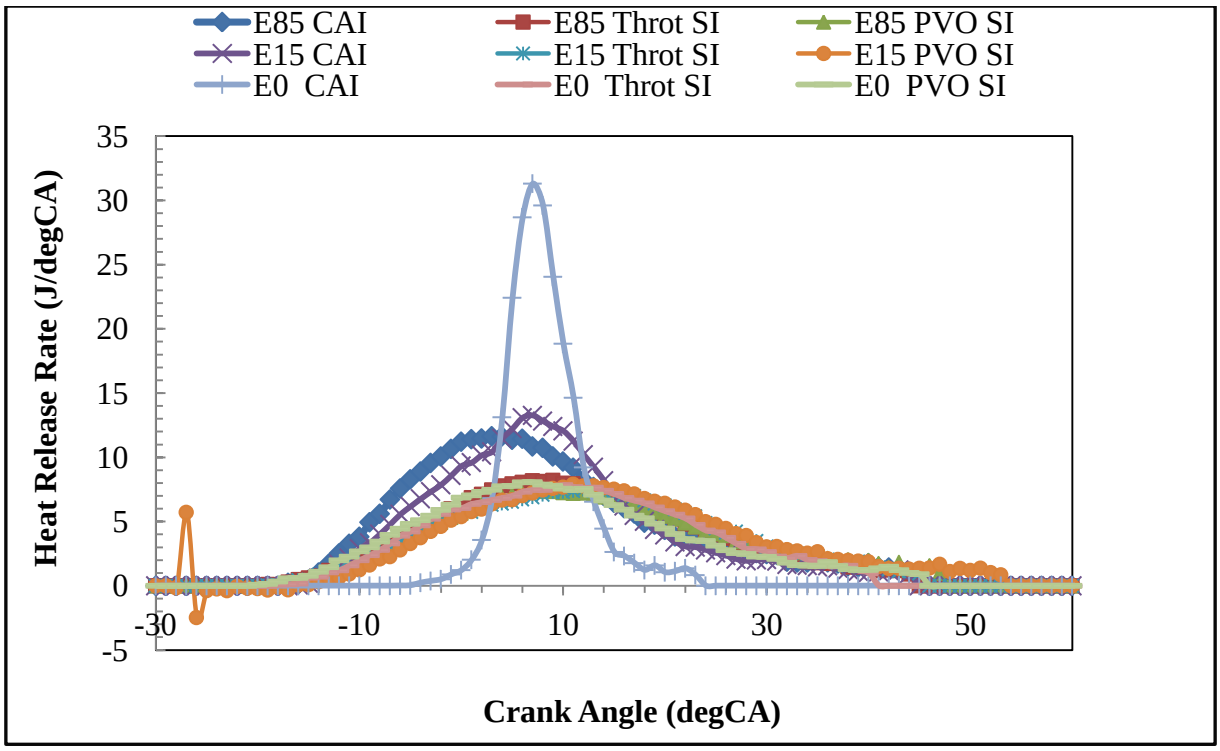


**(e) Heat Release Rate**

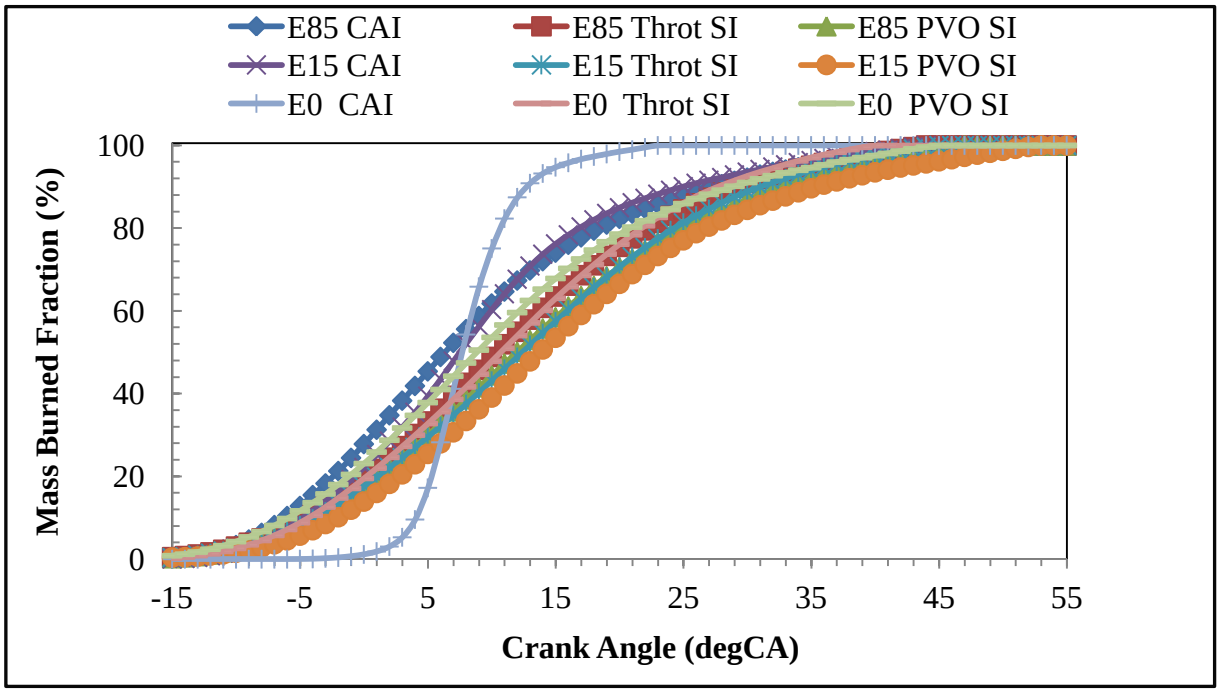


**(f) Mass Burned Fraction**

**Figure 5.22 (ctd) Combustion Analysis**

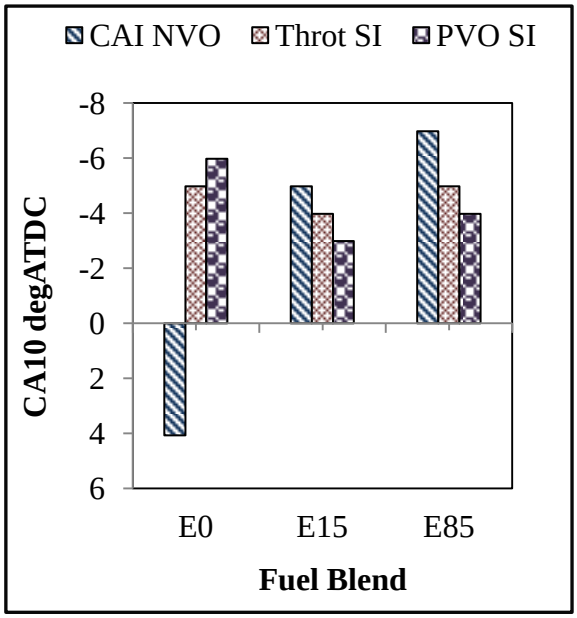


(g) CA10

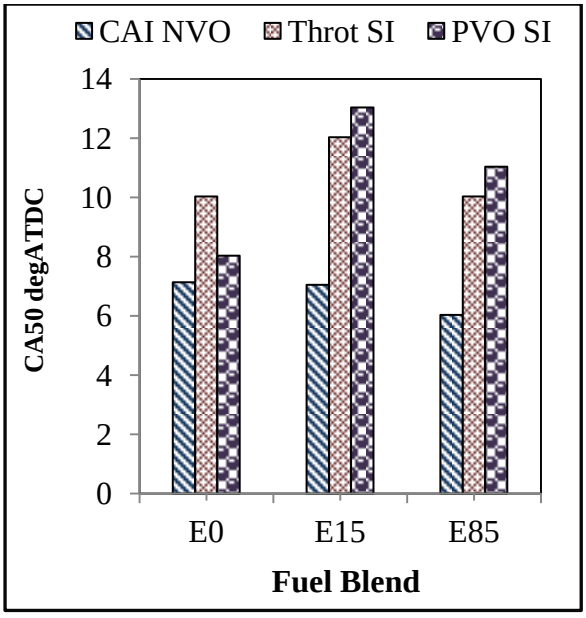


(h) CA50

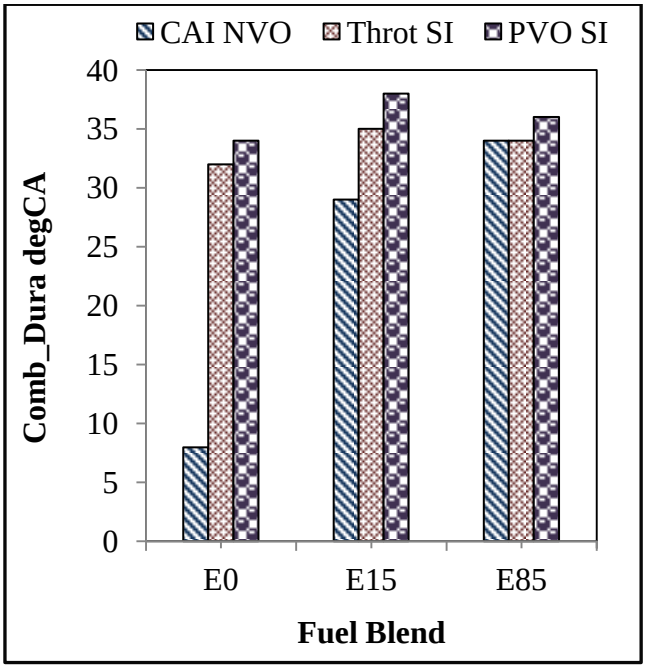


**(i) Combustion Duration**

**Figure 5.22 (ctd) Combustion Analysis**

### 5.8.2 Engine Performance and Efficiency Analysis

Figure 5.23(a) shows the combustion efficiency for the combustion modes and fuel blends with lambda 1.2. It was observed that using E15 and E85 resulted in reduced combustion efficiency in both throttled SI, PVO SI and CAI combustion modes. The reduced combustion efficiency associated with using E15 and E85, are likely to be related to the charge cooling-effects of the ethanol and poor mixture formation that may have resulted in pockets of rich mixture, as indicated by the higher CO and HC emissions (Figure 5.24(a) and (b))

On the thermodynamic efficiency, there was slight increase in the values obtained for PVO SI. In the case of throttled SI and CAI NVO, the use of E15 and E85 have no effects.

Figure 5.23(c) compares the effects of using E15 and E85 on indicated efficiency of the modes. The throttled SI indicated efficiency showed a slightly decreasing trend from 34% in E0 to 33% in E15 and to 32% in E85 respectively. In contrast to throttle SI, slight increase in indicated efficiency was observed in PVO SI increasing from 37% in E0 to 38.8% in E15 and to 40.5% in E85.

In the CAI NVO the indicated thermal efficiency was relatively constant at 37%.

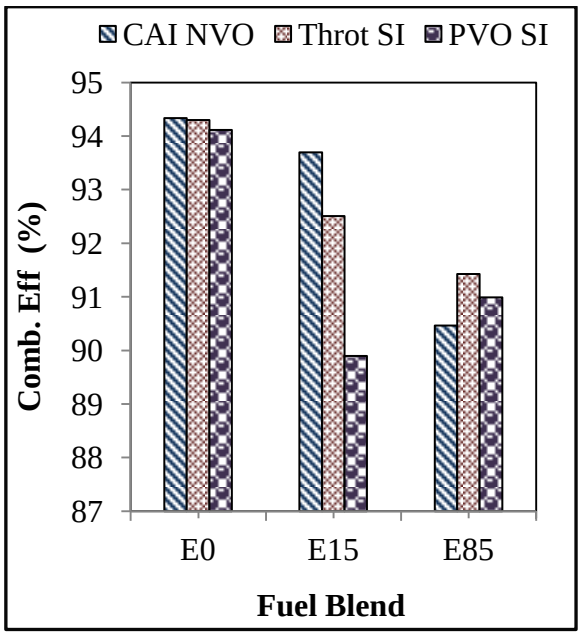


**(a) Combustion Efficiency**

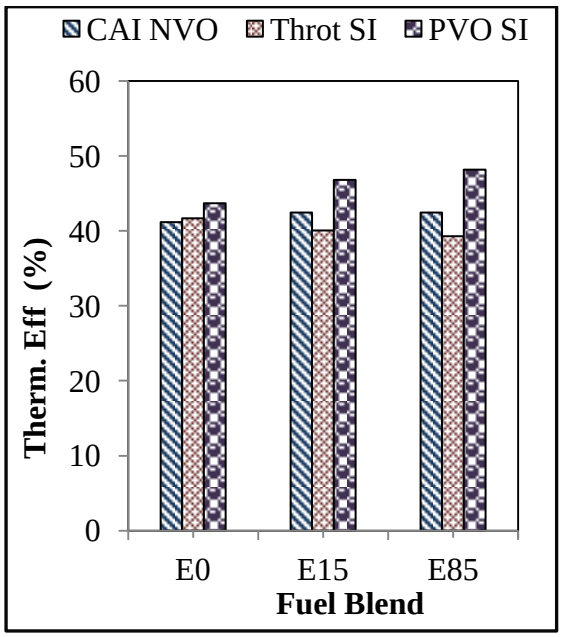


**(b) Thermal Efficiency**

**Figure 5.23 Performance Analysis**

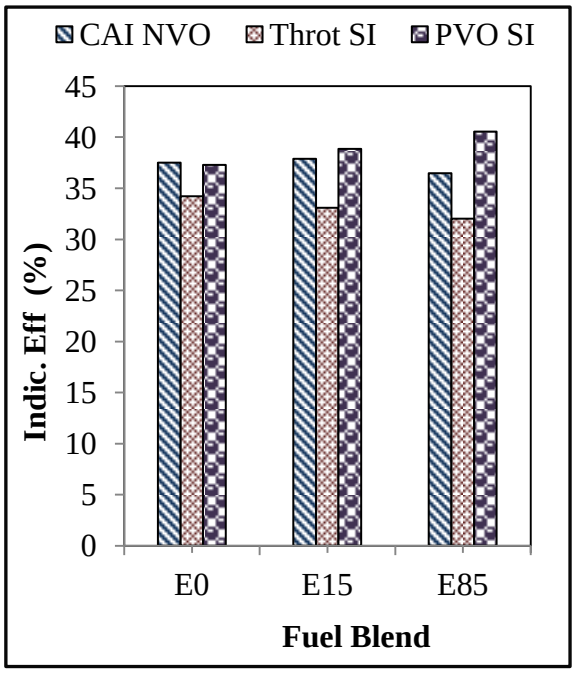


**(c) Indicated Efficiency**

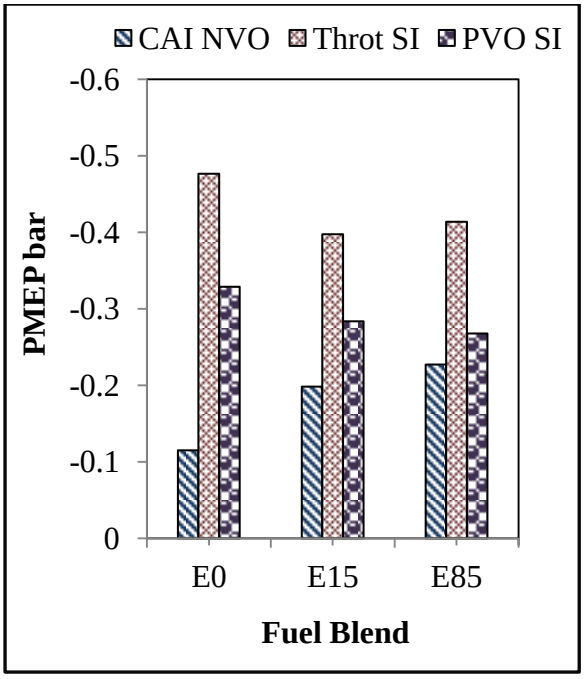


**(d) PMEP**

**Figure 5.23 (ctd) Performance Analysis**

### 5.8.3 Emissions and Fuel Consumption

Figure 5.24(a) shows the CO and UHC emissions in the three combustion modes and fuel blends. As observed Figure 5.24(a), the use of E15 and E85 leads to increase in ISCO emissions and ISHC (Figure 5.24(b)).

In the throttled SI using E15 and E85 increased CO emissions from 5.0 g/KWh in E0 to 9.0g/KWh in E15 to 14.5 g/KWh in E85. In PVO SI it increased from 5.0g/KWh in E0 to 8.0g/KWh in E15 to 9.4g/KWh in E85. In CAI the ISCO increased from 6.7g/KWh in E0 to 6.9g/KWh in E15 to 10.0g/KWh in E85.

As discussed previously, such an increase may be caused by poor ethanol fuel-mixture quality, the wall-wetting effect and low in-cylinder temperature as the percentage of ethanol fuel blend increased in E15 to E85 with the engine operating with lambda 1.2. In addition, the occasional misfires encountered may have also contributed to the increased UHC produced.

It can be seen from Figure 5.24(c) that the use of E15 and E85 using lambda = 1.2 increased NOx emission in CAI combustion. In contrast, the use of E15 and E85 in the throttled SI and PVO SI enabled substantial reduction in NOx emissions. In addition, increased fuel

consumption was observed in using E15 and E85 fuel blends in all the modes shown (Figure 5.24(d)).

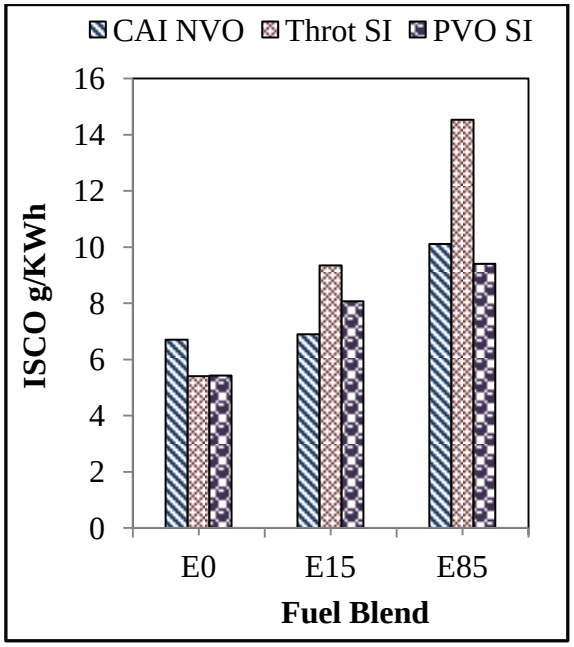


**(a) ISCO**

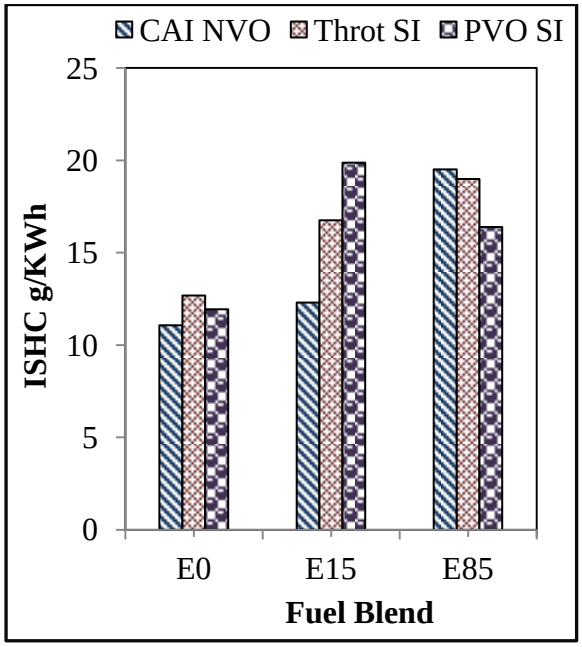


**(b) ISHC**

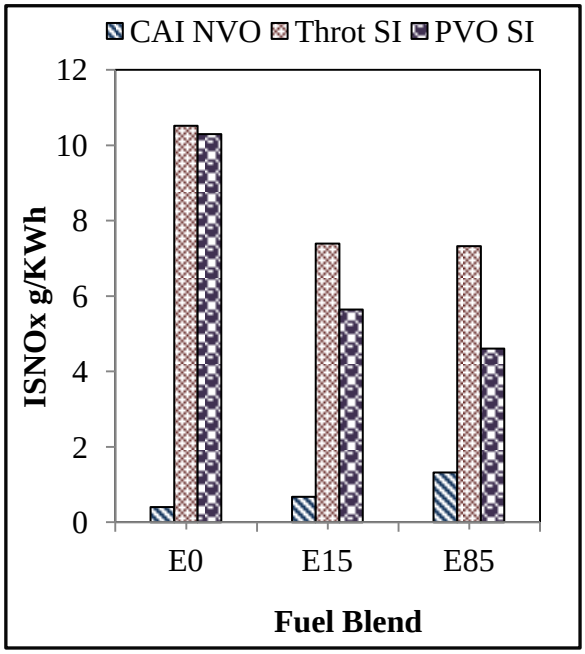


**(c) ISNOx**

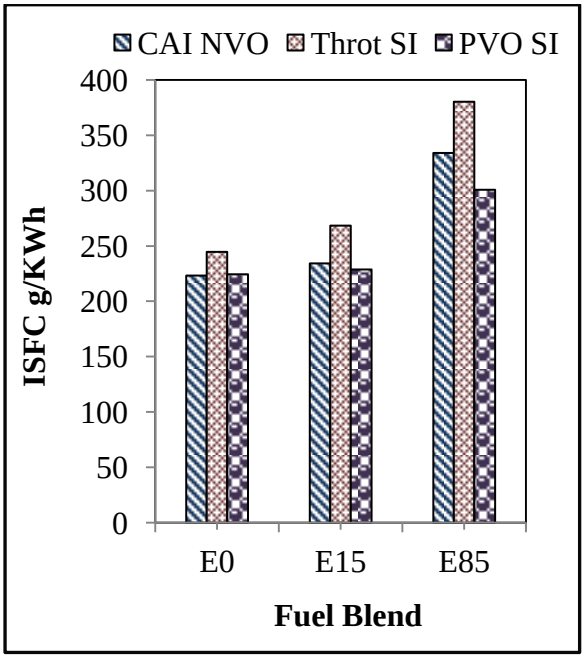


**(d) ISFC**

**Figure 5.24 Gaseous Emissions and Fuel Consumption**

**Particulate Emissions**

It was expected that the particulates will reduce with lambda=1.2, because the aromatic rings responsible for particulate formation are substantially reduced by reduced injection quantity. In using E15 and E85 blends the PN numbers and PN total results for the three modes are shown in Figure 5.25(a) and (b).

In the throttled SI operations, using E15 and E85 lead to substantial reduction in particle formations, and the trend is similar to the previous case of lambda = 1.1.

In the case of PVO SI, Figure 5.25 (b) shows that E15 resulted in a significant rise in the total particle numbers, which was dominated by particles of between 15-20nm in diameter (Figure 5.25(a)). Because of its lower calorific value, a larger volume of E15 was injected over a longer duration. The particulate emissions using E85 was lower than E15.

As shown in Figure 5.25(a), in the CAI NVO mode using E15 and E85 enabled particulate emission reductions, but this mode was characterised by the highest number of particles amongst the three operational modes.

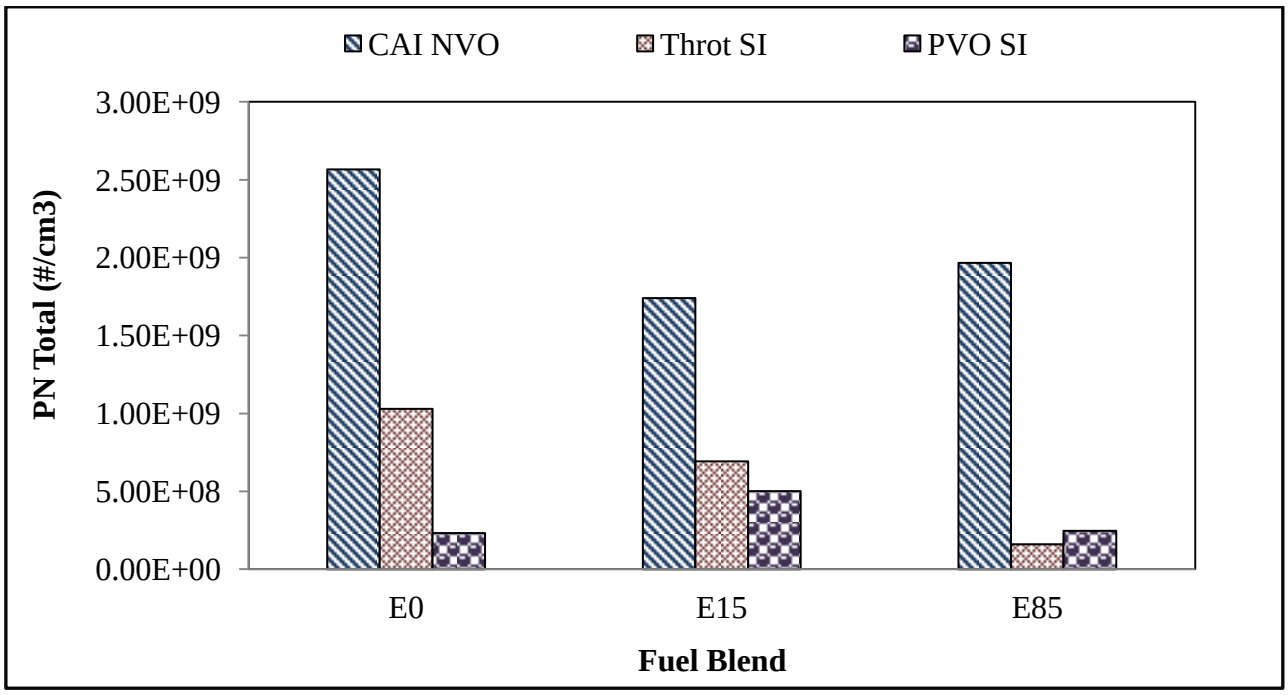


**(a) PN Total**

**Figure 5.25 PN Total and Particulate Number Emissions**

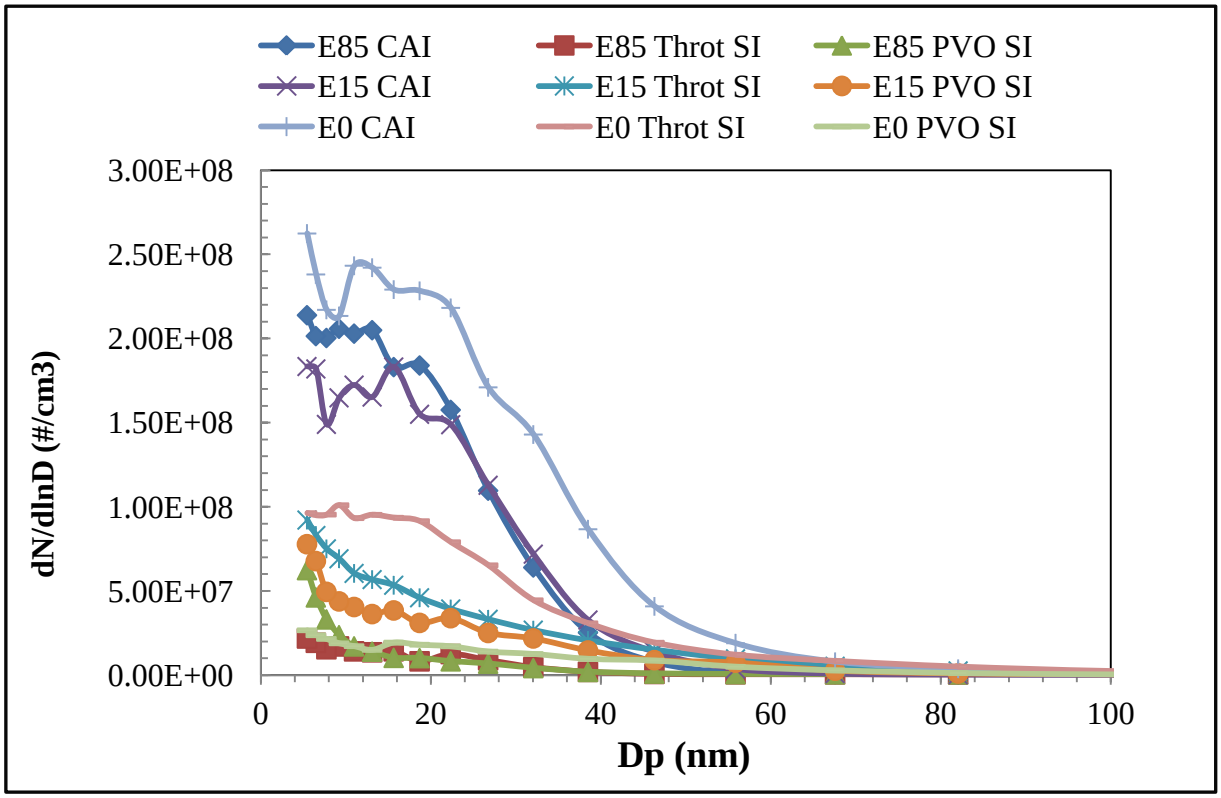


**(b) Particulate Number Emissions**

**Figure 5.25 (ctd) PN Total and Particulate Number Emissions**

**Summary**

The use of E15 and E85 in leaner mixture of lambda 1.2 resulted in longer burn duration, reduced combustion efficiency in all the modes and increased UHC and CO were observed. The observed NOx emissions in CAI combustion increased. There was reduction in particulate emissions size but higher numbers were recorded for all the modes.

## 5.9 Summary

### 5.9.1 Summary of the characteristics of each combustion mode with gasoline

The CAI combustion has very high pressure rise rate, the latest to start but fastest, has improved fuel economy, reduced pumping loss, higher combustion efficiency, lowest NOx emissions, increased particulate emissions in part-load operation.

Throttled SI mode is characterised with higher pumping loss, higher fuel consumption, reduced combustion efficiency, and highest NOx emission.

The PVO SI has higher combustion efficiency, reduced pumping loss like the CAI, reduced particulate emissions, and reduced NOx emissions

### 5.9.2 Summary of the effect of ethanol with stoichiometric mixture

The use of E15 and E85 in lamda 1.0 resulted in reduction in pressure rise rate and longer burn duration in CAI combustion. There was reduction in combustion efficiency in throttle SI and PVO SI. In contrast, there was increase in combustion efficiency in PVO SI as ethanol blend increases from E0 to E85. The ISCO and ISHC were higher in E15 and E85 compared to E0. In the case of PVO SI the ISCO and ISHC decreased as ethanol increases from E0 to E85. In CAI use of ethanol led to slight increase in NOx, but a reduction was recorded in Nox for cases of PVO and throttled SI.
The use of E15 and E85 resulted in higher particulate number emissions but reduced in size.

### 5.9.3 Summary of the effect of ethanol with leaner mixture

The PVO SI suffered from the lowest combustion efficiency but improved gas exchange and indicated efficiencies, and the lowest ISFC over Throttled SI. The addition of ethanol had the most pronounced effect on improving the pressure rise rate of CAI NVO combustion mode.

The CAI NVO mode produced the least CO in E0, E15, and E85 and least ISHC in E15 and E85.

The PVO mode was characterised with the lowest number of particles amongst the three operational modes using E15 and E85.

The presence of ethanol led to reduction of particulate number in CAI combustion because of the oxygenate nature of Ethanol**.**

## Chapter 6 Part-load Performance and Emission Analysis of SI Combustion with EIVC

### 6.1 Introduction

In this work, reduced intake valve-duration by early intake valve-closure (EIVC) was investigated for its potential to improve the indicated fuel consumption over the conventional throttled operation at part-load in a direct-injection gasoline engine. Effects of such operating modes on the gaseous and particulate emissions were also analyzed by means of Horiba exhaust-gas emission analyzers and an Electrostatic Mobility Spectrometer (EMS) based particle analyzer, respectively. Furthermore, the effect of ethanol on the particulate emissions was studied and compared to the throttled SI operating mode.

### 6.2 Engine Operating Conditions

Figure 6.1 shows the valve timings and injection timings used in the 4-stroke EIVC and throttled SI mode operations in this study.

**Mode 1; 4-Stroke Throttle-controlled SI Mode**

This is the conventional spark-ignition mode used in the production gasoline engine. Engine load is controlled by the throttle opening, and its combustion process is initialized by the spark discharge followed by flame propagation. The engine was operated in this mode to obtain the baseline data. In this engine operation mode, fuel was injected earlier in the intake stroke to obtain a homogeneous mixture. To prevent fuel from wetting the piston top, injection timing was set to 420deg CA ATDC.

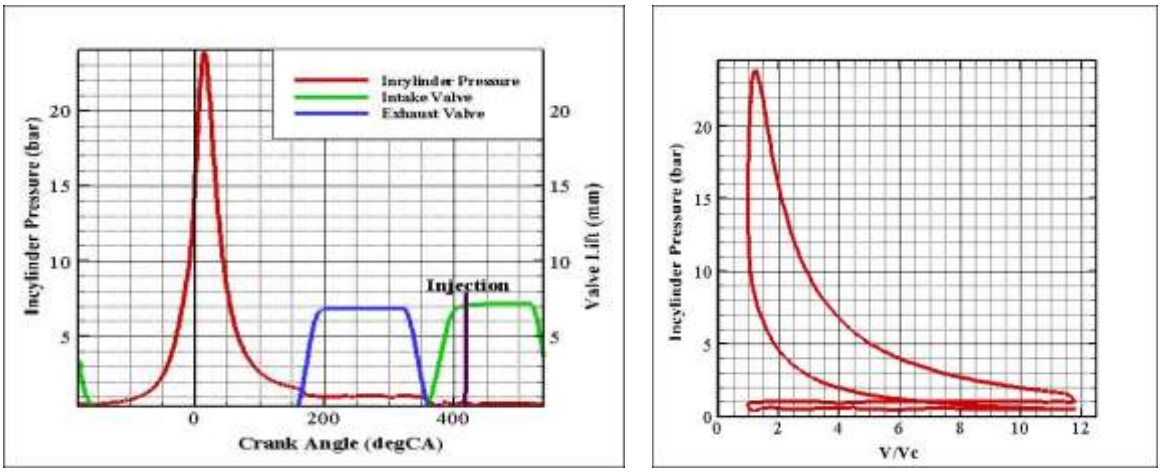


**(a) 4-Stroke throttled SI valve timing and P-V diagram**

**Figure 6.1 Valve Timings and Injection Timings in the 2 Operation Mode**

**Mode 2: 4-Stroke Intake Valve Throttled SI Mode**

In order to reduce the pumping loss caused by the partially-closed intake-throttle at part load, intake valve opening duration can be used to regulate the amount of air let into the cylinder with WOT. In this work, the intake valve opening (IVO) was fixed at the normal timing and the lift was fixed at 2.00mm. The intake valve closing (IVC) was varied to control the intake air-flow and injection timing was set at 420degCA ATDC

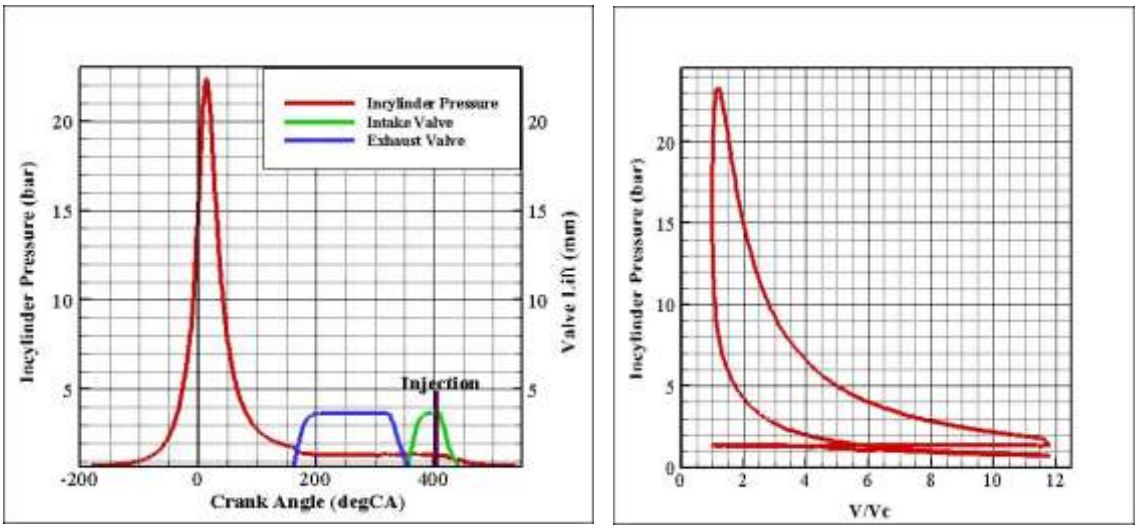


(b) 4-Stroke Early Intake Valve Closure valve timing and P-V diagram

**Figure 6.1 (ctd) Valve Timings and Injection Timings in the 2 Operation Mode**

## 6.3 Results and Discussions on the Throttled SI and EIVC combustion

The engine was supplied with gasoline and its blends with ethanol, E15 (15% ethanol by volume) and E85 (85% ethanol by volume). To enable better comparison of the results of the two different operation modes, the engine was operated at a typical operation condition of 1500rpm and 3.20bar IMEPnet. The net IMEP used was equivalent to that generated in a comparable multi-cylinder production engine at a reference brake-load of 2.62bar BMEP. Spark timing was set to MBT for all operations. The oil and coolant temperature were held at 80$^{o}$C. In order to study the effect of the air/fuel mixture on combustion, performance and emissions, experiments were performed at different lambda values.

### 6.3.1 Combustion Analysis

Figure 6.2 shows and compares the combustion characteristics of the three operation-modes using different fuel blends. It should be noted that in the throttled SI combustion the throttle

was partly opened, while EIVC SI combustion-mode was operated with the wide-open throttle (WOT).

Figure 6.2(a) shows maximum pressure-rise rate as a function of lambda and combustion-mode. It can be seen that the maximum pressure-rise rate for the combustion-modes and fuel blends were below 1.0bar/CA. As shown in Figure 6.2(b), the MBT spark timings were more advanced in the EIVC SI mode than the throttled SI mode due to slower burning velocities as evidenced by the mass-fraction burned curves in Figure 6.2(d) and the corresponding heat release rate results in Figure 6.2(c). As shown in Fig. 6.3(e), the COVimeps for all modes are characterised by very low and nearly constant cycle-to-cycle variability.

In the two modes, the EIVC mode was characterized by the longest combustion duration shown in Figure 6.2(j). This can be explained as follows: the low-intake valve-lift (2mm) and the early closing of the intake valves result in loss of flow momentum inside the cylinder. Moreover, the natural tumble movement is not supported long enough to produce the turbulence required to enhance the combustion initiation and the rate of heat release. In addition, early closing of the intake-valve reduces cylinder gas-temperature and pressure at the end of the compression stroke, at which the flame propagation takes place.

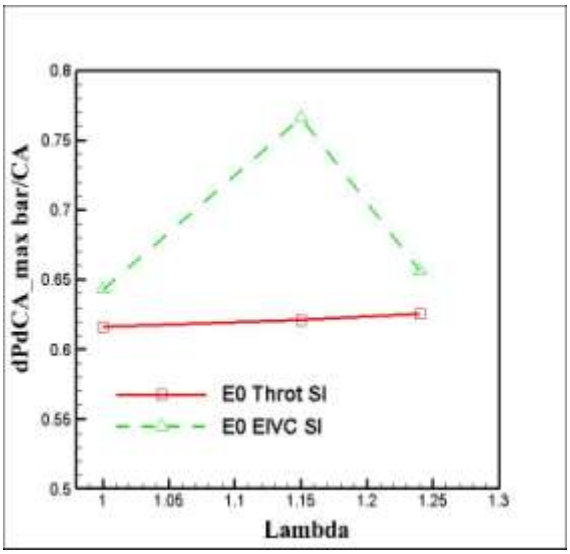


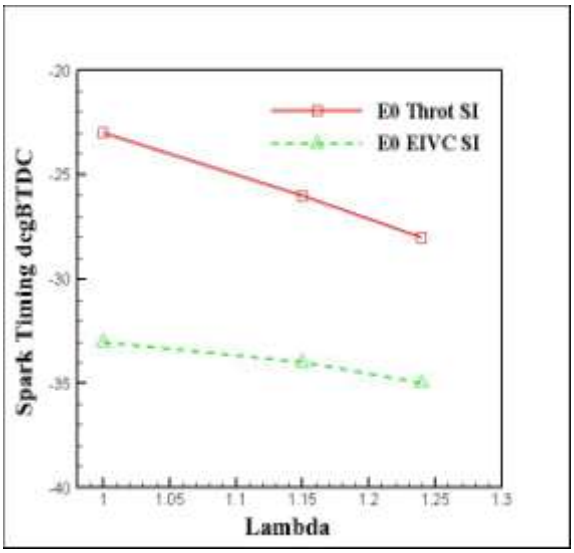


**(a) Maximum Pressure Rise Rate** **(b) MBT Spark Timing**

**Figure 6.2 Combustion Analysis**

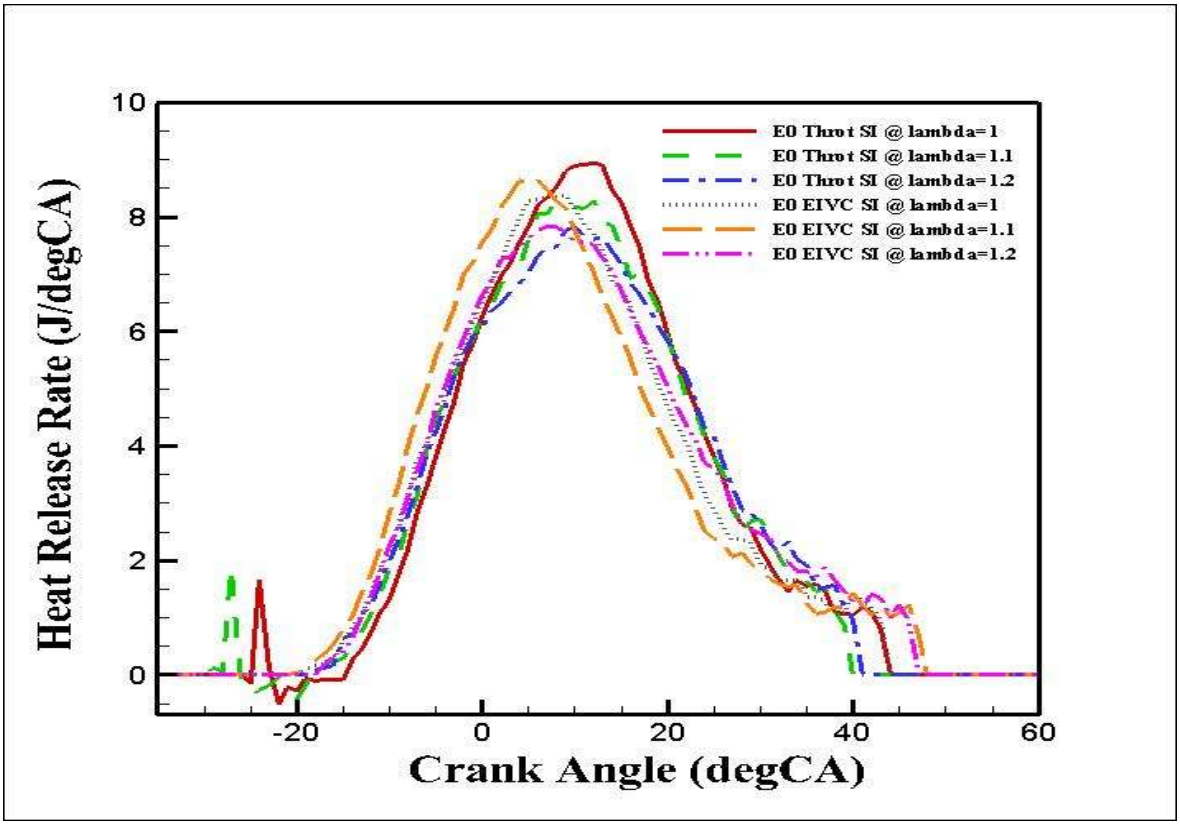


**(c) Heat Release Rate**

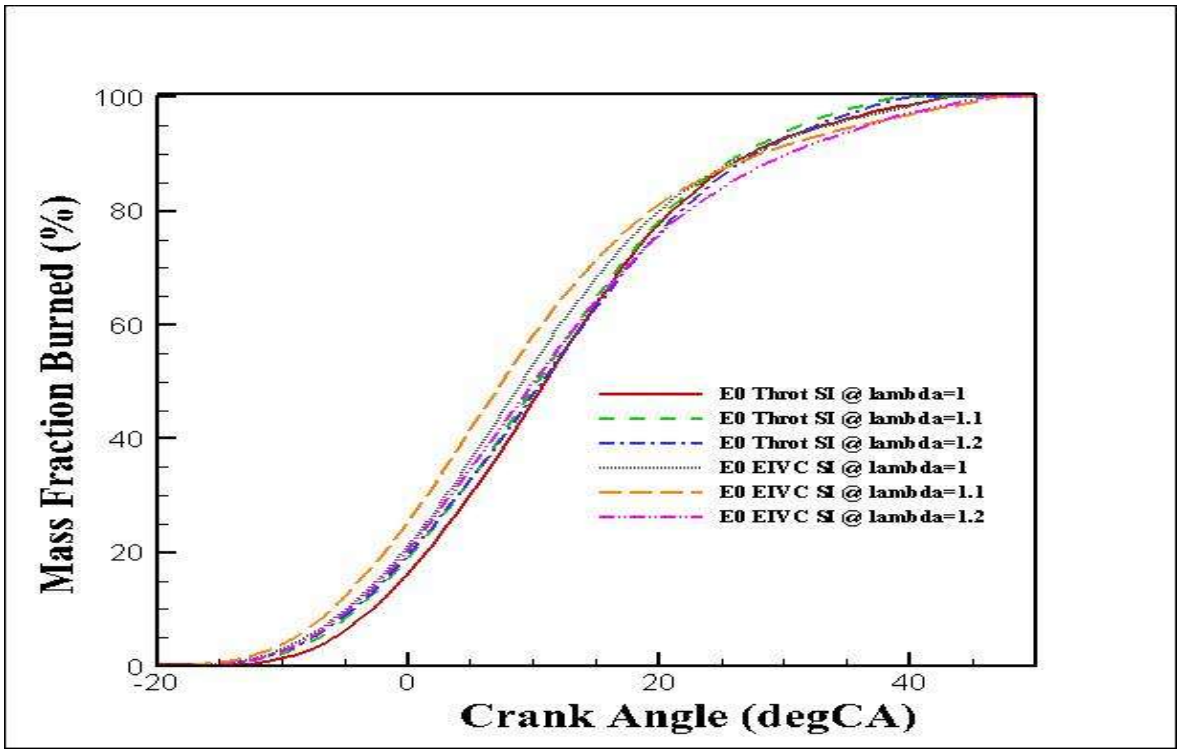


**(d) Mass Fraction Burned**

**Figure 6.2 (ctd) Combustion Analysis**

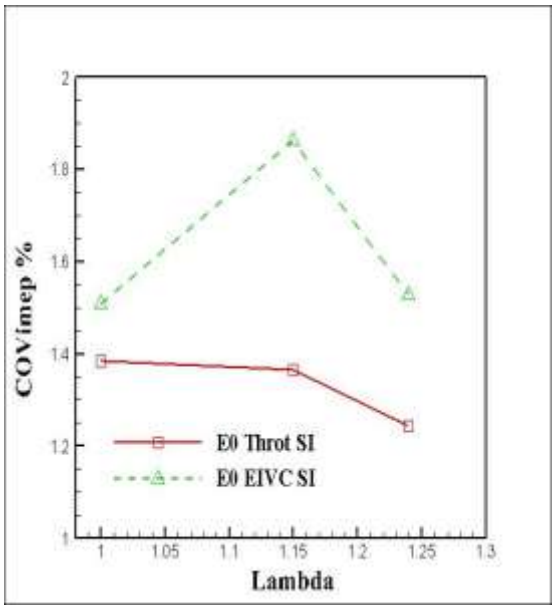


**(e) COV of IMEP**

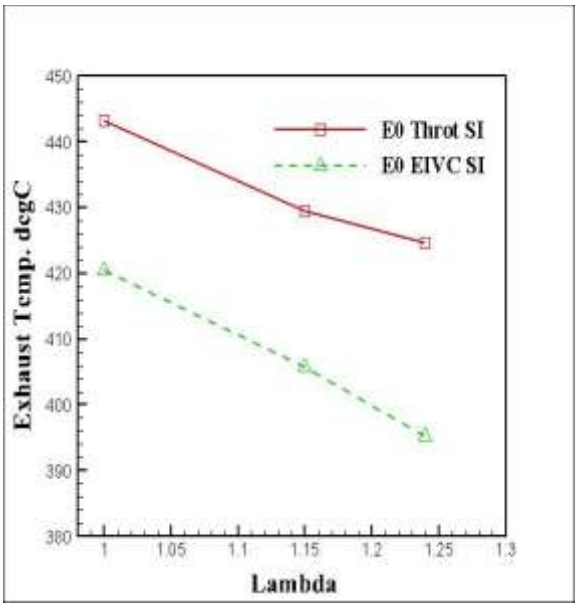


**(f) Exhaust Temperature**

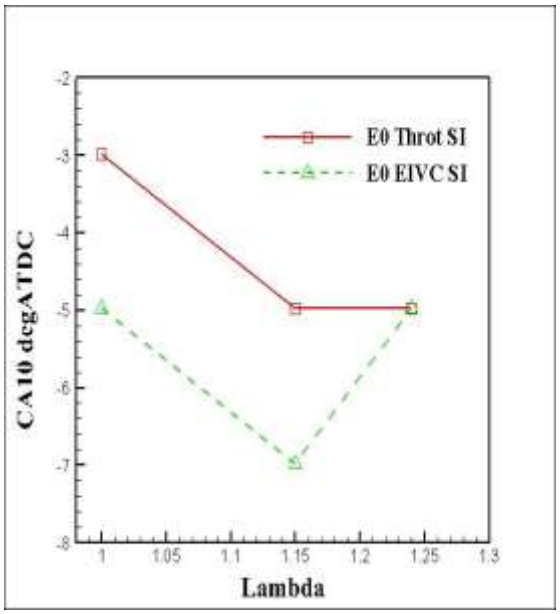


**(g) CA10**

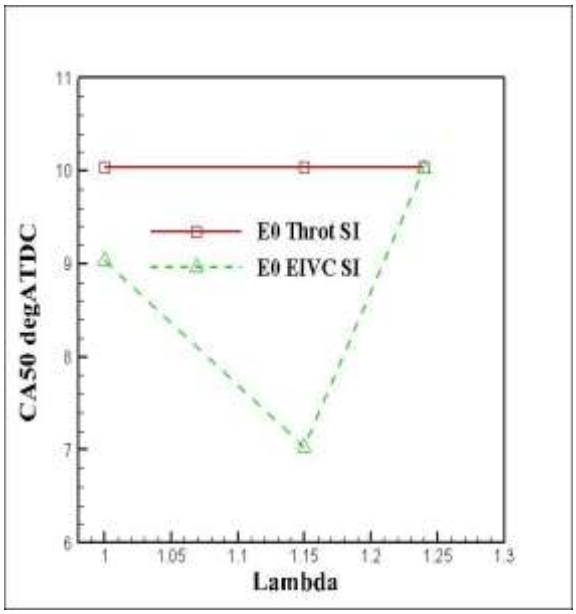


**(h) CA50**

**Figure 6.2 (ctd) Combustion Analysis**

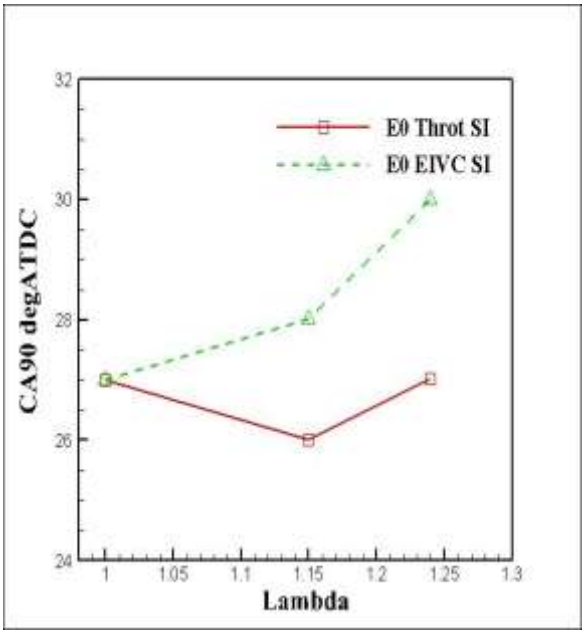


**(i) CA90**

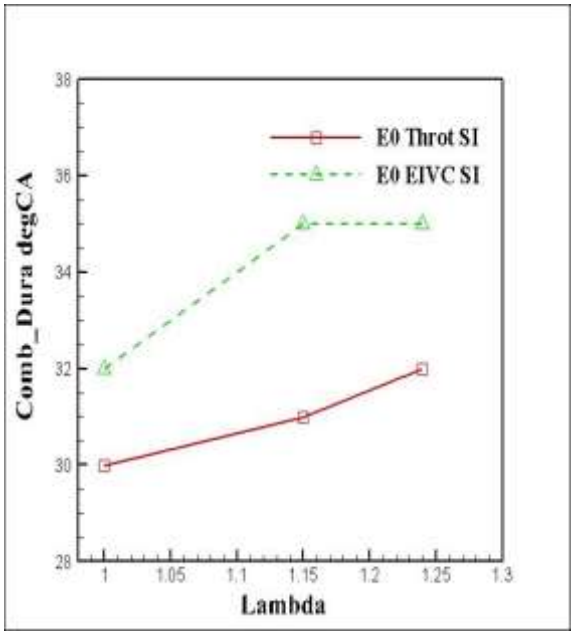


**(j) Combustion Duration**

**Figure 6.2 (ctd) Combustion Analysis**

### 6.3.2 Engine Performance and Efficiency Analysis

Figure 6.3(a) shows the combustion efficiency in the throttled SI and EIVC SI combustion modes. It can be seen that the combustion efficiency of the EIVC combustion is slightly lower than in the throttled SI modes. This is caused by the higher CO and HC emissions as a result of reduced valve-lift and duration as discussed previously.

The theoretical thermodynamic efficiency of the engine is shown in Figure 6.3(b). The EIVC mode exhibits the lowest theoretical thermodynamic efficiency even if the combustion process were assumed complete. This is a result of its longer combustion duration than in the throttled SI.

The gas exchange efficiency in Figure 6.3(c) shows that the EIVC has an average of 91% efficiency brought down by the reduced valve-lift and duration. The throttle SI has the lowest gas-exchange efficiency of 86.6%, the reason for the largest pumping loss seen in Figure 6.3(f).

Figure 6.3(d) compares the net indicated efficiency of the EIVC SI and throttled SI with the lambda sweep of 1 to 1.25. The figure shows an average indicated efficiency of 33.71% in EIVC SI and 33.75% in the throttled SI. The indicated efficiency is similar in EIVC and the

throttled SI. However, the ISFC of the EIVC mode could be further improved by optimising the valve lift, timing, and duration**.**

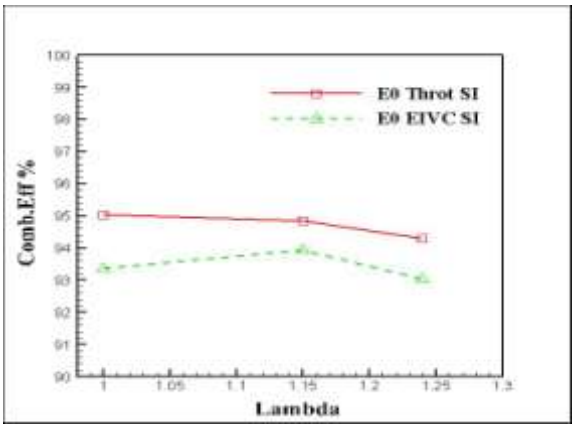


**(a) Combustion Efficiency**

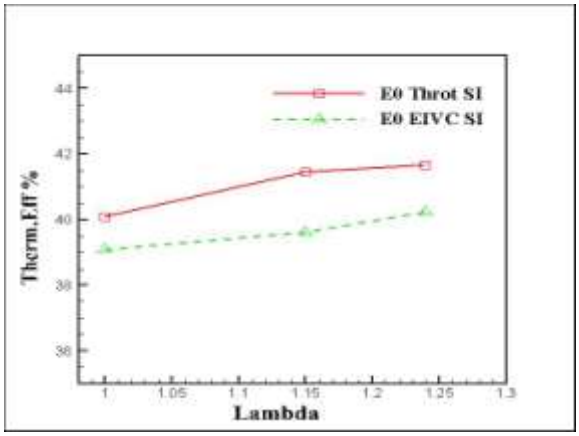


**(b) Thermal Efficiency**

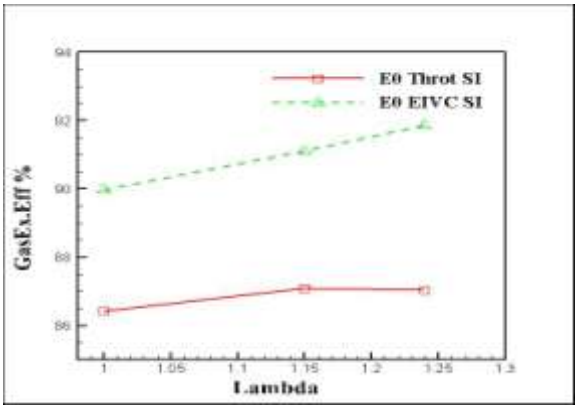


**(c) Gas Exchange Efficiency**

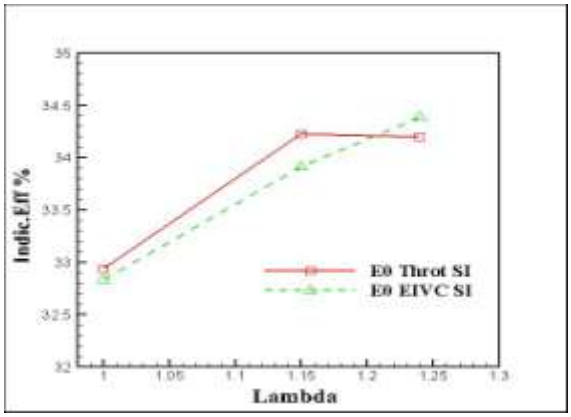


**(d) Indicated Efficiency**

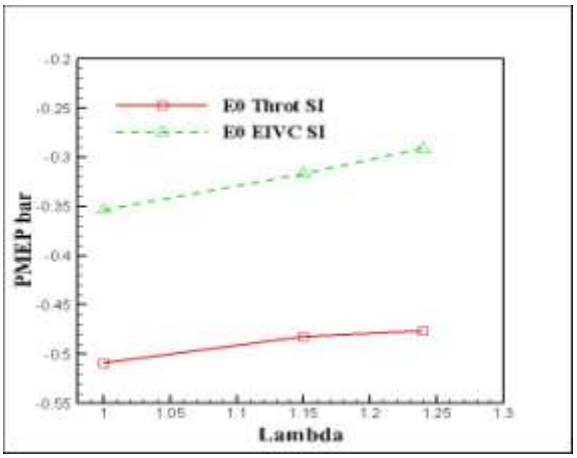


**(e) PMEP**

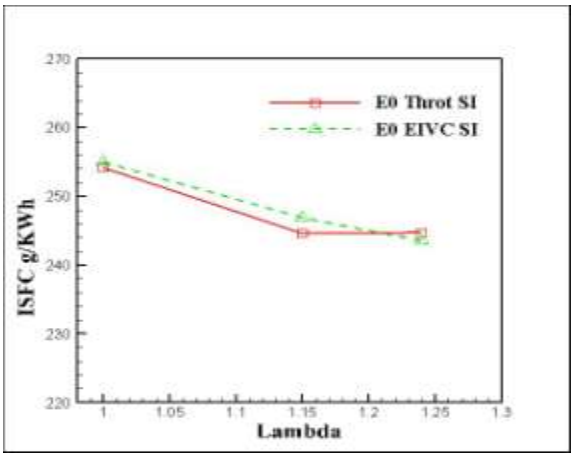


**(f) ISFC**

**Figure 6.3 Performance Analysis**

### 6.3.3 Gaseous Emissions and Fuel Consumption

Figure 6.4(a) shows the CO emission in the throttled SI and EIVC SI combustion at different lambda values. As seen in Figure 6.4(a), the ISCO emission is higher in the EIVC mode than in the throttled SI combustion and it decreases with increasing lambda, reaching a minimum with lambda=1.15. In the throttled SI combustion the CO emission is about 50% lower than in the EIVC with lambda 1 and reaches the same level as that in EIVC with lambda 1.15. As the lambda value is further increased to 1.25, ISCO emissions of the two modes become equal.

Figure 6.4(b) shows the results for ISHC emission for the two modes of operations. The EIVC operation produces about a 25% increase in ISHC emissions compared to the throttled SI combustion.

The higher CO and HC emissions results suggest that there are more locally rich mixtures formed in the EIVC mode. With EIVC, intake-valves are closed early in the induction stroke before BDC, consequently in-cylinder temperature and turbulence are reduced. These resulted in poorer fuel evaporation and incomplete mixing. However, the interaction of fuel injection and intake air-flow during the EIVC mode could have caused more fuel impingement on the piston-crown, when the fuel-spray was deflected by the high-speed air-flow.

Figure 6.4(c) shows the NOx emissions for the two combustion modes. It can be seen that the NOx emission in EIVC and the throttled Si is around 9-13g/KWh.

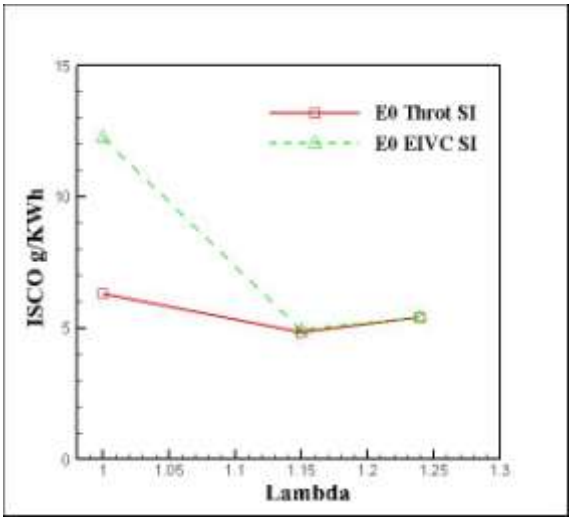


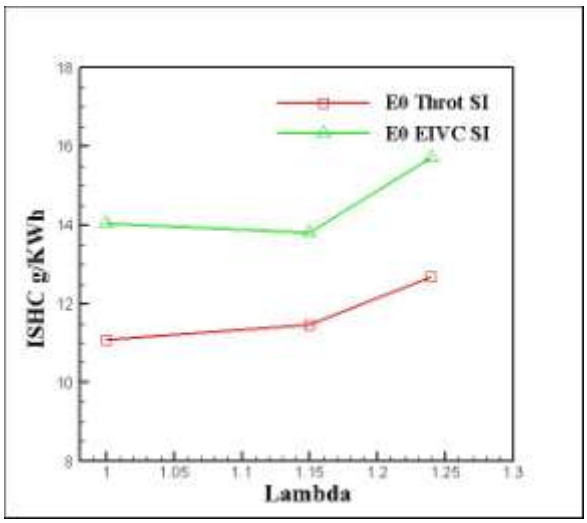


**(a) ISCO** **(b) ISHC**

**Figure 6.4 Gaseous Emissions and Fuel Consumption**

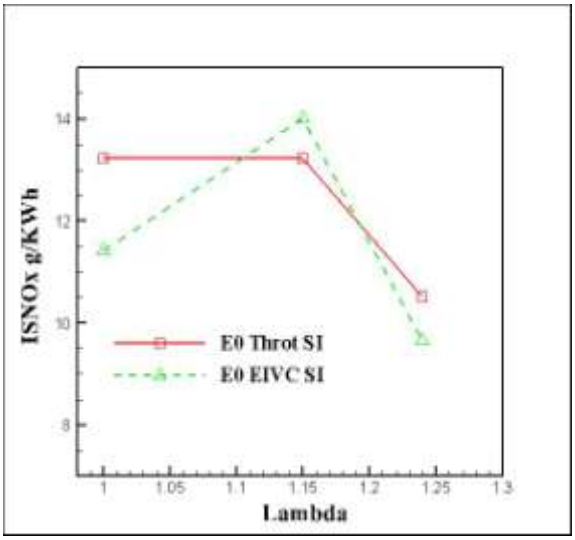


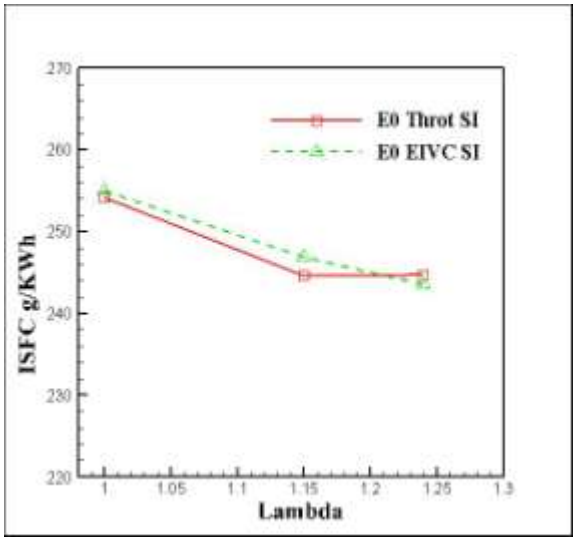


**(c) ISNOx** **(d) ISFC**

**Figure 6.4 (ctd) Gaseous Emissions and Fuel Consumption**

**Particulate Emission**

It can be seen from Figure 6.5(a) and (b) that with lambda = 1, 1.1 and 1.2, the throttled SI mode is characterized by greatest number of particles in total while the EIVC SI showed the least number of particles. For all cases examined, the particles are dominated by the small particles in the range of 20nm, which are typically associated with soot particles in the nucleation mode.

In the case of the EIVC SI operation, fuel was injected into air and residual gas at lower temperature than throttled SI. As a result, there were no soot particles produced from pyrolysis. The majority of particles detected in the exhaust were liquid condensates, as indicated by their much smaller particle sizes in Figure 6.4(b). In addition to the soot particles, there are also a significant number of very small particles measuring 5nm in diameter. Such particles are typically liquid-fuel condensates in the exhaust.

Furthermore, Figures 6.5(a) and (b) show that due to less fuel-rich combustion, the leaner mixture helped reduce the particle emissions of all sizes in the two combustion modes, except a small range of particle sizes in the throttled SI engine, where lambda 1.1 mixture caused a rise in particle emissions.

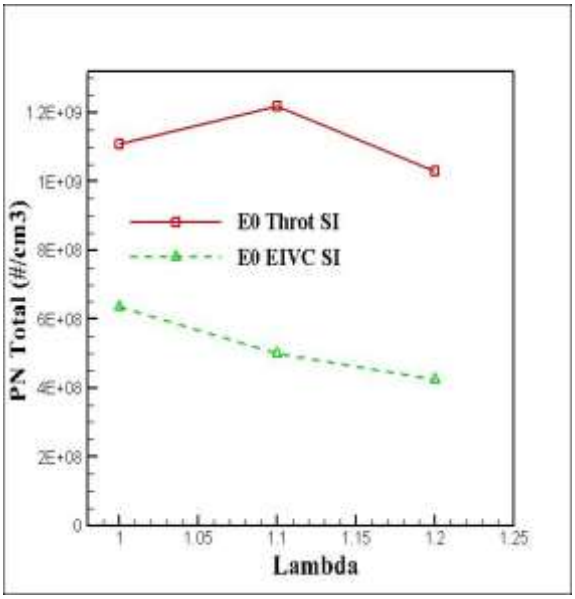


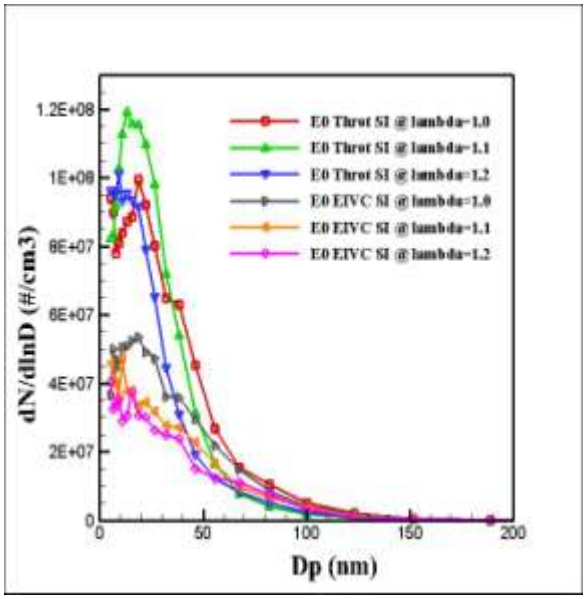


**(a) PN Total** **(b) Particulate Number Emissions**

**Figure 6.5 PN Total and Particulate Number Emissions**

## 6.4 Effects of Gasoline Ethanol Blend E15 on throttled SI and EIVC Combustion

### 6.4.1 Combustion Analysis

Figure 6.6(a) shows maximum pressure-rise rate as a function of lambda in both EIVC SI and the throttled SI combustion. It can be seen that the maximum pressure-rise rate for the two modes with lambda 1.0 was less than 0.7bar/CA, decreasing to less than 0.6 for leaner mixtures of lambda 1.1 and 1.2. However, knocking combustion was not an issue in the operational conditions in this test, although there were occasional misfires.

In contrast, spark timing was retarded (Figure 6.6(b)) in E15 because of the high flame-speed of the blends. As the mixture became leaner at lambda 1.1, spark-timing for throttled SI was further advanced but in EIVC SI timing was retarded. However with lambda 1.2 the spark timing for both modes was advanced to enable enough time for complete combustion.

The two modes are characterised by very low and nearly constant cycle-to-cycle variability as shown by the COVimep results in Figure 6.6(e). Of the two modes, the EIVC mode was characterized by the longest combustion duration at lambda 1.1. This can be explained as follows: the low-intake valve-lift (2mm) and early closing of the intake-valves result in loss of flow momentum inside the cylinder. Moreover, the natural tumble movement is not supported long enough to produce turbulence required to enhance the combustion initiation and the rate

of heat-release. In addition, early closing of the intake-valve and ethanol-blend further reduces cylinder gas-temperature and pressure at the end of the compression stroke, at which the flame propagation takes place.

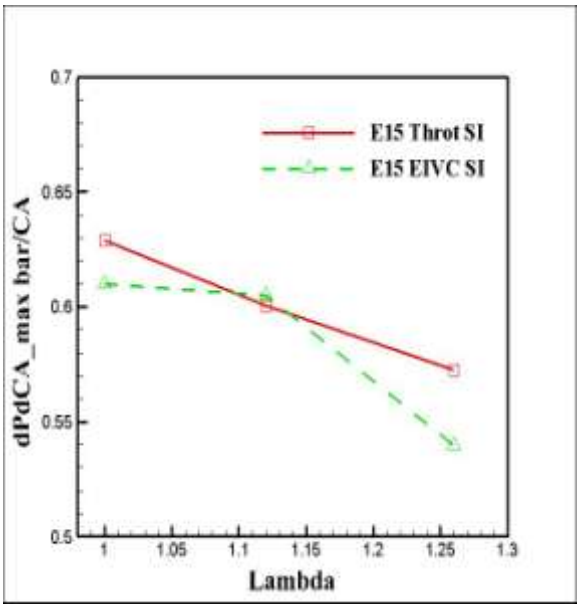


**(a) Maximum Pressure Rise Rate**

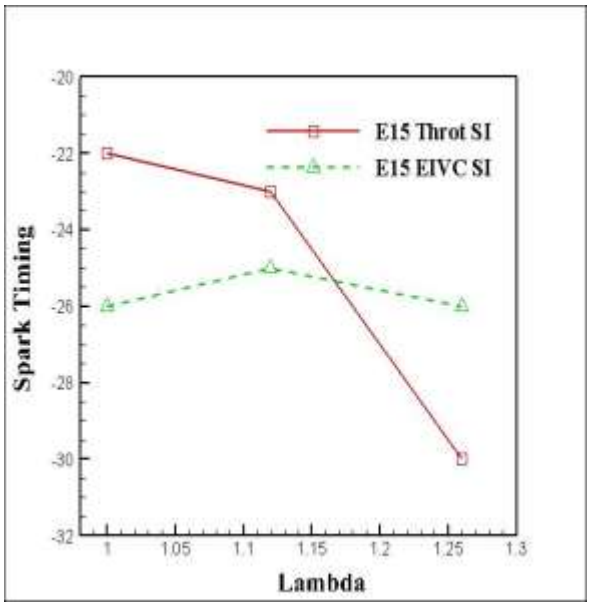


**(b) MBT Spark Timing**

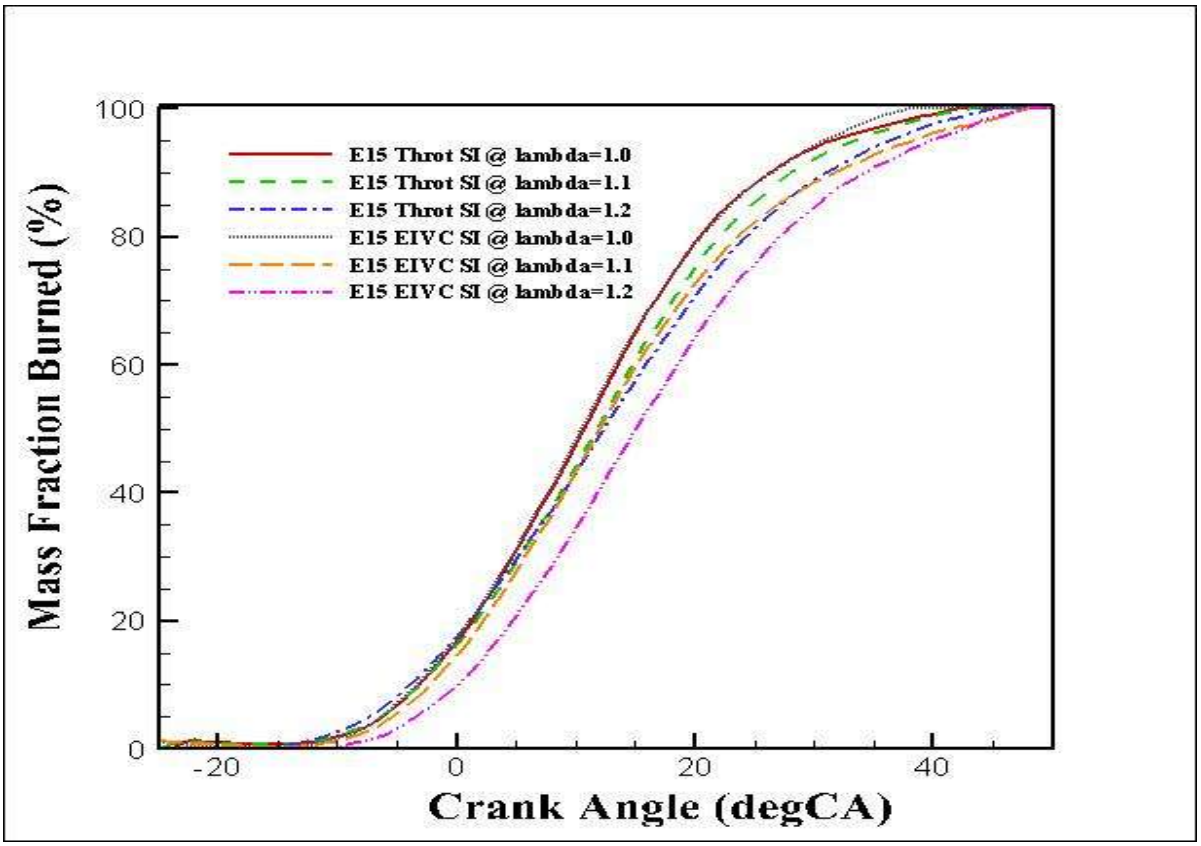


**(c) Mass Fraction Burned**

**Figure 6.6 Combustion Analysis**

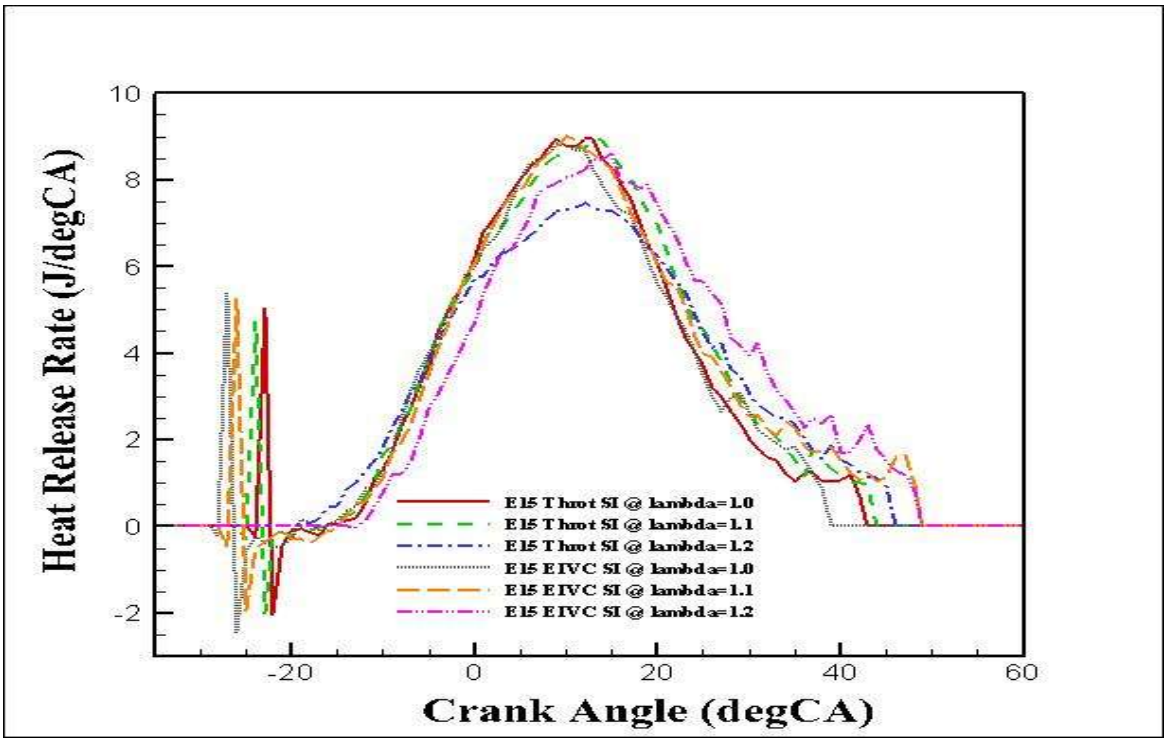


**(d) Heat Release Rate**

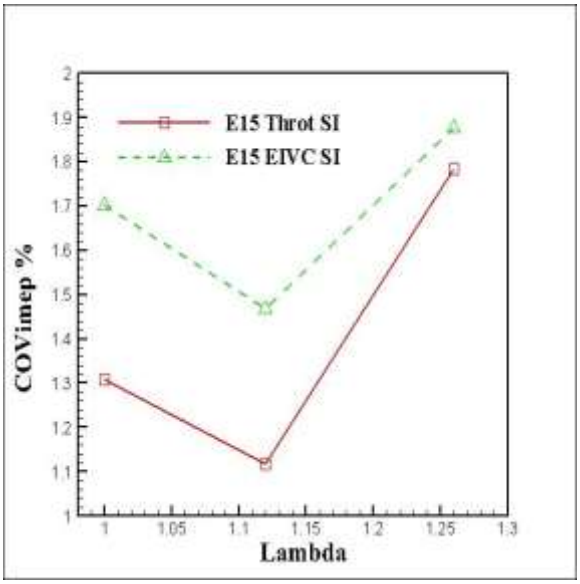


**(e) COV of IMEP**

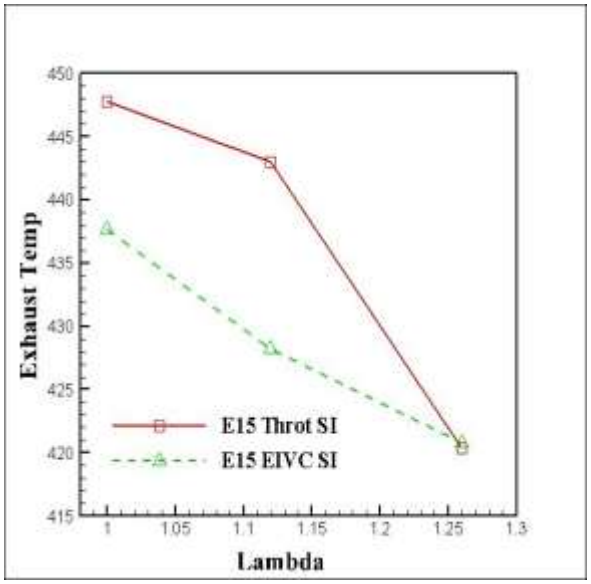


**(f) Exhaust Temperature**

**Figure 6.6 (ctd) Combustion Analysis**

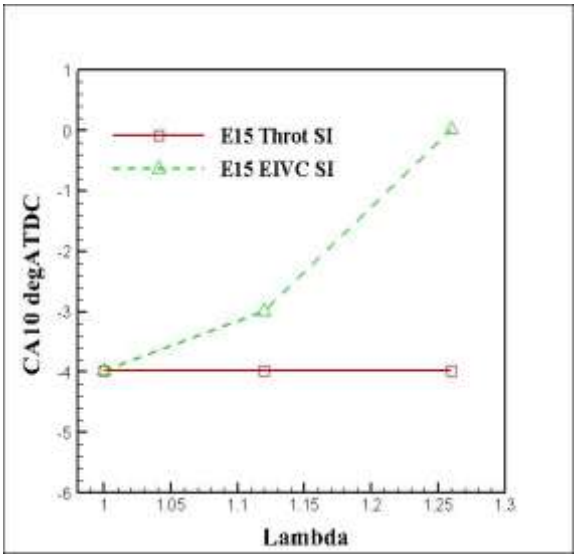


**(g) CA10**

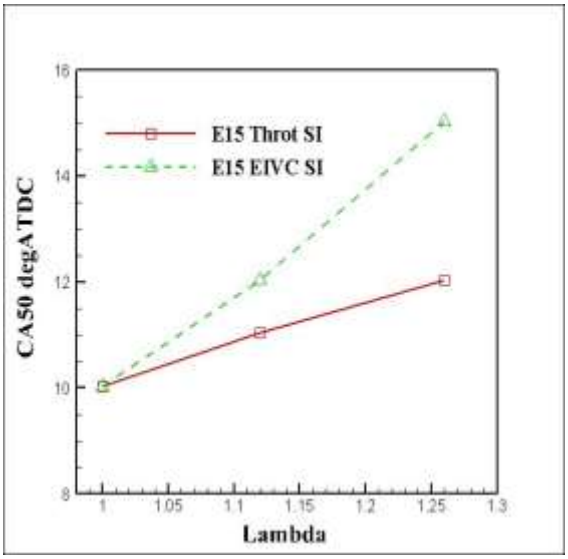


**(h) CA50**

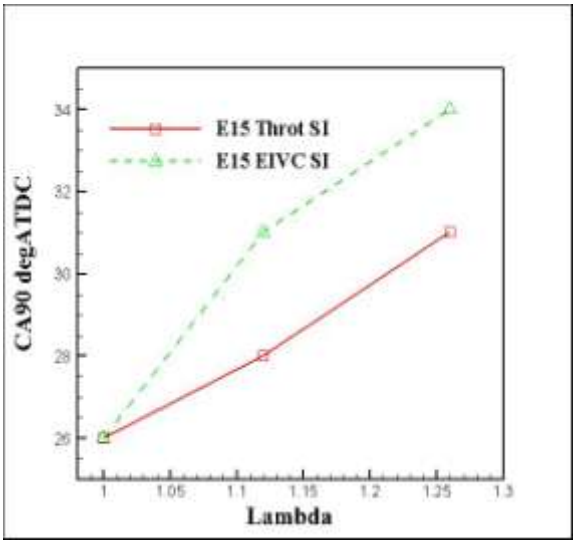


**(i) CA90**

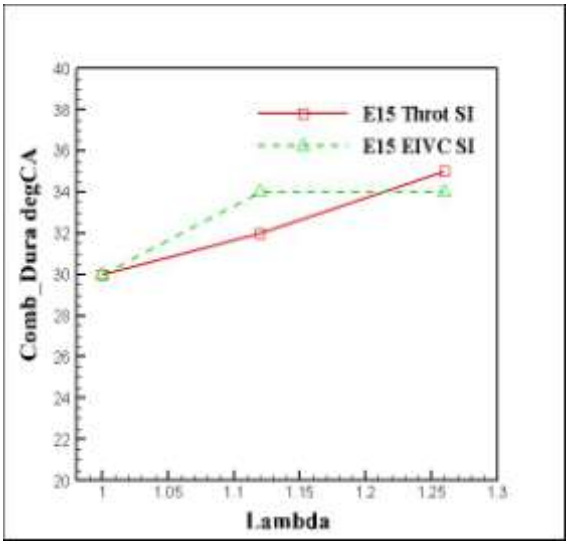


**(j) Combustion Duration**

**Figure 6.6 (ctd) Combustion Analysis**

### 6.4.2 Engine Performance and Efficiency Analysis

Figure 6.7(a) shows the combustion efficiency in throttled SI and EIVC combustion modes. It can be seen that the combustion efficiency in the EIVC varies from 92% with lambda 1.0, increased to 93% with lambda 1.1 then decreased to 92.6% with lambda 1.2.Combustion efficiency was slightly lower than in the throttled SI mode with lambda 1.0 and 1.1, caused by the higher CO and HC emissions as a result of reduced valve lift and duration as discussed previously. In general, combustion efficiencies are lower than that of well designed modern SI engines because of the use of a side-mounted fuel injector and un-optimised combustion chamber in the single-cylinder engine.

In Figure 6.7(b), the EIVC mode resulted in the highest theoretical thermodynamic efficiency, which is contrary to the gasoline (E0) results.

The gas-exchange efficiency in Figure 6.7(c) shows that the EIVC has an average of 92% efficiency for all lambda. The throttle SI has the lowest average gas-exchange efficiency of 88% for all lambda values, the reason for the largest pumping loss seen in Figure 6.7(e).

Figure 6.7(d) compares the net indicated efficiency of the EIVC and throttled SI modes for the lambda sweep of 1 to 1.25. The figure shows an average indicated efficiency of 34.8% in the EIVC and 32.3% in the throttled SI. The indicated efficiency of throttled SI is 7.5% lower in indicated efficiency on average. This resulted in a 7% improvement in ISFC in the EIVC over throttled SI.

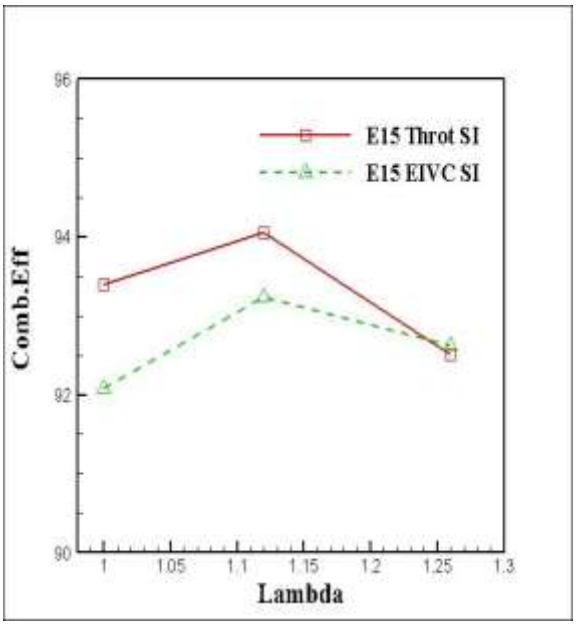


**(a) Combustion Efficiency**

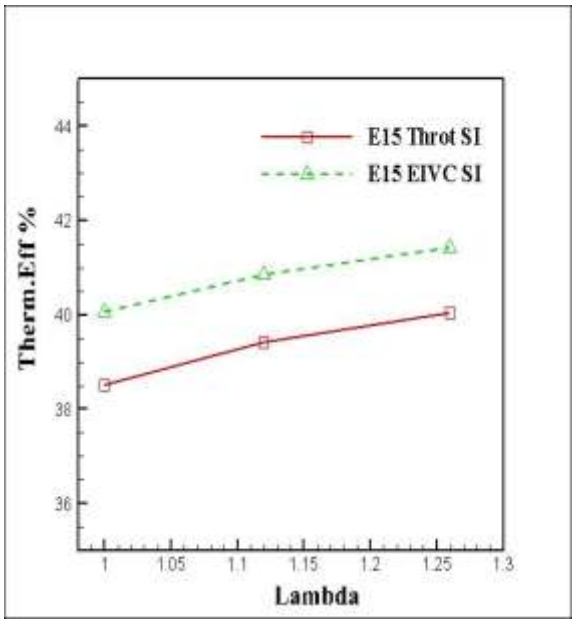


**(b) Thermal Efficiency**

**Figure 6.7 Performance Analysis**

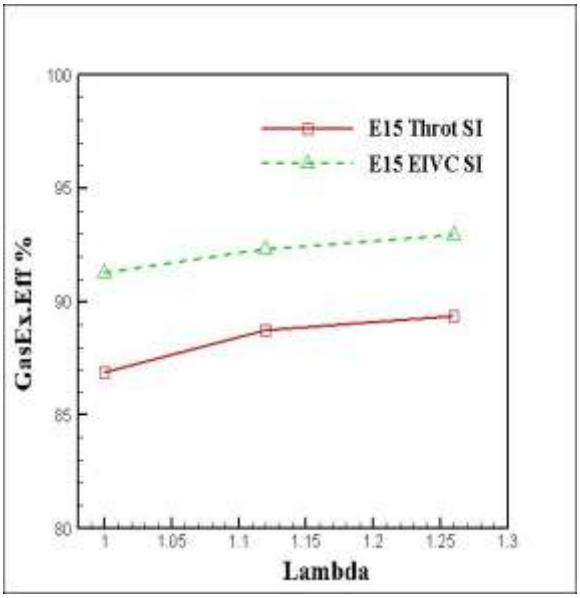


**(c) Gas Exchange Efficiency**

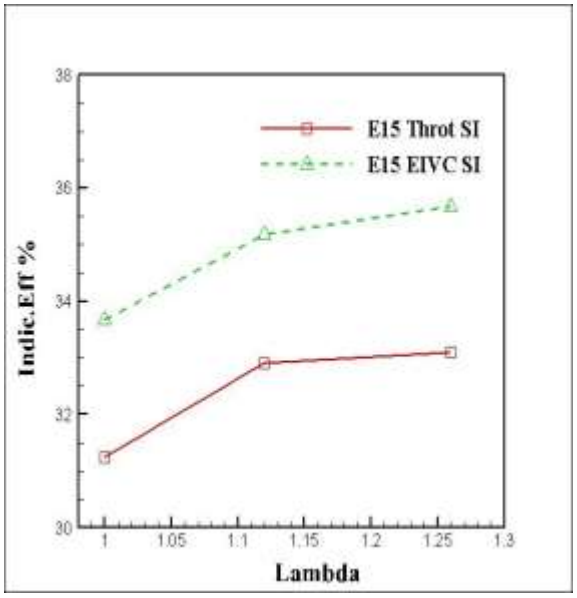


**(d) Indicated Efficiency**

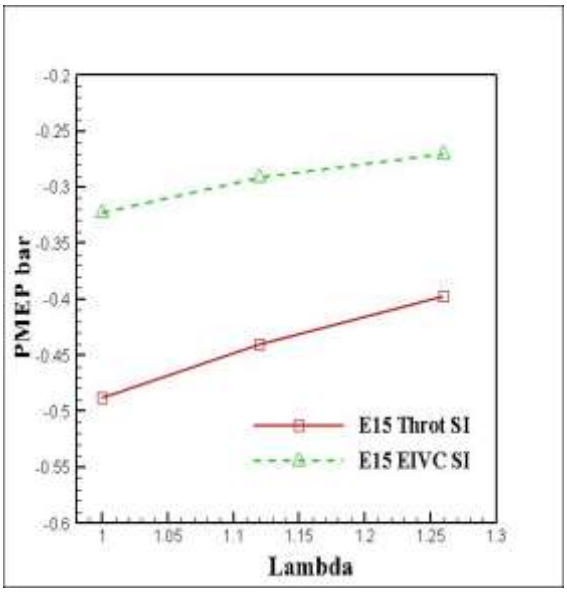


**(e) PMEP**

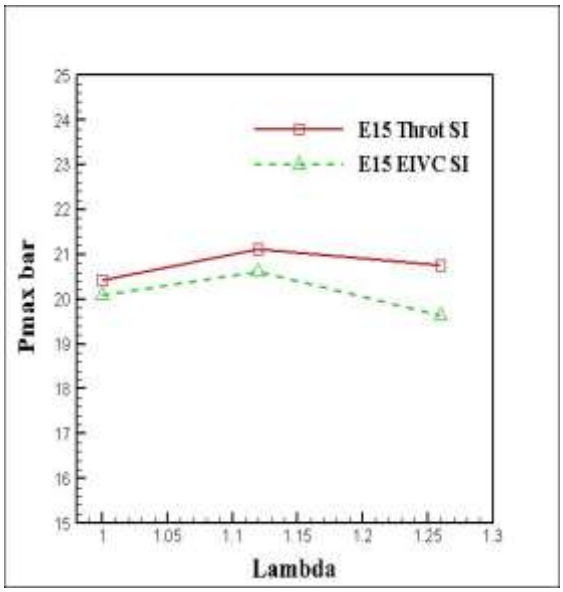


**(f) PMax**

**Figure 6.7 (ctd) Performance Analysis**

### 6.4.3 Fuel Consumption and Emissions

Figure 6.8(a) shows the CO emission in the throttled SI and EIVC SI combustion with lambda values of 1.0, 1.1, and 1.2. As seen in Figure 6.8(a), the ISCO emission is higher in the EIVC mode than in the throttled SI at stoichiometric and it decreased with increased lambda to a minimum at lambda=1.25 at which point it was less than the value recorded in throttled SI. For throttled SI, the CO emission is about 20% lower than in the EIVC with lambda 1 and reaches the same level at that in the EIVC with lambda 1.15. As the lambda value is further

increased to 1.25, there is about a 7% improvement on CO emissions in the EIVC over throttled SI.

Figure 6.8(b) shows the results for ISHC emission for the two modes of operations. The EIVC operation produces higher ISHC with lambda 1.0 and 1.1, but lower value with lambda 1.2 compared to the throttled SI combustion.

The higher CO and HC emissions results suggest that there are more locally rich mixtures formed in the EIVC mode with lambda 1.0 to 1.15. In the EIVC, intake-valves are closed early in the induction stroke before BDC and the in-cylinder temperature in E15 is further reduced.

Figure 6.8(c) shows the NOx emissions for the three combustion modes. It can be seen that the NOx emission in EIVC SI varies from 7.3g/KWh with lambda 1.0 to 8.3g/KWh with lambda 1.1 and decreases to 3.8g/KWh with lambda 1.2. In the throttled SI the values are 10.2g/KWh with lambda 1.0, 11.5g/KWh with lambda 1.1 and 7.4 with lambda 1.2. In comparison on average the NOx emissions in EIVC SI was about 45% lower than the throttled SI combustion mode.

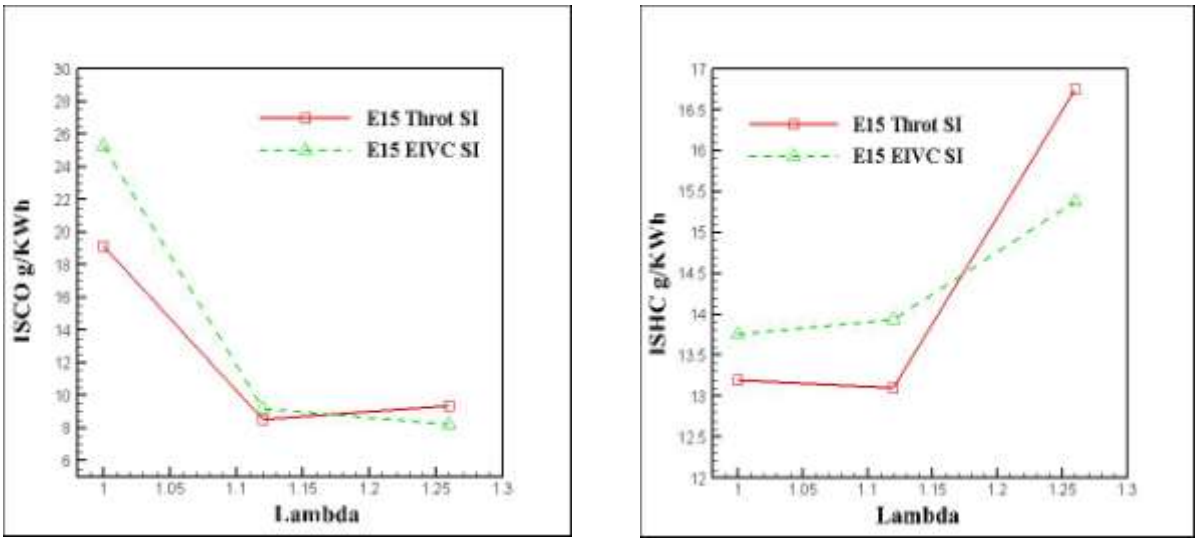


**(a) ISCO** **(b) ISHC**

**Figure 6.8 Gaseous Emissions and Fuel Consumptions**

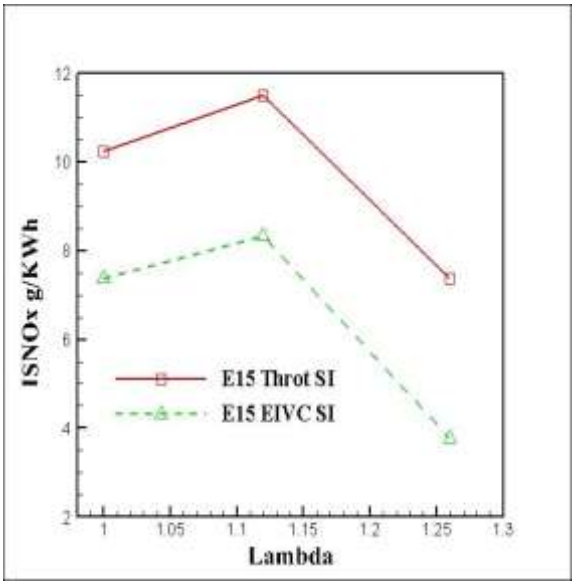


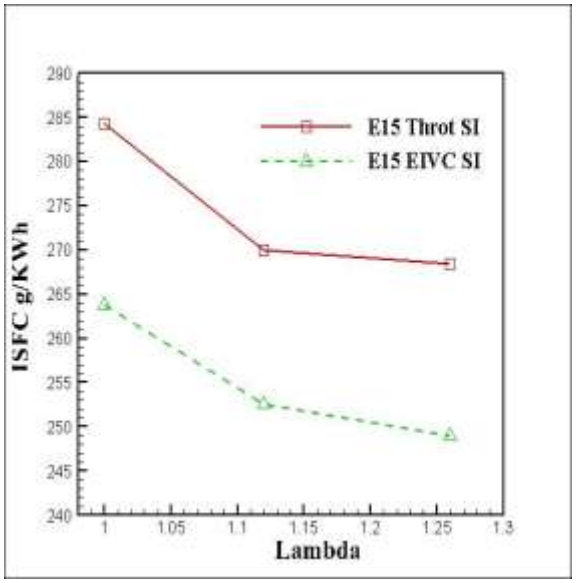


**(c) ISNOx** **(d) ISFC**

**Figure 6.8 (ctd) Gaseous Emissions and Fuel Consumptions**

**Particulate Emission**

Figure 6.9(a) and (b) show the PN total and particulate number emissions with lambda 1.0, 1.1, and 1.2. There is no peak visible in the figure and the lean mixtures shifts the particulate emissions towards smaller size particles in EIVC SI and the throttled SI combustion modes. The EIVC showed the least number of particles (Figure 6.9(a)). For all cases examined, the particles are dominated by the small particles in the range of 20nm, which are typically associated with particulates in the nucleation mode.

In the case of EIVC and the throttled SI operation, fuel was injected into air and residual gas at a much lower temperature. As a result, there was no soot particle likely to be produced from pyrolysis. The majority of particles detected in the exhaust were more likely liquid-condensates, as indicated by their much smaller particle size. In addition, there were also a significant number of very small particles measuring 5nm in diameter. Such particles are typically liquid-fuel condensates in the exhaust.

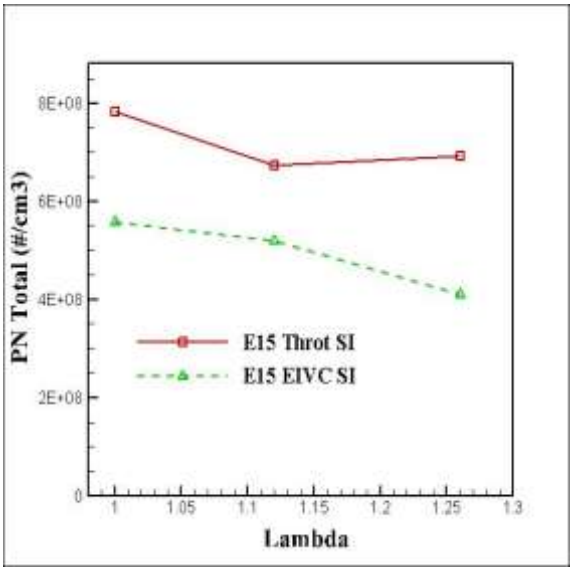


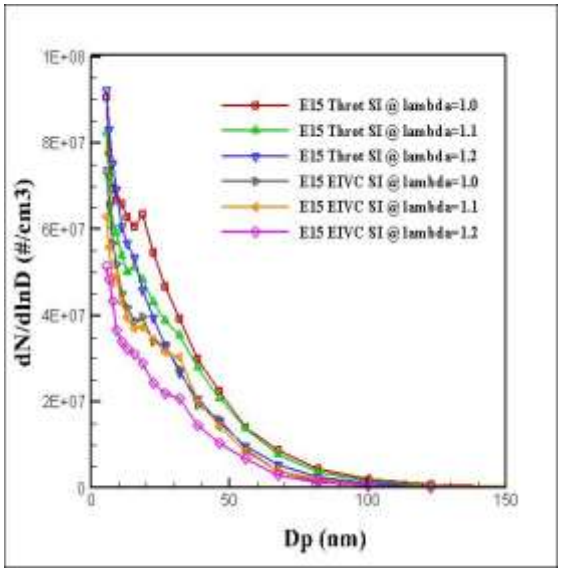


**(a) Total particle numbers** **(b) Particle Numbers and sizes**

**Figure 6.9 Total particle numbers and Particle size distributions**

## 6.5 Effects of Gasoline Ethanol Blend E85 on Throttled SI and EIVC Combustion

### 6.5.1 Combustion Analysis

Figure 6.10 shows and compares the combustion characteristics of the two operation modes in E85 fuel blends with different lambda values. It should be noted that in the throttled SI combustion the throttle was partly opened while EIVC SI combustion mode was operated with the throttle wide open (WOT).

Figure 6.10(a) shows maximum pressure-rise rate as a function of combustion modes and fuel blends. It can be seen that the maximum pressure-rise rate for all the combustion modes was less than 0.8bar/CA. As shown in Figure 6.10(b), the MBT spark-timings were more advanced in EIVC mode than in the throttled mode at lambda 1.0 due to slower burning velocities, as evidenced the mass burned fractions in Figure 6.10(c) and the corresponding heat-release rate in Figure 6.10(d).

Shown in Figure 6.10(e), the COVimeps for all modes were low and did not vary significantly with lambda 1.0 and 1.1. In contrast, in the throttled SI combustion modes with lambda 1.2 it was 4.5%. Although the engine operation was stable, there were occasional misfires and increased fuel consumption. Furthermore the higher charge cooling effect in E85 fuel blend reduced the in-cylinder temperature and combustion duration (Figure 6.11(j)).

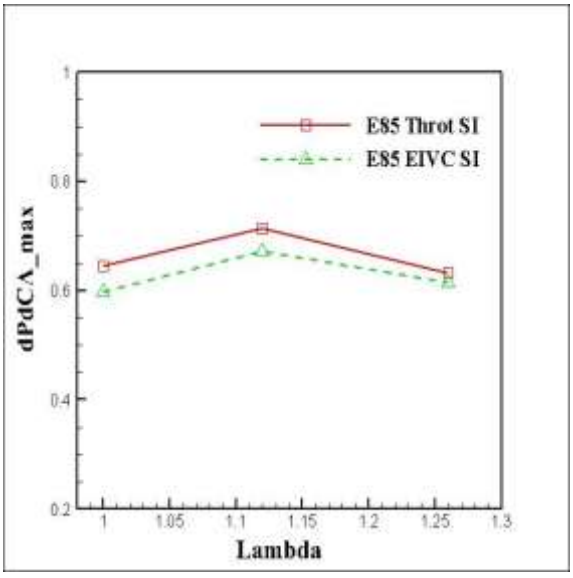


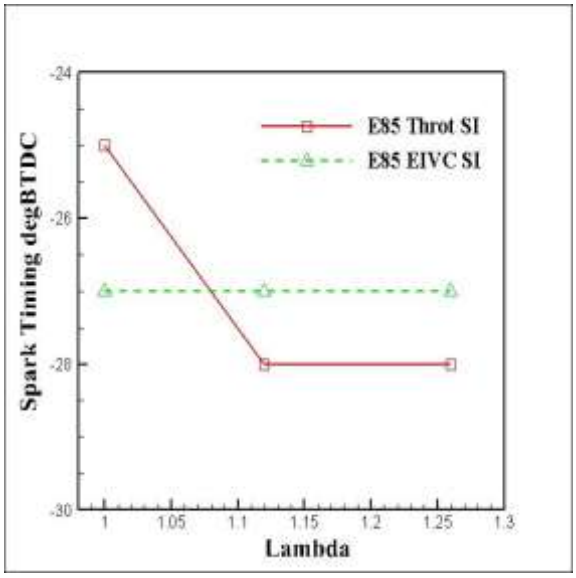


**(a) Maximum Pressure Rise Rate** **(b) MBT Spark Timing**

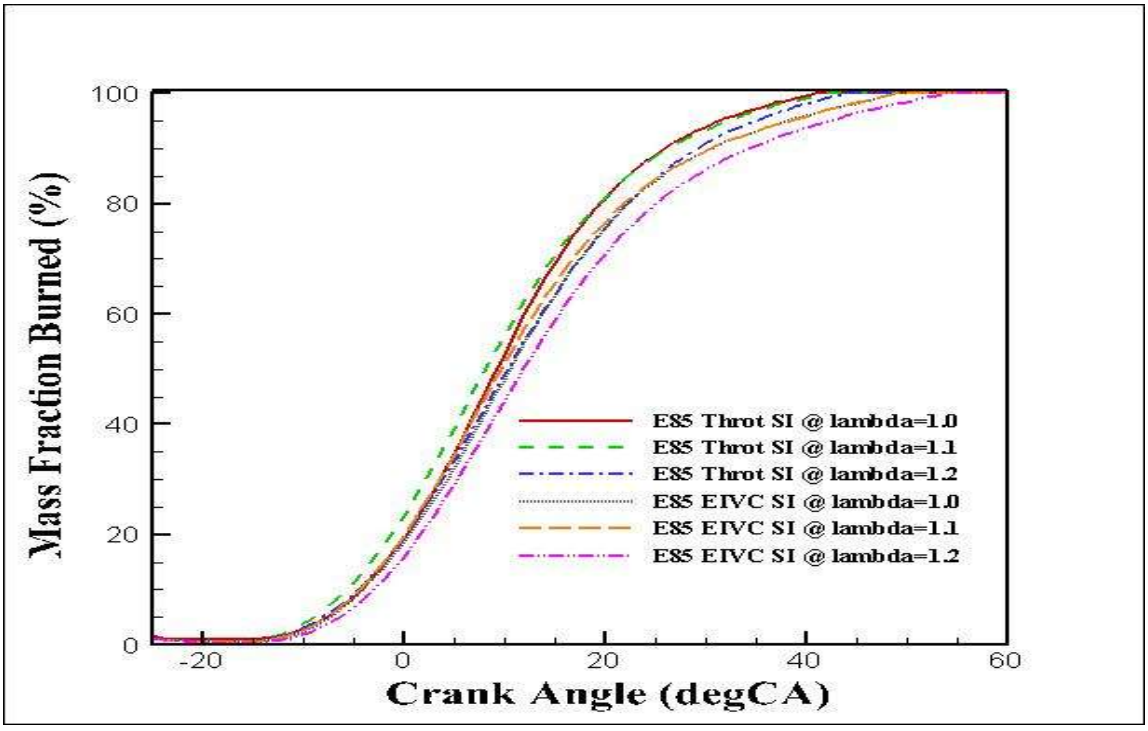


**(c) Mass Burned Fraction**

**Figure 6.10 Combustion Analysis**

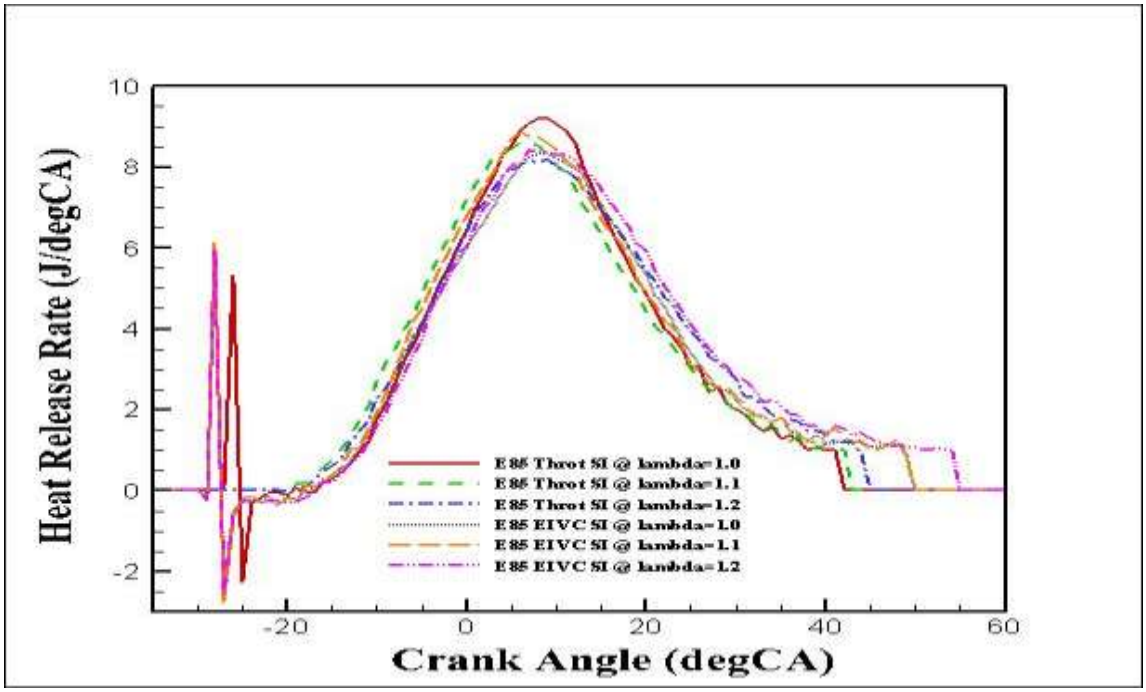


**(d) Heat Release Rate**

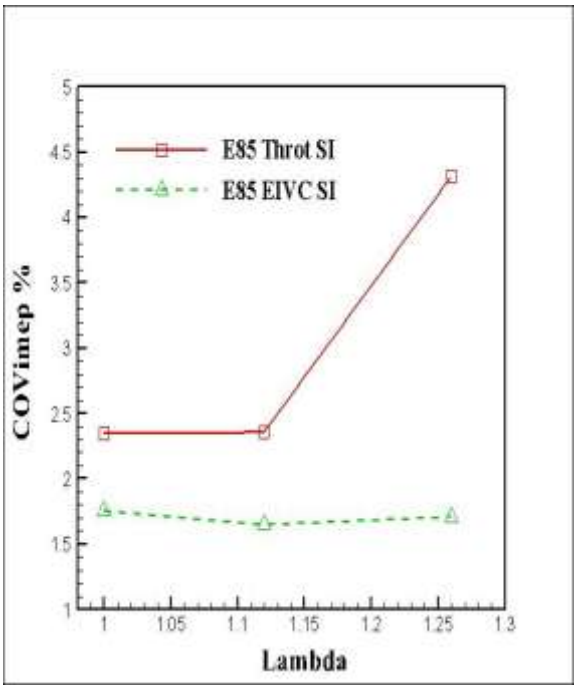


**(e) COV of IMEP**

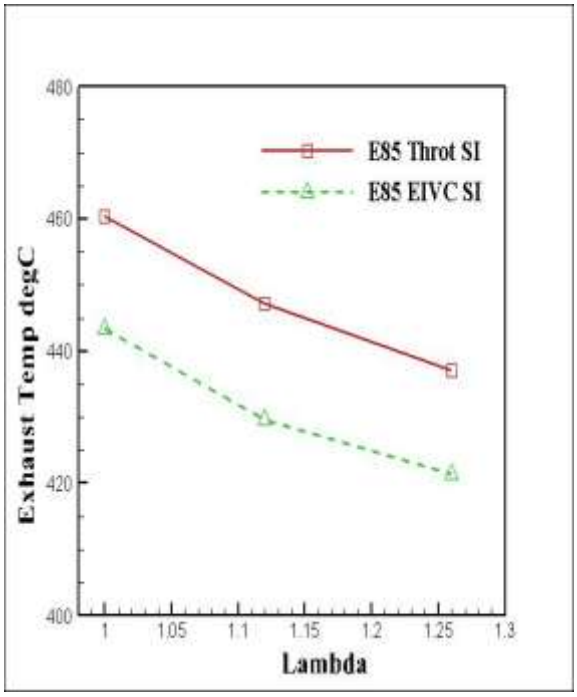


**(f) Exhaust Temperature**

**Figure 6.10 (ctd) Combustion Analysis**

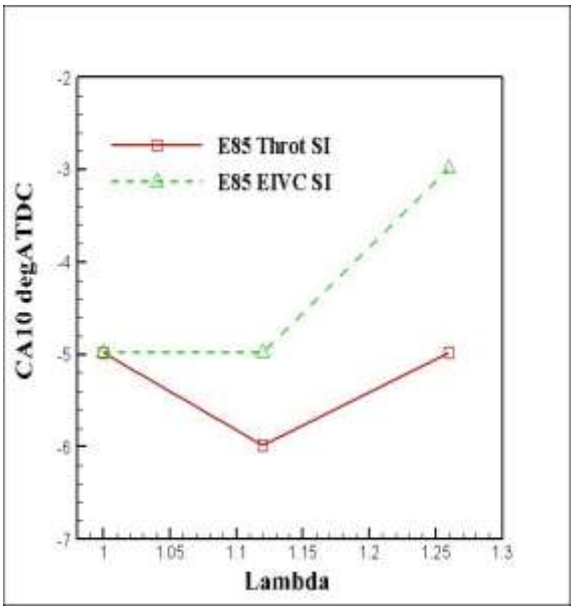


**(g) CA10**

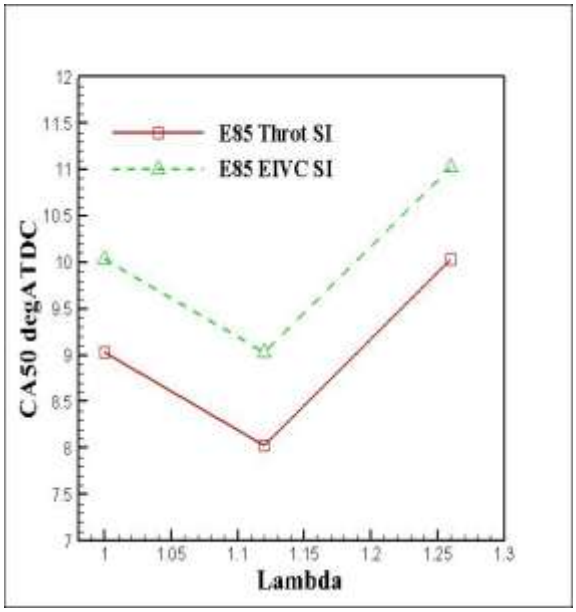


**(h) CA50**

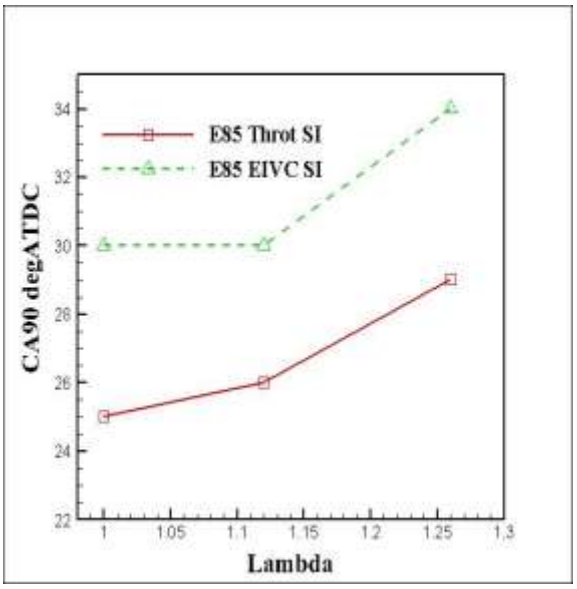


(i) CA90

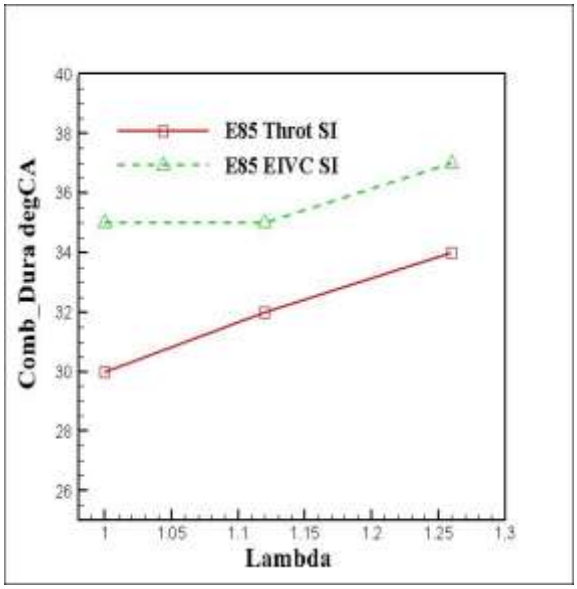


(j) Combustion Duration

**Figure 6.10 (ctd) Combustion Analysis**

### 6.5.2 Engine Performance and Efficiency Analysis

Figure 6.11(a) shows the combustion efficiency in the throttled SI and the EIVC SI combustion modes. The combustion efficiency in the EIVC SI and the throttled SI combustion is the same (92%) with lambda 1.0 but slightly higher in the EIVC with lambda 1.1 and 1.2.

The throttled SI mode exhibits the lowest theoretical thermodynamic efficiency (Figure 6.11(b)). This is a result of its throttling and increased pumping loss, which is much greater than can be found in the EIVC SI combustion mode.

The gas-exchange efficiency in Figure 6.11(c) shows that the EIVC SI and throttled SI are characterised by linearly increasing gas-exchange efficiency with increasing lambda values. The EIVC SI resulted in an average of 91.2% efficiency. The throttle SI has the lowest gas-exchange efficiency (88.2%), the reason for the largest pumping loss seen in Figure 6.11(e).

Figure 6.11(d) compares the net indicated efficiency in the EIVC and throttled SI modes with the lambda sweep of 1 to 1.25. The figure showed an average indicated efficiency of 34.2% in the EIVC and 31.6% in the throttled SI combustion. The indicated efficiency in the EIVC was 2.5% higher than in the throttled SI. This resulted in an average of 7.2% improvement in ISFC (Figure 6.12(e)). Furthermore, it can be seen that the difference in PMEP between EIVC and the throttled SI operations, which averaged 35% (Figure 6.11(e)) is greater than their difference in ISFC. This implies that some other factors may have reduced the benefit of lower PMEP of EIVC than the throttled SI. This could be attributed to the burn duration or other factors unknown at present. However, in this test the combustion duration of EIVC seen in Figure 6.10(j) is longer than in the throttled SI. Therefore the slower flame propagation in the EIVC mode alone is not sufficient to explain the diminishing difference in ISFC and the large difference in PMEP between the two engine operation modes.

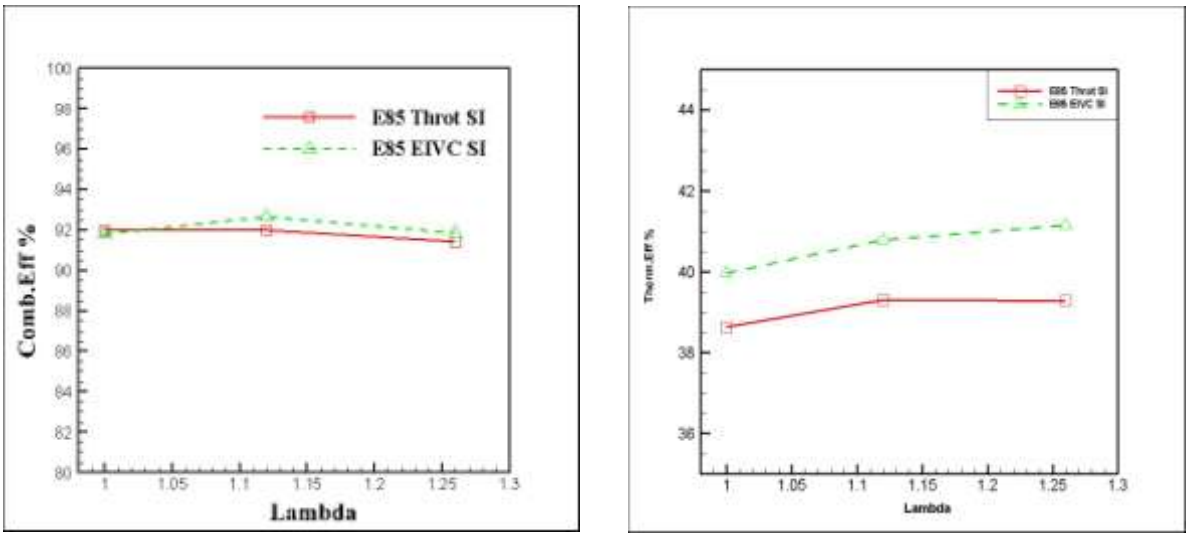


**(a) Combustion Efficiency** **(b) Thermal Efficiency**

**Figure 6.11 Performance Analysis**

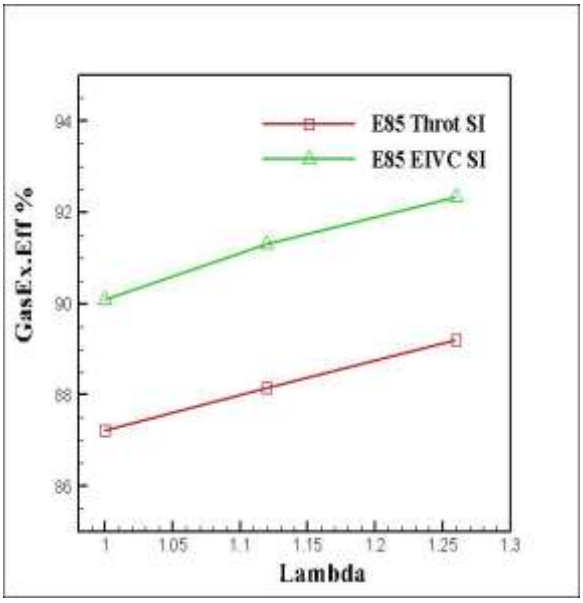


**(c) Gas-Exchange Efficiency**

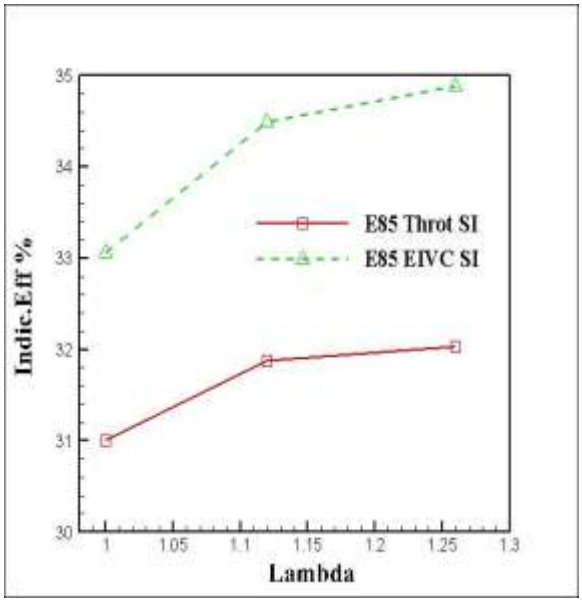


**(d) Indicated Efficiency**

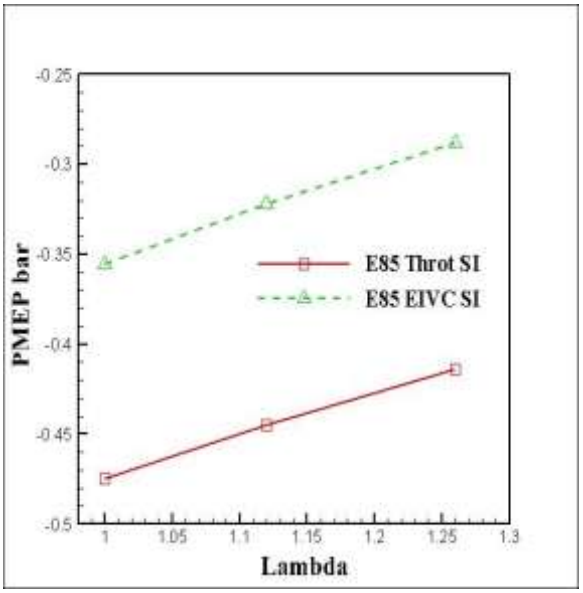


**(e) Pumping Mean Effective Pressure**

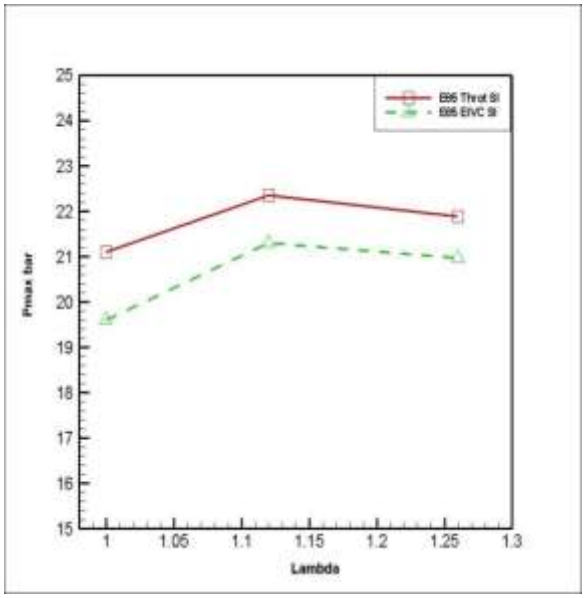


**(f) Maximum Cylinder Pressure**

**Figure 6.11 (ctd) Performance Analysis**

### 6.5.3 Fuel Consumption and Emissions

Figure 6.12(a) shows the CO emission in the throttled SI and the EIVC SI with lambda 1.0, 1.1 and 1.2 values. As seen in Figure 6.12(a), the ISCO emission is slightly higher in the EIVC SI mode than in the throttled SI mode at lambda 1.0 and it decreases with increasing lambda reaching a minimum with lambda=1.25.

Figure 6.12(b) shows the results in ISHC emission for the two modes of operations. The throttled SI operation produces about a 15% increase in ISHC emissions compared to the EIVC SI combustion.

The higher CO and HC emissions results suggest that there are more locally rich mixtures formed in the throttled SI mode. The partly-open throttle-valve, interaction of fuel injection and intake air-flow during the throttled SI mode would have caused more fuel impingement on the piston. In addition the higher charge cooling effects of E85 must have affected the fuel evaporation and led to poor mixture preparation.

Figure 6.12(c) shows the NOx emissions for the three combustion modes. It can be seen that the NOx emission for EIVC SI is higher than in the throttled SI.

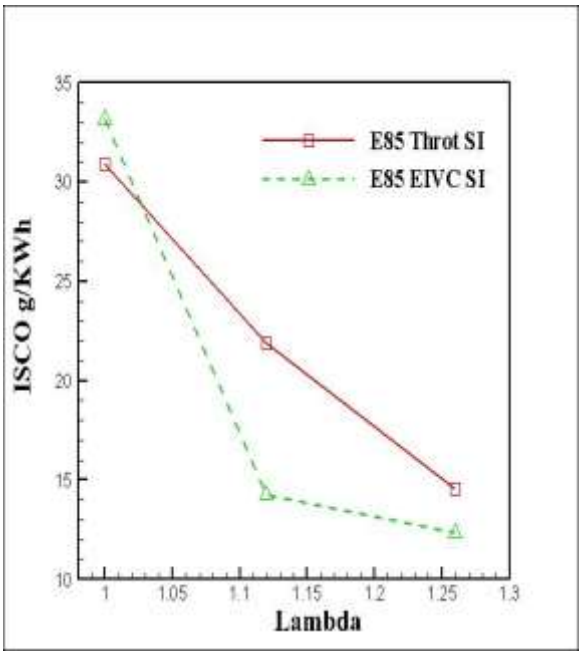


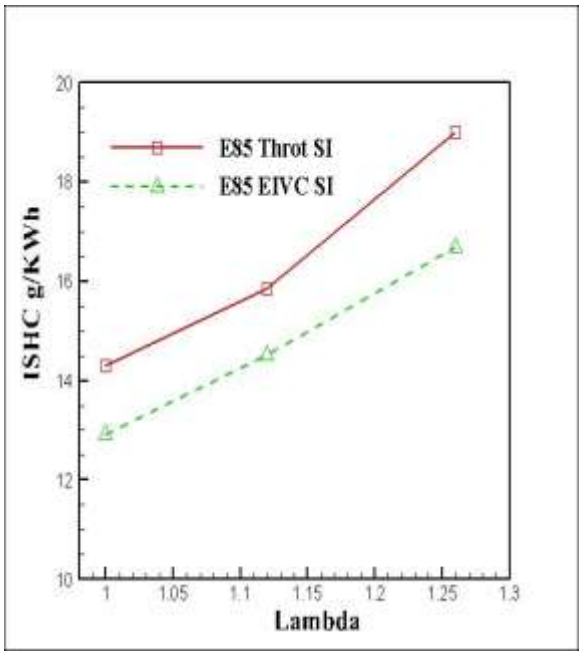


**(a) ISCO** **(b) ISHC**

**Figure 6.12 Gaseous Emissions and Fuel Consumptions**

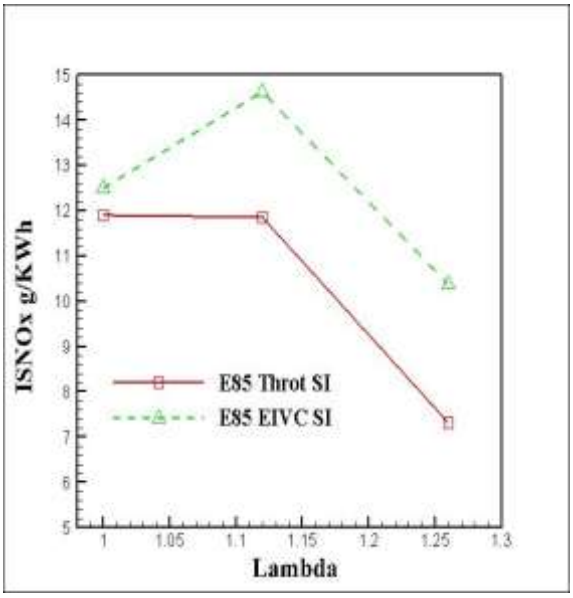


**(c) ISNOx**

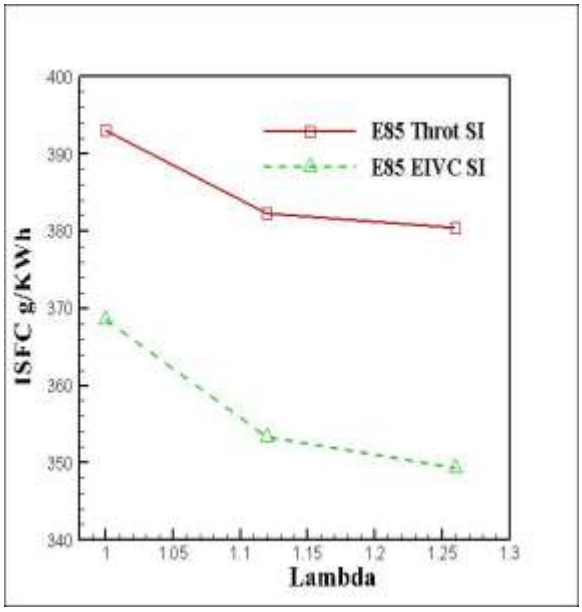


**(d) ISFC**

**Figure 6.12 (ctd) Gaseous Emissions and Fuel Consumptions**

**Particulate Emission**

It can be seen from Figure 6.13(a) and 6.13(b) that with lambda = 1, 1.1, and 1.2 the EIVC SI mode is characterized by the greatest number of particles in total, while the throttled SI showed the least number of particles. For all cases examined, the particles are dominated by the small particles in the range of 20-40nm, which are typically associated with soot particles in the nucleation mode.

In the case of the EIVC SI, Figure 6.13(a) shows that E85 resulted in a significant rise in the total particle numbers, which was dominated by particles of diameter between 15-40nm as shown in Figure 6.13(b).

In the throttled SI operations, the number of particles decreased rapidly in E85. As shown in Figure 6.13(b), the majority of particles were around 20nm in diameter. The absence of peaks in the number of particles with throttled SI suggests that E85 helped to reduce the soot formation.

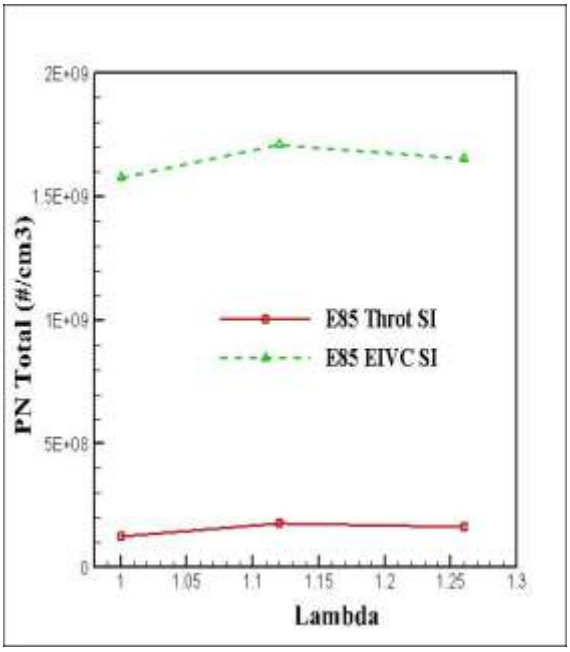


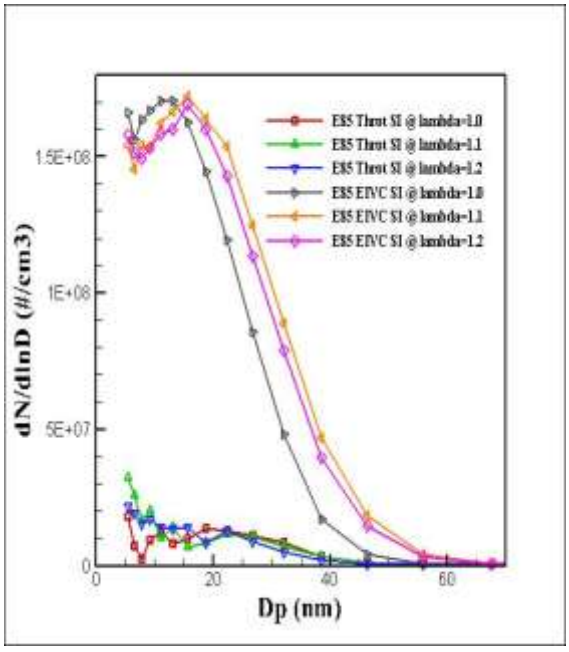


**(a) Total Particle Numbers** **(b) Particcle Number and Size**

**Figure 6.13 Total particle number and and size distribution**

## 6.6 Comparison of Gasoline E0, E15 and E85 at Lambda 1.0

### 6.6.1 Combustion Analysis

Figure 6.14 shows and compares the combustion characteristics of the three operation modes in different fuel blends.

Figure 6.14(a) shows the maximum pressure-rise rate as a function of combustion modes and fuel blends. It can be seen that the maximum pressure-rise rate for all the combustion modes was less than 0.65bar/CA. As shown in Figure 6.14(b), the MBT spark-timings were more advanced in EIVC SI mode than in the throttled mode due to slower burning velocities, as evidenced in the mass burned fractions in figure 6.14(c) and the corresponding heat release rate curves in figure 6.14(d). Furthermore, both E15 and E85 showed a noticeable reduction in the heat- release rate.

As shown in Figure 6.14(e), the COVimep for all modes are below 2.5% and did not vary significantly in the fuel blends and combustion modes studied.

As shown in Figure 6.14(f), E15 and E85 increased exhaust temperature by about 4.5$^{o}$C and 17$^{o}$C respectively over E0 fuel in the throttled SI mode due to spark retard. For the same

reason, in the EIVC SI, E15 and E85 exhaust temperatures were 17$^{o}$C and 23$^{o}$C higher than in E0.

Figure 6.14(g) shows that the overall combustion period tended to increase from the throttled SI to EIVC SI combustion. In the EIVC, the slower burning process is likely to have been caused by decreased turbulence and lower temperature at the end of compression. The effect of ethanol on combustion was mode-dependent and did not show any consistent trend.

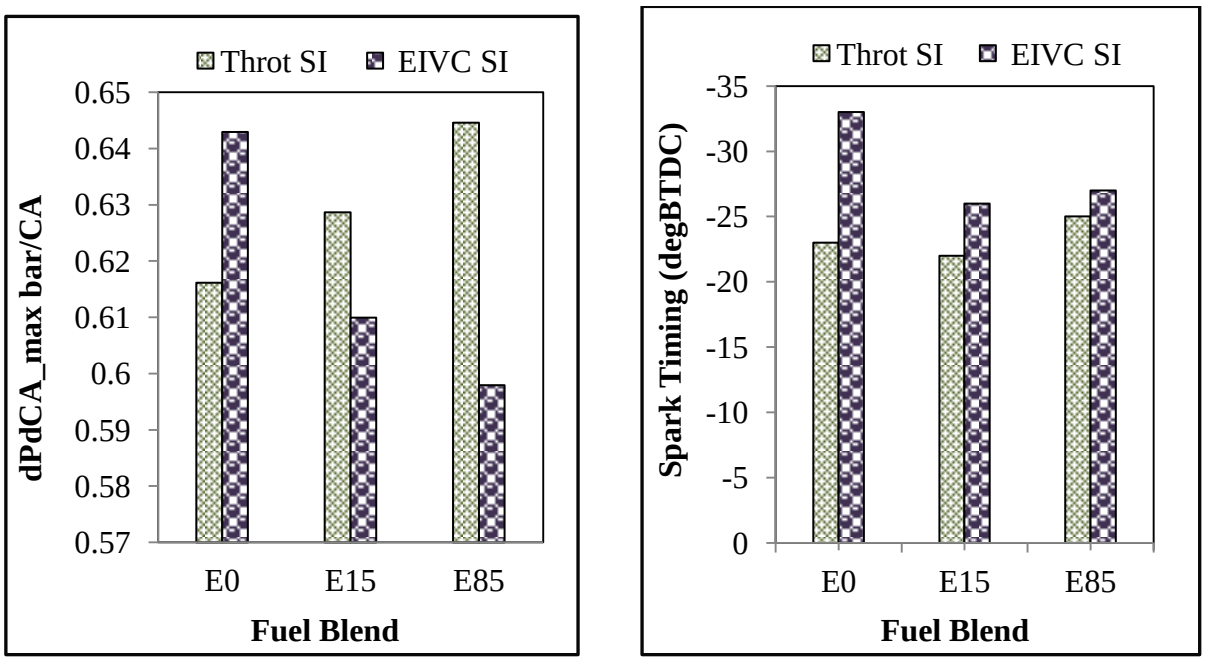


**(a) Maximum Pressure-Rise Rate** **(b) MBT Spark-Timing**

**Figure 6.14 Combustion Analysis**

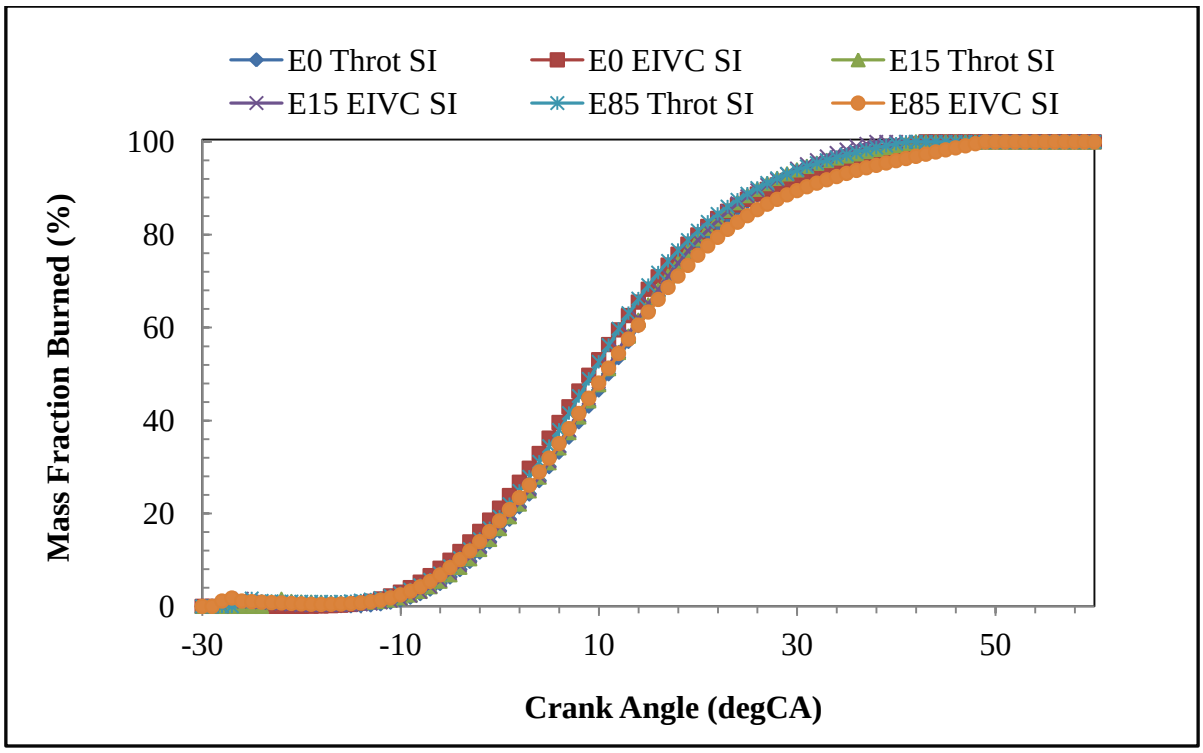


**(c) Mass Fraction Burned**

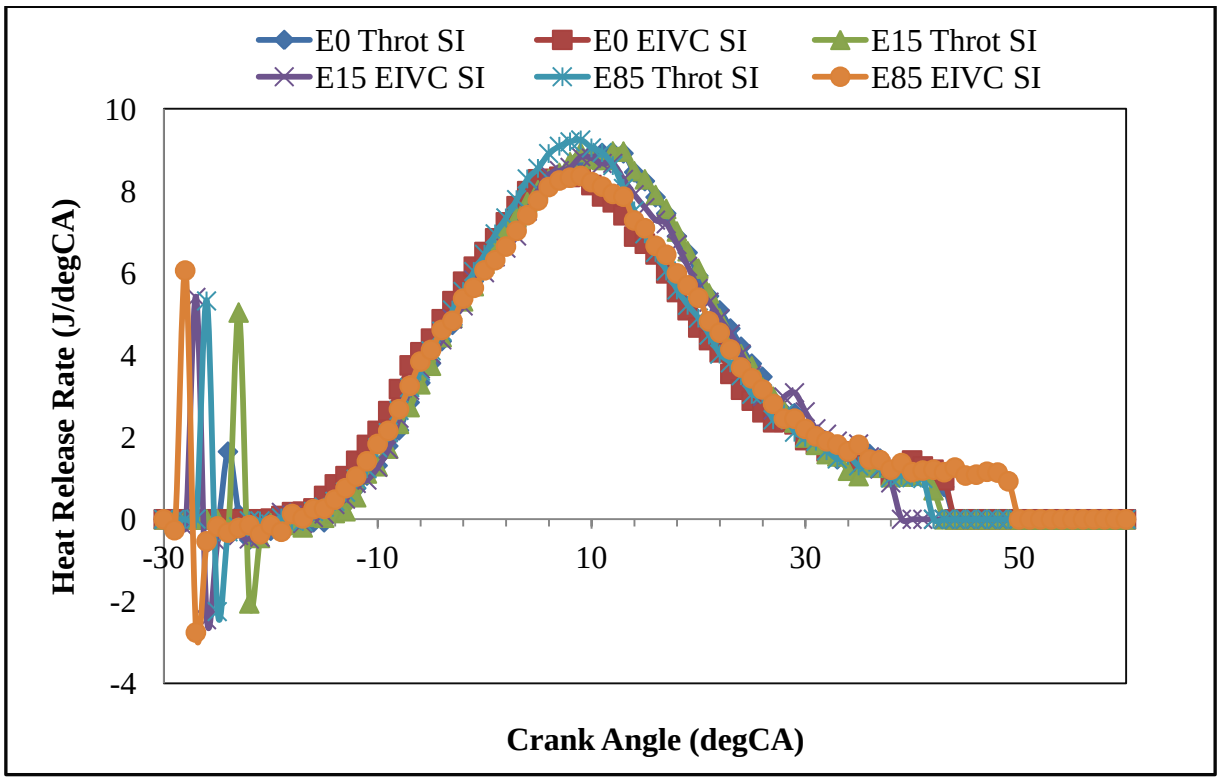


**(d) Heat-Release Rate**

**Figure 6.14 (ctd) Combustion Analysis**

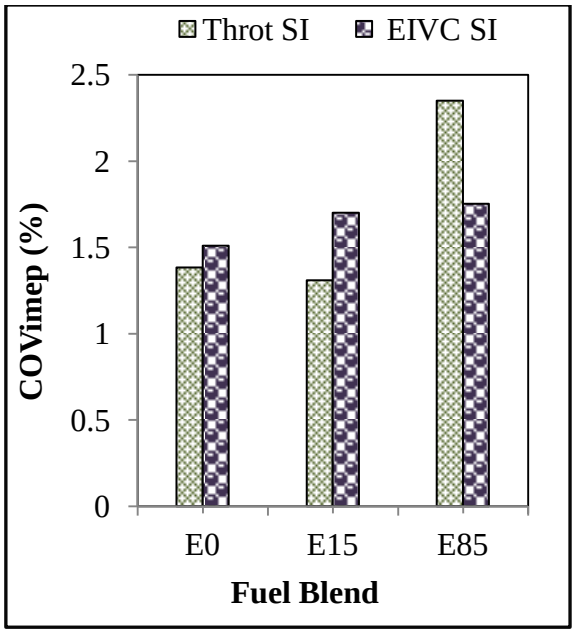


**(e) COV of IMEP**

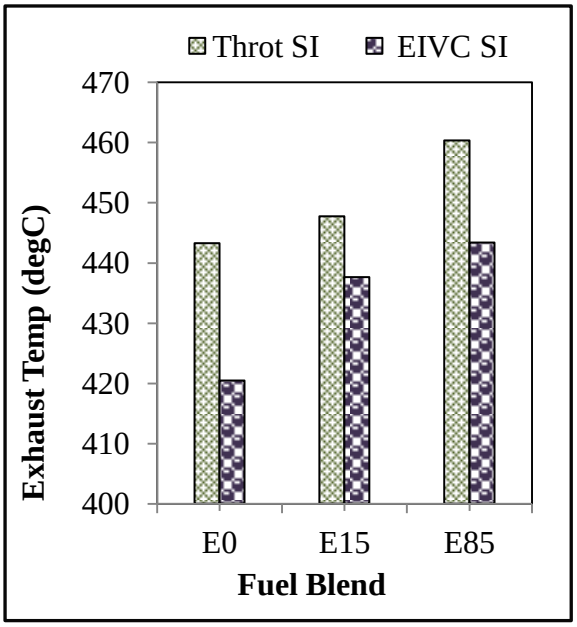


**(f) Exhaust Temperature**

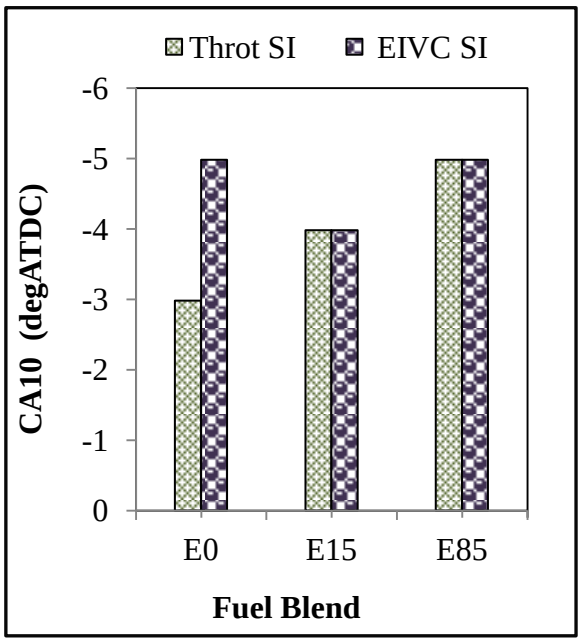


**(g) CA10**

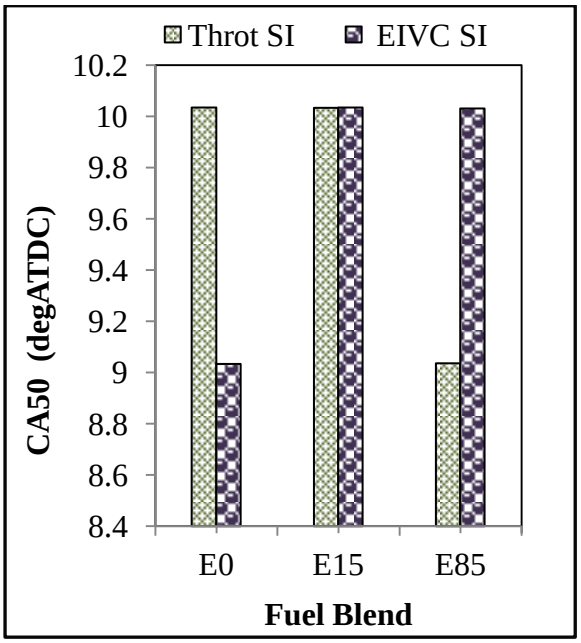


**(h) CA50**

**Figure 6.14 (ctd) Combustion Analysis**

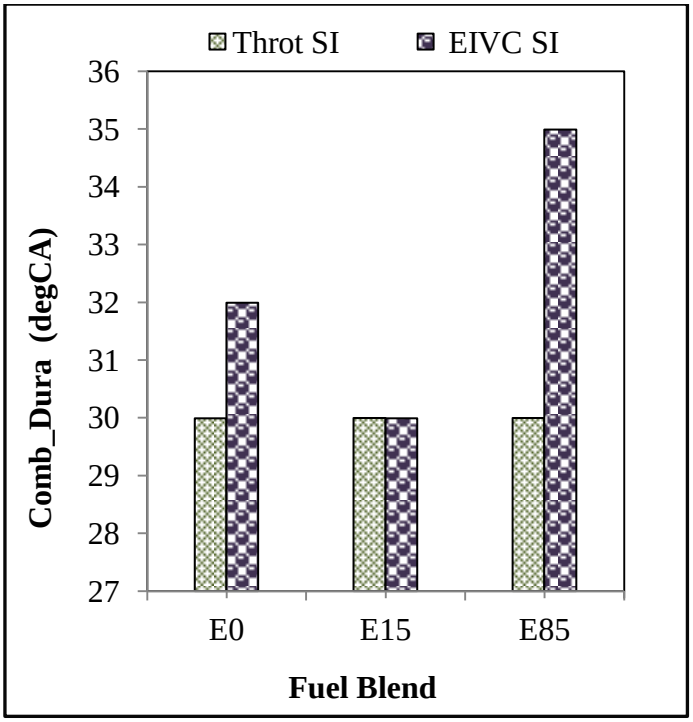


**(i) Combustion Duration**

**Figure 6.14 (ctd) Combustion Analysis**

### 6.6.2 Engine Performance and Efficiency Analysis

Figure 6.15(a) shows the combustion efficiency for the combustion modes and fuel blends. It can be seen that the combustion efficiency in E15 and E85 blends in the throttle SI combustion decreased slightly to 93% in E15 and 92% in E85 in comparison to 95% in E0. The lower combustion efficiency is likely to be related to the charge-cooling effect of the ethanol and poor mixture formation that resulted in pockets of rich mixture, as indicated by the increasingly higher CO emissions (Figure 6.16(a)).

The thermodynamic efficiency of the engine is shown in Figure 6.15(b), the blend in E15 and E85 in the EIVC SI slightly increased the thermodynamic efficiency. In contrast to the EIVC SI, in the throttled SI blends E15 and E85, the efficiency was reduced.

Figure 6.15(c) compares the indicated efficiency of the modes and fuel blends. The throttled SI indicated efficiency shows a slightly decreasing trend: 33% in E0 to 31.2% in E15 and 31.0% in E85, whilst the EIVC exhibits a nearly constant value of 33%. Generally, in the EIVC, efficiency is about 2% higher than in the throttled SI combustion using E15 and E85;

with corresponding fuel savings of 7% in both E15 and E85 (Figure 6.16(d)), due to lower ISHC in E85 shown in Figure 6.16(b) as well as lower pumping loss (Figure 6.15(d)).

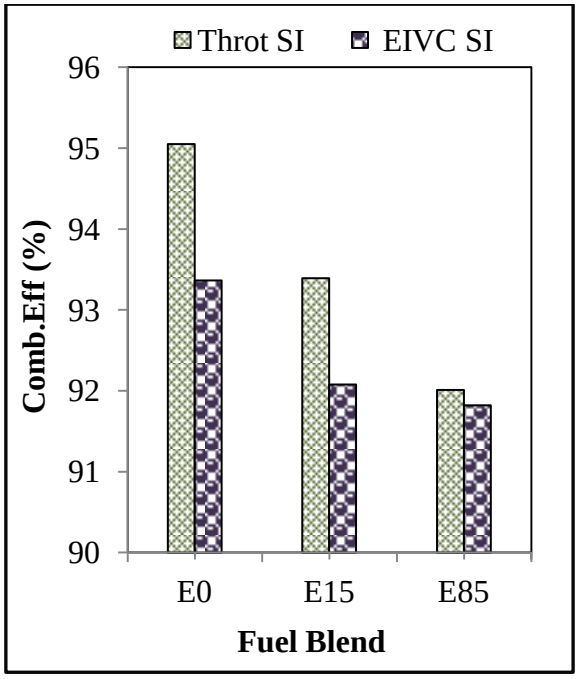


**(a) Combustion Efficiency**

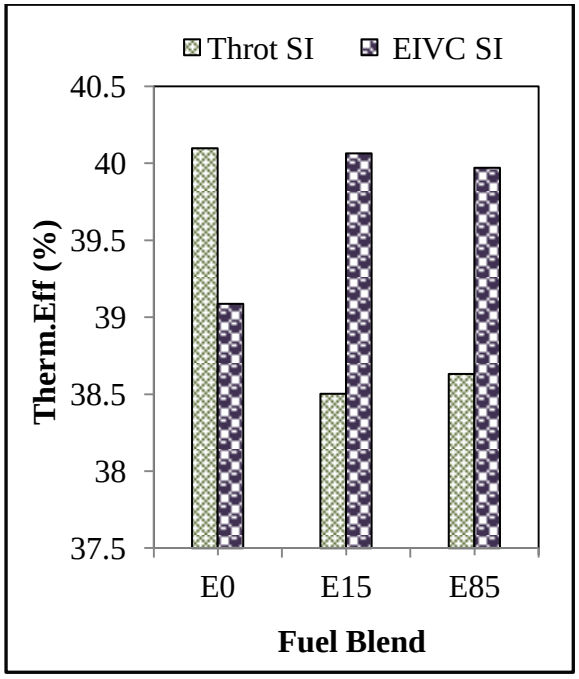


**(b) Thermal Efficiency**

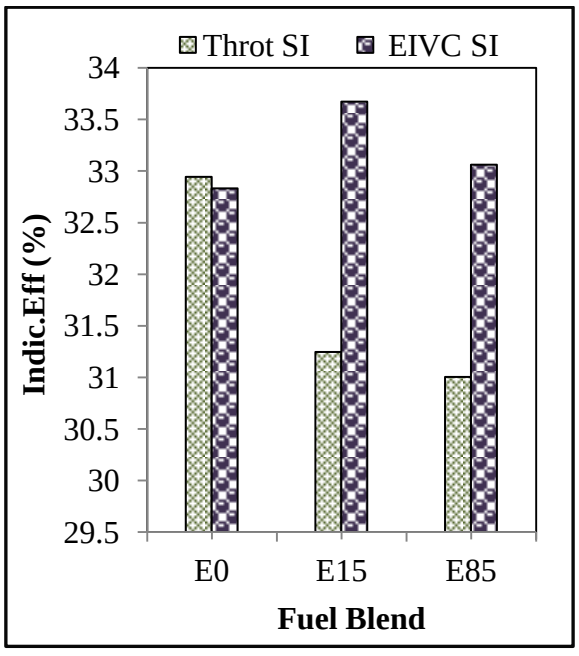


**(c) Indicated Efficiency**

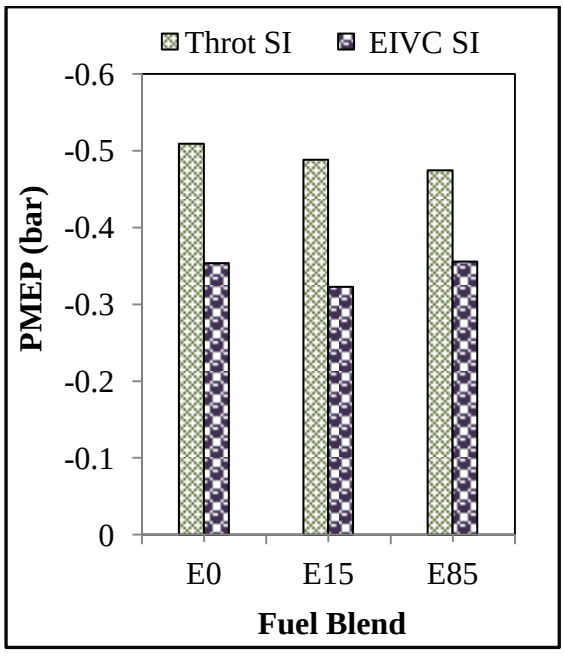


**(d) PMEP**

**Figure 6.15 Performance Efficiency**

### 6.6.3 Gaseous Emissions and Fuel Consumption

Figure 6.16(a) and (b) shows the CO and UHC emissions for the two combustion-modes and fuel-blends. As seen in Figure 6.16(a), the ISCO was higher for EIVC than in throttled SI combustion. In the throttled SI combustion, CO increased from 6.0 g/KWh with gasoline to 31.0 g/KWh as ethanol contents were increased. For EIVC SI it increased from 12.0g/KWh in E0 to 33.0g/KWh in E85. As discussed previously, such an increase may be caused by poor ethanol fuel mixture quality, the wall-wetting effect and low in-cylinder temperature, as the percentage of ethanol fuel blend increased from E0 to E85.

As shown in Figure 6.16(a), the change in ISHC from gasoline and its mixtures with ethanol was much less than the ISCO in the EIVC mode and SI mode.

It can be seen from Figure 6.16(c), that the EIVC mode produced lower NOx emissions in E15 and E85, as a result of lower combustion temperature. However, the two modes display similar trends in ISNOx.

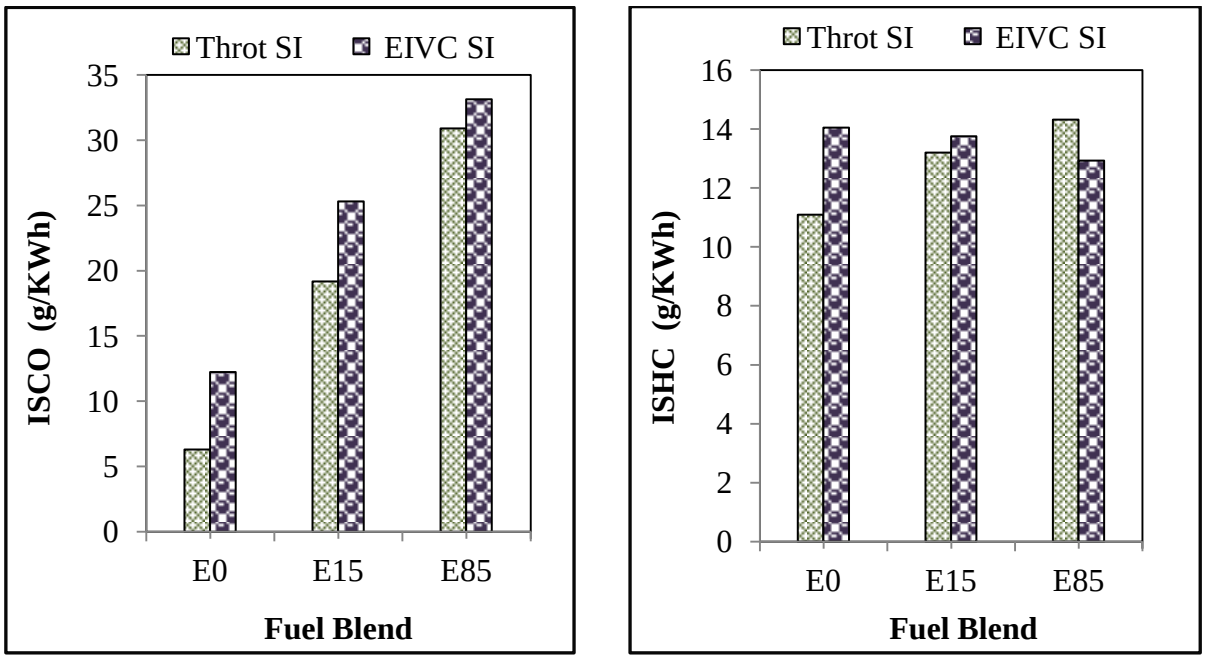


**(a) ISCO** **(b) ISHC**

**Figure 6.16 Gaseous Emissions and Fuel Consumption**

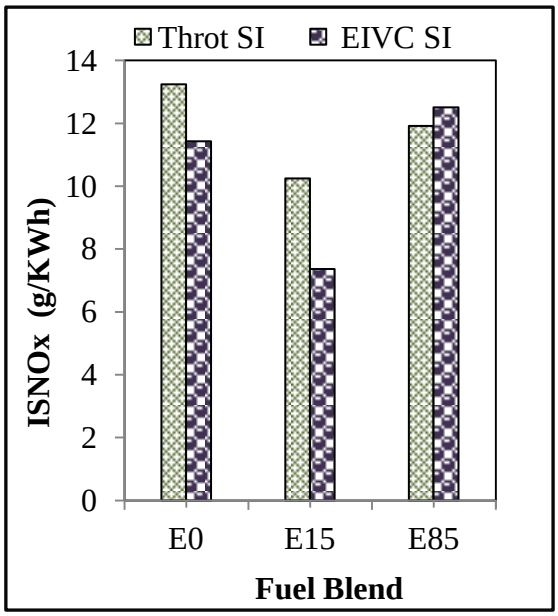


**(c) ISNOx**

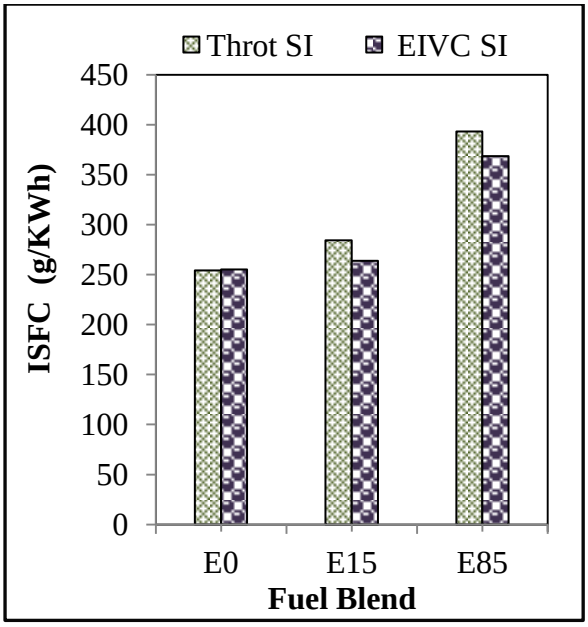


**(d) ISFC**

**Figure 6.16 (ctd) Gaseous Emissions and Fuel Consumption**

**Particulate Emissions**

Figure 6.17(a) shows that the total number of particles varies between different operational modes, in addition the effect of ethanol on particle numbers is also mode-dependent. In the case of throttled SI operations, the number of particles decreased rapidly when the ethanol content was increased from zero to 85%. As shown in Figure 6.17(b), the majority of particles were around 20nm in diameter. The presence of oxygen in E15 and E85 helped to reduce the particulate formation.

In the case of EIVC, Figure 6.17(a) shows a significant rise in the total particle number in E85, dominated by particles of between 15-20nm in diameter, as shown in Figure 6.17(b). This may be explained by the valve- timing and fuel-injection timing (Figure 2). Because of its lower calorific value, a larger volume of E85 was injected over a longer duration and most of the E85 was injected after IVC when the charge temperature was reduced with expansion in the second half of the intake stroke. Furthermore, the charge-cooling effect of E85 was more pronounced in the case of EIVC as injection took place with a fixed intake mass. As a result, the E85 fuel injection occurred in a cooler environment, resulting in reduced evaporation.

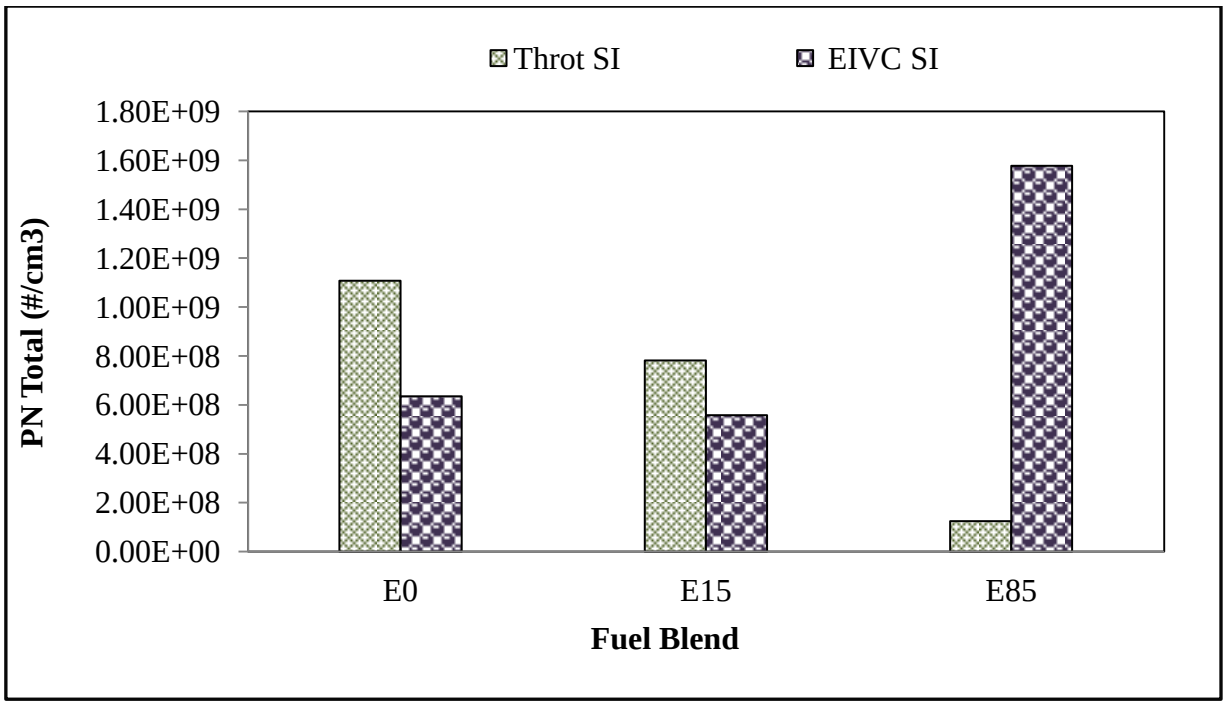


**(a) Total Particle Number Distribution**

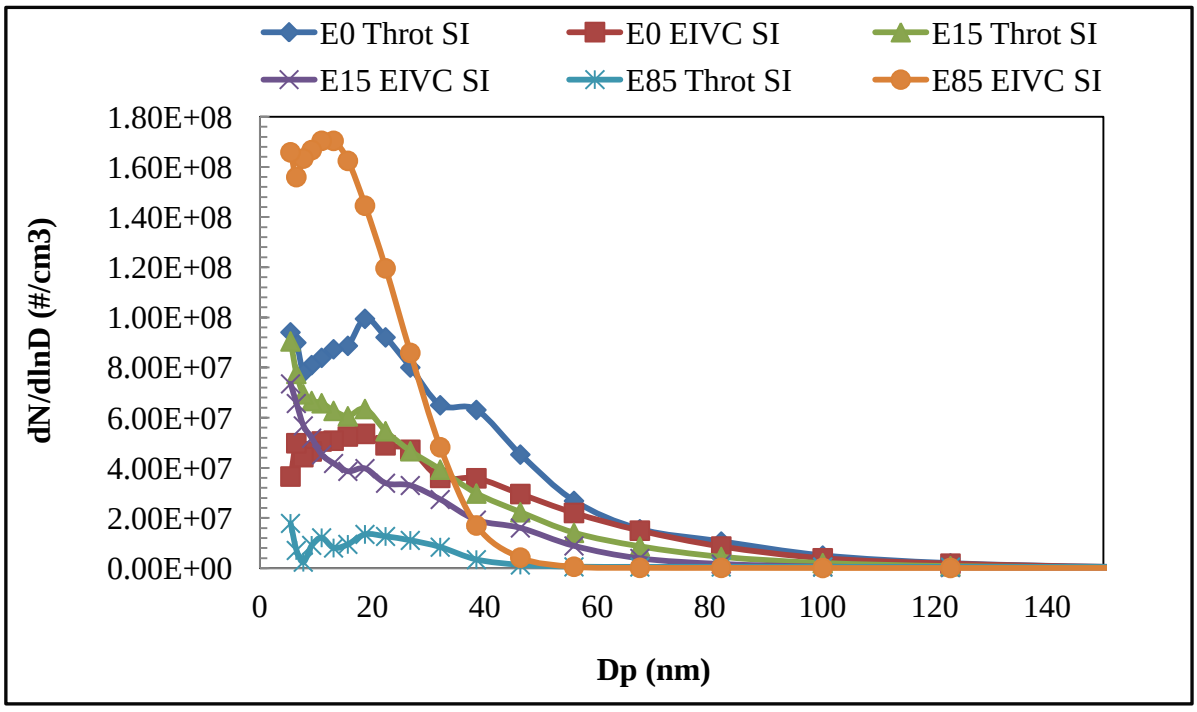


**(b) Particle Number Distribution**

**Figure 6.17 Total Particle Number and size distributions of different fuel blends at lambda 1.0**

## 6.7 Comparison of Gasoline E0, E15 and E85 at Lambda 1.1

### 6.7.1 Combustion Analysis

Figure 6.18(a) shows the maximum pressure-rise rate as a function of combustion-modes and fuel blends. It can be seen that the maximum pressure-rise rate in the two combustion modes were below 0.8bar/CA in the fuel blends. As shown in Figure 6.18(b), the MBT spark-timings were more advanced in the EIVC than in the throttled SI in E0 and E15 due to slower burning velocities, as evidenced by the mass fraction burned (Figure 6.18(c)) and the corresponding heat-release rate (Figure 6.18(d)).

Shown in Figure 6.18(e), the COVimep measured in the modes were low, below 3.0 % and did not vary significantly with the fuel blends and combustion modes studied.

As shown in Figure 6.18(f), E85 increased exhaust temperature by about 18$^{o}$C more than the E0 and E15 fuel blends in the throttled SI mode. For the same reason, the EIVC in E85 exhaust temperature was 24$^{o}$C higher than in E0 and E15. This difference may be due to spark-retard. Although the spark was retarded further using the E15 blend, the exhaust temperature was the same as in E0.

Figure 6.18(i) shows that the overall combustion period was longer in EIVC than in throttled SI. In the case of EIVC, the slower burning process was likely to have been caused by decreased turbulence and lower temperature at the end of compression. The effect of ethanol on combustion was mode-dependent and did not show any consistent trend.

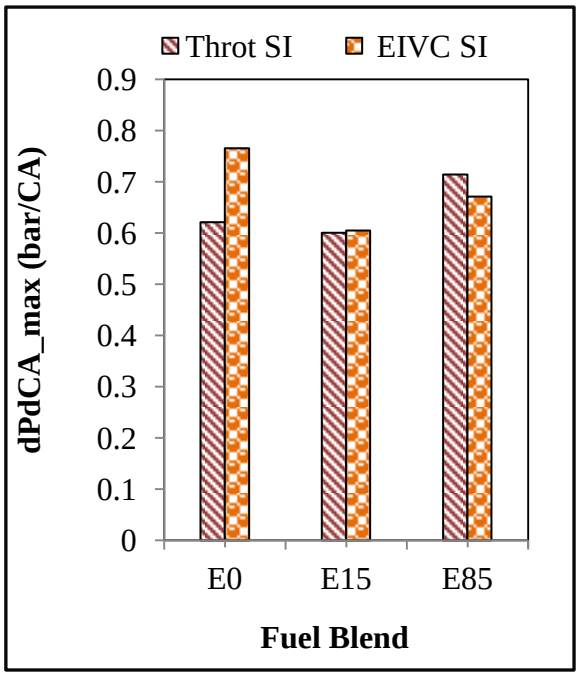


(a) Maximum Pressure Rise Rate

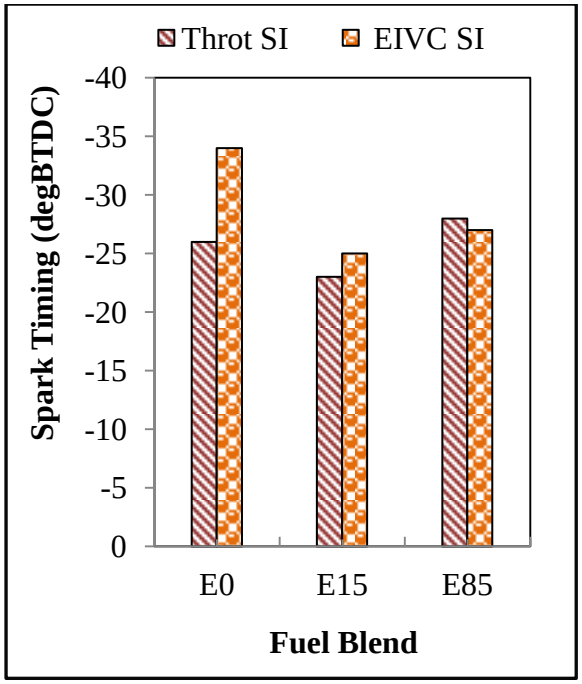


(b) MBT Spark Timing

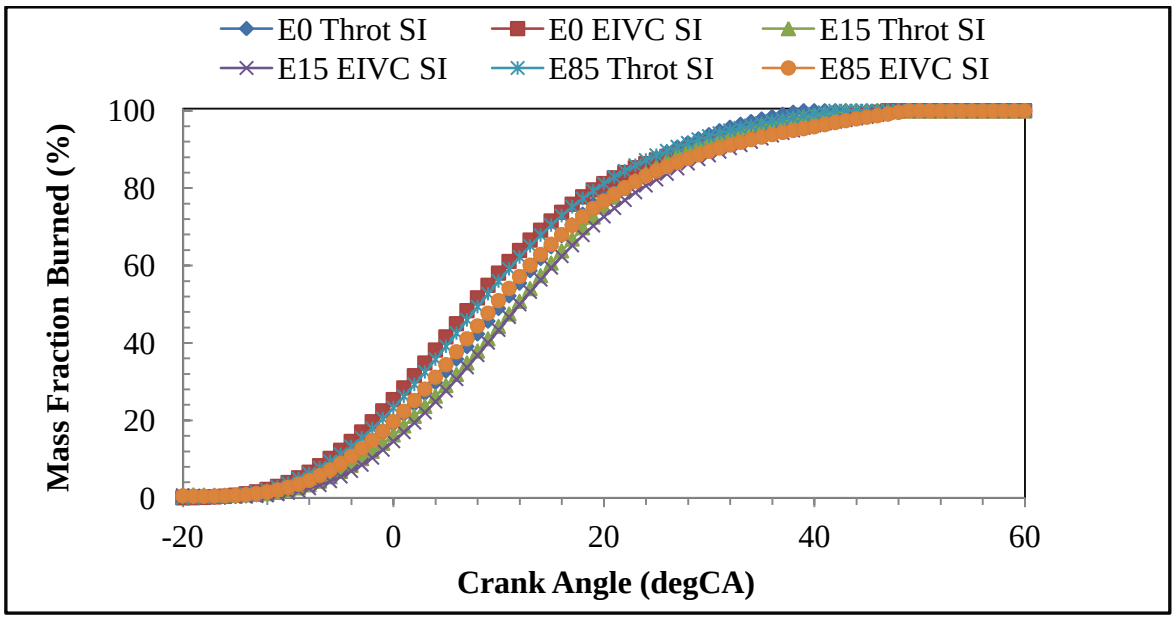


(c) Mass Fraction Burned

**Figure 6.18 Combustion Analysis**

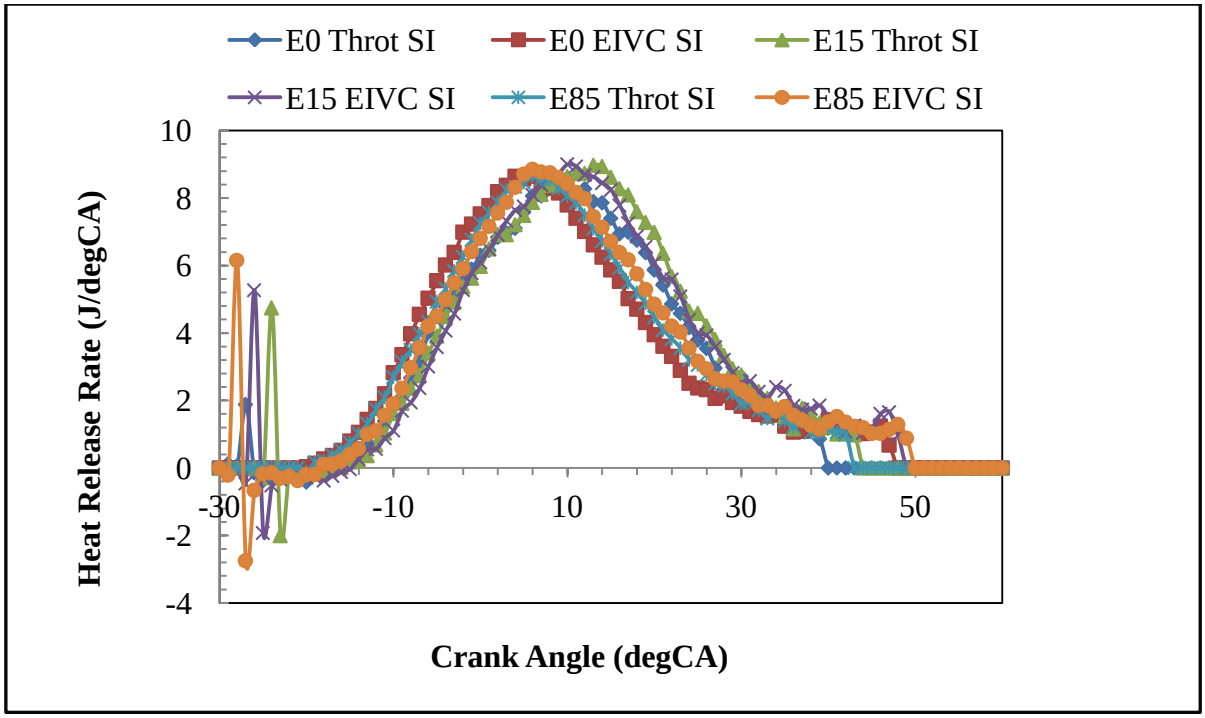


**(d) Heat Release Rate**

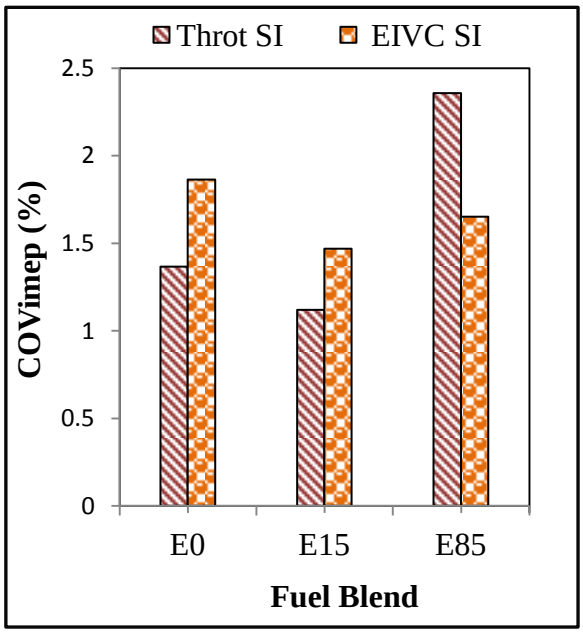


**(e) COV of IMEP**

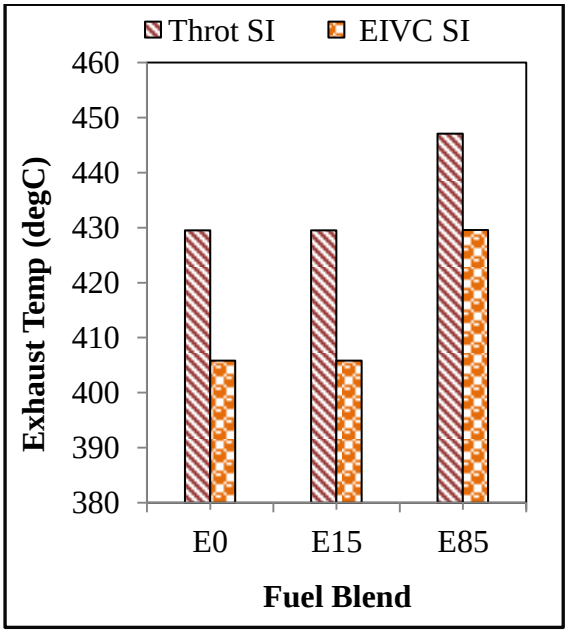


**(f) Exhaust Temperature**

**Figure 6.18 (ctd) Combustion Analysis**

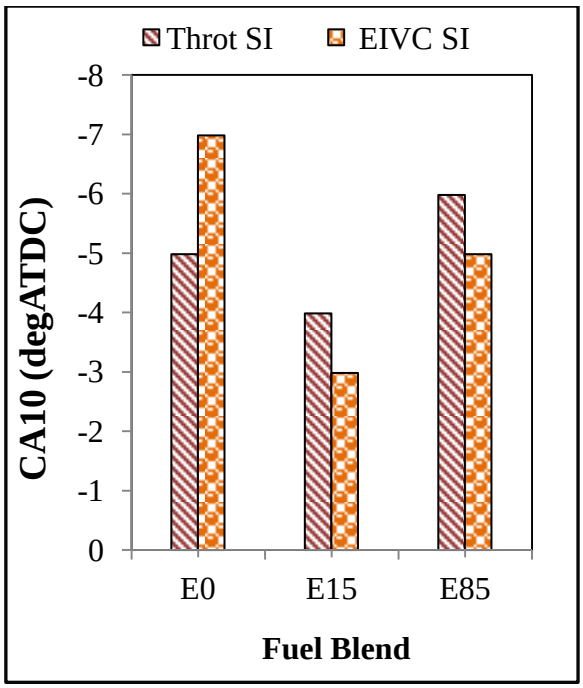


**(g) CA10**

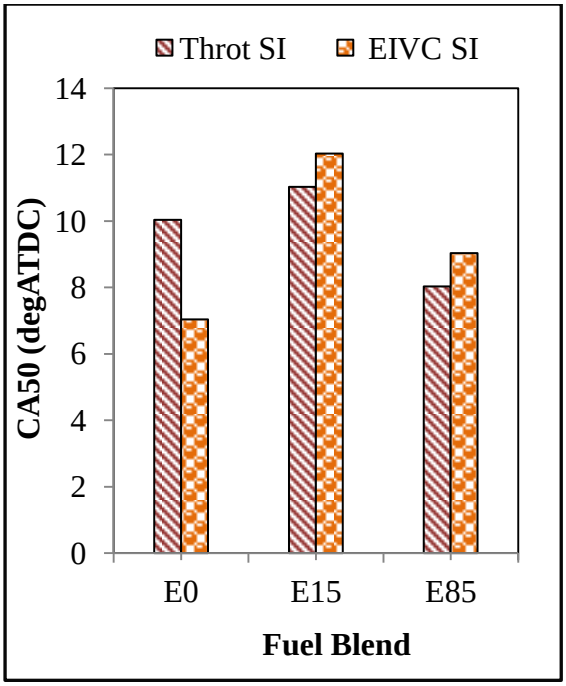


**(h) CA50**

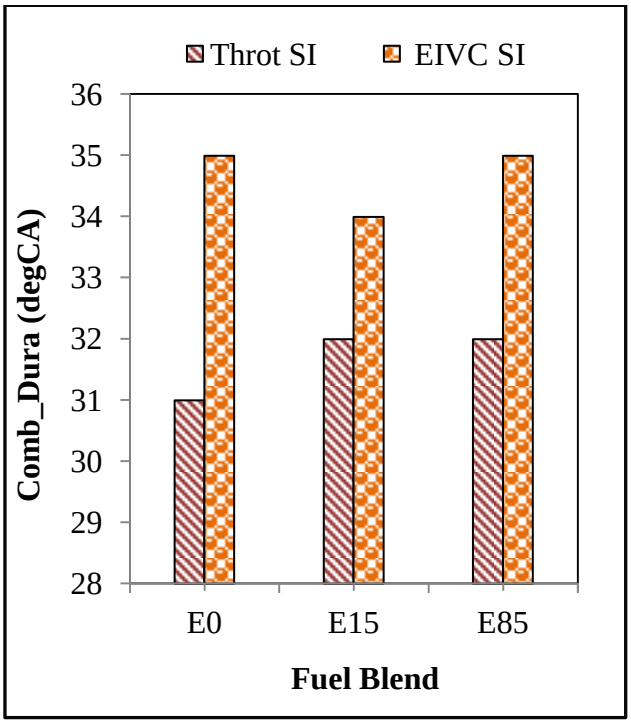


**(i) Combustion Duration**

**Figure 6.18 (ctd) Combustion Analysis**

### 6.7.2 Engine Performance and Efficiency Analysis

Figure 6.19(a) shows the combustion efficiency for the combustion-modes and fuel-blends. It can be seen that the combustion efficiency of the throttle SI combustion decreased slightly to 92% in E85 from 94.9% in E0. As discussed earlier, the lower combustion efficiency is likely to be related to the charge-cooling effects of the ethanol and poor mixture formation that resulted in pockets of rich mixture, as indicated by the increasing CO emissions in E0 to E85 (Figure 6.20(a)).

The EIVC SI combustion efficiency was lower than in throttled SI and the trends are similar to both. This lower efficiency in EIVC SI could be caused by the different mixture-formation process, another likely contributor could be the lower in-cylinder turbulence. Although the reduced valve-lift could result in higher gas velocity past the valves and improve the fuel atomisation process, as discussed earlier, the early closure of the valve would lead to a cooler in-cylinder temperature. Furthermore, the additional charge-cooling effects in E15 and E85 further deteriorated the mixture preparation and hence the higher CO emissions (Figure 6.20(a)).

The thermodynamic efficiency of the engine is shown in Figure 6.19(b). The throttled SI displays greater thermodynamic efficiency in E0. In contrast the EIVC SI displays the greatest thermodynamic efficiency in E15 and E85.

Figure 6.19(c) compares the indicated efficiency of the modes and fuel blends. The throttled SI indicated efficiency shows a slightly decreasing trend to 32.9% in E15 and 31.9% in E85 compared to34% in E0, whilst the EIVC SI did not display a consistent trend. The indicated efficiency increases from 33.9% in E0 to 35% in E15 and decreased to 34.5% in E85. In general, the indicated thermal efficiency in the EIVC SI combustion mode is slightly lower than in the throttled SI combustion. In addition, it was observed that the EIVC SI displays 2.3% and 2.6% greater efficiency using E15 and E85 with corresponding fuel savings of 6.5% and 8% (Figure 6.20(d)), due to moderate ISHC emissions (Figure 6.20(b)) as well as lower pumping loss shown (Figure 6.19(d)). It was observed that in E0 blend, the PMEP in EIVC SI was about 35% better than in throttled SI but the ISFC in EIVC was slightly higher than in the throttled SI. Although, the combustion duration of EIVC SI was long, this does not account for the poor fuel economy. There are likely to be other causes responsible for this poor performance.

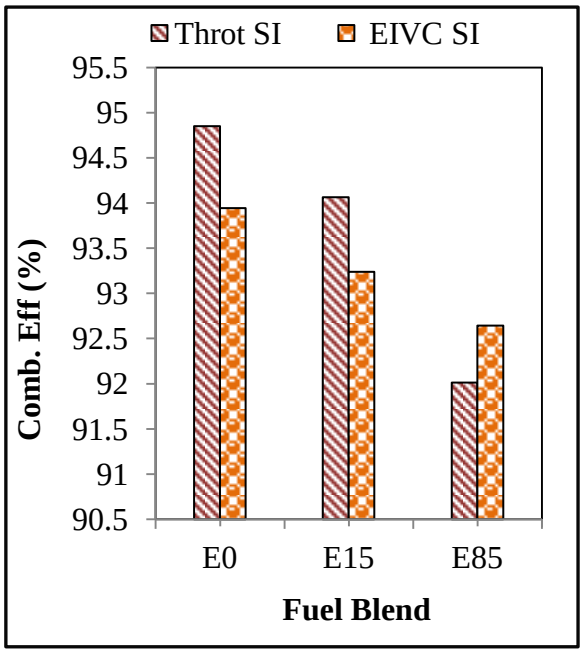


**(a) Combustion Efficiency**

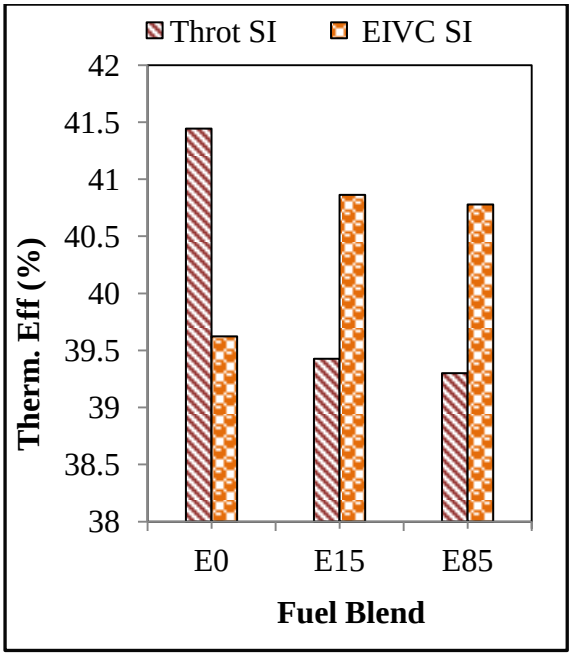


**(b) Thermal Efficiency**

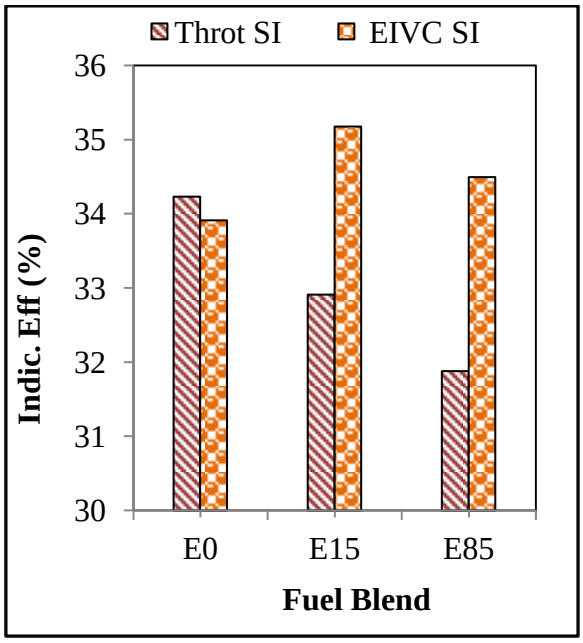


**(c) Indicated Efficiency**

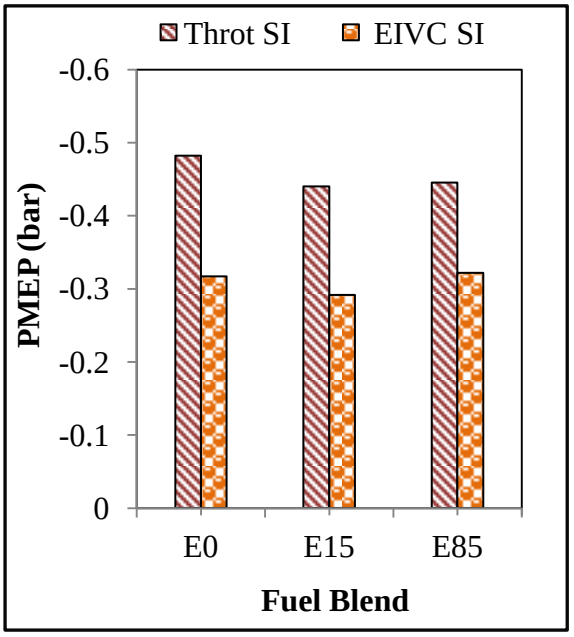


**(d) PMEP**

**Figure 6.19 Performance Analysis**

### 6.7.3 Fuel Consumption and Emissions

Figure 6.20(a) shows the CO and UHC emissions for the three combustion-modes and fuel-blends. As seen in Figure 6.20(a), the ISCO was higher in the throttled SI than in EIVC SI in E85 blend. In the throttled SI combustion CO increased from 4.8 g/KWh in E0 to 21.9 g/KWh

in E85. For EIVC SI, it increased from 4.9g/KWh in E0 to 14.0g/KWh in E85. As discussed previously, such an increase may be caused by poor ethanol fuel mixture quality, the wall-wetting effect and low in-cylinder temperature as the percentage of ethanol fuel blend increased from E0 to E85.

As shown in Figure 6.20(b) the change in ISHC from gasoline and its mixtures with ethanol was relatively constant in the EIVC mode, but exhibits an increasing trend in throttled SI mode.

It can be seen from Figure 6.20(b) that the throttled SI resulted in lower NOx emissions in E0 and E85, but the EIVC resulted in the lowest NOx using E15.

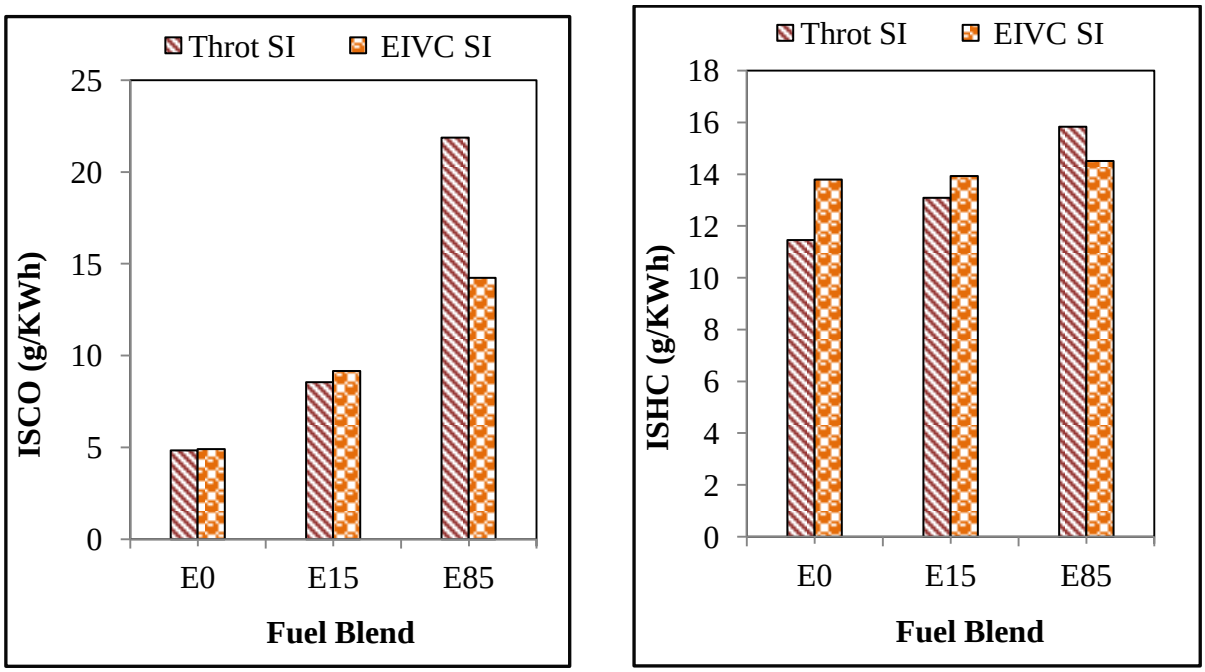


**(a) ISCO** **(b) ISHC**

**Figure 6.20 Gaseous Emissions and Fuel Consumption**

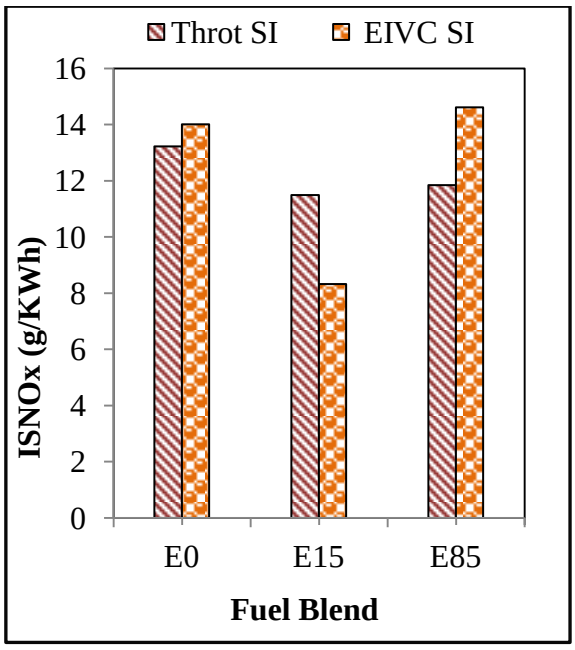


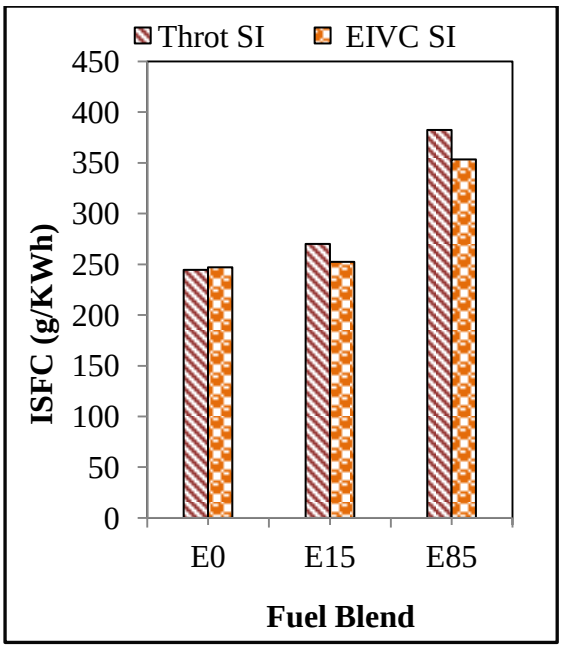


**(c) ISNOx** **(d) ISFC**

**Figure 6.20 (ctd) Gaseous Emissions and Fuel Consumption**

**Particulate Emission**

Figure 6.21(a) shows that the total number of particles varies between different operational modes and the effect of ethanol on particle numbers is also mode-dependent. In the case of throttled SI operations, the number of particles PN decreased rapidly and the peak was removed when the ethanol content was increased from zero to 85%. As shown in Figure 6.21(b), the majority of particles were around 20nm in diameter. The appearance of peaks in the number of particles of around 20nm with gasoline suggests that a higher number of particles of this size were formed and emitted under such operating conditions. The presence of oxygen in E15 and E85 helped to reduce the particle formation.

In the case of EIVC, Figure 6.21(a) shows that E85 resulted in a significant rise in the total particle number, which was dominated by particles of between 15-20nm in diameter, as shown in Figure 6.21(b). This may be explained by the valve-timing and fuel-injection timing (Figure 2). Because of its lower calorific value, a larger volume of E85 was injected over a longer duration and most of E85 was injected after IVC, when the charge temperature was reduced with expansion in the second half of the intake stroke. Furthermore, the charge-cooling effect of E85 was more pronounced in the case of EIVC as injection took place with a fixed intake mass. As a result, the E85 fuel injection occurred in a cooler environment and

with lower in-cylinder pressure resulting in reduced evaporation and longer penetration. This could have led to more liquid impingement on the piston.

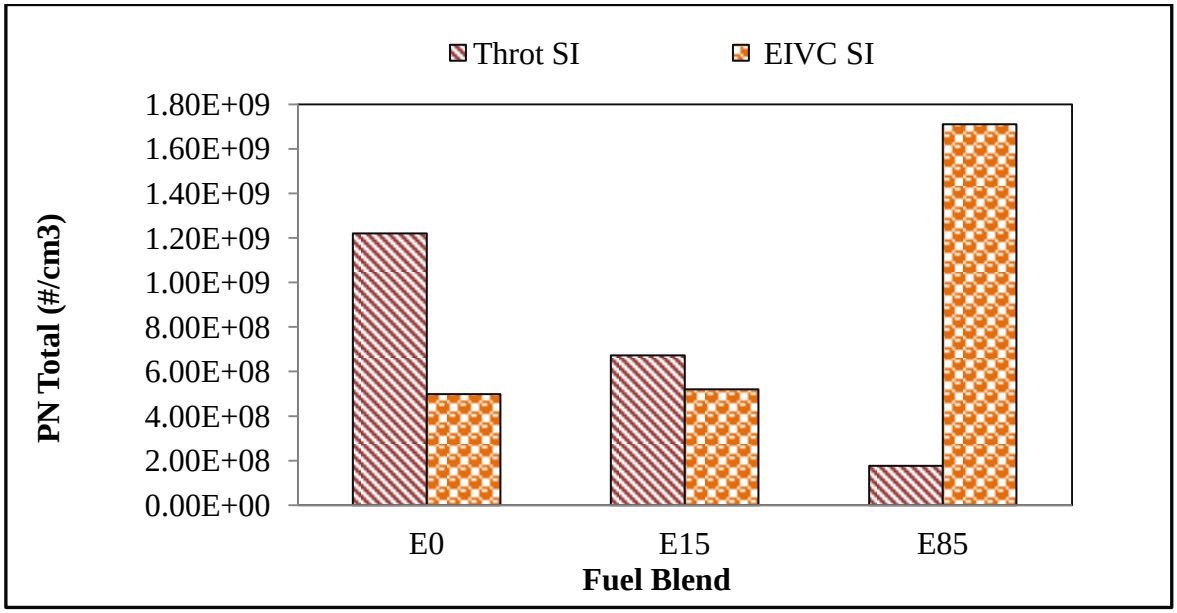


**(a) Total particle numbers**

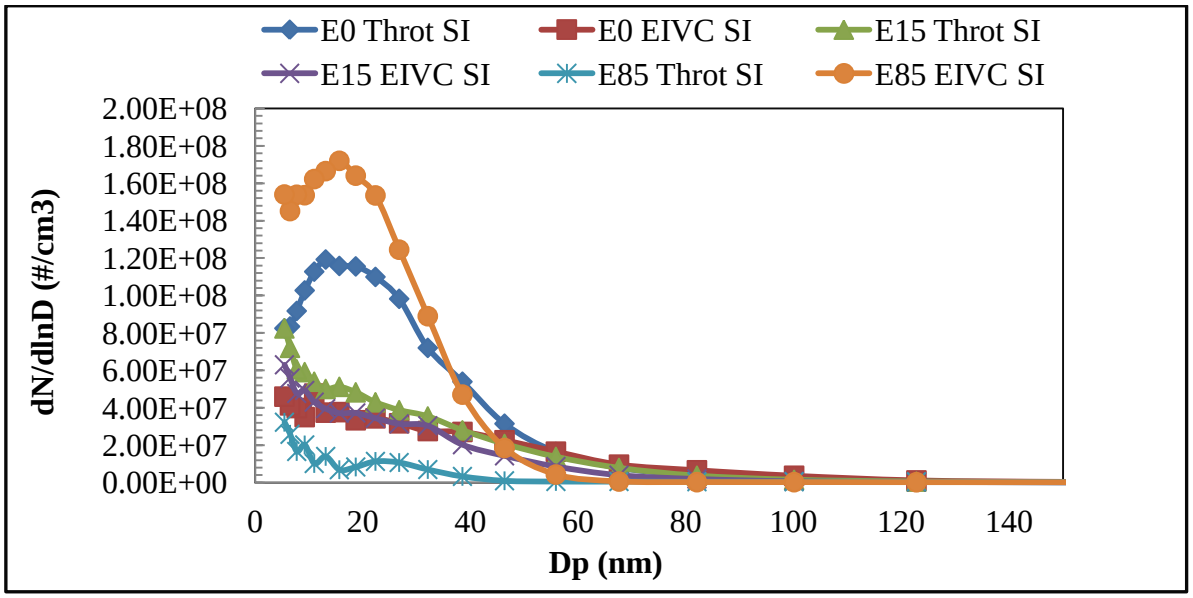


**(b) Particle number and size distributions**

**Figure 6.21 Particle number and size distributions of different fuel blends at lambda 1.1**

## 6.8 Comparison of Gasoline E0, E15 and E85 at Lambda 1.2

### 6.8.1 Combustion Analysis

Figure 6.22(a) shows maximum pressure-rise rate as a function of combustion-modes and fuel-blends. It can be seen that the maximum pressure-rise rate for all the combustion modes was less than 0.7bar/CA. As shown in Figure 6.22(b), the MBT spark timings were more advanced in EIVC SI mode in E0 than the throttled SI mode due to slower burning velocities (Figure 6.22(c)) and the heat-release rate (Figure 6.22(d)). However, in E15 and E85 the EIVC was slightly further retarded than in the throttled SI.

Shown in Figure 6.22(e), the COVimep in E0, E15 and E85 in the EIVC was below 2%. For throttled SI it was below 2% in E0 and E15. However, in E85 it was about 4.5%, this is as a result of the lambda value of 1.2 and the higher charge-cooling effects of ethanol, in addition there was occasional misfire observed.

As shown in Figure 6.22(f), E15 and E85 increased the exhaust temperature by about 4$^{o}$C and 17$^{o}$C respectively, over that in E0 fuel in the throttled SI mode due to spark retard. Similarly, in the EIVC, E15 and E85 blends the exhaust temperatures were 17$^{o}$C and 23$^{o}$C higher than in E0.

Figure 6.22(i) shows that the overall combustion period tended to increase in the throttled SI to EIVC in E0 and E85.

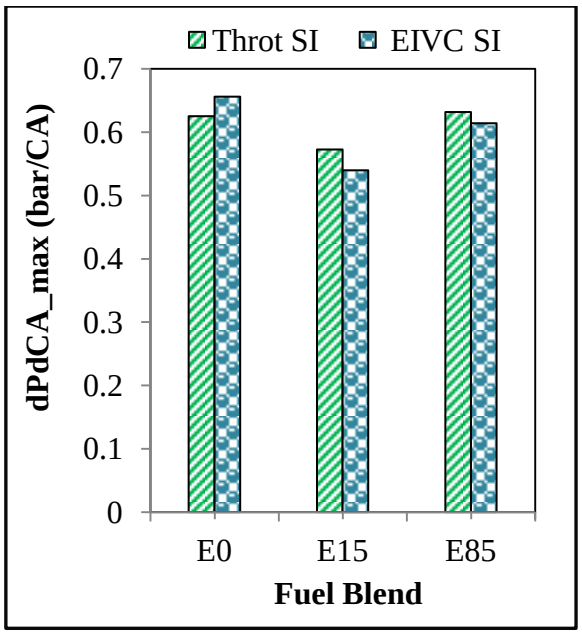


(a) Maximum Pressure Rise Rate

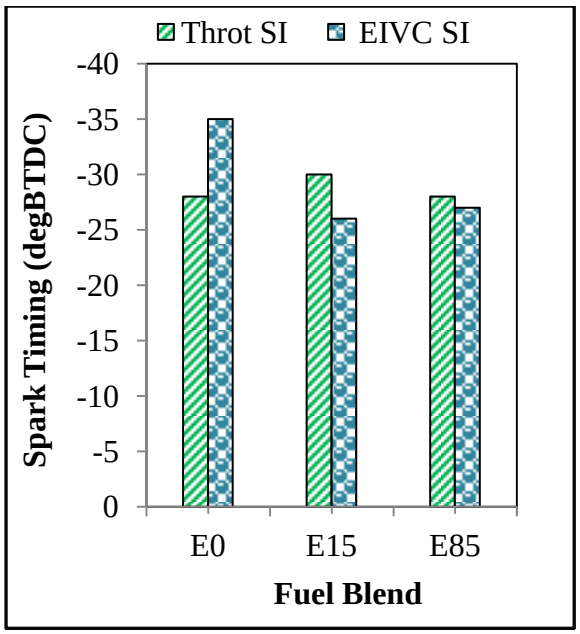


(b) MBT Spark Timing

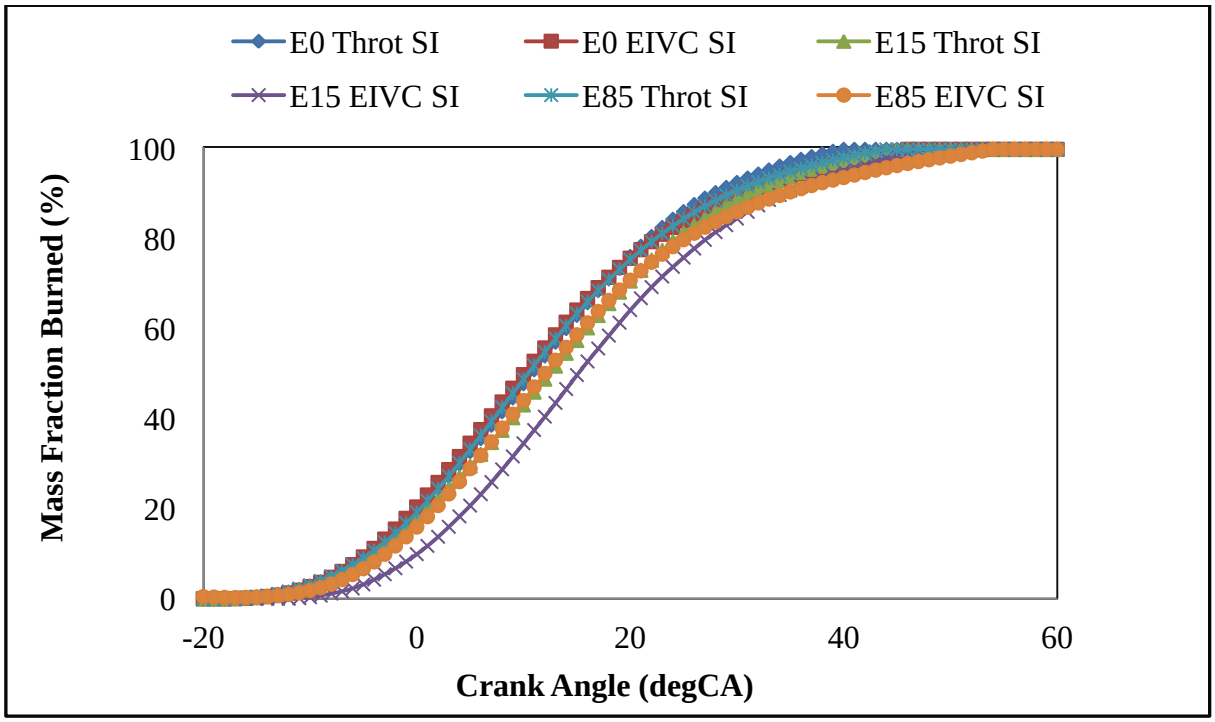


(c) Mass Fraction Burned

**Figure 6.22 Combustion Analysis**

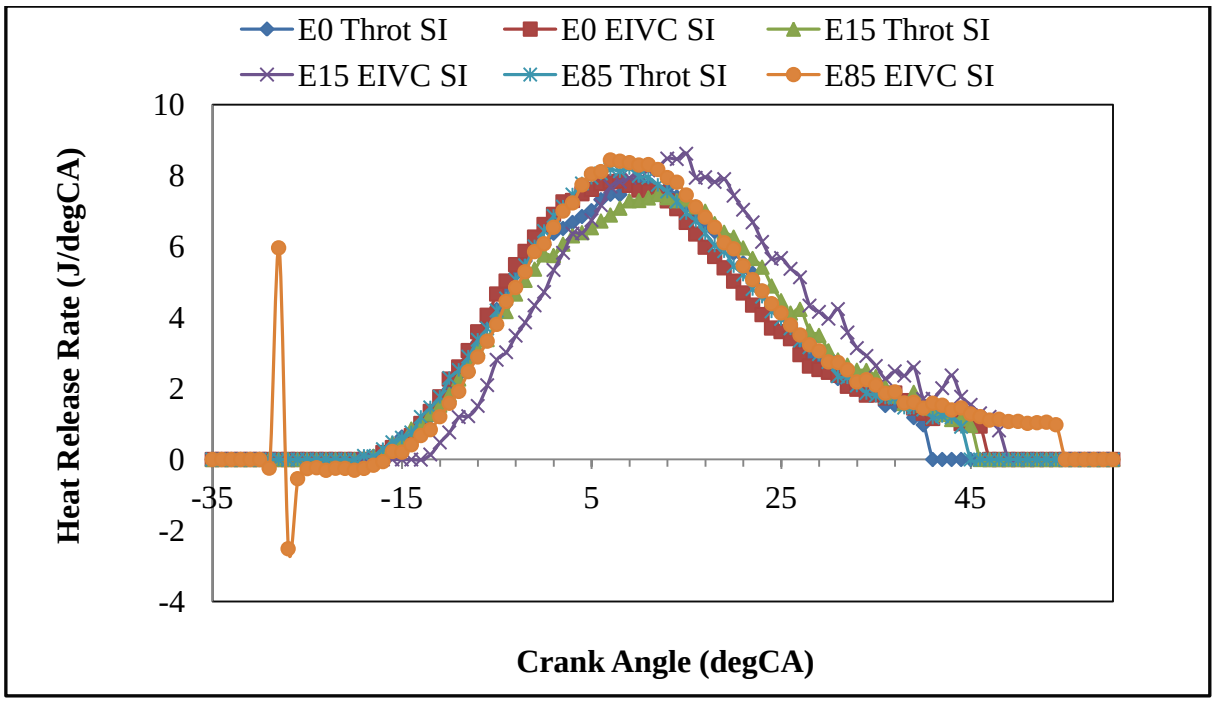


**(d) Heat Release Rate**

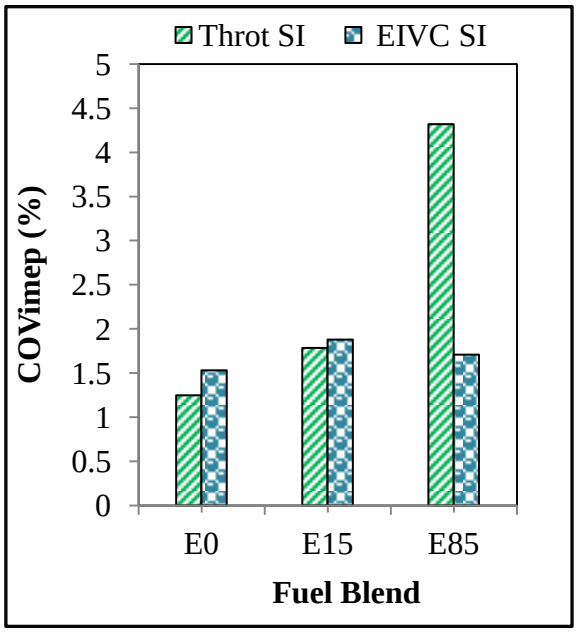


**(e ) COV of IMEP**

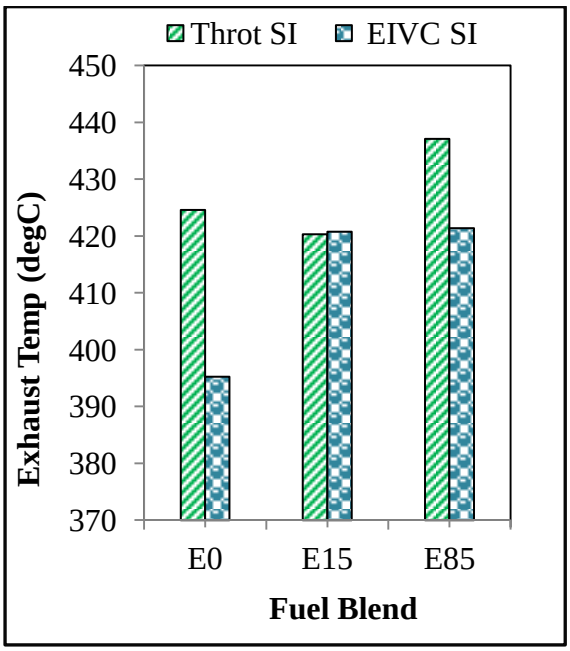


**(f) Exhaust temp**

**Figure 6.22 (ctd) Combustion Analysis**

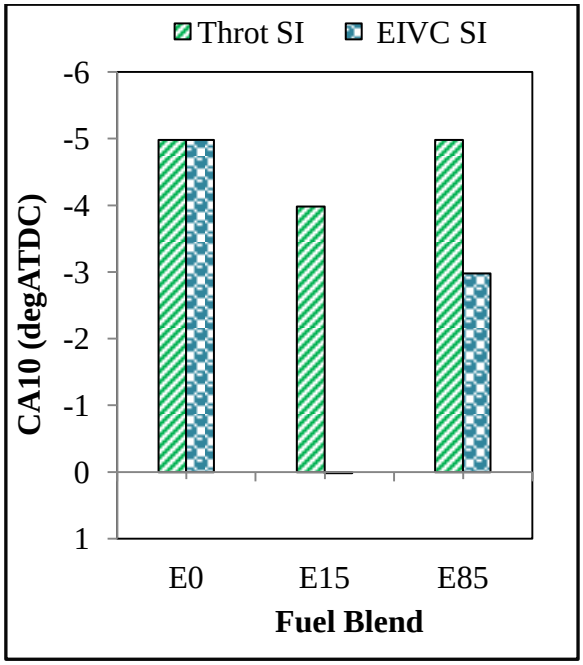


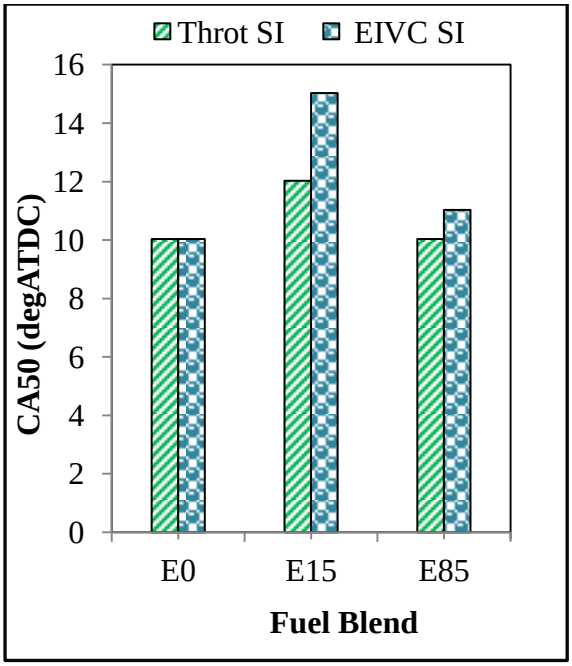


**(g) CA10** **(h) CA50**

**Figure 6.22 (ctd) Combustion Analysis**

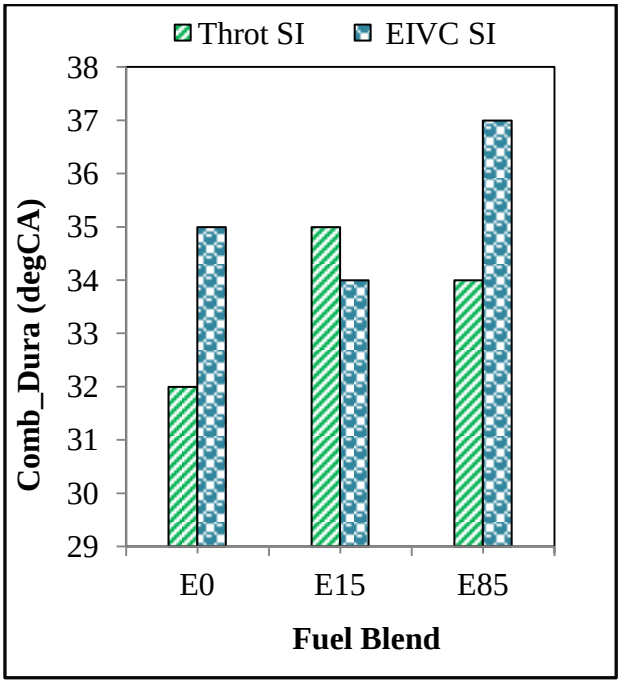


**(i) Combustion Duration**

**Figure 6.22 (ctd) Combustion Analysis**

### 6.8.2 Engine Performance and Efficiency Analysis

Figure 6.23(a) shows the combustion efficiency for the combustion-modes and fuel-blends. It can be seen that the combustion efficiency of the throttle SI combustion decreases slightly from 94.3% in E0 to 92.5% in E15 and 91.4 in E85. The lower combustion efficiency is likely to be related to the charge-cooling effects of the ethanol and poor mixture formation that may have resulted in pockets of rich mixture, as indicated by the increasing higher CO emissions (Figure 6.24(a)).

The EIVC SI combustion efficiency was lower than in the throttled SI operations in E0. This could have been caused by the different mixture formation process in EIVC as well as the lower turbulence. Although the reduced valve-lift could result in higher gas velocity past the valves and improve the fuel-atomisation process, the early closure of the valve would lead to cooler in-cylinder temperature the longer burn duration may not have been enough to complete the combustion process as indicated by the higher HC emissions (Figure 6.24(b)). In E15 and E85 the combustion efficiency in the EIVC was slightly higher than in the throttled SI.

Shown in Figure 6.23(b) is the thermodynamic efficiency of the engine. The throttle SI combustion shows a greater thermodynamic efficiency in E0. The EIVC SI shows greater thermodynamic efficiency in E15 and E85.

Figure 4(c) compares the indicated efficiency of the modes and fuel blends. The throttled SI indicated efficiency shows a slight decrease from 34.2% in E0 to 33% in E15 and to 32% in E85. In contrast, the EIVC SI resulted in an increase to 35.7% in E15 from 34.4% in E0 then decreased to a value of 34.9% in E85. In general, the indicated thermal efficiency in the EIVC SI operation of gasoline is about the same as in the throttled SI combustion operations. In addition, in the EIVC SI, 2.7% and 2.9% greater efficiency was obtained using E15 and E85 with corresponding fuel savings of 8% (Figure 6.24(d)), due to lower ISHC (Figure 6.24(b)) as well as lower pumping loss (Figure 6.23(d)).

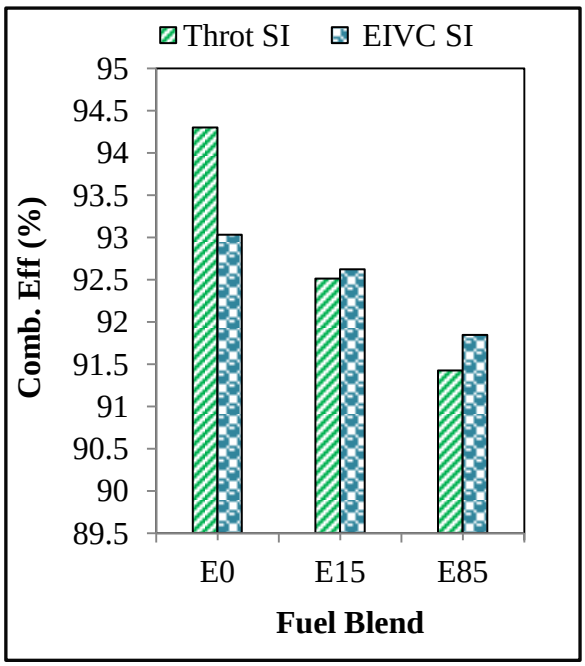


**(a) Combustion Efficiency**

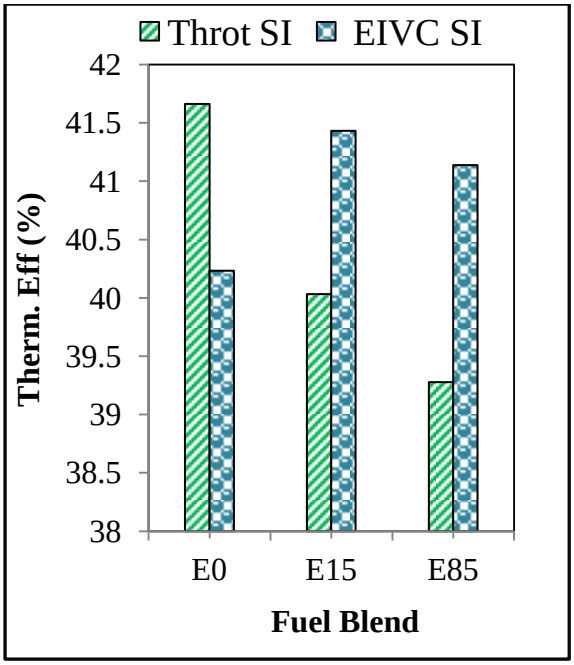


**(b) Thermal Efficiency**

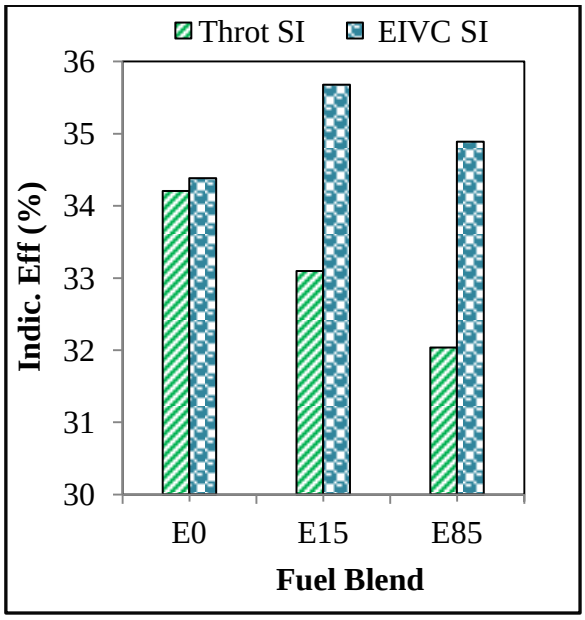


**(c) Indicated Efficiency**

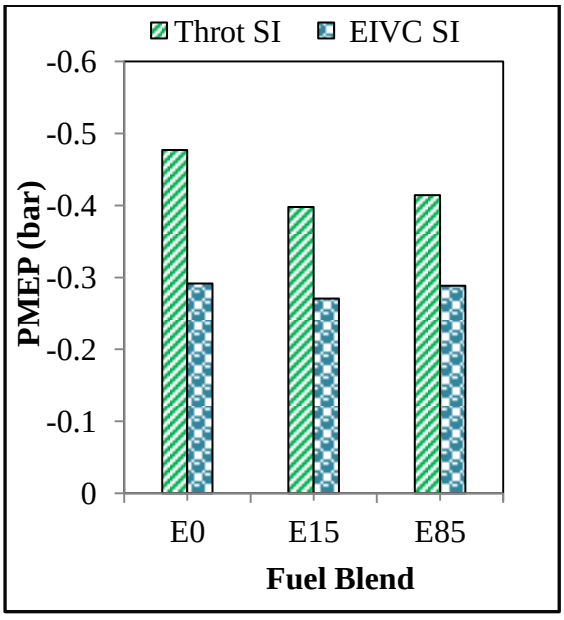


**(d) PMEP**

**Figure 6.23 Performance Analysis**

### 6.8.3 Gaseous Emissions and Fuel Consumption

Figure 6.24(a) shows the CO and UHC emissions for the throttled SI and EIVC combustion-modes and fuel-blends. In Figure 6.24(a), the ISCO was higher in the throttled SI in E15 and E85 than in the EIVC combustion. In the throttled SI combustion, CO increased from 5.4

g/KWh in E0 to 14.0 g/KWh in E85. In the EIVC SI, it increased from 5.4g/KWh in E0 to 12.3g/KWh in E85. As discussed previously, such an increase may be caused by poor ethanol fuel-mixture quality, the wall-wetting effect and low in-cylinder temperature as the percentage of ethanol fuel blend increased from E0 to E85.

As shown in Figure 6.24(b), the change in ISHC from gasoline and its mixtures with ethanol was much less than the ISCO in the throttled SI mode. The EIVC combustion exhibited a similar trend in ISHC with added ethanol content.

It can be seen from Figure 6.24(c) that the EIVC mode produced the lowest NOx emissions in the E15 and E0 blends.

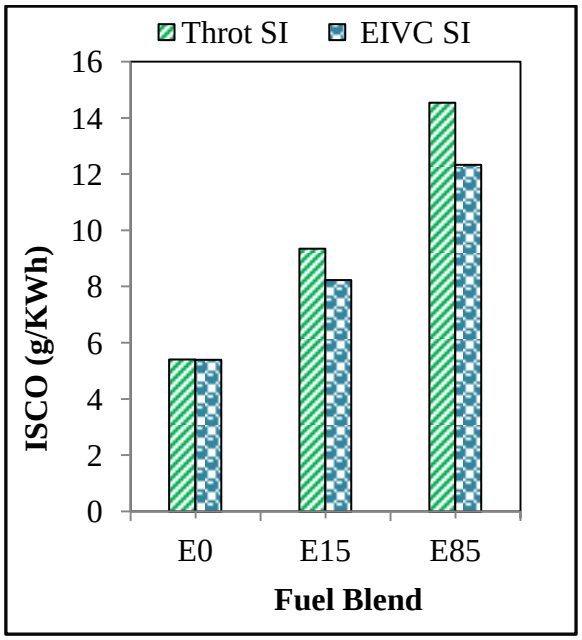


**(a) ISCO**

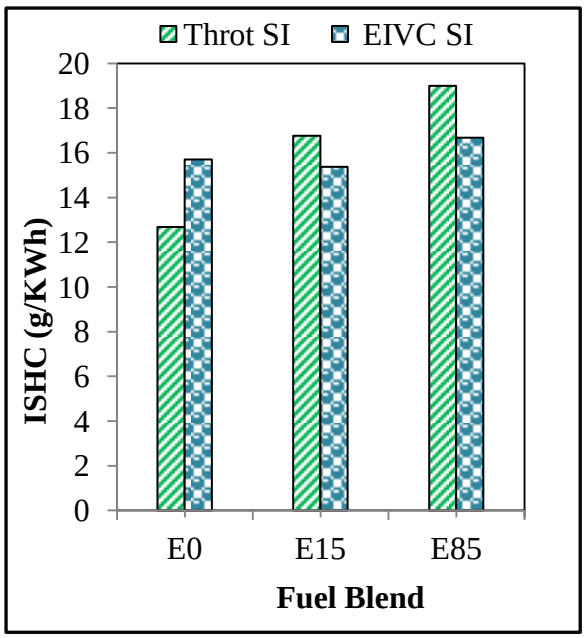


**(b) ISHC**

**Figure 6.24 Gaseous Emissions and Fuel Consumption**

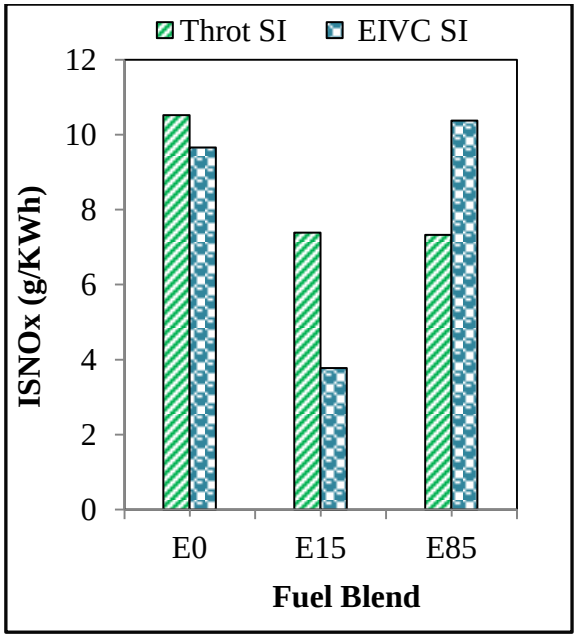


**(c) ISNOx**

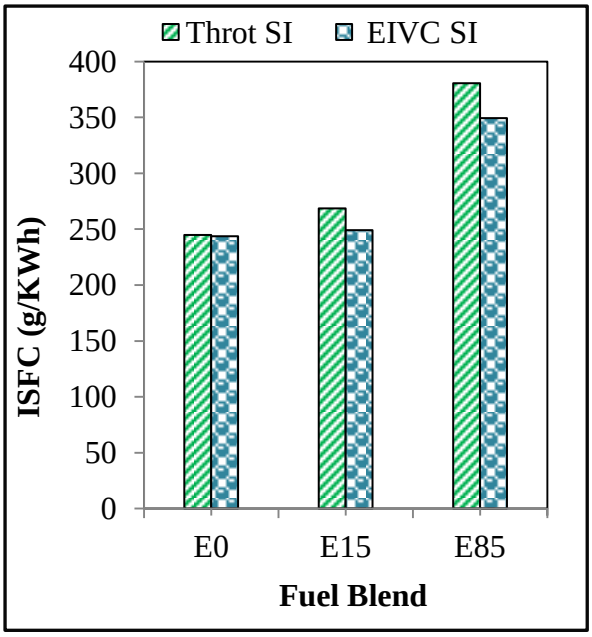


**(d) ISFC**

**Figure 6.24 (ctd) Gaseous Emissions and Fuel Consumption**

**Particulate Emissions**

Figure 6.25(a) shows that the total number of particles varies between different operational modes and the effect of ethanol on particle numbers is also mode-dependent. In the case of throttled SI operations, the number of particles decreased rapidly when the ethanol content was increased from zero to 85%. As shown in Figure 6.25(b), the majority of particles were around 20nm in diameter. The presence of oxygen in E15 and E85 helped to reduce soot formation.

In the case of EIVC, Figure 6.25(a) shows that E85 resulted in a significant rise in the total particle number, which was dominated by particles of between 15-20nm in diameter, as shown in Figure 6.25(b).

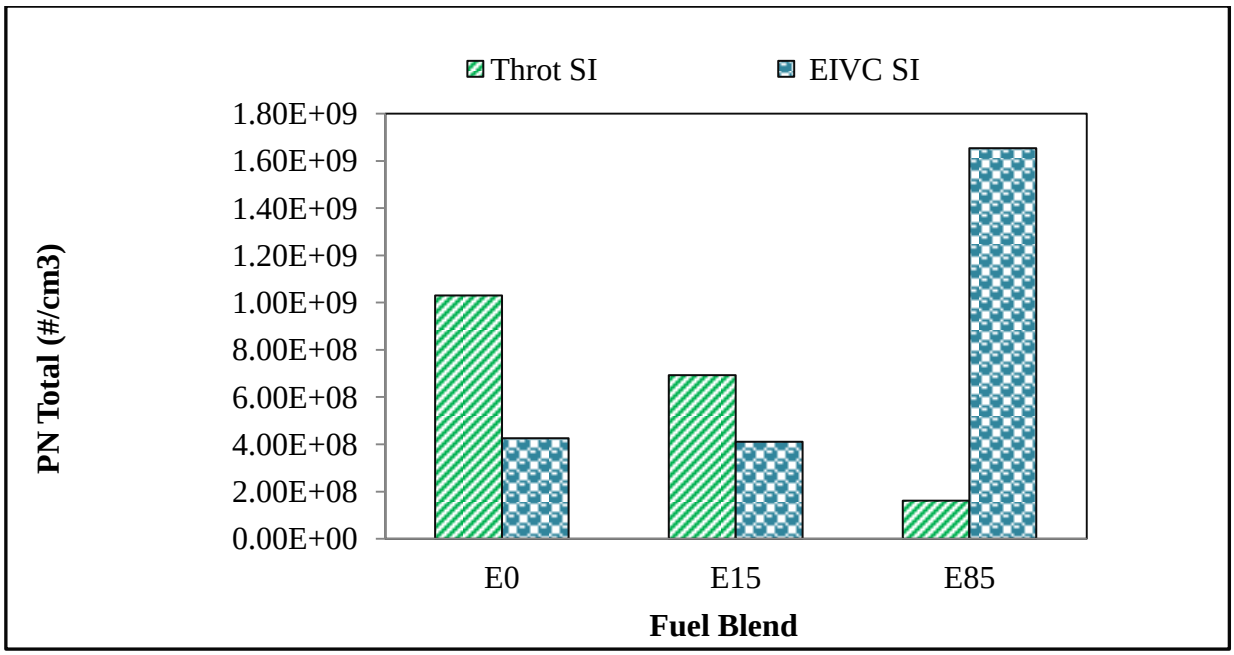


**(a) Total Particle Numbers**

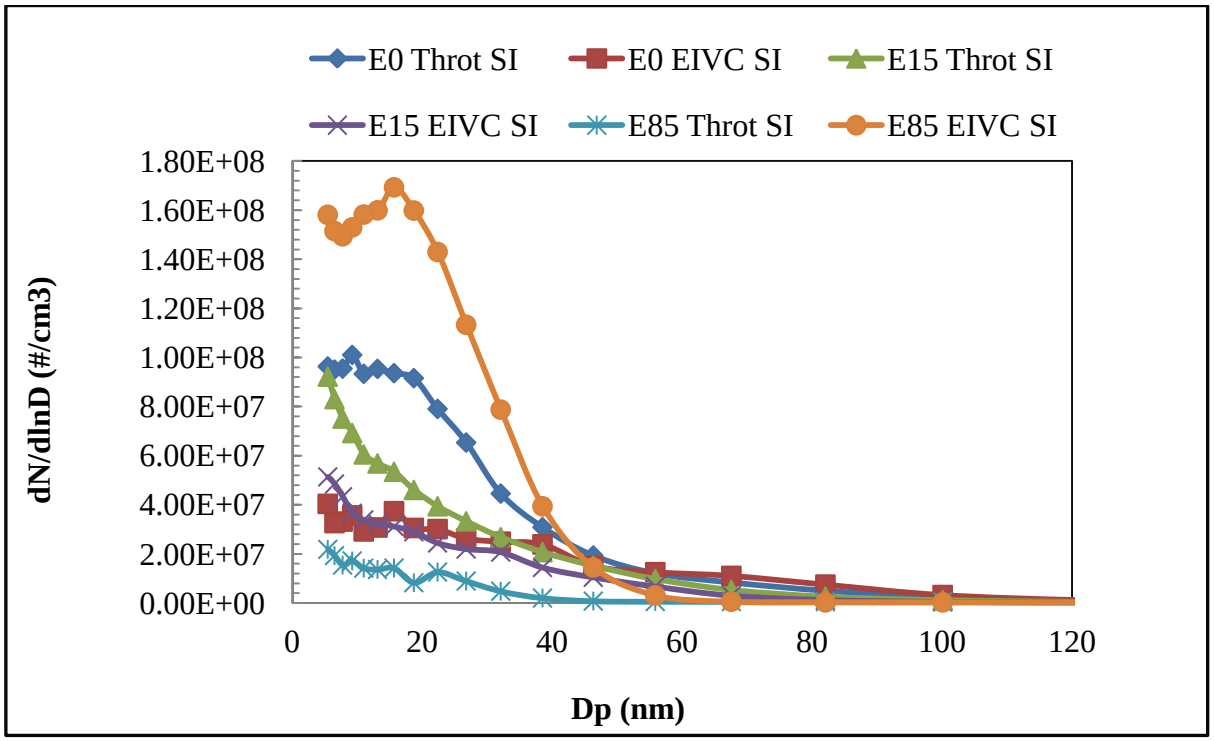


**(b) Particle Number and Size distributions**

**Figure 6.25 Total particle numbers and size distributions of different fuel blends at Lambda 1.2**

## 6.9 Summary

In the two operational modes, at 3.2bar IMEP load condition. A 3.3% improvement in ISFC of EIVC over throttled SI was obtained due to reduced pumping work.
The engine out ISHC emissions for EIVC was on the average 25% higher compared to the throttled SI
The particle size distribution is characterised by a peak between 15nm to 20nm in diameter, indicating the presence of nucleation mode particles. The leaner mixture helps to reduce the total particle emissions for all combustion modes.
Less and smaller particles were detected from the EIVC and throttle SI combustion. Most particles were in the range of a few nanometers related to the unburned hydrocarbons.
The EIVC mode resulted in slower combustion than throttled SI mode due to lower turbulence.

E85 produced the highest ISFC because of the lower calorific value of ethanol than gasoline in all the operational mode study.

In the Throttled SI mode, the presence of ethanol led to significant reduction in the formation and emission of particlulates.

The effect of ethanol was the least evident. In the EIVC mode, E85 produced the largest number of particles as the fuel injection took place in a cooler charge after IVC.

The addition of ethanol caused significant increase in CO emissions from locally rich mixtures due to increased injection durations during the EIVC and Throttled SI modes.

The particle emissions from the DI gasoline engine were dominated by smaller particles characterised with a peak between 10nm to 30nm in diameter. In the Throttled SI mode, the presence of ethanol led to significant reduction in the formation and emission of particlulates.

The EIVC mode was characterised with the lowest number of particles amongst the two operational modes because of the higher in-cylinder charge temperature. The effect of ethanol was the least evident.

However, there is still window of improvement on all three combustion modes by optimising the injection strategy, combustion chamber design, as well as the valve timing and duration used.

# Chapter 7 Conclusions and Future Work

## 7.1 Summary of Engine Operations

The unique 2/4-stroke camless engine has enabled research to be carried out on various combustion modes and engine operations and their performance compared for the same engine configuration, a significant advantage over engine experiments on different engines which have been previously performed. The 2-stroke SI combustion was achieved by simultaneously opening the exhaust and intake valves around BDC at each engine revolution whilst the 2-stroke CAI was readily accomplished with reduced scavenging through earlier closure of the exhaust valves and shorter scavenging duration.

Different 4-stroke operation modes and combustion processes were accomplished through the capability offered by the camless engine, including both SI combustion and CAI combustion. The efficiency and emissions of throttled, EIVC and PVO operations were investigated and analysed. The tests were done by selecting the standard valve timing with throttled SI operation as the baseline. During the EIVC SI operation, the intake valve lift was reduced and the opening duration was shortened. The PVO SI operation was achieved by retarding the exhaust valves well into the intake period and advancing the intake valves into the exhaust stroke.

In the 4-stroke CAI combustion mode, the negative-valve overlap method was employed by closing the exhaust valves early during the exhaust stroke to retain some hot residual gases. The intake valve opening was delayed into the intake to create symmetry about the low pressure top dead centre. The characteristics of both 4 and 2-stroke CAI combustion processes and their effect on efficiency and emissions were compared with the SI combustion operations. The effect ethanol on different combustion processes and engine operation modes was studied.

## 7.2 Conclusions

Substantial results have been obtained and analysed of different engine operations in terms of engine performance, efficiencies and emissions. The main findings will be presented in the order of objectives stated previously in Chapter 1.

### 7.2.1 Effect of Modes of Operations on Efficiency and Emissions

In this section, general characteristics of different engine operation modes will be stated and presented. The range of load was varied from 2.2bar to 8.6 bar IMEP at 1500rpm.

#### 7.2.1.1 4-Stroke Throttled SI mode

This conventional operational mode was chosen as a basis for comparison with the alternative modes of operations. Early injection was used to produce a homogeneous mixture. Combustion was initiated by the use of spark discharge and followed by flame propagation in the premixed fuel and air mixture. The throttled SI operation was characterised by high pumping loss (-0.6 bar at 2.21bar IMEP) due to partly closed throttle at low load.

The combustion and thermal efficiency remained relatively constant at 94% and 39% for the loads considered. However, the indicated efficiency displayed an increase from 28.9% at low load to 36.9% at the highest load, the gas exchange efficiency increased from 78.4% to 99.7% at high loads. This was reflected in an improvement in the ISFC.

The gaseous emissions of ISCO and ISHC were observe to reduce slightly as the load increased.

The ISNOx emissions was observed to increase by about 100% as load increased from 2.2 bar to 8.6 bar.

The particulate emissions was observed to increase as the load increased, and were characterised by particles in the nucleation mode (diameter less than 20nm).

#### 7.2.1.2 4-Stroke Intake Valve Throttled SI Operation

During the intake valve throttled SI operation, load was controlled by the intake valve duration and lift and maintained constant at 3.5 bar IMEP. The combustion efficiency was found to be lower (90%) because of the longer combustion duration than the throttled SI operation. However, due to lower pumping loss, better indicated efficiency was obtained.

The ISCO and ISHC emissions were higher compared to the baseline. The ISNOx was lower than that in throttled SI. The particulate emissions displayed similar particle sizes and numbers to the throttled SI operation.

#### 7.2.1.3 4-Stroke PVO SI Operation

In the positive valve overlap SI operation, the combustion efficiency was lower than in throttled SI but similar to the intake valve throttled SI operation, because of longer combustion duration due to the presence of internal EGR. The PVO SI operation was characterised by the highest indicated efficiency compared to the two previous modes, due to the lowest pumping loss. On the average the recorded indicated efficiency was 42%, which is about 8% to 10% greater than in the previous cases at 3.5 bar IMEP.

The ISCO and ISHC emissions were lower than the intake valve throttled SI but higher than in the baseline SI.

The measured NOx emissions are lowest compared to the two previous modes as a result of increased residual or dilution that reduces the maximum combustion temperature.

The particulate emissions were lower than those from the intake valve throttled SI, but higher than that in baseline throttled SI. The measured particulate number was observed to reduce in size, shifted to smaller size and increased particle number as the PVO duration increased.

#### 7.2.1.4 4-Stroke CAI Operation

The 4-stroke CAI combustion was achieved in the load range of 4.9 to 7.6bar IMEP whilst the residual gas fraction used varied from 19% at maximum load to 49% at minimum load. It was characterised by highest pressure rise rate and fastest combustion rate, compared to all the considered operation modes.

The combustion efficiency was on the average about 94% similar to baseline SI and higher than in PVO SI and intake valve throttled. The indicated efficiency was higher than in the throttled SI. But unlike the throttled SI operation, the indicated efficiency in CAI combustion was observed to decrease with increasing loads.

The most significant advantage of the CAI combustion was the ultra-low NOx emissions. Over 95% reductions from the baseline SI operation was obtained. It was also observed that the ISCO and ISHC emissions were lower than that in the throttled SI operation.

However, more and big particles were produced than the other SI modes due to the difference in the fuel injection timing. The fuel injection into the hot residual gas during the negative valve overlap period was considered to be the cause of increased particulate emissions.

#### 7.2.1.5 2-Stroke Throttle SI Operation

The 2-stroke SI operation was characterised with the lowest combustion efficiency. The ISCO and ISHC emissions were very high increasing up to 189g/KWh and 34g/KWh at the part-load conditions investigated because of inhomogeneous mixture of later injection and incomplete combustion due to high residual gas concentration, which led to the very low ISNOx emission.

The particulate emissions were characterised with smaller particles (less than 10nm in diameter) and similar in trend to the 4-stroke throttled SI operation.

#### 7.2.1.6 2-Stroke CAI Mode

The 2-stroke lean-boost CAI combustion was characterised with the highest combustion efficiency, which varied from 91% at 1.5 bar IMEP_net to 96.8% at 7.4 bar IMEP_net.

The ISCO emission was the lowest recorded in all the modes and was found to decrease as load increased. The ISHC was low and similar to the value obtained in 4-stroke CAI.

The ISNOx was lowest observed in all combustion mode. It was 0.05g/KWh at minimum load and 2.3g/KWh at maximum load of 7.4 bar IMEP_net.

The particulate emissions recorded were lower than the other modes considered and dependent upon the relative air/fuel ratio and injection timing.

### 7.2.2. Effect of Ethanol on Efficiency, Combustion and Emissions

The ethanol blends of E15 and E85 were used to examine the effect of ethanol on engine performance, combustion and emissions. The high octane rating makes it a better candidate substitute to gasoline in motor vehicles. In addition the oxygenate property of ethanol is well known to reduce particulate emissions.

#### 7.2.2.1 Effect of E15

During CAI, PVO, intake valve throttled and throttled SI operations, it was observed that the use of ethanol E15 resulted in slight increase in gas exchange efficiency in all the unthrottled operations, but decrease in combustion efficiency in all the modes were observed, except in PVO where slight increase was observed.

The use of E15 resulted in lower emissions of HC and NOx. The reduction in NOx was due to lower combustion temperature of E15. Though higher ISCO emissions was observed.

In addition E15 resulted in particle mass emissions reduction in all the modes, but greater quantities in smaller particles were observed.

#### 7.2.2.2 Effects of E85

The combustion efficiency was further reduced as ethanol blend was increased to 85%, resulting in highest fuel consumption and CO emission. Except that the PVO operation resulted in reduced ISCO emission.

The particulate emissions in using E85 was observed to reduce in size but shifted to greater number.

In all the modes study it was observed that the best fuel economy in using E15 and E85 are in unthrottled engine operational modes in CAI, PVO and intake valve throttled.

### 7.2.3 Effect of the Relative Air Fuel Ratio

In order to evaluate the effect of the relative air/fuel ration (lambda) on efficiency and emissions of each operational mode, a typical part load condition of 3.2 bar IMEP_net and 1500rpm was chosen.

In all SI modes, the combustion duration became longer and combustion efficiency increased as lambda was increased from 1.0 to 1.2, except the PVO operation which exhibited lower combustion efficiency at lambda 1.2. Similarly, the indicated efficiency was observed to increase slightly as lambda was increased to 1.2 other than PVO.

The effect of lambda was most pronounced in the 4-stroke CAI combustion. Increasing lambda from 1.0 to 1.2 brought down the pressure rise rate from about 5bar/CA to 2bar/CA (fig 5.2(a)), equivalent to 50% reduction.

The ISCO was observed to decrease significantly in the SI modes (50% in EVC, 40% in PVO, 30% in throttled SI). As lambda was increased further to 1.2, the ISCO increased in the throttled and EVC operations, whereas it continued to decrease in PVO. In contrast, the ISCO emission in CAI continuously increased as lambda was increased from 1.0 to 1.2.

The ISHC emissions was highest in PVO, but as lambda was increase from stoichiometric to leaner mixture, the ISHC emissions in PVO reduced to a value lower than that in throttled SI. The CAI combustion resulted in the lowest observed emissions of ISHC.

The lowest ISNOx was observed in CAI combustion, it was below 1g/KWh in using lambda 1.0-1.2.

The particulate emissions in all the modes shifted the peak of particle sizes to very small diameters as lambda increased.

### 7.3 Recommendation for Future Work

Based on the studies performed, further works can be carried out to obtain better understandings and identify operational strategies for the use of alternative fuels and reduced emissions:

**1**. Further study on E10 to E100 to establish what percentage of ethanol is economical when an engine is operated in CAI combustion, EIVC and PVO modes. The PVO and EIVC can be easily implemented on production engines with slight modifications. This will enable better improved fuel economy, reduced particulate emissions, and reduced global warming effects in vehicles running on E15 and E85.

**2**. Since the PVO operation has shown its potential in reducing particulate and possibly other gaseous emissions, the use of E85 during the PVO operations should be studied.

**3**. Optimising the valve timing and valve lift in the CAI, PVO and EIVC operations are another area of research that needs to be investigated.

Finally, the current fuel injector location and piston top are not optimised as shown by the relatively low combustion efficiency results. It is necessary that better fuel injector and an optimised piston top design should be the subject of further research.

## References


1. Chan, C, C., An Overview of Electric Vehicle Technology, Proceedings of the IEEE, Vol 81, NO. 9, 1993.

2. Hongbin Wang., et al., Comparative studies of Drivetrain Systems for electric vehicles, SAE Technical Paper 2013-01-2467, 2013.

3. Heywood, J, B., Internal Combustion Engine Fundamentals. McGraw-Hill, Inc., New York, NY, 1988.

4. Zhao, H., HCCI and CAI engines for the automotive industry. Woodhead Publishing Ltd., Cambridge UK, 2007.

5. Car Emissions and Euro 5, http://www.euro.who.int/mediacentre/PR/2004/20040617.

6. Uk Greenhouse Gas Statistics and Inventory Team, Science and Innovation group, DECC. 5th July 2013.

7. Zhao H., Advanced direct injection combustion engine technologies and development, Volume 1: gasoline and gas engines, Woodhead Publishing, cambridge, 2010

8. Richard van Basshuysen., Gasoline Engine with Direct Injection, MercedesDruck Publishing, Berlin, 2009.

9. Claus, B., and Dietmar, S., "VarioCam Plus – A Highlight of te Porsche 911 Turbo Engine," SAE Technical paper 2001-01-0245, 2001.

10. Sellnau, M., and Rask, E., "Two-Step Variable Valve Actuation for Fuel Economy, Emissions, and performances," SAE Technical paper 2003-01-0029, 2003.

11. Flierl, R., and Kluting, M., "The Third Generation of Valvetrains – New Fully Variable Valvetrains for Throttle-Free Lod Control," SAE Technical Paper 2000-01-1227, 2000

12. Theobald, M A., Lequesne, B., and Henry, R., "Control of Engine Load via Electromagnetic Valve Actuators," SAE Technical Paper 94081, 1994.

13. Wu, H., Chen, J., Li, M., Durret. R. et al., "Iterative Learning Control for a Fully Flexible Valve actuation in a test cell," SAE Int. J. Engines 6(1):2012, doi:10.4271/2012-01-0162, 2012.

14. Postrioti, L., Battistoni, M., Foschini, L., and Flora, R., "Application of a Fully Flexible electro-Hydraulic Camless system to a Research SI Engine," SAE International 2009-01-0075, 2009.

15. Schetcner, M. M., and Levin, B. M., "Camless Engine," SAE Technical paper 960591, 1996.

16. Jeff Allen., and Don Law., "Production Electro-Hydraulic Variable valve-train for a New Generation of I.C. Engines," SAE Technical paper 2002-01-1109, 2002.

17. Turner, C. W., Rabbit, G.R., Balton, C. S., “Design and Control of a Two-Stage Electro-hydraulic valve Actuation,” SAE Technical paper 2004-01-1265, 2004.

18. Kreuter, P., Heuser, P., and Joachim, R-M., “The Meta VVH System – A continuously Variable valve timing system,” SAE Technical Paper 980765, 1998.

19. Takemura, S., Aoyama, S., Sugiyama, T., et al., “A Study of a Continuous Variable valve Event and Lift (VEL) System,” SAE Technical paper 2001-01-0243, 2001.

20. Kreuter, P., Heuser, P., et al., “Variable Valve Actuation – Switchable and Continuously Variable Valve Lifts,” SAE International 2003-01-0026, 2003.

21. Osborne, R.J., stokes, J., Lake, T. H., et al., “Development of a Two-stroke/Four-Stroke Switching Gasoline Engine – The 2/4SIGHT concept,” SAE Technical Paper 2005-01-1137, 2005

22. Tai, C., Tsu-Chin, T., et al., “Using Camless Valvetrain for air Hybrid Optimisation,” SAE Technical Paper 2003-01-0038, 2003

23. Kreuter, P., Heuser, P., and Schebitz, M., “Strategies to Improve SI-Engine performance by means of variable Intake lift, Timing and Duration”. SAE Technical paper 920449, 1992.

24. Vogel, O., Roussopoulos, K., Guzella, L. and Czekaj, J. "Variable Valve Timing Implemented with a Secondary valve on a four cylinder SI engine," SAE Technical Paper 970335, 1997.

25. Kreuter, P., Heuser, P., and Reinicke-Murmann, J., "The Meta VVH System - A Continuously Variable Valve Timing System," SAE Technical Paper 980765, 1998, doi:10.4271/980765.

26. Soderberg, F., and Johansson, B., “Fluid Flow, Combustion and Efficiency with Early or Late Inlet Valve Closing”. SAE paper 972937, 1997.

27. Urata, Y., Umiyama, H., Shimizu, K., Fujiyoshi, Y., Sono Hiroshi., and Fukuo, K “A Study of Vehicle Equipped with Non-Throttling S.I. Engine with Early Intake Valve Closing Mechanism” SAE Paper 930820, 1993.

28. Patel, R., Ladommatos, N., et al., “Comparison between Unthrottled, Single and Two-valve induction Strategies Utilising Direct gasoline Injection: Emissions, Heat-release and Fuel Consumption Analysis,” SAE International 2008-01-1626,2008.

29. Miklanek, L., Vitek, O., Gotfryd, O., and Klir, V., “Study of Unconventional Cycles (Atkinson and Miller) with Mixture Heatings as a Means for the Fuel Economy Improvement of a Throttled SI Engine at Part Load,” SAE Int. J. Engines 5(4), doi:10.4271/2012-01-1678

30. Hong H., Patil-Parvate, G. B., and Gordon, B., “Review and analysis of variable valve Timing Strategies-Eight ways to Approach, “ Proc. IMechE, Part D; J. Automobile Engineering 2004 **218**(1179), 1179-1200, doi:10.1177/095440700421801013

31. Xin, H., Russel, P.D., and Zongxuan, S., "Late Intake valve Closing as an Emissions control Strategy at Tier 2 Bin 5 Engine-Out NOx Level," SAE Technical Paper 2008-01-0637, 2008, doi:10.4271/2008-01-0637

32. Wang, C., Daniel, R., and Ma, X., "Comparison of gasoline (ULG), 2,5-Dimethylfuran 9DMF) and Bio-Ethanol in a DISI Miller Cycle with Late Inlet Valve Closing Time," SAE Technical Paper 2012-01-1147, 2012, doi: 10.4271/2012-01-1147

33. Taylor, J., Fraser, N., Dinglestadt, R., and Hoffmann, H., "Benefits of Late Intake valve Timing Strategies Afforded Through the Use of Intake Cam in Cam Applied to a Gasoline Turbocharged Downsized Engine," ," SAE Technical Paper 2011-01-0360, 2011, doi: 10.4271/2011-01-0360

34. Asmus, T. W., "Valve Events and Engine Operations," SAE Paper, No. 820749, 1982.

35. Rabia, S. M., and Kora, N. S., "Knocking Phenomena in Gasoline with Late-Intake Valve Closing, "SAE Paper, No. 920381, 1992.

36. Onishi, S., et al., Active Thermo-atmosphere Combustion (ATAC) a new combustion process for internal combustion engines, SAE paper 790501, 1979.

37. Thring, R., Homogeneous-Charge Compression-Ignition (HCCI) Engines, SAE paper 892068, 1989.

38. Aoyama Taro ., Yoshiaki Hattori., and Junichi Mizuta., An Experimental Study on Premixed-Charge compression Ignition Gasoline Engine, SAE paper 960081, 1996.

39. Ishibashi Yoichi., and Masahiko Asai., Improving the Exhaust Emissions of Two-Stroke Engines by Applying the Activated Radical combustion., SAE paper 96072, 1996

40. Kontarakis George., Nick Collings., and tom Ma., Demonstration of HCCI Using a Single Cylinder Four-Stroke SI Engine with Modified Valve Timing., SAE paper 2000-01-2870, 2000.

41. Allen Jeff., and Law Don., Variable Valve Actuated Controlled Auto-Ignition: Speed Load Maps and Strategic Regimes of Operation., Sae paper 2002-01-0422

42. Koopmans Lucien., and Ingemar Denbratt., A Four Stroke Camless Engine, Operated in HCCI Mode with commercial gasoline., SAE paper 2001-01-3610, 2001.

43. Zhao, H., et al., Control strategies for steady and transient operation of a 4-stroke gasoline engine with CAI combustion using a 4-variable valve actuating system (4VVAS), SAE paper 2006-01-1083, 2006.

44. Wolters, p., et al., Controlled auto ignition combustion process with electromechanical valve train, SAE paper 2003-01-0032, 2003.

45. Zhao, H., et al., Investigation of CAI combustion with positive valve overlap and enlargement of CAI operating range, SAE paper 2009-01-1104, 2009

46. Scott B. Fiveland., et al., Experimental and Simulated Results Detailing the Sensitivity of Natural gas HCCI Engines to Fuel Composition, SAE Technical Paper 2001-01-3609, 2001.

47. Noraz K. Noran et al., Comparison of HCCI and SI Combustion of Direct Injected CNG at Low Load Condition, SAE Technical Paper 2011-01-1180, 2011.

48. Anil Singh Bika., et al., Hydrogen Fuelled Homogeneous Charge Compression Ignition Engine, SAE Technical Paper 2011-01-0672, 2011

49. Rosati, M. F, and Aleiferis, P.G., Hydrogen SI and HCCI Combustion in a Direct-Injection Optical Engine, SAE Technical paper 2009-01-1921, 2009.

50. Zhao, H., et al., Performance and analysis of a 4-stroke multi-cylinder gasoline with CAI combustion, SAE paper 2002-01-0420, 2002

51. Yan Zhang et al., 2-Stroke CAI combustion operation in a GDI Engine with Poppet Valves, SAE Technical Paper 2012-01-1118, 2012.

52. Cao, L., Zhao, H., and Jiang, X., "Investigation into Controlled Auto-Ignition Combustion in a GDI Engine with Single and Split Fuel Injections," SAE Technical Paper 2007-01-0211, 2007, doi:10.4271/2007-01-021.

53. Amann et al., HCCI Fuels Evaluations-Gasoline Boiling Range Fuels, SAE Technical paper 2005-01-3727, 2005.

54. Alok Kumar., Khatri D S and Babu MKG, "Experimental Investigations on the Performance, Combustion and Emission characteristics of alcohol blended gasoline in a spark Ignition Engine", SAE Technical Paper 2008-28-0068, 2008.

55. Ulrik Larsen et al, Ethanol as a Fuel for Road Transportation, Main Report. Technical University of Denmark, May 2009.

56. Hakan Bayraktar., Theoretical investigation of flame propagation process in an SI engine running on gasoline-ethanol blend. Renew Energy 32 (2007) 758-771, 2007.

57. Marriot D. Craig et al., Development of a Naturally Aspirated Spark Ignition Direct-Injection Flex-Fuel Engine, SAE Technical Paper 2008-01-0319, 2008.

58. Koichi Nakata et al., The Effect of Ethanol Fuel on a Spark Ignition Engine, SAE Technical paper 2006-01-3380, 2006.

59. Celik M. Bahattin., Experimental determination of suitable ethanol-gasoline blend rate at high compression ratio for gasoline engine, Applied Thermal Engineering 28 (2008) 396-404.

60. Rodrigo C. Costa and Jose R. Sodre, Compression ratio effects on an ethanol/gasoline fuelled engine performance, Applied Thermal Engineering 31 (2011) 278-283

61. James E. Anderson et al., Octane Numbers of Ethanol-Gasoline Blends: Measurements and Novel Estimation Method from Molar Composition, SAE Technical paper 2012-01-1274, 2012.

62. Kenneth Kar et al., Measurement of Vapour Pressures and Enthalpies of Vaporization of Gasoline and Ethanol Blends and Their Effects on Mixture Preparation in an SI Engine, SAE Technical Paper 2008-01-0317, 2008.

63. Emmanuel Kasseris and John Heywood., Charge Cooling Effects on Knock Limits in SI DI Engines Using Gasoline/Ethanol Blends: Part 2-Effective Octane Numbers, SAE Technical paper 2012-01-1275, 2012.

64. Emmanuel Kasseris and John Heywood., Charge Cooling Effects on Knock Limits in SI DI Engines Using Gasoline/Ethanol Blends: Part 1-Quantifying Charge Cooling, SAE Technical paper 2012-01-1284, 2012.

65. Tien Mun Foong et al., The Effects of Charge Cooling on the RON of Ethanol/Gasoline Blends, SAE Technical Papers 2013-01-0886, 2013.

66. Takashi Tsunooka et al., High Concentration Ethanol Effect on SI Engine Cold Startability, SAE Technical Paper 2007-01-2038, 2007.

67. Yan Zhang et al., The Combustion and Emission Characteristics of Ethanol on Port Fuel Injection HCCI Engine, SAE Technical Paper 2006-01-0631, 2006

68. Rahbari A, The Effect of EGR on HCCI Engines Using Ethanol as Fuel, SAE Technical Paper 08SFL-0172, 2008

69. Yufeng Li et al., CAI Combustion with methanol and Ethanol in an Air-Assisted Direct Injection SI Engine, SAE Technical Paper 2008-01-1873, 2008.

70. Tongroon M., and Zhao H., "Combustion Characteristics of CAI Combustion with Alcohol Fuels", SAE Paper 2010-01-0843, 2010.

71. Zhang Y., Zhao H., Ojapah M and Cairns A., CAI combustion of gasoline and its mixture with ethanol in a 2-stroke poppet valve DI gasoline engine, Fuel 109 (2013) 661-668

72. Kittleson D B. "Engines and Nanoparticles: A Review". J. Aerosol Sci. Vol. 29. No. 5/6., 1998

73. Eastwood P. "Particulate Emissions from Vehicles". 2008.

74. Kobayashi Y., et al Soot precvursor measurements in benzene and hexane diffusion flames, Combustion and flames 154 (2008) 346-355

75. DeCarlo P F., Slowik J G., Worsnop D R., Davidotis P. and Jimenez J L. "Particle Morphology and Density Characterisation by Combined Mobility and Aerodynamic Diameter Measurements. Part 1: Theory". Aerosol Sci. Technol.38: 2004

76. Maricq, M., Podsiadlik, D., Brehob, D., and Haghgooie, M., "Particulate Emissions from a Direct-Injection Spark-Ignition (DISI) Engine," SAE Technical Paper 1999-01-1530, 1999, doi:10.4271/1999-01-1530.

77. Graskow B R., Kittelson D B., Ahmadi M R and Morris J E, "Exhaust Particulate Emissions from a Direct Injection spark ignition Engine", SAE Technical Paper 1999-01-1145, 1999.

78. Yongha Kim., et al. Fuel Effect on Particle Emissions of a Direct Injection Engine, SAE Technical Paper 2013-01-1559.

79. Khalek I A., Bougher T and Jetter J J. " Particle Emissions from a 2009 Gasoline Direct Injection Engine Using Different Commercially Available Fuels". SAE Technical Paper 2010-01-2117, 2010.

80. Whelan I., Samuel S and Hassaneen A.E., The Effect of Fuel Temperature on Particulate Matter Formation in Gasolione Direct-Injection Engines, SAE Technical Paper 2010-01-1469, 2010.

81. Stephen sakai, Mitchell Hageman and david Rothamer., Effect of Equvalence Ratio on the Particulate Emissions from a Spark-Ignited , Direct –Injected gasoline Engine., SAE Technical Paper 2013-01-1560, 2013.

82. Michael Hedge, Philip Weber, Jess Gingrich, Terrence Alger and Imad Khalek., "Effect of EGR on Particle Emissions from a GDI Engine", SAE International 2011-01-0636, 2011.

83. Lei Zhou et al., Effect of Hot Exhaust Gas Recirculation on the Combustion Charactesistics and Particles Emissions of a Pilot-Ignited Natural Gas Engine, SAE internationa 2013-01-1341, 2013.

84. Aikawa, K., Sakurai, T., and Jetter, J., "Development of a Predictive Model for Gasoline Vehicle Particulate Matter Emissions," SAE Int. J. Fuels Lubr. 3(2):610-622, 2010, doi:10.4271/2010-01-2115.

85. Price, P., Stone, R., Collier, T., and Davies, M., "Particulate Matter and Hydrocarbon Emissions Measurements: Comparing First and Second Generation DISI with PFI in Single Cylinder Optical Engines," SAE Technical Paper 2006-01-1263, 2006, doi:10.4271/2006-01-1263.

86. Arsie, I., Di Iorio, S., and Vaccaro, S., "Experimental Characterization of Nanoparticles Emissions in a Port Fuel Injection Spark Ignition Engine," SAE Technical Paper 2011-24-0208, 2011, doi:10.4271/2011-24-0208, 2011.

87. Price, P., Stone, R., Misztal, J., Xu, H. et al., "Particulate Emissions from a Gasoline Homogeneous Charge Compression Ignition Engine," SAE Technical Paper 2007-01-0209, 2007, doi:10.4271/2007-01-0209, 2007

88. Di Iorio, S., Lazzaro, M., Sementa, P., Vaglieco, B. et al., "Particle Size Distributions from a DI High Performance SI Engine Fuelled with Gasoline-Ethanol Blended Fuels," SAE Technical Paper 2011-24-0211, 2011, doi:10.4271/2011-24-0211, 2011.

89. Price, P., Twiney, B., Stone, R., Kar, K. et al., "Particulate and Hydrocarbon Emissions from a Spray Guided Direct Injection Spark Ignition Engine with Oxygenate Fuel Blends," SAE Technical Paper 2007-01-0472, 2007, doi:10.4271/2007-01-0472.

90. Dimou, I., Kar, K., and Cheng, W., "Particulate Matter Emissions from a Direct Injection Spark Ignition Engine under Cold Fast Idle Conditions for Ethanol-Gasoline Blends," SAE Int. J. Engines 4(1):1738-1746, 2011, doi:10.4271/2011-01-1305.

91. Chen, L., Braisher, M., Crossley, A., Stone, R. et al., "The Influence of Ethanol Blends on Particulate Matter Emissions from Gasoline Direct Injection Engines," SAE Technical Paper 2010-01-0793, 2010, doi:10.4271/2010-01-0793.

92. Fatouraie, M., Wooldridge, M., and Wooldridge, S., "In-Cylinder Particulate Matter and Spray Imaging of Ethanol/Gasoline Blends in a Direct Injection Spark Ignition Engine," SAE Int. J. Fuels Lubr. 6(1):1-10, 2013, doi:10.4271/2013-01-0259, 2013.

93. Di Iorio, S., Lazzaro, M., Sementa, P., Vaglieco, B. et al., "Use of Renewable Oxygenated Fuels in Order to Reduce Particle Emissions from a GDI High Performance Engine," SAE Technical Paper 2011-01-0628, 2011, doi:10.4271/2011-01-0628, 2011.

94. Stokes, J., Hundleby, G.E., Lake, T.H and Christie, M. J., " Development Experience of a Poppet-Valved Two-Stroke Flagship Engine," SAE Technical paper 920778, 1992.

95. Winklmayr, W., Reischl, G.P., Lindner, A.O., and Berner, A., "A New Electromobility Spectrometer for the Measurement of Aerosol Size Distributions in the Size Range from 1 to 1000nm", J.Aerosol Sci, Vol 22. No 3, pp289, 1991.

96. Reischl, G.P., " measurement of Ambient Aerosols by the Differential Mobility Analyser method: Concepts and realization Criteria for the Size Range Between 2 and 500nm", Aerosol Science and Technology 14:5-24 (1991).

97. Pannich Intra and Nakom Tippayawong., " An Overview of Differential Mobility Analysers for Size Classification of nanoimeter-sized aerosol particles", Songklanakarin J.Sci.Technol, 30 (2), 243-256, Mar.-Apr.2008.

98. Anderson,V.F., Anderson, J>E., Wallington, T.J., Mueller,S.A and Nielsen, O.J., "Distillation Curves for Alcohol_Gasoline Blends, Energy Fuels 2010, 24,2683-2691.DO:10.1021/ef9014795

99. Farron, C., Matthias, N., Foster, D., Andrie, M. et al., "Particulate Characteristics for Varying Engine Operation in a Gasoline Spark Ignited, Direct Injection Engine," SAE Technical Paper 2011-01-1220, 2011, doi:10.4271/2011-01-1220.

100. Anderson,V.F., Anderson, J.E., Wallington, T.J., Mueller,S.A and Nielsen, O.J., "Vapour Pressures of Acohol-Gasoline Blends, Energy Fuels 2010, 24, 3647-3654.DO:10.1021/ef100254w.

101. Zhang, Y., Zhao, H., Ojapah, M., and Cairns, A., "Effects of Injection Timing on CAI Operation in a 2/4-Stroke Switchable GDI Engine," SAE Int. J. Engines 5(2):67-75, 2012, doi:10.4271/2011-01-1773.

102. Popuri, S. and Bata, R., "A Performance Study of Iso-Butanol-, Methanol-, and Ethanol-Gasoline Blends Using a Single Cylinder Engine," SAE Technical Paper 932953, 1993, doi:10.4271/932953.

## APPENDIX

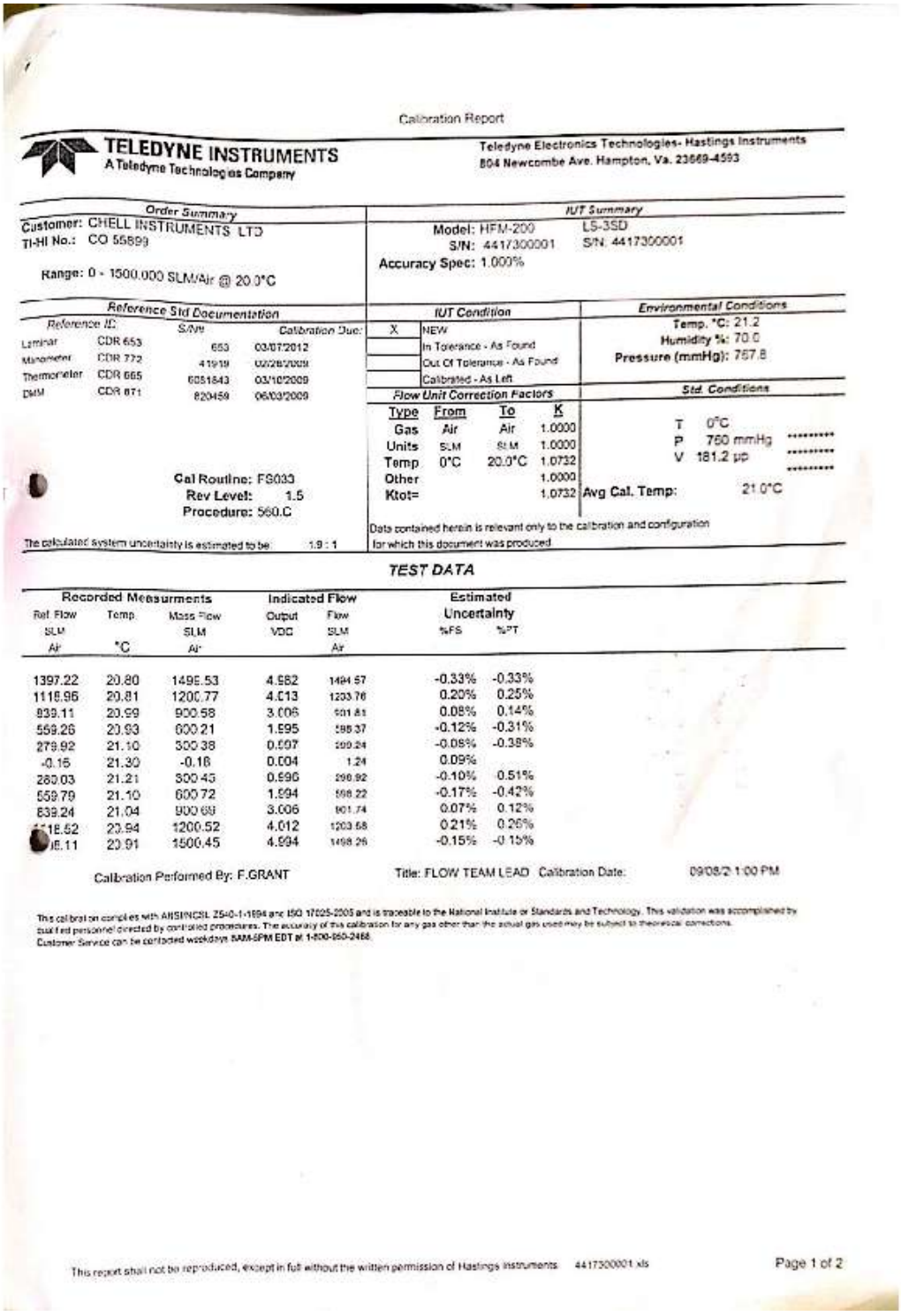

Calibration Report

**TELEDYNE INSTRUMENTS**
A Teledyne Technologies Company

Teledyne Electronics Technologies- Hastings Instruments
804 Newcombe Ave. Hampton, Va. 23669-4593

**Order Summary**

Customer: CHELL INSTRUMENTS LTD
TI-HI No.: CO 55899

Range: 0 - 1500.000 SLM/Air @ 20.0°C

**IUT Summary**

Model: HFM-200 LS-3SD
S/N: 4417300001 S/N: 4417300001
Accuracy Spec: 1.000%

**Reference Std Documentation**

| Reference ID | | S/N# | Calibration Due: |
|---|---|---|---|
| Laminar | CDR 653 | 653 | 03/07/2012 |
| Manometer | CDR 772 | 41919 | 02/26/2009 |
| Thermometer | CDR 665 | 6051843 | 03/10/2009 |
| DMM | CDR 671 | 820459 | 06/03/2009 |

Cal Routine: FS033
Rev Level: 1.5
Procedure: 560.C

The calculated system uncertainty is estimated to be 1.9 : 1

**IUT Condition**

| | |
|---|---|
| X | NEW |
| | In Tolerance - As Found |
| | Out Of Tolerance - As Found |
| | Calibrated - As Left |

**Flow Unit Correction Factors**

| Type | From | To | K |
|---|---|---|---|
| Gas | Air | Air | 1.0000 |
| Units | SLM | SLM | 1.0000 |
| Temp | 0°C | 20.0°C | 1.0732 |
| Other | | | 1.0000 |
| Ktot= | | | 1.0732 |

**Environmental Conditions**

Temp. °C: 21.2
Humidity %: 70.0
Pressure (mmHg): 767.8

**Std. Conditions**

T 0°C
P 760 mmHg *********
V 181.2 µp *********

Avg Cal. Temp: 21.0°C

Data contained herein is relevant only to the calibration and configuration for which this document was produced.

**TEST DATA**

| Recorded Measurments | | | Indicated Flow | | Estimated Uncertainty | |
|---|---|---|---|---|---|---|
| Ref. Flow SLM Air | Temp °C | Mass Flow SLM Air | Output VDC | Flow SLM Air | %FS | %PT |
| 1397.22 | 20.80 | 1495.53 | 4.982 | 1494.57 | -0.33% | -0.33% |
| 1118.96 | 20.81 | 1200.77 | 4.013 | 1203.76 | 0.20% | 0.25% |
| 839.11 | 20.99 | 900.58 | 3.006 | 901.81 | 0.08% | 0.14% |
| 559.26 | 20.93 | 600.21 | 1.995 | 598.37 | -0.12% | -0.31% |
| 279.92 | 21.10 | 300.38 | 0.997 | 299.24 | -0.08% | -0.38% |
| -0.16 | 21.30 | -0.16 | 0.004 | 1.24 | 0.09% | |
| 280.03 | 21.21 | 300.45 | 0.996 | 298.92 | -0.10% | 0.51% |
| 559.79 | 21.10 | 600.72 | 1.994 | 598.22 | -0.17% | -0.42% |
| 839.24 | 21.04 | 900.69 | 3.006 | 901.74 | 0.07% | 0.12% |
| 1118.52 | 20.94 | 1200.52 | 4.012 | 1203.58 | 0.21% | 0.26% |
| 1398.11 | 20.91 | 1500.45 | 4.994 | 1498.26 | -0.15% | -0.15% |

Calibration Performed By: F.GRANT Title: FLOW TEAM LEAD Calibration Date: 09/08/2 1:00 PM

This calibration complies with ANSI/NCSL Z540-1-1994 and ISO 17025-2005 and is traceable to the National Institute of Standards and Technology. This validation was accomplished by qualified personnel directed by controlled procedures. The accuracy of this calibration for any gas other than the actual gas used may be subject to theoretical corrections.
Customer Service can be contacted weekdays 8AM-5PM EDT at 1-800-950-2468.

 4417300001.xls 

**Figure A1 Air Flow Meter Calibration Result (Teledyne)**

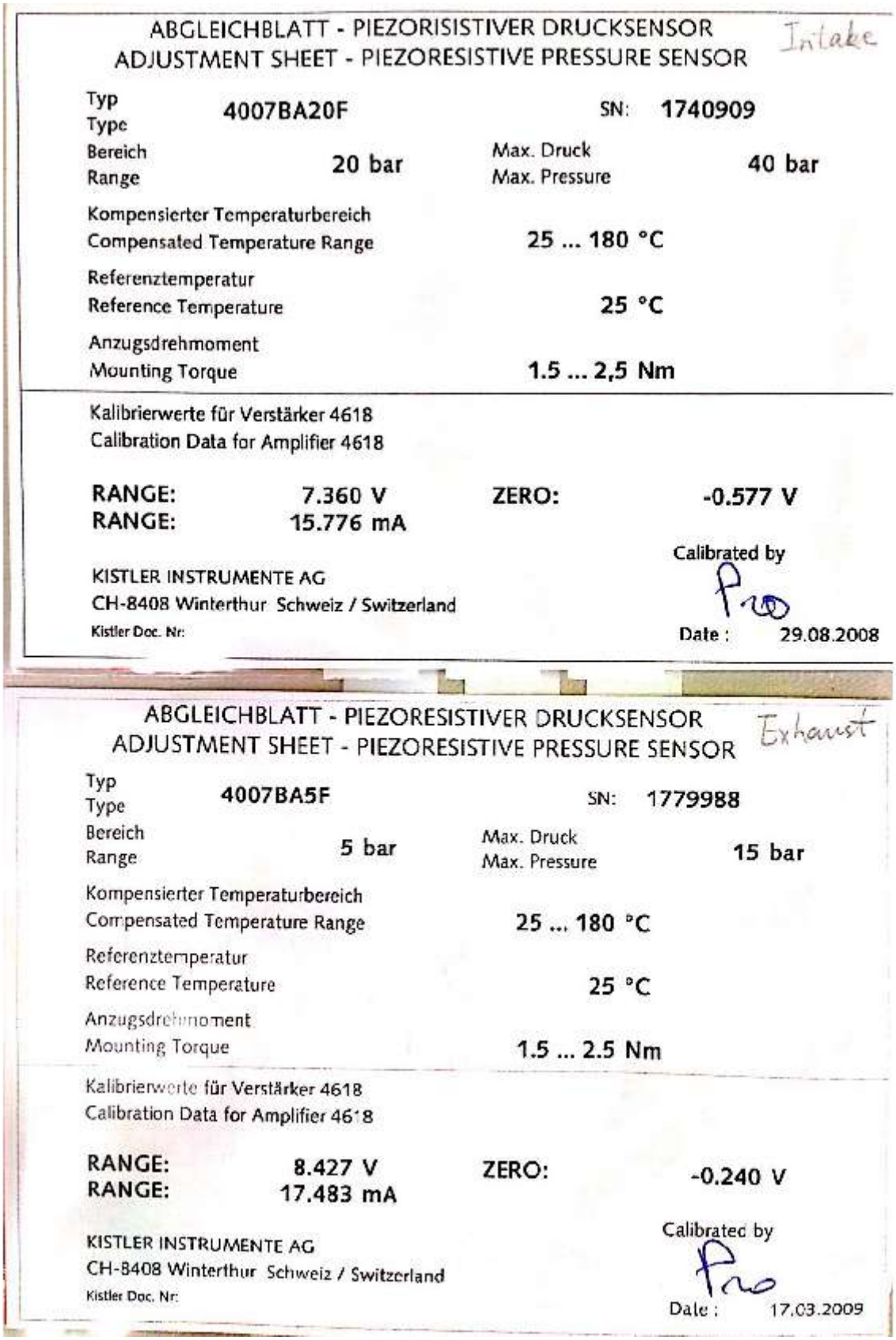

ABGLEICHBLATT - PIEZORISISTIVER DRUCKSENSOR
ADJUSTMENT SHEET - PIEZORESISTIVE PRESSURE SENSOR

Intake

Typ / Type: 4007BA20F — SN: 1740909

Bereich / Range: 20 bar — Max. Druck / Max. Pressure: 40 bar

Kompensierter Temperaturbereich / Compensated Temperature Range: 25 ... 180 °C

Referenztemperatur / Reference Temperature: 25 °C

Anzugsdrehmoment / Mounting Torque: 1.5 ... 2,5 Nm

Kalibrierwerte für Verstärker 4618
Calibration Data for Amplifier 4618

RANGE: 7.360 V — ZERO: -0.577 V
RANGE: 15.776 mA

KISTLER INSTRUMENTE AG
CH-8408 Winterthur Schweiz / Switzerland
Kistler Doc. Nr:

Calibrated by

Date : 29.08.2008

ABGLEICHBLATT - PIEZORESISTIVER DRUCKSENSOR
ADJUSTMENT SHEET - PIEZORESISTIVE PRESSURE SENSOR

Exhaust

Typ / Type: 4007BA5F — SN: 1779988

Bereich / Range: 5 bar — Max. Druck / Max. Pressure: 15 bar

Kompensierter Temperaturbereich / Compensated Temperature Range: 25 ... 180 °C

Referenztemperatur / Reference Temperature: 25 °C

Anzugsdrehmoment / Mounting Torque: 1.5 ... 2.5 Nm

Kalibrierwerte für Verstärker 4618
Calibration Data for Amplifier 4618

RANGE: 8.427 V — ZERO: -0.240 V
RANGE: 17.483 mA

KISTLER INSTRUMENTE AG
CH-8408 Winterthur Schweiz / Switzerland
Kistler Doc. Nr:

Calibrated by

Date : 17.03.2009

**Figure A2 Pressure Sensor Calibration Certificate (Kistler Instrument)**

**My Publications to Date**

**1.** Effects of Ethanol on Part-Load Performance and Emissions in Throttled SI, EIVC, PVO and CAI combustion. Paper abstract accepted by International Journal of Engine Research for April 2015 special edition on use of Biofuel by: **Ojapah M M**, Zhang Y, and Zhao H.

**2**. 4-Stroke CAI/HCCI Operation on a Poppet Valve DI Engine using Gasoline and its Blends with Ethanol. Abstract accepted for SAE April 2015 World Congress with Paper Offer Number: 15PFL-0994, by: **Ojapah M M**, Zhang Y, and Zhao H.

**3**. Particulate Emissions in 2-stroke CAI combustion. Abstract Accepted for SAE April 2015 World Congress with Paper Offer Number: 15PFL-0983, by: **Ojapah M M**, Zhang Y, and Zhao H.

**4**. Effects of Ethanol on Gaseous and PM Emission in 2-Stroke CAI Combustion**.** Accepted for FISITA 2014. Paper number F2014-CET-102**: Ojapah M M**, Zhang Y, and Zhao H

**5**. Effects of Ethanol on Part-load Performance and Emissions Analysis of SI Combustion with EIVC and Throttled Operation and CAI Combustion. Paper no. SAE 2014-01-1611 by: **Ojapah M M**, Zhang Y, and Zhao H

**6.** Effects of Ethanol on Performance and Exhaust Emissions from a DI Spark Ignition Engine with Throttled and Unthrottled Operations. Paper no. SAE 2014-01-1393 by: **Ojapah M M**, Zhang Y, and Zhao H

**7**. Part-load Performance and Emissions Analysis of SI Combustion with EIVC and Throttled Operation and CAI Combustion by: **Ojapah M M**, Zhang Y, and Zhao H. IMechE paper no. C1370/023. 2013

**8**. Analysis of Gaseous and PM emissions of 4-Stroke CAI/HCCI and SI combustion in a DI Gasoline Engine. Paper no: SAE 2013-01-1549 by: **Ojapah M M**, Zhang Y, and Zhao H

**9**. Particulate Matter Emission from Different Combustion Modes in a 2/4 Stroke Switchable Direct Injection Gasoline Engine by: **Ojapah M M**, Zhang Y, and Zhao H. IMechE Paper no: C1328/021. 2011

**10**.2-stroke CAI operation on a poppet valve DI engine fuelled with gasoline and its blends with ethanol. SAE 2013-01-1674 by: Yan Zhang, Hua Zhao, **Mohammed Ojapah**, Alasdair Cairns. Measured the particulates and dyno operation.

**11**. CAI Combustion of Gasoline and its Mixture with Ethanol in a 2-Stroke Poppet Valve DI Gasoline Engine, Fuel 109 (2013) 661-668 by: Zhang Y, Hua Zhao, **Ojapah M** and Alasdair C. Measured the particulates and dyno operation.

**12**. CAI Combustion of Gasoline and its Mixture with Ethanol in a 2-Stroke Poppet Valve DI Gasoline Engine, Fisita2012-A01-013 by: Zhang Y, **Ojapah M** and Zhao H. Measured the particulates and dyno operation.

**13.** Effects of Injection Timing on CAI Operation in a 2/4 Stroke Switchable GDI Engine by: Zhang Y, Zhao H, **Ojapah M**, and Cairns A. SAE Int. J. Engines 5(2):2012, doi 10.4271/2011-01-1773. Measured the particulates and dyno operation.

**14.** 2-Stroke CAI combustion Operation in a GDI Engine with Poppet Valves by: Zhang Yan, **Mohammed Ojapah**, Alasdair cairns, and Hua Zhao. SAE 2012-01-1118. Measured the particulates and dyno operation.

**15.** Analysis of CAI/HCCI combustion in a 2-Stroke poppet valve Engine by: Zhang Y, Zhao H, **Ojapah M**, and Cairns A. IMechE C1328/010 Nov 2011. Measured the particulates and dyno operation.

**16.** Experiment and Analysis of a Direct Injection Gasoline Engine Operating with 2/4 Stroke Cycles of Spark Ignition and Controlled Auto Ignition Combustion by: Zhang Y, Zhao H, **Ojapah M**, and Cairns A. JSAE20119078, SAE 2011-01-1774. Measured the particulates and dyno operation.